

Catalytic Synthesis of Amines:
From Small Molecules to Nitrogen-Containing Polymers

by

Mitchell Robert Perry

B.Sc., The University of Prince Edward Island, 2010

M.Sc., The University of Prince Edward Island, 2012

A THESIS SUBMITTED IN PARTIAL FULFILLMENT OF
THE REQUIREMENTS FOR THE DEGREE OF

DOCTOR OF PHILOSOPHY

in

The Faculty of Graduate and Postdoctoral Studies
(Chemistry)

THE UNIVERSITY OF BRITISH COLUMBIA
(Vancouver)

September 2017

© Mitchell Robert Perry, 2017

Abstract

The research presented in this thesis highlights the utility of *N,O*-chelated complexes of early transition metals for the catalytic synthesis of amines. Two atom economic transformations to make carbon-carbon and carbon-nitrogen bonds, hydroaminoalkylation and hydroamination, were investigated. A significant expansion of the substrate scope of a pre-established catalytic system is presented, and a variety of novel titanium precatalysts were developed and screened for catalytic activity. The products of hydroaminoalkylation were employed as monomers for ring-opening metathesis polymerization using known ruthenium-based catalysts. These amine-containing polymers show interesting rheological behavior attributed to the presence of hydrogen bonding interactions.

The substrate scope of a previously reported tantalum phosphoramidate complex capable of room temperature reactivity was expanded to include a solvent-free protocol. This methodology was shown to afford amine products in comparable or greater yields than the related diluted reactions. Titanium metal was investigated as an alternative to tantalum-based precatalysts. A family of mono-, di-, and tri-substituted phosphoramidate complexes was presented, with mono-phosphoramidates outperforming the others in the catalytic synthesis of amines, despite being susceptible to unwanted ligand redistribution reactions.

The selective mono-alkylation of cyclic diene substrates was shown to generate strained alkene products suitable for use in ring-opening metathesis polymerization. Despite having unsaturated, Lewis-basic moieties, these monomers were polymerized to generate a variety of viscoelastic homopolymers bearing substituted aryl-amines with tunable hydrogen bonding potential. Thermal and rheological analysis revealed behaviours characteristic of hydrogen bonding, such as increased glass transition temperatures, and viscosity dependent on molecular

weight and amine substitution. An expansion of the monomers amenable to polymerization was presented, and a variety of copolymeric structures were synthesized. Efforts focused on pairing amine-containing monomers with those of commodity plastics, such as norbornene. Excellent control over monomer incorporation was achieved in most cases.

Preliminary investigations into useful applications of these novel polymers were presented and include anti-microbial materials, agents for sequestering metal ions, and compatibilizers for polymer blends. These preliminary experimental results show promise and future efforts will focus on realizing the full potential of these unique materials.

Lay Summary

Amines are organic molecules that contain a nitrogen atom. These are important compounds with biological applications, including pharmaceuticals. The synthesis of amines is performed on tonne scale each year and is complicated by the generation of a large amount of waste. This thesis focuses on two simple reactions using metal-based catalysts to generate amines, eliminating the production of waste byproducts. Titanium is investigated as an inexpensive, non-toxic, and “green” alternative to current technologies and aims to reduce the environmental impact of amine synthesis. Next, these amines were incorporated into new plastics that aim to improve the properties of current materials, including the observation that they becoming “stronger” when they are repeatedly stretched. These amine polymers can be incorporated into commodity plastics to modify the properties of these materials to realize new applications. The novel work described in this thesis highlights the synthesis of new small and large amine-containing molecules.

Preface

The research disclosed in this thesis was partially conducted through collaborative efforts with other members of the Schafer Research Group. In consultation with my supervisor, Dr. Laurel Schafer, I designed and conducted all the experiments described herein, except for the specific instances described below.

The synthetic development of phosphoramidate proligands and phosphoramidate tantalum complexes utilized in this research, mainly precatalyst **2**, was performed by Dr. Pierre Garcia and/or Dr. Ying Yin Lau. All thermal and rheological characterization presented in Chapter 3 and Chapter 4 was conducted by either Tannaz Ebrahimi or Tanja Tomkovic, and guided by myself, Dr. Laurel Schafer, and/or Dr. Savvas Hatzikiriakos. UBC BioServices conducted all anti-microbial testing. The polymerization of aminonorbornene **6** using G3 (section 3.4.2) was conducted in collaboration with Nirmalendu Kuanr, under my supervision. However, the experimental design was solely mine. Molecular weight analysis by gel permeation chromatography was performed on an instrument operated and maintained by the Gates Group. All data obtained from X-ray crystallography presented herein was collected by either Scott Ryken or Damon Gilmour. I performed the final refinements with the assistance of Damon Gilmour.

A portion of Chapter 2 was published by Wiley-VCH: Garcia, P., Lau, Y.Y., Perry, M.R., and Schafer, L.L. "Phosphoramidate Tantalum Complexes for Room-Temperature C-H Functionalization: Hydroaminoalkylation Catalysis" *Angew. Chem., Int. Ed.* **2013**, 52, 9144.

A portion of Chapter 3 was published by the Royal Society of Chemistry: Gilmour, D.J., Webster, R.L., Perry, M.R., and Schafer, L.L. "Titanium pyridonates for the homo- and copolymerization of *rac*-lactide and ϵ -caprolactone" *Dalton Trans.*, **2015**, 44, 12411. Another

portion of Chapter 3 was published by the American Chemical Society: Perry, M.R., Ebrahimi, T., Morgan, E., Edwards, P.M., Hatzikiriakos, S.G., and Schafer, L.L. “Catalytic Synthesis of Secondary Amine-Containing Polymers: Variable Hydrogen Bonding for Tunable Rheological Properties” *Macromolecules*, **2016**, 49, 4423. A portion of Chapter 3 was also included in a provisional patent: Perry, M.R., Morgan, E.M., Edwards, P.M., and Schafer, L.L. Nitrogen containing polymers and a one-pot synthesis of these materials. 62/114, 171. Filed Feb 10th, **2015**.

Table of Contents

Abstract.....	ii
Lay Summary	iv
Preface.....	v
Table of Contents	vii
List of Tables	xiii
List of Figures.....	xv
List of Schemes.....	xxiii
List of Compounds.....	xxvi
List of Equations	xxxii
List of Abbreviations and Acronyms	xxxiii
Acknowledgements	xxxvi
Dedication	xxxvii
Chapter 1: Introduction	1
1.1 The Advent of Functional Polymeric Materials.....	1
1.2 Controlled and Living Polymerizations.....	2
1.3 Ring-Opening Metathesis Polymerization.....	3
1.3.1 Mechanistic Aspects of Ring-Opening Metathesis Polymerization	6
1.3.2 Grubbs Metathesis Catalysts.....	8
1.3.3 Copolymer Synthesis	10
1.4 Nitrogen-Containing Polymers	11
1.5 Rheology	17

vii

1.6	Hydrogen bonding	21
1.7	Scope of Thesis	24
Chapter 2: Titanium Phosphoramidate for the Catalytic Synthesis of Amines.....		27
2.1	Introduction.....	27
2.2	Catalytic Synthesis of Amines.....	28
2.3	Hydroaminoalkylation	31
2.4	Hydroamination	34
2.5	Tantalum, Titanium, and the Motivation for New Catalysts	36
2.6	Early Transition Metal Catalysts in Small Molecule Forming Reactions	38
2.6.1	Tantalum Phosphoramidates for Hydroaminoalkylation.....	46
2.6.2	Monophosphoramidate Titanium Complexes.....	57
2.6.3	Diphosphoramidate Titanium Complexes	66
2.6.4	Tri(phosphoramidate) Titanium Complexes.....	74
2.6.5	Monophosphoramidate mono(chloro) Titanium Complexes.....	83
2.7	Titanium Phosphoramidates in C-C and C-N Bond Forming Reactions.....	88
2.7.1	Hydroaminoalkylation with Monophosphoramidate Titanium Species	88
2.7.2	Hydroaminoalkylation with Diphosphoramidate Titanium Species.....	91
2.7.3	Titanium Phosphoramidates for Mono-alkylation of Norbornadiene.....	93
2.8	Hydroamination	95
2.8.1	Intramolecular Hydroamination of Primary Aminoalkenes	96
2.8.2	Hydroamination of Secondary Aminoalkenes	98
2.9	Conclusions.....	100
2.10	Experimental	103

2.10.1	Materials and Methods.....	103
2.10.2	Synthesis and Characterization.....	104
Chapter 3: Hydroaminoalkylation and Ring-Opening Metathesis Polymerization: Synthesis of Nitrogen-Containing Polymers.....		115
3.1	Schafer Chemistry in the Field of Polymeric Materials.....	115
3.2	Tantalum Phosphoramidates: Coupling Hydroaminoalkylation and Ring-Opening Metathesis Polymerization.....	117
3.3	Small Molecule Synthesis by HAA: Selective Formation of ROMP Monomers.....	118
3.3.1	Tantalum-Catalyzed Hydroaminoalkylation: Expansion of Amine Scope.....	124
3.4	Aminonorbornenes in Ring-Opening Metathesis Polymerization.....	126
3.4.1	Polymerization of Aminonorbornene Monomer 6 with G2.....	126
3.4.2	Polymerization of Aminonorbornene monomer 6 with G3	132
3.4.3	Attempted Polymerization of Alkyl-Substituted Substrate, 42.....	136
3.4.4	Living Polymerization of Secondary Amine-Containing Monomers.....	137
3.5	Expansion of Polymer Scope: Polymerization of Aryl-Substituted Monomers	141
3.6	Aminocyclooctene Monomer Synthesis by Hydroaminoalkylation.....	144
3.7	Ring-Opening Metathesis Polymerization of Aminocyclooctenes.....	146
3.8	Probing Hydrogen Bonding by IR Spectroscopy.....	152
3.9	Thermal Analysis of Functionalized Polymers.....	156
3.10	Rheology	160
3.10.1	Rheology of Methoxy-Functionalized Aminonorbornene Polymers.....	160
3.10.2	Rheology of Variously-Substituted Aminonorbornene Polymers	165
3.11	Conclusions.....	166

3.12	Experimental.....	169
3.12.1	Materials and Methods.....	169
3.12.2	Synthesis and Characterization.....	171
Chapter 4: Expansion of Nitrogen-Containing Polymers and Synthesis of Copolymers....		179
4.1	Introduction.....	179
4.2	Attempted Polymerization of Alkyl Amine 42 with G3.....	181
4.3	Derivatization of Cyclohexyl Aminonorbornene Substrate, 42.....	184
4.3.1	Attempted Alkylation with Alkyl Halides to Access Quaternary Amine Monomers	184
4.3.2	Attempted Alkylation of 42 <i>via</i> Reductive Amination.....	185
4.3.3	Attempted Eschweiler-Clarke Alkylation.....	187
4.3.4	Quaternization of Aminonorbornene 42 with HCl	188
4.4	Synthesis and Polymerization of a Tertiary Alkyl Amine Monomer	189
4.4.1	Secondary Amine Derivatization using Benzyl Chloride.....	189
4.4.2	Polymerization of Tertiary Amine Monomer 49 using G2.....	191
4.4.3	Polymerization of 49 using G2: Monitoring Reaction Progress.....	195
4.4.4	Reactivity of G1 and G3 Towards Benzyl Amine Monomer 49	198
4.5	Material Characterization.....	201
4.6	Polymers Containing Both Amine and Alcohol Functionalities.....	205
4.6.1	Thermal Analysis of TBDMS-Protected Polymer, P50.....	213
4.7	Nitrogen-Containing Copolymers.....	215
4.7.1	Copolymers of Amine-Containing and Hydrocarbon Monomers	216
4.7.2	Amine-Containing Copolymers including Hydrocarbon Comonomers	226

4.7.3	Copolymers of Two Amine-Containing Monomers	231
4.8	Potential Applications of Nitrogen-Containing Polymers	236
4.9	Conclusions	239
4.10	Experimental	241
4.10.1	Materials and Methods	241
4.10.2	Synthesis and Characterization	243
Chapter 5: Conclusions and Future Work		248
5.1	Summary	248
5.2	Future Directions	255
5.2.1	Synthesis of Sterically Bulky Mono-Ligated Titanium Complexes	255
5.2.2	Further Investigations and Expansion of H-Bonding in Polymers	256
5.2.3	Post-Polymerization Chemistry	257
5.2.4	Potential Applications for Nitrogen-Containing Polymers	259
5.3	Concluding Remarks	261
References		262
Appendices		276
Appendix A Supplementary Information for Chapter 2		276
A.1	Selected NMR Spectra	276
A.2	Additional Information Regarding the Geometry Index Parameter	289
A.3	Method for Monitoring Hydroaminoalkylation Reactivity	290
Appendix B Supplementary Information for Chapter 3		291
B.1	Selected NMR Spectra of Aminonorbornenes and Other Products	291
B.2	Selected NMR Spectra of Polymers	300

B.3	Additional Information for Chapter 3	307
Appendix C	Supplementary Information for Chapter 4	310
C.1	Selected NMR Spectra of Aminonorbornenes and Other Products.....	310
C.2	Selected NMR Spectra of Polymers	316
C.3	Additional Information for Chapter 4	319
Appendix D	X-Ray Crystallographic Data	324
D.1	X-Ray Crystallographic Data Presented in Chapter 2	324
D.2	X-Ray Crystallographic Data Presented in Chapter 3	332
D.3	X-Ray Crystallographic Data Presented in Chapter 4	334
Appendix E	Additional Formulas and Information	336

List of Tables

Table 1 Room temperature hydroaminoalkylation using 2 under solvent-free conditions.....	50
Table 2 Reactions of silylated substrates using 2 under solvent-free conditions	55
Table 3 Select bond lengths (Å) and angles (°) for monophosphoramidate complex 18	61
Table 4 Select bond lengths (Å) and angles (°) for triphosphoramidate complex 26.....	77
Table 5 Hydroaminoalkylation reactivity of monophosphoramidate titanium complexes generated <i>in situ</i>	90
Table 6 Hydroaminoalkylation activity of isolated diphosphoramidate titanium complexes	93
Table 7 Hydroaminoalkylation of strained diene to generate monoalkylated product 6.....	94
Table 8 Hydroamination of primary aminoalkene 36 using complex 18	97
Table 9 Screening of titanium complexes for intramolecular hydroamination of secondary aminoalkene, 38	99
Table 10 Select bond lengths (Å) and angles (°) for compound 6.....	121
Table 11 Polymerization data for monomer 6	131
Table 12 Polymerization data for monomer 6 using G3.....	133
Table 13 Living polymerization data for monomer 6.....	138
Table 14 Polymerization data for monomer 6 at various times.....	139
Table 15 Polymerization data for monomers 6 and 43-45 to form P6 and P43-45	143
Table 16 Thermal properties of variously substituted amine polymers.....	158
Table 17 Conversion of benzyl monomer 49 to P49 using G2.....	196
Table 18 Comparison of GPC data obtained for P49 synthesized by G1, G2, and G3	200
Table 19 Data for copolymers synthesized from PNB macroinitiators and 6	222
Table 20 Characterization of copolymers synthesized from PNB macroinitiators and 6.....	224

Table 21 Copolymers of NBE or COE and 6 synthesized from sequential or single addition protocols.....	227
Table 22 Percent composition and thermal properties of copolymers of NBE or COE and 6 ...	229
Table 23 Sequestration of Cu(II)SO ₄ with tertiary amine polymer P49	238

List of Figures

Figure 1 Select cyclic alkenes and their respective ring strain values (kcal/mol)	4
Figure 2 Polymers of norbornene from Ziegler-Natta (top) and ROMP (bottom) ^{35, 37}	4
Figure 3 Inter- and intramolecular (backbiting) chain-transfer reactions ^{24, 35}	5
Figure 4 ROMP mechanism: initiation (top), propagation (middle), and termination (bottom) ^{24, 43}	6
Figure 5 Grubbs metathesis catalysts: G1, G2, and G3, respectively	8
Figure 6 Representations of linear copolymers	10
Figure 7 Select uses of amine-containing polymers ¹⁰⁵	12
Figure 8 Donor-induced decomposition of ruthenium alkylidene complexes by unprotected amines ¹²⁶	14
Figure 9 ROMP of unprotected amino-acid derived monomers.....	15
Figure 10 Representation of a parallel plate rheometer	17
Figure 11 Complex modulus (G^*) as represented as a vector diagram comprised of storage modulus (G' , y-axis) and loss modulus (G'' , x-axis).....	19
Figure 12 Typical behaviour of an unlinked (left) and linked or partially linked (right) viscoelastic polymer ^{140, 143-144}	20
Figure 13 Representation of reversible association of hydrogen bonding side groups ¹⁵⁰	22
Figure 14 Hydrolysis of acrylate polymers gives acrylic acid groups with hydrogen bonding potential ¹⁴⁸	23
Figure 15 Select amines and their respective uses.....	27
Figure 16 Common traditional synthetic approaches to amine synthesis.....	28

Figure 17 Catalytic synthesis of amines by Buchwald-Hartwig amination (top), direct C-H amination (middle), and hydroaminomethylation (bottom) ^{218, 223, 230-231}	30
Figure 18 Common <i>N,O</i> -chelating ligands used by the Schafer Group: amidates, ureates, pyridonates, and phosphoramidates	33
Figure 19 Selected titanium complexes bearing <i>N,O</i> -chelating ligands ^{77, 247-248, 258, 261, 264, 318-322}	38
Figure 20 Previous titanium and zirconium <i>N,O</i> -chelated complexes reported by the Schafer Group	40
Figure 21 Titanium complexes bearing aminopyridinato ³⁴¹ and phenylaminopyridinato ³⁴² ligands for hydroaminoalkylation.....	42
Figure 22 Precatalyst development for hydroaminoalkylation catalyzed by tantalum precatalysts ¹⁸³	47
Figure 23 ORTEP of compound 11. Ellipsoids shown at 50% probability. Hydrogen atoms omitted for clarity	52
Figure 24 ¹ H and ³¹ P{ ¹ H} (inset) NMR spectra (300 MHz and 121 MHz, respectively, C ₆ D ₆ , 298 K) of monophosphoramidate complex 18.....	59
Figure 25 ORTEP of complex 18. Ellipsoids shown at 50% probability. Hydrogen atoms removed for clarity.....	60
Figure 26 Idealized square pyramidal and trigonal bipyramidal molecular geometries.....	62
Figure 27 ¹ H and ³¹ P{ ¹ H} (inset) spectra (C ₆ D ₆ , 300 MHz and 121 MHz respectively, 298 K) of monophosphoramidate complex 21	64
Figure 28 Ligand redistribution of complex 21 over time to form diphosphoramidate side product 22 as observed by ³¹ P NMR spectroscopy (C ₆ D ₆ , 121 MHz, 298 K).....	65

Figure 29 ^1H and $^{31}\text{P}\{^1\text{H}\}$ NMR (inset) spectra of complex 22 (C_6D_6 , 300 MHz and 121 MHz, respectively, 298 K).....	68
Figure 30 Diphosphoramidate complexes 19 and 22-25. Yields shown represent isolated percent yields of recrystallized products, except that of 25 which represents the yield of crude product. $^{31}\text{P}\{^1\text{H}\}$ NMR spectroscopy (C_6D_6 , 121 MHz, 298 K).....	69
Figure 31 ORTEP and selected bond lengths and angles for diphosphoramidate complexes 23 (left) and 24 (right). All ellipsoids shown at 50% probability and all hydrogen atoms removed for clarity	72
Figure 32 ORTEP and selected bond lengths and angles for diphosphoramidate complexes 19 (left) and 22 (right). All ellipsoids shown at 50% probability and all hydrogen atoms removed for clarity. Isopropyl groups shown as wire frames for clarity	73
Figure 33 ORTEP of triphosphoramidate complex 26. Ellipsoids shown at 50% probability. Hydrogen atoms omitted for clarity.....	76
Figure 34 ^1H and ^{31}P (inset) spectrum of triphosphoramidate complex 26, (C_6D_6 , 300 MHz and 121 MHz, 298 K).....	79
Figure 35 Variable temperature ^1H NMR spectra of complex 26 (tol- d_8 , 400 MHz).....	80
Figure 36 Variable temperature ^{31}P NMR spectra of complex 26 (tol- d_8 , 400 MHz).....	81
Figure 37 ATR-IR spectra of di- and triphosphoramidate complexes 19 and 26.....	82
Figure 38 ORTEP of complex 28. Ellipsoids shown at 50% probability. Hydrogen atoms removed for clarity.....	85
Figure 39 Synthesis of diphenyl phosphinic ligands from P(III) and P(V) starting materials	86
Figure 40 Synthesis of diphenyl-substituted proligands 30 and 31 from diphenylphosphinic chloride	86

Figure 41 Hydroaminoalkylation screening using monophosphoramidate titanium complexes..	89
Figure 42 Intermolecular hydroaminoalkylation using 4-methoxy- <i>N</i> -methyl aniline and 1-octene. Reactions were conducted using isolated diphosphoramidate complexes 19 and 22-25.....	92
Figure 43 Zirconium pyridonate complex capable of intramolecular hydroamination and hydroaminoalkylation	96
Figure 44 Titanium pyridonate complexes explored by the Schafer Group for the ring opening polymerization of cyclic esters	115
Figure 45 ORTEP of complex 41. Ellipsoids shown at 50% probability. Hydrogen atoms omitted for clarity.....	116
Figure 46 Sequential synthesis of nitrogen-containing polymers by coupling HAA and ROMP methodologies.....	118
Figure 47 Solvent-free HAA using 2 to generate secondary amines in good yields. Isolated percent yields from solution-phase reactivity are shown in parentheses and those solvent-free reactions are shown in red.....	119
Figure 48 Synthesis of strained aminonorbornene 6 <i>via</i> HAA using 2	120
Figure 49 ¹ H NMR spectrum of norbornene monomer 6 (300 MHz, CDCl ₃ , 298 K).....	120
Figure 50 ORTEP of complex 6. Ellipsoids shown at 50% probability. Hydrogen atoms removed for clarity.....	121
Figure 51 Crystal lattice (top) and selected region displaying H-bonding (bottom) of compound 6. N-H-OCH ₃ H-bond distance is 2.168 Å	122
Figure 52 ATR-IR spectra of methoxy-substituted aminonorbornene 6, in the solid-state (black) and the liquid state (red)	123

Figure 53 Room temperature HAA generates mono-functionalized aminonorbornenes in one step	125
Figure 54 ^1H NMR overlay of monomer, 6, (bottom) and polymer, P6, (top) (CDCl_3 , 300 MHz, 298 K)	128
Figure 55 Real-time monitoring of monomer conversion of 6 with G2 as observed by ^1H NMR spectroscopy (600 MHz, THF-d_8 , 298 K). At time 0 min the sample was at $-196\text{ }^\circ\text{C}$	129
Figure 56 Conversion of monomer 6 to P6 with G3.....	134
Figure 57 Conversion of monomer 6 to P6 using G3 as determined by ^1H NMR spectroscopy (400 MHz, THF-d_8 , 298 K).....	135
Figure 58 Conversion (%) of monomer 6 to P6 over time (h) using G2	140
Figure 59 Molecular weight (blue) (M_n , g mol^{-1}) and dispersity (red) (M_w/M_n) vs. conversion (%) of 6 to P6.....	140
Figure 60 Polymerization of aryl-substituted aminonorbornene monomers 6 and 43-45	141
Figure 61 Formation of aminocyclooctene monomers 46 and 47 <i>via</i> HAA.....	145
Figure 62 ^1H NMR spectra (CDCl_3 , 300 MHz, 298 K) of cyclooctene monomers 46 (bottom) and 47 (top).....	146
Figure 63 ROMP of aminocyclooctene monomers 46 and 47 to form P46 and P47, respectively	147
Figure 64 Overlay of ^1H NMR spectra of P46 (bottom) and P47 (top) (CDCl_3 , 300 MHz, 298 K)	148
Figure 65 ATR-IR spectra of neat 6 and the ring-opened polymeric form, P6	153
Figure 66 ATR-IR spectra of monomer 43 and the ring-opened polymeric form, P43.....	154
Figure 67 ATR-IR spectra of P6 and P43-P45 of similar molecular weight.....	155

Figure 68 Overlay of TGA thermograms of aryl-substituted amine homopolymers P6 and P43-45 and commercial PNB	159
Figure 69 Master curves ($T_{\text{ref}} = 120\text{ }^{\circ}\text{C}$) of the viscoelastic moduli (G' & G'') and complex viscosity (η^*) as a function of the angular frequency (ω) for (a) polynorbornene (PNB) ($M_n = 119,700\text{ g mol}^{-1}$, $D = 1.35$), (b) P6 ($M_n = 94,900\text{ g mol}^{-1}$, $D = 1.05$).....	161
Figure 70 Viscoelastic moduli (G' and G'') ($T_{\text{ref}} = 120\text{ }^{\circ}\text{C}$) of P6 samples of various molecular weight.....	162
Figure 71 Scaling of the zero shear viscosity of M_w for P6 ($\eta_0 = 3765\text{ exp (E-4 } M_w)$ versus unfunctionalized PNB ($\eta_0 = 5\text{E-13} M_w^{3.77}$)	163
Figure 72 Complex viscosity (η^*) vs angular frequency master curves for (a) unfunctionalized PNB and (b) P6 of various molecular weight ($T_{\text{ref}} = 120\text{ }^{\circ}\text{C}$)	164
Figure 73 Complex viscosity (η^*) of variously substituted aminonorbornene polymers ($T_{\text{ref}} = 120\text{ }^{\circ}\text{C}$).....	165
Figure 74 ^1H NMR spectra of 42 and G3 (bottom), after 4 h (middle), and 20 h (top) (CDCl_3 , 400 MHz, 298 K). Reaction performed in THF, quenched, and dried <i>in vacuo</i> prior to analysis in CDCl_3	183
Figure 75 ^1H NMR spectrum (CDCl_3 , 300 MHz, 298 K) of compound 49	190
Figure 76 ATR-IR spectra of unprotected, secondary amine monomer, 42 (blue), and benzyl-substituted tertiary amine monomer 49, (red). Inset shows the NH stretching region	191
Figure 77 ^1H NMR (CDCl_3 , 300 MHz, 298 K) spectrum of tertiary benzyl polymer P49.....	193
Figure 78 ATR-IR spectra of neat 49 and the ring-opened polymeric form, P49	194
Figure 79 ^1H NMR spectra overlay of monomer 49 over time with G2 (THF-d_8 , 400 MHz, 298 K)	197

Figure 80 Conversion of benzyl monomer 49 with G1, 100:1	199
Figure 81 Polymerization of benzyl monomer 49 to generate P49 using G1, G2, or G3	200
Figure 82 DSC thermogram of P49 ($M_n = 158,300 \text{ g mol}^{-1}$, $D = 1.11$)	202
Figure 83 Summary of glass transition temperatures from TGA (red) and rheology (black)	202
Figure 84 TGA analysis of secondary aryl amine polymer P49 ($M_n = 158,300 \text{ g mol}^{-1}$, $D = 1.11$)	203
Figure 85 Summary of thermal decomposition data of secondary and tertiary amine polymers. T_d , 5% (red) and T_d , 50% (blue)	204
Figure 86 ^1H NMR spectrum (CDCl_3 , 300 MHz, 298 K) of TBDMS-protected monomer 50 ..	208
Figure 87 ATR-IR overlay of TBDMS-substituted monomer, 50 (blue), and OH-substituted monomer, 51 (red)	209
Figure 88 GPC chromatogram overlay of P51 at T 0 (red) and after sitting in solution for 1 month (blue). Light scattering data is displayed	211
Figure 89 DSC thermogram of TBDMS-protected polymer, P50	213
Figure 90 TGA thermogram of TBDMS-protected polymer, P50	214
Figure 91 ^1H NMR spectrum (300 MHz, CDCl_3 , 298 K) of a copolymer synthesized using of amine-containing macroinitiator 6 and NBE, 5:5	218
Figure 92 ^1H NMR spectrum (CDCl_3 , 300 MHz, 298 K) of a copolymer synthesized using a PNB macroinitiator and 6, 5:5	220
Figure 93 Overlay of ^1H NMR spectra (CDCl_3 , 300 MHz, 298 K) of copolymers synthesized from PNB macroinitiators and 6. The relative incorporation values are shown above the corresponding spectra	223
Figure 94 DSC thermograms of poly(NBE- <i>block</i> -6) of various monomer incorporations	225

Figure 95 Generation of diblock copolymers from NBE or COE and 6 using a sequential addition protocol	226
Figure 96 ^1H NMR spectrum (CDCl_3 , 300 MHz, 298 K) of copolymer from 100:100 NBE:6 (Table 19, Entry 1).....	228
Figure 97 TGA thermograms of copolymers of NBE or COE and 6, described in Table 22	230
Figure 98 DSC thermograms of copolymers of NBE or COE and 6, described in Table 22	231
Figure 99 ^1H NMR spectrum (CDCl_3 , 300 MHz, 298 K) of copolymer synthesized from 6 and 46 (100:100).....	234
Figure 100 TGA thermogram of amine-containing copolymer comprised of 6 and 46	235
Figure 101 Proposed benzyl-monomers to generate tertiary polymers to probe H-bonding effects	257
Figure 102 Idealized square pyramidal and trigonal bipyramidal molecular geometries.....	289
Figure 103 Representative ^1H NMR spectrum (tol-d_8 , 300 MHz, 298 K) for monitoring hydroaminoalkylation reactions between 1-octene and 4-methoxy- <i>N</i> -methyl aniline, and determining yield by ^1H NMR spectroscopy. This reaction went to 41% yield using precatalyst 18.....	290
Figure 104 ORTEP of compound 48 synthesized by adding HCl to monomer 42.....	335

List of Schemes

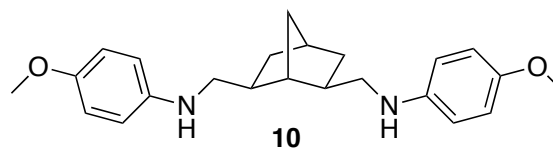
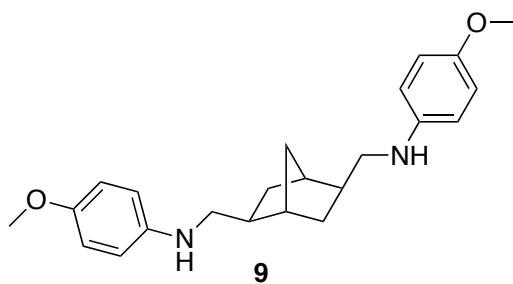
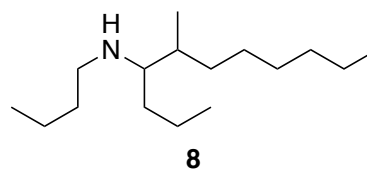
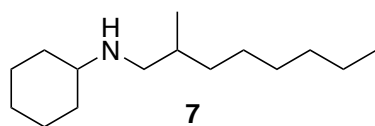
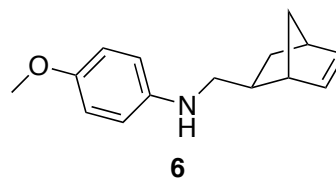
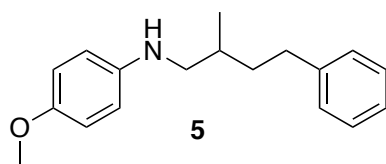
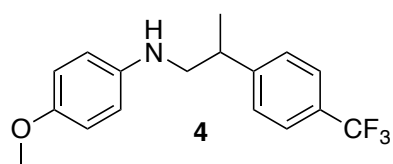
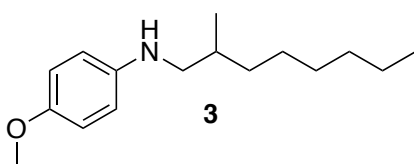
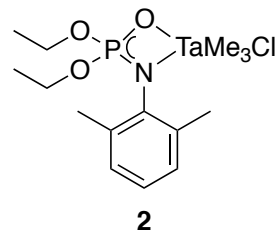
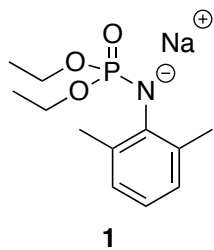
Scheme 1 Synthesis of Nylon 6,6	1
Scheme 2 General ROMP of a cyclic olefin.....	4
Scheme 3 ROMP of an unprotected secondary amine using a highly active molybdenum catalyst ¹³⁶	16
Scheme 4 Hydroaminoalkylation of amines and alkenes	31
Scheme 5 Proposed mechanism for intermolecular hydroaminoalkylation catalyzed by homoleptic early transition metal dimethylamido complexes	32
Scheme 6 Intermolecular (top) and intramolecular (bottom) hydroamination of alkenes.....	34
Scheme 7 Mono(aminopyridonate) titanium complexes for hydroamination ²⁴⁶	43
Scheme 8 Intermolecular hydroaminoalkylation of internal and terminal alkenes with <i>N</i> -methylaniline using a titanium mono(formamidinate) titanium complex ³⁴⁶	44
Scheme 9 Mono(<i>N,O</i>) amido ether titanium complexes capable of hydroamination of aminoalkenes ²⁵⁸	45
Scheme 10 Synthesis of phosphoramidate chloro complex 2 <i>via</i> salt metathesis from 1	48
Scheme 11 Derivatization of 6 with <i>p</i> -nitrobenzenesulfonyl chloride to form product 11	52
Scheme 12 Formation of dialkylated products 9 and 10 by hydroaminoalkylation	53
Scheme 13 Previously reported result of linear regioselectivity with silylated substrates using complex 2 ¹⁸³	54
Scheme 14 Synthesis of monophosphoramidate titanium complex 18	57
Scheme 15 Synthesis of monophosphoramidate titanium complex 21	63
Scheme 16 Synthesis of diphosphoramidate titanium complex 22	67
Scheme 17 Synthesis of diphosphoramidate complex 19 <i>via</i> salt metathesis	71

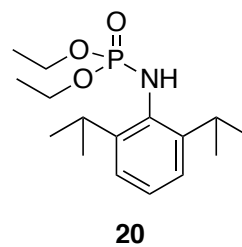
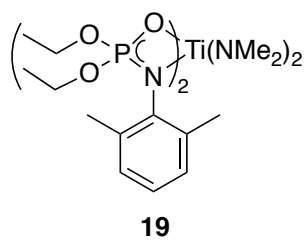
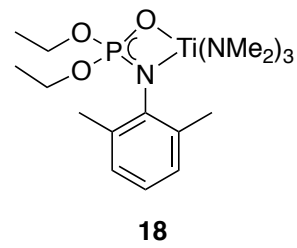
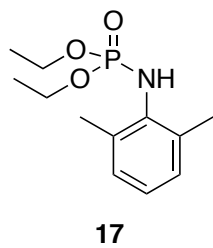
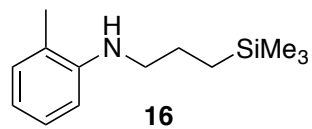
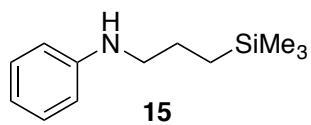
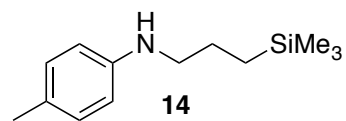
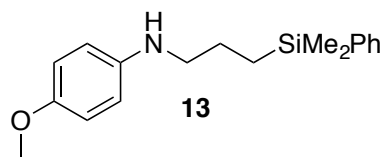
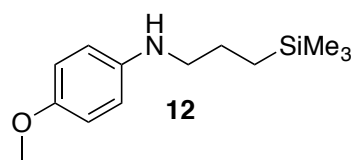
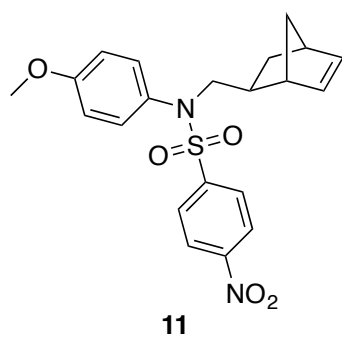
Scheme 18 Synthesis of triphosphoramidate complex 26 <i>via</i> protonolysis.....	75
Scheme 19 Attempted salt metathesis to generate a mono(chloro) titanium complex	83
Scheme 20 Attempted hydroaminoalkylation of <i>N</i> -methylcyclohexylamine and 1-octene using complex 18.....	91
Scheme 21 Polymerization of monomer 6 to form the respective polymer, P6	127
Scheme 22 Attempted polymerization of cyclohexyl-substituted norbornene, 42	137
Scheme 23 Living polymerization of monomer 6 with G2. Propagation continues upon a second aliquot of 6	137
Scheme 24 Polymerization of monomer 47 with added PPh ₃	151
Scheme 25 Attempted polymerization of secondary alkyl amine substrate 42 with G3	182
Scheme 26 Attempted alkylation of cyclohexyl monomer 42 with 1-bromobutane	184
Scheme 27 Synthesis of quaternary ammonium salt <i>via</i> alkylation of 42 with methyl iodide...	185
Scheme 28 Attempted synthesis of tertiary monomers <i>via</i> reductive amination with 42.....	186
Scheme 29 Attempted alkylation of 42 <i>via</i> reductive amination with <i>p</i> -methylbenzaldehyde ..	187
Scheme 30 Attempted Eschweiler-Clarke methylation of 42.....	187
Scheme 31 Alkylation of 42 with benzyl chloride to form tertiary amine monomer 49.....	189
Scheme 32 Polymerization of benzyl amine monomer 49 using G2.....	192
Scheme 33 Protection of 4-(methylanino)phenol with TBDMS-Cl	206
Scheme 34 HAA using silyl ether to produce TBDMS-protected monomer 50	207
Scheme 35 Polymerization of amino alcohol monomer, P51	210
Scheme 36 Polymerization of TBDMS-protected monomer, 50 to generate P50.....	212
Scheme 37 Copolymer synthesis using an amine-containing macroinitiator from 6, and comonomer NBE	217

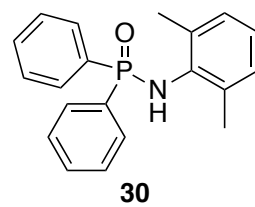
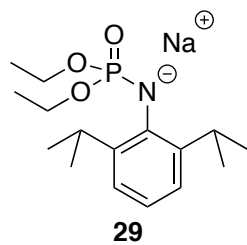
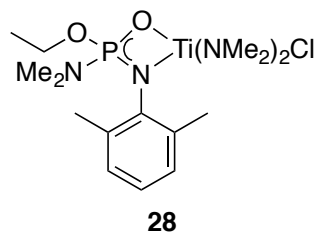
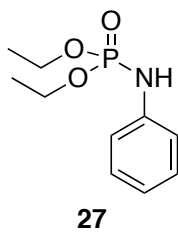
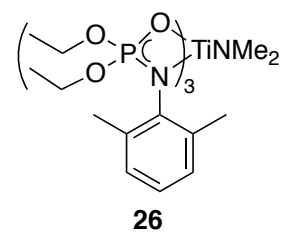
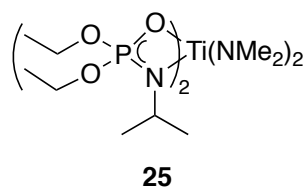
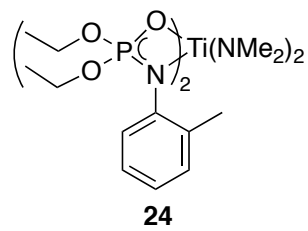
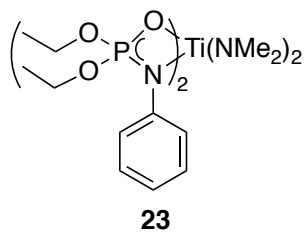
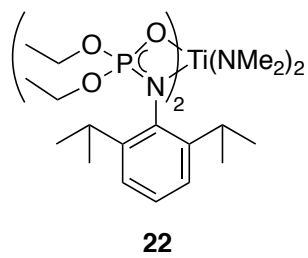
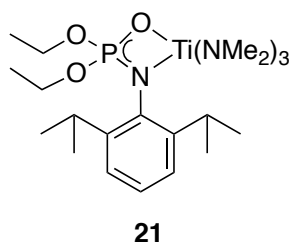
Scheme 38 Copolymer synthesis using a PNB macroinitiator and comonomer 6	219
Scheme 39 Synthesis of copolymers from PNB macroinitiators of various chain lengths	221
Scheme 40 Diblock copolymer synthesis using amine-containing monomers.....	232
Scheme 41 Proposed synthesis of an adamantyl-substituted phosphoramidate complex.....	256
Scheme 42 Protonation of P6 to generated quaternary amine moieties.....	258
Scheme 43 Brominated polymer P44 as a macroinitiator for ATRP.....	259

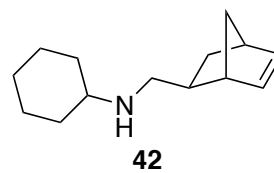
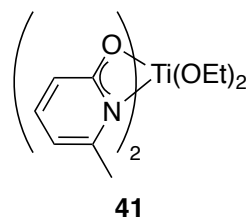
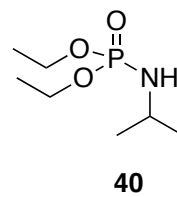
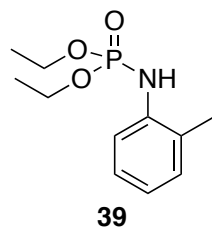
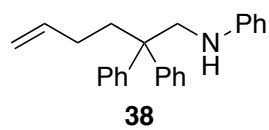
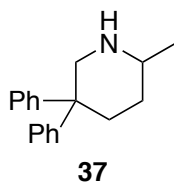
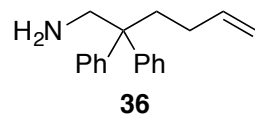
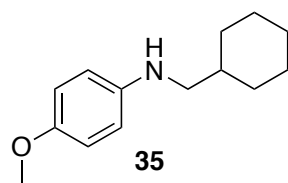
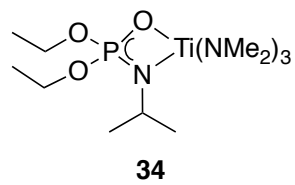
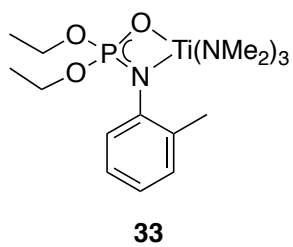
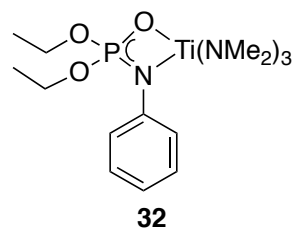
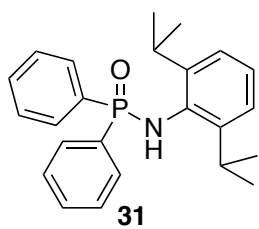
List of Compounds

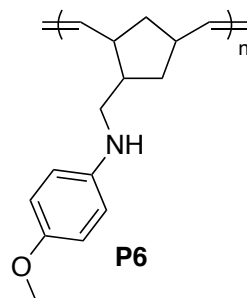
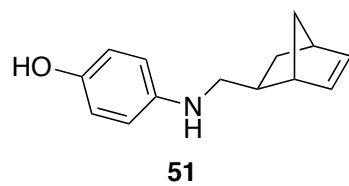
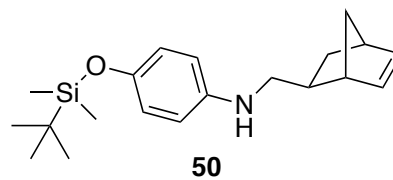
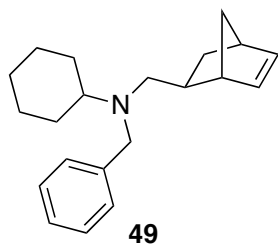
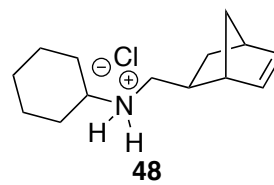
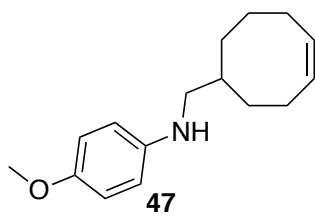
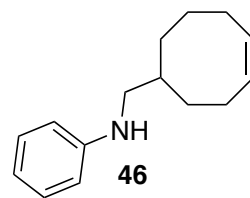
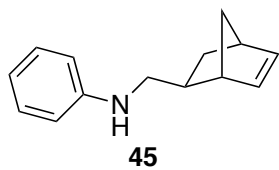
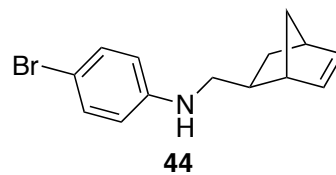
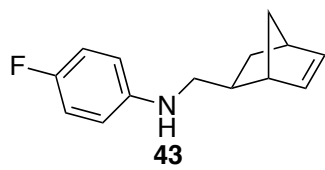
This following list of compounds is intended to act as a reference for the reader:

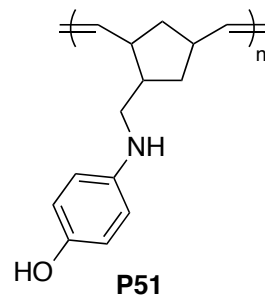
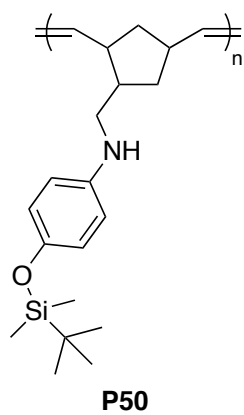
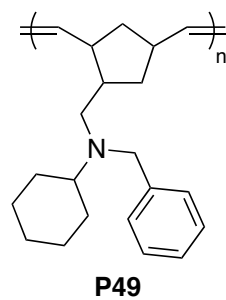
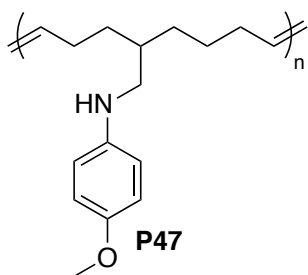
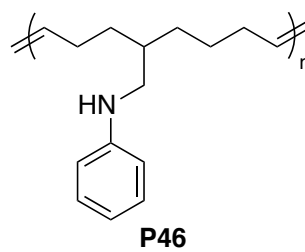
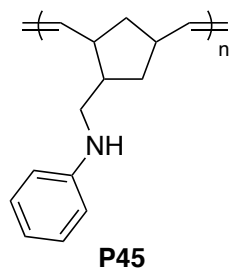
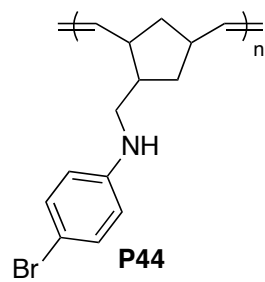
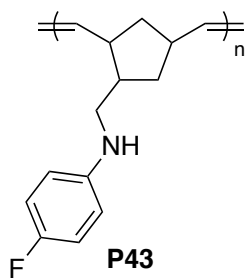












List of Equations

Equation 1 Formula used in the calculation of τ_5 values.....	289
Equation 2 Equation for determining percent yield of hydroaminoalkylation reactions.....	290

List of Abbreviations and Acronyms

AP	aminopyridonate
aq	aqueous
Ar	aryl
ATR	attenuated total reflection
ATRP	atom transfer radical polymerization
B	billion
Boc	<i>tert</i> -butyloxycarbonyl
<i>ca.</i>	circa
calcd	calculated
CDCl ₃	chloroform-d
CI	chemical ionization
COD	cyclooctadiene
COE	cyclooctene
<i>D</i>	dispersity
DCM	dichloromethane
<i>dipp</i>	2,6-diisopropylphenyl
DLS	dynamic light scattering
DMF	dimethylformamide
DP	degree of polymerization
DSC	differential scanning calorimetry
<i>e.g.</i>	exempli gratia
EI	electron ionization
eq.	equivalent
<i>et al.</i>	et alibi
etc.	et cetera
EVE	ethyl vinyl ether
ϵ	epsilon
G1	Grubbs 1 st generation catalyst
G2	Grubbs 2 nd generation catalyst
G3	Grubbs 3 rd generation catalyst
GPC	gel permeation chromatography
h	hour
H-bond	hydrogen bond
HA	hydroamination
HAA	hydroaminoalkylation
HRMS	high resolution mass spectrometry
<i>i.e.</i>	id est

<i>i</i> Pr	isopropyl
IR	infrared
LLS	laser light scattering
LRMS	low resolution mass spectrometry
LS	light scattering
M	molar
<i>m/z</i>	mass-to-charge ratio
MeCN	acetonitrile
mg	milligram
MHz	megahertz
min	minute
<i>M_n</i>	number-average molecular weight
MRSA	methicillin-resistant <i>Staphylococcus aureus</i>
MS	mass spectrometry
MSSA	methicillin-sensitive <i>Staphylococcus aureus</i>
MW	molecular weight
<i>M_w</i>	weight-average molecular weight
NaHMDS	sodium bis(trimethylsilyl)amide
NBD	norbornadiene
NBE	norbornene
<i>n</i> BuLi	<i>n</i> -butyllithium
NHC	<i>N</i> -heterocyclic carbene
NMR	nuclear magnetic resonance
o/n	overnight
ORTEP	Oakridge Thermal Ellipsoid Plot
PMP	<i>para</i> -methoxyphenyl
PNB	polynorbornene
ppm	parts per million
ROMP	ring-opening metathesis polymerization
ROP	ring-opening polymerization
RT	room temperature
sqp	square pyramidal
TBAF	tetrabutylammonium fluoride
TBDMS-Cl	<i>tert</i> -butyldimethylsilyl chloride
tbp	trigonal bipyramidal
<i>t</i> Bu	tertiary butyl
<i>T_d</i> , 5%	5% onset decomposition temperature
<i>T_d</i> , 50%	50% weight loss decomposition temperature
TEA	triethylamine

T_g	glass transition temperature
TGA	thermogravimetric analysis
TMS	trimethylsilyl
tol	toluene
USD	United States Dollar
vs.	versus
VT	variable temperature
xs	excess
κ	kappa
π	pi
σ	sigma

Acknowledgements

This body of work was possible only with the help of several individuals. I would like to acknowledge Dr. Laurel Schafer for her guidance throughout the course of this degree. She has greatly impacted the way I approach fundamental science and will continue to influence and inspire me throughout my independent career.

I would like to express my gratitude to my committee members, Dr. Derek Gates and Dr. Michael Wolf, for valuable input and critique of this document prior to submission. I would also like to acknowledge the efforts of Dr. Ying Yin Lau and Damon Gilmour for their help with proofreading. All comments and suggestions have improved the quality of this thesis.

The completion of the work presented in this document and the presentation of such was made possible through the generous financial contributions of the Natural Sciences and Engineering Research Council, the Dr. Arnold By Travel Fellowship, the Walter C. Sumner Memorial Fellowship, the Gladys Estella Laird Research Fellowship, the University of British Columbia, the Faculty of Graduate Studies, and the National Science Foundation.

Thank you to the people with whom I have had the pleasure of sharing this experience. Special acknowledgement goes to Amber Shukaliak, Damon Gilmour, Nirmal Kuanr, Ying Lau, JM and Nat Lauzon, Pippa Payne, Joe Clarkson, Scott Ryken, Barahman Movassagh, Andreas Wagner, Erin Morgan, and Désirée Sauer. Your help and encouragement both in and out of lab is greatly appreciated.

Dedication

This thesis is dedicated to my parents,

Robert Perry and Dr. Gloria McInnis-Perry,

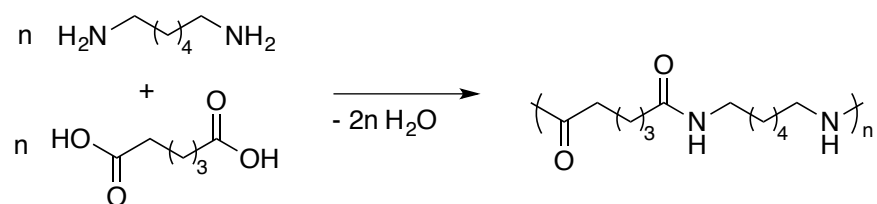
and my brother,

Dr. Benjamin Perry

Chapter 1: Introduction

1.1 The Advent of Functional Polymeric Materials

The 19th century is credited as the beginning of the synthetic polymer industry.¹ Early investigations dealt with the manipulation of naturally occurring polymers including the vulcanization of rubber by Goodyear and the synthesis of gun-cotton (Parkesine) from cellulose and nitric acid, as synthesized by Parkes in *ca.* 1860.² The field of polymer chemistry has advanced significantly in the last century. The development of Nylon, the world's first absolute synthetic fiber, by Carothers at DuPont in the 1930s, was a monumental scientific achievement. This opened a vast new area for revolutionary synthetic materials that improved upon nature's building blocks (Scheme 1).²⁻⁴ The global market for polymer production continues to grow annually, with *ca.* 300 million tons of synthetic polymers being produced in 2015, a growth of *ca.* 4% since 2012.⁵



Scheme 1 Synthesis of Nylon 6,6

The ability to control and manipulate the molecular structure, molecular weight, and dispersity of a polymer is integral to preparing materials with tunable and variable properties.⁶⁻⁷ Due to their ease of synthesis and widespread characteristics, synthetic polymeric materials continue to replace materials such as wood, metal, glass, and natural fibers, offering tailor-made

characteristics.⁸ Furthermore, these synthetic alternatives are typically much lighter than their ‘natural’ counterparts, making them superior materials for some applications.

Several methods to produce polymers that incorporate a variety of functionalities have been developed, including free-radical polymerization of vinyl monomers,⁹ atom-transfer radical polymerization,¹⁰⁻¹¹ organometallic-mediated radical polymerization,^{6, 12} nitroxide-mediated radical polymerization,¹³ reversible addition-fragmentation chain-transfer polymerization,¹⁴⁻¹⁷ ring-opening polymerization,¹⁸⁻²⁰ metal-free protocols,²¹⁻²³ and ring-opening metathesis polymerization.²⁴⁻²⁷ These examples represent only a few of the many synthetic protocols that lead to the functionalized polymers currently dominating the materials market. Despite the significant advancements in the field, the goal remains unchanged; chemists strive to develop advanced synthetic materials with unique and tunable physical and chemical properties.^{3, 28}

1.2 Controlled and Living Polymerizations

From the most simple, fundamental perspective, a polymer is a large molecule comprised of several repeat units. The word polymer derives from Greek, and can be broken down to *poly*, meaning “many”, and *mer* meaning “parts”.⁸ The properties of the resultant material depend on the monomer, the polymer morphology, molecular weight (MW), and the molecular weight distribution (or dispersity, *D*). As such, control over these properties is imperative to predict, manipulate, and exploit the properties of the macromolecule.⁶ The term “living polymerization” was first coined by Szwarc in 1956.²⁹ This term refers to a chain-growth polymerization in which the ability for chain termination has been removed.³⁰⁻³¹ Central to this classification is complete and rapid initiation of every species in the mixture. When initiation rates are high relative to propagation, chain growth occurs consistently within the mixture, ultimately resulting in

materials with low dispersities and well-defined properties. Consequently, MW increases linearly with monomer consumption. Conversely, if initiation is rate limiting, the active propagating species will form at different times and lead to polymeric materials with inconsistent molecular weight, high levels of dispersity, and low levels of control.³² The degree of polymerization (DP), or the number of repeat units in each polymer chain, should match the theoretical value dictated by the monomer-to-initiator ratio. A polymerization can be said to be “living” if these criteria are met, and dispersity values are less than 1.5, although values less than 1.2 are highly desirable.⁹ The ability to control these parameters can lead to macromolecules with defined properties and molecular architectures and are thus the focus of much research effort across the world.

1.3 Ring-Opening Metathesis Polymerization

One such mechanism that can produce polymers of defined molecular weights and low dispersities is ring-opening metathesis polymerization (ROMP). This living polymerization mechanism uses metathesis reactions to generate polymers from cyclic olefins (Scheme 2).³³ While ROMP is a transformation that is relatively new to polymer chemistry, dating back to *ca.* 1950, olefin metathesis has quickly become one of the more versatile synthetic methods to lead to innovative materials and pharmaceuticals, with many chemical technologies having been developed on the basis of this transformation in the past two decades.³⁴ Several commercial products are synthesized *via* ROMP with a few notable examples being Norsorex (polynorbornene), Vestenamer (polycyclooctene), and a variety of products synthesized from dicyclopentadiene (Telene, Metton, Prometa, Pentam), to name a few.³⁵



Scheme 2 General ROMP of a cyclic olefin

The driving force for this reaction is the release of ring strain in cyclic monomers. Typically, cyclic molecules need to possess a ring strain enthalpy greater than 5 kcal/mol to be appropriate candidates for ROMP. A few select monomers and their respective ring strain values are shown in Figure 1.³⁶



Figure 1 Select cyclic alkenes and their respective ring strain values (kcal/mol)

In contrast to Ziegler-Natta polymerization, ROMP generates polymers in a controlled fashion while retaining an unsaturated backbone, as shown in Figure 2.³⁷ This synthetic route is attractive as it allows access to post-polymerization functionalization or hydrogenation.³⁸ However, these unsaturations make secondary-metathesis reactions possible.

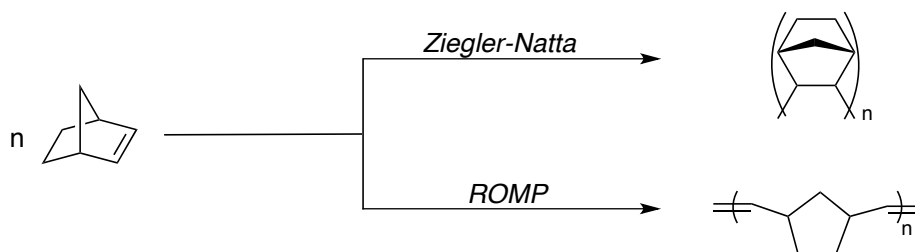
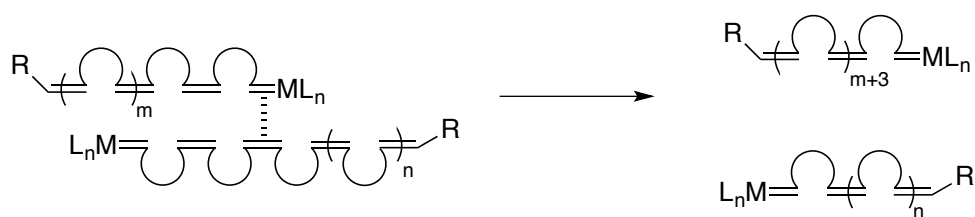


Figure 2 Polymers of norbornene from Ziegler-Natta (top) and ROMP (bottom)^{35, 37}

Intermolecular chain-transfer reactions occur when an active metal-alkylidene reacts with an unsaturation on a different polymer chain. While this does not affect the total number of polymer chains in the mixture, it does increase or decrease the MW accordingly. In intramolecular “back-biting” reactions, the active alkylidene reacts with an unsaturation in the same polymer chain and leads to a cyclic olefin and a species of reduced molecular weight (Figure 3).^{24, 35} Both reactions are typically undesired and lead to unpredictable MWs and increased dispersity values.

Intermolecular Chain Transfer



Intramolecular Chain Transfer

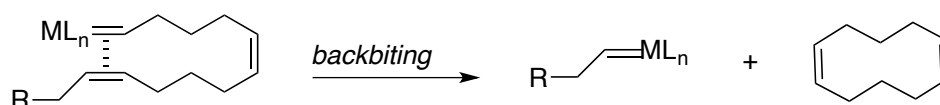


Figure 3 Inter- and intramolecular (backbiting) chain-transfer reactions^{24, 35}

1.3.1 Mechanistic Aspects of Ring-Opening Metathesis Polymerization

In 2005, the Nobel Prize was awarded jointly to Grubbs, Schrock, and the late Chauvin for their work in developing and elucidating the mechanism of olefin metathesis.³⁹ The so-called “Chauvin” mechanism begins by the coordination of an olefin to the metal-alkylidene complex (initiation, Figure 4). A strained metallacyclobutane intermediate is formed *via* a metal-promoted [2+2] cycloaddition before ring-opening produces a new metal-alkylidene species through cycloreversion. Chain growth occurs as this reaction sequence repeats itself and the propagation forms a longer, linear polymer chain. This reaction continues to propagate in the presence of monomer until the feedstock is depleted, or the reaction is terminated *via* the addition of a terminating agent, commonly a vinyl ether, to afford a methylene-terminated polymer chain and an inactive alkylidene.⁴⁰⁻⁴²

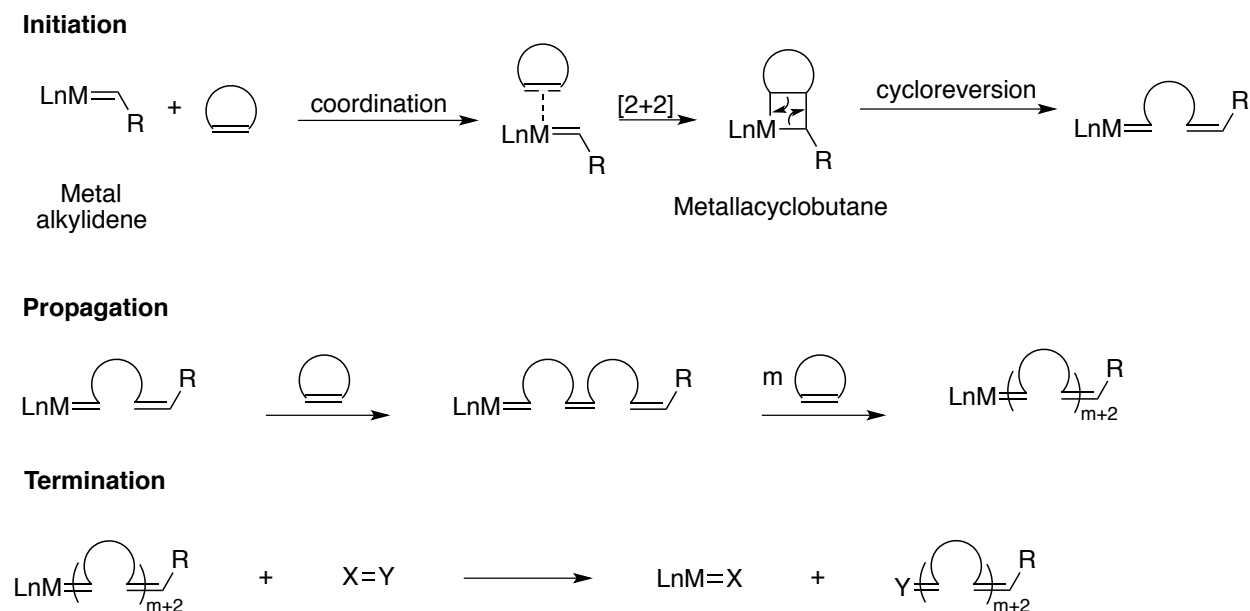


Figure 4 ROMP mechanism: initiation (top), propagation (middle), and termination (bottom)^{24, 43}

It is important to note that ROMP reactions are generally reversible. The propagating species can exist as either the ring-opened alkylidene or the metallacyclobutane, with the reaction conditions, catalyst, and associated ligands dictating this equilibrium.²⁴ Typically, ROMP is best conducted at high concentrations of monomer and low temperatures, and monomers possessing higher ring-strain typically favour polymer over monomer in this equilibrium. However, these monomers are more difficult to control due to their increased propensity to ring-open.⁴⁴

Two dominant classes of metathesis catalysts are those developed by Schrock, based on molybdenum and tungsten, and those developed by Grubbs, that utilize ruthenium-based alkylidenes.²⁴ A comparison between the two classes shows that the former offer more rapid initiation kinetics leading to more well-defined macromolecules. However, the inherent sensitivity of the early transition metal molybdenum and tungsten complexes towards air and moisture, compounded with the lower functional-group tolerance of these species, make ruthenium systems particularly appealing for many chemical transformations.^{25, 43, 45} Hundreds of variants of these ruthenium complexes have been reported.^{43, 46-48} Advancements in the field of ROMP have grown considerably in the last few decades, including metal-free examples.²¹ Regardless of catalyst, the judicious pairing between monomer and initiator, as well as modification of experimental conditions, remains integral to ensure precise control over polymer microstructure and properties. All polymer chemistry presented in this thesis utilizes the ruthenium catalysts developed by Grubbs.

1.3.2 Grubbs Metathesis Catalysts

Within Grubbs systems there exists three main generations as outlined in Figure 5. The Grubbs 1st Generation (G1) catalyst was first reported in 1996 and is comprised of two tricyclohexyl phosphine ligands, as well as two chloro ligands, *trans* to one another.⁴⁹ The Grubbs 2nd Generation (G2) catalyst makes use of a strongly σ -donating *N*-heterocyclic carbene (NHC) ligand in place of one of the phosphine ligands.⁵⁰⁻⁵² Not only does this substitution lead to a complex that is much more water, air, and functional-group tolerant than G1, but G2 has been shown to possess large differences in its reactivity profile. G2 is much more active for metathesis transformations. Initially, this was thought to be due to the strongly σ -donating NHC ligand causing a strong *trans*-influence and promoting a more rapid dissociation of the phosphine ligand. This hypothesis was subsequently shown to be false, and the increased reactivity of G2 is attributed to the greater affinity of the 14-electron complex (*ie.* G2 minus PCy₃) towards the electron-rich, yet π -accepting olefin substrates over the re-binding of the liberated σ -donating phosphine.⁵³⁻⁵⁸

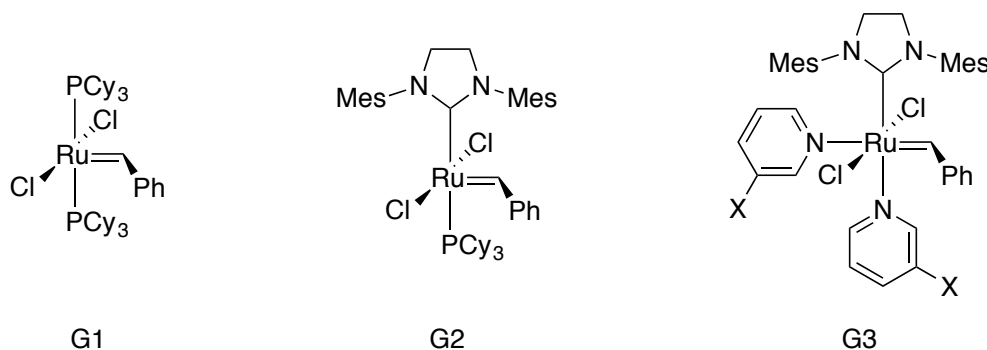


Figure 5 Grubbs metathesis catalysts: G1, G2, and G3, respectively

Although G1 and G2 both initiate catalysis *via* a dissociative mechanism, where the *trans* PCy₃ ligand dissociates before the ruthenium binds an incoming olefin, the rate of G1 initiation (phosphine dissociation) was found to be two orders of magnitude higher than that of G2 initiation, even though G2 displays greater overall reactivity (over two orders of magnitude higher).⁴² The difference lies in the fact that the 14-electron G2-intermediate bearing an NHC (G2 minus the PCy₃ moiety) has a greater affinity for the incoming π -acidic olefins, relative to the competing free σ -donating phosphines (4 orders of magnitude higher). In contrast, recombination of the competing phosphine is more prevalent with the G1 system.^{43, 59} Vougioukalakis *et al.* note that improvements to initiation alone do not necessarily lead to an improved catalyst, since the betterment of the overall system depends on initiation rate, phosphine rebinding potential, and reactivity of the 14-electron intermediate with the incoming olefin. Furthermore, the rate of catalyst decomposition is an integral factor in the development of faster, more robust, and overall “better” catalytic systems.⁴³

To improve initiation rates, the so-called “Grubbs 3rd generation catalyst” (G3) makes use of a substituted-pyridine ligand *trans* to the strongly σ -donating NHC.⁶⁰ Typically, 3-bromopyridine is used as a more labile ligand capable of rapid dissociation, and initiation rates can be increased over a million-fold relative to G2.²⁴ Rapid initiation is a prerequisite for initiators for controlled ROMP in order to afford macromolecules with defined molecular weights and low dispersities. The development of this class of systems has allowed for the precise synthesis of polymer structures using monomers containing a variety of functional groups.^{41, 43, 61-67} Furthermore, the living nature of these transformations has allowed for the construction of many copolymeric structures.^{27, 43, 68-70}

1.3.3 Copolymer Synthesis

The functional group tolerance and living nature of many ROMP reactions has made feasible the predictable synthesis of homopolymers from a variety of monomer feedstocks. Furthermore, the utility of this reaction protocol has allowed for the tailor-made synthesis of polymers containing more than one monomer unit, or copolymers.⁷¹ Copolymers are macromolecules that are comprised of at least two different structural units. For example, A-B copolymers consist of two distinct monomer units, where terpolymers are synthesized from three unique monomers, and can be arranged in any order.

Most common are linear copolymers that consist of a single main chain of covalently linked units, with the arrangement of the monomers in the chain differentiating these classes. For example, A-B linear copolymers can be classified as alternating copolymers if they have a regular pattern of alternating A and B units (A-B-A-B-A-B-A-B) as shown below (Figure 6). The units can also be arranged randomly (A-B-B-B-A-B-A-B-A-A) to give a random copolymer, and if the chain contains segments of entirely A followed by another segment of B (A-A-A-A-A-B-B-B-B-B) the architecture is termed a block copolymer.

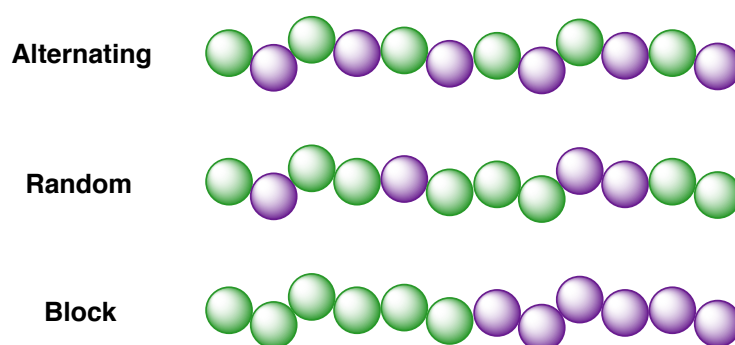


Figure 6 Representations of linear copolymers

Block copolymers are typically synthesized by consuming one feedstock prior to the addition of another monomer. ROMP has become a versatile technique for manufacturing such materials due to its ability to form living polymers, thus insuring copolymers with predictable chain lengths and degree of monomer incorporation. The properties of two or more homopolymers are often desired in one material, *ie.* a combination of toughness and strength. One example is the combination of poly(lactide) (PLA), which is hard, brittle, and possesses a low maximum strain, and thus is limited in its ability to be drawn into fibers, etc. and poly(caprolactone) (PCL), which is tough and possesses a high maximum strain.⁷²⁻⁷³ Blending of these two polymers results in phase separation as these macromolecules are immiscible,⁷⁴⁻⁷⁵ highlighting the need for compatibilization. The formation of a homogenous blend is often not possible and leads to complicated material processing and inconsistent performance. The development of PLA-PCL copolymers is an ever-growing area of research with the goal of covalently linking the properties of these two desirable homopolymers to help alleviate the problems associated with polymer blending.⁷⁶⁻⁷⁹

1.4 Nitrogen-Containing Polymers

Nitrogen-containing polymers display a diverse range of applications. Several examples of the anti-microbial efficacy of these macromolecules have been reported. In particular, protonated amines display strong coordination to the negatively charged cell-wall, making these molecules effective biocides.⁸⁰⁻⁸⁴ The exploitation of the amphiphilic nature (*ie.* polar amine groups and a non-polar backbone) of many amine-containing macromolecules has made these polymers effective compatibilizers for polymer blends.⁸⁵⁻⁸⁷ These are additives that facilitate the association of two otherwise immiscible polymers, making polymer processing more facile.

Other examples of the applications of nitrogen-containing materials are CO₂ uptake,⁸⁸⁻⁹¹ anti-fouling coatings,⁹² drug delivery,⁹³⁻⁹⁷ water purification,⁹⁸⁻⁹⁹ and catalytic materials.^{23-24, 100-104}

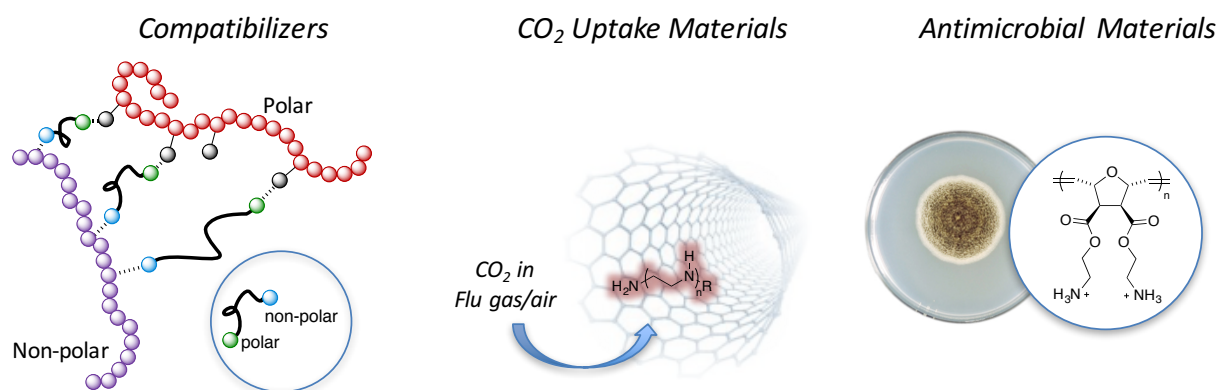


Figure 7 Select uses of amine-containing polymers¹⁰⁵

At the forefront of much research has been the development of functional-group tolerant ROMP catalysts. Significant advances have been achieved by rational ligand design making the incorporation of several functionalities possible. Regardless of this progress, there still exist significant obstacles in the advancement of the field, particularly with the lack of diversity of amine-containing monomers amenable to ROMP, and the efficient synthesis of such starting materials. While amides are known to be compatible with ROMP initiations,^{26, 43, 61, 106} unsaturated amines are poor substrates in metathesis reactions due to the Lewis-basic nature of these monomers, which can interfere unproductively with catalytic activity.⁶⁴ Current strategies for accessing these value-added products are often plagued by multi-step monomer syntheses, including conversion of the amine to an amide, carbamate, or sulfonamide functionality, followed by post-polymerization deprotection,⁶¹ or alternatively, post-polymerization installation of the amine functionality.^{64, 107-112} Alternative methods to these include substrate deactivation by protonation of the amine, although these approaches are not always successful.¹¹³⁻¹¹⁹

Investigations of amines with ruthenium catalysts show that basic amines, such as primary and secondary amines are often incompatible with Grubbs systems. The most successful metathesis reactions are with hindered tertiary amine substrates, as increased steric bulk prevents coordination to the metal centre and deactivation of the catalyst.⁶⁴ These deactivation pathways have been extensively studied, including investigations by Moore, Fogg, and coworkers that show decomposition of these species in the presence of coordinating primary and secondary amine groups.¹²⁰⁻¹²⁹

Subjecting G2 to stoichiometric amounts of primary or secondary amine leads to complete loss of metathesis activity and decomposed ruthenium species, with the elimination of the alkylphosphine moiety being facilitated by the bound amine group.^{26, 58, 112, 126-128, 130} An isolated intermediate shows that the formation of a σ -alkyl species, in which the amine (pyridine) is bound to the ruthenium metal centre after displacement of PCy₃. Subsequent attack by the liberated phosphine on the methyldene carbon is the primary deactivation event for Grubbs systems containing labile phosphine ligands (Figure 8).¹²⁶ Phosphine free systems have also been studied, with the nitrogen substrates being involved in a base-induced decomposition of the metallacyclobutane intermediate.¹²⁹

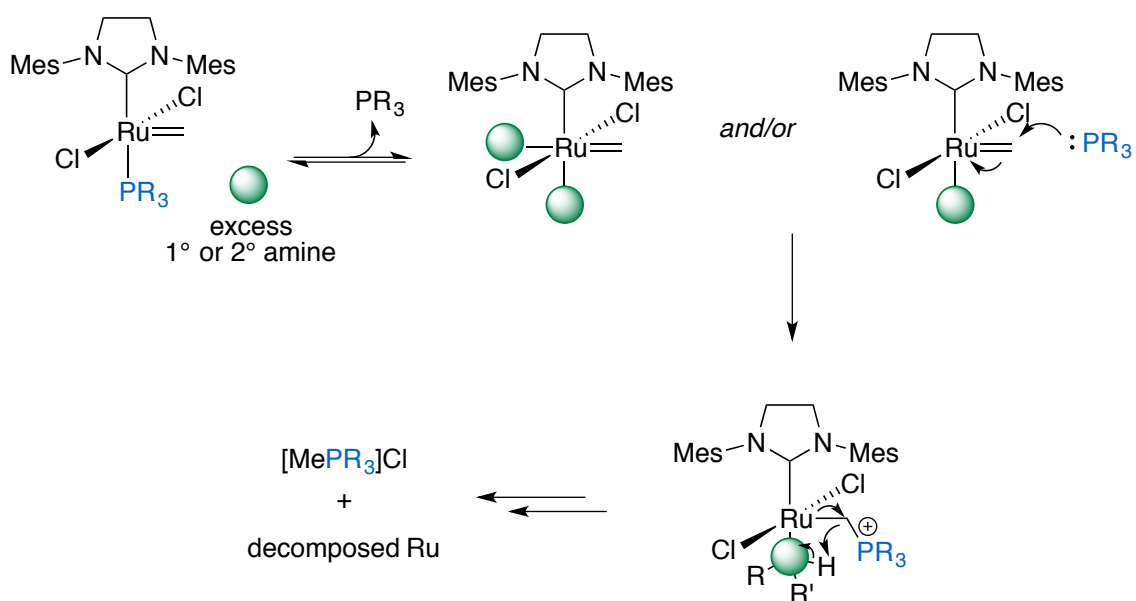


Figure 8 Donor-induced decomposition of ruthenium alkylidene complexes by unprotected amines¹²⁶

Reports of ROMP with unprotected amines have been disclosed, including those with tertiary amines or amino acid derivatives.^{106, 131-132} In 2009, Sutthasupa *et al.* reported amino acid derived monomers bearing protected and unprotected amine groups which were amenable to polymerization with G2.¹³³ The authors point out that both Boc-protected secondary and tertiary amine analogues (**A** and **B**, Figure 9) generate polymeric material in near quantitative yields (>85 %) after 1 h. However, molecular weight values were high (176 Kg mol⁻¹ - 364 Kg mol⁻¹) relative to theoretical values (*ca.* 52 Kg mol⁻¹) and dispersity values (1.83 - 3.10) indicate low levels of control over the polymerization. When unprotected amines **C** and **D** were used, increased reaction times of 20 h were required to form any appreciable amount of polymer, and low catalyst loadings (1 mol%, M:I = 100:1) were detrimental to the reaction, presumably due to the increased concentration of coordinating amine substrate. Higher catalyst loadings (2 - 5 mol %, M:I = 50:1 - 20:1) were required to obtain polymeric product (11 - 81 % yield), and

dispersities were lower than the Boc-analogues, ranging from 1.29 to 1.49. It should be noted that both *endo*, *endo* and *exo*, *exo* isomers of these monomers were studied, with the latter consistently outperforming the former. This observation was attributed to the steric interaction of the *endo* groups inhibiting efficient coordination to the ruthenium centre.^{24, 43, 134-135}

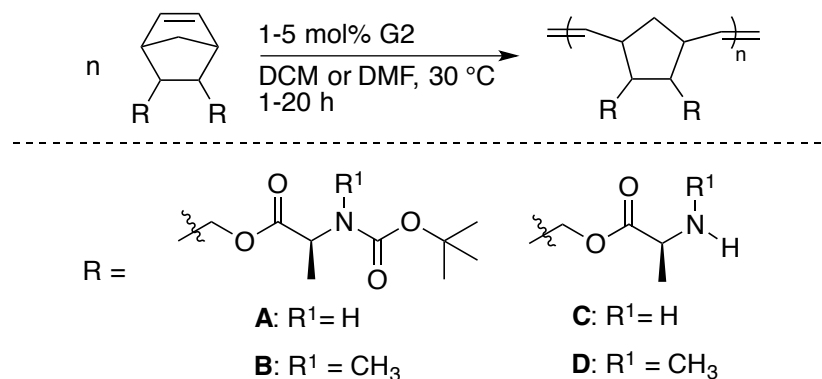
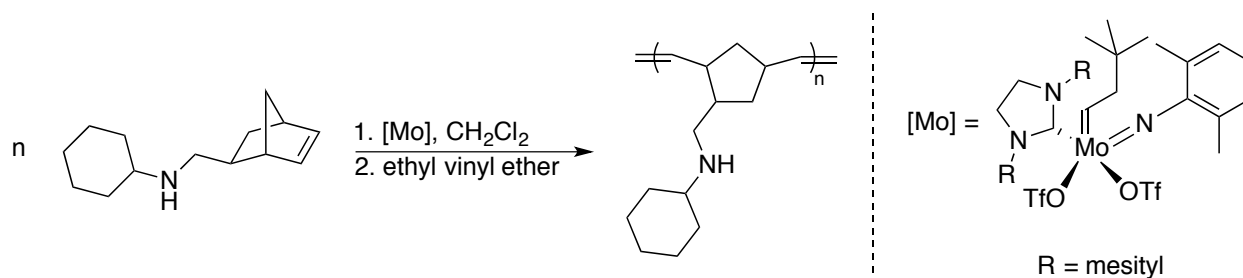


Figure 9 ROMP of unprotected amino-acid derived monomers

Amino acid spacers as well as the potential intramolecular H-bonding interaction between the amino and carbonyl groups are credited for the unexpected success of this family of monomers. Lower dispersities for non-Boc protected substrates **C** and **D** are attributed to the reversible coordination of the amine group, that slows propagation. However, a major drawback to these reports is the laborious, multi-step synthesis of these substrates.¹³³

In 2014, Buchmeiser *et al.* reported a highly active and functional group tolerant molybdenum complex.¹³⁶ Catalytic screening of this complex showed that it is tolerant of unprotected hydroxyl groups and one unprotected secondary amine substrate. ROMP of the secondary amine generates polymeric material in 90% yield, with a molecular weight and

dispersity of 13,100 and 1.10, respectively (Scheme 3).¹³⁶ No further optimization or substrate scope was reported.



Scheme 3 ROMP of an unprotected secondary amine using a highly active molybdenum catalyst¹³⁶

Again, this constitutes a rare example of this class of catalyst being compatible with unprotected primary and secondary amine substrates. Although the group presents only one example of generating polymers from amine-containing substrates using ROMP, the high nucleophilicity and lack of steric protection of this monomer make this example particularly noteworthy. As with the amino-acid derived monomers discussed above, the synthesis of the cyclohexyl-substituted monomer is multi-step and low yielding.^{102, 136-137}

The deleterious impact of amines and amine-containing impurities on ROMP is widely accepted.^{64, 107, 115, 127} While the examples presented above represent a few select cases of polymerization of free amines to date, the controlled polymerization of unprotected, primary and secondary-amine monomers has not been documented as a practical and efficient strategy for accessing this broadly useful class of materials.

1.5 Rheology

The study and analysis of polymeric materials is deeply intertwined with chemical engineering. The material properties of polymers can be studied using rheological measurements that provide integral information regarding the processing potential and future applications of such products. Firstly, rheology is defined as the study of the deformation and flow of matter.¹³⁸⁻¹³⁹ Often, this is concerned with the study of liquids, but also applies to polymers in the melt-phase. The measurement of these rheological parameters is conducted using a rheometer, which detects the materials' behaviour in response to an applied stress.^{138, 140-141} All measurements conducted in this thesis were performed using a parallel plate rheometer, which applies a shear, oscillating force parallel to a fixed plate (Figure 10). There are a few main principles and terms in this field that are pertinent to this thesis and will be discussed in this section.

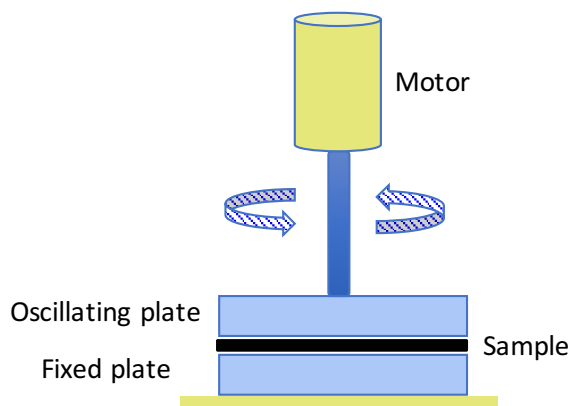


Figure 10 Representation of a parallel plate rheometer

One important property of polymeric materials is their viscosity. Viscosity, η , is the measure of a polymer's resistance to deformation or flow.¹⁴¹ Materials can be classified broadly into categories depending on their viscous behavior. At the two extremes are viscous liquids and elastic solids. Viscous liquids will deform upon the addition of a force. This deformation is irreversible and the material will not resume its original shape upon removal of the stress, as the energy input is released as heat. Water is often given as an example of a purely viscous liquid.¹³⁸⁻
¹³⁹ In contrast, a purely elastic solid will deform reversibly upon the addition of a force. The material will store the applied energy and will reassume its original shape once the force is removed. Steel and concrete represent examples of idealized elastic solids.^{138, 140} Viscoelastic materials display characteristics of both viscous and elastic substances when undergoing deformation. They do not respond linearly to applied stress. Viscoelastic materials will dissipate energy, typically as heat, where purely elastic materials do not. Many synthetic polymers can be classified as viscoelastic and this behavior is manifested in a few key measurements, namely storage modulus and loss modulus.^{138, 140}

The storage modulus (G') is a measure of how much energy a material can store. This is related to the material's elasticity, and thus G' is often referred to as elastic modulus. Conversely, the loss modulus (G'') of a material measures the energy that is dissipated (typically in the form of heat) and is related to how viscous a material is. Dynamic or complex modulus, G^* , is a value that considers both the viscous and elastic components of the materials' response. It is a measure of the overall viscoelastic behavior of the material and is the ratio of the G' and G'' values of a material at a given temperature. Graphically, G^* can be illustrated by the vector diagram shown below, where G' is represented on the y-axis, and loss G'' is on the x-axis. (Figure 11).^{138, 140-141}

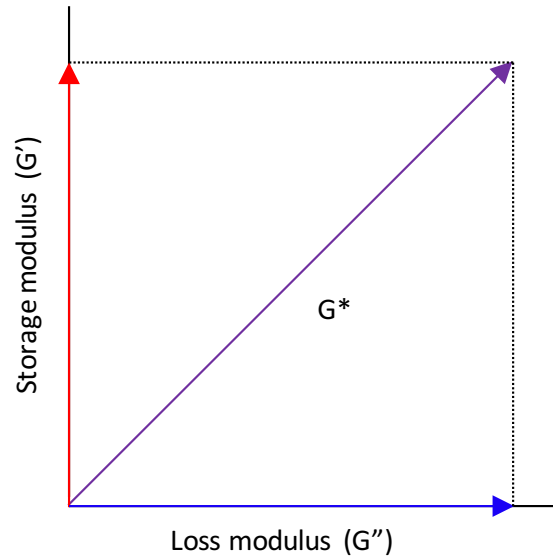


Figure 11 Complex modulus (G^*) as represented as a vector diagram comprised of storage modulus (G' , y-axis) and loss modulus (G'' , x-axis)

Importantly, the values of a material's G' and G'' are useful in determining the polymer's physical state at a given shear rate and temperature. For example, if G' is greater than G'' then the material is more solid-like. Conversely, if G'' is greater than G' the material is said to be liquid-like. Analyzing conventional viscoelastic polymers over a range of frequencies while holding temperature constant (*i.e.* frequency sweep test) shows that liquid-like behavior is observed at low frequencies (Figure 12, left).¹⁴² Here, G'' is greater than G' , as the polymer chains have sufficient time to relax. As frequency increases, there comes a crossover frequency where G' trumps G'' and the material becomes solid-like as the chain entanglements cannot relax on the time scale.^{138, 140, 143} Interestingly, when inter-chain interactions are present, no long term relaxation is observed and the polymer remains as a solid-like material regardless of the angular frequency (Figure 12, right).^{140, 143-144}

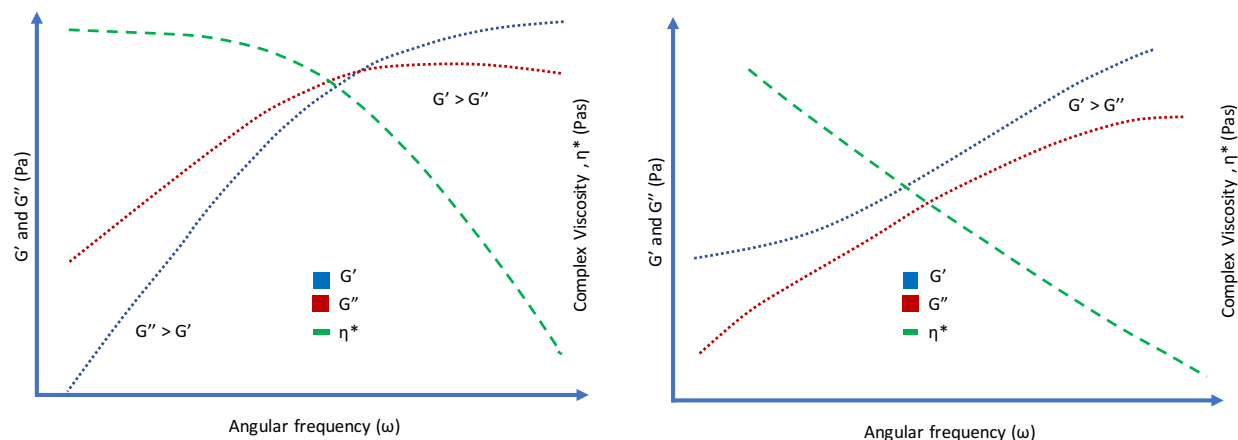


Figure 12 Typical behaviour of an unlinked (left) and linked or partially linked (right) viscoelastic polymer^{140,}

143-144

Complex viscosity, η^* , is a measure of a material's viscosity under specific frequency parameters, where zero-shear viscosity, η_0 , is the measurement of shear deformation of a substance at a shear rate (frequency) approaching zero. Many viscoelastic polymers display behavior known as shear-thinning, where viscosity decreases with increasing shear frequency.¹³⁹ At low shear frequencies, materials that display this behavior will exhibit a plateau in their measured viscosity, as viscosity becomes independent of shear rate. This constant value of viscosity is η_0 and can also be thought of as the resting viscosity of the material and provides insight into molecular interactions throughout the polymer sample.^{141, 145-146} Shear thickening can also be observed when particle-particle interactions are present within the material. At a defined shear rate, these particles, or polymer chains, cannot move freely throughout the network and result in increased viscosity. For example, the presence of H-bonding in polymer samples has been shown to impart this behaviour.¹⁴⁷⁻¹⁵⁰ The making and breaking of reversible bonds between association sites or "sticky-sites" inhibits reptation, or the thermal motion of polymer chains throughout the network.¹⁵¹⁻¹⁵²

The field of rheology offers a valuable complement to the conventional characterization techniques used in chemistry. All the material characterization discussed above provides information regarding the physical properties of bulk materials under various testing conditions. Increased levels of viscosity amongst a breadth of polymer samples provides insight into the inter- and/or intramolecular chain interactions and the potential evidence for network and/or cross-linked structures. These relationships between chemical structure and mechanical properties continue to lead the development of unique polymeric materials for commercial applications.

1.6 Hydrogen bonding

Despite the limitations in synthesizing nitrogen-containing polymers from common Grubbs-type initiators, this class of materials offers a wide range of potential uses. Central to the incorporation of nitrogen-containing groups such as amines, is the ability of these groups to exhibit interesting properties owing to their hydrogen bonding (H-bonding) potential throughout the polymer sample. Indeed, H-bonding within polymeric materials has been extensively investigated and has implications that can lead to enhanced elasticity and/or strength, and tunable viscosity for ease of polymer processing. Furthermore, thermally mendable polymers,^{147, 153} and self-healing¹⁵⁴⁻¹⁵⁶ and self-assembly^{83, 105, 145, 148-150, 157-178} have all been targeted as applications of this niche class of polymeric materials.

In 2014, Lewis *et al.* investigated the efficacy of side-groups capable of H-bonding on the effect of transient supramolecular networks. The ability of these side-chains to H-bond was directly observed by the rheological behavior of these viscoelastic materials. Poly("butyl acrylate)s bearing various H-bonding comonomers, including acrylamidopyridine (AAP), acrylic

acid (AA), carboxethylacrylate (CEA), and ureidopyrimidinone acrylate (UPy) were investigated (Figure 13).¹⁵⁰

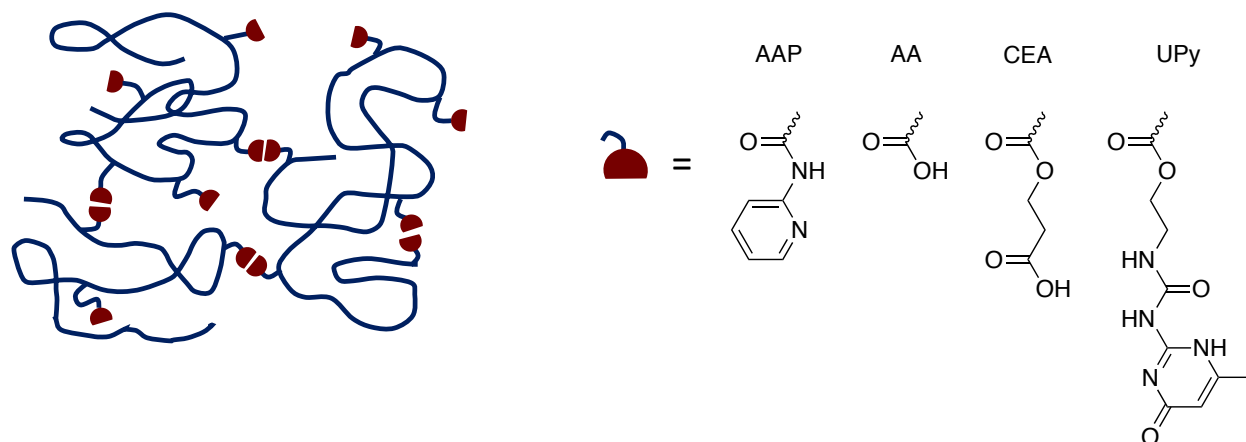


Figure 13 Representation of reversible association of hydrogen bonding side groups¹⁵⁰

Importantly, for polymers bearing weakly H-bonding side groups (AAP, AA, and CEA), G'' far exceeds G' at low frequencies indicating liquid-like behavior. At higher frequencies, there exists an increase in G' and the materials such that the difference between G' and G'' is drastically reduced and the materials behave as solid-like polymer melts. Furthermore, higher glass transition temperatures (T_g) were observed for these polymers capable of creating H-bonding networks, relative to unfunctionalized poly(*n*-butyl acrylate). In contrast, when the stronger H-bonding groups (UPy) were incorporated into the polymer chain, an increase in G' was displayed throughout the frequency sweep test and the polymer behaves as a solid-like material even at low frequencies. This behavior is indicative of transient networks being formed throughout the polymer sample.^{150, 179}

This variation of rheological properties on the presence of H-bonding groups within the polymer sample has also been reported recently by Shabbir *et al.*¹⁴⁸ Poly(*n*-butyl acrylate)s were hydrolyzed to various extents to generate copolymers of the form poly(*n*-butyl acrylate)-*co*-poly(acrylic acid) (Figure 14).

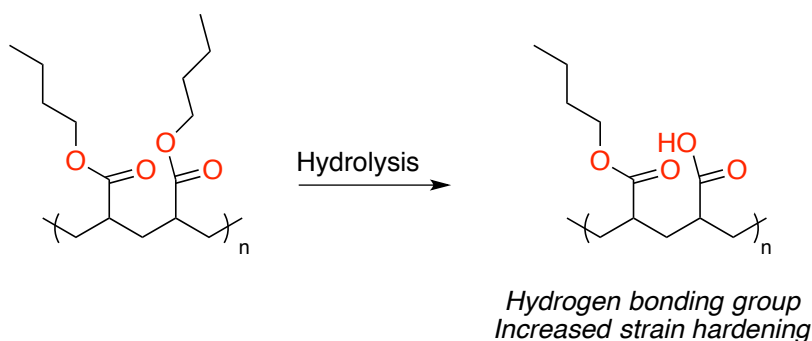


Figure 14 Hydrolysis of acrylate polymers gives acrylic acid groups with hydrogen bonding potential¹⁴⁸

The values of G' and G'' were found to increase linearly with the number of H-bond groups present in the polymer chain (higher amounts of hydrolysis), as this hinders reptation due to the increased chain associations present. Specifically, the unfunctionalized homopolymer, poly(*n*-butyl acrylate), displays classical viscoelastic behavior (*vide supra*) with higher G'' than G' at lower frequencies. A clear crossover point is observed as relaxation is slower than the rotational timescale. The relative difference between G' and G'' decreases as the incorporation of acrylic acid is increased from 0% to 13% as increasing levels of the H-bonding groups are present. When the percent of acrylic acid is increased to 38%, no cross over point is observed and the material behaves solid-like over the entire frequency range. This report highlights that specific tailoring of the viscoelastic properties of polymeric materials is possible by varying the incorporation of H-bonding within the polymeric material.¹⁴⁸

1.7 Scope of Thesis

The central theme of the research presented in this thesis is the development of nitrogen-containing molecules. It deals with the atom-economic, catalytic synthesis of amines from simple alkene and amine starting materials. All chemistry performed in the generation of small molecules was conducted with early transition metal complexes bearing *N,O*-chelating ligands. All polymeric material was synthesized using commercially available or easily-synthesized Grubbs ruthenium catalysts.

The introduction to this thesis highlighted the relevance of functional materials. It discussed the historical aspects to the development of useable, synthetic macromolecules and focused on the importance of controlled and living polymerization techniques. Mechanistic aspects of ROMP, a method used to generate polymeric materials, were detailed. The common problems associated with the incompatibility of amine-containing substrates were explained, as well as the potential benefits of the incorporation of such a moiety into polymeric materials, with H-bonding being of particular interest. An introduction to polymer rheology was presented and focused on the interesting characteristics often observed with amine moieties possessing the potential to form transient polymer networks through H-bonding interactions.

One of the main pillars of the Schafer Research Group is the development of early transition metal catalysts using *N,O*-chelating ligands for the synthesis of amines. Several previous examples of bidentate N,C,O motifs have been disclosed in the literature, including amidates, ureates, sulfonamidates, and pyridonates.¹⁸⁰⁻¹⁸¹ Chapter 2 begins by highlighting the benefits of hydroaminoalkylation and hydroamination over traditional synthetic methods.¹⁸² It extends the research focus to include bulky N,P,O chelating phosphoramidate ligands installed on tantalum.^{105, 183} One tantalum phosphoramidate was previously found to be excellent for

hydroaminoalkylation at room temperature.¹⁸³ To date, this is the only disclosed complex capable of this achievement. The start of the independent research in this thesis begins by discussing the solvent-free, room-temperature reactivity of this complex and increasing its substrate scope. The select mono-alkylation of norbornadiene is highlighted as a key research finding that spawns the latter investigations of Chapter 2. The utility of this N,P,O chelating phosphoramidate motif is expanded to include titanium dimethylamido complexes, with a focus on exploiting this earth-abundant, lowly toxic, and inexpensive metal¹⁸⁴ for analogous C-C bond forming transformations. These complexes are also screened in preliminary C-N bond forming reactions and show good efficacy for hydroamination. Several solid-state molecular structures are presented and discussed.

Chapter 3 builds on the work presented in Chapter 2, by taking advantage of the monoalkylated, internal alkene monomers that can be synthesized at room temperature using a tantalum phosphoramidate complex.¹⁰⁵ A variety of substrates derived from norbornadiene and differing amines were synthesized and characterized. The cyclic diene scope was increased to include 1,5-cyclooctadiene, with two substrates being synthesized for direct comparison to the norbornene variants. Aryl-substituted substrates were found to be excellent candidates for ROMP using Grubbs catalysts, despite bearing sterically unhindered, unprotected, secondary amine groups. Alkyl-substituted aminonorbornenes were not suitable substrates for this transformation. This atom-economic synthesis of aminonorbornene substrates for ROMP offers a facile route to otherwise difficult and wasteful syntheses of these monomers. Homopolymers of aminonorbornene substrates were synthesized using ROMP and tested for their rheological properties.¹⁰⁵ Interestingly, the free aryl amine groups impart various viscoelastic behaviour

depending on their H-bonding capabilities and provide information regarding the transient molecular interactions present in these novel materials.

Chapter 4 focuses on capitalizing on this unexpected and unique compatibility of secondary amines with Grubbs catalysts. A variety of copolymers are synthesized. Specific focus is drawn to linear A-B copolymers where the relative incorporation values of the amine comonomer is varied, with intentions to exploit the potential of these value-added amine-containing segments by incorporating them with inexpensive hydrocarbon comonomers. These copolymers were synthesized using a “block” and “random” approach, with little differences being observed by thermal analysis techniques.

All major discoveries and observations in this thesis are summarized in Chapter 5. Insights into future development of the research ideas presented in this body of work are discussed after relevant conclusions, with key future works being focused on the potential applications and expansion of the molecules and protocols developed in this thesis.

Chapter 2: Titanium Phosphoramidate for the Catalytic Synthesis of Amines

2.1 Introduction

Amines are important small molecules for a variety of applications. The biological relevance of these nitrogen-containing molecules ensure their usefulness in pharmaceutical sciences.¹⁸⁵ Other fields of use are the fine chemical and agricultural industries which produce and utilize amines for applications ranging from water and flu-gas purification and detergents to fertilizers and chemicals for crop protection.¹⁸⁶ Figure 15 shows a few select amines and their uses.

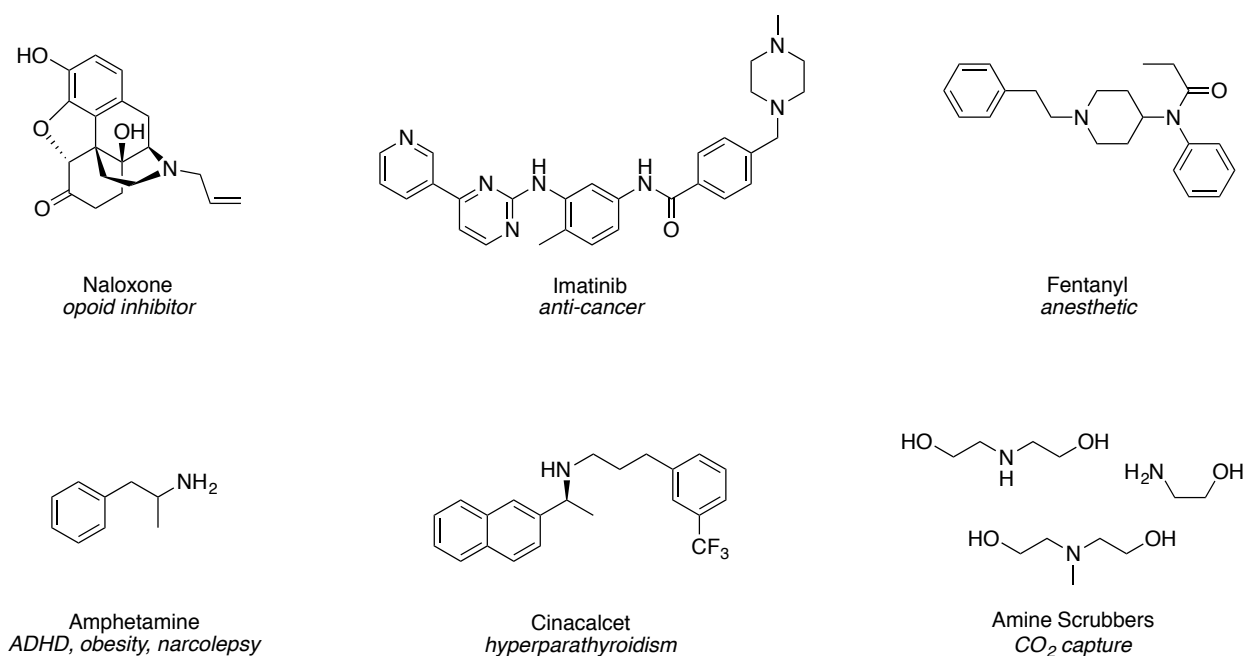


Figure 15 Select amines and their respective uses

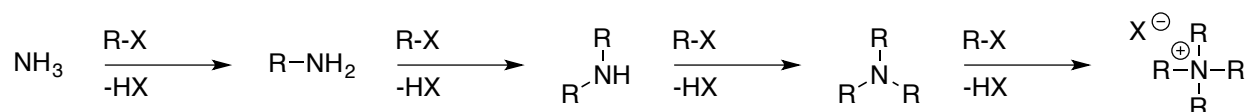
The widespread use of these molecules makes the demand for such compounds prolific. The global market for amines was valued at *ca.* 14B USD in 2015. This value is projected to increase at an annual rate of 8% and is estimated to be valued at *ca.* 20B USD in the year

2020.¹⁸⁷ Thus, research into fundamental chemical transformations that generate these essential molecules efficiently is of utmost importance. The following sections describe select examples of synthetic protocols used to furnish amine molecules.

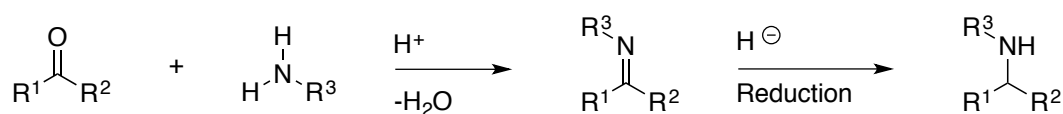
2.2 Catalytic Synthesis of Amines

Amines can be generated by a variety of synthetic methods. Traditional strategies include *N*-alkylation,¹⁸⁸ Eschweiler-Clarke methylation,¹⁸⁹⁻¹⁹¹ reductive amination,¹⁹²⁻¹⁹⁵ Gabriel synthesis,¹⁹⁶⁻¹⁹⁸ and Ullmann coupling,¹⁹⁹⁻²⁰⁰ to name a few. While these protocols are inherently useful in the generation of amines, they are plagued by harsh reaction conditions, the use of stoichiometric additives, chemoselectivity issues, and the generation of significant amounts of waste. Figure 16 details a few of these synthetic protocols.

N-alkylation



Reductive amination



Gabriel synthesis

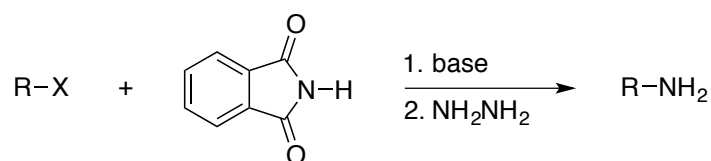
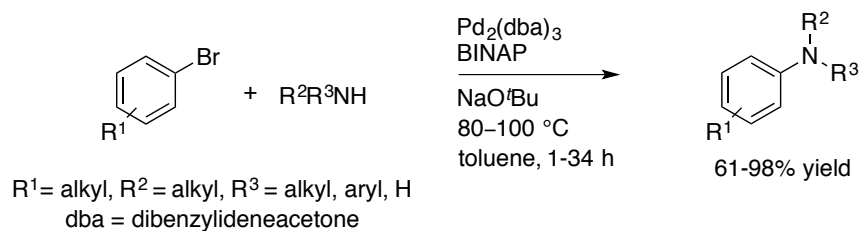


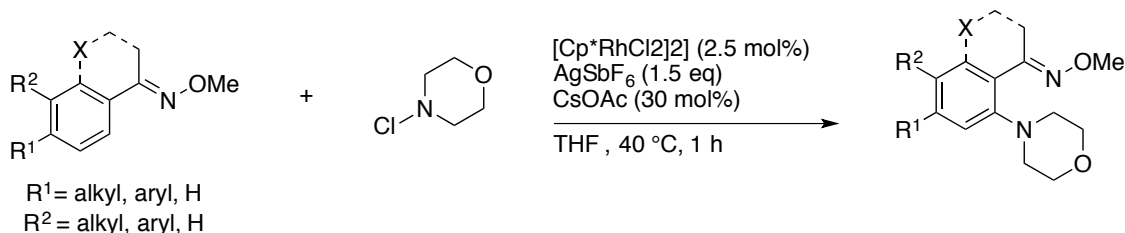
Figure 16 Common traditional synthetic approaches to amine synthesis

One of the most important applications of modern organometallic chemistry is the utilization of transition metal complexes to catalyze chemical reactions in an efficient and selective manner. Due to the growing demand for amines, the development of efficient, catalytic methodologies to synthesize these products is of interest.² Ideally, these processes would be in line with the principles of Green Chemistry: be atom-economic, catalytic, prevent waste, use non-toxic components, all while operating under catalytic conditions, at low temperatures, and with limited need for solvents.²⁰¹ Other protocols for the development of amines through efficient metal-catalyzed transformations have been developed to help circumvent these restrictions. These approaches include, but are not limited to, Buchwald-Hartwig amination,²⁰²⁻²⁰⁸ direct C-H amination,²⁰⁹⁻²¹⁸ and hydroaminomethylation (Figure 17).²¹⁹⁻²²⁹

Buchwald-Hartwig Amination



Direct C-H Amination



Hydroaminomethylation

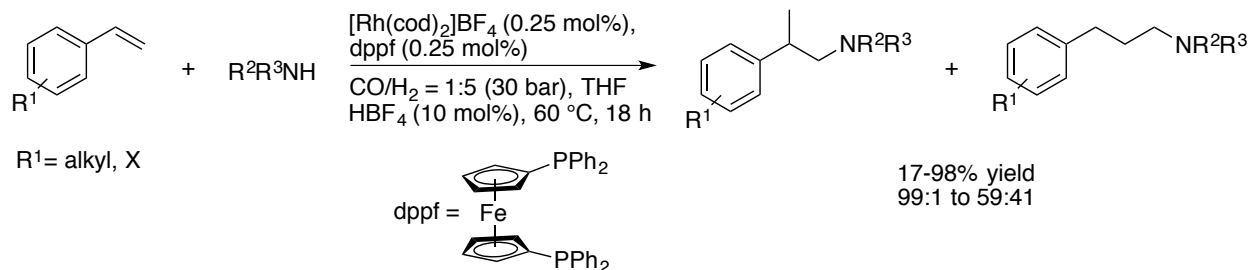


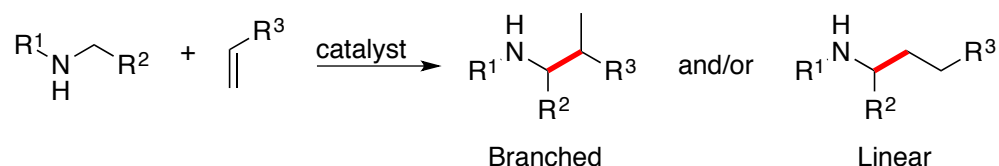
Figure 17 Catalytic synthesis of amines by Buchwald-Hartwig amination (top), direct C-H amination (middle), and hydroaminomethylation (bottom)^{218, 223, 230-231}

Two alternative methodologies, hydroaminoalkylation (HAA)^{105, 181-183, 232-239} and hydroamination (HA),^{181, 232, 240-266} are the main pillars of the Schafer Group. They both generate amines in a single step from olefins and simple amine substrates. Furthermore, these starting materials are often commercially available and no prefunctionalization of the alkene is required. These catalytic transformations offer facile methods to generate new, value-added amine

products and are particularly appealing when non-toxic, earth-abundant, early transition metal-based precatalysts are utilized. These reactions are discussed in more detail below.

2.3 Hydroaminoalkylation

HAA is a C-C bond forming reaction α to a nitrogen atom (Scheme 4). This methodology offers an atom-economic conversion of simple starting materials, namely alkenes and amines, into higher substituted products.^{182, 267-268} This emerging catalytic transformation is an attractive reaction for further development.



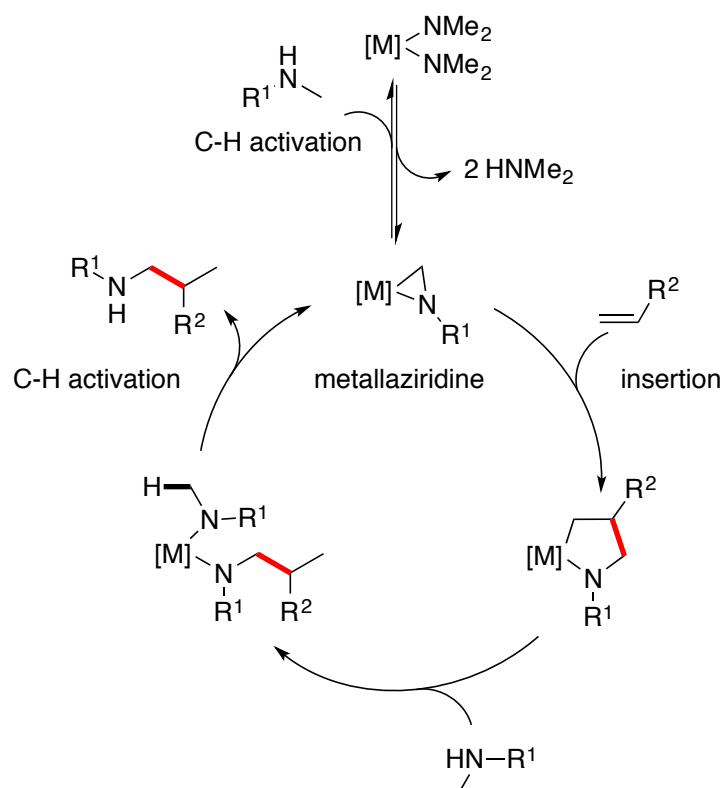
Scheme 4 Hydroaminoalkylation of amines and alkenes

The first reports of HAA were disclosed independently by Maspero,²⁶⁹ and later Nugent,²⁷⁰ in the early 1980s. Homoleptic dimethylamido complexes of tantalum, niobium, or zirconium were shown to be successful in catalyzing the alkylation of dimethylamine, α to the nitrogen atom, with ethylene, propylene or 1-hexene. However, high temperatures (>160 °C) were required and yields were 38% at best.

The field of HAA catalysis remained dormant until 2007 when Hartwig *et al.* reported the HAA between *N*-arylamines and terminal alkenes, using $\text{Ta}(\text{NMe}_2)_5$ as a catalyst.²⁷¹ Although high temperatures were required (160-165 °C), the reaction times were reduced (27-67 h) and yields were drastically improved (50-96%). A propensity to form the branched regioisomer was

observed.²⁷¹ Conversely, when late transition metals are used, linear isomers are obtained.²⁷²⁻²⁷³

The regioselectivity can be rationalized by the insertion of the alkene into the metal-carbon bond of the reactive metallaziridine. The mechanism for HAA was proposed by Nugent and is shown below (Scheme 5).²⁷⁴⁻²⁷⁵



Scheme 5 Proposed mechanism for intermolecular hydroaminoalkylation catalyzed by homoleptic early transition metal dimethylamido complexes

Inspired by the advancements in the field, the Schafer Group sought to take advantage of ligand modified reactivity in HAA and disclosed mono- and diamidate tantalum complexes in 2009.²³⁴ These complexes allowed for an increase in substrate scope and reduction in reaction temperatures to 110 °C for select substrates. Another attractive ligand set is that of *N,O*-chelating phosphoramidates. Complexes bearing these ligands are proposed to be more active HAA

catalysts. Relative to amidates, the phosphoramidate ligand motif is more electron-withdrawing, a characteristic reported previously to increase the activity of known HAA catalysts.²⁷⁴ Phosphoramidates offer tunable steric bulk and electronic properties at both phosphorus and nitrogen atoms, as well as facile modular synthesis (Figure 18).¹⁸³ Furthermore, phosphoramidates exhibit a tetrahedral geometry about the phosphorus atom, creating a more sterically encumbered metal centre, relative to amidate ligands which bind in a trigonal planar geometry. This characteristic is central to this thesis and will be discussed and exploited further in Chapter 2.

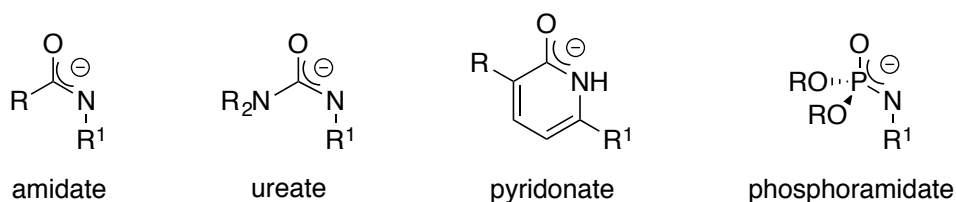
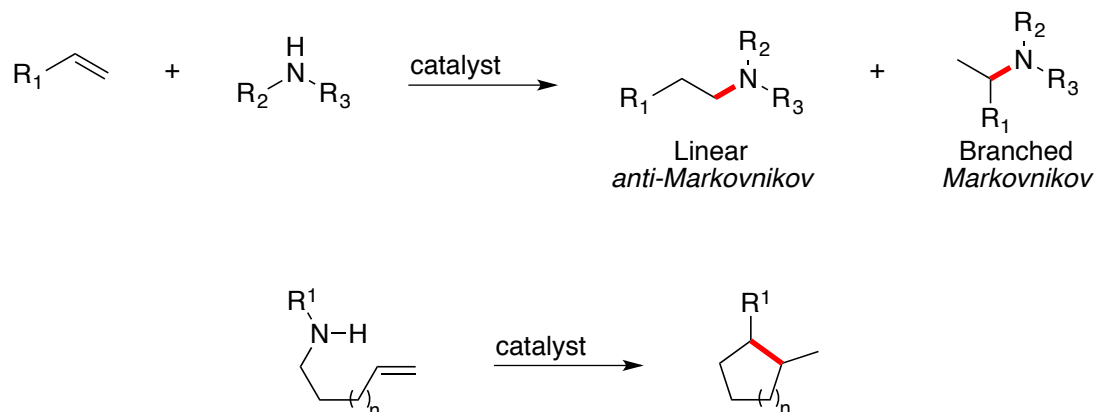


Figure 18 Common *N,O*-chelating ligands used by the Schafer Group: amidates, ureates, pyridonates, and phosphoramidates

2.4 Hydroamination

HA is the addition of an N-H bond across a C-C unsaturation. This transformation results in a newly formed C-N bond as shown below in Scheme 6.^{261, 276-282} Much like the HAA reaction shown above, HA is an efficient, atom-economic reaction that utilizes readily available, simple amine and alkene feedstocks.



Scheme 6 Intermolecular (top) and intramolecular (bottom) hydroamination of alkenes

Overall, the addition of an amine across an alkene is nearly thermodynamically neutral. However, the high activation barrier associated with adding an electron-rich amine across π -systems makes the direct addition of amines across a C-C unsaturation difficult and highlights the need for effective catalysts to facilitate this transformation.²⁸² Alkynes undergo HA more readily than alkenes, as the alkyne π -bond is *ca.* 70 kJ/mol weaker than the π -bond of a typical alkene.²⁷⁸ Furthermore, the reduced steric accessibility associated with the HA of substituted alkenes, relative to alkynes, rationalizes the persistent difficulties associated with this reaction.²⁷⁷ While effective catalytic systems have been developed for the HA of alkynes, a general synthetic approach to the synthesis of unactivated alkenes with unprotected amines remains the focus of much current research.²⁸²

Several catalytic systems for HA have been developed based on metals from across the periodic table.^{240, 252, 276-279, 283-294, 261, 281-282, 295-302} Systems based on Group 4 metals, namely zirconium and titanium, offer some of the best selectivities with unprotected amines.³⁰³ These observations, coupled with the low cost and toxicity of titanium, make these titanium-based systems very attractive for tackling the research challenges targeted in this thesis.

Many synthetic issues associated with efficient C-C and C-N bond formation have been targeted. However, many challenges in the field persist. Several catalytic systems still require high reaction temperatures and/or long reaction times to afford the desired amines in appreciable yields. Furthermore, the careful choice of metal catalyst remains essential to overcome these challenges, with early transition metals offering low-cost, non-toxic alternatives to their late metal counterparts. The following sections detail the investigations into HA and HAA using early transition metal catalysts. It begins by introducing and building on pre-established results using a phosphoramidate tantalum precatalyst with the focus of expanding the conditions of this complex to include solvent-free reactivity. Chapter 2 explores the utility of phosphoramidate titanium complexes in catalysis, with the goal being the development of cost-effective, sustainable alternatives to the tantalum congener previously explored by the Schafer Group.¹⁸³

2.5 Tantalum, Titanium, and the Motivation for New Catalysts

The investigations of tantalum-catalyzed HAA described above, as well as other successes in the field, demonstrate the marked success of this metal in HAA catalysis. Perhaps troublesome is the estimation that there are approximately 50 years left of tantalum resources remaining, highlighting the importance of increased recycling efforts or the discovery of suitable replacements.³⁰⁴ There is a need for viable alternative catalysts for this C-H alkylation reaction.³⁰⁵⁻³⁰⁶

Tantalum has a long and interesting history. It was discovered in Sweden in 1802 as a component of tantalite, a mineral composed of a mixture of tantalum and niobium. Tantalum is a lustrous metal that is highly corrosion resistant and ductile. Because of this, it has been widely used as a component of alloys; the metal has further application as capacitors for mobile phones and other commonly used electronic devices.³⁰⁷⁻³⁰⁹ It has been used extensively in medical implants,³¹⁰ such as hip and knee replacements, due to its inertness in the body and low levels of irritation.³¹¹ The widespread use of this metal has undoubtedly led to the pending shortage.

The socioeconomic environment surrounding the metal has caused an inconsistent global market regarding its trade. Coltan, a short-hand term referring to the minerals columbite and tantalite, is a conflict resource, or a natural resource that is directly mined in a conflict zone and used to perpetuate fighting. The term is also applied to a variety of metals with the main offenders being tin, tungsten, tantalum, and gold (3TGs). Tantalum is often cited as fueling the war in the DPR Congo, a conflict that is often referred to as the most violent and deadliest since WWII.³¹²⁻³¹³ This atmosphere has led many nations to boycott the import of coltan from DPR Congo, Rwanda, and Burundi, three nations with large reserves and deposits.^{312, 314} Since 2014, a shift has been made to obtain these minerals from more politically and economically stable

nations such as Canada, Finland, Brazil, Australia, and USA. Perhaps this troubled situation is befitting of the element; its name stems from Greek mythology and has formed the etymology of the word tantalize. Although the African countries mentioned above account for only a small percent of the world's production, it has significantly tarnished the reputation of this otherwise useful metal.

Another metal that is central to this thesis is titanium. Titanium is the second most abundant transition metal in the Earth's crust.¹⁸¹ It is lightweight and highly corrosion resistant. Coupled with its biocompatibility, these beneficial characteristics have allowed the use of this inexpensive metal to gain considerable research interests in the past decade. Titanium represents a cost-effective alternative to tantalum, often cited as being ten times cheaper.^{184, 315-316}

A range of titanium-based catalysts bearing *N,O*-chelating ligands have been synthesized and have been shown to be capable of chemistry from HA^{180-181, 232-233, 241-242, 247-248, 250, 252, 264-265, 303} and HAA^{181, 232, 239, 268, 317} to polymer chemistry, focusing on the ROP of cyclic esters^{76, 181} and Ziegler-Natta olefin polymerization.^{181, 318} Previously, it was shown that tantalum phosphoramidates were amongst the leading examples of precatalysts capable of performing HAA.¹⁸³ In keeping with the principles of Green Chemistry, titanium analogues are targeted. Specifically, *N,O*-chelates of titanium that could harness the reactivity for the amine forming reactions discussed above, while avoiding the unattractive characteristics of tantalum are of interest. Figure 19 below details select examples of *N,O*-chelated complexes of titanium in the literature and their respective uses, with one recent book chapter and review article providing a more comprehensive overview of the field and highlighting the utility of this ligand set.¹⁸⁰⁻¹⁸¹ While several examples of titanium complexes bearing *N,O*-chelates have been reported, ranging from salen, salan, and quinolate species, the following sections of this thesis detail the

investigation of titanium complexes bearing mono-anionic ligands that form 4-membered metallacycles and the exploitation of these complexes in catalysis. This is done to have direct comparison to other 3-membered *N,O*-chelating ligands discussed below.

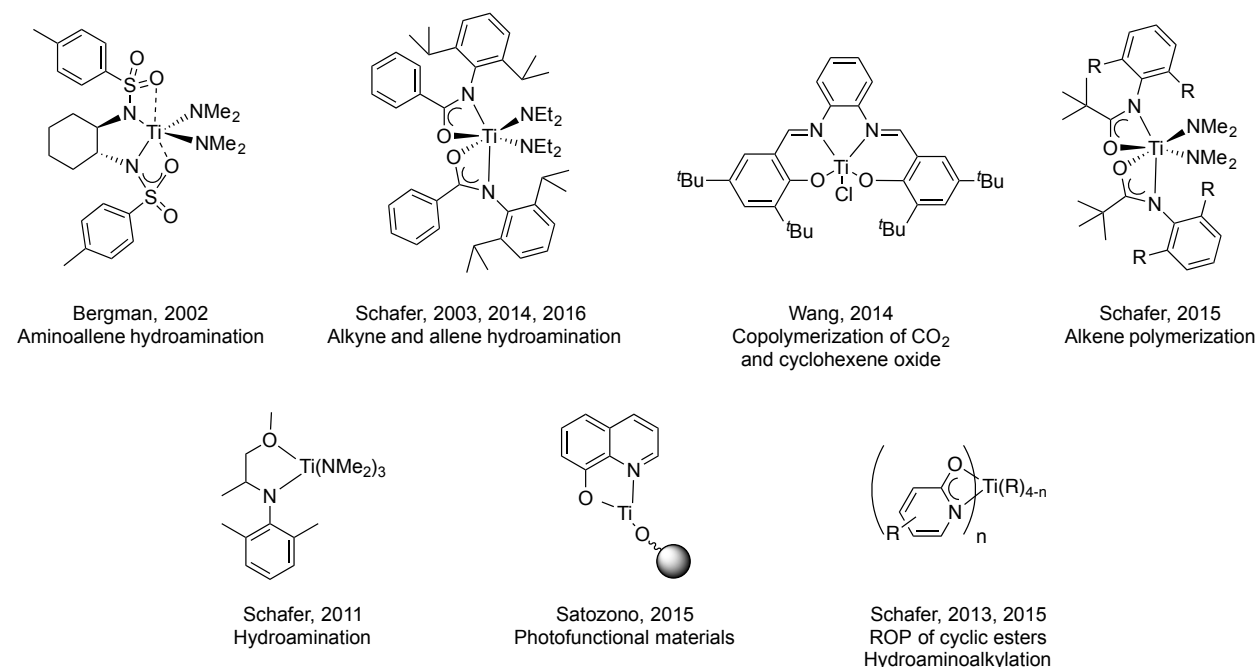


Figure 19 Selected titanium complexes bearing *N,O*-chelating ligands^{77, 247-248, 258, 261, 264, 318-322}

2.6 Early Transition Metal Catalysts in Small Molecule Forming Reactions

A longstanding goal in the Schafer Group has been to synthesize environmentally-friendly and reactive complexes for the formation of new C-C and C-N bonds. Specifically, early transition metals that are inexpensive, environmentally-benign, and biocompatible are the focus of much research. The most pertinent literature to this chapter is discussed below, and highlights the work done by members of the Schafer Group and other leading researchers in the field.

In recent years, the Schafer Group and others have published a breadth of reports on the synthesis of mono- and di(*N,O*)-chelated complexes of Group 3, 4, and 5 metals having applications in the formation of small molecules.^{76-77, 181, 183, 232, 252, 292, 318, 323-327} Tantalum complexes bearing one and two amidate ligands (κ^2 -*N,O*) have proven effective in the HAA of amines.^{234, 327} Yttrium complexes bearing one and two amidates have been competent in the HA and the amination of aminoalkenes^{254, 328} and amidation of aldehydes.³²⁹ *N,O*-chelating pyridonates of titanium have shown efficacy in the polymerization of cyclic esters.⁷⁷ Several examples of HA catalysts have been reported including diureate zirconium^{243, 259} and diamidate zirconium and titanium complexes for this C-N bond forming reaction.^{241, 243, 245, 248, 253-254, 259, 330-332} Furthermore, the latter complexes have been utilized in olefin polymerization.³²³ Yttrium complexes bearing three *N,O*-chelating amidates were reported for the polymerization of *rac*-lactide⁷⁷ and ϵ -caprolactone.³³³

The various coordination modes of *N,O*-chelating ligands have been explored by the Schafer Group and found to be highly dependent on the metal and ligand used. For example, in 2013 Payne *et al.* disclosed the first example of a Group 4 tri(*N,O*)-chelated complex. This investigation focused on the chelation of three or four amidate ligands with titanium, zirconium, or hafnium (Figure 20).³³⁴

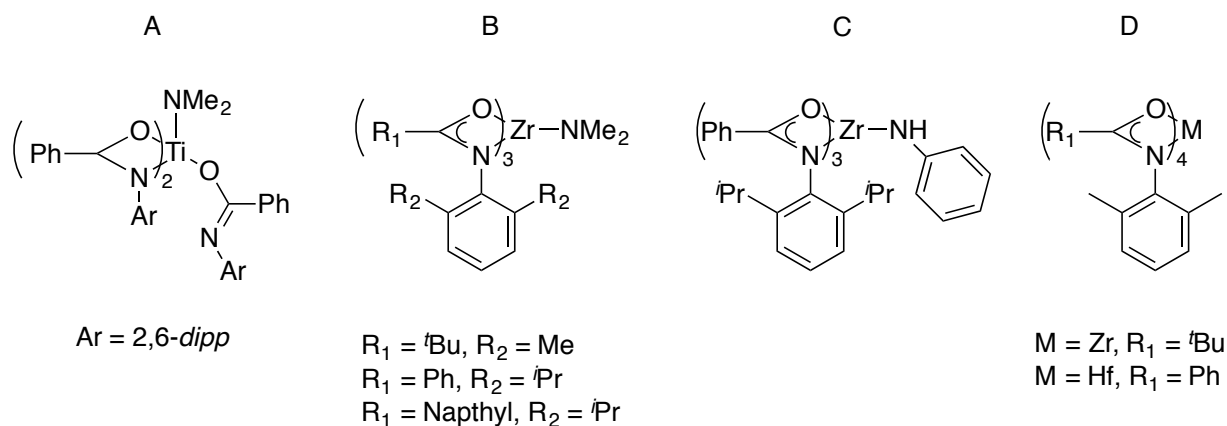


Figure 20 Previous titanium and zirconium *N,O*-chelated complexes reported by the Schafer Group

Different binding modes were observed in the solid-state when zirconium and hafnium were used. The larger zirconium metal centre (*ca.* 1.55 Å)³³⁵ was found to support three $\kappa^2\text{-}N,O$ ligands (B and C, Figure 20), whereas titanium, having a smaller atomic radius (*ca.* 1.40 Å),³³⁵ has one of these three chelates bound in a $\kappa^1\text{-}O$ fashion to alleviate steric strain imparted by the bulky chelates (A, Figure 20). Hafnium (atomic radius *ca.* 1.55 Å)³³⁵⁻³³⁶ could support three and four *N,O*-chelating ligands, all bound in a $\kappa^2\text{-}N,O$ chelating fashion.³³⁴ Homoleptic complexes of zirconium and hafnium (D, Figure 20) were synthesized either from the tetrabenzyl metal starting material ($M(\text{CH}_2\text{Ph})_4$), or from $M(\text{NMe}_2)_4$ species. Importantly, mono(amidate)tri(amido) complexes of titanium, zirconium, or hafnium have never been successfully prepared due to the lack of adequate steric protection imparted by the amidate ligands and rapid ligand redistribution to form the diamidate species. Diamidate species have been shown to be competent for a variety of catalytic transformations in the past, including HA and HAA.^{180, 242, 245, 247-248, 250-254, 257, 259, 263, 318, 323, 326, 329, 331, 337-339}

The binding modes of *N,O*-chelating pyridonate ligands and the generation of the respective titanium complexes was investigated by Chong *et al.* in 2015.³⁴⁰ In this example,

combining three equivalents of proligand with $\text{Ti}(\text{NMe}_2)_4$ gave a tripyridonate complex in good yield (91%) and all *N,O*-chelates were bound in a κ^2 -fashion, as demonstrated by X-ray crystallography. Using this approach, a Ti^{III} species was accessed upon exposure of this compound to an excess of benzylamine. The resulting reduced species has two κ^2 -pyridonates and one pyridonate bound κ^1 through oxygen. Presumably, the presence of two neutrally bound benzylamine ligands prevents all the bidentate ligands from binding in κ^2 -fashion, as the 7-coordinate titanium species is already very sterically crowded.

Doye *et al.* have also reported titanium complexes bearing *N,N*-chelating ligands. These include a related diaminopyridinato complex for the HAA of alkenes and styrenes,³⁴¹ and a diphenylaminopyridinato titanium complex for the HAA of styrene and butadiene substrates (Figure 21).³⁴² These catalytic systems offer interesting reactivity for HAA, with these complexes preferentially generating the linear isomers over the branched. The use of titanium amidate catalysts for this reaction has not yet been reported.

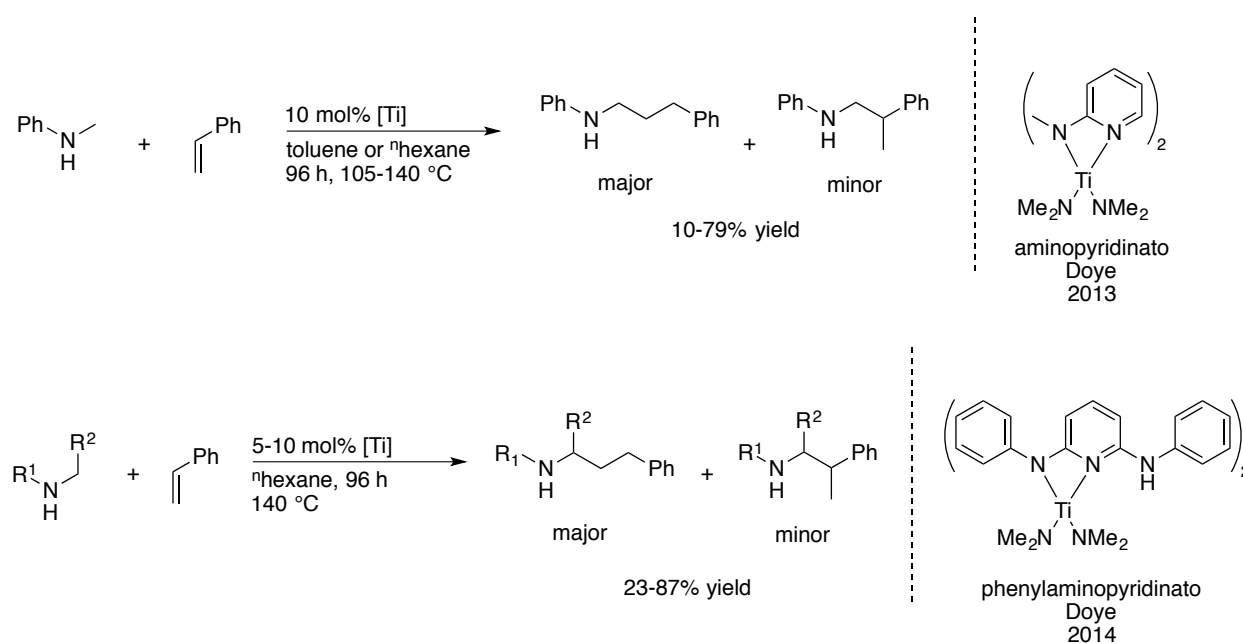
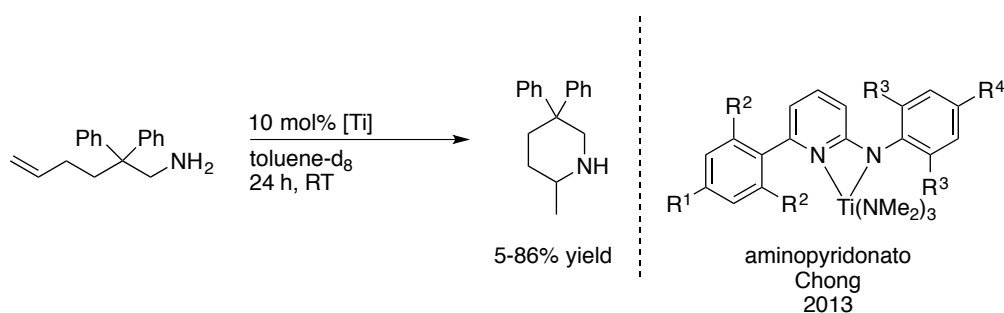


Figure 21 Titanium complexes bearing aminopyridinato³⁴¹ and phenylaminopyridinato³⁴² ligands for hydroaminoalkylation

Tri(amido) titanium complexes bearing one κ^2 -*N,N*-chelate are known and have shown efficacy in a variety of chemical transformations. A few select examples are described below. Specifically, Chong *et al.* have reported titanium complexes bearing 2-aminopyridonate (AP) ligands in 2013.²⁴⁶ These bulky *N,N*-bidentate ligands were installed onto titanium *via* protonolysis with $\text{Ti}(\text{NMe}_2)_4$ and a variety of substitution patterns were explored in good yields (80-98%) (Scheme 7). The compounds were isolable yellow solids and could be purified by crystallization from hexanes. Attempts to isolate di(AP)-ligated titanium complexes were unsuccessful, even when heated with an equimolar mixture of proligand to homoleptic starting material for extended periods of time at 100 °C. The authors do mention the potential formation of a minor amount of diligated complex, although this species could not be isolated.²⁴⁶



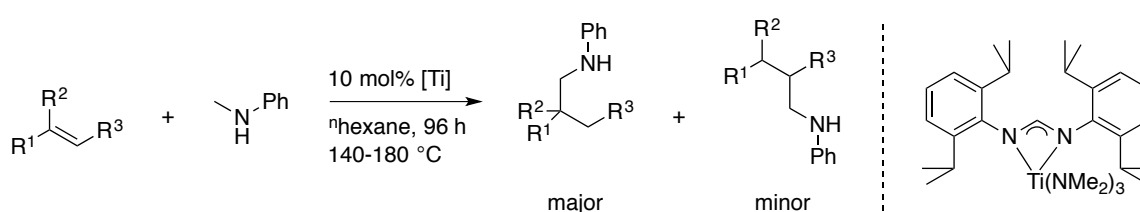
Scheme 7 Mono(aminopyridonato) titanium complexes for hydroamination²⁴⁶

These complexes were found to be competent for room temperature intramolecular HA of aminoalkenes in 24 h. Depending on the substitution pattern of the AP ligand, the respective complex could form exclusively a 6-membered ring through HA in good yields (86%). However, when increasing the steric bulk from methyl ($R^1=R^2=R^3=R^4=Me$) to isopropyl ($R^1=R^4=H$, $R^2=Me$, $R^3=iPr$) the authors note a drastic reduction in the catalytic activity (86% to 20%, respectively). The authors are careful to note that the activity of the so called $ApTi(NMe_2)_3$ family of complexes increases with decreasing amounts of steric congestion. Furthermore, they report the screening of the Group 4 AP analogues using *in situ* catalyst generation with $M(NMe_2)_4$ ($M = Ti, Zr, Hf$) and found that the Ti congeners were superior to the others. This is noteworthy because catalysis using homoleptic $Ti(NMe_2)_4$ gave a mixture of HA and HAA products (9:1) and reaches only 50% after 24 h. This example highlights the significance of steric bulk, whereby complexes must possess enough steric congestion to prevent dimerization and/or ligand redistribution, while sterically accessible metal centres are required to promote reactivity.

Other examples include the Group 4 amidinate titanium complexes bearing one *N,N*-chelate and three dimethylamido ligands reported by Eisen *et al.* in 2013.³⁴³ When one equivalent of $Ti(NMe_2)_4$ was subjected to one, two, or three equivalents of proligand, the

exclusive formation of pentacoordinate mono(formamidinate)tris(dimethylamido) titanium complexes was observed and products were isolated in excellent yields (>90%). Changing the conditions to alter the reaction temperature or time did not affect the resulting product, attributed to the large steric bulk of the *N,N*-chelate. These mono(formamidinate) complexes were then exploited for the polymerization of α -olefins.³⁴³⁻³⁴⁵

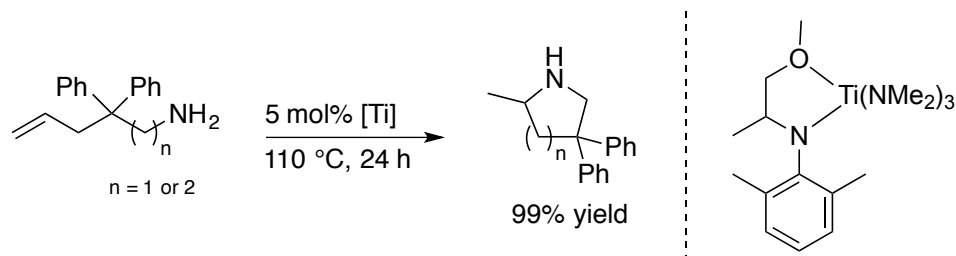
Doye *et al.* later facilitated the C-C bond forming HAA reaction between secondary amines and internal and terminal alkenes using the mono(formamidinate) titanium catalyst shown in Scheme 8.³⁴⁶ These complexes were easily synthesized and isolated due to their increased steric protection around the titanium centre that prevents dimerization and/or ligand redistribution.



Scheme 8 Intermolecular hydroaminoalkylation of internal and terminal alkenes with *N*-methylaniline using a titanium mono(formamidinate) titanium complex³⁴⁶

Furthermore, Ayinla and Schafer have reported an *N,O*-chelating amino ether ligand having a two carbon backbone to give a 5-membered metallacycle, with the respective zirconium and titanium complexes being isolable in good yields (72-86%).²⁵⁸ These complexes were screened for HA of aminoalkene substrates to form cyclic, nitrogen-containing heterocycles in excellent yields (Scheme 9). The titanium and zirconium complexes were isolable and analyzed in the solid-state. The titanium complexes show a N-Ti-O bite angle of *ca.* 73.7°, which is larger than the bite angle of the smaller *N,O*-chelates that form a 4-membered metallacycle (amidates,

ureates, phosphoramidates, *vide infra*) and provides access into isolable, reactive, mono-ligated, titanium complexes.²⁵⁸ To date, no mono-ligated *N,O*-chelated titanium systems have been reported where the complex exists as a 4-membered metallacycle.



Scheme 9 Mono(*N,O*) amido ether titanium complexes capable of hydroamination of aminoalkenes²⁵⁸

The examples discussed above highlight the importance of sterically accessible complexes bearing three labile dimethylamido ligands and one sterically bulky chelate to prevent the formation of dichelated complexes. With the success achieved with titanium amidates, pyridonates, and amino ethers as catalysts for amine synthesis, it was envisioned that new titanium catalysts could be developed. The sterically demanding phosphoramidate ligand provided a promising avenue to be explored in combination with titanium. It was of interest to use this more sterically bulky, electron withdrawing, N,P,O chelate to access mono *N,O*-chelates of titanium that would avoid dimerization and/or redistribution reactions while remaining active in catalysis. The following sections discuss these synthetic investigations. The successes achieved with a tantalum phosphoramidate complex is highlighted, with a focus on expanding the substrate scope amenable to the solvent-free, room-temperature synthesis of amines. Secondly, efforts to install the bulky phosphoramidate ligand motif onto titanium starting materials is discussed, and complexes bearing one, two, and three bulky *N,O*-chelates are presented. These complexes are screened for HAA and HA activity.

2.6.1 Tantalum Phosphoramidates for Hydroaminoalkylation

In 2013, the synthesis and reactivity of tantalum phosphoramidate complexes was investigated by the Schafer Group (Dr. Pierre Garcia and Dr. Ying Lau) in an attempt to circumvent the high reaction temperatures and long reaction times often necessary for HAA.¹⁸³ Screening of a variety of tantalum phosphoramidate complexes was conducted using 4-methoxy-*N*-methylaniline to be consistent with previous literature reports.^{234-237, 271, 275, 330, 347} Figure 22 shows some of the many complexes that were screened, either as isolated complexes or from species generated *in situ*, for this carbon-carbon bond forming transformation. As shown below, many systems require high reaction temperatures (>100 °C) and reach low conversions after 20 hours. When the phosphoramidate ligand motif was combined with an electron-withdrawing chloro ligand and labile methyl ligands, the resulting complexes were active for room temperature HAA, owing to the more sterically accessible, electrophilic metal-centre. Importantly, the *N,O*-chelate provides adequate steric bulk that prevents dimerization and an easily modifiable ligand for further precatalyst optimization.

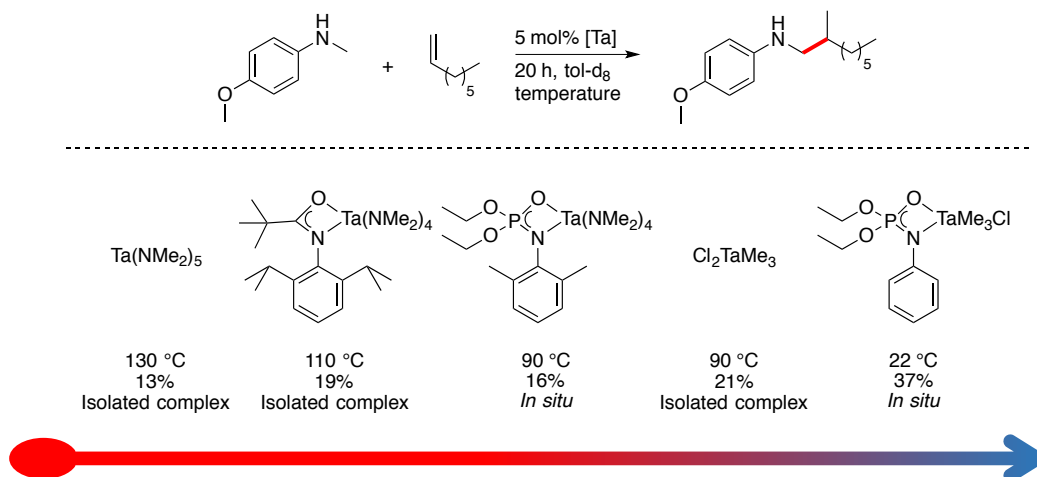
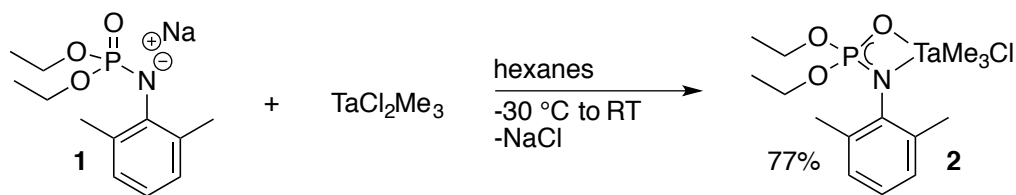


Figure 22 Precatalyst development for hydroaminoalkylation catalyzed by tantalum precatalysts¹⁸³

After further development efforts performed by Dr. Garcia and Dr. Lau, complex **2** (Scheme 10) bearing methyl substituents at the 2- and 6- positions of the aryl ring was identified as the most active complex. Compound **2** can be easily synthesized *via* salt-metathesis between the sodium-salt of the desired proligand and TaCl_2Me_3 . After removal of the NaCl *via* filtration, the complex can be recrystallized from hexanes and isolated as a yellow solid in good yields (77%). Compound **2** is highly reactive to air and moisture and is light and temperature sensitive. These characteristics make the handling and use of this complex difficult; however, the exquisite reactivity afforded by this complex make it a valuable tool for HAA. This represents the first and only reported example of room temperature HAA.



Scheme 10 Synthesis of phosphoramidate chloro complex **2** *via* salt metathesis from **1**

In addition to targeting mild reaction conditions for improving energy efficiency in catalytic transformations, the principles of Green Chemistry encourage the elimination of the use of solvent.³⁴⁸ Indeed, transition metal catalyzed C-H functionalization reactions have recently evolved to include solvent-free reaction protocols.^{271, 349-351} Therefore, it was of interest to the author to investigate if **2** was effective under solvent-free reaction conditions, thus eliminating the solvent waste generated in this transformation. The following sections describe work that was done by the author, using complex **2**, which was developed by Dr. Garcia and Dr. Lau.

A variety of substrates were shown to be tolerant to solvent-free reaction conditions (Table 1). Typically, neat conditions offered comparable or improved yields relative to reactions conducted in toluene. For example, the reaction between 1-octene and 4-methoxy-*N*-methylaniline gave **3** in only 84% yield after 20 h in toluene, whereas 96% yield of product **3** is obtained under neat conditions in the same amount of time (Entry 1). Interestingly, the reaction involving 4-trifluoromethylstyrene to generate product **4** (Entry 2) suffers decreased yields (62% *vs.* 78%, after 168 h), but maintains a comparable level of regioselectivity (1.7:1 *vs.* 1.8:1 branched/linear). A notable contrast exists in the reaction between *N*-methylcyclohexylamine and 1-octene. The reaction gives 71% yield in the absence of solvent after only 20 h while it takes 168 h to reach 62% yield in solution. Furthermore, it was found that certain neat reactions

(Entries 4^d and 5^d) required only 6 h to reach comparable yields to those requiring 20 h in toluene, drastically reducing the time required to form products **6** and **7**, respectively.

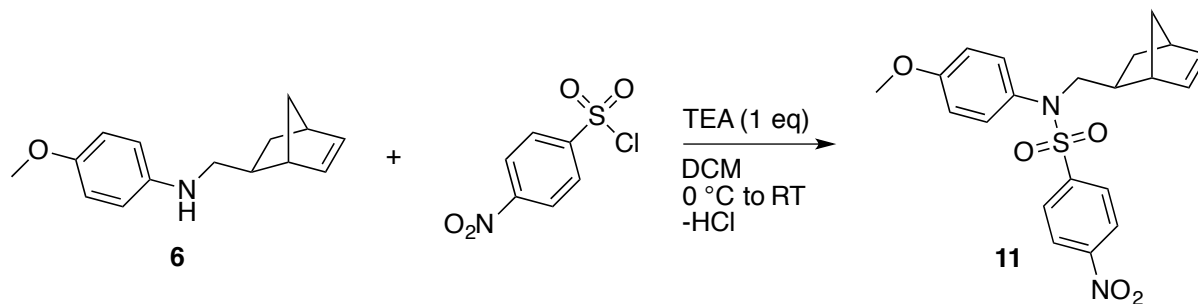
Table 1 Room temperature hydroaminoalkylation using 2 under solvent-free conditions

$ \begin{array}{c} \text{R}^1\text{-N(H)-} \\ + \quad 1.5 \quad \begin{array}{c} \text{R}^2 \\ \text{C}=\text{C} \\ \text{R}^3 \end{array} \\ \xrightarrow[\text{neat, 20 h, RT}]{10 \text{ mol\% [Ta]}} \text{R}^1\text{-N(H)-CH(R}^3\text{)-CH}_2\text{R}^2 \end{array} $				
<div style="text-align: right;"> 2 </div>				
Entry ^a	Amine	Alkene	Product	Yield (%) ^b
1			 3	96
2			 4	62 ^c [1.7:1]
3			 5	86
4			 6	54 58 ^{d,e} 61 ^f
5			 7	71 65 ^d
6			 8	20

^aReactions conducted with 1 mmol amine and 1.5 mmol of alkene for 20 h at room temperature, unless otherwise stated. ^bIsolated yields of the major product reported after column chromatography. Branched/linear ratio ([b:l]) determined by GC-MS. ^cReaction time was 168 h. ^dReaction time was 6 h. ^e1 mmol:1 mmol amine/alkene. ^f5 mmol alkene used.

Notably, all reactions yielded the branched regioisomers preferentially, which is in agreement with previous results when early transition metals are used.¹⁸³ In one case, a cyclic diene, norbornadiene (NBD) was employed to generate monoalkylated product **6**. Low yields of this reaction (54%, Entry 4) were observed and attributed to the generation of small amounts of dialkylated products, as indicated by GC-MS analysis (*vide supra*, Scheme 12). Alternatively, equimolar amounts of amine and alkene were reacted using the same conditions to avoid over alkylation (Entry 4^e). Regardless, a trace amount of **9** and **10** was observed by GC-MS in this case, although the yield of isolated **6** remained comparable. Most importantly, the synthesis of the norbornene-containing product **6** was shown to be scalable to 5 mmol of amine (0.66 g) with comparable yields (Entry 4^f). The remaining strained alkene moiety present in this product allows a synthetic handle for further chemical transformations, with ROMP being an appealing avenue for future investigation (*vide infra*).

In the case when using NBD to generate product **6** (Entry 4), two possible diastereomers are possible. Pleasingly, only one product is observed by GC-MS and NMR spectroscopic analysis. To determine the nature of the obtained isomer, product **6** was derivatized with a nosyl group to aid crystallization to determine the stereoisomer generated (Scheme 11). A white solid, **11**, was recovered in excellent yield (>95%).



Scheme 11 Derivatization of **6** with *p*-nitrobenzenesulfonyl chloride to form product **11**

Crystals suitable for X-ray crystallography of compound **11** were obtained by slow evaporation of a saturated solution in acetonitrile and show the formation of the *exo*-isomer in the solid-state (Figure 23). All bond lengths and angles are in good agreement with expected values. A full list of bond lengths and angles can be found in Appendix C (Table A 1).¹⁸³

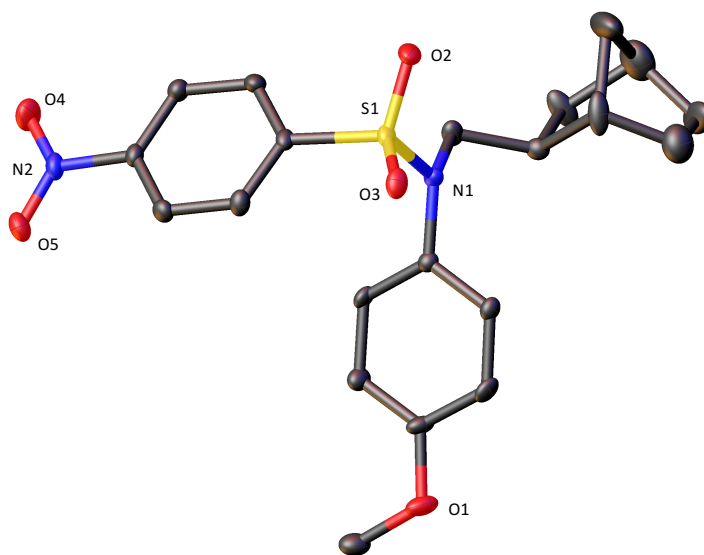
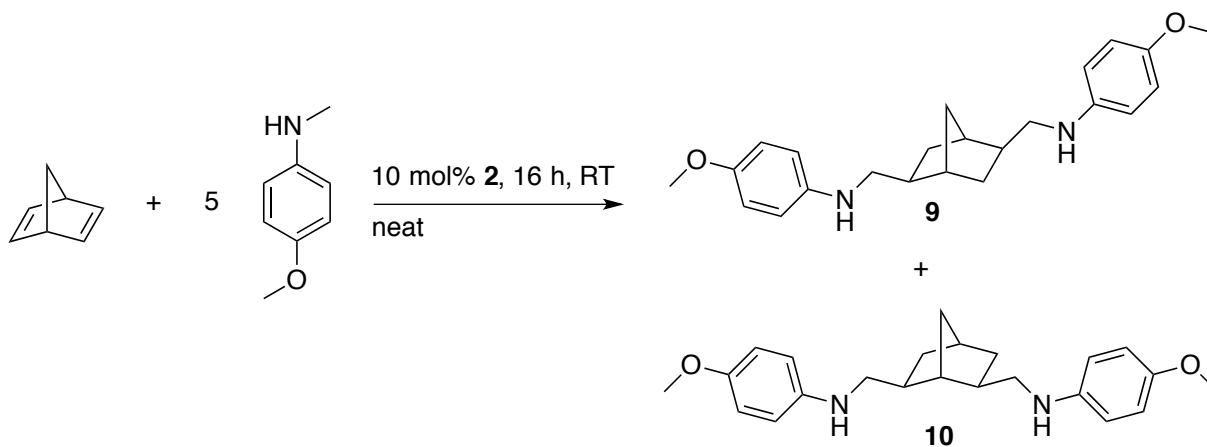


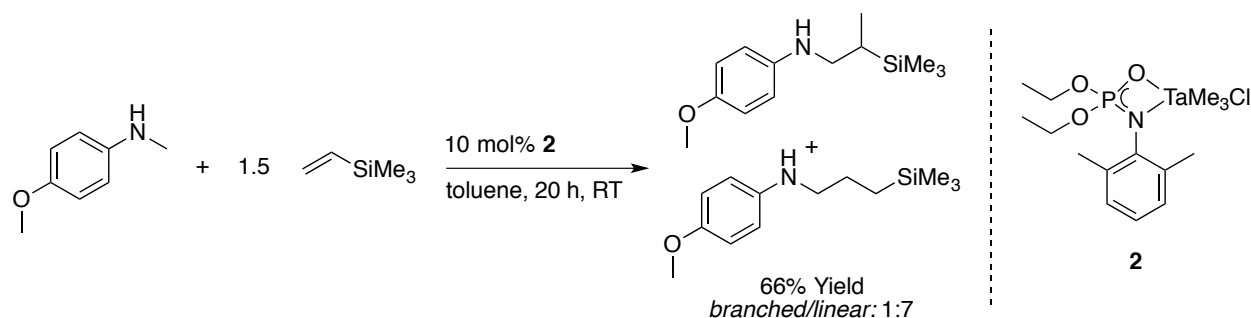
Figure 23 ORTEP of compound **11**. Ellipsoids shown at 50% probability. Hydrogen atoms omitted for clarity

The dialkylated side-products were synthesized and characterized independently by reacting an excess of 4-methoxy-*N*-methylaniline (5 eq.) and NBD to confirm the identity of the undesired **9** and **10** (Scheme 12). Analysis of the crude solid (after removing tantalum salts *via* filtration) by GC-MS showed two products in near equal ratio, as well as unreacted starting materials and proligand. The mixture was purified *via* column chromatography (hexanes/ethyl acetate) to give a mixture of isomers shown below in 10% yield. This mixture could not be separated further. The products are the 2,5-substituted compound **9** (Scheme 12, top) and 2,6-substituted regioisomer **10** (Scheme 12, bottom). Each of these substituents could exist as either *endo*- or *exo*-diastereomeric centres; however, as mono-alkylation generates exclusively *exo*-diastereomers (*vide supra*, Figure 23) it is proposed that both substituents in the dialkylated products exist in the *exo*-conformation.



Scheme 12 Formation of dialkylated products **9 and **10** by hydroaminoalkylation**

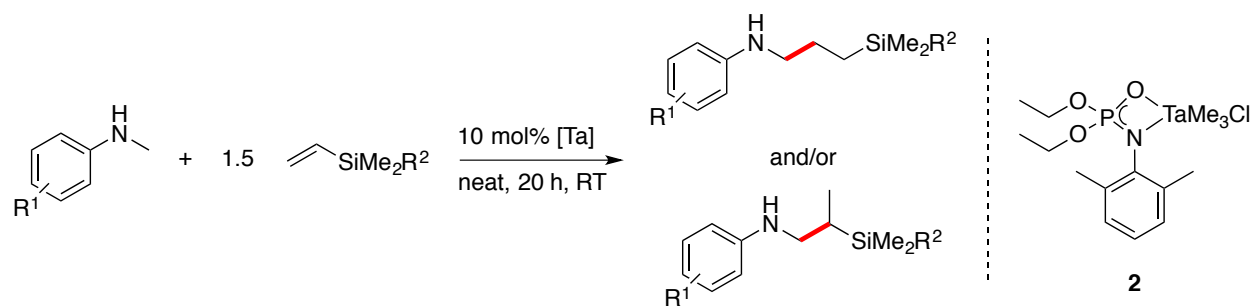
The reported investigation using complex **2** highlights a reversal in regioselectivity when a silylated substrate is used. Specifically, when vinyltrimethylsilane was reacted with 4-methoxy-*N*-methylaniline in toluene, the linear product formed preferentially over the branched, in a ratio of 1:7 and overall yield of 66% (Scheme 13).¹⁸³



Scheme 13 Previously reported result of linear regioselectivity with silylated substrates using complex **2**¹⁸³

This represented one of the first examples of Group 5 complexes generating the linear isomer over the branched product, and is attributed to the β -silicon effect of these substrates.^{271, 330} We were curious to see if vinyltrimethylsilane and other silylated substrates would behave similarly under solvent-free conditions and also wanted to increase the breadth of silylated products capable of being synthesized by HAA using **2**. Table 2 outlines the substrates that have been screened in this transformation.

Table 2 Reactions of silylated substrates using 2 under solvent-free conditions



Entry ^a	Amine	Alkene	Product	Yield (%) ^b [b:l] ^c
1			 12	67 [1:7.3]
2			 13	65 [1:19.0]
3			 14	60 [1:9.0]
4			 15	27 [1:16.0]
5			 16	<5 ^d

^aReactions conducted with 1 mmol amine and 1.5 mmol of alkene. ^bIsolated yields of the major isomer reported after purification by column chromatography. ^cBranched/linear ratio ([b:l]) determined by GC-MS. ^dConversion as determined by ¹H NMR spectroscopy.

The reaction of 4-methoxy-*N*-methylaniline and vinyltrimethylsilane (Table 2, Entry 1) to generate **12** under neat conditions reaches yields (67%) and shows regioselectivity (1:7.3) comparable to solution phase reactivity (66%, 1:7.3). While no differences between solution-phase and neat-reactivity were observed, it was still of interest to probe the differences in regioselectivity of substrates comprised of silyl groups to expand the potential of this reaction. The preliminary results show that *para*-substitution about the aryl ring of the amine is important for obtaining higher yields (Entries 1 and 3 vs. Entry 4), as the electron-donating methyl and methoxy groups facilitate greater reactivity. Interestingly, *ortho*-substituted amine substrate 2-methyl-*N*-methylaniline (Entry 5) was not well tolerated and reached <5% conversion. This result is attributed to the steric bulk of this substrate. These preliminary results indicate the potential utility of the tantalum catalyst to selectively generate linear regioisomers over their branched counterparts.

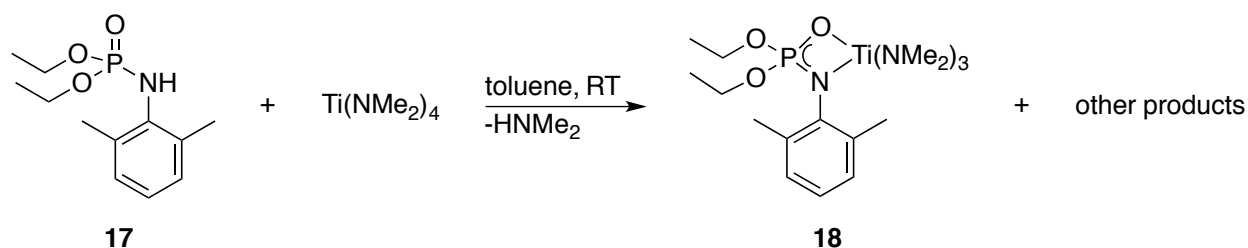
This section discussed the expansion of the substrates utilized in HAA using complex **2**. Specifically, it focused on employing a solvent-free protocol to increase the appeal of this phosphoramidate tantalum precatalyst. In many cases, the productivity of **2** was shown to be increased in the absence of solvent, relative to the analogous reactions conducted in toluene. This section also included the presentation of a variety of silylated amine products synthesized using **2**, with higher levels of the respective linear regioisomers being formed over the branched counterparts, an observation attributed to the β -silicon effect.¹⁸³

With these promising HAA results in hand, it was of interest to us to expand the pairing of the bulky phosphoramidate proligand to include titanium-based starting materials, rather than tantalum. This would offer an alternative complex with this inexpensive metal for amine-generating catalytic reactions.

2.6.2 Monophosphoramidate Titanium Complexes

Initial attempts began by attempting to synthesize monophosphoramidate complexes bearing three labile dimethylamido ligands to promote reactivity. Following the procedure described previously,³³⁴ we attempted to synthesize these complexes *via* protonolysis. As the phosphoramidate ligand motif is more sterically bulky than the commonly used amidate ligands, due to the tetrahedral phosphorus centre (*vide supra*), we envisioned that the exclusive formation of monophosphoramidate titanium complexes could be accessed and provide reactive complexes with sterically accessible metal centres that would avoid dimerization and/or ligand redistribution.

Homoleptic $\text{Ti}(\text{NMe}_2)_4$ was combined with an equimolar amount of phosphoramidate **17**. Analysis of the crude mixture by ^1H and ^{31}P NMR spectroscopy revealed a mixture of products as indicated by several sets of resonances being observed for the phosphoramidate ligand in the ^1H NMR spectrum (Scheme 14). Furthermore, two resonances were observed in the $^{31}\text{P}\{^1\text{H}\}$ NMR spectrum at 7.1 ppm and 5.9 ppm, whereas only one resonance was expected. The phosphoramidate proligand, **17**, has one distinct ^{31}P resonance at *ca.* 4.3 ppm.



Scheme 14 Synthesis of monophosphoramidate titanium complex **18**

Recrystallization of the material yielded the diphosphoramidate species, **19**, as red crystals (*vide infra*). The filtrate was reduced and isolation of monophosphoramidate species could be achieved through successive recrystallizations. Eventually, mono(phosphoramidate)tris(dimethylamido) titanium species **18** could be obtained as a yellow solid, albeit in low yield (<10 %).

Analysis of **18** by ^1H and ^{31}P NMR spectroscopy was performed (Figure 24). One phosphorus resonance was observed at 7.1 ppm (inset, Figure 24). Two sharp singlets were observed in the ^1H NMR spectrum. One singlet, attributed to the dimethylamido group, appears at 3.3 ppm (yellow circle, 18H), while the singlet at 2.5 ppm (blue circle, 6H) is consistent with two equivalent aryl methyl (ArCH_3)₂ groups. The ethoxy moieties of the phosphoramidate show a characteristic triplet at 1.0 ppm (red circle, 6H) and multiplet between 3.9 ppm and 3.8 ppm (green circle, 4H) and the 3:1 ratio between the dimethylamido (yellow circle, 18H) and ethoxy methyl groups of the phosphoramidate support the presence of a monophosphoramidate species in solution.

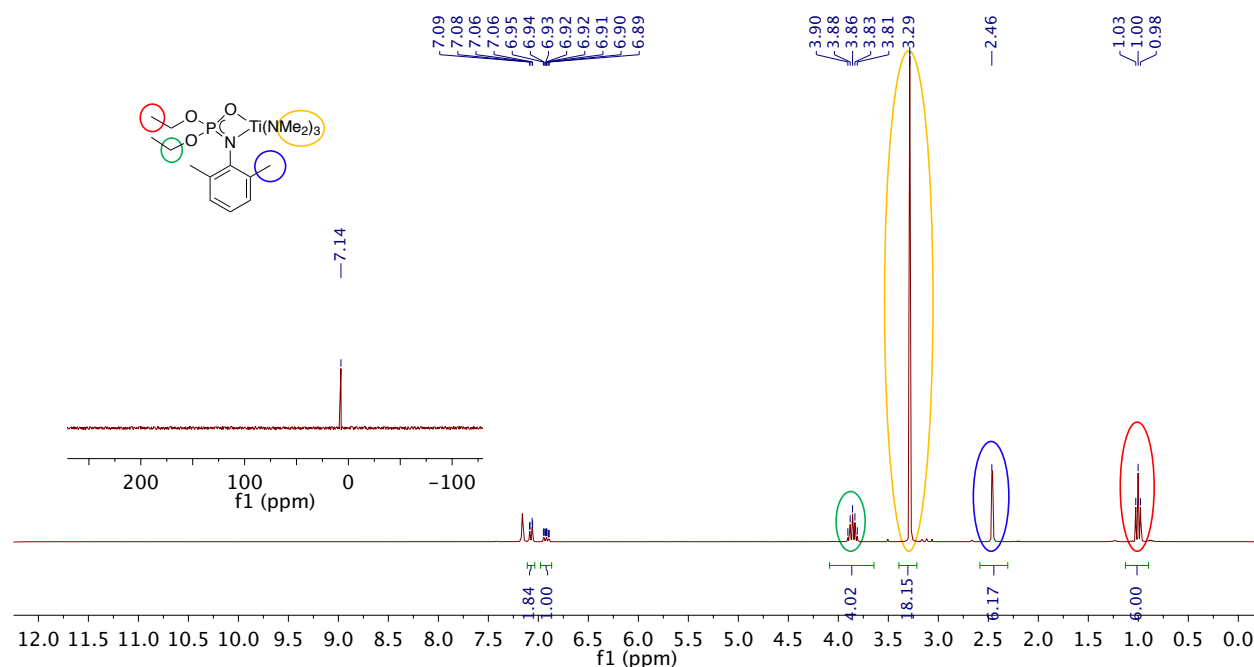


Figure 24 ^1H and $^{31}\text{P}\{^1\text{H}\}$ (inset) NMR spectra (300 MHz and 121 MHz, respectively, C_6D_6 , 298 K) of monophosphoramidate complex **18**

Complex **18** was found to be stable in the solid-state for months, but significant ligand redistribution occurred within minutes while in solution at room temperature, making acquisition of a diagnostic ^{13}C NMR spectrum difficult. Fortunately, complex **18** was isolable as crystalline material suitable for X-ray crystallography after removing all volatiles *in vacuo* (Figure 25).

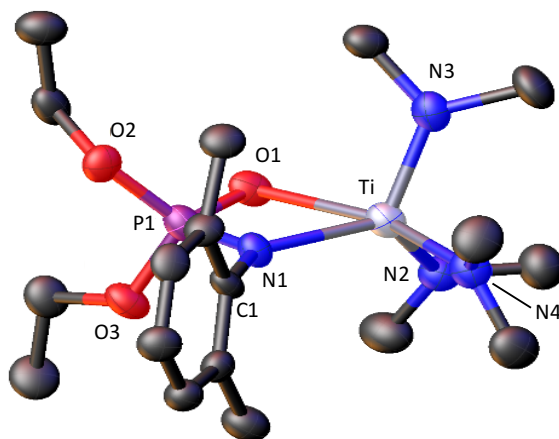


Figure 25 ORTEP of complex 18. Ellipsoids shown at 50% probability. Hydrogen atoms removed for clarity

The solid-state molecular structure shows the *N,O*-chelate bound κ^2 to maximize bonding interactions with the electron deficient titanium centre. The delocalization about the chelate is unsymmetrical with the Ti-N1 bond length of 2.107(7) Å being shorter than the Ti-O1 bond length of 2.223(6) Å (Table 3). This observation is noted for the previously reported tantalum monophosphoramidate complex **2**, which has a Ta-O bond length of 2.190(2) Å and a Ta-N bond length of 2.135(3) Å.¹⁸³ The chelate is bound to complex **18** with a tight bite angle to the metal, with the O1-Ti-N1 angle being 67.3(3)° and a N1-P1-O1 angle of 102.3(4)°. This is in good agreement relative to complex **2**, which has a O-Ta-N bond angle of 66.68(9)°.¹⁸³

Table 3 Select bond lengths (Å) and angles (°) for monophosphoramidate complex 18

Bond length (Å)		Bond angle (°)	
Ti-O1	2.223(6)	N1-P1-O1	102.3(4)
Ti-N1	2.107(7)	O1-Ti-N1	67.3(3)
P1-O1	1.514(6)	O1-Ti-N3	95.9(3)
P1-N1	1.570(8)	N1-Ti-N3	121.2(3)
P1-O2	1.570(7)	N2-Ti-N3	113.5(3)
P1-O3	1.567(6)	N3-Ti-N4	95.6(3)
Ti-N2	1.922(8)	N1-Ti-N2	112.8(3)
Ti-N3	1.893(7)	N1-Ti-N4	93.5(3)
Ti-N4	1.931(8)		
N1-C1	1.433(11)		

The bond lengths of the delocalized ligand backbone P1-O1 of 1.514(6) Å and P1-N1 of 1.570(8) Å are in reasonable agreement with tantalum complex **2** (P-O 1.516(2) Å and P-N 1.616(3) Å).¹⁸³ These bond lengths are in good agreement with the delocalized π -character present in the ligand motif. Interestingly, the three amido ligands display a trend in bond length depending on their position relative to the plane of the *N,O*-chelate. The amido N4-Me₂ ligand lies closest to the plane of the *N,O*-chelate has the longest Ti-N bond (1.931(8) Å), indicating the strong *trans* influence of the chelate. N2-Me₂ lies slightly below this plane and possesses a Ti-N2 length of 1.922(8) Å. The N3-Me₂ lies most perpendicular to this plane and has the shortest Ti-N bond length of 1.893(7) Å, consistent with significant multiple bond character.

The classification of the geometry of 5-coordinate complexes can be assessed by using geometry index or structure parameter, τ_5 .³⁵² The geometry is classified as a 5-coordinate idealized square-pyramid (spp) when the τ_5 value is 0, or an idealized trigonal bipyramidal (tbp) complex when the τ_5 value is 1 (Figure 26).

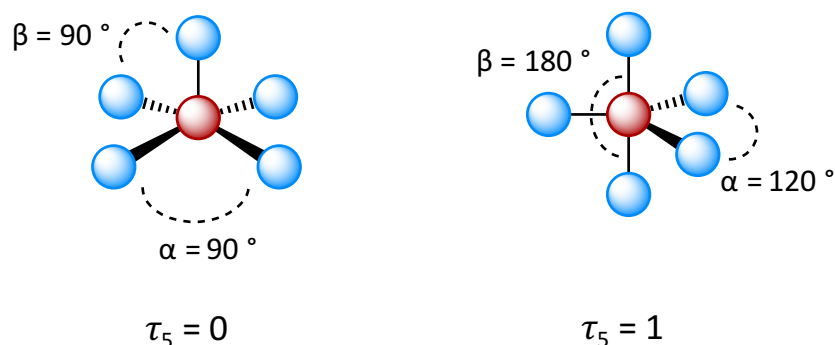
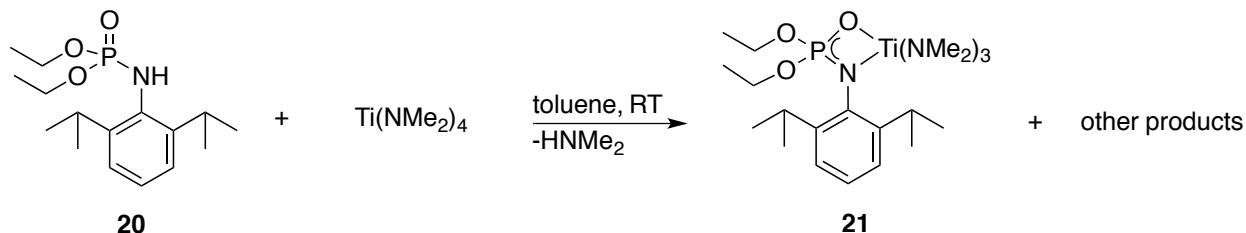


Figure 26 Idealized square pyramidal and trigonal bipyramidal molecular geometries

Monophosphoramidate complex **18** possesses a τ_5 value of 0.43 and is therefore not definitively assigned as sqp or tbp, but is best considered as sqp considering τ_5 and the significant axial π -bond character observed in the solid-state. The deviations from conventional geometries are thought to be largely due to the constraints of the tightly bound phosphoramidate.

Exclusive formation of **18** proved difficult, even under dilute reaction conditions at low temperatures ($-30\text{ }^{\circ}\text{C}$ to RT), and after short reaction times (10 minutes) as evidenced by significant amounts of diphosphoramidate species, **19**, observed by ^1H and ^{31}P NMR spectroscopy. Furthermore, using a large excess of $\text{Ti}(\text{NMe}_2)_4$ (40 eq.) did not eliminate the formation of the diligated species. As shown with a bulky AP ligand (Scheme 7) disclosed by Chong *et al.*, the formation of tris(dimethylamido) titanium species bearing one κ^2 -ligand is possible.²⁴⁶ In this vein, a more sterically bulky 2,6-diisopropylphenyl (*dipp*) substituted phosphoramidate proligand, **20**, was used in an attempt to generate mono-substituted products (Scheme 15).



Scheme 15 Synthesis of monophosphoramidate titanium complex **21**

A toluene solution of proligand **20** (1 eq.) was added to a stirring toluene solution of homoleptic titanium starting material (1 eq.). The mixture was stirred overnight at room temperature before all volatiles were removed and an orange oil was obtained. A crude spectrum (^{31}P NMR spectroscopy) displayed two resonances (6.3 ppm, *mono* and 5.3 ppm, *di*). Again, the diphosphoramidate side product, **22**, could be removed by successive recrystallizations using toluene. Reduction of the filtrate revealed the desired mono(phosphoramidate)tri(amido) complex, **21**. Mass spectrometry showed the expected parent mass for the pentacoordinate complex (492 m/z) and a mass-to-charge ratio of 448, which represent a loss of 44 molecular weight units, a commonly observed occurrence when ionizing complexes bearing labile dimethylamido ligands. The complex was analyzed by HRMS and gave a parent mass of 492.27139 (calcd: 492.27088). The ^1H NMR spectrum of complex **21** shows clear resonances attributed to the dimethylamido and *dipp* ligands in a 3-to-2 ratio (3.3 ppm, s, 18H, $3\times\text{N}(\text{CH}_3)_2$: 1.4 ppm, d, 12H, $2\times\text{CH}(\text{CH}_3)_2$). The expected resonance for the ethoxy moieties are also present and agree well with predicted values. Aryl protons are overlapped with resonances of the C_6D_6 used for spectroscopy (7.2 ppm). Furthermore, one ^{31}P resonance was observed (6.3 ppm) (Figure 27), which is downfield to the related diphosphoramidate analogue. Fortunately, the increased steric bulk allowed for analysis by ^{13}C NMR spectroscopy, with the spectrum

displaying one set of resonances (see Appendix A for spectrum). However, exclusive formation of monophosphoramidate species still proved elusive.

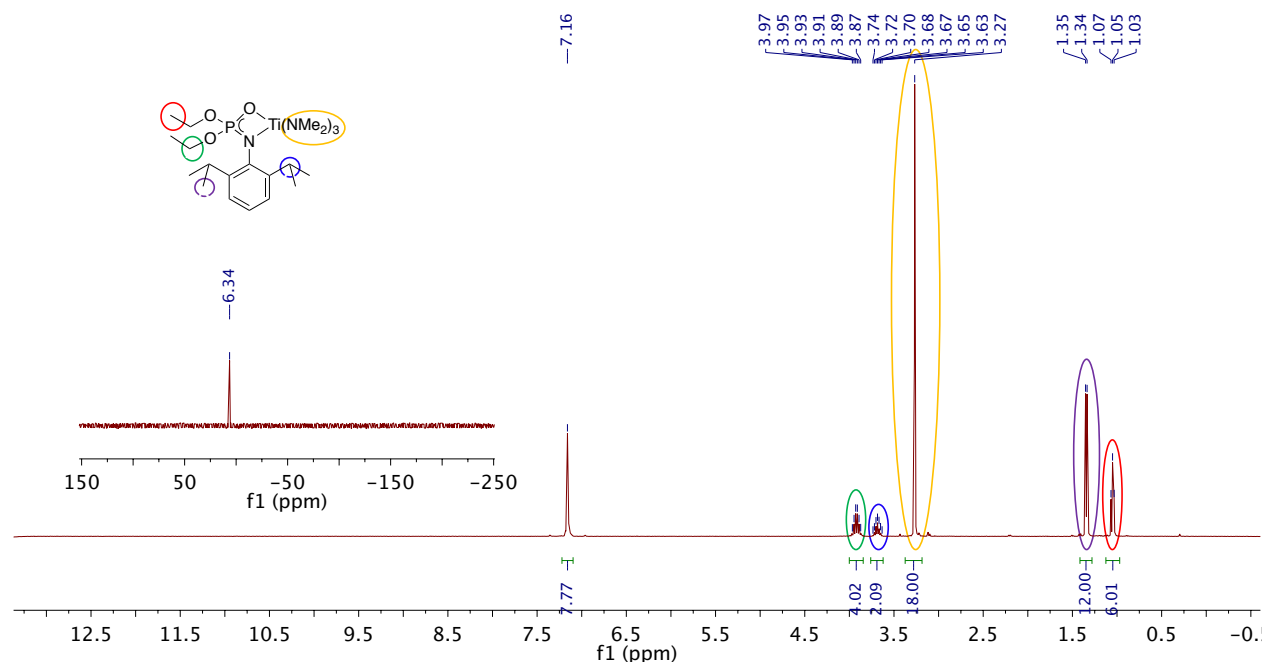


Figure 27 ^1H and $^{31}\text{P}\{^1\text{H}\}$ (inset) spectra (C_6D_6 , 300 MHz and 121 MHz respectively, 298 K) of monophosphoramidate complex **21**

The same solution-phase behavior observed for **18** was observed with complex **21** despite bearing bulkier *dipp* groups, albeit at seemingly slower rates. Figure 28 (bottom) shows the ^{31}P NMR spectrum of complex **21**. The top spectrum displays the same sample after being kept in C_6D_6 at room temperature in a J. Young NMR tube for *ca.* 1 month.

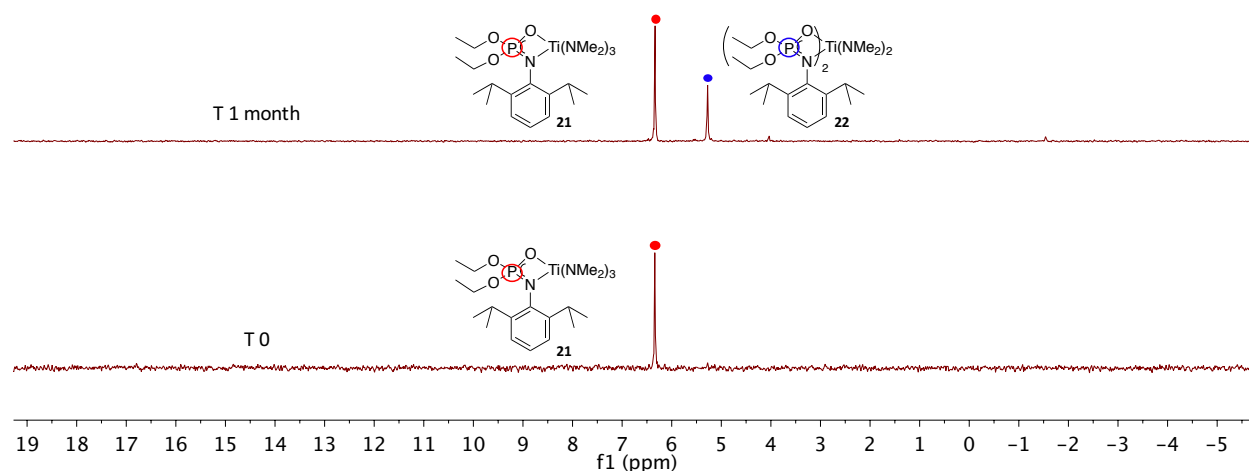


Figure 28 Ligand redistribution of complex 21 over time to form diphosphoramidate side product 22 as observed by ^{31}P NMR spectroscopy (C_6D_6 , 121 MHz, 298 K)

As noted above, all attempts to isolate monophosphoramidate complexes exclusively were plagued by ligand redistribution to form disubstituted-analogues. We were curious to see if we could access monophosphoramidates through disproportionation of the easily formed diphosphoramidate species. Diphosphoramidate complex **19** was dissolved in toluene and added to a J. Young NMR tube. Neat $\text{Ti}(\text{NMe}_2)_4$ (10 eq.) was added the NMR tube was sealed and agitated. No formation of a monophosphoramidate complex was observed by ^1H or ^{31}P NMR spectroscopy. The NMR tube was heated to $145\text{ }^\circ\text{C}$ overnight and analyzed again by ^1H and ^{31}P NMR spectroscopy. Again, no formation of monophosphoramidate species was observed.

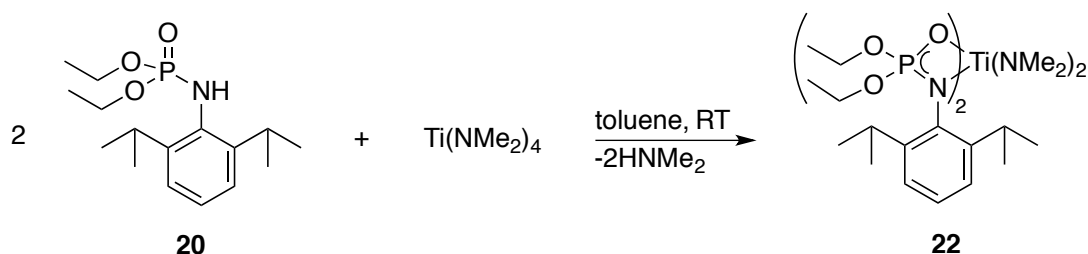
The exclusive formation and isolation of monophosphoramidate titanium complexes were complicated by the persistent formation of diphosphoramidate species. As discussed in the introduction (Figure 19), many examples of di(*N,O*)-chelated titanium complexes have been reported to be competent for HA and HAA activity. As no reports of diphosphoramidate titanium

species are present in the literature, it was of interest to explore the application of these easily formed complexes as potential catalysts for C-C and C-N bond forming reactions.

2.6.3 Diphosphoramidate Titanium Complexes

The exclusive formation of titanium complexes bearing one *N,O*-chelating phosphoramidate ligand was not successful under any of the conditions employed. However, these studies did elucidate the conditions and potential for the facile synthesis of Diphosphoramidate titanium species. Indeed, many HA and HAA reactions are facilitated by complexes bearing two amidate *N,O*-chelates. No reports of diphosphoramidate titanium complexes are present in the literature. Therefore, we were curious to see if a range of these complexes could be investigated for use in these small molecule transformations.

The synthesis of diphosphoramidate complexes began by subjecting two equivalents of proligand **20**, bearing *dipp* groups, to $\text{Ti}(\text{NMe}_2)_4$ in a protonolysis reaction. Specifically, **20** (2 eq.) was dissolved in toluene in a 20 mL scintillation vial and stirred vigorously. To this was added a yellow solution of $\text{Ti}(\text{NMe}_2)_4$ (1 eq.). While adding the colourless proligand solution dropwise, the resulting solution turned orange and then deep red in colour. The mixture was left to stir overnight before all solvent and volatiles were removed *in vacuo* (Scheme 16). Analysis of the crude solid showed one resonance in the ^{31}P NMR spectrum at 5.3 ppm, indicating exclusive formation of diphosphoramidate product. The crude red solid could be crystallized from hot toluene to afford red plates of complex **22** in 64% yield. This yield could be improved by sequential recrystallizations of the mother liquor to give an overall yield of 85%. Figure 29 shows the ^1H and ^{31}P NMR spectra of the crystalline product.



Scheme 16 Synthesis of diphosphoramidate titanium complex 22

Only one set of resonances for the *N,O*-chelate is visible in the ^1H NMR spectrum indicating a symmetric molecule in solution at room temperature. Consistent with the monophosphoramidate species, **18** and **21**, discussed previously in Section 2.6.5, the characteristic dimethylamido singlet resonates at 3.3 ppm (orange circle, 12H). The expected triplet is visible at 1.2 ppm (purple circle, 12H) and integration of this signal is consistent with being assigned to the methyl groups of the four equivalent ethoxy ligands. The isopropyl groups of the phosphoramidate give rise to the expected resonances; a well-resolved doublet is visible at 1.5 ppm (green circle, 24H), and the expected septet for the methyne protons appears at *ca.* 4.0 ppm (blue circle, 4H), albeit overlapped by the methylene groups of the ethoxy moiety (yellow circle, 8H). The one-to-one ratio between phosphoramidate methyl protons and those of the dimethylamido ligand support the presence of the expected diphosphoramidate bis(dimethylamido) species in solution.

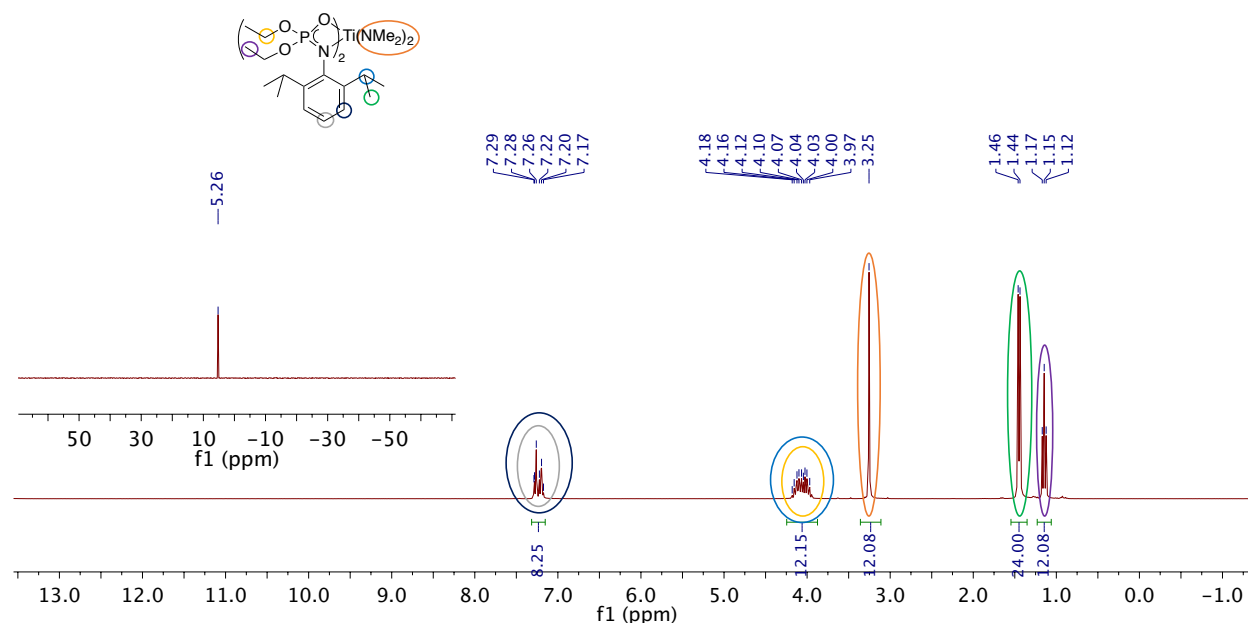


Figure 29 ^1H and $^{31}\text{P}\{^1\text{H}\}$ NMR (inset) spectra of complex **22** (C_6D_6 , 300 MHz and 121 MHz, respectively, 298 K)

Furthermore, the $^{31}\text{P}\{^1\text{H}\}$ NMR spectrum gives one sharp singlet at 5.3 ppm (inset, Figure 29), indicating that both phosphoramidate ligands are equivalent on the NMR timescale. The nature of the complex was further supported by HRMS that shows a m/z of 758.37725 relative to the calculated value of 758.37806. Elemental analysis gave a percent composition of C, 56.91; H, 8.87; N, 7.12, which is in good agreement to the calculated values of C, 56.84; H, 8.74; N, 7.36. Complex **22** was also analyzed in the solid-state by X-ray crystallography (Figure 31).

The ease of synthesizing and isolating complex **22** provided motivation to synthesize a family of substituted diphosphoramidate complexes, **19** and **22-25**, bearing two dimethylamido ligands. Substitution about the aryl-ring was varied, and different *N*-substituted derivatives were incorporated. The changes in ligand structure were done to draw conclusions regarding the reactivity of these complexes in small molecule transformations detailed in Section 2.7 (*vide*

infra). All aryl-substituted complexes, **19** and **22-24**, were obtained as red solids and could be recrystallized easily from saturated solutions in either toluene, hexanes, or diethyl ether. The characteristic resonance of the dimethylamido moiety ranged from 3.5 ppm to 3.2 ppm. In one case, the synthesis could be scaled to use 2.5 g of proligand to generate complex **24** in 91% yield. Figure 30 displays the complexes that were synthesized. Percent yields listed for aryl-substituted complexes represent that of recrystallized products. The percent yield given for complex **25** represents that of crude, yet clean product. This complex is an oil (see Appendix A for spectra). Alkyl-substituted complex **25** displays a significant downfield shift in the ^{31}P NMR spectrum relative to the aryl variants, with the phosphorus resonating at 11.0 ppm.

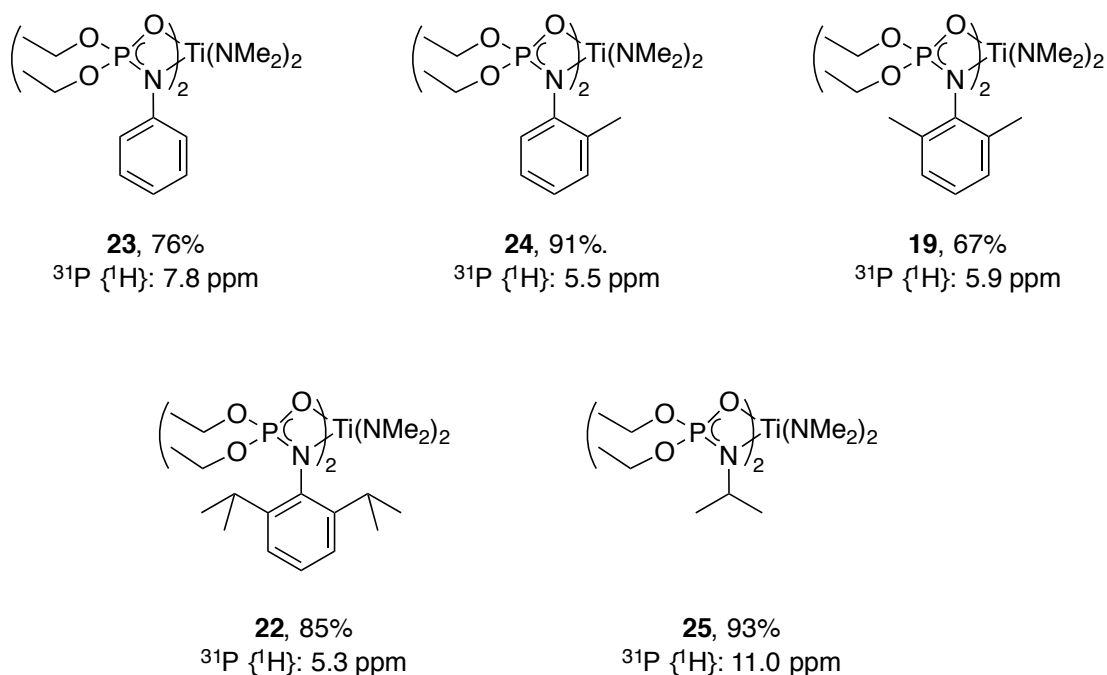
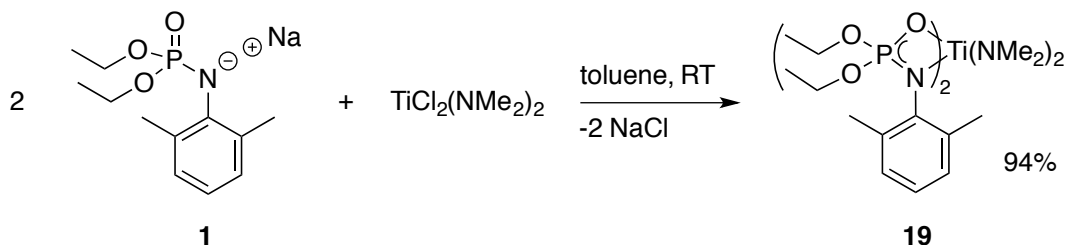


Figure 30 Diphosphoramidate complexes **19** and **22-25**. Yields shown represent isolated percent yields of recrystallized products, except that of **25** which represents the yield of crude product. $^{31}\text{P}\{^1\text{H}\}$ NMR spectroscopy (C_6D_6 , 121 MHz, 298 K)

All compounds listed in Figure 30 were fully characterized, including ^1H , ^{13}C , and ^{31}P NMR spectroscopy, HRMS and/or EA, and IR (ATR) spectroscopy. All diphosphoramidate complexes, **19** and **22-25**, display only one resonance when analyzed by ^{31}P NMR spectroscopy (7.8-5.3 ppm for aryl variants **19** and **22-24**, and 11.0 ppm for alkyl-substituted **25**), indicating symmetry within the complexes in solution. Comparison between mono- and diphosphoramidate complexes bearing 2,6-dimethyl substitution, **18** (mono) and **19** (di) vs. those bearing *dipp* groups **21** (mono) and **22** (di), shows that the mono-*N,O* chelated systems show more downfield ^{31}P NMR resonances than their disubstituted counterparts (7.1 ppm vs. 5.9 ppm for **18** and **21**, and 6.3 ppm vs. 5.3 ppm for **19** and **22**). Furthermore, all ^1H NMR spectra were easily defined by one set of resonances attributed to the phosphoramidate relative to a sharp singlet of the equivalent dimethylamido ligands (3.5 ppm-3.0 ppm).

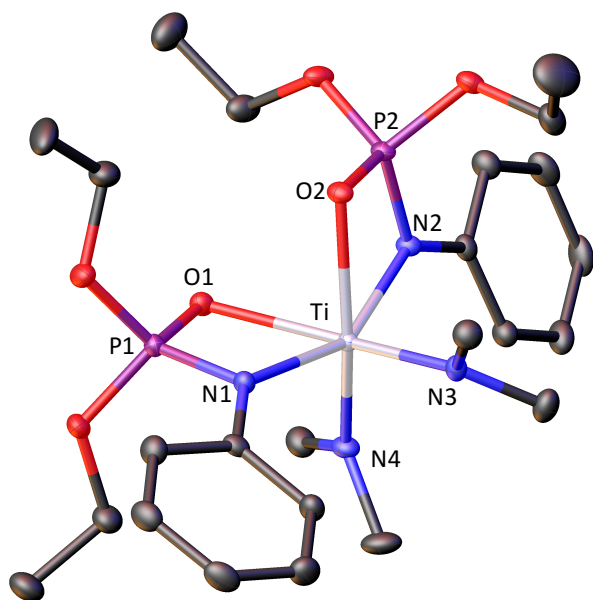
These complexes could also be synthesized *via* salt metathesis using $\text{TiCl}_2(\text{NMe}_2)_2$. In one select example, complex **19** was formed in excellent yield (94%) by reacting the two equivalents of the sodium-salt **1** with $\text{Ti}(\text{NMe}_2)_2\text{Cl}_2$ (Scheme 17). Complex **19** was obtained as a red solid and all characterization is consistent with the expected values obtained from the protonolysis route described above.



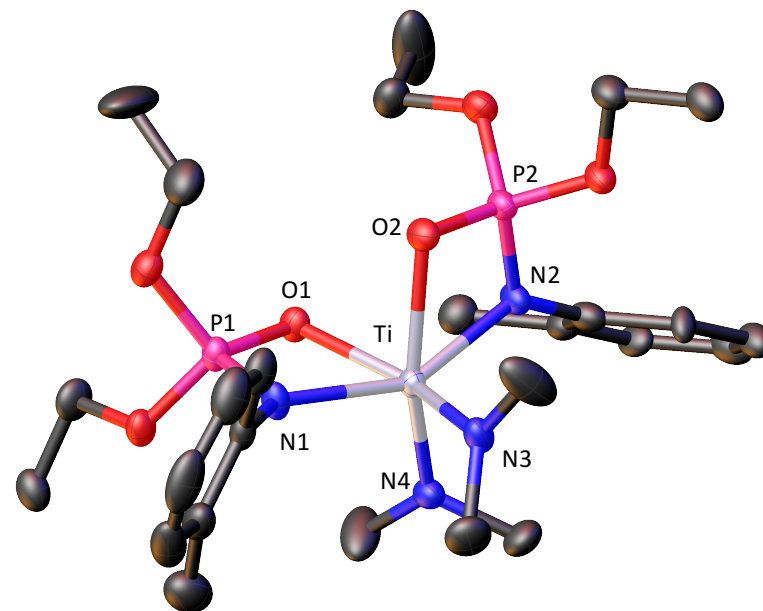
Scheme 17 Synthesis of diphosphoramidate complex **19** *via* salt metathesis

Although the yield obtained by salt metathesis is higher than that when using protonolysis, this method requires the additional steps of synthesizing the sodium salt of the ligand and the removal of the NaCl *via* filtration. However, the desired complex **19** can be isolated easily in both cases.

Solid-state molecular structures could be obtained in cases where aryl-substituted *N,O*-chelates were used. Crystals of complexes **19** and **22-24** could be grown by cooling saturated toluene or hexanes solutions. The solid-state molecular structures of these complexes are shown in Figure 31 and Figure 32 and relevant bond lengths and angles are depicted in the corresponding tables. In all cases, the two phosphoramidate ligands bind κ^2 -*N,O* in the solid-state and the complexes are best described as 6-coordinate distorted octahedral in their geometry. The nitrogen atoms of the chelate are also specifically orientated *trans* to each other to alleviate steric interactions. This has been described previously by the Schafer Group.³³⁸

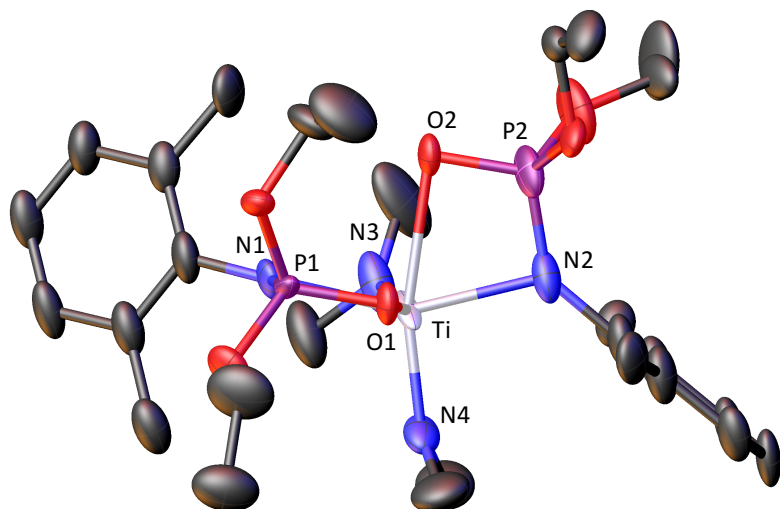


Bond Length (Å)		Bond Angle (°)	
Ti-O1	2.1924(15)	O1-Ti-N1	67.84(6)
Ti-N1	2.1304(19)	O2-Ti-N2	67.65(7)
Ti-O2	2.1838(16)	O2-Ti-N4	160.52(7)
Ti-N2	2.1603(19)	N1-Ti-N2	153.87(7)
Ti-N3	1.900(2)	O1-Ti-N3	158.80(8)
Ti-N4	1.9036(19)	N3-Ti-N4	102.27(9)

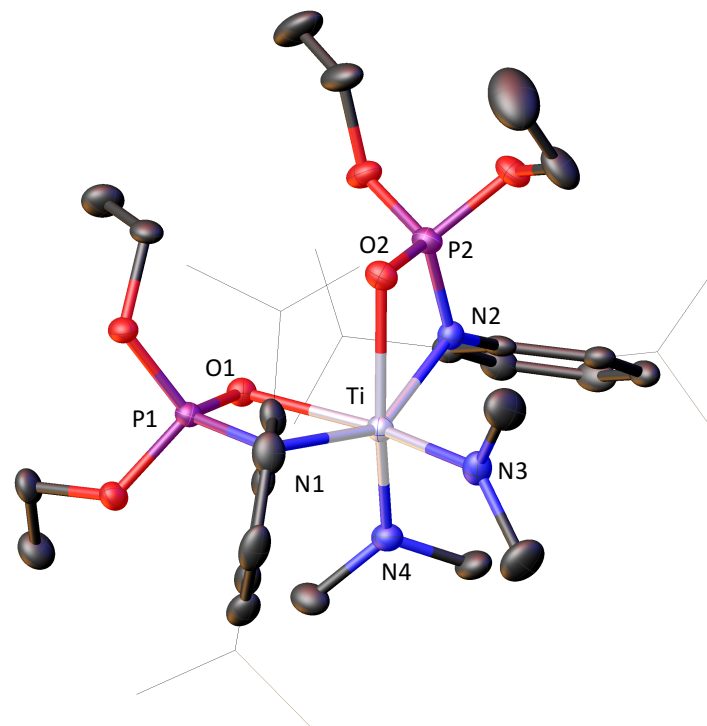


Bond Length (Å)		Bond Angle (°)	
Ti-O1	2.226(2)	O1-Ti-N1	67.80(8)
Ti-N1	2.099(3)	O2-Ti-N2	67.61(9)
Ti-O2	2.208(2)	O2-Ti-N4	161.74(10)
Ti-N2	2.120(3)	N1-Ti-N2	151.55(9)
Ti-N3	1.908(3)	O1-Ti-N3	161.33(10)
Ti-N4	1.911(3)	N3-Ti-N4	95.28(11)

Figure 31 ORTEP and selected bond lengths and angles for diphosphoramidate complexes 23 (left) and 24 (right). All ellipsoids shown at 50% probability and all hydrogen atoms removed for clarity



Bond Length (Å)		Bond Angle (°)	
Ti-O1	2.208(2)	O1-Ti-N1	67.61(9)
Ti-N1	2.120(3)	O2-Ti-N2	67.61(9)
Ti-O2	2.208(2)	O2-Ti-N4	161.74(10)
Ti-N2	2.208(2)	N1-Ti-N2	149.956(5)
Ti-N3	1.911(3)	O1-Ti-N3	94.28(11)
Ti-N4	1.911(3)	N3-Ti-N4	98.548(5)



Bond Length (Å)		Bond Angle (°)	
Ti-O1	2.2533(16)	O1-Ti-N1	66.19(6)
Ti-N1	2.1577(19)	O2-Ti-N2	68.26(7)
Ti-O2	2.1929(15)	O2-Ti-N4	161.98(8)
Ti-N2	2.1038(19)	N1-Ti-N2	147.86(7)
Ti-N3	1.898(2)	O1-Ti-N3	160.39(8)
Ti-N4	1.915(2)	N3-Ti-N4	95.74(9)

Figure 32 ORTEP and selected bond lengths and angles for diphosphoramidate complexes 19 (left) and 22 (right). All ellipsoids shown at 50% probability and all hydrogen atoms removed for clarity. Isopropyl groups shown as wire frames for clarity

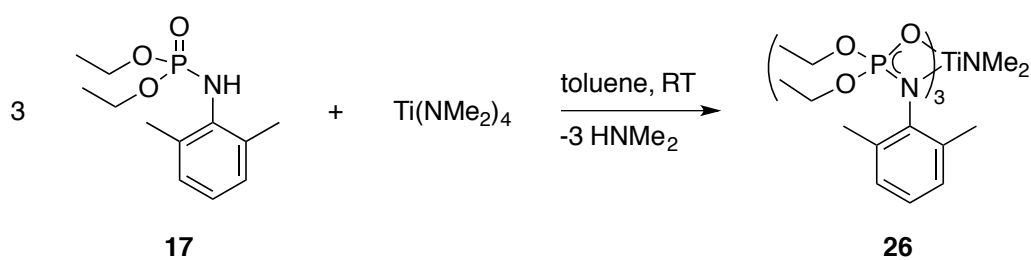
No significant change in the bite angle of the ligand was observed when varying the *ortho*-substitution on the phosphoramidate aryl group, with these O-Ti-N angles being consistently between 66.19(6)° and 67.84(6)°. In comparison to the monophosphoramidate **18** bearing 2,6-dimethyl groups, compound **19** has a slightly shorter Ti-O1 bond (2.208(2) Å vs. 2.223(6) Å) and a slightly longer Ti-N1 bond (2.120(3) Å vs. 2.107(7) Å). This is perhaps owing to the increased steric congestion about the metal centre when going from a 5-coordinate monophosphoramidate to a 6-coordinate diphosphoramidate species. As steric bulk increases in the *ortho*-positions, the N1-Ti-N2 bond angle of the chelate deviates further from the idealized linearity of 180°. For example, the N1-Ti-N2 angle of complex **23** and **24** is 153.87(7)° and 151.55(9)°, respectively, whereas complex **22** bearing bulky *dipp* groups has a more obtuse angle of 147.86(7)° to alleviate the steric strain.

2.6.4 Tri(phosphoramidate) Titanium Complexes

Inspired by the work by Payne *et al.*,³³⁴ it was of interest to see if titanium complexes bearing more than two *N,O*-chelates could be accessed. Complexes bearing three and four *N,O*-chelates have been reported.^{329, 333-334} In these cases, less sterically bulky ligands, amidates and pyridonates, were used. It was also of interest to see if the bulky phosphoramidate ligand motif would be amenable to the synthesis of tri- and tetraphosphoramidate complexes of titanium.

Proligand **17** (3 eq.) was added to a 20 mL scintillation vial and dissolved in toluene. A solution of Ti(NMe₂)₄ (1 eq.) was added dropwise to the proligand solution causing the mixture to become dark red in colour. The reaction was let stir overnight at room temperature before all volatiles were removed *in vacuo* to give a red solid in 96% yield (Scheme 18). Recrystallization of the mixture could easily be conducted using a minimum amount of hot toluene to dissolve the

crude solid and placing the vial in a $-30\text{ }^{\circ}\text{C}$ freezer overnight. The complex crystallized as red plates and could be washed with cold hexanes, 67% yield. Improved yields from crystallization could be achieved by reducing the volume of the mother liquor and cooling to $-30\text{ }^{\circ}\text{C}$.



Scheme 18 Synthesis of triphosphoramidate complex **26** *via* protonolysis

Firstly, the solid was analyzed by X-ray crystallography. Figure 33 shows the ORTEP of complex **26** obtained from crystals that were grown from cooling a hot solution in toluene. Relevant bond lengths and angles are displayed in Table 4.

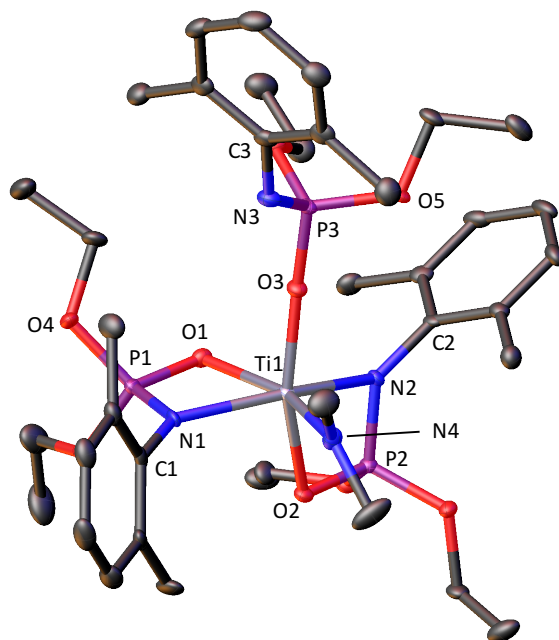


Figure 33 ORTEP of triphosphoramidate complex **26**. Ellipsoids shown at 50% probability. Hydrogen atoms omitted for clarity

As in the case with the diphosphoramidates, **26** is a six-coordinate distorted octahedral compound. All three phosphoramidates are uniquely bound to the metal centre. Two *N,O*-chelates are bound κ^2 , with both nitrogen atoms (N1 and N2) positioned *trans* to one another, while the other adopts a κ^1 -binding mode through oxygen. The first κ^2 -chelate (N1-P1-O1) has a similar bonding environment as the complexes discussed above previously. The dimethylamido ligand (N4Me₂) lies pseudo-*trans* to oxygen (O1), having a bond angle (O1-Ti-N4) of 162.50(8)°. Both κ^2 -*N,O* chelates possess similar O-Ti-N bite angles of 68.66(8)° and 69.20(8)°. As with the previous compounds, the κ^2 -*N,O*-chelate is unsymmetrically bound, with a shorter Ti-N1 bond length (2.068(2) Å) than Ti-O1 bond length (2.2022(18) Å). However, in the absence of a second dimethylamido ligand, O2 lies *trans* to κ^1 -O3. This results in a shorter Ti-O2

bond length (2.0492(19) Å) relative to Ti-N2, which lies *trans* to N1, which has a bond length of 2.152(2) Å.

Table 4 Select bond lengths (Å) and angles (°) for triphosphoramidate complex 26

Bond length (Å)		Bond angle (°)	
Ti-O1	2.2022(18)	O1-Ti-N1	68.66(8)
Ti-N1	2.068(2)	O1-P1-N1	101.98(10)
Ti-O2	2.0492(19)	O2-Ti-N2	69.20(8)
Ti-N2	2.152(2)	O2-P2-N2	100.59(11)
Ti-O3	1.8909(19)	N1-Ti-N2	152.56(9)
Ti-N4	1.889(2)	O1-Ti-N4	162.50(8)
O3-P3	1.5302(19)	O1-P1-O4	111.44(10)
P3-N3	1.528(2)	O3-Ti-N4	96.38(9)
P3-O5	1.5890(19)	O2-Ti-O3	160.49(8)
N1-C1	1.435(3)	O1-Ti-O2	87.96(7)
N2-C2	1.433(3)	O1-Ti-O3	90.49(8)
N3-C3	1.400(4)	P3-O3-Ti	174.67(13)

The third phosphoramidate is bound κ^1 in the solid-state, presumably to relieve steric congestion about the metal centre with three bulky *N,O* donor ligands. Opening of the ligand with the Ti-O bond retained, rather than the Ti-N bond, is expected, as this observation has been noted previously in tri(amidate)mono(amido) titanium complexes and is attributed to steric congestion and strong titanium-oxygen bond strengths.³³⁴ The Ti-O3 bond (1.8909(19) Å) is the closest contact between the metal and the phosphoramidate that is observed in any of the complexes that have been discussed. The P3-O3-Ti bond angle is almost linear (174.67(13) °), further corroborating a strong bonding interaction with significant π -character. The Ti-N4 bond length (1.889(2) Å) matches that in triamidate complexes of titanium, and is in good agreement with M-N multiple bond character.³³⁸ The Ti-amido bond length observed (1.889(2) Å) is in

good agreement with the di(κ^2 -*N,O*)phosphoramidate titanium species discussed above, as well as the di(amidate)bis(dimethylamido) titanium species previously reported.³³⁸

Compound **26** shares many similar structural features to an analogous triamidate titanium system (A in Figure 20). The shortening of the Ti-O bond length in the κ^1 -*O* ligand is also observed with the amidate Ti- κ^1 -*O* bond length of 1.857(1). Additionally, the linearity along the Ti-O-P trajectory is also consistent with the triamidate, which at 151.3(1)° is slightly more bent. Furthermore, complex **26** was further characterized by HRMS; a *m/z* ratio of 860.32945 was found, relative to the calculated value 860.32874 (C₃₈H₆₃N₄O₉P₃Ti). Elemental analysis also showed expected values of 52.74 C; 7.69 H, 6.60 N, which were in good agreement with calculated values (53.03 C; 7.38 H, 6.51 N). The solid was analyzed in solution by ¹H and ³¹P NMR spectroscopy (Figure 34). At room temperature, a separate set of resonances can be distinguished for the aryl (CH₃)₂ groups of the κ^1 -*N,O* chelate at 2.6 ppm and the two κ^2 ligands (2.5 ppm). Complex **26** also displays broad resonances attributed to the methyl groups of the ethoxy moieties (0.8-1.3 ppm). The dimethylamido ligand gives rise to a sharp singlet as expected. The ³¹P NMR spectrum displays three distinct resonances in a 1:1:1 ratio; a sharp singlet at 8.0 ppm is attributed to the ligand bound in a κ^1 -*O* fashion and two broad singlets (1.1 and -26.2 ppm) assigned to the two inequivalent κ^2 -*N,O* chelates. The broadness of these resonances suggests fluxionality of these groups at room temperature.

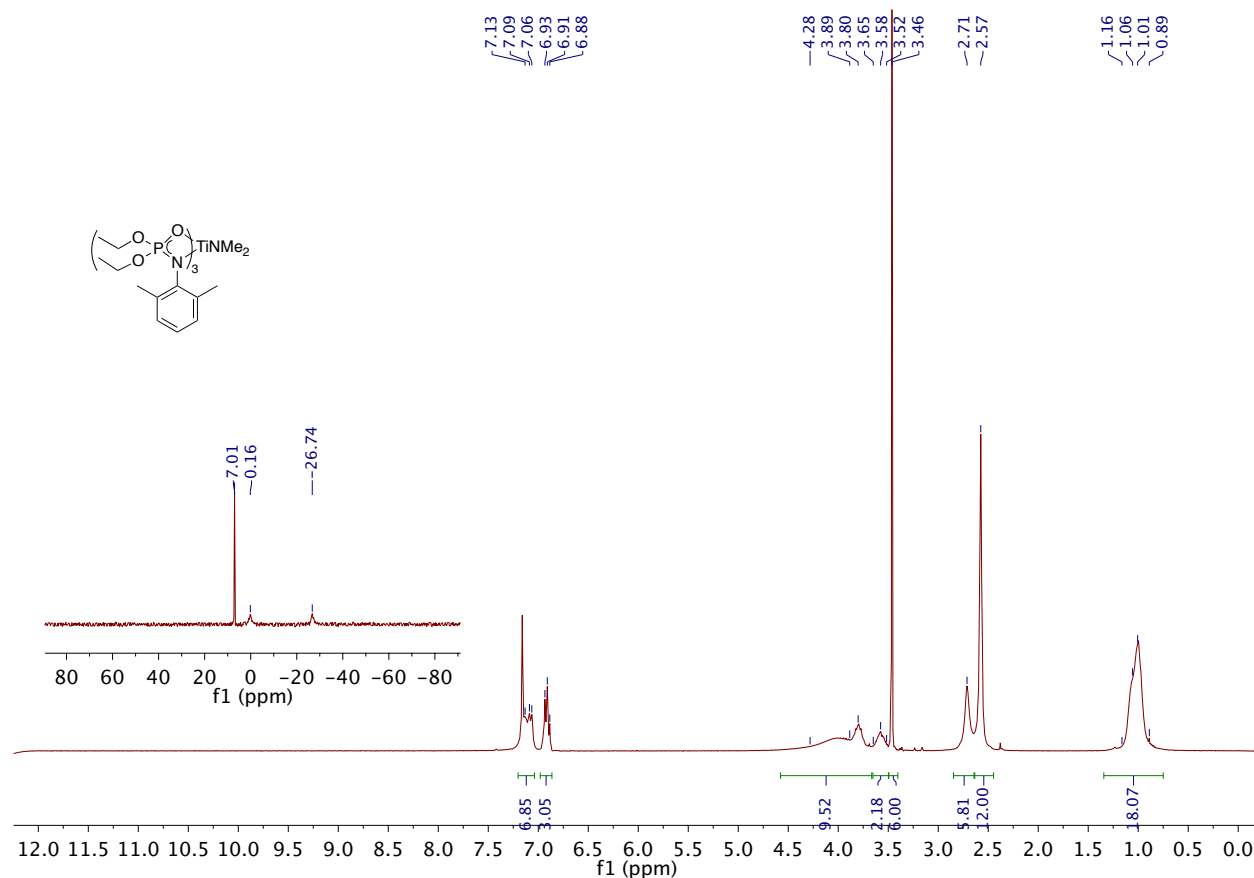


Figure 34 ¹H and ³¹P (inset) spectrum of triphosphoramidate complex 26, (C₆D₆, 300 MHz and 121 MHz, 298 K)

The fluxionality of the complex was investigated by variable temperature (VT) ¹H and ³¹P NMR spectroscopy in toluene-d₈ (Figure 35 and Figure 36). At low temperatures (-15 °C) the resonances of the ethoxy moieties resolve into doublets of quartets (4.7-4.1 ppm), suggesting that the methylene protons are diastereotopic at and below this temperature. The methyl groups also resolve into distinct resonances and display clear triplets between 1.3-0.8 ppm. The aniline CH₃ groups are resolved into singlets ranging from 2.83-2.53 ppm. The broad ³¹P NMR signals become sharp as the equilibrium between κ²- and κ¹-ligands are slower than the NMR timescale.

Integration of these ^{31}P signals is consistent with a 1:1:1 ratio, as expected for the three *N,O*-chelates.

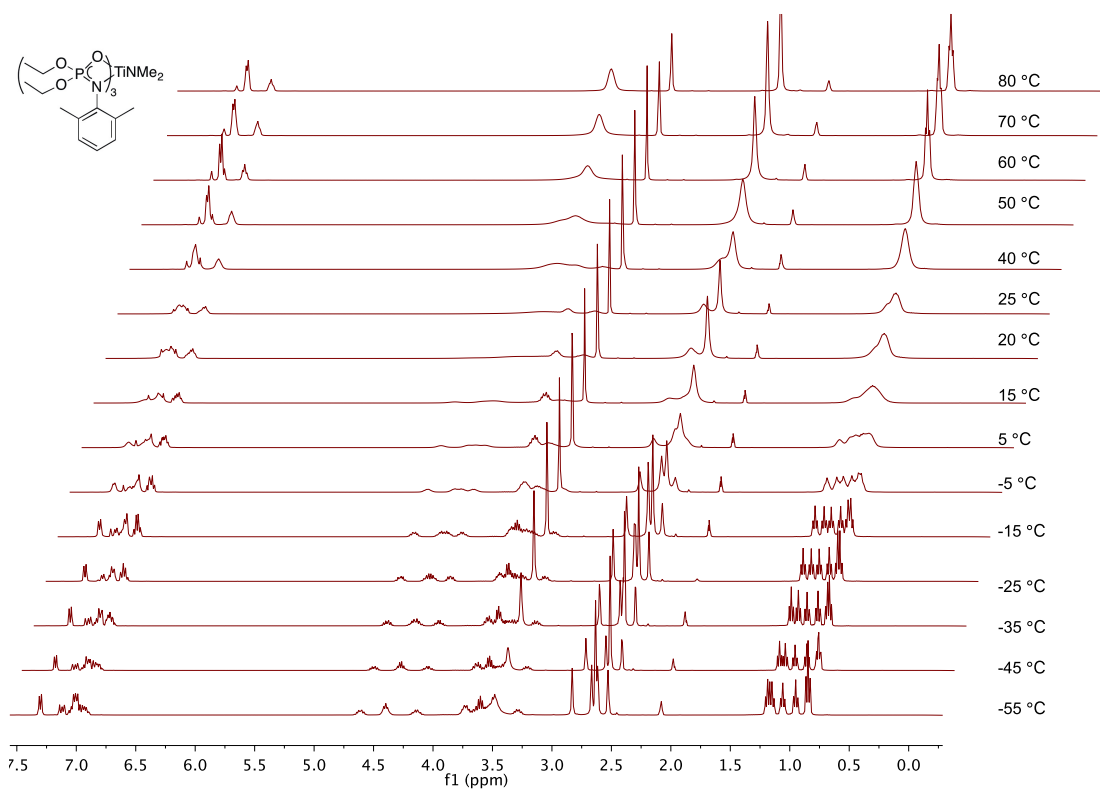


Figure 35 Variable temperature ^1H NMR spectra of complex 26 (tol- d_8 , 400 MHz)

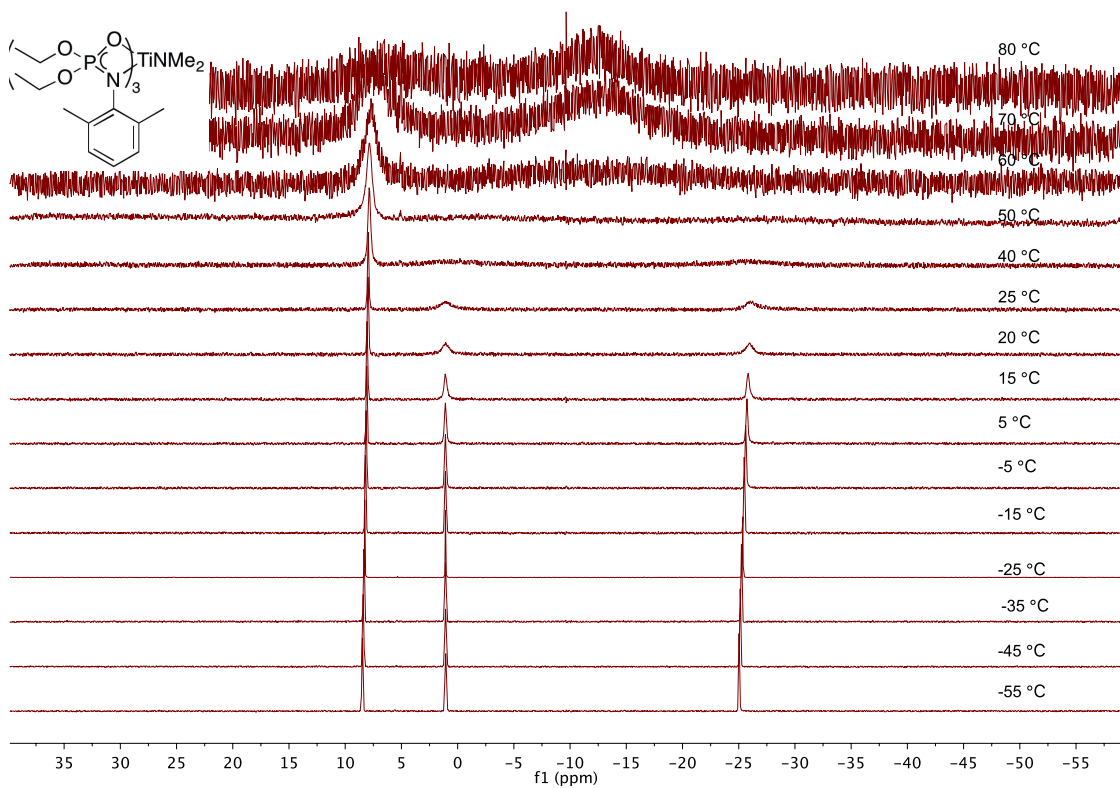


Figure 36 Variable temperature ^{31}P NMR spectra of complex **26** (tol- d_8 , 400 MHz)

It was of interest to see if these separate binding modes would be visible by ATR-IR spectroscopy. No obvious differences exist between the di- and triphosphoramidate complexes, **19** and **26**, by IR spectroscopy, as shown below in Figure 37.

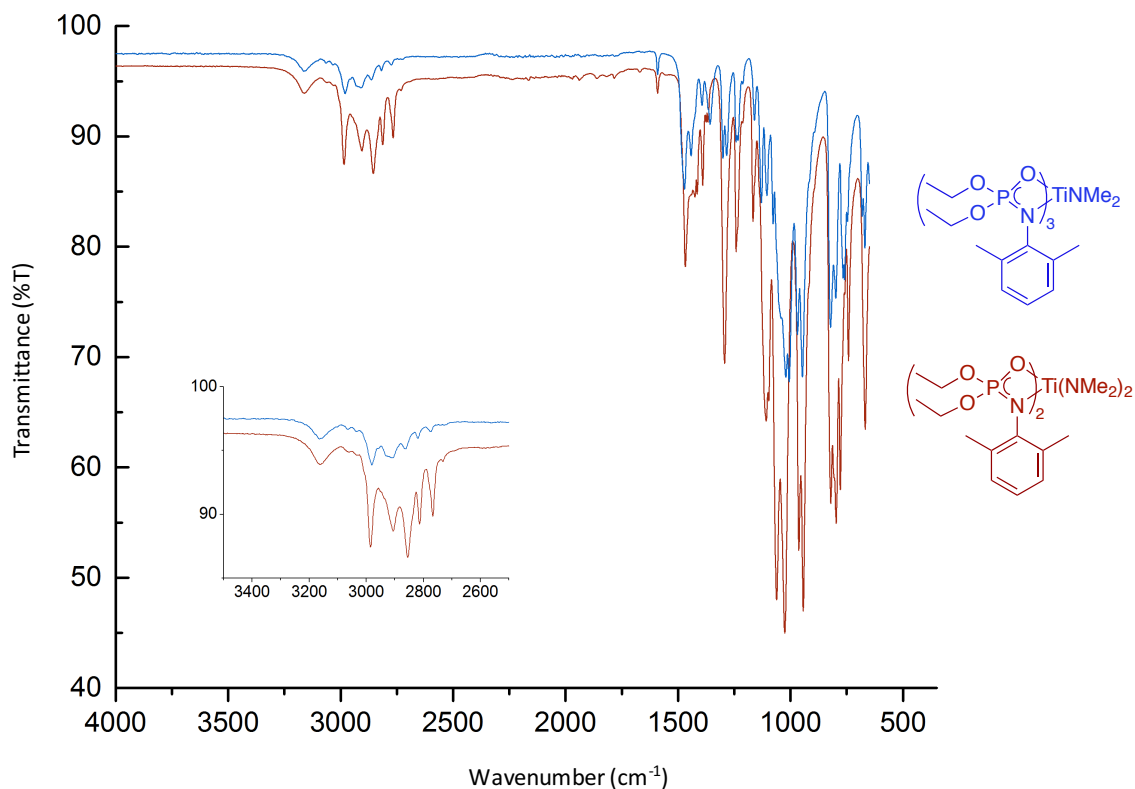


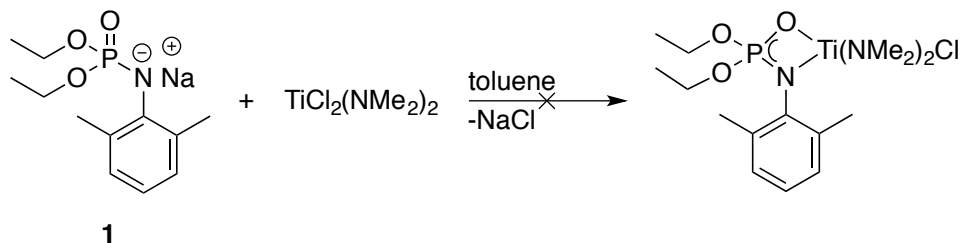
Figure 37 ATR-IR spectra of di- and triphosphoramidate complexes 19 and 26

It was of interest to see if higher substituted phosphoramidate complexes of titanium could be obtained, namely tetraphosphoramidates. In this vein, four equivalents of proligand **27**, bearing unsubstituted phenyl substituents, were combined with 1 eq. of $\text{Ti}(\text{NMe}_2)_4$. Only the respective trisubstituted species was formed, with mass spectrometry revealing a parent mass of 732 m/z , which corresponds to a tri(*N,O*)-ligated complex with no dimethylamido ligand (presumably lost in the ionization process). No higher mass fragments were detected. These results indicated that the phosphoramidate ligand motif was too bulky to facilitate the formation of complexes bearing four *N,O*-chelates around the small titanium metal centre.

2.6.5 Monophosphoramidatemono(chloro) Titanium Complexes

The incorporation of chloro ligands into early transition metal complexes has been shown to increase reactivity in HAA reactions.²⁷⁴ In 2013, the Schafer Group exploited this observation and was able to garner room temperature HAA of terminal alkenes and secondary amines using tantalum complex **2**.¹⁸³ It was shown that the anionic chloro ligand was imperative for creating an electrophilic metal centre, thereby achieving room temperature C-C bond formation. The respective dimethylamido analogues required elevated temperature (90 °C) to reach moderate yields (19%). Therefore, it was of interest to us to see if a chloro ligand could be installed easily onto titanium complexes bearing a phosphoramidate chelate.

Attempts to synthesize mono(phosphoramidate)di(amido)mono(chloro) complexes of titanium began by performing salt-metathesis using the previously disclosed ligand salt, **1**. The mixed titanium dichloro starting material was chosen to access mono(chloro) titanium species in agreement with previously disclosed literature.^{238, 353} Contrary to examples previously discussed (eg. salt metathesis reactions involving sodium salts of phosphoramidates to generate **2** and **19**), these reactions were carried out in toluene, as $\text{TiCl}_2(\text{NMe}_2)_2$ is sparingly soluble in hexanes (Scheme 19).



Scheme 19 Attempted salt metathesis to generate a mono(chloro) titanium complex

Specifically, the sodium salt **1** was suspended in toluene and cooled to $-30\text{ }^{\circ}\text{C}$. $\text{TiCl}_2(\text{NMe}_2)_2$ (1 eq.) was dissolved in toluene to generate a red solution which was cooled to $-30\text{ }^{\circ}\text{C}$. The proligand suspension was added dropwise to the stirring metal precursor to ensure an excess of metal throughout the addition. The mixture became orange in colour and was let warm to room temperature and stir overnight. The suspension was filtered through Celite® and the filtrate was reduced *in vacuo*.

A variety of inequivalent phosphorus signals (8 total) were observed *via* $^{31}\text{P}\{^1\text{H}\}$ NMR spectroscopy indicating that exclusive formation of the targeted compound was not possible under these conditions. The mono(chloro) compound targeted possesses a molecular weight of 427 g/mol. LRMS-EI of the crude material gave a mass-to-charge ratio corresponding to the desired complex, albeit in minor amounts, and that which corresponds to the desired compound minus a dimethylamido ligand (minus 44 *m/z*). However, a variety of higher mass-to-charge ratios were present in the spectrum that correspond to diphosphoramidate species and/or fragments of these complexes (*eg.* 648 *m/z*).

The solid was recrystallized from hot toluene to give a minor amount of crystalline product that could be analyzed by X-ray crystallography (Figure 38). Interestingly, this unexpected complex is the result of ligand based reactivity, with a dimethylamido fragment replacing an ethoxy moiety in the phosphoramidate backbone. Full characterization of this complex, **28**, was not possible due to the small quantity of material isolated.

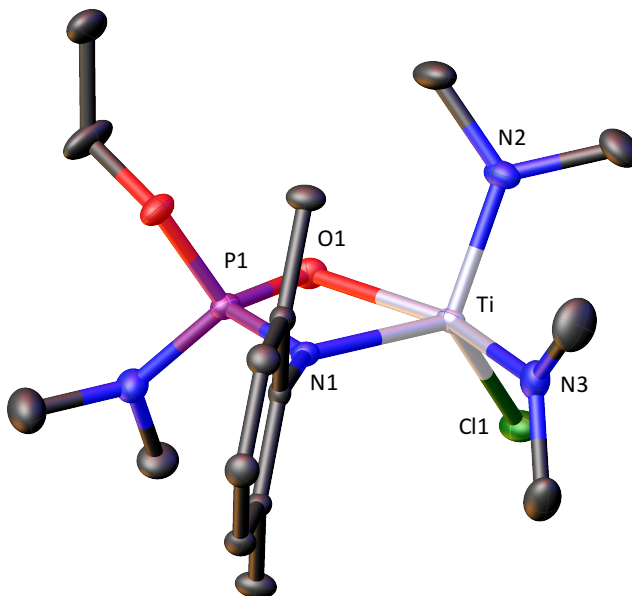


Figure 38 ORTEP of complex 28. Ellipsoids shown at 50% probability. Hydrogen atoms removed for clarity

These types of substituted phosphoramidate side products have been noted previously in our group by GC-MS, but never isolated in the solid-state. Increasing the steric bulk by using **29**, having *dipp* groups, did not circumvent the ligand redistribution and no desired product could be isolated. One potential way to mitigate the observed ligand reactivity would to be use ligands of phosphinic derivatives (Figure 39). These *N,O*-chelates can be synthesized using two common literature procedures. Proligands of this type could be prepared from either the phosphorus (III) or (V) starting materials and can be isolated in good yields as white solids. All characterization was in good agreement with reported values.³⁵⁴⁻³⁵⁶

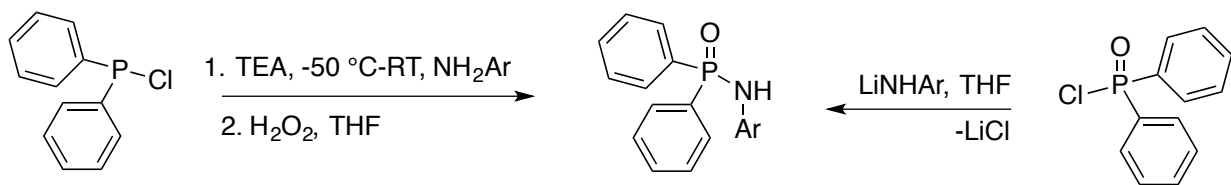


Figure 39 Synthesis of diphenyl phosphinic ligands from P(III) and P(V) starting materials

Proligand **30**, bearing 2,6-dimethylphenyl substitution, was chosen to have a direct comparison to previously reported work (Figure 40). The sodium-salt of proligand **30** was suspended in toluene and cooled to -30°C . Meanwhile, $\text{Ti}(\text{NMe}_2)_2\text{Cl}_2$ was dissolved in toluene, forming a red solution, and cooled to -30°C . The ligand solution was added dropwise to the stirring solution of the titanium starting material and the mixture was left to stir overnight, during which time the mixture became darker in colour. After the allotted time, the mixture was filtered through Celite® and the filtrate was reduced *in vacuo*.

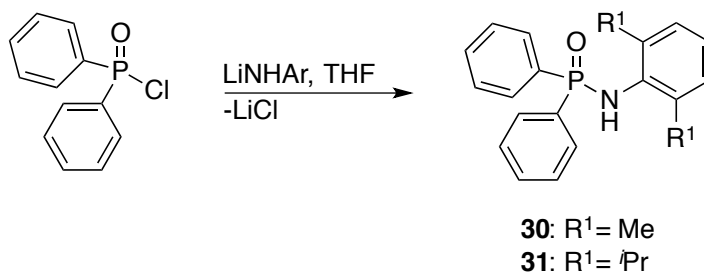


Figure 40 Synthesis of diphenyl-substituted proligands **30** and **31** from diphenylphosphinic chloride

Analysis of the crude red solid by ^1H NMR spectroscopy indicated a mixture of mono- and di(*N,O*)-chelated titanium species. Unfortunately, these complexes could not be successfully separated *via* recrystallization. Furthermore, a black solid isolated from the recrystallization of the mother liquor, possessed aryl resonances in the ^1H NMR spectrum, but no signal in the ^{31}P

NMR spectrum, indicating a product of ligand decomposition. No crystals suitable for X-ray crystallography could be obtained despite a variety of attempts using various solvents and solvent mixtures.

The analogous experiment was conducted using the sodium salt of the bulkier *dipp* derivative, **31**, to impart steric protection. After filtering and removing all volatiles, the crude solid was analyzed by LRMS-EI. The expected mass-to-charge ratio (547.20 m/z) was not observed in the mass spectrum, although this phenomenon is commonly observed. A species with the same mass of a mono(*N,O*)mono(chloro) fragment was present (460 m/z). However, mass-to-charge ratios corresponding to a variety of unwanted side products were also observed in the spectrum. Importantly, a mono(*N,O*)tri(amido) titanium species could be observed (557 m/z). This indicates ligand redistribution, as the starting material possesses only two dimethylamido ligands. Furthermore, the fragments of this triamido complex that correspond to the loss of this species' dimethylamido ligands were present (512, 468, and 424 m/z).

Interestingly, while no di(*N,O*)mono(dimethylamido)mono(chloro) species were observed by mass spectrometry, m/z ratios corresponding to a di(*N,O*)bis(dimethylamido) titanium species (889 m/z), and the di(*N,O*)mono(dimethylamido) and di(*N,O*) fragments (844 m/z) were present in the crude mixture. This solid could not be further purified, and no crystals suitable for X-ray crystallography could be obtained. However, this data supports the idea that these *N,O*-chelates are not sterically bulky enough to be used in the formation of mono(*N,O*) ligated complexes and lead to ligand redistribution to form disubstituted analogues, as noted before while investigating the synthesis of mono(phosphoramidate)tris(dimethylamido) complexes in Section 2.6.3.

2.7 Titanium Phosphoramidates in C-C and C-N Bond Forming Reactions

Phosphoramidate titanium species were screened for catalytic activity in the C-C and C-N bond forming HAA and HA reactions, respectively. HAA reactivity is typically monitored using standard screening reactions of 4-methoxy-*N*-methyl aniline and 1-octene. Yields were calculated by observing the disappearance of the *ortho*-protons of the starting material vs. the *ortho*-protons of the product (see Appendix A.3). The product mixture was also analyzed by GC-MS to verify that only one product was formed in the reaction. The yield of the reaction could also be obtained by isolating the desired product *via* column chromatography.

The HA reaction, a C-N bond formation α to an amine, was also investigated using the titanium complexes described above. Here, conversions and yields were monitored by comparing well-resolved product peaks to trimethoxybenzene, a common internal standard used in HA reactions.²⁴⁶ In this section, the effects of these sterically bulky ligands on these two titanium-mitigated reactions are explored.

2.7.1 Hydroaminoalkylation with Monophosphoramidate Titanium Species

The efficacy of monophosphoramidate titanium complexes in HAA was investigated. Despite the propensity of these complexes to undergo ligand redistribution in solution, the sterically accessible metal centre and the presence of three labile dimethylamido ligands made these complexes prime candidates for catalytic screening in HAA. Regardless, the screening of these monophosphoramidate complexes, **18**, **21**, and **32-34**, was attempted with these precatalysts prepared *in situ* (Figure 41). Specifically, a toluene- d_8 solution of proligand was added to a 20 mL scintillation vial containing a stirring toluene- d_8 solution of $Ti(NMe_2)_4$. This solution was then added *via* pipette to a J. Young NMR tube containing a toluene- d_8 solution of

amine and alkene substrates. The NMR tube was sealed and placed in a preheated oil bath for a predetermined period. After this time, the vessel was exposed to air to quench any reactivity. Table 5 displays the results of these species in our standard screening reaction between 4-methoxy-*N*-methylaniline and 1-octene. All reaction products were further verified by GC-MS to ensure only one product was formed.

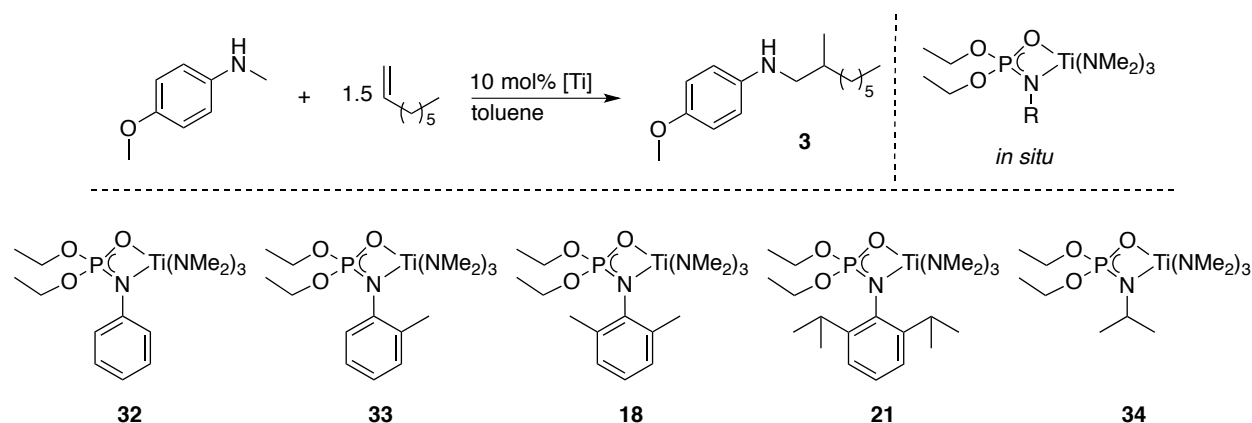
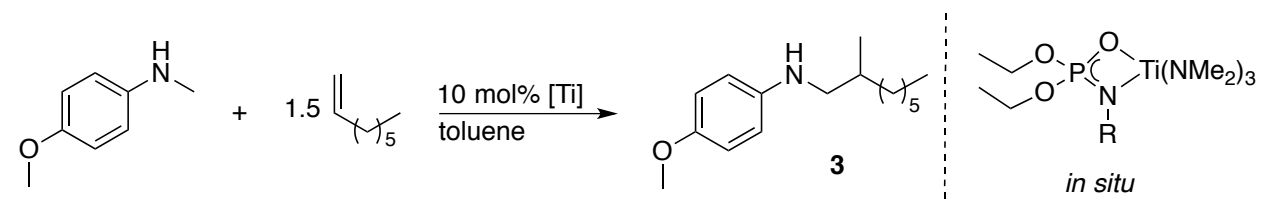


Figure 41 Hydroaminoalkylation screening using monophosphoramidate titanium complexes

Modest conversions to form product **3** were observed, with no aryl-substituted complex generating the desired compound in greater than 50% conversion at 130 °C. Longer reaction times did lead to increased conversions (Entry 2 vs. Entry 3, Entry 4 vs. Entry 5, and Entry 7 vs. Entry 8), although conversions were limited to 45% even after 164 h at this temperature. More forcing temperatures were required to reach higher conversions, with complex **18** reaching 90% after 96 h at 165 °C (Entry 6). Interestingly, *N*-aryl substituted complex **34** was the most competent of this series, and converted >95% of the reactants to product **3** at 164 h at 130 °C (Entry 9). Quantitative conversion could also be achieved in 96 h using 165 °C as the reaction temperature. However, this does not compare favourably with the state-of-the-art titanium

catalysts, which can perform this transformation to generate similar products at lower temperatures (105 °C) after just 24 h, often using 5 mol% catalyst loadings.²⁶⁷

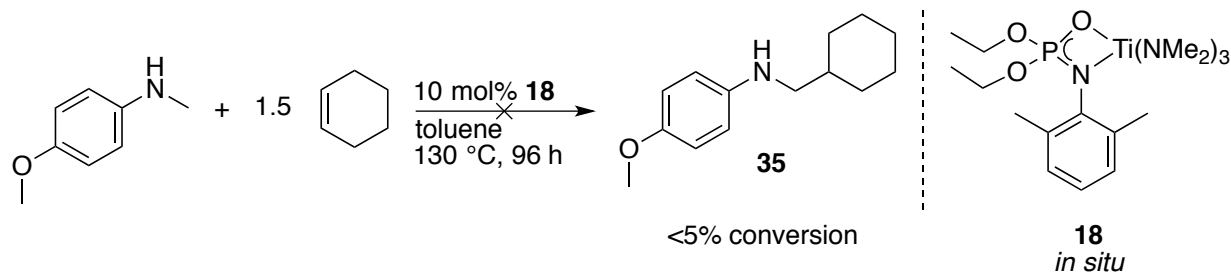
Table 5 Hydroaminoalkylation reactivity of monophosphoramidate titanium complexes generated *in situ*



Entry ^a	Complex	Time (h)	Temperature (°C)	Conversion (%) ^b
1	32	164	130	45
2	33	24	130	20
3	33	164	130	36
4	18	24	130	14
5	18	164	130	32
6 ^c	18	96	165	90
7	21	24	130	31
8	21	164	130	39
9	34	164	130	>95
10 ^c	34	96	165	>95

^aReactions conducted with precatalysts generated *in situ* using the following conditions: [amine]:[alkene]:[cat] 1:1.5:0.1. Reactions were conducted at 130 (°C), in sealed J. Young NMR tubes using tol-d₈ (1 mL). ^bDetermined by ¹H NMR spectroscopy. Only the branched diastereomer was observed by ¹H NMR spectroscopy and GC-MS. ^cConducted at 165 °C.

Complex **18** was screened for the HAA of cyclohexene, a common internal alkene substrate (Scheme 20). Unsurprisingly, <5% conversion was observed, even after 96 h at 165 °C, as HAA is rarely achievable with internal, unactivated alkene substrates.²³⁸



Scheme 20 Attempted hydroaminoalkylation of *N*-methylcyclohexylamine and 1-octene using complex **18**

These results indicate that monophosphoramidate complexes of titanium are modest candidates for HAA reactivity under these conditions. Presumably, the sluggish reactivity is due to the presence of diphosphoramidate species existing due to ligand redistribution. Interestingly, quantitative conversion was observed when *N*-alkyl substituted complex **34** was used, indicating that the electronic factors imparted by this substitution pattern increases the reactivity of this complex. Steric parameters should also be considered, as the reactivity of isopropyl-substituted **34** is superior to phenyl-substituted complex **32** of similar size (Entry 9 vs. Entry 1).

2.7.2 Hydroaminoalkylation with Diphosphoramidate Titanium Species

Diphosphoramidate species were screened for HAA reactivity using the standard screening reaction between 4-methoxy-*N*-methyl aniline and 1-octene (Figure 42), as described for monophosphoramidate complexes in Section 2.7.1. The facile synthesis and isolation of these complexes allowed for the screening to be conducted using isolated precatalysts.

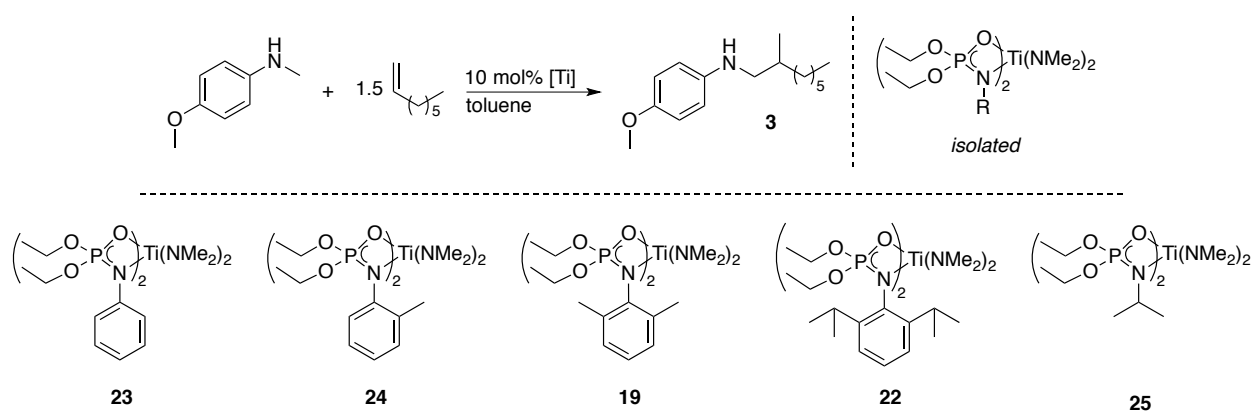
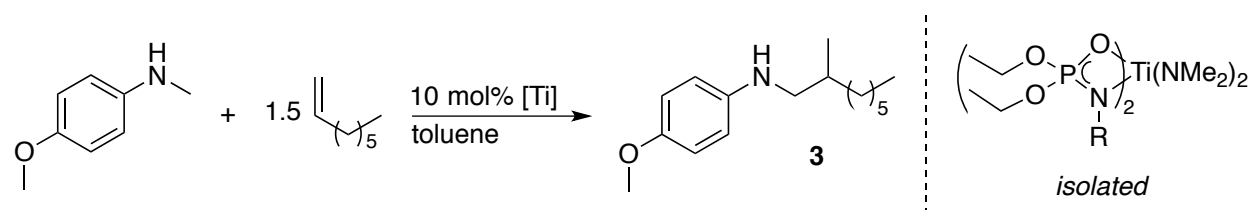


Figure 42 Intermolecular hydroaminoalkylation using 4-methoxy-*N*-methyl aniline and 1-octene. Reactions were conducted using isolated diphosphoramidate complexes **19** and **22-25**

Low conversions were observed at 130 °C with aryl-substituted complex **22** reaching a mere 13% conversion after reacting for 164 h, while *N*-alkyl-substituted complex **25** reached 18% at 130 °C after 96 h (Table 6, Entry 6). As was shown with the monophosphoramidate species, the conversion was promoted by increasing reaction temperatures. Complex **19** was shown to increase from 9% at 130 °C (Entry 3) to 41% at 165 °C (Entry 4), although all reactivity was limited to less than 50% conversion.

It is important to note that the reaction using monophosphoramidate complex **18** generated *in situ* (Table 5, Entry 6) contained unavoidable amounts of **19** (the di-substituted species of the same substitution pattern about the aryl ring). Complex **18** reached 90% conversion at 165 °C after 96 h, whereas isolated complex **19** reached only 9% under analogous reaction conditions (Table 6, Entry 3). These results indicate that monophosphoramidate species are more competent than their diphosphoramidate counterparts, but unfortunately are known to undergo deleterious ligand redistribution in solution, preventing the exploitation of their full catalytic potential.

Table 6 Hydroaminoalkylation activity of isolated diphosphoramidate titanium complexes



Entry ^a	Complex	Time (h)	Temperature (°C)	Conversion (%) ^b
1	23	96	130	<5
2	24	164	130	<5
3	19	96	130	9
4 ^c	19	96	165	41
5	22	164	130	13
6	25	96	130	18
7 ^d	26	164	165	<5

^aReaction conditions: [amine]:[alkene]:[cat] = 1:1.5:0.1. Reactions were conducted at 130 (°C), in sealed J. Young NMR tubes using tol-d₈ (1 mL). ^bDetermined by ¹H NMR spectroscopy. Only the branched diastereomer was observed by ¹H NMR spectroscopy and GC-MS. ^cReaction conducted at 165 °C. ^dReaction conducted with triphosphoramidate complex **26**.

As expected, the tri(phosphoramidate)mono(dimethylamido) titanium complex **26** shows negligible activity for the HAA between 4-methoxy-*N*-methylaniline and 1-octene owing to the presence of large amounts of steric bulk around the reactive metal centre and the lack of requisite dimethylamido ligands to form the active tantalaziridine.^{181, 234, 239, 334}

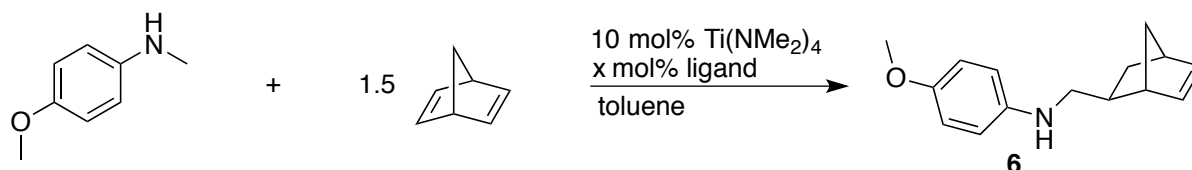
2.7.3 Titanium Phosphoramidates for Mono-alkylation of Norbornadiene

HAA is very challenging when using internal alkenes. As discussed previously, Chong *et al.* have disclosed one such transformation using a tantalum pyridonate complex.²³⁸ However, activity has been observed when using activated internal alkenes, such as cyclooctene (COE) and norbornene (NBE).^{234, 238} These products are particularly interesting owing to the fact that they possess high levels of ring strain and have the potential to be used in ROMP (*vide infra*). Indeed,

the HAA of commercially available substrates to form monomers for ROMP in one-step is a desirable goal as alternative avenues into these starting materials are laborious (see Chapter 3).

An inherent challenge associated with using strained dienes as substrates is the potential selectivity issue that could lead to the generation of dialkylated products (Scheme 12). The sluggish activity of titanium phosphoramidates in intermolecular HAA led us to investigate these complexes as potential catalysts for these reactive internal alkene substrates, where selectivity is desired. Ultimately, monoalkylated products were targeted such that the remaining internal alkene could be further exploited. We began by using NBD and 4-methoxy-*N*-methyl-aniline (Table 7).

Table 7 Hydroaminoalkylation of strained diene to generate monoalkylated product 6



Entry ^a	Ligand (mol%)	Complex	Temp (°C)	Time (h)	Yield (%) ^b
1	0	$\text{Ti}(\text{NMe}_2)_4$	145	240	25
2	10	18	110	240	10
3	10	18	145	240	24
4	20	19	145	240	12

^aReactions performed in sealed J. Young NMR tubes using $\text{Ti}(\text{NMe}_2)_4$ (0.13 mmol), 4-methoxy-*N*-methylaniline (1.3 mmol), norbornadiene (2.0 mmol), and toluene- d_8 (1 mL). Titanium complexes **18** and **19** were generated *in situ*. ^bIsolated yields after column chromatography (95:5 hexanes:ethyl acetate).

Interestingly, the HAA of NBD provides only monoalkylated product **6** regardless of the titanium species employed. Dialkylated products **9** and **10** were not observed. This contrasts with the reactivity of the more active tantalum chloro complex **2** discussed previously. However, no

improvement over homoleptic $\text{Ti}(\text{NMe}_2)_4$ was observed when using monophosphoramidate complex **18**. Diphosphoramidate complex **19** was markedly worse than $\text{Ti}(\text{NMe}_2)_4$ and **18**, again highlighting the inability of these bulky complexes to be competent precatalysts for HAA under these conditions.

The goal of the research presented in this section was to generate monoalkylated products using a strained diene substrate and phosphoramidate titanium complexes. Despite the ring-strain of NBD, high reaction temperatures (145 °C), and long reaction times (240 h), only modest yields of **6** were obtained. While it was pleasing that all reactions resulted in the exclusive formation of the desired monoalkylated product, the poor performance of these titanium species ultimately prevents their use for the efficient generation of amine-containing NBE monomers for ROMP. This transformation will be discussed further in Section 3.3 with tantalum complex **2** being utilized in the formation of these valuable monomers.

2.8 Hydroamination

The preliminary results obtained from the HAA screening reactions discussed above led us to investigate these complexes for the C-N bond forming reaction, HA. Indeed, many Group 4 complexes that have shown efficacy for HAA are also competent for C-N bond formation. Furthermore, most known *N,O*-chelated titanium-based HA catalysts are bis-ligated. In fact, unwanted HAA side-products are sometimes observed when cyclizing aminoalkenes,^{233, 245, 268, 317, 347, 357-358} highlighting the need for chemoselectivity between these two reactions (Figure 43). However, using HA to form C-N bonds is entropically favoured when using intramolecular substrates, and typically leads to the preferential formation of the HA products.²³² It should be noted that there are no reported examples of titanium-catalyzed intermolecular HA of alkenes.

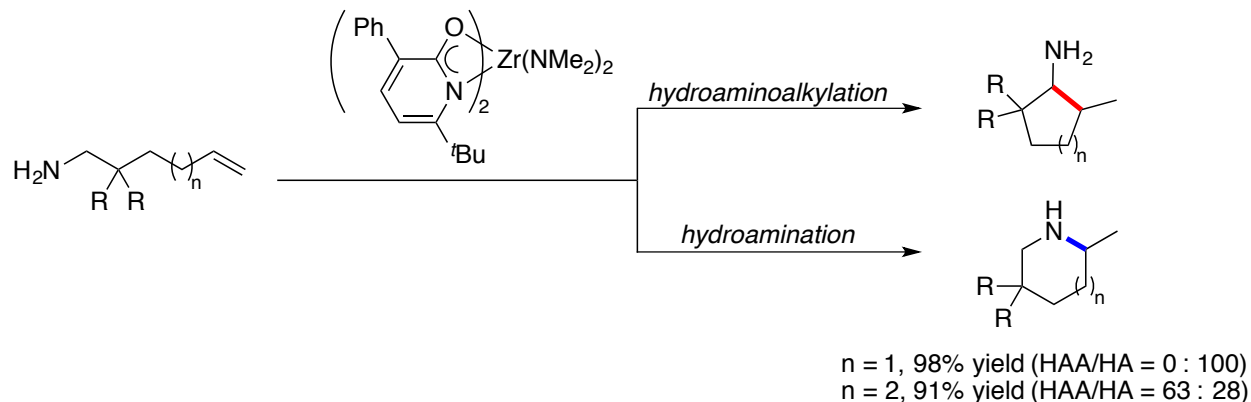


Figure 43 Zirconium pyridonate complex capable of intramolecular hydroamination and hydroaminoalkylation

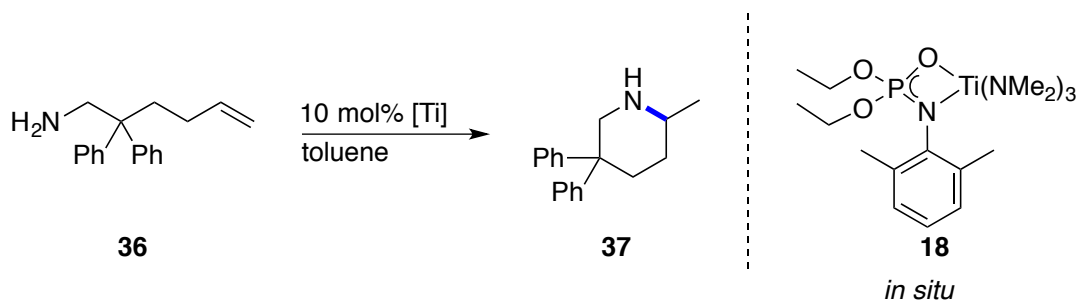
In this vein, we chose to screen the mono- and diphosphoramidate titanium complexes discussed above for HA activity. We opted to use primary aminoalkene **36** for a direct comparison to the work done by Chong *et al.*,^{232, 246} as well as to probe whether complexes **18** and/or **19** show any bias toward HAA when cyclizing this primary aminoalkene. These complexes were chosen to maintain consistent ligand substitution between catalytic screening reactions.

2.8.1 Intramolecular Hydroamination of Primary Aminoalkenes

Screening of compound **36** in HA reactivity was done using the conditions established by Chong *et al.*²⁴⁶ This primary aminoalkene was subjected to 10 mol% of monophosphoramidate titanium complex **18** or diphosphoramidate titanium complex **19**. Both species were screened using complexes generated *in situ*. Specifically, a toluene- d_8 solution of prolignand (either 1 or 2 eq.) was added to a stirring toluene- d_8 solution of $Ti(NMe_2)_4$. The precatalyst mixture was then

added to a J. Young NMR tube containing a toluene- d_8 solution of the aminoalkene substrate. The vessel was sealed and placed in a preheated oil bath for a predetermined period. After the allotted time, the mixture was exposed to air to quench the reaction. The results of these reactions are presented in Table 8.

Table 8 Hydroamination of primary aminoalkene **36 using complex **18****



Entry ^a	Complex	Time (h)	Temperature (°C)	Conversion (%) ^b
1	18	4	100	>95
2	18	4	80	>95
3	18	2	80	>95
4	18	1	65	38
5	18	4	65	82
6	18	6	65	86
7	18	24	25	54
8	18	168	25	>95
9 ^c	19	4	80	<5

^aReaction conditions: [aminoalkene]:[Ti]:[proligand]= 1:0.1:0.1. Reactions were conducted in sealed J. Young NMR tubes using tol- d_8 (1 mL). ^bConversion determined using ^1H NMR spectroscopy by monitoring the disappearance of the olefinic peaks in the starting material relative to a well-resolved product peak. Only the hydroamination product was observed by ^1H NMR spectroscopy and GC-MS. ^cDiphosphoramidate **19** was used and generated *in situ*.

Gratifyingly, complex **18** generated the 6-membered HA product, **37**, exclusively under all conditions employed. No HAA side-products were observed *via* ^1H NMR spectroscopy or GC-MS analysis. Full conversion of the aminoalkene **36** was observed after 4 h at 100 °C (Table

8, Entry 1). The reaction temperature could be reduced to 80 °C with conversion being complete after 2 h (Entry 3). The cyclization did proceed at lower reaction temperatures; however, conversions were reduced to 38% after 1 h at 65 °C (Entry 4) and 86% after 6 h at 65 °C (Entry 6). Room temperature conversion was observed, with complex **18** converting 54% of **36** to the cyclized product **37** after 24 h (Entry 7) and quantitative conversion was observed after 168 h at this temperature (Entry 8). While these results are exciting as they represent the first examples of mono(*N,O*)-chelated phosphoramidates employed for HA, it should be noted that the AP titanium complexes developed by Chong can cyclize a range of primary aminoalkene substrates under much milder conditions at 5 mol% catalyst loading.²⁴⁶

Complex **18** was screened *in situ* knowing that the formation of the disubstituted analogue was present. To ensure that it was indeed the mono-species facilitating this transformation, we screened diphosphoramidate complex **19** for this reaction (Table 8, Entry 9). No significant conversion was observed using this precatalyst (generated *in situ*), providing confidence that this species was not contributing meaningfully to conversion values. However, it is noted that the “real” catalyst loading values of monophosphoramidate complex **18** are significantly affected by the formation of this inactive bis(*N,O*)-chelated species.

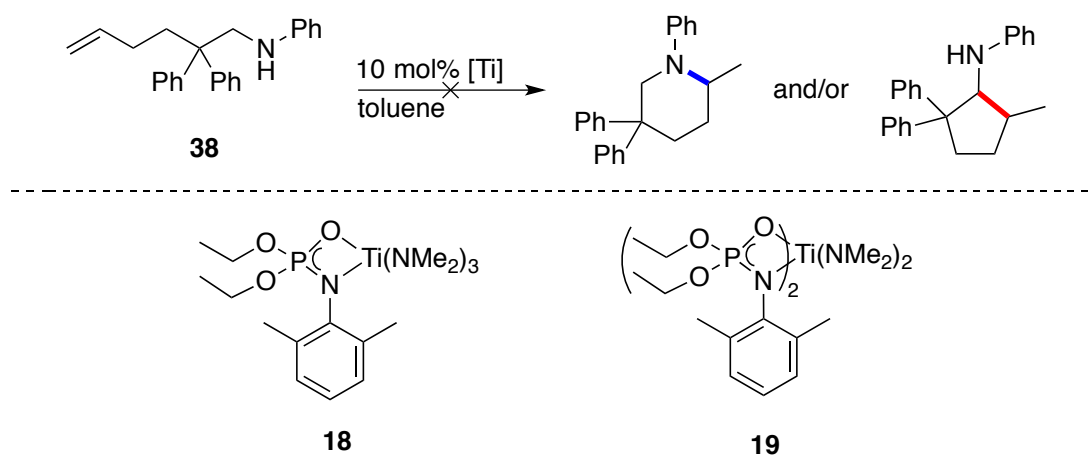
2.8.2 Hydroamination of Secondary Aminoalkenes

The intramolecularhydroamination of secondary aminoalkenes using early transition metals is known to be challenging. Group 4 complexes of zirconium are more competent for this reaction, whereas the titanium-catalyzed HA of aminoalkenes has been proposed to proceed exclusively *via* a [2+2] cycloaddition mechanism.³⁵⁹⁻³⁶⁰ Here, a titanium imido species is a requisite for the formation of a 4-membered metallacycle, which goes on to form the desired

cyclized product, thereby eliminating the possibility of secondary amine substrates for this transformation. However, it was of interest to us to perform preliminary screening reactions with complexes **18** and **25** to see if any HA or HAA activity would be observed.

Mono- and diphosphoramidate titanium complexes **18** and **19**, respectively, were formed *in situ* and screened for the HA of the secondary aminoalkenes, using *N*-(2,2-diphenylhex-5-en-1-yl)aniline, **38**. The reactions were screened at both 70 °C and 145 °C (Table 9).

Table 9 Screening of titanium complexes for intramolecular hydroamination of secondary aminoalkene, 38



Entry ^a	Complex	Ligand eq. (%)	Temperature (°C)	Time (h)	Conversion (%) ^b
1	Ti(NMe ₂) ₄	0	70	80	<5
2	Ti(NMe ₂) ₄	0	145	80	5
3	18	10	70	80	<5
4	19	10	145	80	<5
5	18	20	70	80	<5
6	19	20	145	80	<5

^aReactions conducted with titanium phosphoramidate complexes generated *in situ*. Reaction conditions: [aminoalkene]:[Ti]:[ligand] = 1:0.1:x in 1 mL of toluene. ^bConversion determined using ¹H NMR spectroscopy by monitoring the disappearance of the olefinic peaks in the starting material relative to a well-resolved product peak.

None of the homoleptic tetrakis(dimethylamido) titanium, mono- or diphosphoramidate precatalysts were effective at this transformation, even under the most forcing conditions of 145

°C for over 3 days. These results are not surprising given the paucity of reported early transition metal complexes capable of this transformation; secondary aminoalkenes cannot access the requisite metal-imido intermediate required for Group 4 catalytic HA.^{232, 267, 361}

2.9 Conclusions

Chapter 2 described an investigation into the catalytic synthesis of amines. These nitrogen-containing products are used as commodity products including fine-chemicals. Traditional syntheses rely on multi-step protocols or toxic metal catalysts. Two emerging protocols were studied, namely HAA and HA, which are C-C and C-N bond forming reactions, respectively. These protocols allow access to amine products in a one-step, atom-economic reaction. Several examples of precatalysts utilized in these transformations have been discussed, with arguably the most impactful and important being those based on easily synthesized *N,O*-chelating ligands, such as phosphoramidates. Furthermore, titanium, an earth-abundant, non-toxic metal was the focus of this chapter. A new group of titanium complexes with phosphoramidate ligands was presented.

Sterically accessible metal complexes bearing one bulky phosphoramidate ligand were characterized and discussed. While this bulky, tetrahedral ligand motif did allow for the isolation and solid-state characterization of one complex, **18**, the exclusive formation of these complexes proved difficult due to ligand redistribution. In contrast to the amido ether example discussed previously, which creates a larger 5-membered metallacycle, phosphoramidates have tighter bite angles and the resultant 4-membered metallacycles are not adequately large enough to spatially hinder the formation of diphosphoramidate species. Furthermore, while the *N,O*-chelating phosphoramidate motif possesses increased steric bulk relative to amidate and pyridonate

ligands, this bulk is situated on the nitrogen and phosphorus atoms. The oxygen atom of the chelate does not possess enough steric hindrance to prevent the observed ligand redistribution to form more stable, bis-ligated complexes.

These diphosphoramidate complexes were readily synthesized and isolable which allowed for solid-state characterization for all aryl-substituted species. Triphosphoramidate titanium species were also found to be easily synthesized and isolated. Variable temperature ^1H and ^{31}P NMR spectroscopy, as well as solid-state analysis, provided insight into the binding mode of these chelates, with one ligand binding $\kappa^1\text{-O}$ as consistent with triamidate complexes of titanium. The bulky ligand set did not allow for tetra(*N,O*) complexes to be accessed owing to the relatively small atomic radius of titanium. Attempts to synthesize derivatives containing an electron-withdrawing chloro ligand were not possible due to ligand redistribution. One unpredicted product, **28**, was isolated *via* crystallization and characterized in the solid-state. It showed unexpected ligand based reactivity where an ethoxy moiety was substituted for a dimethylamido group.

Monophosphoramidate complexes were screened using an *in situ* catalyst preparation despite knowingly containing diphosphoramidate side-products. Moderate activity for HAA of secondary amines and terminal alkenes was observed, with the most success coming from forcing conditions of 165 °C and 96 h. The analogous diphosphoramidate reached only 45% under these conditions, presumably due to the large amount of steric bulk preventing access to the reactive metal-centre. HA of primary aminoalkenes gave exclusive formation of the 6-membered cyclic product while no 5-membered HAA product was observed. Conversions were quantitative after 2 hours at 80 °C while full conversion was observed after 1 week at room temperature. Diphosphoramidate titanium species again proved too bulky to facilitate this

transformation, with negligible reactivity being observed under analogous conditions. Furthermore, preliminary screening reactions were performed to investigate the HAA activity of these complexes with specific attention given to the generation of monoalkylated products for their use as monomers for ROMP. While the reactivity of these activated alkenes in HAA was more promising than other substrates screened, the use of these complexes did not lead to an efficient, high yielding transformation. Although these results are an interesting proof of concept, as no examples of HAA or HA using titanium phosphoramidate complexes exist in the literature, they are not competitive with the existing titanium catalysts developed by Chong²⁴⁶ and Doye.³⁴¹⁻

342

2.10 Experimental

2.10.1 Materials and Methods

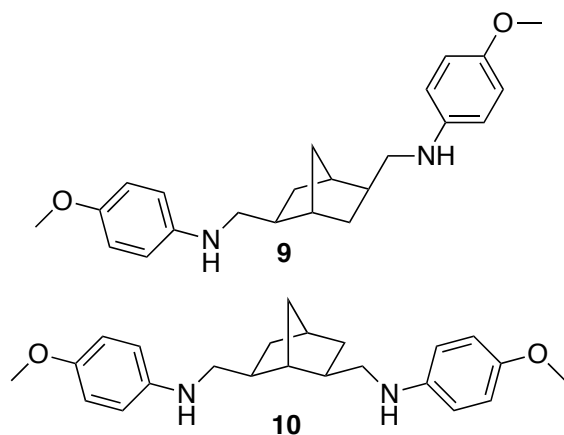
General Methods. Synthesis of metal complexes and subsequent reactions involving these precatalysts were performed under an inert atmosphere of nitrogen using standard Schlenk line or glove box techniques. Hexanes, toluene, tetrahydrofuran, and diethyl ether were purified by passing over a column of activated aluminum and degassed *via* successive free-pump-thaw cycles or deoxygenated by sparging with N₂ prior to use. Dichloromethane was dried over CaH₂ and distilled. Toluene-d₈ and benzene-d₆ were distilled from sodium, degassed *via* three successive freeze-pump-thaw cycles, and stored over 4 Å molecular sieves in the glove box. Solvents for chromatography (ACS grade or above) were used as received from commercial sources. All chemicals were purchased from commercial sources and used as received, unless otherwise stated. Thin layer chromatography (TLC) was performed on Whatman Partisil K6F UV₂₅₄ pre-coated TLC plates. Silica gel F60 (230-400 mesh) was used as purchased from Silicycle. All characterization of products synthesized by hydroaminoalkylation or hydroamination not presented in this chapter, including aminonorbornene **6**, can be found in the following references or in the experimental section of Chapter 3.^{105, 183, 238, 246, 340} spectra are presented in the relevant appendix. Characterization and corresponding spectra of nosylated compound **11** can be found in the following reference.¹⁸³ Phosphoramidate proligands were synthesized using methods described below. All characterization data is consistent with that reported in the literature. Ligand salts, such as **1** were synthesized according to literature procedures and used without further characterization.¹⁸³ The specific proligands and corresponding references are as follows: **17**,^{183, 362} **20**,¹⁸³ **27**,^{183, 362-365} **39**,^{183, 365-366} **40**.^{183, 366}

Instrumentation

NMR spectroscopy was performed on a Bruker Avance 300 MHz, 400 MHz, or 600 MHz spectrometer at 298 K unless otherwise stated. All coupling values are $^3J_{\text{H-H}}$ and reported in Hz. Abbreviations for NMR assignments for peaks are as follows: s = singlet; d = doublet; t = triplet; q = quartet; sept = septet, m = multiplet; br = broad. GC-MS was performed on an Agilent 7890A system using helium as the carrier gas. High-resolution mass spectra (HRMS) were acquired from a Waters/Micromass LCT spectrometer. IR spectra were obtained on either a Nicolet 4700 FTIR (NaCl) or a Perkin Elmer Frontier (ATR) spectrometer.

2.10.2 Synthesis and Characterization

Characterization of dialkylated side-products of hydroaminoalkylation

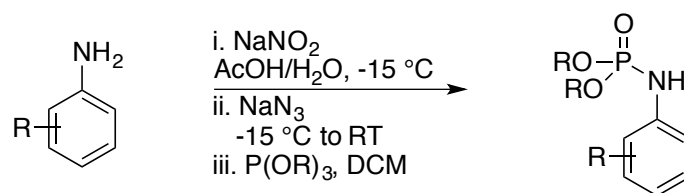


9 and **10**. Known compounds.¹⁰⁵ To a vial containing **2** (0.1 eq., 0.06 g, 0.10 mmol), *para*-methoxy-*N*-methylaniline (5.0 eq., 0.15 g, 1.10 mmol) and norbornadiene (1.0 eq., 0.02 g, 0.22 mmol) were added to afford a yellow solution. The mixture was stirred for 16 h at RT causing the reaction to become viscous and red. Purification

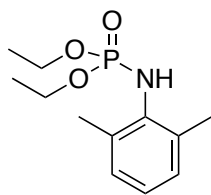
via column chromatography (hexanes/ethyl acetate, 9:1) yielded a yellow oil consisting of a mixture of isomers in a 1:1 ratio, as determined by GC-MS analysis, 0.08 g, **10**. This mixture could not be separated further. ^1H NMR (300 MHz, CDCl_3): δ 6.82 (d, $^3J = 9.0$, 8H, $4 \times \text{ArH}$), 6.61 (d, $^3J = 9.0$, 8H, $4 \times \text{ArH}$), 3.78 (s, 12H $4 \times \text{OCH}_3$), 3.31 (br s, 4H, $4 \times \text{NH}$), 2.91 (m, 8H,

4×NCH₂), 2.18 (m, 3H, 3×CH), 1.71 (m, 4H, 2×CH₂), 1.49 (m, 4H, 2×CH₂), 1.29 (m, 5H, 5×CH), 1.17 (m, 4H, 2×CH₂). ¹³C NMR (75 MHz, CDCl₃): δ 152.1 (4×C), 142.9 (4×C), 115.0 (8×CH), 114.2 (4×CH), 114.1 (4×CH), 56.0 (4×CH₃), 50.4 (2×CH₂), 50.3 (2×CH₂), 42.7 (2×CH₂), 42.4 (2×CH), 41.7 (CH₂), 39.5 (3×CH), 36.4 (2×CH), 36.1 (2×CH₂), 35.3 (CH₂), 32.7 (CH₂). IR (NaCl, cm⁻¹): 3392, 2937, 1511, 1231, 819. HRMS-ESI (m/z): calcd: 367.2386; found 367.2379.

General Procedure A: Preparing aryl-substituted phosphoramidate proligands



Aryl-substituted phosphoramidate proligands were synthesized per reported procedures.^{183, 364} The desired aniline was dissolved in a mixture of glacial AcOH /H₂O (1:1) and cooled to -15 °C. Next, NaNO₂ (1.4 eq.) was added in 3 portions over 10 minutes and the mixture was let stir for approximately 10 minutes. NaN₃ (1.5 eq.) was added portion-wise and the reaction brought to room temperature. After 45 min, the reaction was extracted with CH₂Cl₂ and neutralized with saturated NaHCO₃ (aq). P(OR)₃ (1.5 eq.) was added in one portion to the resulting organic layer and the reaction was stirred overnight. Hydrolysis with 5 M HCl (aq), extraction with CH₂Cl₂, washing with brine, and drying over MgSO₄ afforded crude products after removal of the volatiles *in vacuo*. Sonication in pentane and filtering the suspension yielded off-white solid that was sublimed under reduced pressure to afford a white crystalline product.

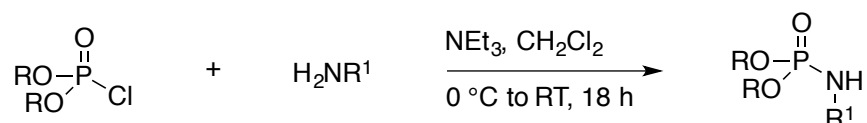


17

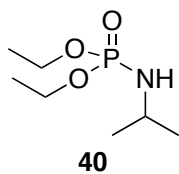
17. Known compound¹⁸³ synthesized using **General Procedure A** using 2,6-dimethylaniline (3.9 g, 32 mmol, 4.0 mL) to afford **18** as white crystalline material after sublimation, 6.31 g, 76%. ¹H NMR (300 MHz, CDCl₃): δ 7.04-6.95 (m, 3H), 4.14-4.04 (m, 5H), 2.37 (s, 6H), 1.27 (t, ³J = 7.3 Hz, 6H);

¹³C{¹H} NMR (75 MHz, CDCl₃): δ 136.0 (2×C), 135.1 (C), 128.6 (2×CH), 126.2 (CH), 63.2 (CH₂) 62.1 (CH₂), 19.2 (2×CH₃), 16.5 (CH₃), 16.3 (CH₃). ³¹P{¹H} NMR (121 MHz, CDCl₃) δ 4.24. **EA:** Calculated for C₁₂H₂₀NO₃P: C 56.02, H 7.84, N 5.44; O 18.66; found: C 56.09, H 7.82, N 5.37.

General Procedure B: Preparing alkyl-substituted phosphoramidate proligands



Primary alkylamine (23 mmol) and triethylamine (3.3 mL, 25 mmol) were dissolved in anhydrous CH₂Cl₂ (50 mL) and cooled to 0 °C using an ice bath. Chlorophosphate (3.6 mL, 25 mmol) was added dropwise over approximately 5 minutes and the mixture was warmed to room temperature and stirred overnight. All volatiles were removed *in vacuo* and the crude material was purified by flash chromatography (1 % MeOH in DCM) to obtain the desired product.



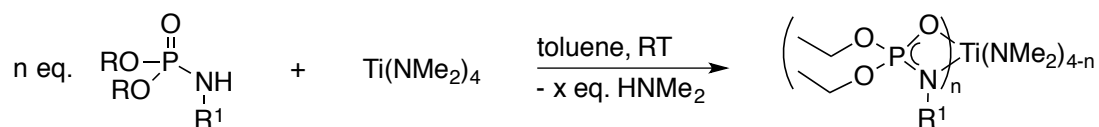
40

40. Known compound^{183, 366} synthesized using **General Procedure B** using isopropylamine (1.9 mL, 22.6 mmol), trimethylamine (3.34 mL, 24.82 mmol) and ClP(O)(OEt)₂ (3.56 mL, 24.82 mmol). Further purification was conducted

via distillation under reduced pressure to yield **40** as a colourless oil (3.8 g, 86%). ¹H {³¹P}

NMR (300 MHz, C₆D₆): δ 4.98 (s, 1H), 4.05-3.88 (m, 4H), 3.36-3.25 (m, 1H), 1.15 (d, $^3J = 6.0$ Hz, 6H), 1.10 (t, $^3J = 7.5$ Hz, 6H). **¹³C{¹H} NMR** (75 MHz, C₆D₆): δ 61.5 (2×CH₂), 43.8 (CH), 25.2 (2×CH₃), 16.4 (2×CH₃). **³¹P{¹H} NMR** (121 MHz, CDCl₃): δ 10.4. **IR** (NaCl, cm⁻¹): 3223, 2977, 2950, 1477. **HRMS-EI** (m/z): Calculated for C₇H₁₈NO₃P: 194.09461; found: 194.09448.

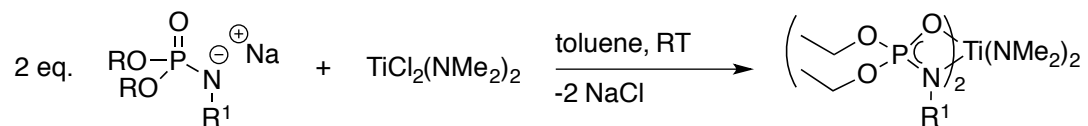
General Procedure C: Preparing phosphoramidate complexes of titanium *via* protonolysis



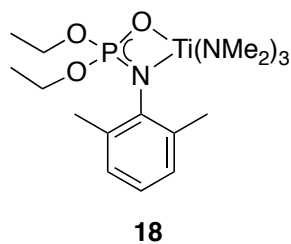
Di- and triphosphoramidate complexes of titanium were prepared by adding dropwise a solution of proligand (2 eq. for bis-complexes and 3 eq. for trisubstituted complexes in toluene (~5 mL) to a stirring solution of Ti(NMe₂)₄ in toluene (~5 mL). The red mixture was let stir overnight before all volatiles were removed *in vacuo*. The crude red solids could be recrystallized from saturated solutions of toluene or hexanes to yield red needles, or ether to yield red plates. Alkyl substituted complexes were isolated as red oils and could not be crystallized. All reactivity discussed was conducted using alkyl-substituted phosphoramidate was done so using crude complexes.

Monophosphoramidate complexes were prepared similarly to that described above, although the proligand solution was added to a stirring mixture of Ti(NMe₂)₄ to ensure an excess of metal-to-proligand during the addition. All other steps were analogous to those described above.

General Procedure D: Preparing phosphoramidate complexes of titanium *via* salt metathesis



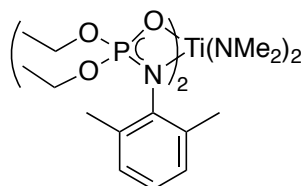
Diphosphoramidate complex **19** was also prepared *via* salt metathesis. The sodium-salt **1** was synthesized by combining a solution of proligand **17** in hexanes to a solution containing an equimolar amount of NaHMDS in hexanes (~8 mL). The mixture was stirred at room temperature overnight before all volatiles were removed *in vacuo*. The off-white solid was washed with hexanes several times until the washings became colourless. The resulting white solid, **1**, was dried *in vacuo* and used without further characterization. **1** (0.17 g, 0.60 mmol) was suspended in hexanes and added to a stirring solution of $\text{TiCl}_2(\text{NMe}_2)_2$ (0.06 g, 0.30 mmol) in hexanes. The mixture was let stir overnight before being filtered through a plug of Celite®. The filtrate was dried *in vacuo* to yield a red solid (0.18 g, 94%). All characterization was consistent with **19** prepared *via* protonolysis using **General Procedure C**.



18. Prepared using **General Procedure C**, using proligand **17** (0.49 g, 1.9 mmol) and $\text{Ti}(\text{NMe}_2)_4$ (0.43 g, 1.9 mmol) and isolated as an orange solid after removal of diphosphoramidate side product by several recrystallizations. This complex could not be characterized by ^{13}C NMR

spectroscopy or mass spectrometry due to its instability and propensity to form the

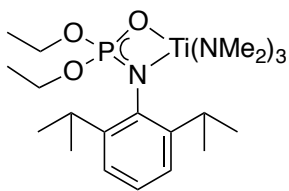
diphosphoramidate analogue. Therefore, no yield is given. The red solid was isolated in poor yields and characterized by the following methods: ^1H NMR (300 MHz, C_6D_6): δ 7.09-7.06 (m, 2H, $2\times\text{ArH}$), 6.95-6.89 (m, 1H, ArH), 3.90-3.81 (m, 4H, $2\times\text{OCH}_2\text{CH}_3$), 3.29 (s, 18H, $3\times\text{N}(\text{CH}_3)_2$), 2.46 (s, 6H, ArCH_3), 1.00 (t, $^3J = 6.0$ Hz, 6H, $2\times\text{OCH}_2\text{CH}_3$). $^{31}\text{P}\{^1\text{H}\}$ NMR (75 MHz, C_6D_6): δ 7.14. Acquisition of a quality ^{13}C NMR spectrum was not possible due to ligand redistribution in solution.



19

19. Prepared using **General Procedure C**, using proligand **17** (0.20 g, 0.78 mmol) and $\text{Ti}(\text{NMe}_2)_4$ (0.09 g, 0.39 mmol) and isolated as a red solid 0.21 g, 84%. ^1H NMR (400 MHz, C_6D_6): δ 7.12 (m, 4H, $4\times\text{ArH}$), 6.96 (m, 2H, $2\times\text{ArH}$), 4.04 (m, 8H, $4\times\text{CH}_2\text{CH}_3$), 3.16 (s, 12H, $2\times\text{N}(\text{CH}_3)_2$), 2.66 (s, 12H, $4\times\text{ArCH}_3$), 1.06 (t, $^3J = 7.2$ Hz, 12H, $4\times\text{CH}_2\text{CH}_3$). $^{13}\text{C}\{^1\text{H}\}$ NMR (100 MHz, C_6D_6): δ 144.2 ($2\times\text{C}$), 144.1 ($2\times\text{C}$), 135.1 ($2\times\text{CH}$), 135.0 ($2\times\text{CH}$), 123.5 (CH), 123.5 (CH), 62.8 ($4\times\text{CH}_2$), 48.5 ($4\times\text{CH}_3$), 19.8 ($4\times\text{CH}_3$), 16.5 ($2\times\text{CH}_3$), 16.4 ($2\times\text{CH}_3$). $^{31}\text{P}\{^1\text{H}\}$ NMR (162 MHz, C_6D_6): δ 5.94. IR (ATR, cm^{-1}): 3164, 2854, 1467, 1293, 1025. HRMS-EI (m/z): Calculated for $\text{C}_{28}\text{H}_{50}\text{N}_4\text{O}_6\text{P}_2\text{Ti}$: 648.26882; found: 648.26882. EA: Calculated for $\text{C}_{28}\text{H}_{50}\text{N}_4\text{O}_6\text{P}_2\text{Ti}$: C, 51.86; H, 7.77; N, 8.64; found: C, 51.99; H, 7.78; N, 8.42.

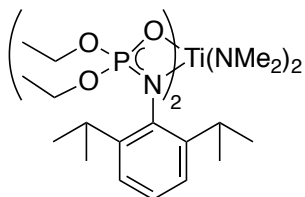
19 could also be prepared using **General Procedure D**, using **1** (0.17 g, 0.61 mmol) and $\text{Ti}(\text{NMe}_2)_2\text{Cl}_2$ (0.06 g, 0.30 mmol) to give a red solid, 0.19 g, 96%. All characterization agreed to that of **19** when using **General Method C** described above.



21

21. Prepared using **General Procedure C**, using proligand **20** (0.14 g, 0.45 mmol) and $\text{Ti}(\text{NMe}_2)_4$ (0.10 g, 0.45 mmol) and isolated as an orange solid. No yield is given due to the propensity of this complex to undergo ligand redistribution to form the diphosphoramidate species at

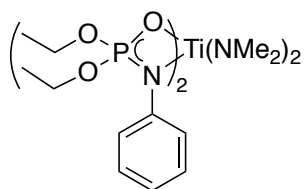
room temperature. ^1H NMR (400 MHz, C_6D_6): δ 7.24-7.11 (overlapped, m, 3H, ArH), 3.92 (m, 4H, CH_2CH_3), 3.68 (sept, $^3J = 8.0$ Hz, 2H, $2 \times \text{CHCH}_3$), 3.27 (s, 18H, $3 \times (\text{CH}_3)_2$), 1.35 (d, $^3J = 8.0$ Hz, 12H, $2 \times \text{CH}(\text{CH}_3)_2$), 1.05 (t, $^3J = 8.0$ Hz, 6H, $2 \times \text{OCH}_2\text{CH}_3$). $^{13}\text{C}\{^1\text{H}\}$ NMR (100 MHz, C_6D_6): δ 145.0 (C), 144.9 (C), 140.3 (C), 124.6 (CH), 123.8 (CH), 123.7 (CH), 63.1 (CH_2), 63.0 (CH_2), 46.9 ($2 \times \text{CH}$), 28.1 ($4 \times \text{CH}_3$), 25.1 ($2 \times \text{CH}_3$), 16.4 ($3 \times \text{CH}_3$), 16.3 ($3 \times \text{CH}_3$). $^{31}\text{P}\{^1\text{H}\}$ NMR (162 MHz, C_6D_6): δ 6.34. **HRMS-EI** (m/z): Calculated for $\text{C}_{22}\text{H}_{45}\text{N}_4\text{O}_3\text{PTi}$: 492.27088; found: 492.27139.



22

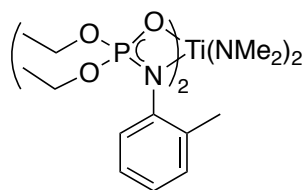
22. Prepared using **General Procedure C**, using proligand **20** (0.20 g, 0.65 mmol) and $\text{Ti}(\text{NMe}_2)_4$ (0.07 g, 0.32 mmol) and isolated as a red solid 0.21 g, 85%. ^1H NMR (300 MHz, C_6D_6): δ 7.29-7.17 (m, 6H, $6 \times \text{ArH}$), 4.18-3.97 (m, 12H, $4 \times \text{CH}_2\text{CH}_3$ and $4 \times \text{CH}(\text{CH}_3)_2$), 3.25 (s,

12H, $2 \times \text{N}(\text{CH}_3)_2$), 1.45 (d, $^3J = 6.0$ Hz, 24H, $4 \times \text{CH}(\text{CH}_3)_2$), 1.15 (t, $^3J = 6.0$ Hz, 12H, $4 \times \text{CH}_2\text{CH}_3$). $^{13}\text{C}\{^1\text{H}\}$ NMR (100 MHz, C_6D_6): δ 145.7 (C), 145.6 (C), 141.1 ($2 \times \text{C}$), 141.0 ($2 \times \text{C}$), 124.5 ($2 \times \text{CH}$), 123.7 ($2 \times \text{CH}$), 123.7 ($2 \times \text{CH}$), 63.1 ($2 \times \text{CH}_2$), 63.0 ($2 \times \text{CH}_2$), 49.44 ($4 \times \text{CH}$), 27.2 ($8 \times \text{CH}_3$), 25.8 ($4 \times \text{CH}_3$), 16.4 ($2 \times \text{CH}_3$), 16.3 ($2 \times \text{CH}_3$). $^{31}\text{P}\{^1\text{H}\}$ NMR (121 MHz, C_6D_6): δ 5.26. **IR** (ATR, cm^{-1}): 3141, 2867, 1466, 1228, 1030. **HRMS-EI** (m/z): Calculated for $\text{C}_{36}\text{H}_{66}\text{N}_4\text{O}_6\text{P}_2\text{Ti}$: 758.37806; found: 758.37725. **EA**: Calculated for $\text{C}_{36}\text{H}_{66}\text{N}_4\text{O}_6\text{P}_2\text{Ti}$: C, 56.84; H, 8.74; N, 7.36; found: C, 56.91; H, 8.87; N, 7.12.



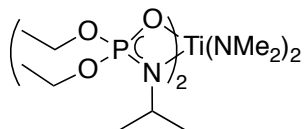
23

23. Prepared using **General Procedure C**, using proligand **27** (0.10 g, 0.44 mmol) and $\text{Ti}(\text{NMe}_2)_4$ (0.05 g, 0.22 mmol) and isolated as a red solid 0.10 g, 76%. ^1H NMR (300 MHz, C_6D_6): δ 7.46-7.43 (m, 4H, 4 \times ArH), 7.34-7.31 (m, 2H, 2 \times ArH), 6.95-6.93 (m, 2H, 2 \times ArH), 4.10-4.02 (m, 8H, 4 \times CH_2CH_3), 3.46 (s, 12H, 2 \times $\text{N}(\text{CH}_3)_2$), 1.02 (t, $^3J = 7.2$ Hz, 12H, 4 \times CH_2CH_3). $^{13}\text{C}\{^1\text{H}\}$ NMR (100 MHz, C_6D_6): δ 147.8 (C), 147.8 (C), 129.2 (4 \times CH), 122.7 (CH), 122.6 (CH), 121.1 (4 \times CH), 62.7 (2 \times CH_2), 62.6 (2 \times CH_2), 48.2 (4 \times CH_2CH_3), 16.4 (2 \times CH_3), 16.3 (2 \times CH_3). $^{31}\text{P}\{^1\text{H}\}$ NMR (162 MHz, C_6D_6): δ 7.78. IR (ATR, cm^{-1}): 3169, 2908, 1500, 1224, 1022. HRMS-EI (m/z): Calculated for $\text{C}_{24}\text{H}_{42}\text{N}_4\text{O}_6\text{P}_2\text{Ti}$: 592.20591; found: 592.20610. EA: Calculated for $\text{C}_{24}\text{H}_{42}\text{N}_4\text{O}_6\text{P}_2\text{Ti}$: C, 48.66; H, 7.15; N, 9.46; found: C, 48.98; H, 7.28; N, 9.24.



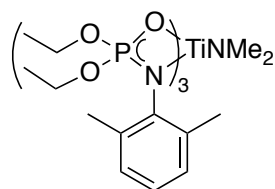
24

24. Prepared using **General Procedure C**, using proligand **39** (2.0 g, 8.2 mmol) and $\text{Ti}(\text{NMe}_2)_4$ (0.92 g, 4.1 mmol) and isolated as a red solid 2.31 g, 91%. ^1H NMR (300 MHz, C_6D_6): δ 7.14 (m, 2H, 2 \times ArH), 6.89 (m, 4H, 6 \times ArH), 6.69 (m, 2H, 2 \times ArH), 3.91 (q, $^3J = 6.0$ Hz, 8H, 4 \times CH_2CH_3), 2.96 (s, 12H, 2 \times $\text{N}(\text{CH}_3)_2$), 2.31 (s, 6H, 2 \times ArCH₃), 0.79 (t, $^3J = 6.0$ Hz, 12H, 4 \times CH_2CH_3). $^{13}\text{C}\{^1\text{H}\}$ NMR (100 MHz, C_6D_6): δ 146.2 (C), 146.1 (C), 134.3 (CH), 134.2 (CH), 130.4 (C), 130.3 (C), 126.1 (2 \times CH), 126.1 (2 \times CH), 123.5 (CH), 123.5 (CH), 62.9 (2 \times CH_2), 62.9 (2 \times CH_2), 48.6 (4 \times CH₃), 19.2 (2 \times CH₃), 16.5 (2 \times CH₃), 16.4 (2 \times CH₃). $^{31}\text{P}\{^1\text{H}\}$ NMR (161 MHz, C_6D_6): 5.54. IR (ATR, cm^{-1}): 3186, 2925, 1501, 1234, 974. HRMS-EI (m/z): Calculated for $\text{C}_{24}\text{H}_{40}\text{N}_3\text{O}_6\text{P}_2\text{Ti}$ (minus $\text{N}(\text{CH}_3)_2$): 576.18718; found: 576.18690.



25

25. Prepared using **General Procedure C**, using proligand **40** (0.18 g, 0.94 mmol) and $\text{Ti}(\text{NMe}_2)_4$ (0.11 g, 0.47 mmol) and isolated as a red oil, 0.23 g, 93 %. ^1H NMR (300 MHz, C_6D_6): δ 4.20-3.91 (m, 10H, $2\times\text{CH}(\text{CH}_3)_2$ and $4\times\text{CH}_2\text{CH}_3$), 3.49 (s, 12H, $2\times\text{N}(\text{CH}_3)_2$), 1.46 (d, $^3J = 6.0$ Hz, 12H, $4\times\text{CH}(\text{CH}_3)_2$), 1.14 (t, $^3J = 6.0$ Hz, 12H, $4\times\text{CH}_2\text{CH}_3$). $^{13}\text{C}\{^1\text{H}\}$ NMR (75 MHz, C_6D_6): 61.7 ($2\times\text{CH}_2$), 61.7 ($2\times\text{CH}_2$), 49.0 ($2\times\text{CH}_3$), 49.0 ($2\times\text{CH}_3$), 48.5 ($4\times\text{CH}_3$), 26.8 (CH), 26.7 (CH), 16.7 ($2\times\text{CH}_3$), 16.6 ($2\times\text{CH}_3$). $^{31}\text{P}\{^1\text{H}\}$ NMR (121 MHz, C_6D_6): 10.98. **HRMS-EI** (m/z): Calculated for $\text{C}_{16}\text{H}_{40}\text{N}_3\text{O}_6\text{P}_2\text{Ti}$ (minus NMe_2): 480.18718; found: 480.18745.



26

26. Prepared using **General Procedure C**, using proligand **17** (0.31 g, 1.20 mmol) and $\text{Ti}(\text{NMe}_2)_4$ (0.09 g, 0.40 mmol) and isolated as a red solid 0.35 g, 95%. ^1H NMR (300 MHz, C_6D_6): δ 7.13-7.06 (overlapped m, 6H, $6\times\text{ArH}$), 6.93-6.88 (m, 3H, $3\times\text{ArH}$), 4.28-3.80 (overlapped m, 10 H, $5\times\text{OCH}_2\text{CH}$), 3.65-3.52 (m, 2H, OCH_2CH_3), 3.46 (s, 6H, $2\times\text{N}(\text{CH}_3)_2$), 2.71 (s, 6H, $2\times\text{ArCH}_3$), 2.57 (s, 12H, $4\times\text{ArCH}_3$), 1.16-0.89 (m, 18H, $6\times\text{OCH}_2\text{CH}_3$). $^{31}\text{P}\{^1\text{H}\}$ NMR (162 MHz, C_6D_6): δ 7.01, 0.16, -26.74. **IR** (ATR, cm^{-1}): 3161, 2980, 2918, 1472. **HRMS-EI** (m/z) Calculated for $\text{C}_{38}\text{H}_{63}\text{N}_4\text{O}_9\text{P}_3\text{Ti}$: 860.32874; found: 860.32945. **EA**: calculated for $\text{C}_{38}\text{H}_{63}\text{N}_4\text{O}_9\text{P}_3\text{Ti}$: 53.03 C; 7.38 H, 6.51 N; found: 52.74 C; 7.69 H, 6.60 N. $^{13}\text{C}\{^1\text{H}\}$ NMR signals are broad due to the complex's fluxionality in solution.

General Procedure E: Screening for HA or HAA reactivity using isolated complexes

Reactions were set up in a glovebox filled with nitrogen. Hydroaminoalkylation reactions were conducted in tol-d_8 (1 mL). Hydroamination reactions were conducted in a solution of trimethoxybenzene in tol-d_8 (0.5 M, 1 mL). Substrates were weighed into a 20 mL scintillation vial and dissolved in tol-d_8 for hydroaminoalkylation reactions and a solution of internal standard (0.5 M, tol-d_8) for hydroaminations reactions. The desired complex was weighed into a separate scintillation vial and dissolved in tol-d_8 (0.5 mL). The substrate solution was added to the precatalyst solution before the reaction mixture was transferred to a J. Young NMR tube. The tube was sealed and heated in a preheated oil bath for the allotted time. Conversions of hydroaminoalkylation reactions were calculated by comparing relative integrations of the *ortho*-aryl protons of starting material to product. Conversions for hydroamination reactions were determined by comparing the relative integrations of product to trimethoxybenzene. All reactions were further analyzed by GC-MS to verify conversions and determine the presence of any potential side products present.

General Procedure F: Screening for HA or HAA reactivity using complexes generated *in situ*

A precatalyst mixture was prepared by dissolving the desired amount of ligand in tol-d_8 (or a 0.5 M solution of internal standard in tol-d_8). $\text{Ti}(\text{NMe}_2)_4$ was weighed into a scintillation vial and dissolved in tol-d_8 (or a 0.5 M solution of internal standard in tol-d_8). The ligand mixture was added to a stirring solution of $\text{Ti}(\text{NMe}_2)_4$ to ensure an excess of metal. The substrate solution was added to a J. Young NMR tube containing a tol-d_8 solution of substrates. The vessel was

sealed, and heated in a preheated oil bath for the desired time. The reactions were quenched by exposing to air. All reactions were conducted in a total of 1 mL of tol-d₈. A typical example is as follows:

Ti(NMe₂)₄ (0.050 mmol, 0.01 g) was weighed into a 20 mL scintillation vial and dissolved in a solution of tol-d₈ and TMB (0.25 mL, 0.50 M). The solution was stirred with a magnetic stirring bar. A solution of proligand **17** (0.050 mmol, 0.01 g, 0.25 mL tol-d₈ and TMB) was added dropwise to the titanium solution. Meanwhile, 1-octene (0.75 mmol, 0.08 g) and 4-methoxy-*N*-methylaniline (0.50 mmol, 0.07 g) were weighed into a separate 20 mL scintillation vial and dissolved in the toluene/internal standard mixture (0.5 mL) and transferred to a J. Young NMR tube. The substrate solution was transferred to the precatalyst mixture. The NMR tube was then placed in a preheated oil bath. The NMR tube was removed from the bath after the reaction time was completed and exposed to atmospheric oxygen to quench the catalyst.

Chapter 3: Hydroaminoalkylation and Ring-Opening Metathesis Polymerization: Synthesis of Nitrogen-Containing Polymers

3.1 Schafer Chemistry in the Field of Polymeric Materials

The advent of polymer chemistry in the Schafer Group dates to the early 2000s. Complexes of yttrium bearing *N,O*-chelating amidate ligands were developed as initiators for the polymerization of cyclic esters to form biodegradable polymers.^{329, 333} In 2015, titanium and zirconium amidate complexes were reported for the synthesis of ultra-high molecular weight polyethylene.³¹⁸

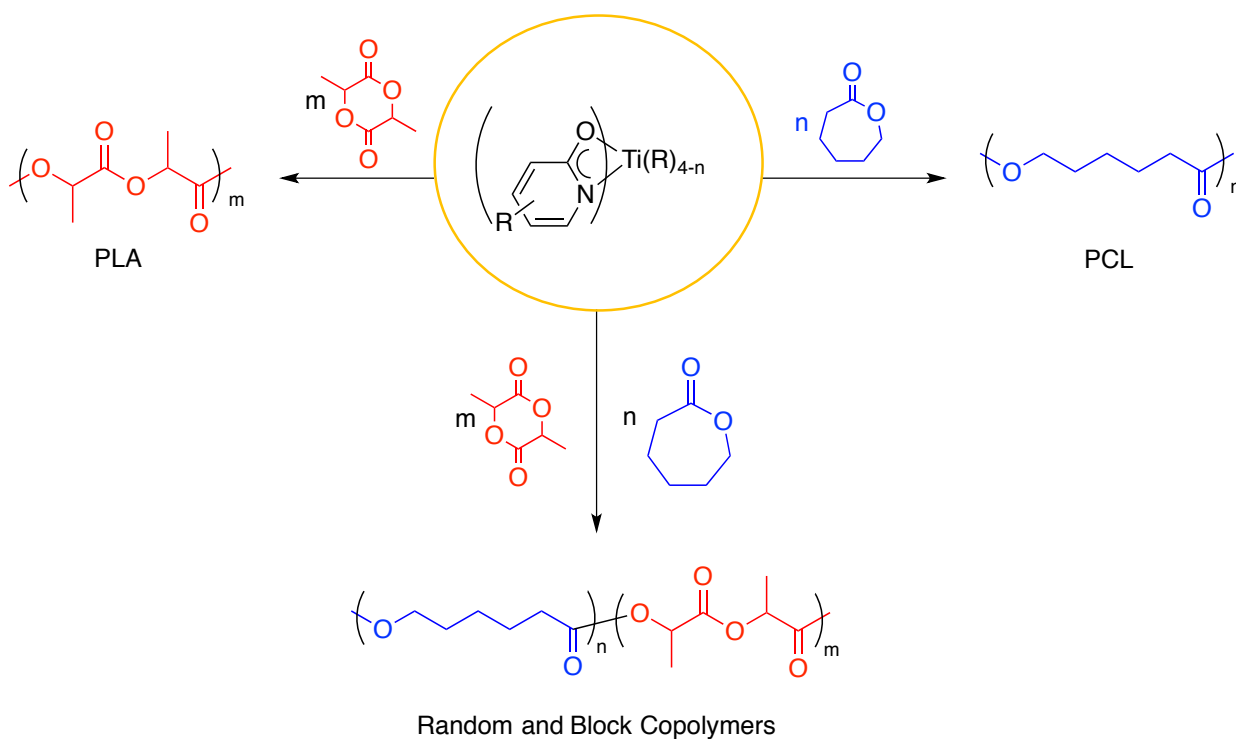


Figure 44 Titanium pyridonate complexes explored by the Schafer Group for the ring opening polymerization of cyclic esters

Titanium amidates and pyridonates were later exploited for their utility in the synthesis of macromolecules. Random copolymers of cyclic esters, namely lactide (LA) and ϵ -caprolactone (ϵ -CL), were achieved and led to well-defined biodegradable polymers (PLA and PCL) with low dispersities. These titanium complexes are among the leading examples of titanium initiators for PLA and PCL syntheses.⁷⁷ Shortly after, the Group released a full disclosure that included several other titanium pyridonate initiators that were competent for the homopolymerization of *rac*-LA and ϵ -CL, and the random and block copolymerization of these monomers (Figure 44).³²² Figure 45 shows one such complex; a di(pyridonate)di(ethoxide) titanium complex, **41**, that is an active initiator for the ROP of LA and ϵ -CL, leading to well-defined homo- and copolymers with low dispersities.⁷⁶

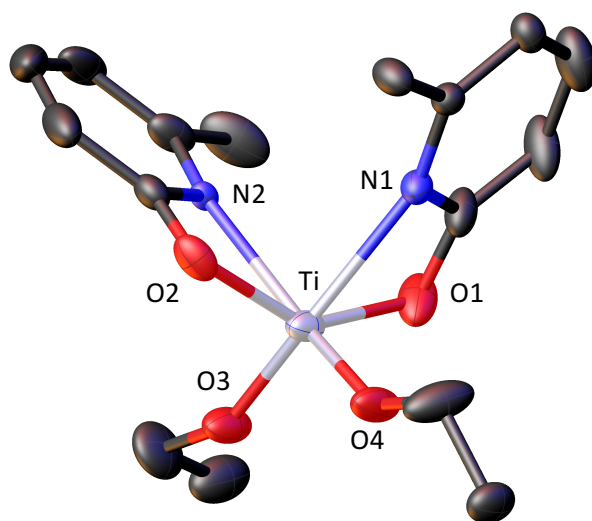


Figure 45 ORTEP of complex **41**. Ellipsoids shown at 50% probability. Hydrogen atoms omitted for clarity

Aside from their utility in the synthesis of polymeric material, *N,O*-chelated complexes have been used to synthesize small amine-containing molecules for use as calcium channel blockers. These biologically active small molecules products may have direct applications as

treatments for chronic pain and/or prostate cancer.³⁶⁷ While these molecules are important synthetic targets, we were curious to see if we could employ these *N,O*-chelated complexes to generate products for the efficient synthesis macromolecular amine-containing products. In line with our interests in polymer chemistry, we were enticed to synthesize a particular class of potential monomers, strained norbornenes bearing pendant amines from HAA, for use in ROMP.

As discussed in Chapter 2, the use of these nitrogen-containing monomers is often plagued by their lack of efficient, atom-economic syntheses. Unfortunately, titanium phosphoramidate complexes described in Section 2.7.3 (page 93) did not prove efficient for the synthesis of potential ROMP monomers, however, tantalum phosphoramidate complex **2** has been shown to be effective for the HAA of NBD to generate monoalkylated product **6** (see Figure 47).¹⁸³ As such, we attempted to expand the amine substrate scope potential of tantalum-catalyzed HAA to include other strained aminonorbornene products with the aim of using these materials for ROMP.

3.2 Tantalum Phosphoramidates: Coupling Hydroaminoalkylation and Ring-Opening Metathesis Polymerization

Ring-opening metathesis polymerization (ROMP) has become one of the most widespread polymerization technologies used in recent years.²⁴ Many initiators are tolerant to a variety of functional groups, including amides, alcohols, aldehydes, ketones, and esters.²⁴ However, some functional groups, including strong Lewis-bases (unhindered amines, phosphines, isonitriles, thiols, etc.) are often problematic, forming inactive ruthenium-based species, and require protection.¹²⁶⁻¹²⁹

While the synthesis of a variety of macromolecular structures and architectures is viable, some classes of polymers are hampered by the lack of efficient syntheses to access the requisite monomers. We envisioned that HAA could be used in this regard to generate nitrogen-containing substrates for ROMP in an efficient manner. This synthetic methodology is appealing and advantageous over other more traditional syntheses because HAA offers an atom-economic, solvent-free, and room temperature route to access higher amines from inexpensive, commercially available substrates Figure 46.

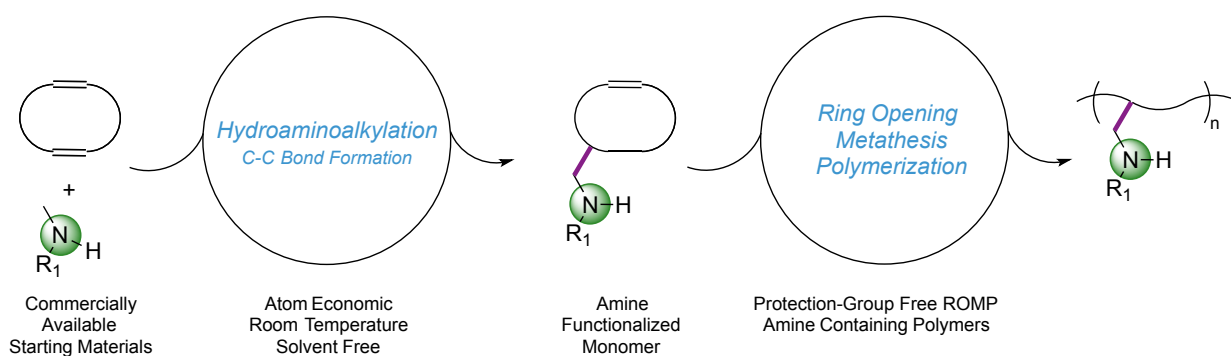


Figure 46 Sequential synthesis of nitrogen-containing polymers by coupling HAA and ROMP methodologies

3.3 Small Molecule Synthesis by HAA: Selective Formation of ROMP Monomers

As discussed in the Section 2.6.1, (page 46) the solvent-free, room temperature reactivity of tantalum phosphoramidate complex **2** was investigated. A small subset of products generated from this protocol is highlighted below (Figure 47), with compound **6** being noteworthy for its potential for future chemical transformations.¹⁸³ This chapter discusses the use of complex **2** to generate monoalkylated compound **6**. Characterization of **6** is discussed in full, including the solid-state molecular structure of this secondary amine. Focus is given to the interesting H-

bonding interactions present in the solid-state, foreshadowing the interesting potential properties of amine-containing polymers. Following these discussions is the expansion of the aminonorbornene products synthesized by complex **2** and the polymerization behavior of this family of unique and interesting molecules.

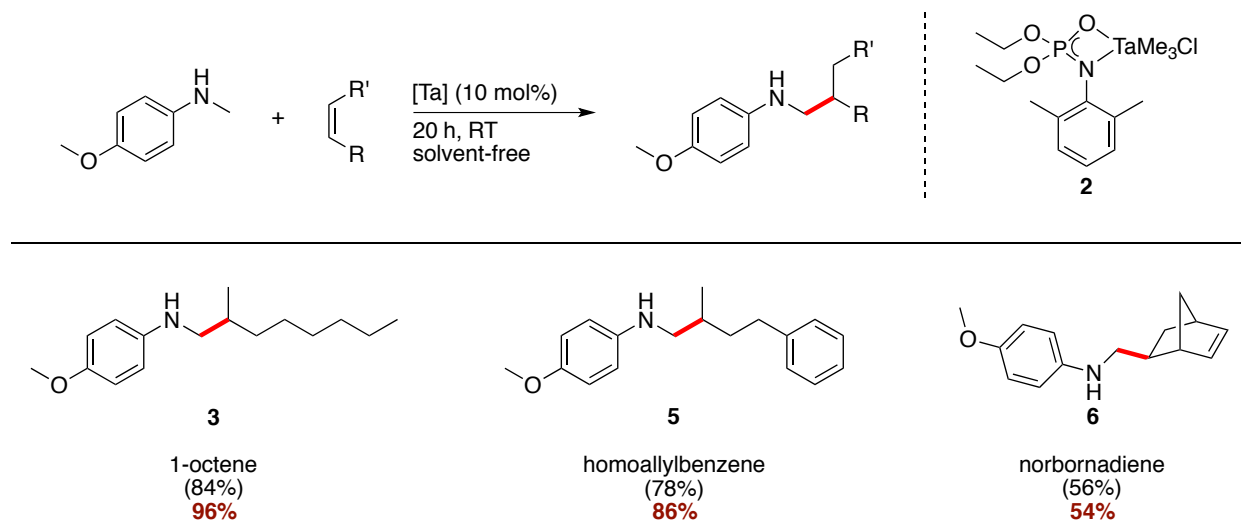


Figure 47 Solvent-free HAA using **2** to generate secondary amines in good yields. Isolated percent yields from solution-phase reactivity are shown in parentheses and those solvent-free reactions are shown in red

Complex **2** was shown to be effective for the regio- and diastereoselective synthesis of aminonorbornenes as evidenced by the formation of the new C-C bond (shown in red) under solvent-free conditions at room temperature. The synthesis of monomer **6** was performed according to the previously published literature report.¹⁸³ One set of signals was observed by ¹H NMR spectroscopy indicating the selective formation of one isomer (Figure 48). Convincingly, analysis of the crude mixture by GC-MS revealed only one species with the desired mass-to-charge ratio (*m/z*) of 229.3 for the desired monoalkylated product, **6**.

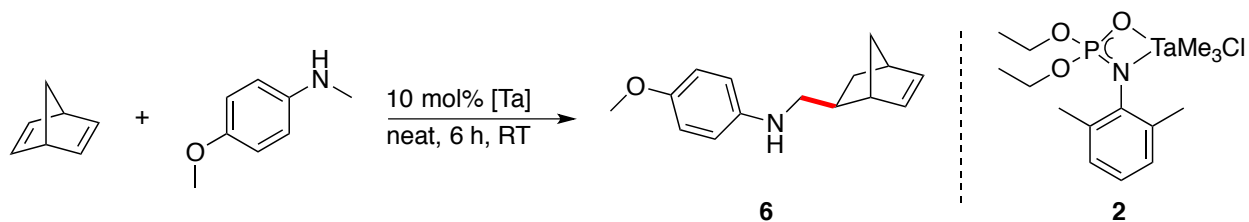


Figure 48 Synthesis of strained aminonorbornene **6** *via* HAA using **2**

This monomer was targeted as the analysis of this product by ^1H NMR spectroscopy (Figure 49) gave clearly resolved, diagnostic resonances, specifically for the methoxy methyl group (3.8 ppm, orange circle) and the olefinic protons at 6.1 ppm (blue circle).

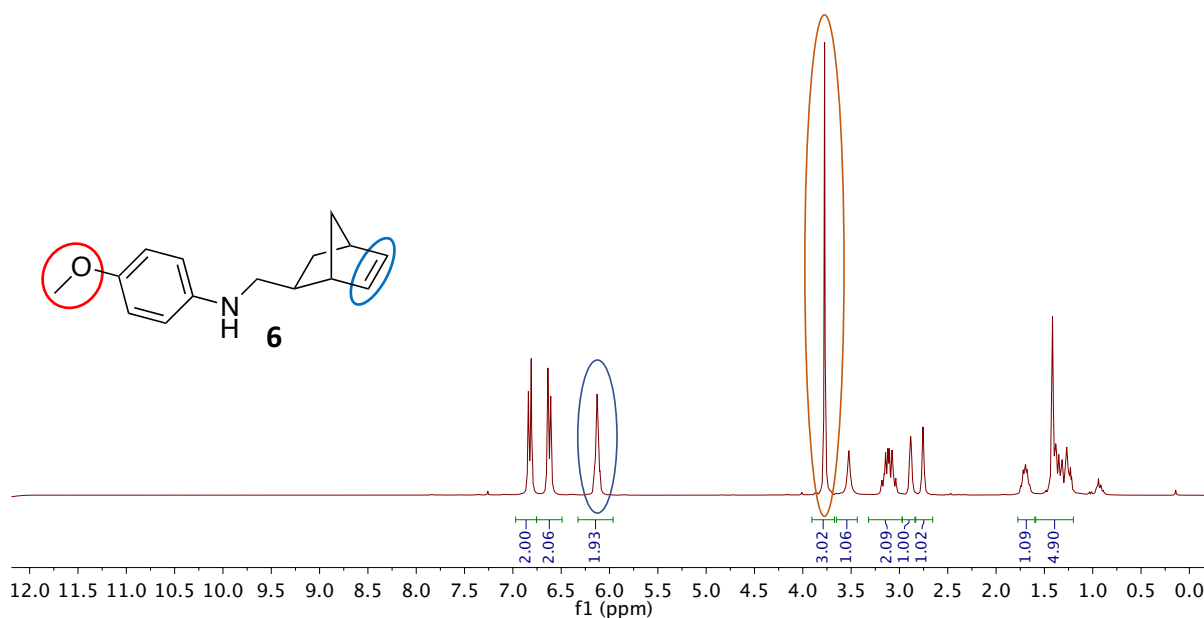


Figure 49 ^1H NMR spectrum of norbornene monomer **6** (300 MHz, CDCl_3 , 298 K)

Colourless crystals of the compound were grown from a dilute solution of hexanes, after leaving the solution undisturbed at room temperature for several weeks. The solid-state molecular structure of compound **6**, could be obtained by X-ray diffraction (Figure 50) to provide the ORTEP shown below.

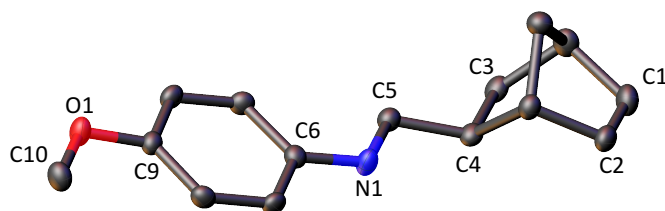


Figure 50 ORTEP of complex **6**. Ellipsoids shown at 50% probability. Hydrogen atoms removed for clarity

The ORTEP shown above confirms the diastereoselectivity of the reaction and the exclusive formation the *exo*-diastereomer, as supported by GC-MS analysis, which is consistent with the nosyl-substituted analogue **11**, discussed previously (Figure 23, Section 2.6.1, page 52). Table 10 details the relevant bond lengths (Å) and bond angles (°).

Table 10 Select bond lengths (Å) and angles (°) for compound **6**

Bond length (Å)		Bond angle (°)	
C1-C2	1.332(4)	C3-C4-C5	112.0(2)
C3-C4	1.554(3)	C4-C5-N1	110.5(2)
C5-N1	1.456(3)	C5-N1-C6	121.2(2)
N1-C6	1.386(3)	C4-O1-C10	117.05(19)
C9-O1	1.384(3)		
O1-C10	1.425(3)		

More interesting is Figure 51 that displays the ordering in the crystal lattice. The arrangement of molecules is such that the H-bond donating amine moieties are near the H-bond accepting methoxy substituents. This foreshadows potential inter- and intramolecular H-bonding interactions in the resultant polymers (*vide infra*).

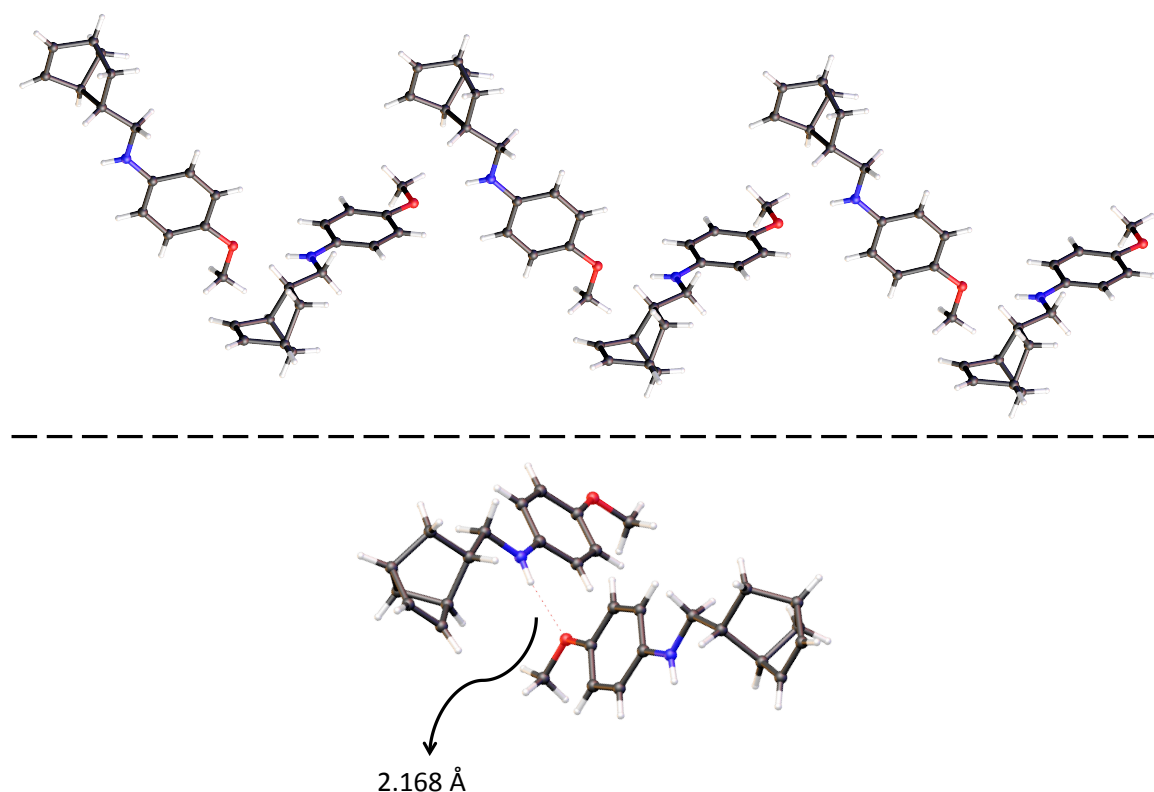


Figure 51 Crystal lattice (top) and selected region displaying H-bonding (bottom) of compound 6. N-H-OCH₃ H-bond distance is 2.168 Å

The strength of H-bonds can be categorized depending on the distance between donor, specifically the H-atom, and acceptor groups. These categories are weak (2.2-3.2 Å), medium (1.5-2.2 Å), and strong (1.2-1.5 Å) depending on the contact lengths observed in the solid-state molecular structure.³⁶⁸⁻³⁶⁹ If the lattice is examined more closely, the intermolecular NH-OCH₃

H-bond has a distance of 2.168 Å, which can be considered a medium H-bonding interaction. Furthermore, the IR spectra of the crystalline monomer were compared to the neat, liquid sample (Figure 52). The ordering and H-bonding interaction can be visible in the N-H stretching region. The solid, crystalline sample of **6** (black trace, ATR) displays a sharp, well defined absorbance at 3383 cm⁻¹, whereas the neat, liquid sample of compound **6** (red trace, ATR) displays a broadened absorbance between 3468 cm⁻¹ and 3330 cm⁻¹ as these N-H interactions are more dynamic in the liquid state.

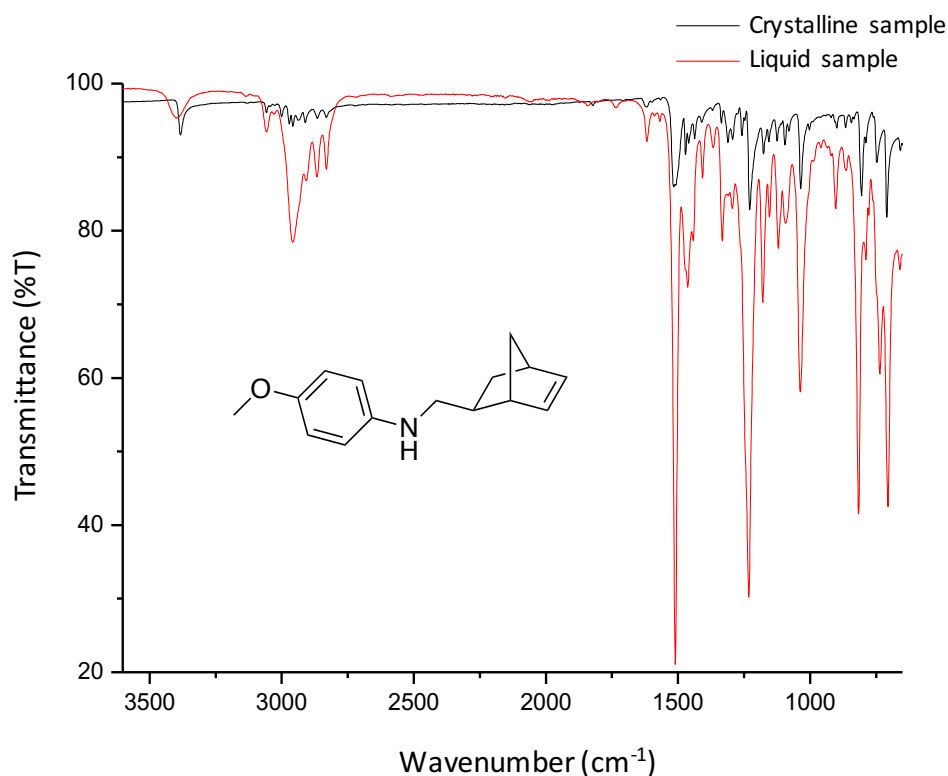


Figure 52 ATR-IR spectra of methoxy-substituted aminonorbornene **6**, in the solid-state (black) and the liquid state (red)

3.3.1 Tantalum-Catalyzed Hydroaminoalkylation: Expansion of Amine Scope

The success of synthesizing compound **6** *via* HAA led us to investigate the synthesis of a variety of other strained aminonorbornenes by varying the starting amine. The compounds shown in Figure 53 were synthesized in an analogous, solvent-free protocol to allow for direct comparisons to be made to previous work by the Schafer Group that describes the room-temperature, solvent-free HAA.¹⁸³ The products of HAA were isolated *via* column chromatography (10:1 hexanes/ethyl acetate, unless otherwise stated) with yields ranging from 41% to 56% for all aminonorbornenes synthesized. Moderate yields are attributed to small quantities of dialkylated product, as observed by GC-MS (See Chapter 2), and Lewis-acid catalyzed homopolymerization of NBD by the tantalum catalyst. Independent control reactions show that the tantalum phosphoramidate complex **2** is capable of polymerizing NBD at room temperature, as evidenced by the solid gel-like material generated when stirring an excess of NBD in the presence of **2** for 1 hour. This material was not isolated or characterized independently due to its poor solubility in common organic solvents. To address the challenge of this unwanted side reaction, the ratio of the alkene and amine starting materials could be decreased to 1:1, and the reaction time reduced to 6 hours, to reduce the propensity to form undesired polymeric side products. However, product yields were not significantly affected and remained comparable to those obtained under previous reaction conditions.

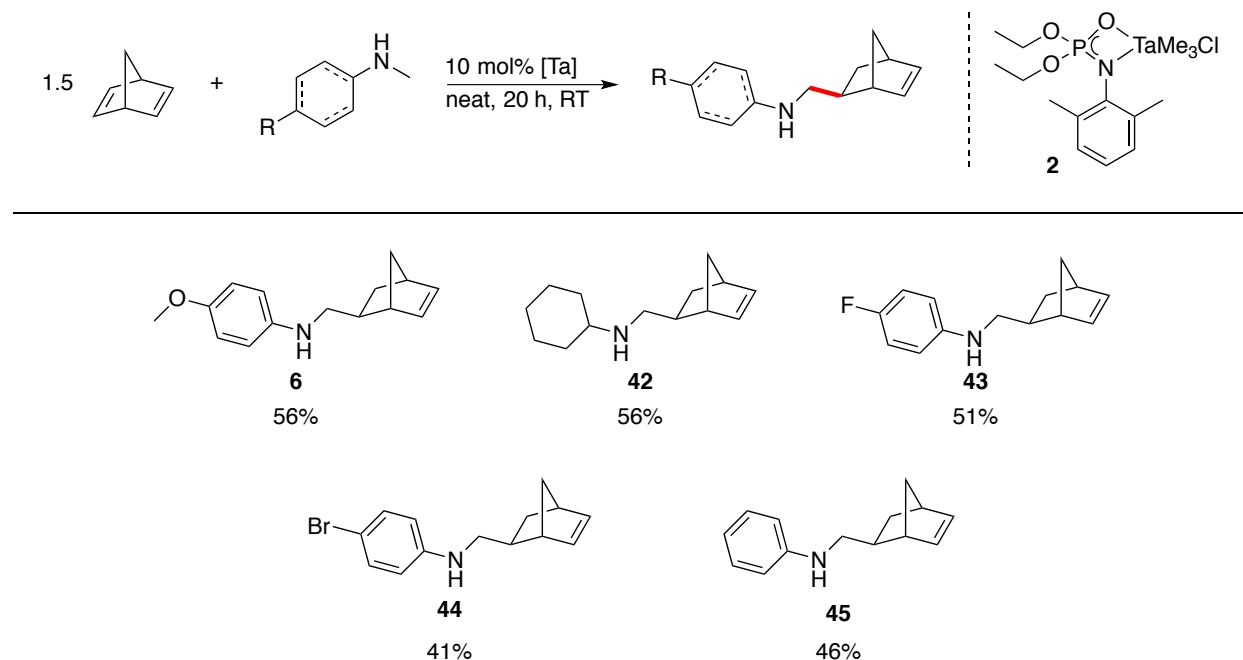


Figure 53 Room temperature HAA generates mono-functionalized aminonorbornenes in one step

Purification of all aryl-substituted products, **6** and **43-45** listed in Figure 53 was conducted *via* column chromatography (hexanes/ethyl acetate) to afford the products as colourless or yellow oils after drying *in vacuo*. Alkyl-substituted product **42** was easily purified by isocratic elution using a hexanes/triethylamine mixture (14:1) to remove tantalum salts and residual ligand. All reactions listed above were found to be diastereoselective. The diastereomer was determined to be the *exo*-product by comparing ^1H NMR and GC-MS data to previously isolated compound **11** (Figure 23 and Figure 50). In the case of *para*-bromo substituted NBE product **44**, yields are reduced due to the formation of what is believed to be polyaniline or polyaniline-like products formed by the homopolymerization of the amine starting material. After HAA to form *para*-brominated product **44** was completed, large amounts of solid material

were removed *via* filtration and could not be identified due to poor solubility in common organic solvents. The mixture was then purified by column chromatography (10:1 hexanes/ethyl acetate) to afford **44** as a yellow oil in 41% yield. The synthesis of this small family of compounds by HAA allowed for the comparison between aryl- and alkyl-substituted substrates in ROMP. Furthermore, the varying substitution of these aryl-substituted monomers allowed for direct comparisons between these monomers. The polymerization reactivity of these molecules is discussed in the following sections.

3.4 Aminonorbornenes in Ring-Opening Metathesis Polymerization

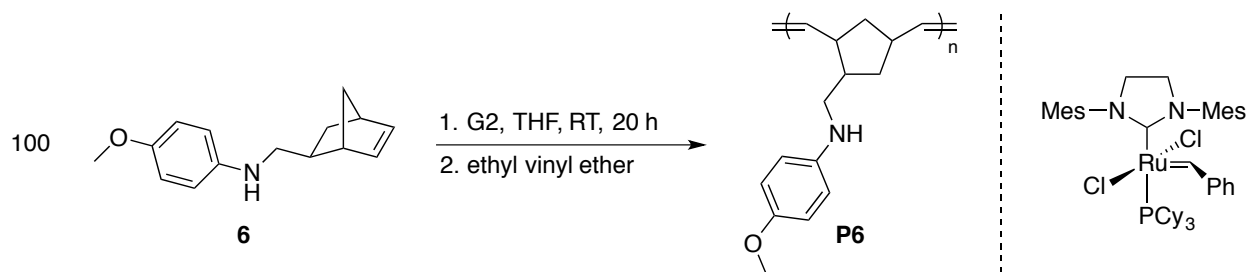
3.4.1 Polymerization of Aminonorbornene Monomer **6 with G2**

The HAA of NBD with a variety of secondary amines yielded facile access to monoalkylated, strained internal alkene products. While these products contain a large amount of ring strain, the driving force for ROMP, the potential incompatibility of the unprotected amine group with ruthenium alkylidenes could lead to hampered reactivity. Previous literature describes several failed attempts at polymerizing unprotected primary and secondary amines, with the reaction proceeding only if protection of the Lewis-basic amine moiety was conducted.^{43, 64, 126-}

¹²⁸ Of course, such amine protection routes could be adopted, if required, as HAA affords the efficient syntheses of these monomers relative to other traditional approaches.

Initial investigations into the polymerization of the secondary amine substituted-norbornene compound **6** were conducted using conditions modified from the literature that describe the polymerization of amino acid-derived monomers. These compounds require extended reaction times of 20 hours to reach full conversion.¹³³ Specifically, commercially available G2 was chosen as the initiator. The methoxy-substituted NBE substrate (**6**, 100 eq.)

was added to a vial containing a magnetic stir bar before THF was added (anhydrous, 1 mL) to dissolve the oil. A solution of G2 was added to the stirring mixture of monomer and was left to react overnight. After 20 hours, ethyl vinyl ether (5 eq.) was added and the mixture was let stir for 30 min to quench the polymerization. The resultant solution was added to a vortex of cold hexanes (xs, 100 mL) to generate a white precipitate, **P6**, that could be isolated *via* gravity filtration and dried *in vacuo* (quantitative yield, >95%) (Scheme 21).



Scheme 21 Polymerization of monomer **6** to form the respective polymer, **P6**

The precipitated product was analyzed by ^1H NMR spectroscopy (CDCl_3 , 300 MHz, 298 K) after drying *in vacuo* overnight. Figure 54 shows a stacked plot of the monomer, **6**, (bottom) and polymer, **P6**, (top). The disappearance of monomer olefinic peaks at 6.1 ppm was observed (blue circle, bottom) and new olefinic resonances of product appeared at 5.3 ppm (blue circle, top). The broad olefinic resonance is consistent with a *trans* bias, which appears further downfield relative to the *cis* arrangement, as reported for NBE polymers synthesized from G2,³⁷⁰ although the overlapping resonances and downfield shoulder complicated definitive integration.¹⁰⁵ Furthermore, broadening of aryl resonances of **6** (green circle, bottom) relative to those of the **P6** (green circle, top) is a telling characteristic of polymeric material. This broadening of signals is present across the entire polymer spectrum (top).

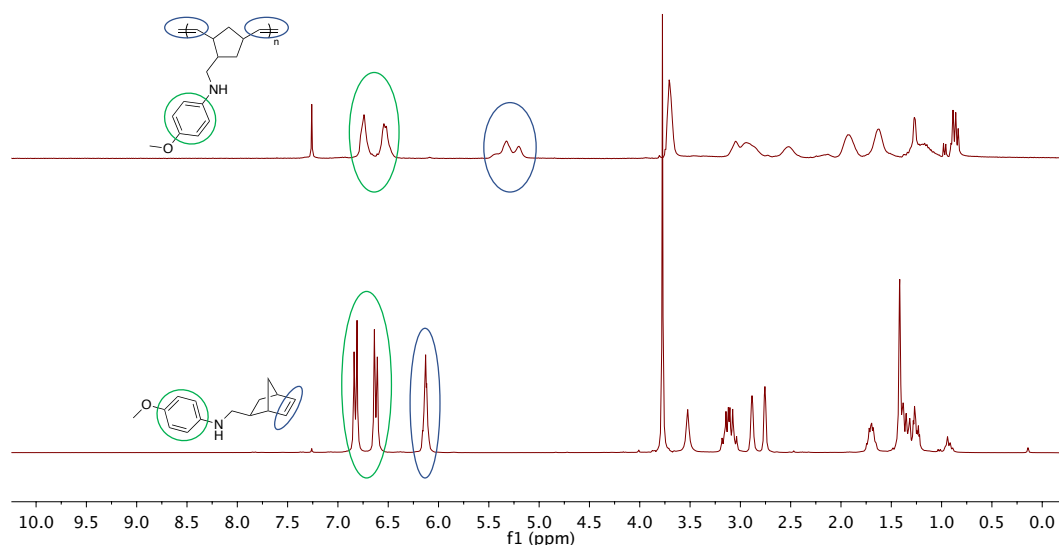


Figure 54 ^1H NMR overlay of monomer, **6**, (bottom) and polymer, **P6**, (top) (CDCl_3 , 300 MHz, 298 K)

The product was also analyzed by IR spectroscopy (ATR) and showed N-H stretching frequencies at 3395 cm^{-1} . Perhaps most convincing are the results of gel permeation chromatography (GPC). The experimental molecular weight (M_n) of this polymer was found to be $25,800\text{ g mol}^{-1}$, which is in good agreement to the theoretical value of $22,900\text{ g mol}^{-1}$ (monomer $\text{MW} \times [\text{M}:\text{I}]$). A low dispersity of 1.07 was also observed, indicating a well-controlled polymerization. MALDI-TOF mass spectrometry gave results consistent with the monomer repeat unit (229 g mol^{-1}) and phenyl and methylene end groups (see Appendix B for spectra), although these were not visible by ^1H NMR spectroscopy due to overlapping aryl-resonances. Furthermore, MALDI-TOF was not found to be an appropriate method to analyze these samples for molecular weight, as aggregation through hydrogen bonding undoubtedly leads to difficulties in the ionization and detection processes.

To discover the optimal reaction time for polymerization, the conversion of **6** to **P6** was monitored in real time using ^1H NMR spectroscopy with a sealed, J. Young NMR tube using THF- d_8 as the solvent. Specifically, monomer **6** (100 eq.) was dissolved in 0.5 mL THF- d_8 . A solution of G2 (1 eq., 0.5 mL THF- d_8) was added to the NMR tube *via* pipette. The solution was added to a J. Young NMR tube, the vessel was sealed, immediately removed from the glovebox, and frozen using liquid nitrogen. The solution was let warm to room temperature in the spectrometer before data acquisition began. Figure 55 shows conversion, determined by the relative integrations of monomer resonances at 6.1 ppm to polymer resonances at 5.3 ppm, relative to time.

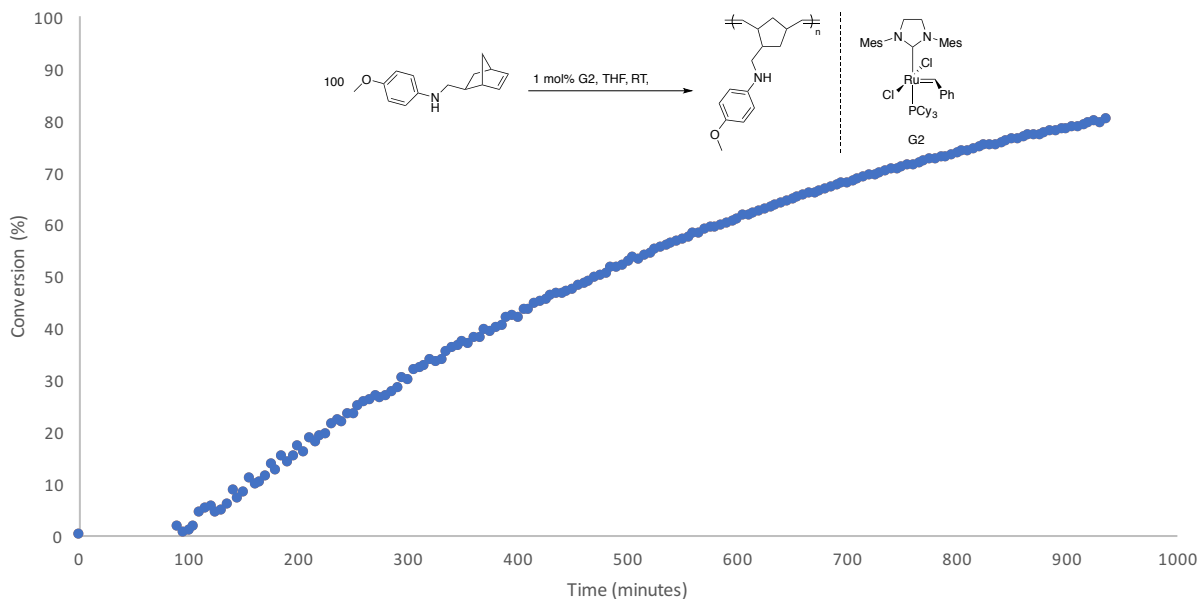


Figure 55 Real-time monitoring of monomer conversion of **6** with G2 as observed by ^1H NMR spectroscopy (600 MHz, THF- d_8 , 298 K). At time 0 min the sample was at $-196\text{ }^\circ\text{C}$

The initial period of inconsistent temperature gave high signal-to-noise ratios and led to inaccurate integration of signals as the reaction mixture warmed to room temperature inside the spectrometer. Furthermore, the conduction of this experiment in an NMR tube potentially prevented effective propagation due to lack of adequate mass transfer. Therefore, no data is presented for the first *ca.* 100 minutes of this monitoring process. This graph shows that full conversion of the feedstock was sluggish and consistent with the other free amine-containing monomers.¹³³ Interestingly, no polymerization was observed under these conditions while using G1, potentially due to this catalyst's more rapid initiation and irreversible coordination of the amine group to the ruthenium species. Regardless, the polymerization of **6** with G2 was an unexpected discovery and led us to further investigate the efficacy of this transformation.

Armed with these insights into the progress of the polymerization reaction with monomer **6**, we were curious to see if we could synthesize polymers with variable molecular weights. Analogous polymerization was conducted using monomer-to-initiator ratios (M:I) from 20 to 1000 (Table 11). All polymerizations were conducted using a monomer concentration of 0.1 mg/mL. The quantity of G2 was kept consistent to minimize error associated with weighing less than 5 mg of catalyst. Monomer quantities were varied to produce the desired M:I values and the volume of solvent was adjusted accordingly. Values listed in Table 11 represent average values of triplicate experiments.¹⁰⁵

Table 11 Polymerization data for monomer 6

Entry ^a	M:I ^b	% Yield ^c	M_n (g mol ⁻¹) ^d	DP ^e	\bar{D} ^f
1	100	>95	25,800	113	1.07
2	20	>95	4,300	19	1.19
3	50	>95	11,100	49	1.04
4	200	>95	51,200	223	1.08
5 ^g	1000	40	91,500	399	1.04
6 ^h	1000	40	108,200	471	1.01

^aValues represent averages of triplicate experiments. All experiments were conducted in Teflon-sealed, 20 mL scintillation vials at room temperature. All reactions were conducted using a monomer concentration of 0.1 mg/mL. ^bMonomer-to-initiator ratio. ^cCalculated from gravimetric analysis. ^dDetermined by GPC using dn/dc values calculated by 100% mass recovery methods. ^eDegree of polymerization = M_n /MW g mol⁻¹. ^fDispersity = M_w/M_n . ^gReaction performed in duplicate. ^hSingle reaction performed in chloroform.

Various M:I ratios were chosen to generate polymeric materials, **P6**, having a breadth of molecular weights. Good levels of control were achieved for M:I values up to 200 (Entry 4). Values of \bar{D} remained under 1.2 for these ratios and good agreement between theoretical and expected DP values was observed. Interestingly, when M:I values were increased to 1000:1 (Entry 5) the percent yield decreased to 40%. Experimental M_n values (obtained from GPC analysis) were limited to approximately 100 kg mol⁻¹, although \bar{D} remained low (1.04). No significant increase in MW was achieved when the polymerization was conducted using chloroform (Entry 6) to increase the solubility of the growing polymer chain and promote efficient initiation in a non-coordinating solvent.⁵³ Increased MW values could not be achieved at longer reaction times (40 h). It is plausible that the propagation is hindered by the increased amine loading present in these reactions (1000:1), potentially a result of the coordinating amine moieties sequestering the catalyst upon increased monomer conversion. Nevertheless, the

synthetic protocol invoked and the unique class of monomers used above allowed access to polymers bearing unprotected secondary amines from ROMP using conventional ruthenium initiators. Importantly, these macromolecules could be generated in two synthetic steps, HAA and ROMP, from commercially available substrates to afford new-to-the-world materials with unbroached potential.

The isolated polymeric materials display a change in colour over time. Leaving a solution of **P6** in CDCl₃ at room temperature, overnight, resulted in a discolouring of the mixture from colourless to dark brown. No precipitation was observed over this time. This behavior was also observed with lower molecular weight amines, including the monomer. Changes in colour were observed when the macromolecules were stored in the solid-state, albeit at seemingly lower rates (*ca.* 7 days). However, the polymers remain intact overtime despite this colour change, as evidenced from consistent MW determination by GPC analysis. Polymers retained similar molecular weights over a period of approximately 12 months. A sample of $M_n = 29,320 \text{ g mol}^{-1}$ was stored in the solid-state for approximately 1 year. The colour changed from off-white to dark brown. Despite this visual change, molecular weight remained consistent ($M_n = 30,260 \text{ g mol}^{-1}$) indicating no secondary metathesis and/or chain scission had occurred. We attribute this colour change to the unwanted oxidation of the amine moiety.

3.4.2 Polymerization of Aminonorbornene monomer 6 with G3

The sluggish reactivity of G2 towards the secondary aryl-amine monomers discussed in previous sections led us to explore other catalysts for this transformation. The long reaction times required to reach full conversion are potentially due to the initiation rates of G2. G3 is

known for its fast rate of initiation, up to a million-fold greater than G2,⁶⁰ and was explored to try and circumvent this sluggish reactivity.

Methoxy-substituted monomer **6** was subjected to the standard polymerization conditions. The reaction was conducted in a sealed J. Young NMR tube using 100 eq. of monomer **6**, G3, and 1 mL THF-d₈. The reaction progress was monitored by ¹H NMR spectroscopy. Figure 56 displays the reaction progress at various times. Surprisingly, the reaction progress when G3 was used was observed to be more sluggish relative to G2 (Table 12). It takes approximately 8 hours to reach 50% conversion (Entry 7) and approximately 30 h for the monomer to be over 90% consumed (Entry 7).

Table 12 Polymerization data for monomer 6 using G3

Entry^a	Time (h)	Conversion (%)^b
1	0	1.1
2	1	9.9
3	2	17.4
4	3	24.2
5	4	29.1
6	6	42.5
7	8	51.7
8	12	66.7
9	24	87.4
10	27	90.8
11	30	92.1

^aReactions carried out in a sealed J. Young NMR tube at room temperature in THF-d₈. Spectra were recorded on a 400 MHz spectrometer. Total reaction concentration was 0.1 g/mL with respect to monomer. ^bDetermined by ¹H NMR spectroscopy.

Central to this problem is undoubtedly the presence of the nucleophilic amine complicating efficient propagation of the olefin. Seemingly, this hindrance is magnified by the rapid dissociation of the labile pyridine ligand of G3 allowing the reversible interaction with the nucleophilic amine substrate to occur more readily than G2, thereby slowing propagation.

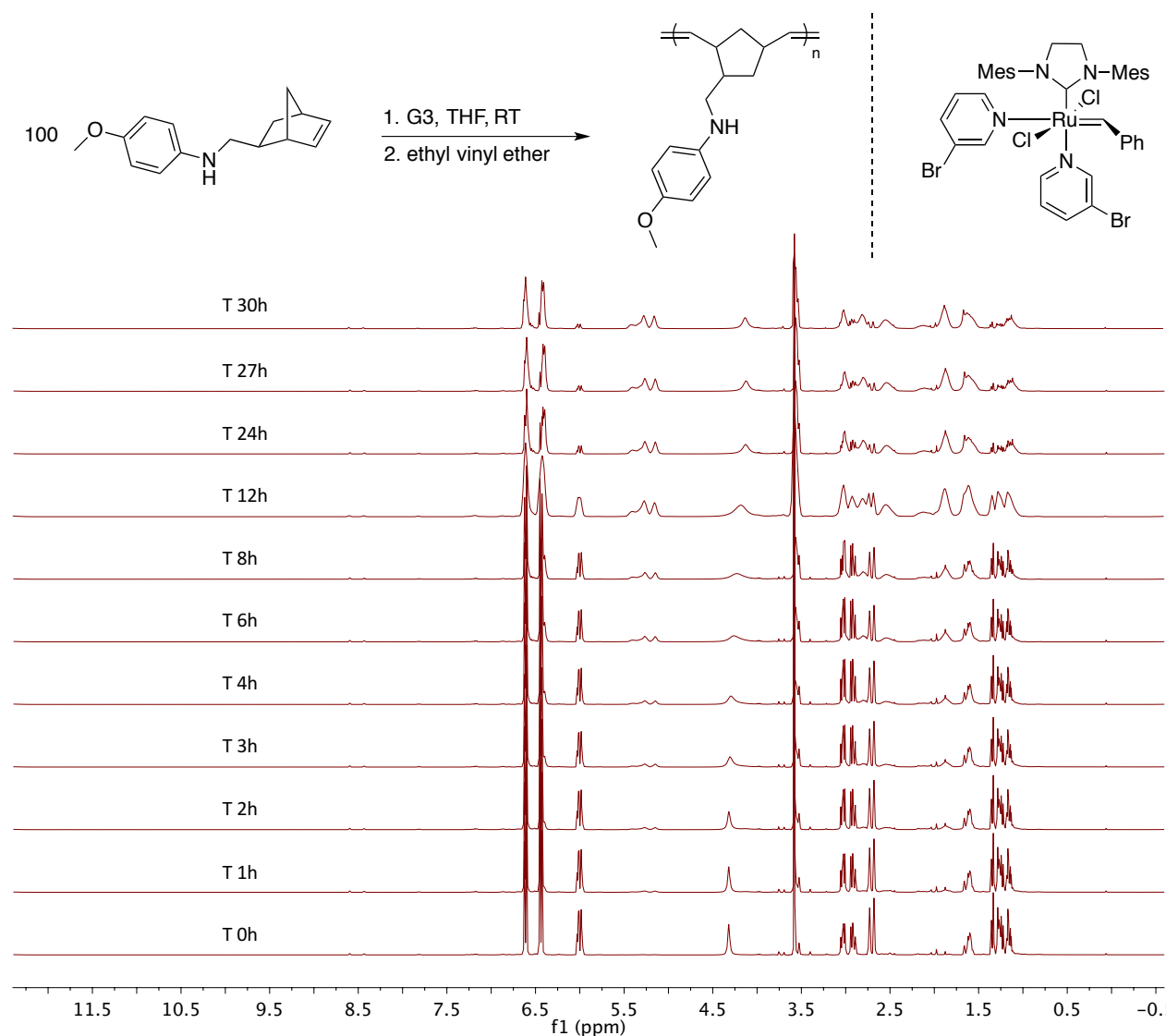


Figure 56 Conversion of monomer 6 to P6 with G3

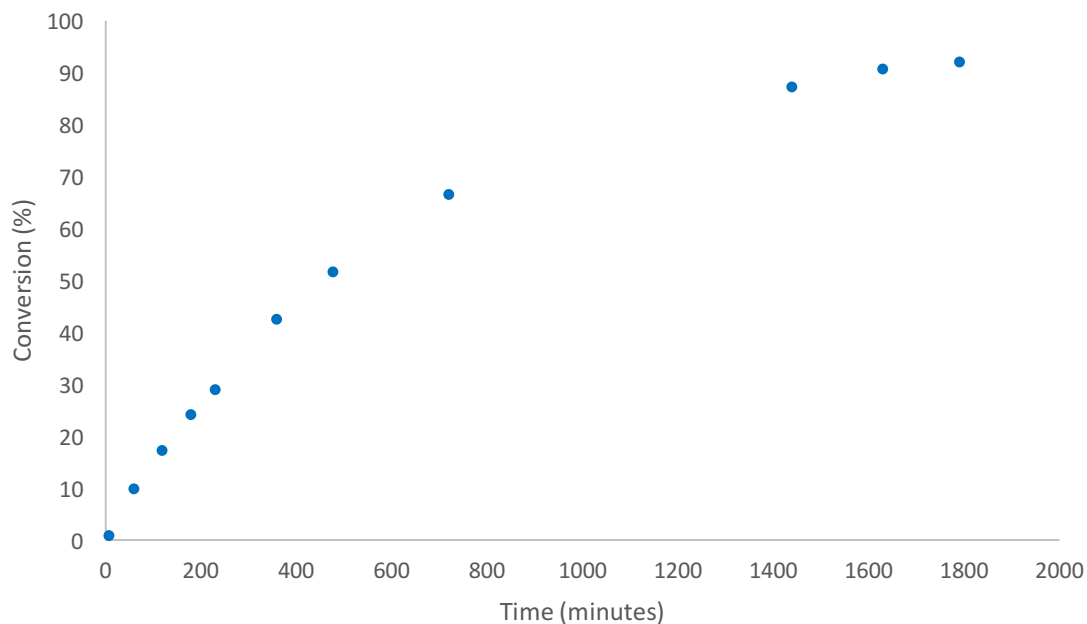


Figure 57 Conversion of monomer 6 to P6 using G3 as determined by ^1H NMR spectroscopy (400 MHz, THF-d_8 , 298 K)

Upon full conversion of monomer (~30 h), the polymerization was quenched with ethyl vinyl ether (2 drops) and the mixture was added to a vortex of cold methanol to precipitate the polymer. The white solid, **P6**, was collected in 71% yield after drying *in vacuo*. GPC analysis on the white solid gave an M_n value of 32,900 g mol^{-1} and a D of 1.14.

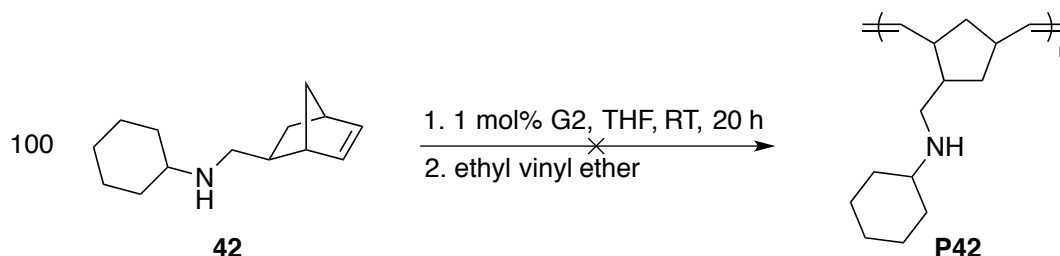
G1 was not successful in polymerizing these secondary amine substrates under the same conditions (RT, 20 h, M:I = 100:1). Analysis by ^1H NMR spectroscopy showed no conversion of **6** to its polymeric form. Presumably, the fast initiation of G1 relative to G2 allows for the coordination of the amine and low levels of catalytic activity are insufficient to facilitate monomer conversion. G2 is known to be a slower catalyst in terms of its initiation rate *vs.* G1.

G2 is undoubtedly affected by the coordinating amine groups, as evidenced by the sluggish conversion of monomer. However, propagation occurs and polymeric materials with high levels of control are obtained. Interestingly, when G3 (a catalyst with an initiation rate 6 orders of magnitude greater than G1) is used, the reaction proceeds, although consumption of monomer is slow and full conversion requires *ca.* 30 hours at room temperature. These results indicate that judicious choice of catalyst is imperative to generate amine-containing polymers using Grubbs catalysts. Fast initiation is not the determining characteristic of whether amine-containing monomers will produce polymer (*ie.* G2 outperforms G1), and otherwise rapidly propagating catalysts (G3) do not necessarily lead to increased conversion profiles (*ie.* G3 is more sluggish than G2). The interplay between these steps is important to consider, as the coordinating amine group interferes with the polymerization progress. The reversible coordination events ultimately lead to polymeric material with predictable MW and low *D* values, although reaction times are long.

3.4.3 Attempted Polymerization of Alkyl-Substituted Substrate, **42**

With these promising preliminary results of aryl-substituted polynorbornene, **P6**, in hand, we were curious to see if cyclohexyl amine-substituted substrate **42** would also be susceptible to ROMP under our established conditions (Scheme 22). The analogous reaction using **42** was conducted. After 20 hours, the mixture was quenched and added to a vortex of cold hexanes. No polymer formation was observed in the ¹H NMR spectrum and no isolable material could be obtained by precipitation. This result was unsurprising as strongly nucleophilic substrates, such as primary and secondary amines, are known to inhibit ruthenium-catalyzed ROMP.¹²⁶⁻¹²⁷ The success of aryl-substituted amine **6** is likely due to the reduced nucleophilicity of this amine

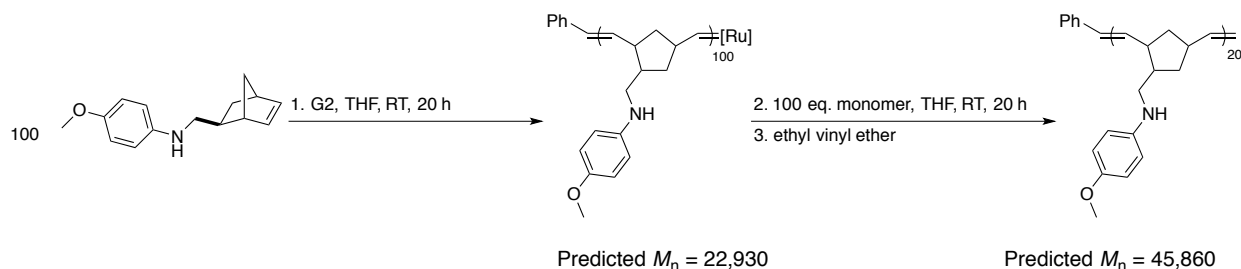
group. Of course, one way to circumvent this is by the addition of steric bulk by converting the substrate to a tertiary amine. An investigation into the polymerization of monomers bearing tertiary amines will be discussed in subsequent sections of this thesis.



Scheme 22 Attempted polymerization of cyclohexyl-substituted norbornene, 42

3.4.4 Living Polymerization of Secondary Amine-Containing Monomers

The low \bar{D} and predictable DP values presented in Table 11 imply that the ROMP of unprotected secondary aryl amines is living in nature. One characteristic feature of a living polymerization is the ability of the propagating species to stay active in the absence of feedstock. Thus, upon addition of a second aliquot of monomer, the polymerization is revived and can continue to propagate until deliberate termination, and will generate a polymer of higher molecular weight.^{24, 29}



Scheme 23 Living polymerization of monomer 6 with G2. Propagation continues upon a second aliquot of 6

Two parallel reactions were conducted to further probe the living character of this reaction. In both cases, 100 eq. of monomer **6** were dissolved in THF, before being added to a vial containing G2 (1 eq.). After 20 hours, one vial was quenched with ethyl vinyl ether. The product was precipitated from cold hexanes and analyzed by GPC. The second reaction was subjected to another 100 eq. of monomer **6** and left to stir for an additional 20 hours. After this time, the polymerization was quenched with ethyl vinyl ether, the product was precipitated from cold hexanes and analyzed by GPC (Table 13). In both cases, low dispersities are observed as well as high yields. The DP is in good agreement with expected values.

Table 13 Living polymerization data for monomer 6

Entry ^a	Time (h)	Total eq. M1	Yield (%) ^b	M_n (g mol ⁻¹) ^c	DP ^d	\bar{D} ^e
1	20	100	94	28,450	124	1.05
2	20 + 20	100+100	>95	48,700	212	1.07

^aTwo parallel reactions were conducted in 20 mL scintillation vials in THF (M:I = 100:1, 0.1 g/mL). After 20 h, vial 1 was quenched with excess ethyl vinyl ether. An additional 100 eq. of monomer in THF (0.1 g/mL) was added to vial 2 and the reaction was let stir for an additional 20 h before being quenched. ^bCalculated from gravimetric analysis. ^cCalculated by GPC using dn/dc values from 100% mass recovery methods. ^dDegree of polymerization = M_n/MW g mol⁻¹. ^eDispersity = M_w/M_n .

Living polymerization is also defined by a linear increase in MW with respect to conversion. The progress of the conversion of monomer to polymer was also studied by setting up parallel reactions and quenching them at predetermined times (Table 14). Conversion to product **P6** could be easily obtained from ¹H NMR spectroscopy of the crude mixtures and GPC analysis of the purified polymers gave insights into chain lengths and dispersity of the species obtained at various time points. Specifically, approximately 100 mg of **6** was added to a 20 mL scintillation vial. The appropriate quantity of G2 (~4 mg) was dissolved in 1 mL THF-d₈ before

being added to the monomer. The mixture was allowed to stir for the desired amount of time before being quenched by the addition of an excess of ethyl vinyl ether. Conversion of monomer to product could be obtained using ^1H NMR spectroscopy by comparing relative integrations of the respective olefinic regions (as in Figure 54). Data for reaction times less than 5 hours were difficult to obtain, as the lower molecular weights at these times made isolation of the product difficult. These data are consistent with the preliminary results from *in situ*, real-time monitoring by ^1H NMR spectroscopy presented in Figure 55.

Table 14 Polymerization data for monomer 6 at various times

Entry ^a	Time (h)	Conversion (%) ^b	$M_{n, \text{th}}$ ^c	$M_{n, \text{exp}}$ (g mol ⁻¹) ^d	\bar{D} ^e
1	5	26	5,962	8,615	1.10
2	10	51	11,633	13,080	1.08
3	15	70	16,052	16,870	1.06
4	20	80	18,346	20,050	1.07

^aAll reactions were conducted in Teflon-sealed, 20 mL scintillation vials at room temperature for 20 h and a monomer concentration of 0.1 mg/mL. M:I = 100:1. ^bDetermined by ^1H NMR spectroscopy. ^cMonomer MW×M:I×conversion. ^dDetermined by GPC using dn/dc values calculated by 100% mass recovery methods. ^eDispersity = M_w/M_n .

It was observed that the physical morphology of the polymers was different as conversion increased. Lower conversions produced a more flocculent, powder-like material, whereas higher conversions (and higher molecular weights) gave larger, more coagulated, species that were more easily isolable once precipitated using hexanes. Figure 58 displays a near-linear increase in molecular weight with increasing conversions, in good agreement with the ^1H NMR experiment discussed above, indicating that the consumption of monomer is contributing to increasing the molecular weight of propagating chains. This observation is consistent with addition-type

polymerization mechanisms. Furthermore, M_n values of **P6** increased as expected while maintaining a low dispersity throughout the reaction, as depicted in Figure 59.

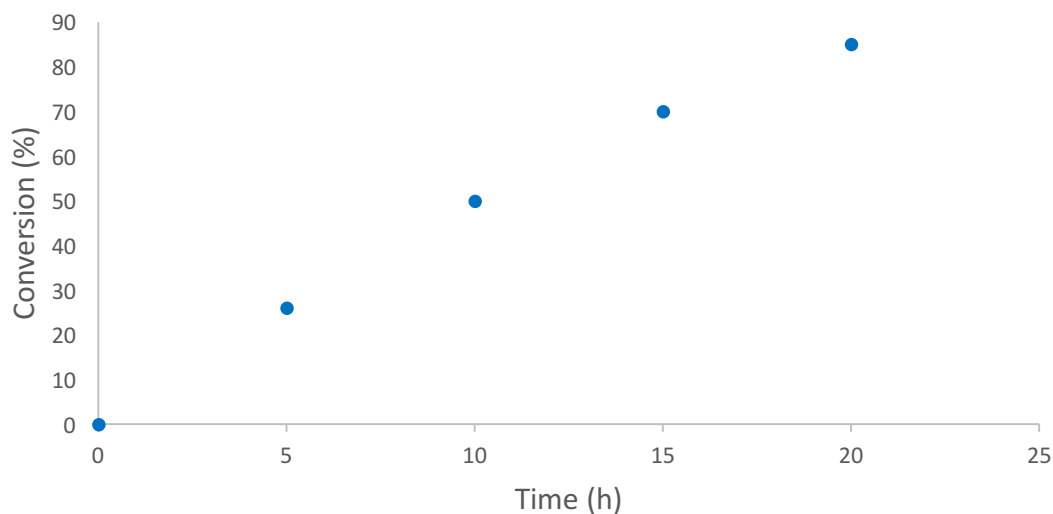


Figure 58 Conversion (%) of monomer 6 to P6 over time (h) using G2

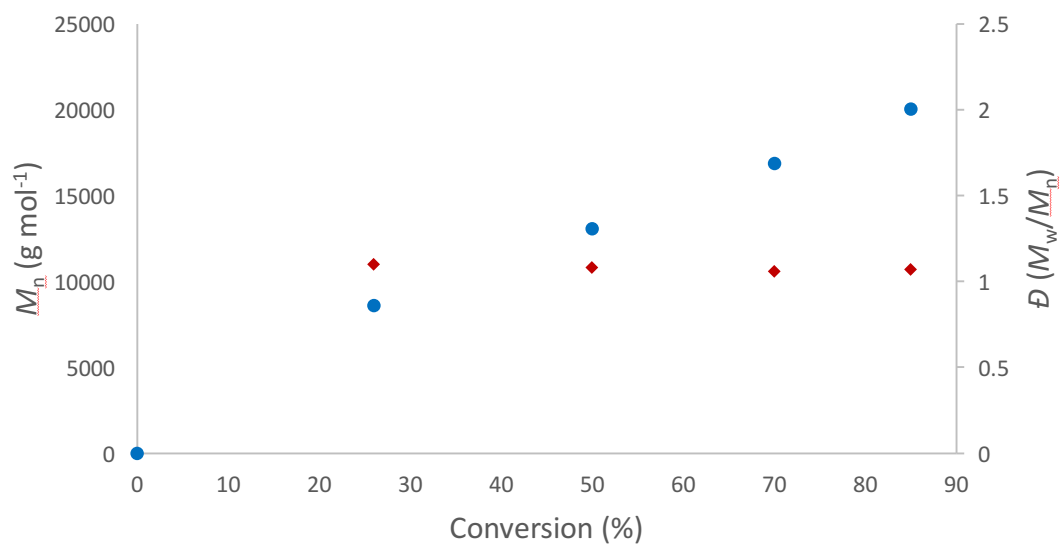


Figure 59 Molecular weight (blue) (M_n , g mol⁻¹) and dispersity (red) (M_w/M_n) vs. conversion (%) of 6 to P6

The successful polymerization of monomer **6** leading to methoxy-substituted polymers allowed us to gain insight into the reaction profile of this monomer. Surprisingly, the sluggish reactivity of this monomer still allowed for polymeric material having low *D* levels. Next, we decided to explore the synthesis of variously-substituted amine-containing monomers to observe potential differences in their reactivity towards G2, and to furnish a family of amine-containing polymers with hopes of accessing polymeric materials with differing properties dictated by the substitution about the aryl ring. The following section describes these efforts.

3.5 Expansion of Polymer Scope: Polymerization of Aryl-Substituted Monomers

The promising results obtained with monomer **6** inspired us to polymerize the other aryl-substituted monomers **43-45** discussed above. Using our optimized conditions, we subjected 100 eq. of the desired aryl-substituted monomers to G2 (1 eq.) in THF (0.1 mg/mL). After reacting for 20 hours the mixtures were quenched with ethyl vinyl ether, let stir for a minimum of 30 min, and product was precipitated using an excess of cold hexanes (Figure 60).

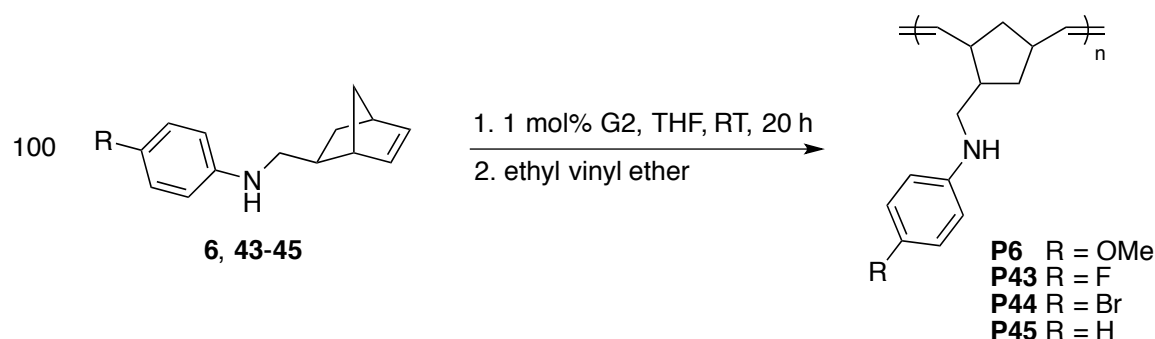
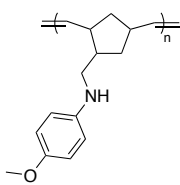
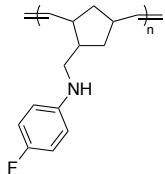
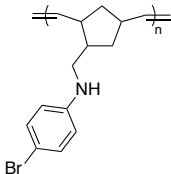
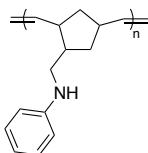


Figure 60 Polymerization of aryl-substituted aminonorbornene monomers **6** and **43-45**

Gratifyingly, all polymerization attempts with aryl-substituted monomers were successful, resulting in white or off-white polymers after precipitation and filtration. Again, these

polymers displayed the same discolouration in the solution-state, with once colourless solutions turning dark over time. Table 15 details the polymerization data obtained for these polymers (**P6** and **P43-P45**). In all cases the experimental molecular weight (from GPC) is in good agreement with theoretical values. These numbers differ in the polymers synthesized due to the different molecular weight values of the respective monomers. DP values agree close with those expected, determined by the M:I ratio (100:1), and indicates high levels of molecular weight control (*i.e.* DP agrees closely with M:I). As before, low levels of dispersity are obtained. Most pleasingly, the polymerization reactions between the specific monomers give consistent molecular weight and dispersity data, as well as quantitative isolated yields.

Table 15 Polymerization data for monomers 6 and 43-45 to form P6 and P43-45

Entry ^a	Repeat Unit	Yield (%) ^b	M_n (g mol ⁻¹) ^c	DP ^d	\bar{D} ^e
1		>95	24,230	106	1.09
2		>95	24,750	108	1.08
3		>95	28,450	124	1.05
4		>95	21,530	101	1.04
5		>95	19,730	91	1.06
6		>95	30,800	110	1.14
7		>95	29,860	107	1.06
8		>95	18,620	93	1.12
9			19,410	97	1.09

^aAll reactions were conducted in Teflon-sealed, 20 mL scintillation vials at room temperature for 20 h and a monomer concentration of 0.1 mg/mL. M:I = 100:1. ^bCalculated from gravimetric analysis. ^cDetermined by GPC using dn/dc values calculated by 100% mass recovery methods. ^dDegree of polymerization: M_n/MW g mol⁻¹. ^eDispersity = M_w/M_n .

These materials have the potential to have different properties depending on their substitution pattern, particularly with respect to their H-bonding potential. An in-depth investigation into the rheological properties of these polymers is discussed in Section 3.10 (*vide infra*, page 160).

3.6 Aminocyclooctene Monomer Synthesis by Hydroaminoalkylation

The success of polymerization of monomers **6** and **43-45** led us to investigate other monomers. Of interest were those that provide more flexible, linear backbones once ring-opened, as these more closely resemble polyethylene. The ‘amphiphilic’ nature of such nitrogen-containing polymers could provide access to applications as compatibilizers for hydrocarbon polymers (polyethylene, polypropylene, etc.) with more polar polymers (Nylon, polyurethane, etc.).³⁷¹

The diene used in HAA was changed to COD. Specifically, the products of HAA between COD and *N*-methylaniline or 4-methoxy-*N*-methylaniline were targeted. While the former product, **46**, has been described in a previously reported publication from the Schafer Group using a tantalum amidate complex,²³⁴ we opted to expand the substrate scope of the tantalum phosphoramidate complex, **2**, to include the 8-membered cyclic diene. Formation of these products (**46** and **47**) was realized in moderate to good yields following a modified HAA procedure. It was found that increasing the temperature to 70 °C and using 5 equivalents of diene led to improved formation of the desired mono-alkylation products (Figure 61). As with the NBD-derived monomers, COD-derived monomer synthesis proceeded both neat and in the solution phase. Isolated yields ranged from 45-75% for these monomers. A full optimization for monomer **47** was not performed.

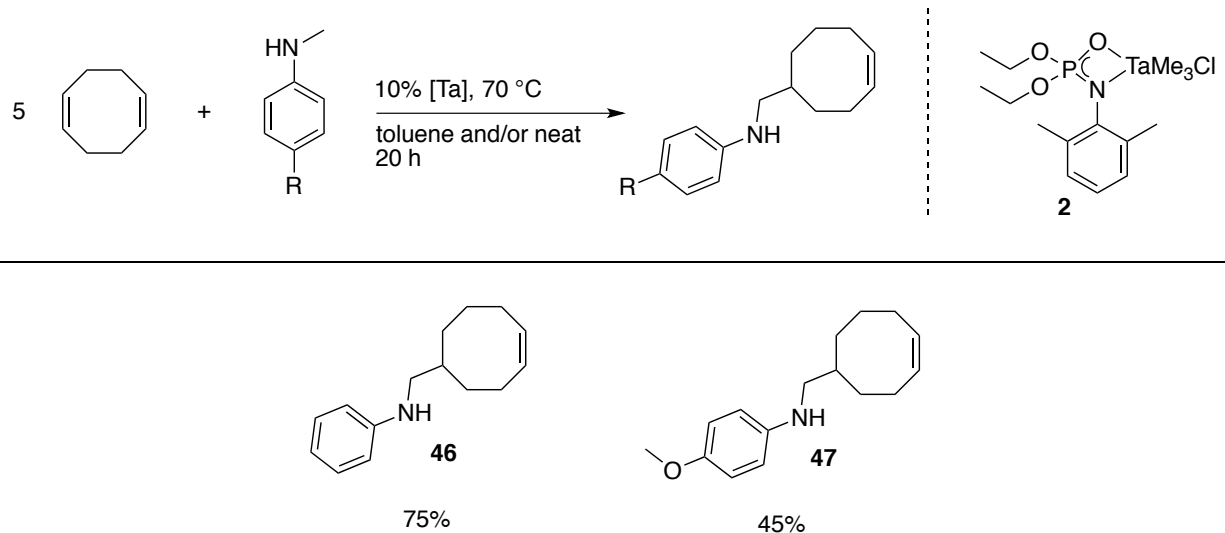


Figure 61 Formation of aminocyclooctene monomers **46** and **47** *via* HAA

Both COD-derived monomers, **46** and **47**, were isolated *via* column chromatography (hexanes/ethyl acetate 10:1) as pale yellow or colourless oils. ¹H NMR spectroscopic analysis of both compounds revealed the expected olefinic resonances between 5.8 and 5.6 ppm (Figure 62, yellow circles). Monomer, **47**, (top) displays a sharp singlet at 3.8 ppm (top, green circle) of the methoxy methyl group. The aniline-substituted monomer, **46**, (bottom) displays a sharp triplet assigned to the *p*-Ar proton of the amine moiety (bottom, red circle). Both spectra display a broad singlet of the N-H group at 3.3 (top, purple circle) and 3.7 ppm (bottom, purple circle).

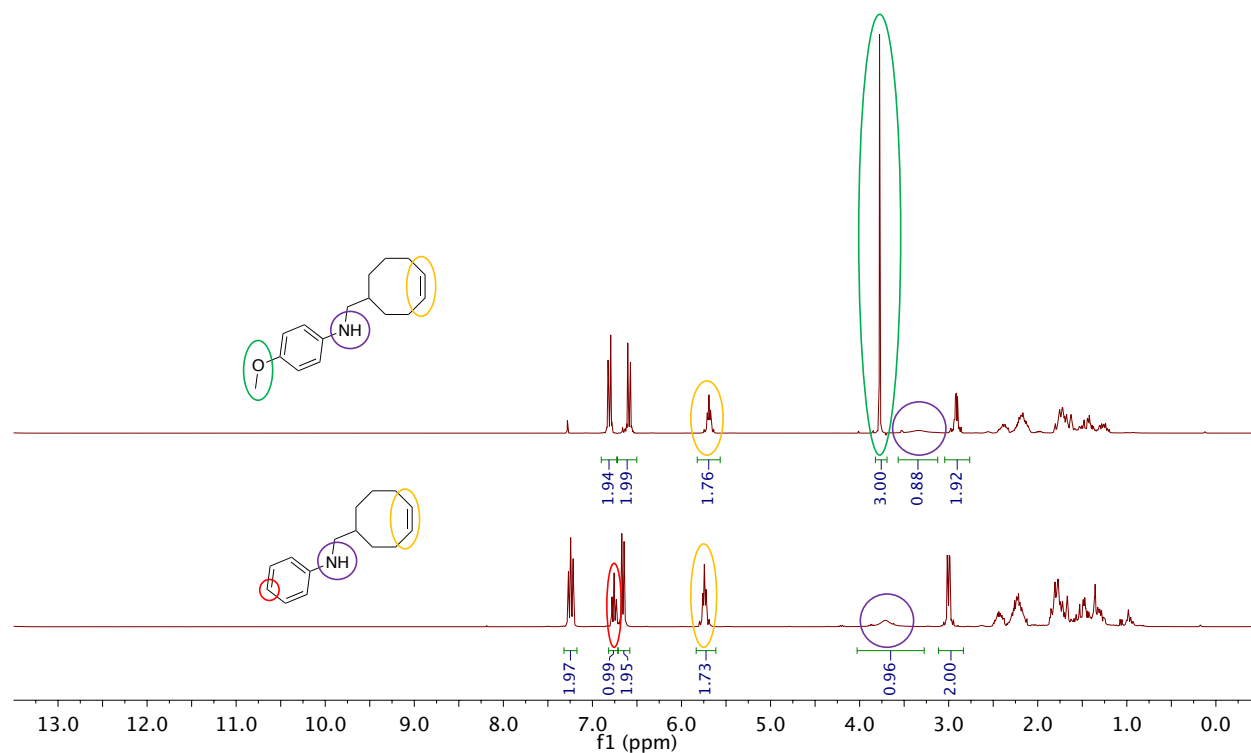


Figure 62 ^1H NMR spectra (CDCl_3 , 300 MHz, 298 K) of cyclooctene monomers **46** (bottom) and **47** (top)

Compound **47** was analyzed by HRMS and gave the experimental value of 246.1855 m/z (calcd; 246.1858 m/z). All other characterization is in good agreement with expected values. All characterization of monomer **46** agreed with published values.²³⁴ The polymerization behavior of these monomers was analyzed using G2 for direct comparison to the aminonorbornenes discussed above. These investigations are highlighted in the following section.

3.7 Ring-Opening Metathesis Polymerization of Aminocyclooctenes

Investigations into the polymerization of aminocyclooctene monomers **46** and **47** began by subjecting these monomers to the conditions established for the NBE derivatives (discussed

previously). Delightfully, these cyclic aminocyclooctenes, **46** and **47**, could be polymerized using G2 (1:100 M:I) and yielded off-white polymers **P46** and **P47**, respectively, in good yields (92 and 76%, respectively) after precipitation and extensive washing using cold methanol. Analysis of the polymers by ^1H NMR spectroscopy revealed that these cyclooctene-based monomers show an unsurprisingly strong *trans* bias of approximately *ca.* 86% based on the relative integrations of resonances at 5.39 (*trans*) and 5.35 (*cis*). These polymers were found to be much easier to precipitate and isolate relative to the NBE-homologues, presumably due to the increased propensity for these flexible long chains to associate more closely to each other in comparison to the NBE-based polymers. The polymers could be removed from the supernatant without the need for gravity filtration. Instead, the mother liquor could be easily decanted to allow for facile isolation of the solid material.

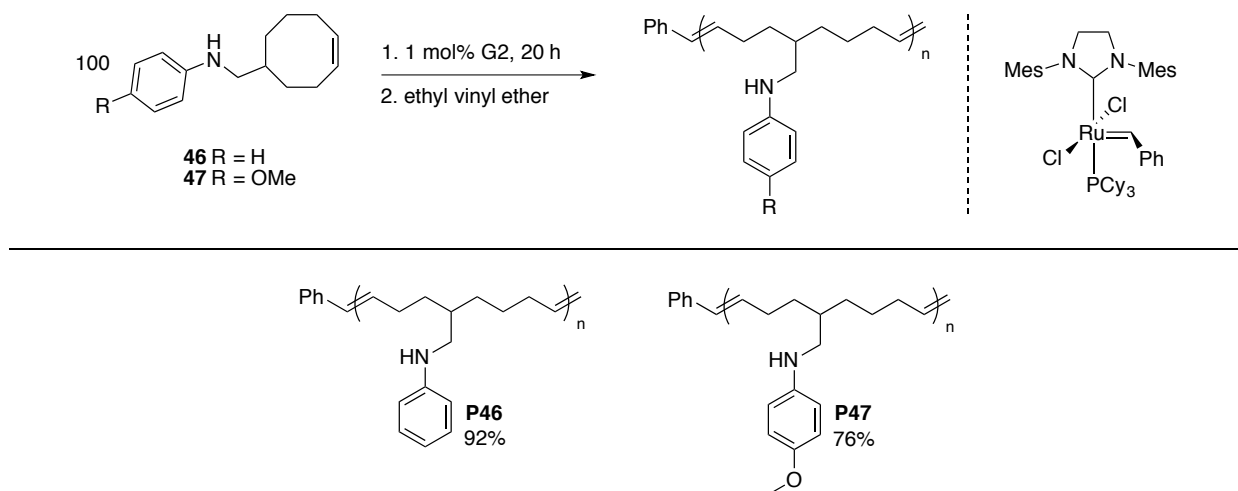


Figure 63 ROMP of aminocyclooctene monomers **46** and **47** to form **P46** and **P47**, respectively

Characterization of these polymers, **P46** and **P47**, by ^1H NMR spectroscopy revealed similar broadening of resonances as displayed in the case of aminonorbornene polymers discussed previously, indicating polymeric material. Resonances of the olefinic groups of each

polymer are observed between 5.5 and 5.3 ppm (Figure 64, blue circles). The NH group, observed at 3.7 ppm for **P46** (bottom, purple circle) and confirms the presence of secondary amino groups in the polymeric material. This resonance is overlapped by the methoxy methyl group at 3.7 ppm in **P47** (top, green circle).

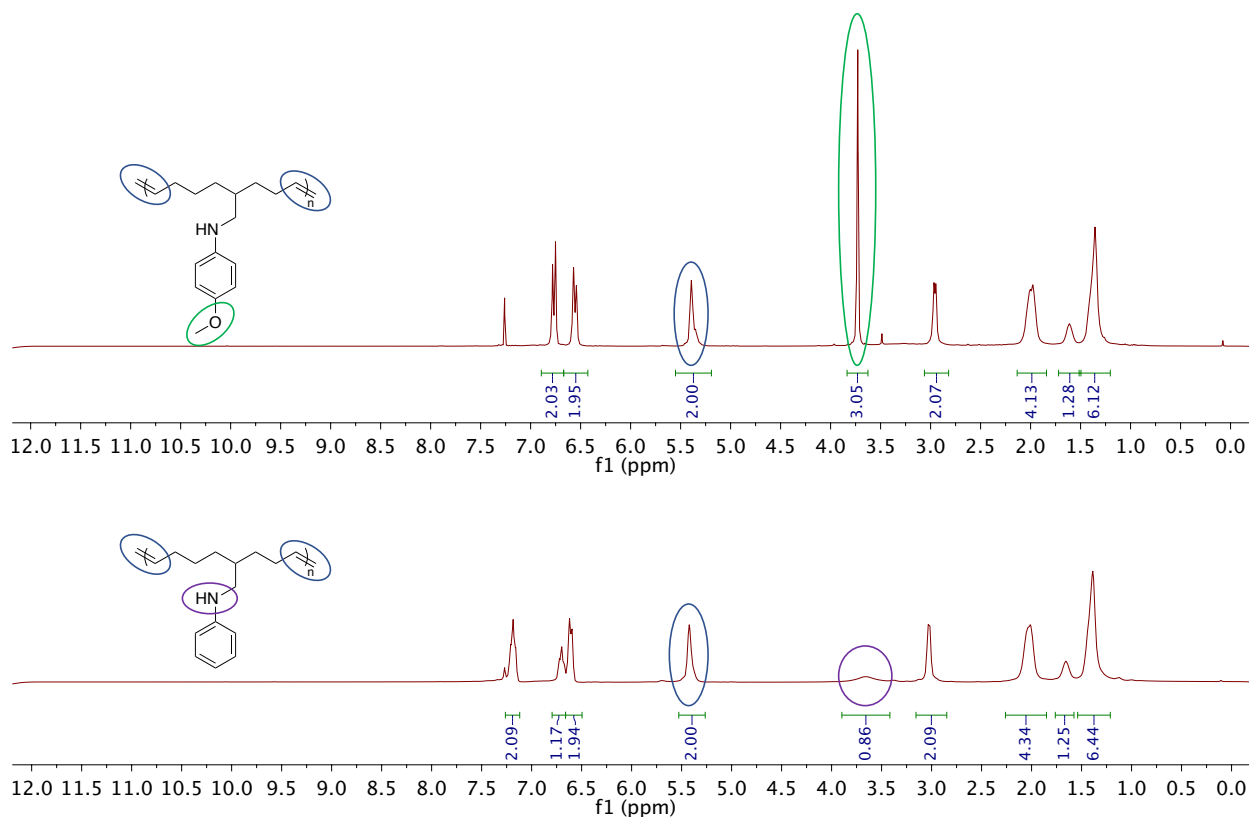


Figure 64 Overlay of ^1H NMR spectra of **P46** (bottom) and **P47** (top) (CDCl_3 , 300 MHz, 298 K)

Polymer solubility in THF is a prerequisite for accurate MW determination by LLS-GPC. However, after re-precipitation and drying these polymers *in vacuo*, **P46** and **P47** became insoluble in common organic solvents. This phenomenon has been reported previously with polymers of flexible backbones derived from ROMP, and is attributed to the high degrees of crystallinity and intermolecular chain-association.³⁷² Therefore, removing residual solvent molecules trapped between neighbouring chains in the drying process gives a polymer with poor

solubility characteristics. This issue was magnified by the H-bonding potential of the polymer chains, coupled with the highly flexible backbone; increasing H-bonding character and polarity is known to disfavor polymer solubility—a process involving solvation, swelling, and dissolution.³⁷³

One way to circumvent this problem is to dissolve the polymer in a minimum amount of hot CHCl_3 . The volatiles could then be removed to “near-dryness” and dissolved in THF for GPC analysis. This methodology produces limitations in molecular weight determination, as dn/dc values are calculated using 100% mass recovery methods, meaning accurate concentrations are imperative. Regardless, GPC analysis was performed to obtain preliminary molecular weight data. The polymer samples could be dissolved in THF for GPC analysis; however, these polymers gave inconsistent GPC traces, often showing low molecular weight shoulders and/or bimodal character. Low molecular weight species (eluent with long retention times) were postulated to be oligomers. Reliable molecular weight data was not obtained and acquisition of accurate dispersity values was hampered by significant tailing in the GPC traces.

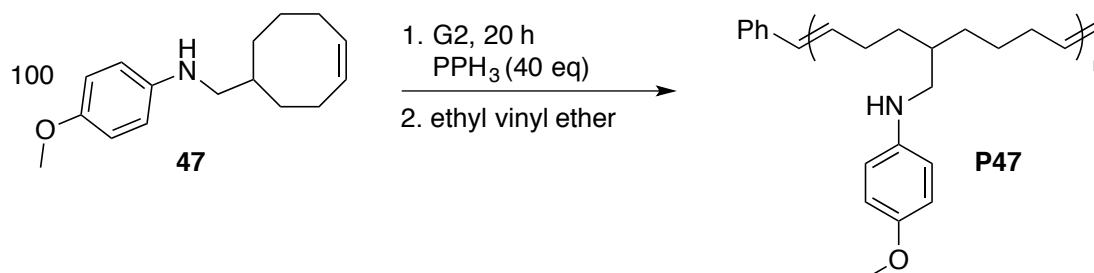
Another potential reason for the poorly-behaved materials was postulated to be secondary metathesis reactions, between either inter- or intramolecular backbones. In theory, the metathesis between two polymer chains (or an intramolecular interaction between one polymer chain) is possible. This “back-biting” event could give rise to a cyclic polymer and oligomeric species, as well as broadened levels of dispersity. To prevent the occurrence of such events, the polymerization was conducted for shorter reaction times (1.5 hours) and worked-up as described above. After precipitation into cold methanol, a gooey solid was collected and dried (65% yield). GPC data was again unfruitful and light-scattering traces showed large amounts of lower molecular weight material. The lower isolated yields of this reaction indicate that conversion of

monomer-to-polymer was incomplete after 1.5 hours (also supported by reduced isolated yields), as expected with the less-strained cyclooctene monomers. Species with longer elution times (lower MW) were observed in the GPC analysis and could potentially be attributed to monomer trapped in the polymer matrix. However, doping GPC samples with minor amounts pure monomer did not provide supporting evidence for this hypothesis, as the pure monomer gave rise to a distinct, well-resolved signal with a longer elution time than the unknown species in question. Furthermore, the presence of residual monomer is unlikely, as no monomer was observed ^1H NMR spectroscopy.

Cyclooctene (COE) is a monomer known to undergo rapid polymerization with G2 at room temperature.³⁷⁴⁻³⁷⁵ Addition of COE after polymerization of the amine-containing monomer, **P46** or **P47**, was hypothesized to generate higher MW copolymeric materials and eliminate the presence of oligomers from the mixture, provided these oligomers possess active alkylidene end groups. Therefore, 100 eq. of COE was added after 1.5 hours. Instant polymerization of COE was observed and led to a solid material that was insoluble in common organic solvents, indicating a high MW copolymer, and unable to be analyzed by conventional methods including GPC.

The presence of persistent lower molecular weight species observed in the GPC analysis led us to believe that the high activity G2 catalyst was potentially responsible for the formation of oligomers through secondary metathesis, or “back-biting”, reactions. As G1 was found incompatible with aminocyclooctene monomers **46** and **47**, we attempted to slow the activity of G2 by the addition of PPh_3 (40 eq.), to slow the catalytic activity (Scheme 24). The results of this experiment could potentially lead to more well-defined macromolecules with predictable

solubility profiles and give insight into the catalyst's activity in the polymerization of nitrogen-functionalized cyclooctene monomers **46** and/or **47**.



Scheme 24 Polymerization of monomer **47** with added PPh_3

This reaction was conducted in a 20 mL scintillation vial. Monomer **47** (0.1 g, 100 eq.) was dissolved in (0.5 mL) THF. To this solution was added a solution containing **G2** (4.2 mg, 1 eq. and PPh_3 (40 eq.) in THF (0.5 mL). The catalyst solution was added to the stirring solution of monomer and the mixture was let react for 3 hours before being quenched with ethyl vinyl ether. The desired polymer was collected by precipitation using cold MeOH (100 mL) and gravity filtration. The yield of this reaction was decreased significantly relative to reactions when no PPh_3 was added, with only 21% of the theoretical maximum yield of polymeric material being recovered. Characterization by GPC showed a monomodal, well-defined trace was obtained that could be analyzed without undesirable, low MW species observed previously. A M_n value of 17,420 was observed ($M_{n,\text{th}} = 24,537$ at 100% conversion) with a modest dispersity ($D = 1.6$). The addition of PPh_3 slows the initiation step (phosphine de-coordination). Rapid initiation imperative for controlled/living polymerization reactions.

While these results suggest that this methodology is viable for producing amino cyclooctene-derived polymers, the inability to obtain reliable, consistent MW data by GPC

analysis without the use of additives, and the difficulties associated with polymer solubility led us to focus specifically on aminonorbornene systems. The following sections highlight further characterization of these unique macromolecules with a focus on probing the H-bonding events occurring throughout **P6** and **P43-P45**.

3.8 Probing Hydrogen Bonding by IR Spectroscopy

Another possible way to observe H-bonding is by IR spectroscopy. In systems displaying H-bonding, the X-H (X = N or O) stretching frequency becomes broadened in solution, as the bonding interactions effectively change the vibrational frequency of the X-H bond. Concomitantly, X-H bond becomes longer, and therefore weaker, from these inter and/or intramolecular H-bonding associations. Theoretically, this would result in a red shift (shift to lower frequency) of that particular absorbance, however, often times this difference is less than 10 cm^{-1} .³⁷⁶

ATR-IR spectroscopy was performed on monomer **6** and the respective polymer, **P6**, with the respective spectra overlaid in Figure 65. No significant changes between the monomeric and polymeric form of these amines could be observed, specifically in the region at *ca.* 3500 cm^{-1} . The same behavior was also observed when the samples were analyzed in a solution of DCM. The analogous comparison between monomer **43** and polymer **P43** was performed (Figure 66). Again, no obvious difference in the spectra were observed, especially when comparing the N-H stretching frequencies of the monomer to those of the polymer at *ca.* $3400\text{-}3500\text{ cm}^{-1}$.

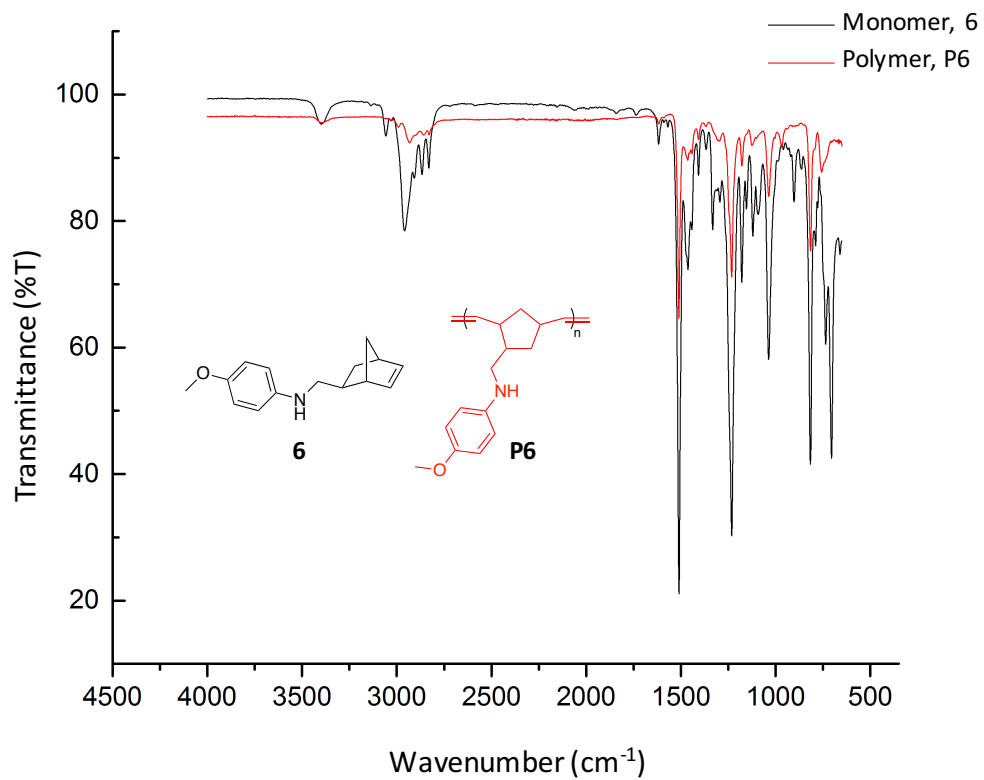


Figure 65 ATR-IR spectra of neat **6** and the ring-opened polymeric form, **P6**

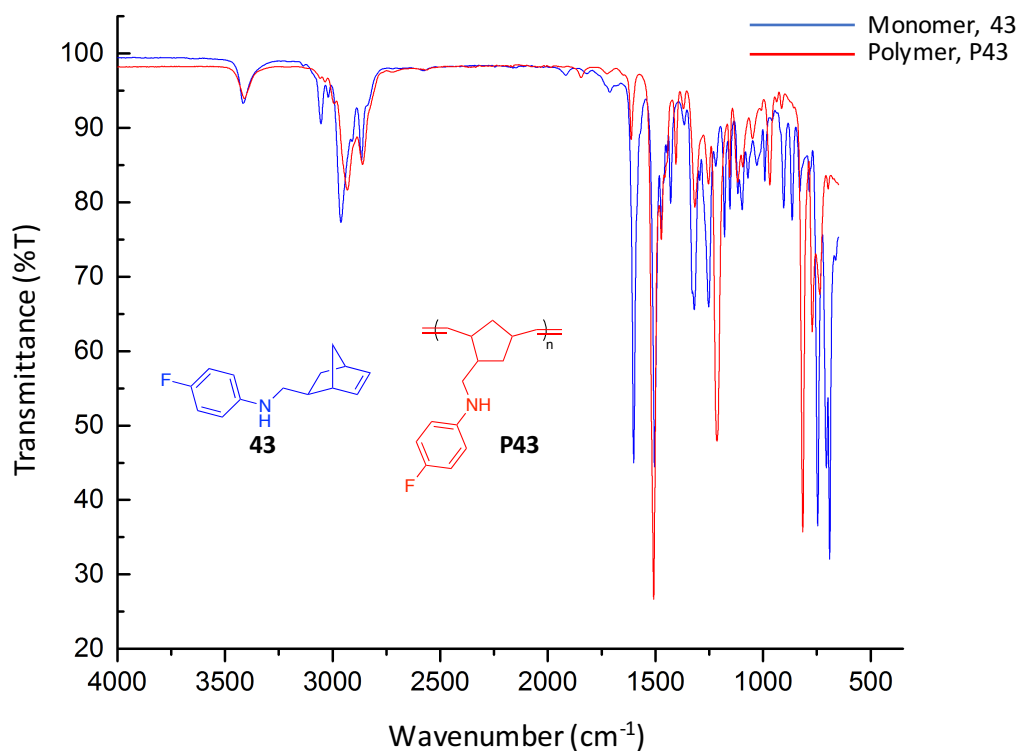


Figure 66 ATR-IR spectra of monomer 43 and the ring-opened polymeric form, P43

Furthermore, if the substituted polymers are compared, all having similar DP values, no significant changes in the spectra are observed, despite each polymer having different substitution on its aryl ring (Figure 67). The inset image displays the N-H stretching region of the polymer samples, with no observed shifts in the N-H stretching regions, and no obvious changes in intensity when the offset of these spectra is considered.

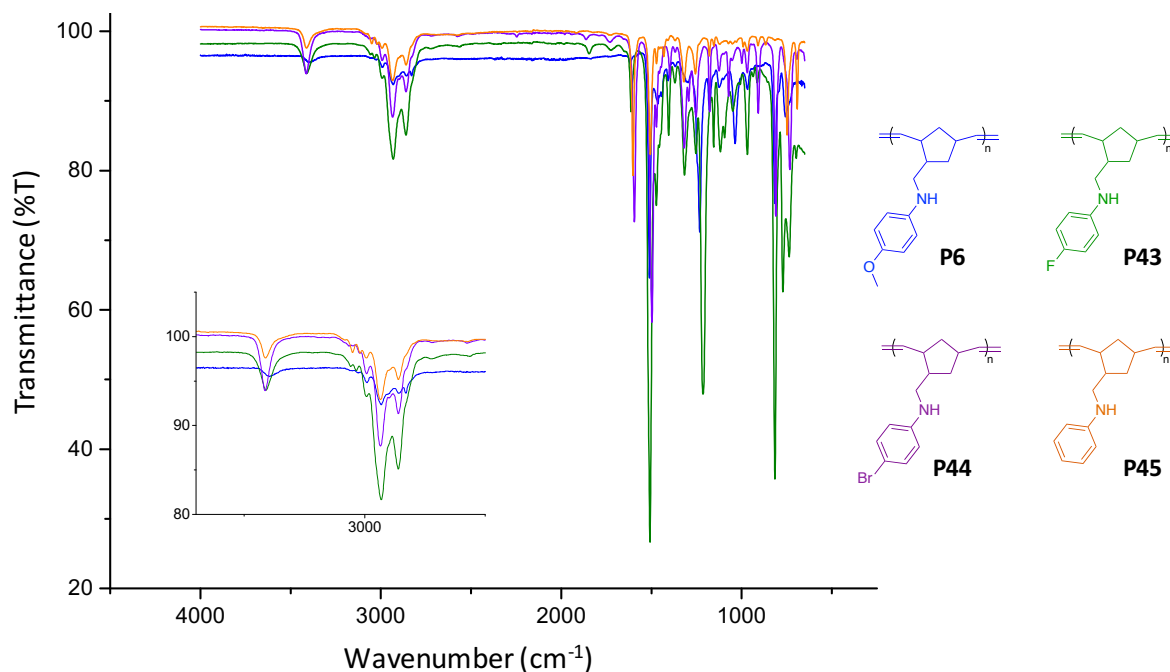


Figure 67 ATR-IR spectra of P6 and P43-P45 of similar molecular weight

While IR spectroscopy is sometimes used in the literature to decipher the presence and strength of H-bonding interactions as previously mentioned, the differences observed are usually relatively small, often being limited to *ca.* 10 wavenumbers. Unfortunately, no obvious differences in this range were observed in the substrates and products discussed in this chapter. Specifically, the N-H stretching frequencies of either the monomers and/or polymers bearing various substitution about the aryl ring show consistent N-H stretching frequencies, as shown in the inset image of Figure 67, and cannot be used to make strong conclusions regarding any H-bonding interactions. This is potentially due to the interaction of the nitrogen moieties being involved in H-bonding interactions, making these absorbance values occur at consistent, sharp wavenumbers. One other way to gain insight into the potential H-bonding interactions present in

these materials is through the analysis of their thermal and rheological properties. The following sections describe a detailed investigation into these potential differences.

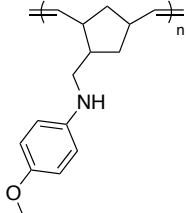
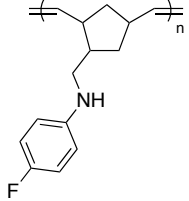
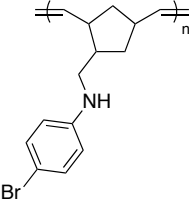
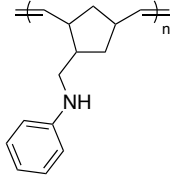
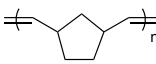
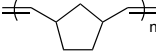
3.9 Thermal Analysis of Functionalized Polymers

The polymers discussed in Section 3.5 (page 141) were analyzed by thermogravimetric analysis (TGA) and differential scanning calorimetry (DSC) to obtain information regarding their thermal characteristics. Table 16 details the thermal properties of these materials relative to unfunctionalized PNB and reveals the sensitivity of the properties to small changes in the H-bond acceptor of the respective repeat units. Glass transition temperatures (T_g) were measured using DSC as well as isochronal dynamic temperature sweep tests. Unfunctionalized PNB (Entry 5, $M_n = 55,300$) possessed a T_g of 48.5 °C, which in good agreement with literature values,³⁷⁷ while aryl-substituted polymers were found to have higher T_g values consistent with enhanced intermolecular interactions and hindered segmental motions, potentially due to H-bonding interactions or π -stacking.¹⁵⁰

All samples were analyzed by TGA to obtain 5% and 50% decomposition values ($T_{d, 5\%}$ and $T_{d, 50\%}$, respectively). Unfunctionalized PNB (Entry 5) has a high thermal stability, with 5% decomposition temperature at 423 °C followed by intense degradation of the polymer backbone resulting in a 50% decomposition temperature of 434 °C. Aniline-substituted polymers **P6** and **P43-P45** (Entries 1-4) possess much lower thermal stabilities, with onset decomposition temperatures between 231-387 °C, suggesting their decreased ability to form closely stacked, crystalline morphologies, as bulky pendant groups inhibit inter- and/or intramolecular chain stacking, relative to unsubstituted PNB ($T_{d, 5\%} = 432$ °C). Furthermore, the 50% decomposition temperature of aryl-substituted polymers typically range from 434-446 °C (with *para*-bromo

polymer **P44** having a $T_{d, 50\%} = 342\text{ }^{\circ}\text{C}$) which is comparable to unfunctionalized PNB ($T_{d, 50\%} = 448\text{ }^{\circ}\text{C}$). **P44** possesses an early onset decomposition temperature of $231\text{ }^{\circ}\text{C}$ ($T_{d, 50\%}$), with the rapid elimination of *ca.* 30% of the samples' weight at this temperature; a value in close agreement with the molar composition of bromine in the sample (brominated monomer **44**, $\text{C}_{14}\text{H}_{16}\text{BrN}$, has a molar composition of: C, 60.45; H, 5.80; Br, 28.72; N, 5.03) suggesting that thermal elimination of this group can occur. Commercial PNB (Entry 6), which contains industrial stabilizers and plasticizers, possesses a much higher M_n ($>2,000,000\text{ g mol}^{-1}$). This material possesses a $T_{d, 50\%} = 431\text{ }^{\circ}\text{C}$ which is in good agreement with the synthesized PNB of much lower M_n values, however, with a much lower onset decomposition temperature ($T_{d, 5\%} = 174\text{ }^{\circ}\text{C}$). This is attributed to the presence of commercial additives and/or stabilizers and presumed increased level of dispersity (although not measured due to this material's insolubility). Furthermore, the presence of these additives prevents the total decomposition below $600\text{ }^{\circ}\text{C}$. Thermal decomposition results (TGA) can be found in Figure 68, which displays TGA thermograms for the polymers described in this section.

Table 16 Thermal properties of variously substituted amine polymers

Entry ^a	Repeat Unit	DP ^b and \bar{D}	T_g (°C) ^{c,d}	T_d (°C) ^{e,f}
1		113 $\bar{D} = 1.07$	61.7 ^c 60.7 ^d	333 ^e 434 ^f
2		95 $\bar{D} = 1.05$	62.3 ^c 65.4 ^d	336 ^e 439 ^f
3		109 $\bar{D} = 1.10$	82.3 ^c 68.6 ^d	231 ^e 342 ^f
4		95 $\bar{D} = 1.11$	58.4 ^c 59.5 ^d	387 ^e 446 ^f
5		588 $\bar{D} = 2.15$	48.5 ^c	432 ^e 448 ^f
6 ^g	 commercial	>21,240	>300 ^c	174 ^e 431 ^f

^aEntries represent average values of triplicate experiments. ^bDegree of polymerization: M_n /MW(g mol⁻¹). ^c T_g as calculated from DSC thermograms. ^d T_g as calculated from isochronal dynamic temperature sweep tests. ^e T_d , 5% and ^f T_d , 50% as calculated by TGA analysis. ^gCommercial PNB, M_n >2,000,000 g mol⁻¹.

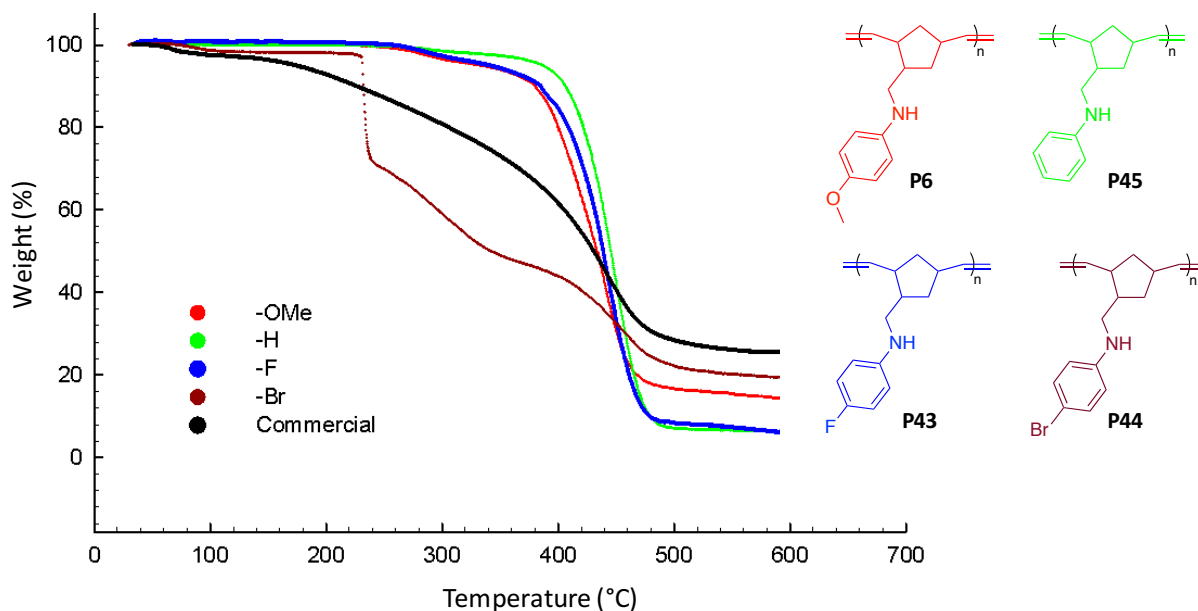


Figure 68 Overlay of TGA thermograms of aryl-substituted amine homopolymers P6 and P43-45 and commercial PNB

The results discussed above suggest that the addition of aryl-amine pendant groups do impart increased thermal stability, as observed from the increase in the increased $T_{d,50\%}$ values of **P6**, **P43**, and **P45** relative to commercial PNB, although they remain consistent with PNB of lower MW synthesized without additives or stabilizers. The relative differences imparted by the degrees to which H-bonding is or is not occurring is difficult to observe with this technique. As such, we turned our attention to other techniques to probe this behaviour. The following section describes the investigations into polymer rheology to assess the potential viscoelastic properties of these aminonorbornene polymers and gain insight into the H-bonding events occurring within the polymer in the melt phase.

3.10 Rheology

3.10.1 Rheology of Methoxy-Functionalized Aminonorbornene Polymers

The presence of the H-bond donor amine functionalities and the H-bond accepting methoxy groups were anticipated to impact melt viscoelastic measurements, relative to unfunctionalized polynorbornene (PNB). Figure 69 shows representative master-curves of the viscoelastic moduli of unfunctionalized PNB ($M_n = 119,700 \text{ g mol}^{-1}$, $D = 1.35$, graph a, left) and methoxy-functionalized polymer, **P6**, of comparable molecular weight ($M_n = 94,900 \text{ g mol}^{-1}$, $D = 1.05$). The unfunctionalized PNB displays a classical frequency dependence expected for linear, mono-disperse polymers. A plateau modulus, G_N^o is nearly reached in storage modulus (G'). These unfunctionalized PNB polymers are highly entangled with an entanglement molecular weight $M_e = 2,091 \text{ g mol}^{-1}$, meaning all polymers studied are highly entangled.¹⁰⁵ A maximum in the loss modulus (G'') is observed before the crossover frequency.

At low frequencies, G'' is greater than G' , meaning the polymer chains behave like viscoelastic liquids; chains can relax and dissipate energy at these frequencies. After the crossover point storage modulus becomes dominant as the frequency of deformation is too high for chains to relax, meaning the material behaves as a viscoelastic solid. Interestingly, the methoxy-functionalized polymer **P6** (graph b, right) reveals solid-like elastic behavior over the entire frequency range. These results indicate large differences in viscoelastic behaviour, potentially due to the formation of transient supramolecular networks due to H-bonding interactions.^{4, 166}

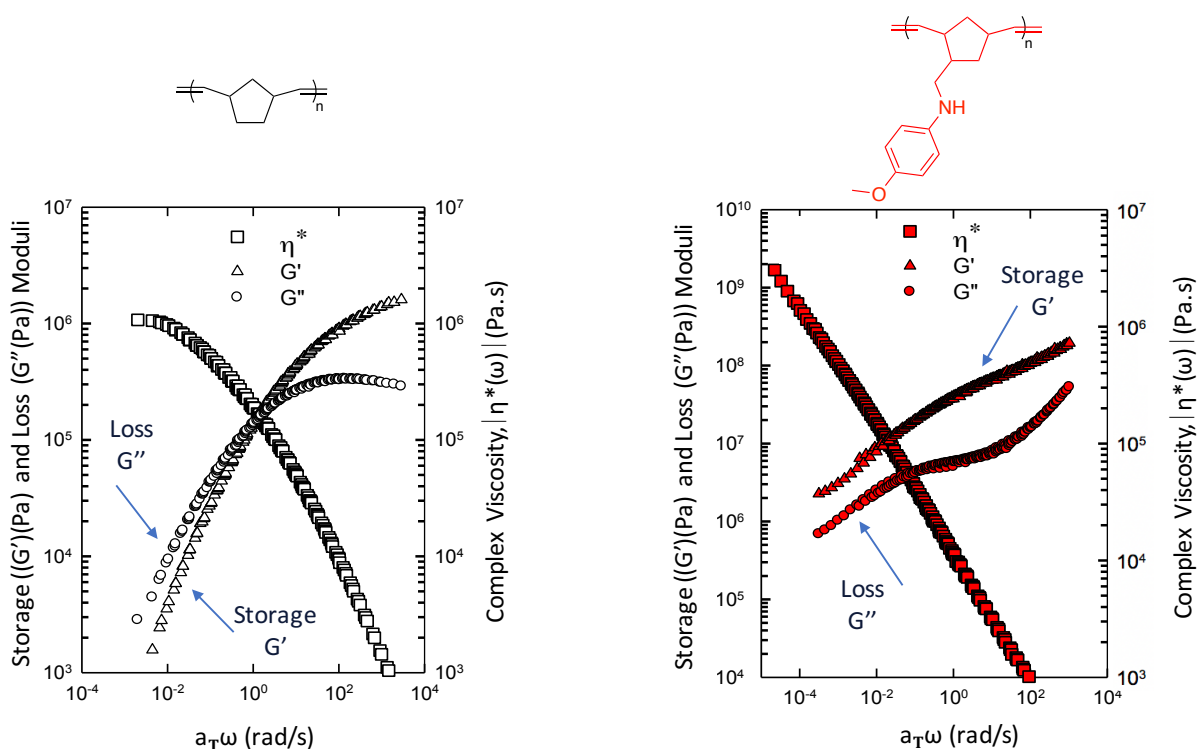


Figure 69 Master curves ($T_{\text{ref}} = 120\text{ }^{\circ}\text{C}$) of the viscoelastic moduli (G' & G'') and complex viscosity (η^*) as a function of the angular frequency (ω) for (a) polynorbornene (PNB) ($M_n = 119,700\text{ g mol}^{-1}$, $D = 1.35$), (b) P6 ($M_n = 94,900\text{ g mol}^{-1}$, $D = 1.05$)

The dominance of storage modulus over loss modulus was found to be dependent on the molecular weight of the functionalized polymer. Figure 70 shows an overlay of **P6** samples of various molecular weights. At lower molecular weights ($M_n = 4,300\text{ g mol}^{-1}$, green trace) loss modulus is dominant over the entire frequency range. However, as molecular weight, and the number of H-bond donors and acceptors increases, a solid response is observed. These results agree well with the acrylic acid copolymers discussed previously.¹⁴⁸ Polymer **P6** having M_n 55,200 g mol^{-1} (blue trace) and M_n 94,200 g mol^{-1} (red trace) have G' values that are dominant over G'' . Again, no cross-over frequency is observed. Furthermore, values of both storage and loss moduli increase by an order of magnitude at the corresponding frequencies as molecular

weight is increased. This is in good agreement with the increasing number of H-bonding amine and methoxy moieties present in the materials.

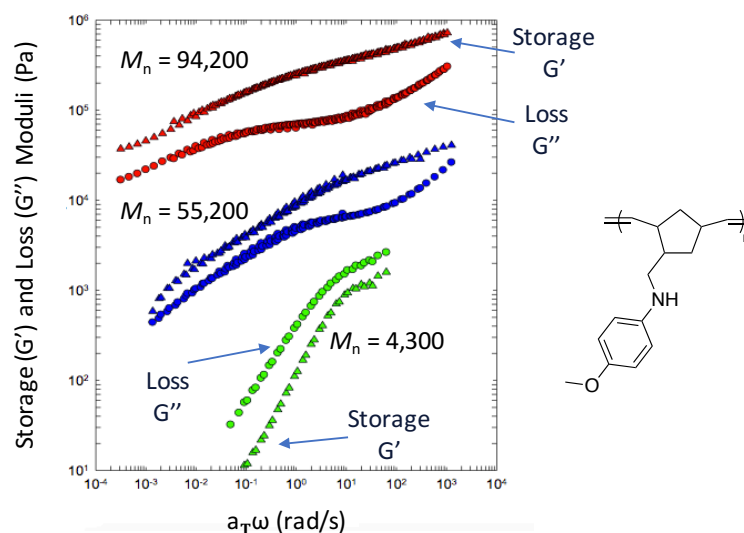


Figure 70 Viscoelastic moduli (G' and G'') ($T_{\text{ref}} = 120\text{ }^{\circ}\text{C}$) of P6 samples of various molecular weight

A similar trend is observed when examining the zero-shear viscosity (η_0). An exponential increase in viscosity is observed for methoxy-substituted **P6** of various M_n (Figure 71, red trace). This behaviour has been reported for branched polymer stars and other polymers with groups capable of H-bonding.^{148, 378} These groups have a pronounced effect on the relaxation capabilities of these materials. H-bond partners can provide additional friction that slows down the relaxation of chains, increasing the viscoelastic moduli relative to native, unfunctionalized polymers. Contrary to this, unfunctionalized PNB (Figure 71, black trace) obeys a Power-law relationship that is consistent with linear monodisperse polymers, where, η_0 increases linearly with increasing molecular weight values.

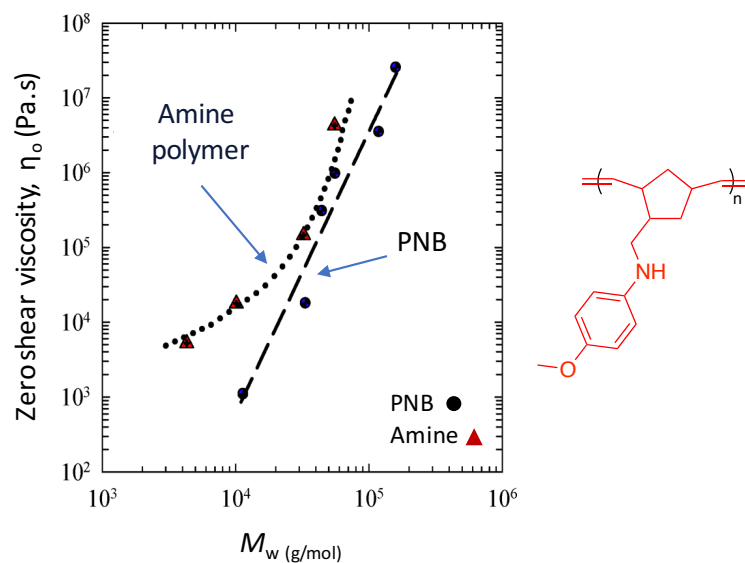


Figure 71 Scaling of the zero shear viscosity of M_w for P6 ($\eta_0 = 3765 \exp(E-4 M_w)$) versus unfunctionalized PNB ($\eta_0 = 5E-13M_w^{3.77}$)

Figure 72 shows the complex viscosity master curves for unfunctionalized PNB (left) and **P6** (right) ($T_{\text{ref}} = 120^\circ\text{C}$). When amine-functionalized polymers are subjected to high frequencies, the complex viscosity is independent of molecular weight as short segment relaxation is dominant, as is known for linear monodisperse polymers.¹³⁹ The plateau in the complex viscosity at low frequencies (zero-shear viscosity) becomes less defined as molecular weight increases, and shows an upturn due to the increased presence of moieties capable of H-bonding. These partners are proposed to align and provide additional friction/increased reptation.¹⁵¹⁻¹⁵² In other words, the thermal motion of polymer chains is restricted as increased levels and participation of H-bonding is present in the material.

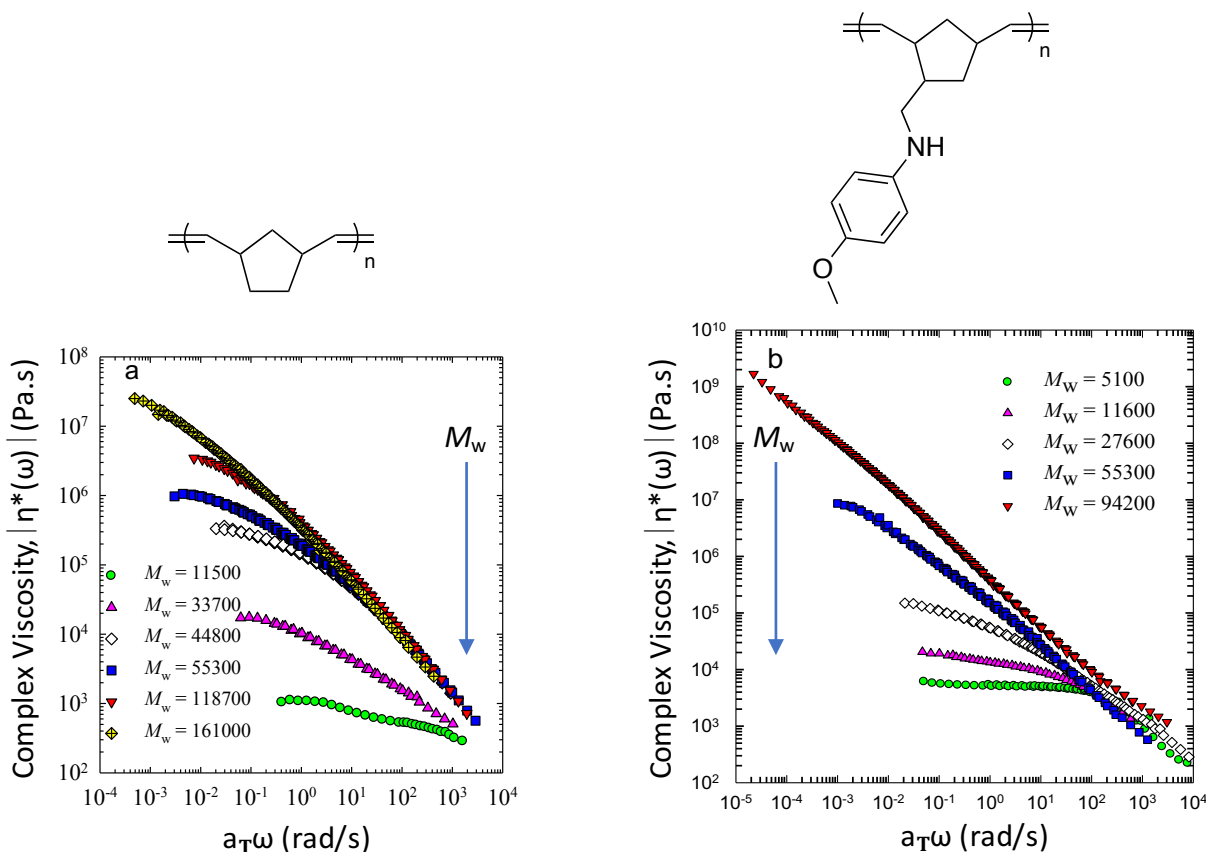


Figure 72 Complex viscosity (η^*) vs angular frequency master curves for (a) unfunctionalized PNB and (b) P6 of various molecular weight ($T_{\text{ref}} = 120^\circ\text{C}$)

The results obtained from analyzing methoxy-substituted polymer **P6** by rheology indicated the presence of H-bonding occurring within the polymer sample. The formation of these transient networks was found to be dependent on polymer MW, with increasing MW leading to higher levels H-bonding, consistent with the increased levels of H-bonding donors and acceptors present in the sample. The ability of aminonorbornene polymers to H-bond should vary depending on the substitution about the aryl ring. In this vein, we subjected our other substituted aryl-amine polymers, **P43-P45** to these rheological measurements to probe these differences.

3.10.2 Rheology of Variously-Substituted Aminonorbornene Polymers

The interesting viscoelastic properties of methoxy-substituted aminonorbornene polymers, **P6**, led us to study polymers bearing other aryl-substitution. It was of interest to us to investigate the specificity of this trend towards the *para*-functionality. Polymers of different molecular weights, but comparable DP values were studied (M_n values vary due to the difference in monomer MW. All polymers were synthesized using M:I of 100:1). Master curves of complex viscosity for these polymers are presented in Figure 73 ($T_{\text{ref}} = 120\text{ }^{\circ}\text{C}$). These samples have similar chain lengths ($\text{DP} \cong 100$) but differ in the substitution of the H-bond acceptor (OMe, F, Br, and H) on the aryl group.

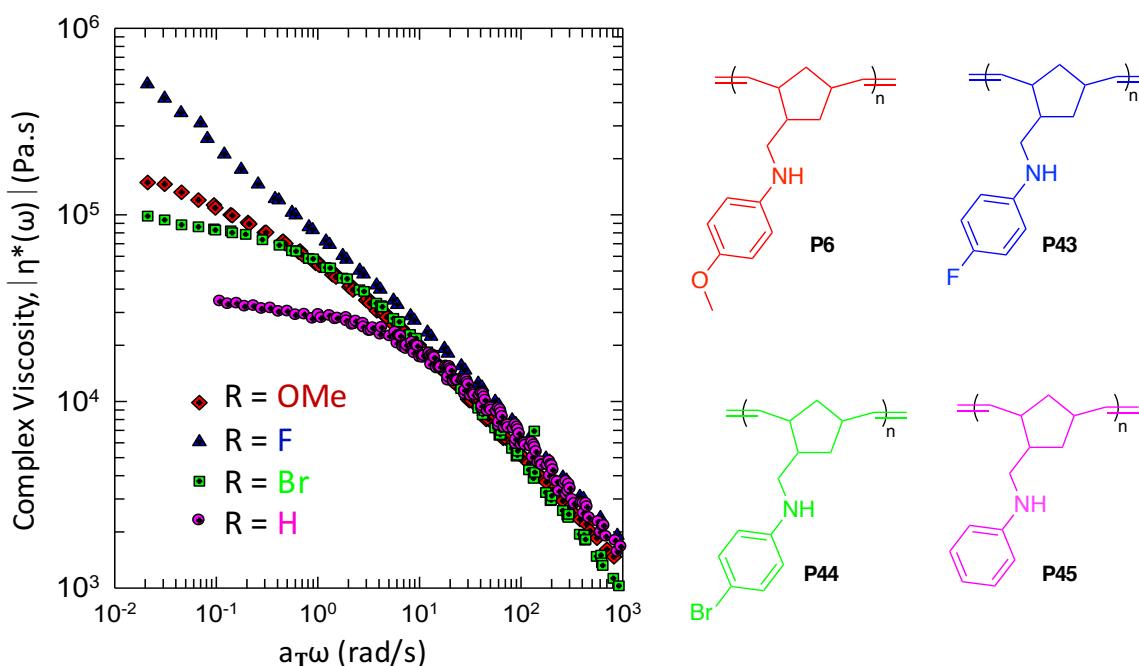


Figure 73 Complex viscosity (η^*) of variously substituted aminonorbornene polymers ($T_{\text{ref}} = 120\text{ }^{\circ}\text{C}$)

Figure 73 shows that the *para*-substitution on the aryl ring changes the rheological behavior of the material, evidenced by the different values of η_0 and the degrees of shear thinning

exhibited. None of the studied samples have reached the terminal region (η_0 at low frequencies) yet, suggesting solid-like microstructures arising from H-bonded networks. The *para*-fluorinated polymer, **P43**, has the most profound shear thinning behavior, followed by the *para*-methoxy, **P6**, and *para*-bromo, **P44**, polymer. As expected, the unsubstituted aniline derivative, **P45**, possesses the least amount of shear thinning at these frequencies, potentially due to its relative difference in H-bonding potential. These results reflect the extent of H-bonding capable by these differently substituted pendant amine groups. These trends map onto the H-bond acceptor character of the *para*-substituents and demonstrate that the viscoelastic properties of these polymers changes significantly with these substituents while the amine functionality remains consistent between all samples.

3.11 Conclusions

Chapter 3 detailed the investigation into the synthesis and characterization of strained aminonorbornene monomers by HAA using a known tantalum phosphoramidate catalyst. This atom-economic, single step synthesis afforded a variety of mono-substituted, alkyl and aryl amine products. These secondary amine products were found to be the *exo*-diastereomer either through comparison to known compounds in the literature, or by analysis of their solid-state molecular structures when possible. Furthermore, only one diastereomer was observed when the crude reaction mixtures were analyzed by GC-MS.

These secondary aminonorbornene products were then subjected to standard polymerization conditions using a known ruthenium metathesis catalyst, G2. Remarkably, secondary aryl-amine substrates polymerized to give the respective polymeric materials with

high levels of MW control and low dispersities. Subsequent experiments reveal that this transformation displays living behaviour. Typically, the polymerization of primary and/or secondary amines requires protection and deprotection protocols to arrive at the desired products. However, the products of HAA did not require protection of the amine group and polymerization proceeded smoothly for aryl-amines. Unsurprisingly, the secondary alkyl amine product, **42**, was not amenable to polymerization using G2 due to the strongly nucleophilic nature of the amine group causing irreversible catalyst deactivation. No productive propagation was observed.

The presence of a free, secondary amine group allows for potential exploitation of the H-bonding potential in the resultant polymeric materials. Unfortunately, no obvious differences in the IR spectra of the variously-substituted amine polymers was observed, potentially due to the insensitivity of the instrumentation or the static environment of the H-bonded amine groups in the solid-state. Thermal characterization by TGA and DSC showed differences in the T_g values of the materials, with *para*-brominated polymer having the most obvious difference as the thermal loss of the halogen group is clear. Potential exploitation of this characteristic is discussed in Chapter 5. T_g values of all amine-functionalized polymers were higher than unfunctionalized PNB and vary depending on the *para*-substituted on the aryl ring, although being relatively consistent between these samples and ranging from *ca.* 60-69 °C.

The H-bonding potential in these polymeric materials was best studied using rheological techniques. The viscoelastic properties of these polymers began by studying methoxy-substituted aminonorborene, **P6**, which showed viscoelastic properties atypical of ‘classical’ materials. At low MWs, loss modulus remained dominant over the entire frequency range and when MW increased a reversal in this trend was observed. The increased number of H-bonding partners in the sample led to storage modulus (G') becoming dominant over loss modulus (G'') as friction

and reptation was increased. No cross-over point was observed for the frequency range studied and these results are corroborated by other materials that invoke H-bonding.³⁷⁸ Viscosity was also observed to increase exponentially with MW due to the H-bonding partners present in the material, whereas unfunctionalized PNB displays a linear increase in viscosity with MW. Furthermore, differences in viscosity were observed between the variously-substituted polymers, an observation attributed to the respective H-bonding potential of these groups. Stronger H-bonding groups -F and -OMe displayed higher viscosities relative to the weaker H-bonding groups -H and -Br. These trends point to potential applications where materials with tunable, specific viscosity parameters are desirable.

The results presented in Chapter 3 show that the polymerization of secondary-aryl amines is possible with G2, a result that has been rarely reported. Coupled with the HAA, the synthesis of these monomers allows access to polymeric materials that are novel and possess untapped potential. Chapter 4 will detail an expansion into the amine and alkene partners realizable in this transformation, with a focus on exploiting the H-bonding capabilities and potentials of these new-to-the-world materials by coupling them with comonomers in the formation of novel copolymeric materials.

3.12 Experimental

General Details. All chemistry was performed in a nitrogen-filled glovebox or using standard Schlenk techniques unless otherwise stated. All hydroaminoalkylation substrates were purchased from Aldrich and purified by either sublimation or distillation from calcium hydride and degassed by three successive freeze-pump-thaw cycles before use. Anhydrous solvents were obtained from an activated alumina tower and degassed prior to use. Benzene- d_6 and toluene- d_8 were dried over activated 4 Å molecular sieves and degassed prior to use. GC-MS was performed on an Agilent 7890A GC system. High-resolution EI mass spectra (HRMS) were acquired from a Waters/Micromass LCT spectrometer. IR spectra were obtained on either a Nicolet 4700 FTIR (NaCl) or a Perkin Elmer Frontier (ATR) spectrometer. HAA products were synthesized following a literature procedure and all characterization matches reported values.¹⁸³ G1 and G2 were purchased from Aldrich and used as received. Polynorbornene was prepared following a published literature procedure.⁸¹ High molecular weight, commercial-grade polynorbornene ($M_n = \sim 2,000,000 \text{ g mol}^{-1}$) was purchased from Monomer-Polymer and Dajac Labs and used as received.

3.12.1 Materials and Methods

NMR Spectroscopy

NMR spectroscopy was performed on a Bruker Avance 300 MHz, 400 MHz, or 600 MHz spectrometer at 298 K unless otherwise stated. All coupling values are $^3J_{\text{H-H}}$ and reported in Hz. Abbreviations for NMR assignments for peaks are as follows: s = singlet; d = doublet; t = triplet; q = quartet; sept = septet, m = multiplet; br = broad. Chemical shift values for polymers are listed as the most abundant peaks in the spectra.

Gel Permeation Chromatography

All GPC analysis was conducted on polymers precipitated 3 times using an appropriate solvent (typically hexanes or methanol) and dried *in vacuo* prior to being dried overnight in a vacuum oven. Analysis was performed using Agilent GPC equipped with a Viscostar-II, opti-lab T-rEX and miniDAWN TREOS detectors. GPC analysis was conducted in THF using a flow rate of 0.5 mL/min at 40 °C. All dn/dc values were calculated from 100% mass recovery methods. All samples were analyzed at a concentration of approximately 2 mg mL⁻¹.

Differential Scanning Calorimetry

Thermal properties of the samples were measured on a TA instruments Q2000 differential scanning calorimeter calibrated using indium. Analyses were performed in an inert atmosphere (nitrogen) with samples of approximately 5-6 mg in an aluminum pan. All analyses were conducted in duplicate to ensure consistency amongst the data. Samples were heated to 200 °C with a heating rate of 10 °C/min. They were held isothermally at 200 °C for 1 min to eliminate any thermal history followed by gradual cooling to -20 °C with a cooling rate of 5 °C/min. The samples were then reheated to 200 °C with a heating rate of 10 °C/min. The glass transition temperatures were determined from the second heating ramp and are reported as the midpoint of the transition.

Thermogravimetric Analysis

Thermal decomposition results were obtained using a thermogravimetric analysis Shimadzu TGA-50 instrument. A heating rate of 20 °C/min was used. Data was typically obtained between

30 to 600 °C. All data was collected for samples under an inert atmosphere of nitrogen. Duplicate runs were performed to ensure consistency amongst the data.

Linear Melt Viscoelasticity

Shear measurements were performed using a MCR 501/502 rheometer (Anton Paar), equipped with 8 mm parallel plates. Dynamic time sweep measurements were carried out at an angular frequency of 2 Hz at 120 °C to examine the thermal stability of the samples. Isochronal dynamic temperature sweep tests were performed at 0.1 Hz with a heating rate of 1 °C/min. The dynamic linear viscoelastic measurements were carried out within the linear viscoelastic regime at temperatures in the range from 90 to 160 °C. The dynamic measurements were conducted in the range of 0.01–100 Hz at a strain of 1%. A gap of 0.5 mm was used to minimize edge effects and ensure a reasonable aspect ratio of plate radius and gap.

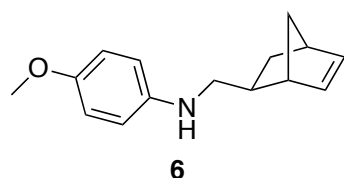
3.12.2 Synthesis and Characterization

General Procedure for Aminonorbornene Synthesis

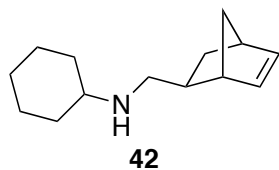
The synthesis of most monomers presented in this chapter has been disclosed in the following citation, and all relevant spectra can be found within this publication.¹⁰⁵ All monomers were synthesized using tantalum phosphoramidate precatalyst **2**^{12, 183} described in this chapter and Chapter 2, and were isolated as colourless or pale yellow oils. HAA produced only one diastereomer of monoalkylated product, as shown by GC-MS analysis of the crude reaction mixture. It was previously confirmed to be the *exo*-diastereomer by X-ray crystallography,^{105, 183} and by comparison to similar compounds in the literature.²⁷¹ All other diastereomers were assigned by analogy to this compound. In some instances, over alkylation of the diene was

observed. All monomers were purified by column chromatography (SiliaFlash F-60, 230-400 mesh) using the solvent systems listed below for the individual compounds.

A typical is described for the synthesis of **6**:

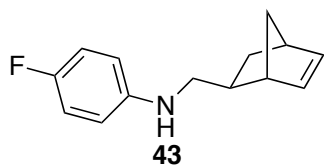


6. Known compound.^{105, 183} To a vial containing tantalum phosphoramidate precatalyst (0.10 eq., 51.7 mg, 0.1 mmol), 4-methoxy-*N*-methylaniline (0.137 g, 1.0 mmol) and an excess of norbornadiene (0.146 g, 1.5 mmol) were added to afford a yellow solution. The reaction was let stir for 20 h at room temperature, during which time the mixture turned red. After the allotted time, the mixture was exposed to air, concentrated *in vacuo* and purified *via* column chromatography (hexanes/ethyl acetate 95:5) yielded a yellow oil 0.13 g, 56 %. **¹H NMR** (300 MHz, CDCl₃): δ 6.83 (d, ³*J* = 9.0 Hz, 2H, 2×Ar*H*), 6.63 (d, ³*J* = 9.0 Hz, 2H, 2×Ar*H*), 6.14-6.12 (m, 2H, (CH)₂), 3.77 (s, 3H, OCH₃), 3.52 (br s, 1H, NH), 3.18-3.04 (m, 2H, CH₂), 2.88 (s, 1H, CH), 2.76 (s, 1H, CH), 1.75-1.68 (m, 1H, CH), 1.42-1.23 (m, 4H, 2×CH₂). **¹³C{¹H} NMR** (75 MHz, CDCl₃): δ 152.0 (C), 142.9 (C), 136.8 (CH), 136.5 (CH), 115.0 (2×CH), 114.0 (2×CH), 55.9 (CH₃), 50.7 (CH₂), 45.4 (CH₂), 44.6 (CH), 41.8 (CH), 39.1 (CH), 31.4 (CH₂). **IR** (NaCl, cm⁻¹): 3396, 2960, 2866, 1514. **HRMS-ESI** (*m/z*): calcd: 229.1467; found: 229.1467.

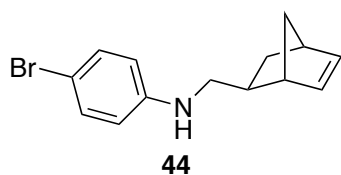


42. Known compound.¹⁰⁵ This product was isolated as a colourless oil after column chromatography (hexanes/triethylamine 14:1) 0.67 g, 56% **¹H NMR** (300 MHz, CDCl₃): δ 6.08-6.00 (m, 2H, (CH)₂), 2.78-2.77 (m, 1H, NH), 2.68-2.56 (m, 3H, CH₂ + CH), 2.43-2.33 (m, 1H, CH), 1.87-1.83 (m, 2H, CH₂), 1.74-1.68 (m, 2H, CH₂), 1.61-1.47 (m, 2H, 2×CH), 1.30-0.99 (m, 10H, 5×CH₂). **¹³C{¹H} NMR** (75

MHz, CDCl₃): δ 136.7 (CH), 136.6 (CH), 57.2 (CH), 53.0 (CH₂), 45.3 (CH₂), 44.7 (CH), 41.8 (CH), 39.6 (CH), 33.8 (2 \times CH₂), 31.7 (CH₂), 26.3 (CH₂), 25.2 (2 \times CH₂). **IR** (ATR, cm⁻¹): 3056, 2926, 1737, 1450, 1127. **HRMS-ESI** (m/z): calcd: 206.1909; found: 206.1902.

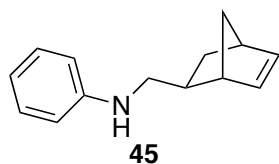


43. Known compound.¹⁰⁵ This product was isolated as a yellow oil after column chromatography (hexanes/ethyl acetate 90:10), 0.18 g, 51% **¹H NMR** (300 MHz, CDCl₃): δ 6.92-6.86 (m, 2H, 2 \times ArH) 6.57-6.53 (m, 2H, 2 \times ArH), 6.13-6.07 (m, 2H, (CH)₂), 3.38 (overlapped br s, 1H, NH), 3.15-3.01 (m, 2H, CH₂), 2.85-2.86 (m, 1H, CH), 2.73-2.72 (m, 1H, CH), 1.71-1.62 (m, 1H, CH), 1.42-1.32 (m, 3H, CH + CH₂), 1.27-1.19 (m, 1H, CH). **¹³C{¹H} NMR** (75 MHz, CDCl₃): δ 155.8 (d, ¹J_{C-F} = 235 Hz, C), 145.0 (2 \times CH), 136.9 (CH), 136.5 (C), 115.9 (CH), 115.6 (CH), 113.6 (CH), 113.5 (CH), 50.5 (CH₂), 45.4 (CH), 44.6 (CH₂), 41.8 (CH), 39.1 (CH), 31.4 (CH₂). **¹⁹F{¹H} NMR** (282 MHz, CDCl₃): δ -128.8. **IR** (ATR, cm⁻¹): 3425, 2964, 2869, 1509. **HRMS-ESI** (m/z) calcd: 218.1345; found: 218.1348.



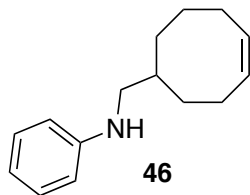
44. Known compound.¹⁰⁵ Any solid formed during the reaction was filtered through a column of silica gel using DCM as the mobile phase. The filtrate was reduced and was purified by column chromatography (hexanes/ethyl acetate 90:10) 0.44 g, 41% **¹H NMR** (300 MHz, CDCl₃): δ 7.28-7.25 (m, 2H, 2 \times ArH), 6.51-6.48 (m, 2H, 2 \times ArH), 6.12 (br s, 2H, (CH)₂), 3.76 (br s, 1H, NH), 3.17-3.02 (m, 2H, CH₂), 2.89-2.88 (m, 1H, CH), 2.73-2.72 (s, 1H, CH), 1.68-1.63 (m, 1H, CH), 1.41-1.20 (m, 4H, 2 \times CH₂). **¹³C{¹H} NMR** (75 MHz, CDCl₃): δ 147.5 (C), 136.9 (CH), 136.4 (CH), 131.9 (2 \times CH), 114.2 (2 \times CH), 108.5 (C), 49.6 (CH₂), 45.3 (CH), 44.5 (CH₂), 41.8 (CH),

38.9 (CH), 31.3 (CH₂). **IR** (ATR, cm⁻¹): 3417, 3344, 2963, 2867, 1595, 1497. **HRMS-ESI** (*m/z*): calcd: 278.0544; found: 278.0539.



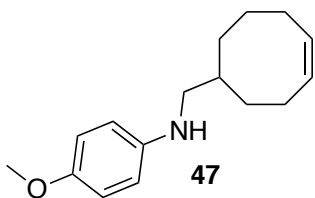
45. Known compound.¹⁰⁵ This product was isolated as a yellow oil after column chromatography (hexanes/ethyl acetate 95:5) 0.92 g, 46% ¹H **NMR** (300 MHz, CDCl₃): δ 7.21-7.16 (m, 2H, 2×ArH), 6.77-6.68 (m, 1H, ArH), 6.65-6.61 (m, 2H, 2×ArH), 6.13-6.07 (m, 2H, (CH)₂), 3.81 (br s, 1H, NH), 3.21-3.05 (m, 2H, CH₂), 2.85 (s, 1H, CH), 2.73 (s, 1H, CH), 1.74-1.65 (m, 1H, CH), 1.36-1.20 (m, 4H, 2×CH₂). ¹³C{¹H} **NMR** (75 MHz, CDCl₃): δ 148.5 (C), 136.9 (CH), 136.6 (CH), 129.4 (2×CH), 117.3 (CH), 112.9 (2×CH), 49.8 (CH₂), 45.4 (CH), 44.6 (CH₂), 41.8 (CH), 39.1 (CH), 31.4 (CH₂). **IR** (ATR, cm⁻¹): 1504, 1601, 2961.

Monomers derived from cyclooctadiene were prepared following the procedure for norbornadiene homologues described above.¹⁰⁵ All monomers were synthesized using the tantalum phosphoramidate precatalyst **2** described in this chapter. In some cases, heating to 70 °C and using 5 eq. of diene was used, although yields were not significantly improved. The examples described below were synthesized using 1.5 eq. of diene and 10 mol% tantalum precatalyst. A reaction time of 20 h was used.



46. Known compound.⁵ A yellow oil was obtained after purification by column chromatography (10:1 hexanes/ethyl acetate), 0.10 g, 75% yield. All characterization is consistent with the previous literature report. ¹H **NMR** (300 MHz, CDCl₃): δ 7.24 (t, ³J = 8.0 Hz, 2H, CH), 6.76 (t, ³J = 7.2 Hz, 1H, CH), 6.66 (d,

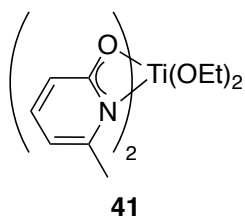
$^3J = 8.0$ Hz, 2H, CH), 5.74 (m, 2H, 2×CH), 3.71 (br s, 1H, NH), 3.01 (m, 2H, CH₂), 2.49-2.12 (m, 4H, 2×CH₂), 1.86-1.24 (m, 6H, 3×CH₂), 1.0 (m, 1H, CH). **¹³C NMR** (75 MHz, CDCl₃): δ 148.7 (C), 130.3 (CH), 130.1 (CH), 129.3 (2×CH), 117.0 (CH), 112.7 (2×CH), 51.7 (CH₂), 37.8 (CH), 33.5 (CH₂), 31.2 (CH₂), 28.3 (CH₂), 26.0 (CH₂), 24.9 (CH₂). **HRMS-ESI** (*m/z*): calcd: 216.1748; found: 216.1752.



47

47. A yellow oil was obtained after purification by column chromatography (10:1 hexanes/ethyl acetate), 0.06 g, 45%. **¹H NMR** (300 MHz, CDCl₃): δ 6.80-6.77 (m, 2H, 2×CH), 6.58-6.55 (m, 2H, 2×CH), 5.90-5.65 (m, 2H, 2×CH), 3.76 (s, 3H, CH₃), 3.32 (br s, 1H, NH), 2.90 (m, 2H, CH₂), 2.37-2.15 (m, 4H, 2×CH₂), 1.74-1.22 (m, 7H, 3×CH₂, CH). **¹³C{¹H} NMR** (75 MHz, CDCl₃): δ 151.9 (C), 143.1 (C), 130.3 (CH), 130.2 (CH), 115.02 (2×CH), 114.0 (2×CH), 55.9 (CH₂), 52.8 (CH₃), 37.9 (CH), 33.5 (CH₂), 31.3 (CH₂), 28.3 (CH₂), 26.0 (CH₂), 25.0 (CH₂). **IR** (ATR, cm⁻¹): 3407, 2913, 1510, 1232, 1037, 816, 723. **HRMS-ESI** (*m/z*): calcd: 246.1858; found: 246.1855.

Titanium Pyridonate Complexes



41

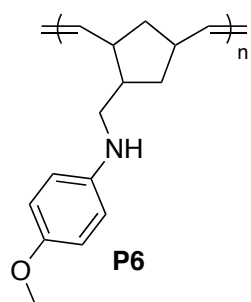
41. Known compound.⁷⁶ In a glovebox of N₂, proligand was weighed into a vial (0.51 g, 4.7 mmol) and suspended in toluene (2 mL). Ti(NMe₂)₄ (0.53 g, 2.3 mmol) was weighed in a vial and dissolved in toluene (2 mL). The yellow solution of titanium was added dropwise to the amide resulting in a red solution. Residual titanium mixture was rinsed into the reaction vessel with an additional 2 mL of toluene. The mixture was let stir overnight before the volatiles, were reduced *in vacuo*. The red/orange solid was dissolved in toluene (5 mL). Ethanol (0.28 mL) was added dropwise

via a microsyringe causing the solution to turn yellow. The mixture was stirred overnight, filtered through celite, and reduced *in vacuo* to afford a yellow powder (0.77 g, 92%). **¹H NMR** (300 MHz, C₆D₆): δ 7.04-6.98 (m, 2H, 2 \times CH), 6.37-6.34 (m, 2H, 2 \times CH), 5.99 (m, 2H, 2 \times CH), 4.60 (q, 3J = 6.0 Hz, 4H, 2 \times CH₂), 2.24 (s, 6H, 2 \times CH₃), 1.32 (t, 3J = 6.0 Hz, 6H, 2 \times CH₃). **¹³C NMR** (75 MHz, C₆D₆): δ 172.9 (2 \times C), 152.9 (2 \times C), 141.4 (2 \times CH), 112.5 (2 \times CH), 106.2 (2 \times CH), 73.4 (2 \times CH₂), 21.2 (2 \times CH₃), 18.8 (2 \times CH₃). **HRMS-EI** (m/z): calcd: 354.1059; found 354.1061. **EA**: calcd: C, 54.3; H, 6.3; N, 7.9; found: C, 54.2; H, 6.4; N, 8.2.

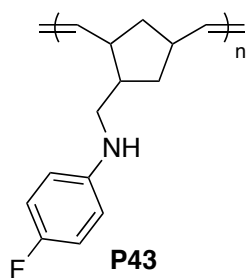
General procedure for polymer synthesis

The synthesis of polymers presented in this chapter has been disclosed in the following citation, and all relevant spectra can be found within this publication.¹⁰⁵ A typical polymerization reaction is described for the polymerization of methoxy-substituted norbornene monomer, **6** to generate **P6**. A solution of monomer **6** (100 eq., 0.20 g, 0.87 mmol) in 2 mL of dry, degassed THF was prepared under a nitrogen atmosphere and stirred using a magnetic stir bar. To this stirring mixture was added a solution of Grubbs second generation catalyst (1 eq., 7.4 mg, 0.009 mmol). The mixture was stirred at room temperature (22 °C) for 20 h and quenched by adding ethyl vinyl ether (excess, 5 eq. vs. [Ru]). After stirring for an additional 30 min, the reaction was added dropwise to a vortex of cold hexanes (-35 °C) to give an off-white, flocculent solid (**P6**). The precipitated polymer was collected by filtration, dried *in vacuo* overnight, and the percent yield was calculated gravimetrically (0.168 g, 84%). Characterization exclusive of GPC was typically conducted on material isolated from the first precipitation. Additional purification required for GPC was conducted using a THF/hexanes system and the polymer was dried *in*

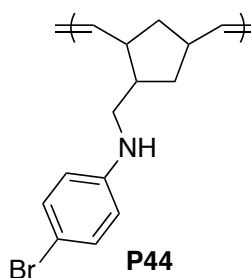
vacuo to constant weight prior to drying in a vacuum oven overnight. All dn/dc values were calculated from 100% mass recovery methods. Resonances are labeled as broad singlets (br s) in cases where no distinct splitting or multiplicity could be determined.



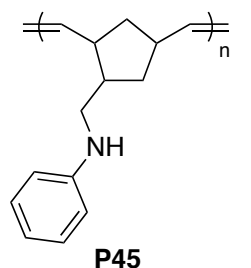
P6. Known compound.¹⁰⁵ ¹H NMR (300 MHz, CDCl₃): δ 6.77-6.74 (m, 2H), 6.57-6.53 (m, 2H), 5.42-5.20 (m, 2H), 3.75 (br s, 3H), 3.11-2.95 (m, 3H), 2.53 (br s, 1H), 1.93 (br s, 2H), 1.64 (br s, 2H), 1.18 (br s, 1H). **IR** (ATR, cm⁻¹): 3395, 2963, 2869, 1511.



P43. Known compound.¹⁰⁵ ¹H NMR (300 MHz, CDCl₃): δ 6.88-6.82 (m, 2H), 6.50-6.46 (m, 2H), 5.45-5.23 (m, 2H), 3.56 (br s 1H), 2.99-2.90 (m, 3H), 2.53 (br s, 1H), 1.95 (br s, 2H), 1.65 (br s, 2H), 1.20 (br s, 1H). **IR** (ATR, cm⁻¹): 3414, 2931, 2861, 1508.



P44. Known compound.¹⁰⁵ ¹H NMR (300 MHz, CDCl₃): δ 7.21 (br s, 2H), 6.41 (br s, 2H), 5.45-5.24 (m, 2H), 3.76 (br s, 1H), 3.01 (br s, 3H), 2.53 (br s, 1H), 1.95 (br s, 2H), 1.64 (br s, 2H), 1.18 (overlapped br s, 1H). **IR** (ATR, cm⁻¹): 3413, 2934, 2860, 1594, 1497.



P45. Known compound.¹⁰⁵ ¹H NMR (300 MHz, CDCl₃): δ 7.20 (br s, 2H), 6.72-6.60 (m, 3H), 5.40-5.28 (m, 2H), 3.91 (br s, 1H), 3.13-2.95 (m, 3H), 2.60 (br s, 1H), 2.01 (br s, 2H), 1.71 (br s, 2H), 1.27 (br s, 1H). **IR** (ATR,

cm^{-1}): 3407, 2931, 2858, 1601, 1505.

Chapter 4: Expansion of Nitrogen-Containing Polymers and Synthesis of Copolymers

4.1 Introduction

Chapter 3 detailed the investigation of the atom-economic and selective syntheses of HAA products and the characterization of these aminonorbornenes. The exploration of the polymerization of these monomers and the testing of the thermal and rheological properties of these new-to-the-world materials was described. Indeed, these small and macromolecular structures proved interesting; all aryl-substituted monomers bearing pendant secondary amines were polymerized and the resultant macromolecules displayed fascinating viscoelastic behavior. These physical properties suggested that H-bonding interactions are present in these polymers. Building upon this proof of concept, Chapter 4 details the expansion of the monomers amenable to this protocol, including an aminonorbornene bearing an alkyl amine pendant group. It concludes by discussing the thermal properties of these various macromolecules in an attempt to understand and exploit the H-bonding potential of these materials.

One noteworthy observation was the inability of Grubbs catalyst, G2, to produce polymer from alkyl-substituted secondary amine substrate **42**. In contrast to the *N*-aryl amines discussed in Chapter 3, alkyl amines possess greater nucleophilicity and thus are more likely to coordinate non-productively to the ruthenium centre and prevent polymerization. Chapter 4 begins by investigating if this limitation could be overcome by utilizing other generations of Grubbs' catalysts, which can initiate polymerization and/or propagate more readily than G2. An investigation into the synthesis of tertiary and quaternary monomer derivatives ensues, with these molecules being targeted to access *N*-alkyl polymers. These monomers would lead to

different H-bonding effects and may have potential applications as materials suitable for metal scavenging or as anti-microbial materials.

Other homopolymers containing various amine and alkene partners are investigated to expand the scope of materials amenable to this strategy. Ultimately, we aim to selectively tune a material for a given application. To realize this objective, other amine groups are implemented in the HAA reaction to furnish monomers that afford diverse H-bonding potential in the resultant polymeric materials. Monomers derived from COD (HAA products **46** and **47**) are also described to probe the effect of a flexible polymer backbone. The linear, polyethylene and H-bonding nature of these polymers could allow for efficient blending with commercial polymers such as polyethylene, polyurethanes, and Nylon.

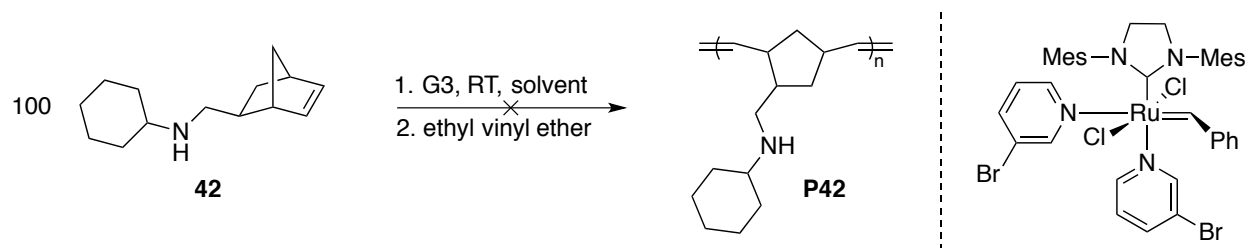
The synthesis of homopolymers is just one exciting avenue to explore with these products of HAA. To further probe the interesting properties brought forth by the amine functional group, it was of interest to synthesize copolymers made in combination with other commercially available, inexpensive monomers, such as NBE and COE. Of particular interest was the production and analysis of copolymers containing low amounts of amine incorporation to explore the extent to which the properties of these novel polymers could be exploited. Ideally, low percentages of amine would still affect the thermal and viscoelastic properties of these value-added polymers, while keeping the overall cost low. Furthermore, precise control over the level of amine-monomer incorporation could lead to copolymers with variable, and tunable properties that depend on the level of H-bonding imparted by the percentage of amine functionality present. A discussion on the synthesis of these homo- and copolymers is presented below, with one example of a copolymer bearing two different amine-containing monomers being included.

4.2 Attempted Polymerization of Alkyl Amine **42** with G3

It is well documented that the polymerization of unprotected, unhindered, secondary amines is often not feasible with conventional Grubbs-type ruthenium catalysts. As mentioned previously, the use of these substrates often results in a Lewis-base, donor-induced decomposition, investigated extensively by Fogg and coworkers.^{24, 26, 64, 126-129} However, secondary aryl amine monomers could be polymerized with high levels of control, although propagation was sluggish, requiring *ca.* 20 h to reach full conversion. Unfortunately, the polymerization of secondary alkyl amine monomer **42** was not achieved under analogous conditions, presumably due to the increased nucleophilicity of this monomer. We were curious if we could overcome the challenges associated with this more nucleophilic amine substrate simply by changing the catalyst employed.

As discussed in Chapter 1, G2 is known to be relatively sluggish with respect to the initiation step of the polymerization. It should be noted that alkyl amine substrate **42** has been reported by Buchmeiser *et al.* to be polymerized by a highly-active molybdenum metathesis catalyst.¹³⁶ This report required laborious monomer synthesis of the alkyl amine substrate, highlighting the need for improved protocols. We were curious to see if using a ruthenium initiator with faster initiation and propagation rates would allow us to access this polymeric motif. The so-called “Grubbs third-generation catalyst” (G3) has a much faster initiation rate relative to G1 and G2 analogues. G3 was also shown to be compatible with the aryl amine monomer **6** in Chapter 3, leading to polymers with controlled MW and *D* values. We were interested to see if a faster initiating system could circumvent the decomposition pathways and lead to productive polymer formation with **42** (Scheme 25). To do this, we investigated the polymerization of **42** in THF, a coordinating solvent, and DCM, a non-coordinating solvent, to

ensure that solvent interactions with the initiator were not hampering productive initiation or propagation of this substrate. DCM is known to promote the requisite dissociation of the axial donor prior to catalytic turnover.⁵³



Scheme 25 Attempted polymerization of secondary alkyl amine substrate 42 with G3

Compound **42** was added to a vial containing a magnetic stir bar. To this vial was added a solution of G3 in either THF or DCM (1 mL). The mixtures were left to stir for 4 hours, after which time a small aliquot was removed from each sample and quenched with ethyl vinyl ether. When polymerizing the secondary aryl amine monomers detailed in Chapter 3, the notable shift in olefinic resonances from the monomer at 6.1 ppm to the ring-opened species at 5.3 ppm was diagnostic of polymerization. When using G3 and **42**, no observable change in the olefinic resonance was noted, regardless of the solvent used (Figure 74). Instead, an off-white, salt-like solid was obtained. Subjecting this material to mass spectrometry revealed a molecular ion peak of 207.6 *m/z*, corresponding to protonated starting material. Furthermore, no evidence of polymerization was observed after 20 h.

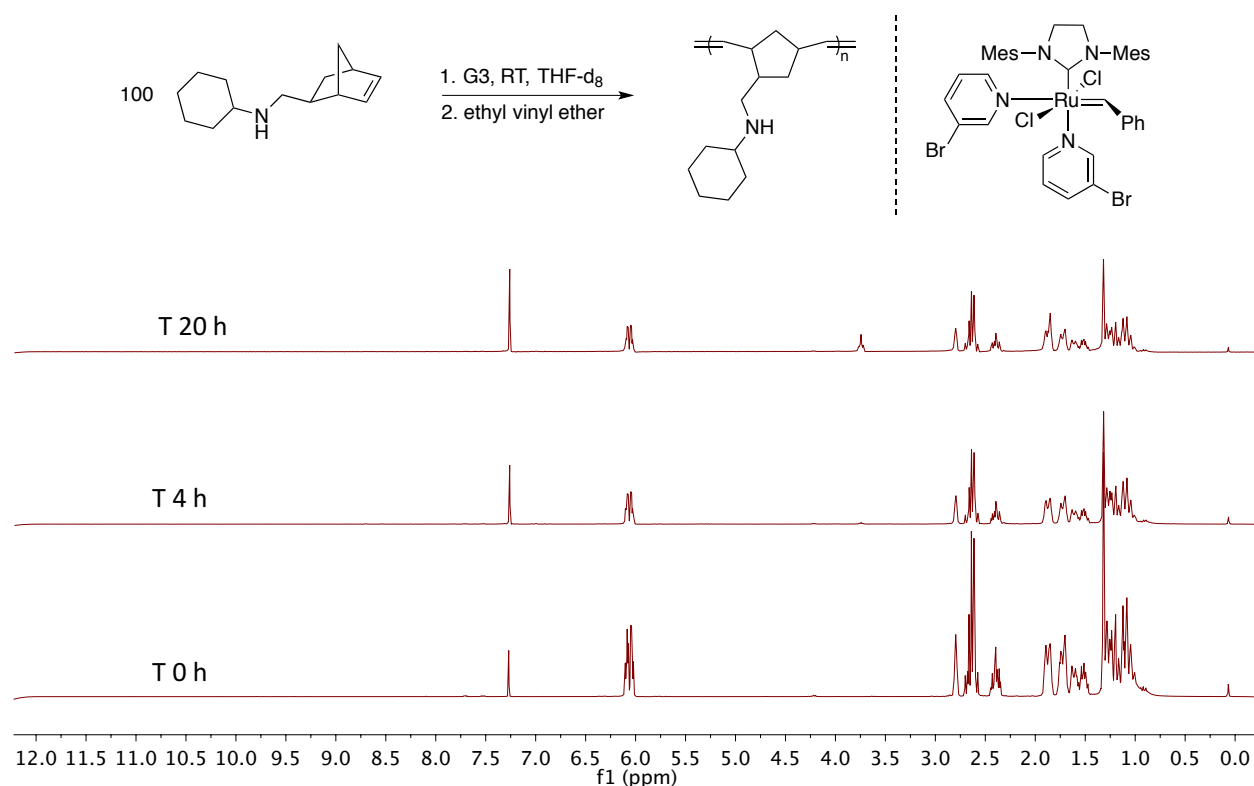


Figure 74 ^1H NMR spectra of **42** and **G3** (bottom), after 4 h (middle), and 20 h (top) (CDCl_3 , 400 MHz, 298 K). Reaction performed in THF, quenched, and dried *in vacuo* prior to analysis in CDCl_3

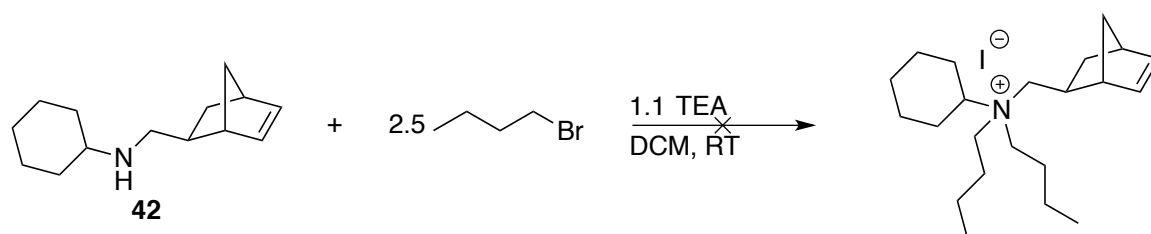
Unfortunately, the polymerization of **42** was unsuccessful despite using a more rapidly initiating and propagating ruthenium catalyst. Presumably, the sterically accessible secondary alkyl amine irreversibly coordinates to the ruthenium centre and leads to decomposition. Attempts to crystallize products from reacting stoichiometric amounts of **G2** or **G3** with **42** have been unsuccessful thus far. One common way to access alkyl amine polymers through ruthenium-catalyzed ROMP is to convert the secondary amine to a tertiary or quaternary amine, thereby avoiding decomposition through increased steric protection. These tertiary amine polymers have shown promise for metal-scavenging procedures.³⁷⁹⁻³⁸⁰ The quaternary amine products are sometimes compatible with Grubbs catalysts,³⁸¹ and have been shown to be

candidates for anti-microbial activity.⁹² The following sections describe efforts to access tertiary and quaternary derivatives of secondary HAA products.

4.3 Derivatization of Cyclohexyl Aminonorbornene Substrate, **42**

4.3.1 Attempted Alkylation with Alkyl Halides to Access Quaternary Amine Monomers

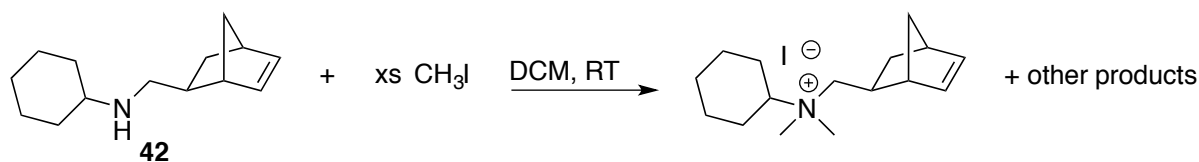
An increase in steric protection about the nitrogen atom was first attempted *via* alkylation. Efforts to quaternize substrate **42** to the respective ammonium salt was attempted by adding an excess of 1-bromobutane (Scheme 26). No precipitate was observed after stirring a solution of **42** and 2.5 eq. of the alkyl halide in DCM overnight in the presence of triethylamine (TEA). The reaction mixture was concentrated *in vacuo* to reveal a white solid. The solid was analyzed by MS and gave mass-to-charge (m/z) ratios corresponding to alkylated triethylamine (158.4 m/z) and monoalkylated starting material (261.1 m/z). No quaternary product was observed by mass spectrometry. All attempts to separate this mixture by recrystallization or column chromatography were unsuccessful.



Scheme 26 Attempted alkylation of cyclohexyl monomer **42** with 1-bromobutane

It was postulated that the *n*-butyl groups coupled with the cyclohexyl moiety were too sterically bulky to allow the formation of the quaternary product. Thus, methylation was attempted using methyl iodide (Scheme 27). TEA was not used due to the previous observation

of alkylated triethylamine. The starting amine, **42**, was added to a 20 mL vial and stirred vigorously. Methyl iodide (3 eq.) was syringed into the vessel and a white solid formed that immediately precipitated from the solution.



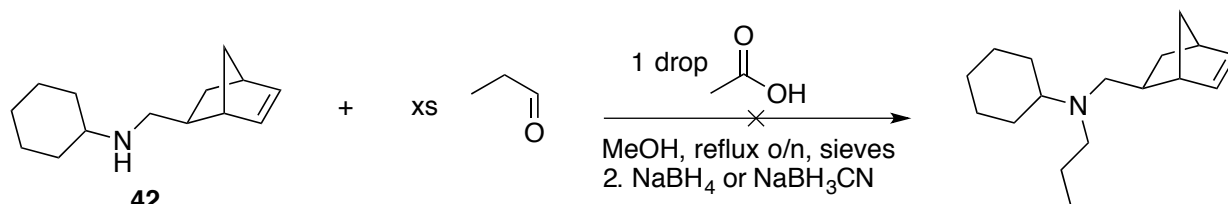
Scheme 27 Synthesis of quaternary ammonium salt *via* alkylation of **42** with methyl iodide

A sample of this mixture was analyzed by mass spectrometry and found to possess the *m/z* corresponding to the desired quaternary amine product (235.6 *m/z*). The tertiary-alkylated product was also observed (219.4 *m/z*). Recrystallization from MeOH or ether yielded the tertiary amine product as a white solid *via* recrystallization from hot methanol, albeit in low yield (<10%). The quaternary amine product was found to be present in the filtrate, but could not be purified despite successive recrystallization attempts in a variety of solvent mixtures. Furthermore, the exclusive formation of the quaternary amine could not be achieved if an additional aliquot (2.5 eq.) of methyl iodide was added to the mixture. The persistent presence of residual tertiary amine side-product consistently complicated purification and isolation of the quaternary amine. The difficulties associated with selective product formation and isolation led us to explore alternative methods of accessing saturated amine products.

4.3.2 Attempted Alkylation of **42** *via* Reductive Amination

The difficulty associated with selective alkylation of the amine moiety on this substrate led us to investigate the efficacy of reductive amination to generate specifically tertiary amine

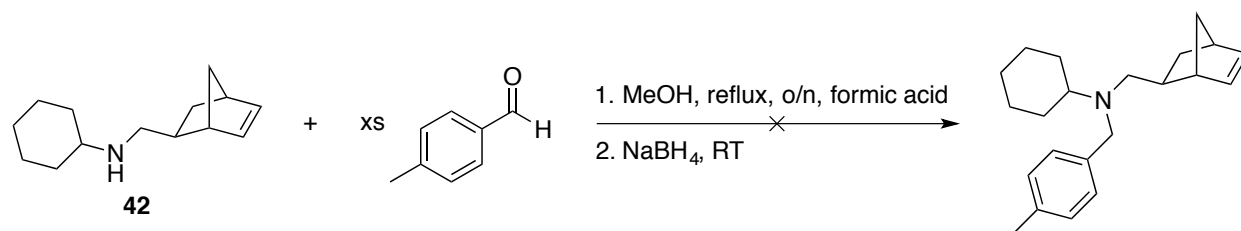
products. Following procedures modified from the literature,^{12, 382-383} cyclohexyl-substituted aminonorbornene **42** was combined with propanal (1 eq.) and dissolved in methanol (Scheme 28).



Scheme 28 Attempted synthesis of tertiary monomers *via* reductive amination with **42**

The solution was left to reflux for 48 hours after the addition of a catalytic amount of acetic acid. No product was obtained as evidenced by GC-MS analysis of the crude mixture. The reaction was repeated using an excess of aldehyde (5 eq.) and the mixture was refluxed overnight in a sealed ampoule to avoid loss of the aldehyde through evaporation as the reaction temperature exceeded the relatively low boiling point (BP) of propanal (*ca.* 50 °C). Molecular sieves were used to remove excess water generated through condensation. After the desired reaction time, NaBH₄ or NaBH₃CN (4 eq.) was added to the mixture to reduce any enamine or imine products which could be susceptible to hydrolysis. The mixture was left to stir overnight before being analyzed by GC-MS. No product was observed in the chromatogram, instead only unreacted starting materials were present.

A less volatile aldehyde, *p*-methylbenzaldehyde, was chosen (BP *ca.* 205 °C) to circumvent the issues with volatility encountered when using lower boiling starting materials. The reaction was conducted in a round bottom flask under a positive flow of nitrogen, and in the presence of molecular sieves to remove any water formed during the condensation (Scheme 29).

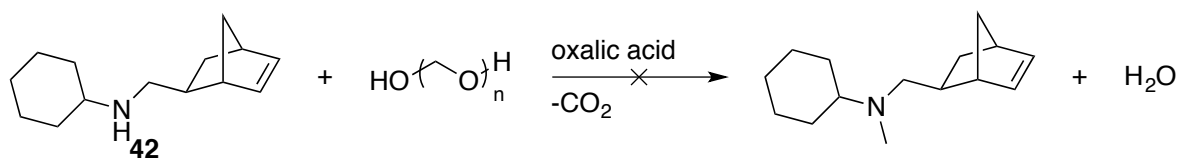


Scheme 29 Attempted alkylation of **42** *via* reductive amination with *p*-methylbenzaldehyde

The reaction vessel was heated overnight at refluxing temperatures (80 °C). After this time, the mixture was filtered using a glass filter frit and the filtrate was analyzed by GC-MS. No product was observed by this method and again the analysis showed unreacted starting materials. Alternative alkylation methods were explored next.

4.3.3 Attempted Eschweiler-Clarke Alkylation

Alkylation of substrate **42** was attempted using Eschweiler-Clarke methylation conditions obtained from the literature.¹⁸⁹ This solvent-free protocol has been shown to be an effective method for alkylation of primary and secondary amines using formaldehyde (or paraformaldehyde). A 250 mL Schlenk flask was charged with **42**, paraformaldehyde (1 eq.), and oxalic acid dihydrate (5 eq.) (Scheme 30).



Scheme 30 Attempted Eschweiler-Clarke methylation of **42**

The flask was purged with N₂, sealed, and heated for 1 hour at 100 °C. Analysis of the crude product by GC-MS revealed full consumption of the secondary amine starting material and

a product having a m/z of 236.2. Interestingly, this mass corresponds to dimethylated product. However, ^1H and ^{13}C NMR spectroscopy revealed consumption of the olefinic peaks of the starting olefin (6.1-6.0 ppm and 136.7 ppm and 136.6 ppm, respectively). This product was not further characterized. The use of this route towards alkylation for the synthesis of tertiary amines as potential monomers was deemed unsuccessful and other methods for derivatization of **42** were explored.

4.3.4 Quaternization of Aminonorbornene **42** with HCl

As discussed previously, the selective alkylation attempts of monomer **42** were surprisingly unsuccessful, often generating inseparable mixtures of products when alkyl halides were used. Amines are easily protonated with acid.³⁸⁴⁻³⁸⁶ The HCl salt of **42** was prepared to yield **48**. White needles of compound **48** were obtained from a DCM solution and analyzed by X-ray diffraction (60%). Analysis of the solid-state molecular structure shows the *exo*-diastereomer, consistent with previously observed diastereoselectivity for tantalum-catalyzed HAA using **2**. This solid-state molecular structure can be found in Appendix D.3 (Figure 104).

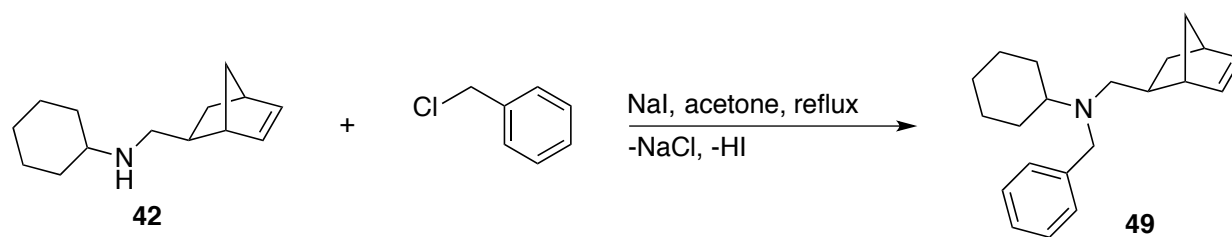
Subjecting compound **48** to standard polymerization conditions was not successful. Specifically, polymerizations using THF, CHCl_3 , or DCM as solvent with G2 as catalyst did not lead to any productive metathesis by ^1H NMR spectroscopy, as no change in the olefinic resonances of **48** were observed after 20 h. The unsuccessful polymerization of **48** led us to explore alternative avenues. We opted to target tertiary amine derivatives, as these are commonly reported as suitable monomers for ROMP.^{26, 43, 64-65}

4.4 Synthesis and Polymerization of a Tertiary Alkyl Amine Monomer

All attempts to alkylate aminonorbornene **42** discussed in the previous sections were met with limited success. However, tertiary amine products could be observed as byproducts. Benzyl chloride has been shown to be a useful alkylating agent for secondary amines,³⁸⁷⁻³⁸⁹ and similar tertiary amine products have been shown to be compatible with Grubbs-type systems.^{64, 390-395} Furthermore, if polymerization is successful with this newly formed tertiary amine, the effects of potential π -stacking observed with aryl amine polymers (Chapter 3) may potentially be mimicked by the benzyl group. The following sections describe the synthesis, characterization, and polymerization of an *N*-benzyl derivative of aminonorbornene substrate **42**.

4.4.1 Secondary Amine Derivatization using Benzyl Chloride

Benzyl chloride (1.5 eq.) was used to alkylate secondary amine **42**. In this synthesis, sodium iodide (1.5 eq.) was used in a Finkelstein-type protocol in acetone (Scheme 31). The mixture was refluxed overnight and let cool to room temperature. The byproduct NaCl was removed by simple gravity filtration.



Scheme 31 Alkylation of **42** with benzyl chloride to form tertiary amine monomer **49**

Pleasingly, only one product peak was observed by GC-MS analysis of the crude reaction mixture. This product was of the desired mass-to-charge ratio (296 *m/z*), supporting the selective

formation of compound **49**. The product was purified *via* a simple back extraction protocol using HCl (6M) and DCM, followed by basification of the aqueous layer with NaHCO₃ (aq, saturated) and re-extraction with DCM. Compound **49** was obtained as a pale, yellow oil in 88% yield after removal of all volatile components and purification *via* column chromatography (hexanes/ethyl acetate, 9:1). ¹H NMR spectroscopy revealed the expected resonances for the newly installed benzyl group at 7.4-7.2 ppm (ArH) and 3.7 ppm (ArCH₂N) in a ratio of 5:2 (Figure 75). The olefinic resonances of compound **49** appear at 6.1 ppm.

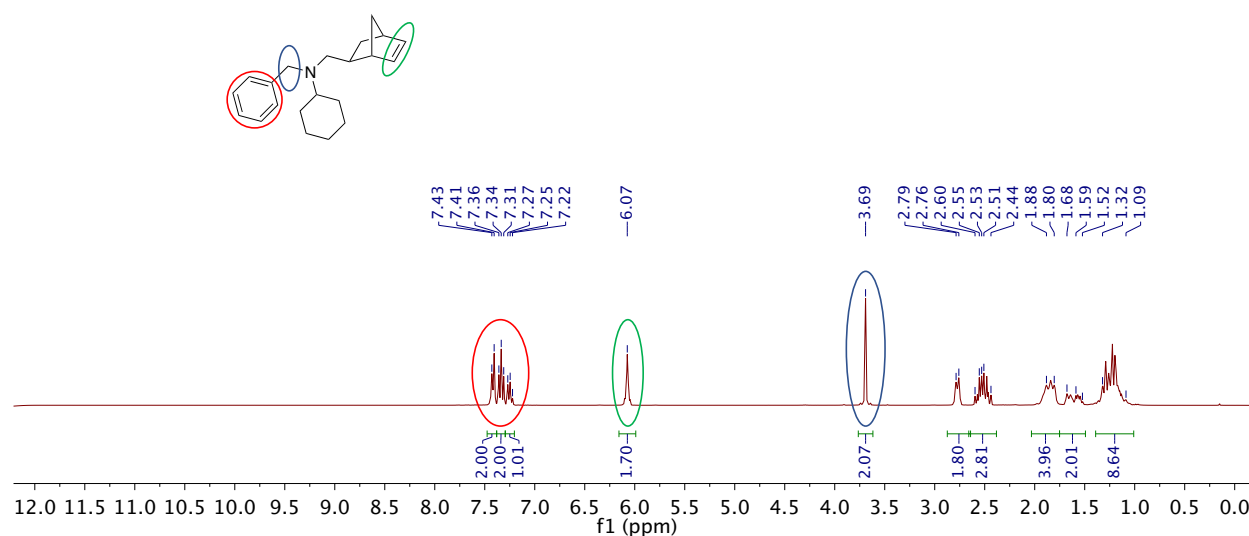


Figure 75 ¹H NMR spectrum (CDCl₃, 300 MHz, 298 K) of compound **49**

High resolution mass spectrometry (HRMS) gave a parent mass of 295.23016 *m/z* relative to the calculated value of 295.23000 *m/z* (C₂₁H₂₉N). Analysis of the oil by ATR-IR spectroscopy showed the disappearance of the N-H stretch of the starting material (3675 cm⁻¹, inlay of Figure 76), supporting the transformation of secondary amine starting material to the desired tertiary amine product.

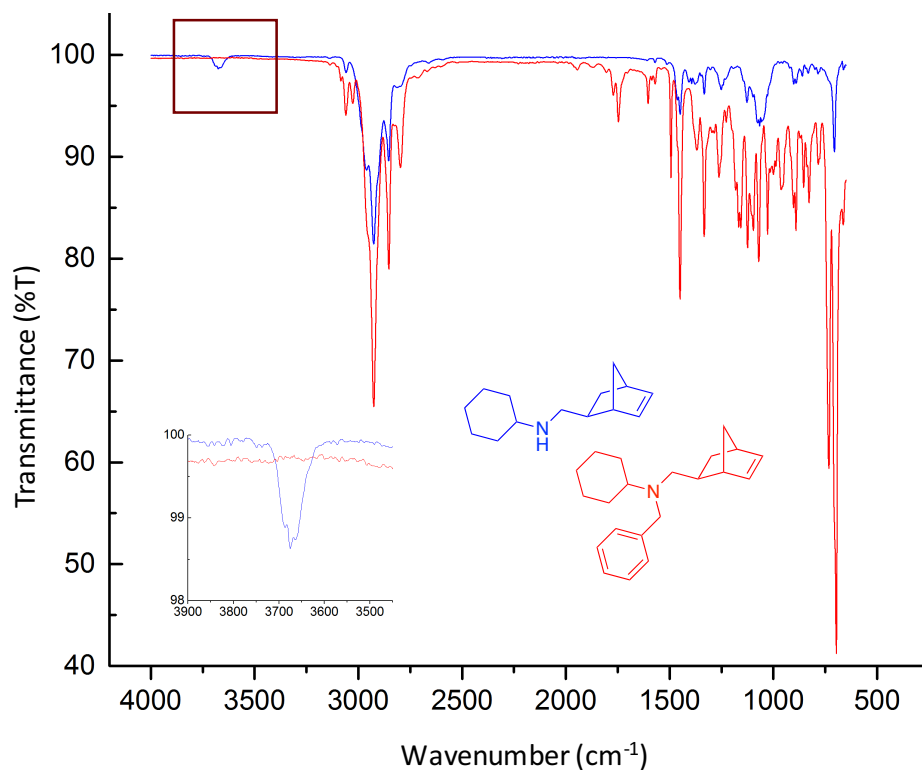


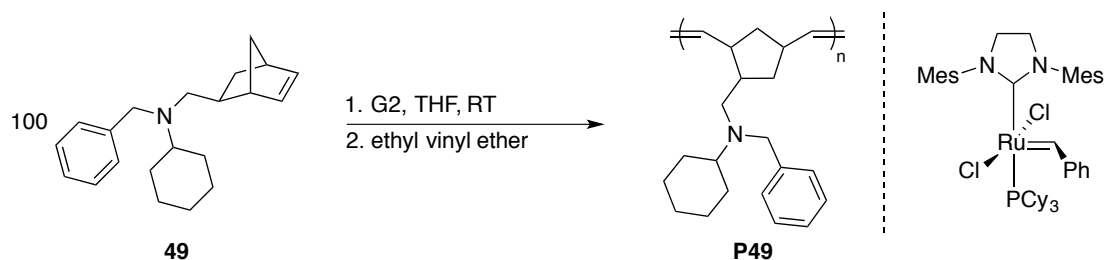
Figure 76 ATR-IR spectra of unprotected, secondary amine monomer, **42** (blue), and benzyl-substituted tertiary amine monomer **49**, (red). Inset shows the NH stretching region

4.4.2 Polymerization of Tertiary Amine Monomer **49** using G2

Previous polymerization studies using aryl-amine monomers **6** and **43-45** required long reaction times of 20 h to reach full conversion. Central to this sluggish reactivity was believed to be the reversible coordination of the aminonorbornene monomers to the ruthenium metal centre. The success of selectively alkylating compound **42** to generate **49** provided an avenue to compare similar secondary and tertiary amine monomers.

The polymerization of benzyl-amine monomer, **49**, was first attempted using G2. The monomer was subjected to our standard polymerization conditions (100 eq., RT, THF, 0.1

mg/mL) (Scheme 32). An aliquot of the reaction mixture was taken after 2 hours and analyzed by ^1H NMR spectroscopy.



Scheme 32 Polymerization of benzyl amine monomer **49** using **G2**

Gratifyingly, full conversion of monomer **49** was observed, with olefinic resonances once appearing at 6.1 ppm no longer visible by ^1H NMR spectroscopy. Concomitant formation of new resonances between 5.3 and 5.2 ppm were observed. The mixture was added to a vortex (100 mL) of cold methanol to precipitate a white solid having a similar appearance to the secondary aryl amine homopolymers (**P6** and **P43-P45**) discussed in Chapter 3. This solid was isolated *via* gravity filtration and dried *in vacuo* to obtain the desired material in 86% yield. Figure 77 displays the ^1H NMR spectrum of the polymer after complete drying. The resonances of the benzyl group are clearly resolved in the analysis of the polymeric material, with signals assigned to the ArH and ArCH_2N groups appearing between 7.3-7.2 ppm and 3.7-3.5 ppm, respectively.

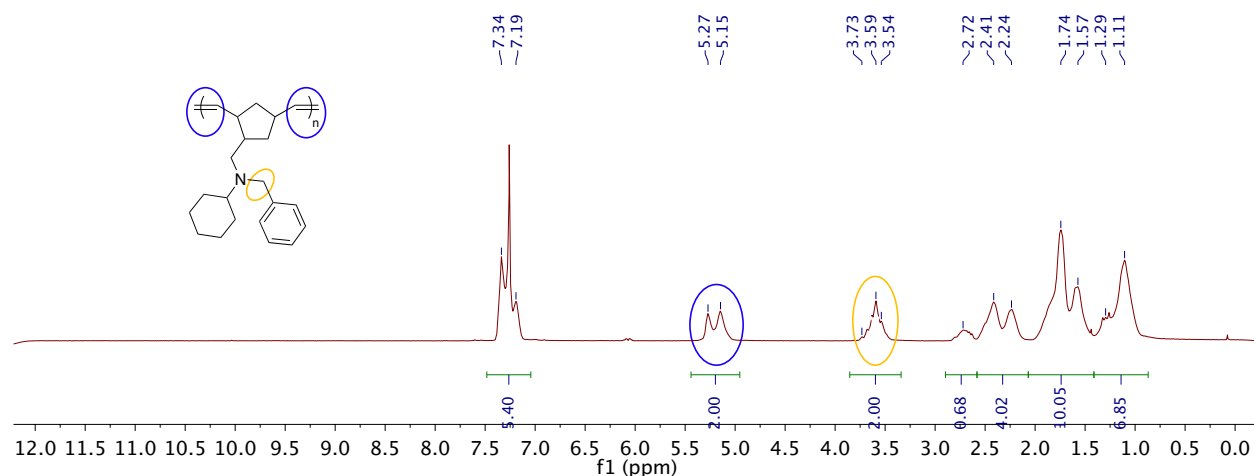


Figure 77 ^1H NMR (CDCl₃, 300 MHz, 298 K) spectrum of tertiary benzyl polymer P49

Elemental analysis was performed on **P49**. Theoretical values (listed in parenthesis, end groups not considered to be consistent with homopolymers discussed in Chapter 3) correspond with those found experimentally and are listed as follows: 84.51 %C (vs. 85.37% theoretical), 10.32 %H (vs. 9.89%), and 4.44 %N (vs. 4.74). Most importantly, the nitrogen incorporation matched closely with expected values. Analysis of the white solid by ATR-IR spectroscopy showed little differences relative to the monomer, which was expected as the ring-opened polymer contains similar functional groups to the starting material (Figure 78).

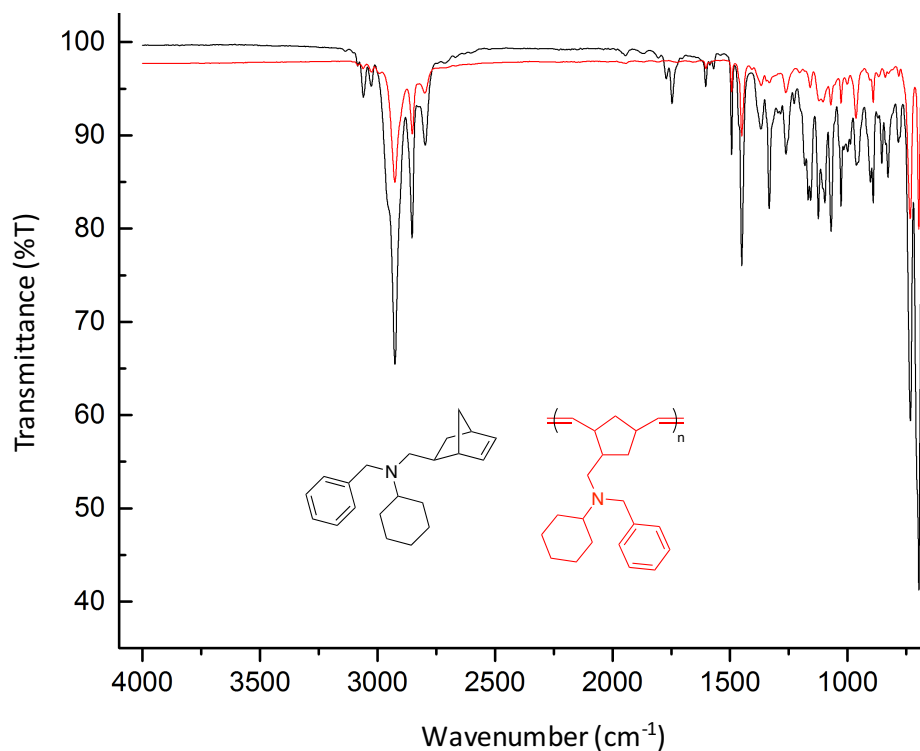


Figure 78 ATR-IR spectra of neat **49** and the ring-opened polymeric form, **P49**

Analysis of the **P49** by GPC gave a M_n value of $158,300 \text{ g mol}^{-1}$, far exceeding the theoretical value (at full conversion) of $29,542 \text{ g mol}^{-1}$. This could indicate that initiation of the ruthenium catalyst is incomplete during this reaction (*vide infra*), leading to chains of greater MW than expected. Interestingly, the \bar{D} of the sample remained relatively low at 1.11. MALDI-TOF mass spectrometry (see Appendix C) confirms the nature of the repeat unit present in the polymer, as peaks were separated by a difference corresponding to the MW of the **49** (295 g/mol). The unexpectedly high MW value obtained could potentially be due to self-assembly within the sample causing formation of higher-ordered species in solution.

Satisfyingly, this benzyl-protected amine polymer, **P49**, is white in colour. As discussed in Section 3.7, the secondary amine-containing polymers discolour over time, with this behavior seemingly becoming more drastic in the solution phase due to oxidation of the aryl-substituted amine moieties. The benzyl-protected variant not only allows for the polymerization of the alkyl amine derivative, but also affords polymers that are white and do not display the undesired oxidation leading to coloured products. Most importantly, the steric protection introduced led to full conversion monomer **49** in no more than 2 h. Intrigued by these results, we were curious to monitor the reactivity of this monomer to gain insight into its reaction profile thereby having a direct comparison to the secondary amine monomers discussed in Chapter 3.

4.4.3 Polymerization of **49** using **G2**: Monitoring Reaction Progress

While it was gratifying that benzyl-protected monomer **49** was susceptible to the standard polymerization conditions, it was of interest to obtain more information about the reaction to potentially allow for optimized conditions. A more rigorous monitoring of the behavior of **49** with **G2** was conducted. Specifically, **49** (100 eq., 0.05g) was dissolved in THF- d_8 (0.3 mL) in a 20 mL scintillation vial and stirred vigorously. Meanwhile, **G2** (1 eq.) was dissolved in THF- d_8 (0.2 mL) and added to the monomer solution before the total mixture was transferred to a J. Young NMR tube *via* pipette. The reaction was monitored by 1H NMR spectroscopy (Table 17). After 5 minutes, 83% of **49** was converted to **P49** and full conversion was reached in less than 10 minutes. These results are also shown in an overlay of 1H NMR spectra (Figure 79). It should be noted that premixing of catalyst and monomer solution in a vial with rapid stirring before transferring to the NMR tube was found to be imperative. Combining the **G2** solution into an

NMR tube containing **49** led to rapid polymerization and solidification of the aminonorbornene and prevented subsequent analysis by ^1H NMR spectroscopy.

Table 17 Conversion of benzyl monomer 49 to P49 using G2

Entry^a	Time (min)	Conversion (%)^b
1	5	82.5
2	7	98.2
3	8	99.7
4	9	100

^aReactions carried out in a sealed J. Young NMR tube at room temperature in THF- d_8 . Total reaction concentration was 0.1 g/mL with respect to monomer. ^bDetermined by ^1H NMR spectroscopy (THF- d_8 , 400 MHz, 298 K).

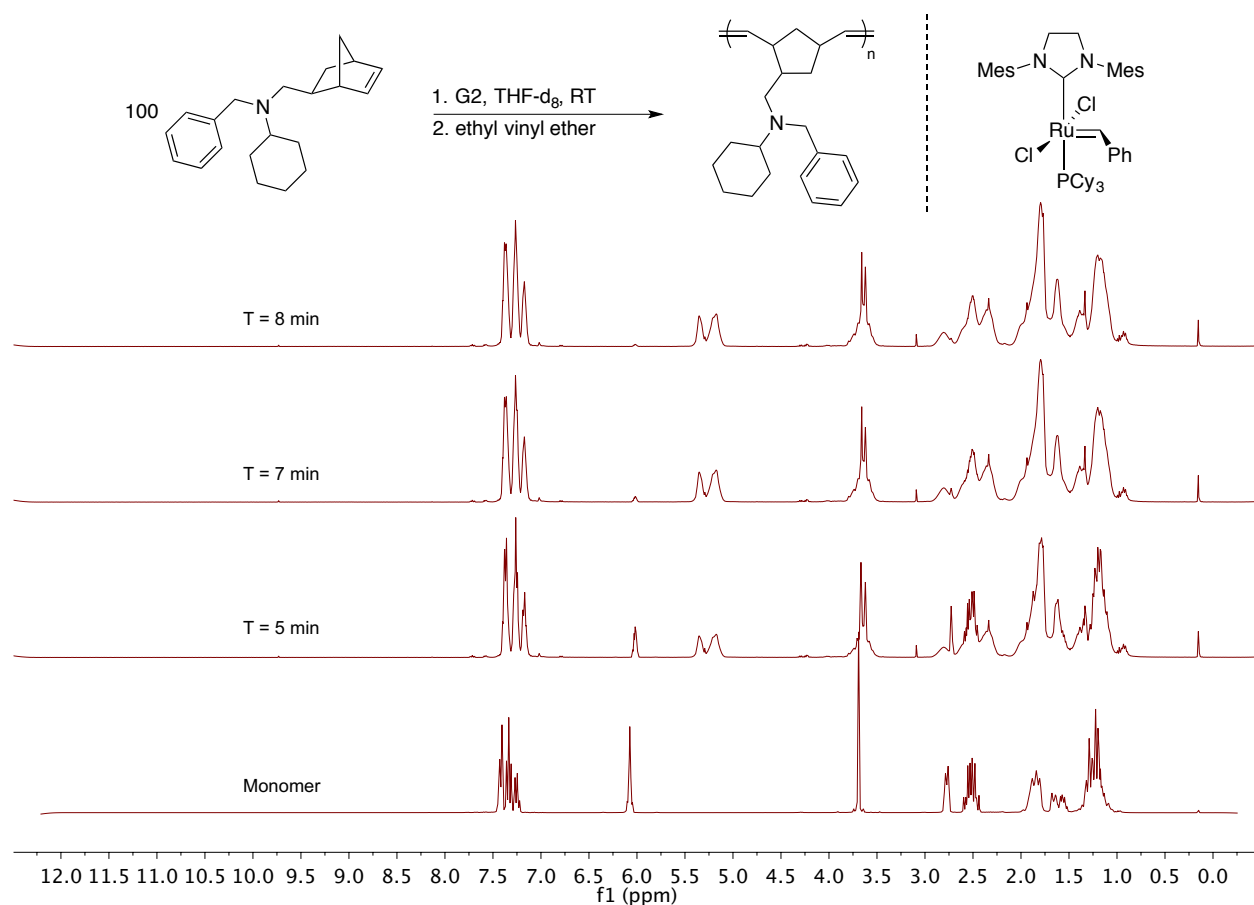


Figure 79 ^1H NMR spectra overlay of monomer 49 over time with G2 (THF- d_8 , 400 MHz, 298 K)

After full conversion of monomer was observed (10 minutes) the polymerization was quenched by the addition of ethyl vinyl ether. The polymer was isolated by precipitation using a vortex of cold methanol (100 mL). A yield of 86% was obtained by gravimetric analysis. Again, GPC analysis of the material gave a high M_n value of 249,100 g mol^{-1} relative to the theoretical value of 29,547 g mol^{-1} , although the D remained low at 1.16. We were curious to see if the discrepancy in experimental and theoretical MW values by GPC would be affected by using other Grubbs catalysts. These experiments are discussed in the sections below.

4.4.4 Reactivity of G1 and G3 Towards Benzyl Amine Monomer **49**

The rapid conversion of *N*-benzyl monomer **49** using G2 led us to investigate other Grubbs catalysts for this transformation. Of interest was G1, as propagation rates are slower relative to G2. We were curious to see if this catalyst would generate polymers with MWs closer to theoretical values. Furthermore, G1 is appealing as it is relatively inexpensive and more easily synthesized than its second-generation counterpart. Also interesting is the fact that secondary amine-containing monomers **6** and **43-45** were previously found to be incompatible with G1. These characteristics could potentially circumvent the unpredictable MW observed when using G2.

The monitoring of the conversion of **49** to **P49** with G1 was conducted as with G2 described above. Figure 80 displays the overlay of ¹H NMR spectra taken at various time points. Pleasingly, the conversion of monomer **49** proceeds rapidly at room temperature. The reaction was quenched with an excess of ethyl vinyl ether after approximately 20 minutes. The polymer was precipitated using cold MeOH. Again, white solid was observed, collected, and dried *in vacuo*, resulting in a 24% yield. Poor yields are attributed to the small quantities of **P49** generated, as this experiment was conducted with *ca.* 50 mg of **49**. Analysis of **P49** by GPC gave a M_n of 63,610 g mol⁻¹ and a low D of 1.01. An expected increase in *trans* content is observed relative to **P49** generated from G2, as G1 is known to generate polymers with higher *trans* content.^{33, 370, 396-397} The *trans* alkene groups resonate further downfield than their *cis* counterparts, and are visible at *ca.* 5.3 ppm.

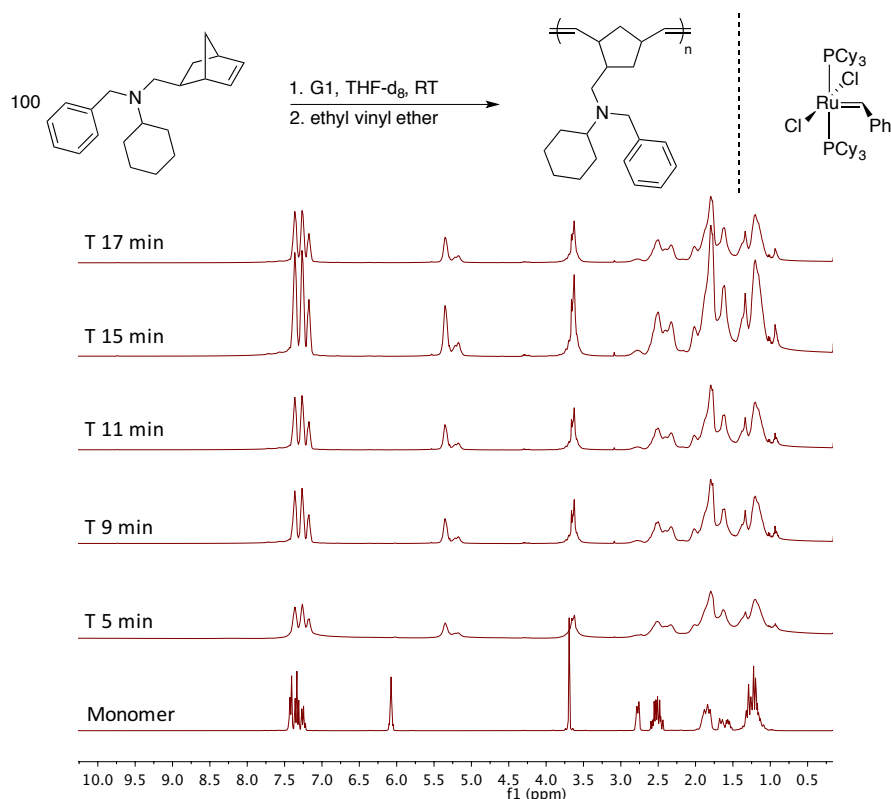


Figure 80 Conversion of benzyl monomer **49** with G1, 100:1

The reactivity of monomer **49** towards G3 was also investigated under analogous conditions. Polymerization of this monomer also resulted in isolable polymers, albeit at a low isolated yield of 27%. These low yields are due, in part, to the problems associated with isolating small amounts of polymeric material, as *ca.* 50 mg of monomer was used in this experiment. The white solid was analyzed by GPC and gave a M_n value of 52,180 g mol⁻¹ and \bar{D} of 1.03.

Comparison of the polymer, **P49**, synthesized by G1, G2, and G3 (Figure 81) is detailed below in Table 18. Interestingly, the more rapidly initiating ruthenium species G1 and G3 generate polymer with a $M_{n, \text{exp}}$ value far closer to $M_{n, \text{th}}$, relative to the more slowly initiating G2.

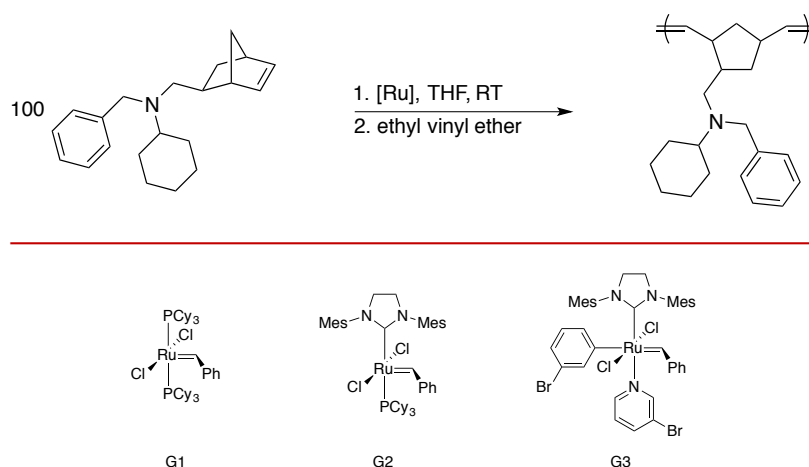


Figure 81 Polymerization of benzyl monomer 49 to generate P49 using G1, G2, or G3

Table 18 Comparison of GPC data obtained for P49 synthesized by G1, G2, and G3

Entry ^a	Initiator	Yield (%) ^b	$M_{n,th}$ ^c	$M_{n,exp}$ ^d	\bar{D} ^e
1	G1	24	29,547	63,620	1.01
2	G2	86	29,547	249,100	1.16
3	G3	27	29,547	52,180	1.03

^aReactions were conducted in 0.5 mL THF-d₈ in a sealed J. Young NMR tube using a M:I = 100 and a monomer concentration of 0.1 mg/mL. ^bCalculated from gravimetric analysis. ^cTheoretical MW, Monomer MW×[M:I]×conversion. ^dDetermined from GPC using 100% mass recovery methods. ^eDispersity = M_w/M_n .

The high MW polymer obtained when G2 is used indicates incomplete initiation of the active species resulting in an increased M:I. When coupled with rapid propagation, a less controlled polymer results. This is also reflected by the higher \bar{D} value obtained when G2 is used (Entry 2) relative to when G1 and G3 (Entries 1 and 3). Although all entries have low \bar{D} values and can be considered to be controlled polymerizations. Lower yields are also observed when either G1 and G3 are used despite near quantitative conversion being reached. This result is attributed, in part, to the drastically reduced molecular weights relative to Entry 2 and, more

likely, the difficulties associated with collecting the small quantities of material generated (<50 mg).

4.5 Material Characterization

The successful synthesis of tertiary amine-containing polymer, **P49**, allowed us to probe the differences with secondary amine polymers. As mentioned previously, the presence of H-bonding in polymers has been shown to increase the T_g values of such materials.^{150, 179}

The thermal properties of tertiary amine polymer **P49** ($M_n = 158,300 \text{ g mol}^{-1}$, $D = 1.11$) were investigated by DSC. A well-defined T_g was observed at 42.7 °C (Figure 82, blue circle). Interestingly, this value is approximately 30 °C lower than the secondary-amine polymers studied in Section 3.10 (summarized in Figure 83) meaning **P49** can go from glassy to rubbery morphology more readily than the secondary-amine counterparts. While this could be attributable to the increase in steric bulk about the nitrogen atom, which may prevent close intermolecular chain interactions from occurring, the elimination of the H-bond donor would also be expected to affect this transition temperature. Specifically, the elimination of the H-bond donor is hypothesized to decrease the inter- and/or intramolecular chain interactions thereby resulting in a decreased T_g . This result highlights how modification of the amine moiety allows tuning of the T_g , an integral physical characteristic of the material.³⁹⁸

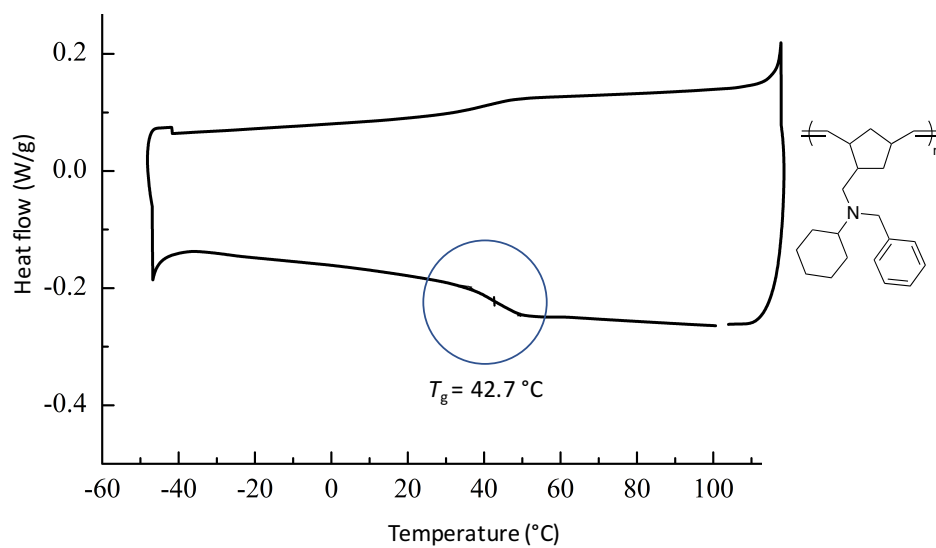


Figure 82 DSC thermogram of P49 ($M_n = 158,300\text{ g mol}^{-1}$, $D = 1.11$)

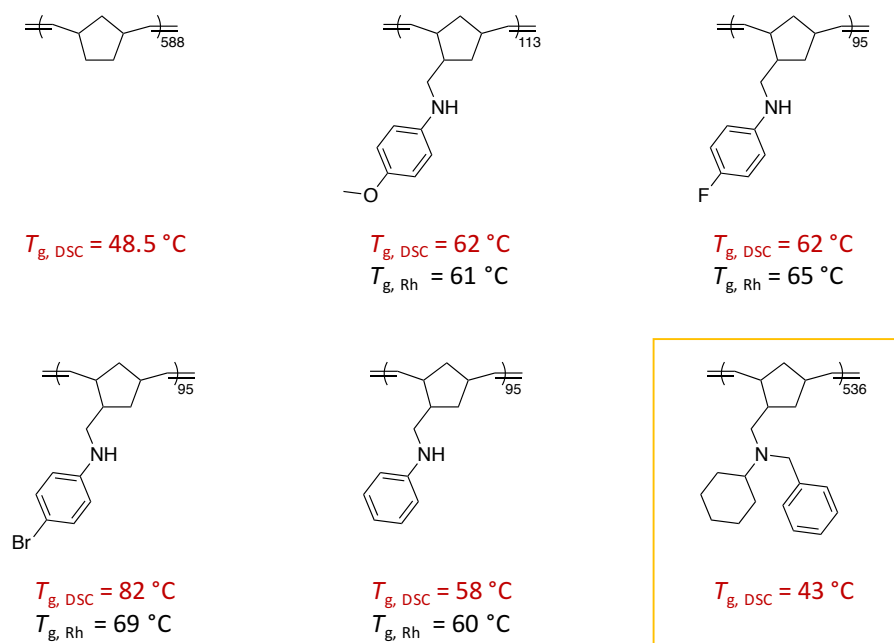


Figure 83 Summary of glass transition temperatures from TGA (red) and rheology (black)

Corroborating results were obtained when the polymer was analyzed by TGA (Figure 84). Much like the other secondary amine-containing polymers studied (except for brominated polymer **P44**), **P49** displays a smooth thermal decomposition. A much lower onset temperature relative to most other aryl-amine polymers studied in Chapter (compared in Figure 85) was observed, attributed to the differing atomic composition and greater monomer molecular weight of this polymer sample.

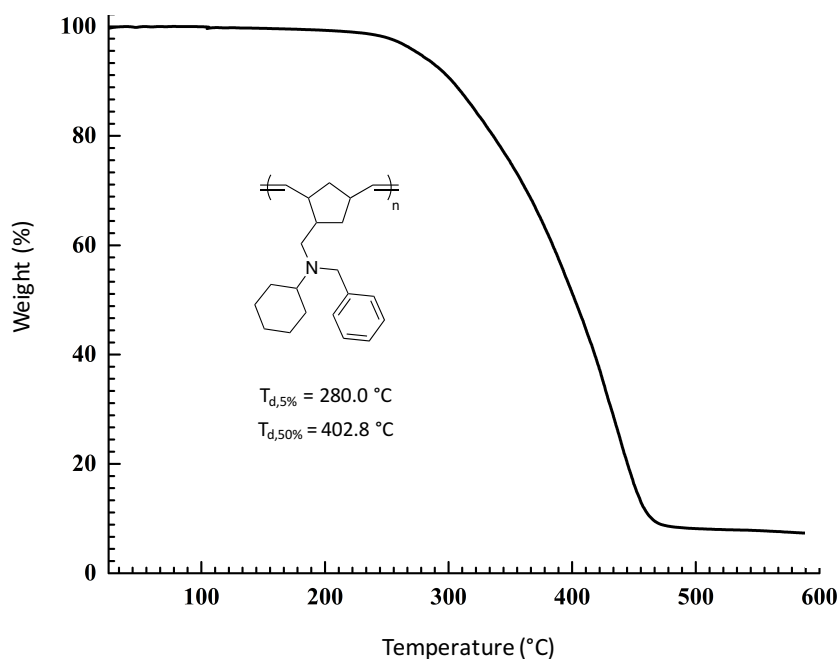


Figure 84 TGA analysis of secondary aryl amine polymer **P49** ($M_n = 158,300 \text{ g mol}^{-1}$, $D = 1.11$)

Tertiary amine-containing polymer **P49** began decomposing at 280 °C ($T_{d, 5\%}$), whereas other secondary aryl amine polymers, which have significant H-bonding potential, did not begin decomposition until approximately 30 °C higher, presumably due to the strength imparted by inter and/or intramolecular interactions of these groups (Figure 85). Interestingly, the $T_{d, 50\%}$ of the tertiary alkyl amine polymer **P49** was found to be 402 °C, a value lower than that of the

polymers bearing secondary-amines, attributed to the elimination of the benzyl protecting group and the relative differences in chemical composition of this tertiary polymer.

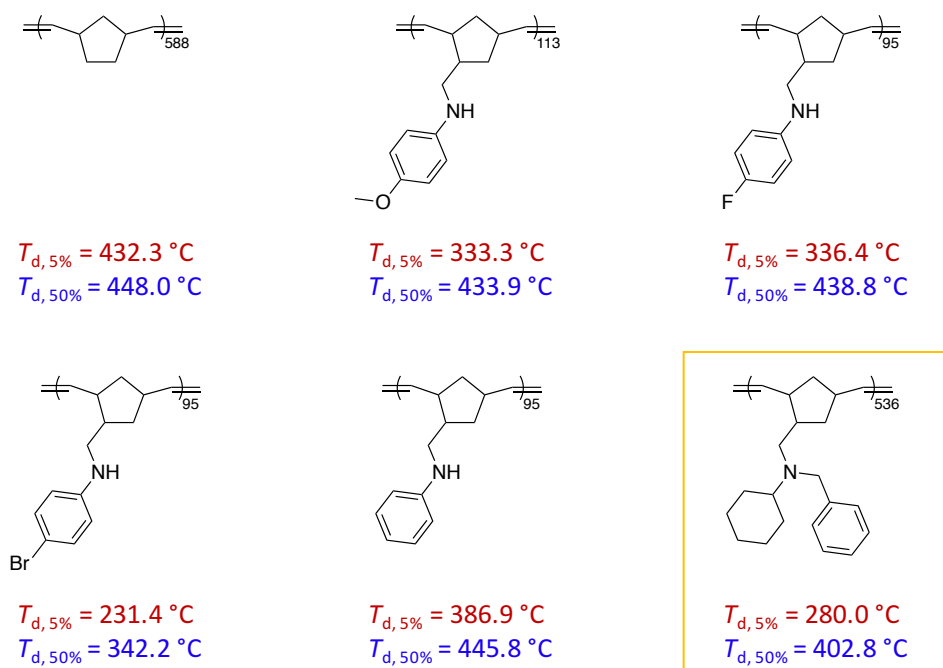


Figure 85 Summary of thermal decomposition data of secondary and tertiary amine polymers. $T_{d,5\%}$ (red) and $T_{d,50\%}$ (blue)

Overall, the investigation of tertiary amine monomer **49** provided valuable insight into the polymerization behavior of the unprotected amines studied in this thesis. Relative to aryl amine monomers **6** and **43-45**, tertiary monomer **49** was rapidly converted to polymer in the presence of Grubbs catalysts. Importantly, G2 leads to full conversion of monomer in minutes, while aryl-substituted secondary amine monomers require upwards of 20 h to reach quantitative conversions. Also noteworthy is the fact that G1 does not tolerate the secondary aryl amine monomers studied, whereas monomer **49** propagates readily in the presence of the first-

generation catalyst. Regardless the of choice of ruthenium catalyst employed, polymer with low levels of \bar{D} are obtained in all cases.

4.6 Polymers Containing Both Amine and Alcohol Functionalities

Incorporating nitrogen functionality into the polymer chain was shown to have dramatic effects on the resultant material properties, with H-bonding considered to be a major factor in determining the thermal and rheological characteristics observed. Interestingly, when tertiary polymer **P49** was analyzed by TGA and DSC, a reduction in thermal stability and T_g was observed. This observation is certainly due, in part, to the decreased interaction between polymer chains. Contrary to this, if the incorporation of stronger H-bonding groups is possible, an increase in these properties should be observed. Thus, the expansion of secondary-amine monomers to include the incorporation of a hydroxyl group in the *para*-position is the focus of this section.

One initial limitation to this proposed hypothesis is that the tantalum precatalyst, **2**, used in the synthesis of monomers by HAA is not compatible with free -OH groups. Therefore, the hydroxyl group of 4-(methyamino)phenol required protection before HAA. The ammonium sulfate salt chosen as it could be obtained cheaply from commercial sources and could be treated with base to give the desired starting material, 4-(methyamino)phenol.

Subsequently, 4-(methyamino)phenol was protected using TBDMS-Cl (Scheme 33).³⁹⁹⁻

⁴⁰⁰ Here, 4-(methyamino)phenol was dissolved in DCM and stirred with a magnetic stir bar. TBDMS-Cl (1 eq.) was added to the mixture in one portion before a DCM solution of imidazole (1.2 eq.) was added. Instantaneous formation of a white solid was observed and the mixture was left to stir overnight, or until full consumption of the starting alcohol was observed by TLC

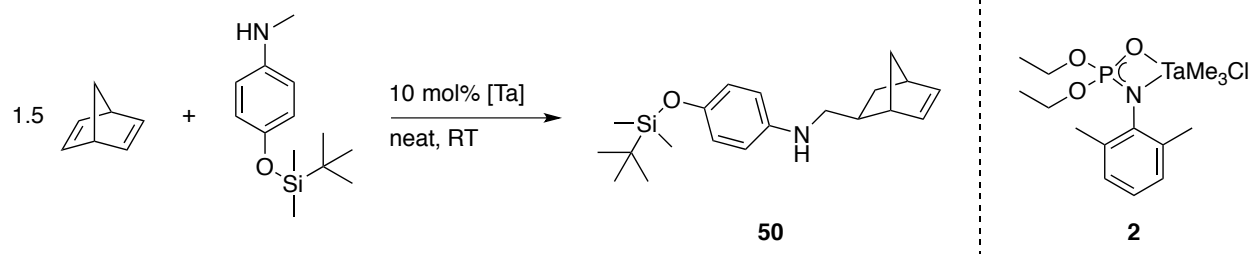
(hexanes/ethyl acetate, 9:1). The product was isolated as a yellow liquid after extraction with 1 M NaOH to give 4.8 g (95 % yield) of the desired silyl ether. Further purification was achieved *via* vacuum distillation to afford a colourless liquid.



Scheme 33 Protection of 4-(methylamino)phenol with TBDMSCl

Distinct resonances attributed to the TBDMS group were visible in the ¹H NMR spectrum at 1.1 ppm and 0.3 ppm. These signals correspond to the three equivalent methyl groups of the 'butyl group, SiC(CH₃)₃, (9H), and the two equivalent methyl groups of the silicon-based protecting group, Si(CH₃)₂, (6H). Importantly, the *NH* resonance is visible at 2.7 ppm. Furthermore, HRMS confirmed the *m/z* of the desired product, 237.15510, which agrees well with the calculated value of 237.15489.

This silyl ether was then employed in HAA using the established conditions with NBD to afford monomer **50**. After 20 h, the crude mixture was purified by column chromatography to afford the desired product in 92% yield (0.69 g) as a colourless oil (Scheme 34).



Scheme 34 HAA using silyl ether to produce TBDMS-protected monomer 50

Characterization of this compound by ^1H NMR spectroscopy revealed the characteristic resonances similar to the other aminonorbornene monomers discussed previously. The ^1H NMR spectrum is displayed in Figure 86. Distinct resonances corresponding to the t -butyl group at 1.0 ppm (9H, red circle) and the two equivalent methyl groups (6H, blue circle) were observed. The olefinic protons (6.1 ppm, 2H, yellow circle) and the NH proton (3.5 ppm, 1H, green circle) give rise to resonances that are consistent with other monomers synthesized by HAA. Furthermore, HRMS gives a m/z of 329.21706, which is in good agreement with the calculated value for $\text{C}_{20}\text{H}_{31}\text{NOSi}$ (329.21749 m/z).

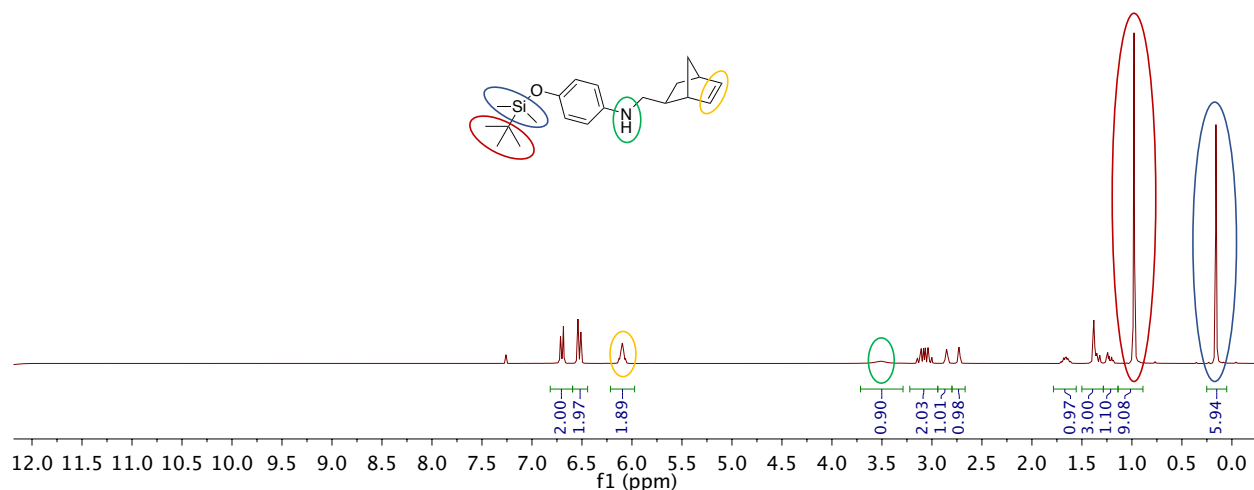


Figure 86 ^1H NMR spectrum (CDCl_3 , 300 MHz, 298 K) of TBDMS-protected monomer **50**

Removal of the silyl-protecting group was possible using tetra-*n*-butylammonium fluoride (TBAF) to generate the desired alcohol, **51**. A white solid was obtained in 60% yield after aqueous workup and sublimation under reduced pressure. ^1H NMR spectroscopy shows the disappearance of all methyl groups attributed to the silyl-protecting group and concomitant appearance of a resonance assigned to the OH moiety (4.0 ppm, 1H, overlapped). Furthermore, HRMS gives the desired parent mass of 215.13090 m/z (calculated 215.13101 m/z). Comparison of the IR spectra of the protected and non-protected aminonorbornenes is displayed in Figure 87.

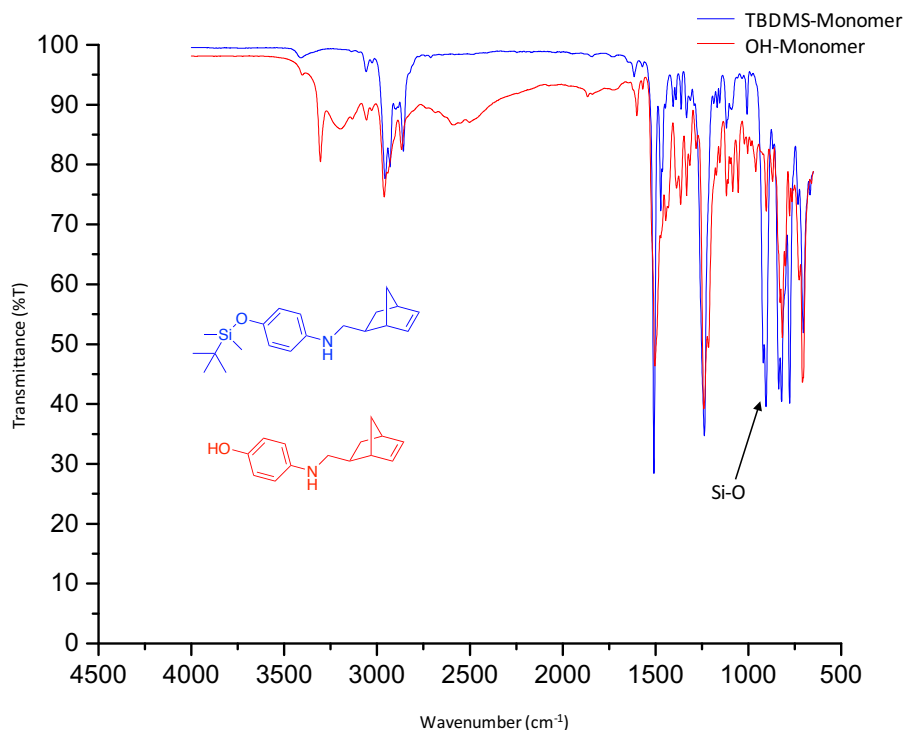


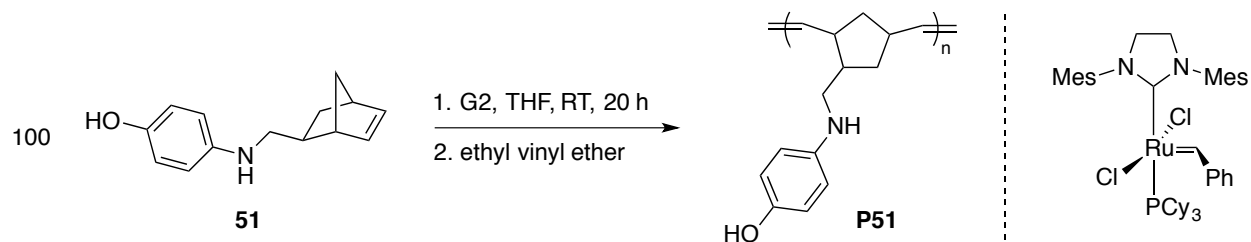
Figure 87 ATR-IR overlay of TBDMS-substituted monomer, **50** (blue), and OH-substituted monomer, **51** (red)

The N-H stretch is consistent between both monomers, occurring at 3418 cm⁻¹ and 3414 cm⁻¹ for the silyl ether and alcohol, respectively. However, this signal is distorted by the absorbance in the OH stretching region at *ca.* 3225 cm⁻¹ for alcohol substrate **51**. A strong, sharp absorption is observed for the Si-O stretch at *ca.* 905 cm⁻¹ for the silyl ether, **50**. Interestingly, two distinct absorptions are observed for the alcohol moiety of monomer **50**. A sharp signal at 3304 cm⁻¹ as well as a broadened absorbance at 3193 cm⁻¹. This broadening is characteristic of H-bonding as varying degrees of intermolecular interaction are averaged over the slightly different absorptions.⁴⁰¹

Alternatively, compound **51** could be accessed by subjecting a crude HAA mixture containing **50** to deprotection conditions in a one-pot protocol. After reacting the starting

materials for 20 h as described above, the mixture was diluted with 5 mL THF and TBAF (1.0 eq. vs. aniline) was added *via* syringe. The mixture was let stir for 1 hour, or until complete deprotection was observed by TLC. However, isolation of the species was complicated, presumably due to the residual tantalum salts in the mixture. In either case, isolation and purification of the alcohol product, **51**, was found to be difficult. Rapid colour change and decomposition was observed, especially in the solution state, presumably due to oxidation to the respective benzoquinone-derivative.⁴⁰²

Polymerization of alcohol **51** was achieved under the standard conditions (Scheme 35). The polymerization required the monomer to be freshly sublimed and used immediately to prevent unwanted side reactions. A white polymeric solid could be collected in quantitative yield (>95%) after precipitation of the polymer from cold hexanes.



Scheme 35 Polymerization of amino alcohol monomer, P51

Analysis of this polymeric material by ¹H NMR spectroscopy revealed a broad singlet at 7.3 ppm (1H), as expected for the OH moiety. Pleasingly, analysis by GPC gave a $M_n = 39,440$ g mol⁻¹ and a $D = 1.01$. However, the solubility of this polymer was found to decrease drastically over time. The sample was left in solution over the course of 1 month. After this time, the solvent was removed and the dried polymer was no longer completely soluble in common solvents, including THF. The original solution used for GPC analysis (2 mg mL⁻¹ THF solution)

was filtered and the soluble portion was analyzed by GPC. Figure 88 displays the GPC traces of the light-scattering (LS) data of the same solution immediately after synthesis and purification (T 0, red trace) and after sitting in solution for 1 month (T 1 month, blue trace). An overlay that displays data from RI and LS detectors can be found in Appendix C.3 (page 319). The same decrease in solubility was observed when the polymer was stored in the solid-state for approximately the same length of time (~1 month). Coupled with longer elution times, these observations suggest a self-assembly, which is magnified relative to the other secondary-amine polymers, owing to the potentially strong H-bonding interactions imparted by the OH groups.⁴⁰³⁻
⁴⁰⁴ Regardless, this phenomenon limited the potential utility of this **P51** and prevented further characterization.

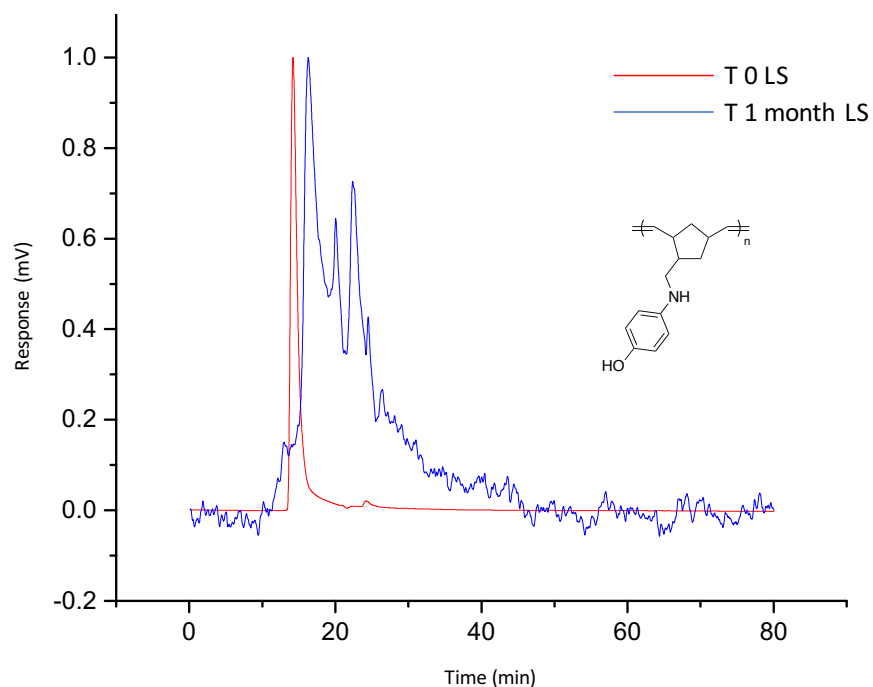
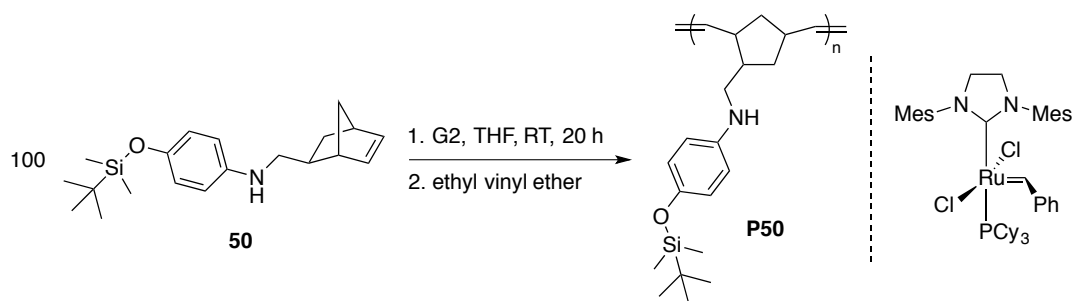


**Figure 88 GPC chromatogram overlay of P51 at T 0 (red) and after sitting in solution for 1 month (blue).
 Light scattering data is displayed**

The poor solubility profile of this polymer, hypothesized to be due to the strong H-bonding associations of the hydroxyl groups, could be avoided by using the TBDMS-protected aminoalkene, **50** for the polymerization reaction (Scheme 36). Following the analogous polymerization conditions, a white solid was obtained in good yield (77%). GPC analysis gave a $M_n = 39,930 \text{ g mol}^{-1}$ ($M_{n, \text{th}} = 32,956 \text{ g mol}^{-1}$) and $D = 1.22$. Analysis by ^1H NMR spectroscopy showed the expected signals of the TBDMS protecting group at 1.0 ppm (9H) and 0.1 ppm (6H), respectively. Thankfully, this polymer displayed a consistent solubility profile over time, with this material being indefinitely soluble in solvents such as THF.



Scheme 36 Polymerization of TBDMS-protected monomer, **50** to generate **P50**

Elemental analysis agrees well with calculated values (calcd: C: 72.89; H: 9.48; N: 4.25; found: C: 72.94; H: 9.87; N: 4.20). Particularly important is the close correlation between calculated and experimental values for the relative quantity of nitrogen present in the material. It was of interest to investigate the thermal properties of **P50** to have comparison to secondary amine polymers discussed in Chapter 3.

4.6.1 Thermal Analysis of TBDMS-Protected Polymer, P50

Polymeric thermal properties were studied by TGA and DSC. TBDMS-protected polymer **P50** displays a T_g value of 72.4 °C (Figure 89). Surprisingly, this value is higher than all polymers discussed in Section 3.9. In particular, **P50** displays an increased T_g relative to the methoxy-substituted analogue (**P6**, $T_g \cong 61$ °C). It was expected that adding a considerable amount of steric bulk to the pendant group would hinder association between neighbouring polymer chains and decrease T_g , as was observed with 3° benzyl amine polymer **P49**. However, in this case, the secondary amine still possesses the ability to H-bond through the free NH group. The electropositive TBDMS group could modify the electronic character of oxygen atom in **P50** in comparison to the methoxy moiety of **P6**. Furthermore, silyl ethers have been shown to be effective H-bond acceptors.⁴⁰⁵

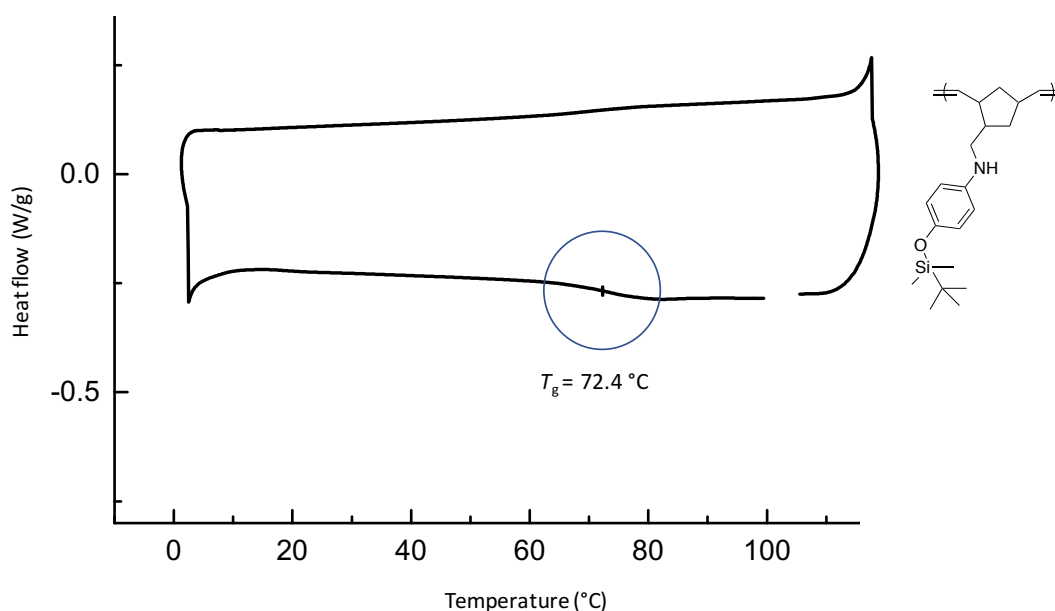


Figure 89 DSC thermogram of TBDMS-protected polymer, P50

The thermal stability of **P50** was monitored by TGA. The polymer began degradation at 378 °C ($T_{d, 5\%}$) and displayed a smooth decomposition profile (Figure 90). The $T_{d, 50\%}$ was measured to be 429 °C. Interestingly, both decomposition temperatures are consistent with those discussed in Table 16, despite this polymer having a considerably higher T_g . This implies that the presence of the silyl protecting group hinders the segmental motion of polymer chains (*ie.* leads to an increased T_g) but does not significantly impact the overall thermal stability of the polymer itself. Indeed, **P50** could theoretically be deprotected to afford an alcohol polymer (*ie.* **P51**), however, the difficulties associated with **P51** discussed above discouraged further investigation into this polymeric motif.

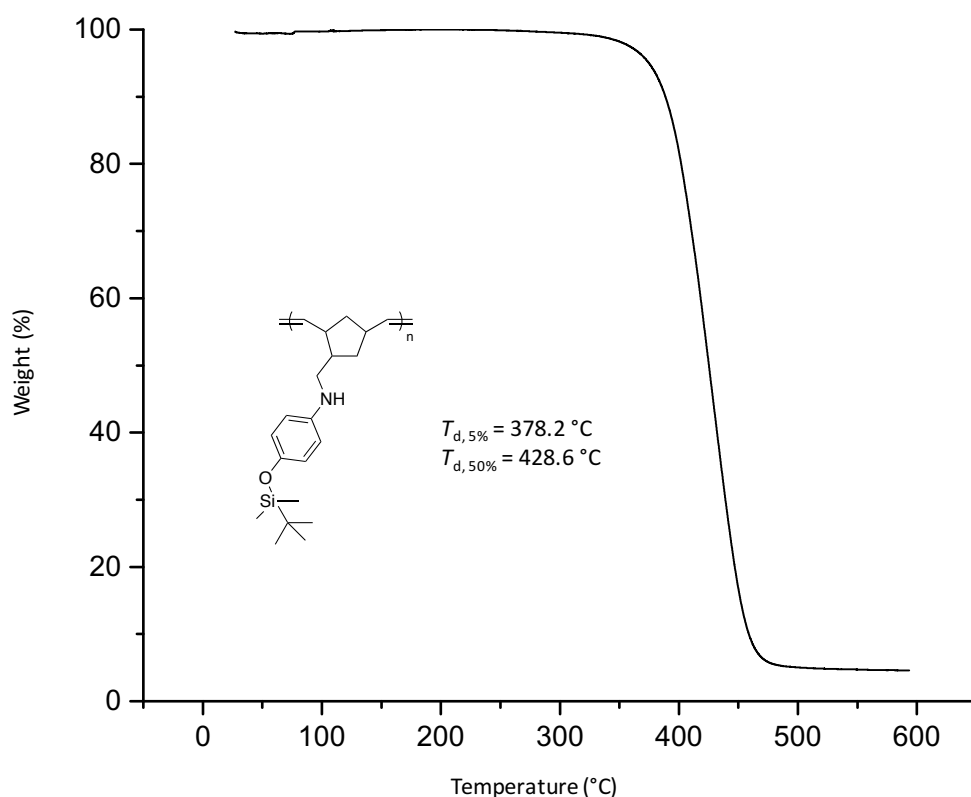


Figure 90 TGA thermogram of TBDMS-protected polymer, **P50**

The results presented in this section indicate that the thermal properties of the polymeric materials can be manipulated by changing the donor and acceptor groups. Strongly H-bonding moieties, as in alcohol monomer **51**, lead to polymers having unpredictable and undesirable solubility characteristics. Presumably, the increased molecular interactions imparted by the OH groups promote cross-linking and self-assembly and inhibit solubility. Interestingly, the protected monomer **50** led to soluble polymeric material, **P50**, that displayed increased thermal stability, namely T_g and T_d values, relative to the comparable methoxy-substituted polymer, **P6**. All of these observations indicate that polymer characteristics depend heavily on the nature of the H-bond donor and acceptor groups, especially considering that the absence of an effective H-bond donor (*ie.* tertiary amine polymer **P49**) results in reduced thermal stability and lower T_g values within these polymeric materials.

4.7 Nitrogen-Containing Copolymers

The unique class of aminonorbornene substrates synthesized by HAA created an interesting avenue into polymer chemistry. The synthesis of novel amine-containing homopolymers was the focus of Chapter 3 and the beginning of Chapter 4. These polymers displayed interesting and variable thermal and rheological properties depending on the amine moiety present in the material. One potential way to harness and exploit the characteristics of these unique amine-containing macromolecules is to incorporate them into copolymeric structures. ROMP has been utilized extensively to access these architectures and a variety of different comonomers have been used.^{26, 43, 406-407}

Copolymeric materials could potentially be used as compatibilizers for polymers blends of immiscible, less polar (*eg.* polyethylene, polypropylene, etc.) and more polar (*eg.* Nylon)

polymers. The immiscibility of these otherwise incompatible polymers hinders the processing of these materials, leading to phase-separation. The advantages of using polymers consisting of segments, or blocks, bearing pendant secondary amines is two-fold. Firstly, the incorporation of such a ‘block’ would lead to a more polar segment, creating the potential to interact with more polar polymers. Secondly, the incorporation of these groups with potential H-bonding capabilities could lead to improved properties of the material overall.

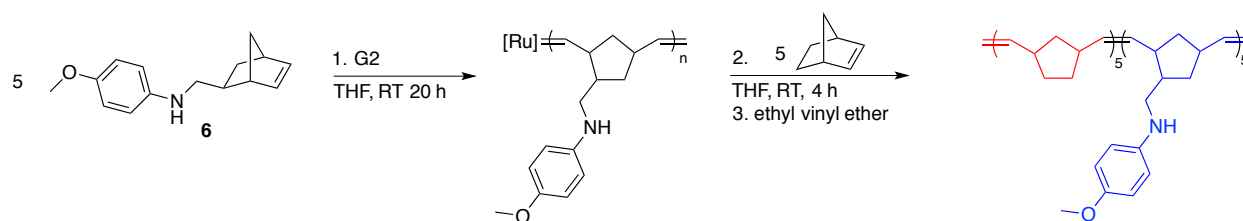
Ideally, low levels of amine-incorporation would still affect the behavior of the resultant copolymer, and materials with different properties could potentially result just from varied amine-incorporation. NBE was chosen as the comonomer for initial investigations. This hydrocarbon is particularly appealing as it is relatively inexpensive and is known to have rapid polymerization behavior with Grubbs catalysts.^{43, 408} Aminonorbornene **P6** was chosen as the amine-containing comonomer as this monomer was most extensively studied in Chapter 3. Furthermore, the methoxy moiety present in **6** provides a convenient handle for analysis by ¹H NMR spectroscopy. The following sections describe the synthesis of copolymers comprised of nitrogen-containing monomers and unsubstituted hydrocarbon comonomers. A synthetic strategy for the facile development of these materials and preliminary thermal characterization of such polymers is presented.

4.7.1 Copolymers of Amine-Containing and Hydrocarbon Monomers

Initial investigations into the synthesis of nitrogen-containing copolymers combining **6** with NBE began by probing the importance of the order of addition. Preliminary experiments utilized a monomer ratio of 5:5 to promote the solubility of the resulting species to aid

characterization. Each monomer was added in a sequential manner to promote the formation of distinct AB block copolymers.

We began by polymerizing aminonorbornene monomer **6** first to form an amine-containing “macroinitiation”, or pentamer, from which the hydrocarbon block could be grown. A two-step procedure was implemented where the slowly propagating **6** was given 20 h to reach full conversion in the presence of G2 (Scheme 37). Next, a solution of NBE (5 eq.) in THF was added and the mixture was left to react for an additional 4 hours before quenching with ethyl vinyl ether (Scheme 37).



Scheme 37 Copolymer synthesis using an amine-containing macroinitiator from **6**, and comonomer NBE

An off-white solid was collected in 53% yield after precipitation from cold MeOH and isolation *via* filtration. Low yields are attributed to the oligomeric nature of the material and the small quantities of both monomers used in the reaction. However, analysis of the material by ^1H NMR spectroscopy provided insight into the percent incorporation of each monomer (Figure 91).

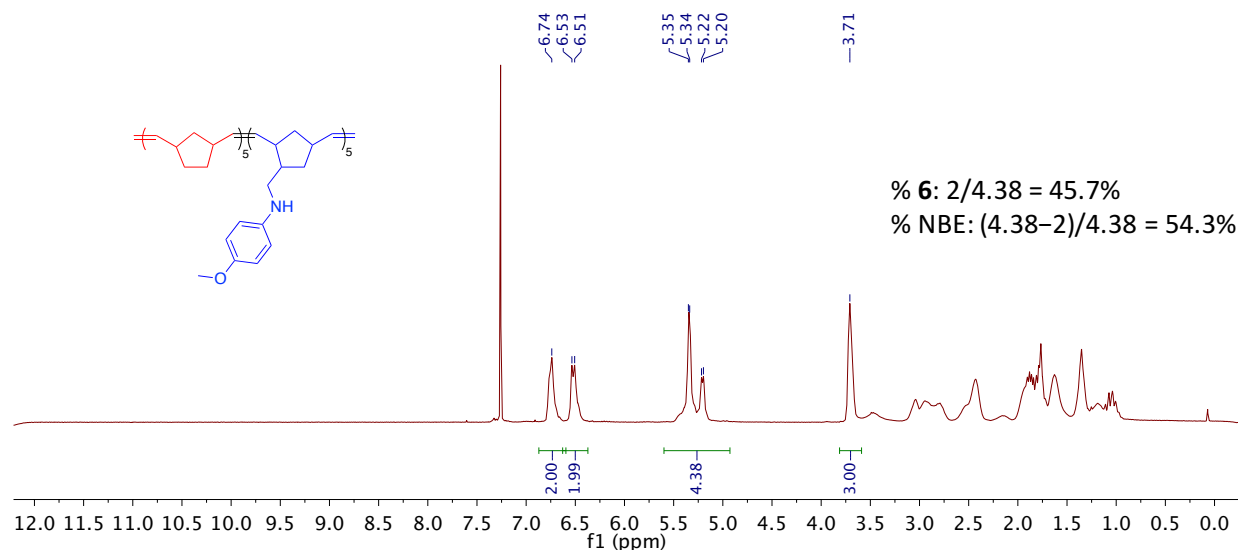
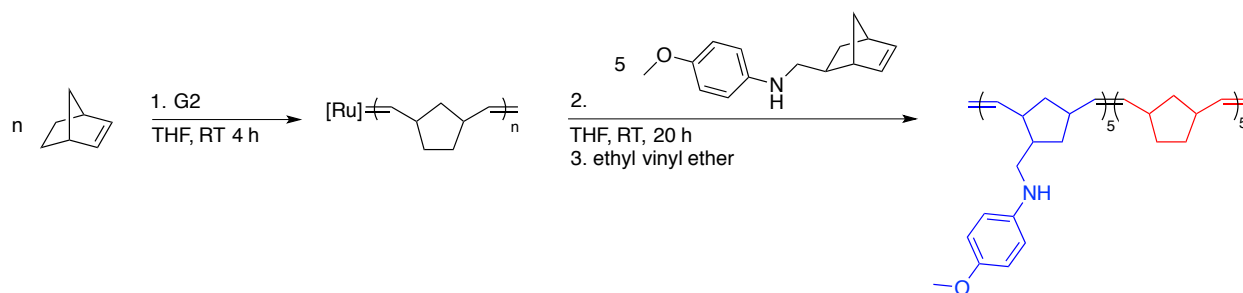


Figure 91 ^1H NMR spectrum (300 MHz, CDCl_3 , 298 K) of a copolymer synthesized using of amine-containing macroinitiator **6** and NBE, 5:5

The presence of the methoxy moiety (3.7 ppm) provided a convenient handle by which to obtain monomer incorporation values. This experiment resulted in material with 46% incorporation of amine-containing comonomer, **6**, and 54% NBE, calculated using the equations displayed in Figure 91. These percent incorporation values determined by ^1H NMR spectroscopy are in good agreement with the expected theoretical value of 50:50.

Elemental analysis was performed on the sample and gave elemental composition values listed as follows, with calculated values shown in brackets: 4.04% N (3.98%); 81.08% C (82.00%); 9.30% H (9.46%). These values are in excellent agreement with the calculated percent composition data and support the formation of the expected decamer resulting from the monomer ratio of 5:5. Unfortunately, end group analysis by ^1H NMR spectroscopy was unsuccessful due to overlapping, broad signals. GPC analysis gave a M_n value of $9,310 \text{ g mol}^{-1}$, which is considerably higher than the $M_{n, \text{th}}$ value of $1,617 \text{ g mol}^{-1}$, and a D of 2.19.

Alternatively, the order of addition could be reversed, with the copolymer being synthesized using a PNB macroinitiator and an amine-containing comonomer, **6**. Reacting the more rapidly polymerizing NBE first would ensure total consumption of monomer before the addition of the second comonomer. This experiment was conducted as described above, with a pentamer of NBE (5 eq.) being polymerized with G2 over 4 h. A solution of **6** (5 eq.) in THF was added and the resulting solution left to react for 20 h before termination with ethyl vinyl ether (Scheme 38).



Scheme 38 Copolymer synthesis using a PNB macroinitiator and comonomer **6**

In this case, the material could be isolated in quantitative yield (>95%) after precipitation and filtration. The off-white solid was analyzed by ^1H NMR spectroscopy and found to be composed of *ca.* 50 % NBE and 50% amine-containing comonomer, **6** (Figure 92). Again, these numbers are in excellent agreement to the expected ratio of 50:50.

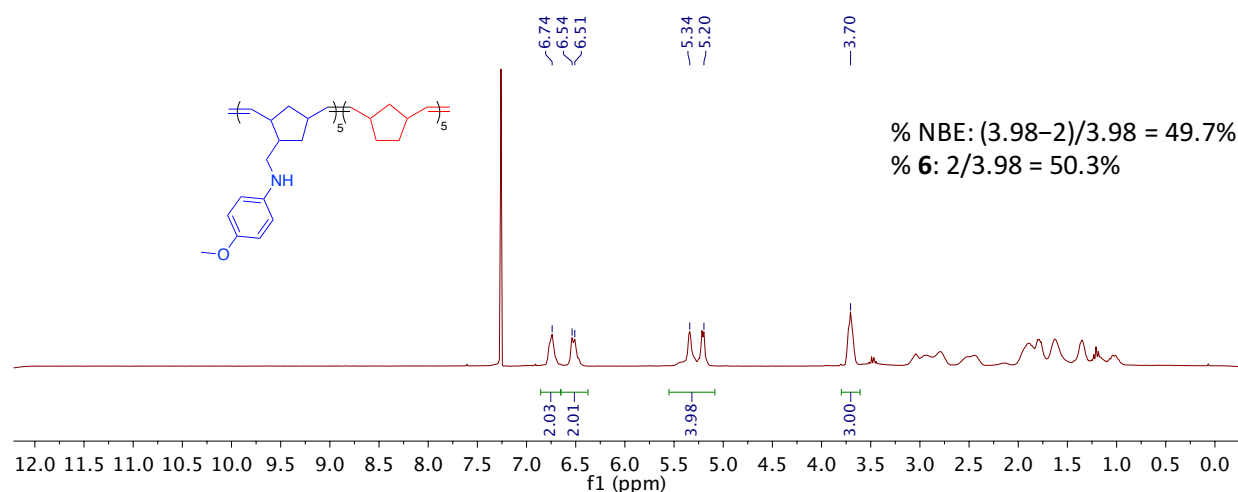


Figure 92 ^1H NMR spectrum (CDCl_3 , 300 MHz, 298 K) of a copolymer synthesized using a PNB macroinitiator and **6**, 5:5

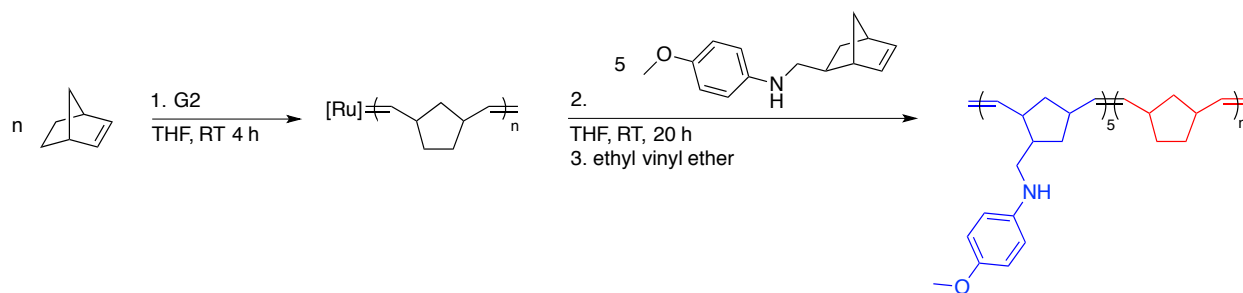
Data obtained from GPC analysis show an experimental M_n of $67,340 \text{ g mol}^{-1}$ which far exceeds the $M_{n, \text{th}}$ of $1,617 \text{ g mol}^{-1}$. Higher than expected MW values are attributed to the rapid polymerization of the strained, unfunctionalized NBE monomer and potential complications with GPC analysis of copolymeric materials.⁴⁰⁹⁻⁴¹¹ Difficulties have been previously encountered when attempting to synthesize controlled, low MW polymers of NBE.¹⁰⁵ However, the dispersity of this polymer sample was decreased relative to the opposite order of addition, and was measured to be 1.20.

Interestingly, the lower \bar{D} obtained when using PNB macroinitiator implies consistent initiation of comonomer **6**. Although deviations from expected MW values indicate rapid, uncontrolled polymerization of the hydrocarbon block. In contrast, when an amine-containing macroinitiator was used, lower MW values were obtained and \bar{D} was high. This implies propagation of the NBE is not consistent throughout the mixture, potentially due to the

ruthenium alkylidene existing in an inactive state. Thus, NBE is only able to propagate upon the reversible decoordination of the amine moiety and results in a broadened \bar{D} .

Ideally, amine-containing copolymers could be synthesized with control over the level of nitrogen incorporation. In doing so, the resulting materials would be theoretically tunable in their H-bonding potential, and synthesized per the desired application. Furthermore, larger hydrocarbon blocks would be desirable. For example, the starting monomer for this copolymer, NBE, is inexpensive and commercially available. PNB, or Norsorex®, is synthesized on a bulk industrial scale and used in applications ranging from anti-slip and anti-vibrational coatings to oil absorbing materials.⁴¹²⁻⁴¹⁴ We were curious to see how variable levels of amine incorporation would affect the resultant material's properties. Fortunately, the percent incorporation values presented above in the synthesis of pentamers are in excellent agreement with theoretical values, and implies that precise control over amine incorporation could be achieved.

It was decided that the hydrocarbon macroinitiator, PNB, would be used for future experiments despite the higher MW values obtained, as low values of \bar{D} were desired. Copolymers were synthesized with various molar equivalents of NBE and 5 eq. of amine-containing comonomer **6** (Scheme 39).



Scheme 39 Synthesis of copolymers from PNB macroinitiators of various chain lengths

Table 19 lists the results of polymerization reactions conducted using various monomer ratios, in a sequential addition procedure. Monomer **6** (5 eq.) was used in all cases, while the relative molar ratio of NBE was varied. Percent yields range from modest to excellent, with lower values being attributed to the difficulties associated with isolating small amounts of material. Again, GPC analysis provided $M_{n, \text{exp}}$ values surpassing theoretical values, a common observation in copolymer analysis. Values of \bar{D} varied greatly between experiments and is due to the difficulties in controlling the synthesis of the PNB macroinitiators used.

Table 19 Data for copolymers synthesized from PNB macroinitiators and 6

Entry ^a	NBE: 6 ^b	Yield (%) ^c	%NBE : % 6 theoretical ^d	%NBE : % 6 experimental ^e	$M_{n, \text{theo}}$ ^f	$M_{n, \text{exp}}$ ^g	\bar{D} ^h
1	5:5	97	50.0 : 50.0	50.3 : 49.7	1,617	67,340	1.20
2	10:5	55	66.7 : 33.3	74.9 : 25.1	2,088	35,540	1.46
3	25:5	66	83.3 : 16.7	87.6 : 12.4	3,501	27,510	1.82
4	50:5	100	90.9 : 9.1	95.8 : 4.2	5,855	121,500	1.27

^aAll entries represent data obtained from single experiments. ^bMonomer ratio relative to G2. ^cCalculated from gravimetric analysis. ^dTheoretical monomer percent (NBE : **6**). ^eDetermined by ¹H NMR spectroscopy. ^fMolar ratio×monomer MW. ^gDetermined by GPC using dn/dc values calculated by 100% mass recovery methods. ^hDispersity = M_w/M_n .

Most importantly, Entries 1-4 show a predictable, consistent increase in the percent of NBE in the material. This observation was observed by ¹H NMR spectroscopy and is illustrated in Figure 93. The integration values of the olefinic region (between 5.5 ppm and 5.0 ppm, yellow circle) increases relative to the methoxy resonance assigned to the nitrogen-containing polymer (3.7 ppm, purple circle). Experimental levels of monomer incorporation are listed above the corresponding spectra.

Table 20 Characterization of copolymers synthesized from PNB macroinitiators and 6

Entry ^a	NBE:6	%NBE : %6 ^c	%NBE : %6 ^d	EA, calcd (%C, %H, %N)	EA, found (%C, %H, %N)
1	5:5	50 : 50	50.3 : 49.7	82.00 9.46 3.98	81.15 9.11 4.23
2	10:5	66.7 : 33.3	74.9 : 25.1	84.54 9.73 3.14	84.30 10.11 2.76
3	25:5	83.3 : 16.7	87.6 : 12.4	85.78 9.93 2.00	83.34 10.12 1.81
4	50:5	90.9 : 9.1	95.8 : 4.2	87.16 10.34 1.17	87.11 11.15 0.60

^aAll entries represent data obtained from single experiments. ^bMonomer-to-monomer ratio relative to G2. ^cTheoretical monomer percent (NBE:6). ^dDetermined by ¹H NMR spectroscopy.

Entries 2-4 were subjected to DSC analysis (Figure 94). The 5:5 decamer, Entry 1, was not analyzed by DSC as the low quantities of material required to obtain the desired monomer-to-initiator values resulted in little polymer obtained for subsequent analysis. Higher monomer ratios (*ie.* 50:5, blue trace) display a T_g value of *ca.* 43 °C, occurring across a broad range of temperatures. When monomer ratios are reduced to 25:5 and 10:5, the lower relative incorporation of NBE gives rise to two distinct T_g values. These polymers, shown in the black and red traces, respectively, possess $T_{g,1}$ values between *ca.* 36 °C and 38 °C, and a $T_{g,2}$ value of *ca.* 56 °C (although subtle in the case of 25:5, black trace), attributed to the two distinct regions in the copolymer. Importantly, these values are both different than that of homo-PNB, which possessed a T_g value of *ca.* 49 °C and the amine-containing homopolymer, **P6** (T_g of *ca.* 61 °C) (see Section 3.9, Table 16).

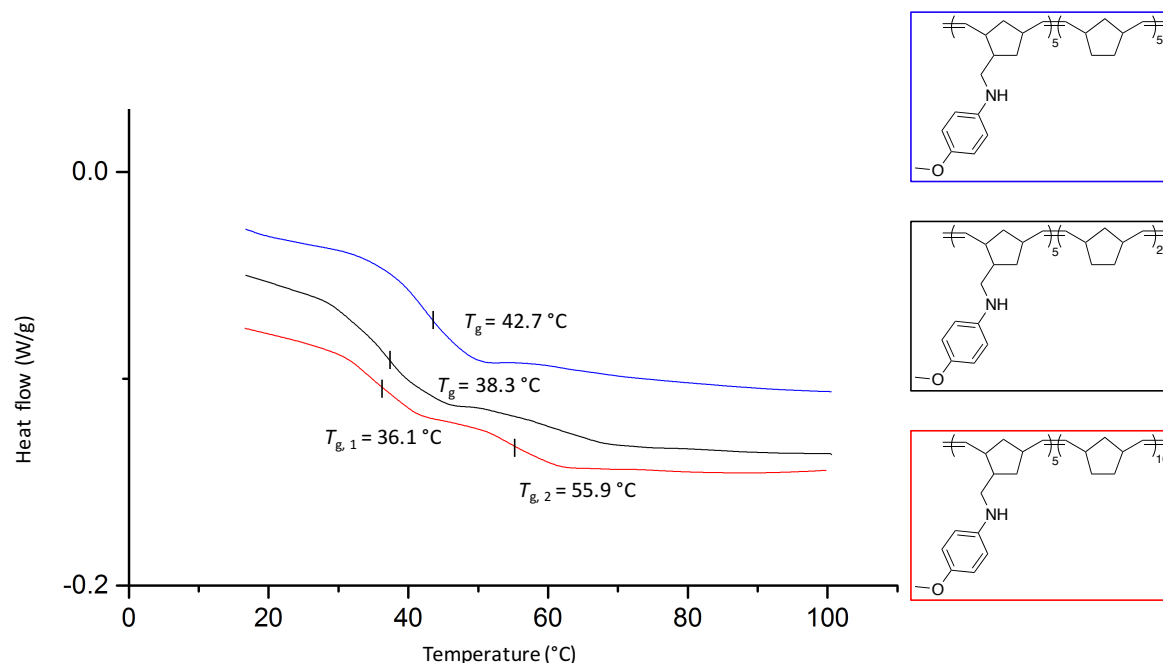


Figure 94 DSC thermograms of poly(NBE-*block*-6) of various monomer incorporations

These results demonstrate that changing the molar ratio in these amine-containing copolymers directly effects the thermal properties of the resultant materials. Lower levels of amine incorporation result in two distinct T_g values to be observed as both blocks give rise to distinct thermal transitions. When the levels of NBE are increased, the T_g arising from the amine-containing portion becomes expectedly less present in the thermogram. Interestingly, as the chain length of NBE is increased, the T_g value changes consistently to higher values. Although this trend was observed with only 3 samples, the increased T_g values observed with low amine incorporation indicates that the thermal properties of inexpensive PNB can be tailored by introducing these unique nitrogen-containing segments.

4.7.2 Amine-Containing Copolymers including Hydrocarbon Comonomers

The interesting results presented above led us to investigate other hydrocarbon comonomers, including COE. This monomer could offer potential benefits when blending with polyethylene, as the ring-opened octene possesses an analogous, linear, flexible backbone. Again, methoxy-substituted amine-containing monomer **6** was chosen as the second comonomer due to its convenient NMR characteristics as well as the in depth understanding of this monomer gained from experiments conducted in Chapter 3 and Chapter 4.

To begin, two polymers were synthesized using a sequential addition protocol expected to generate diblock copolymers (Figure 95), following the experimental procedure described in the previous section. In each case, hydrocarbon comonomer, either NBE or COE, was polymerized first to have direct comparison to the work discussed above and to ensure full, rapid formation of the hydrocarbon macroinitiator prior to building the amine fragment. (Entries 1 and 2, Table 21). These experiments were conducted using monomer-to-monomer ratios of 100:100 to generate copolymers of higher MWs and to probe the effect of longer amine-containing fragments.

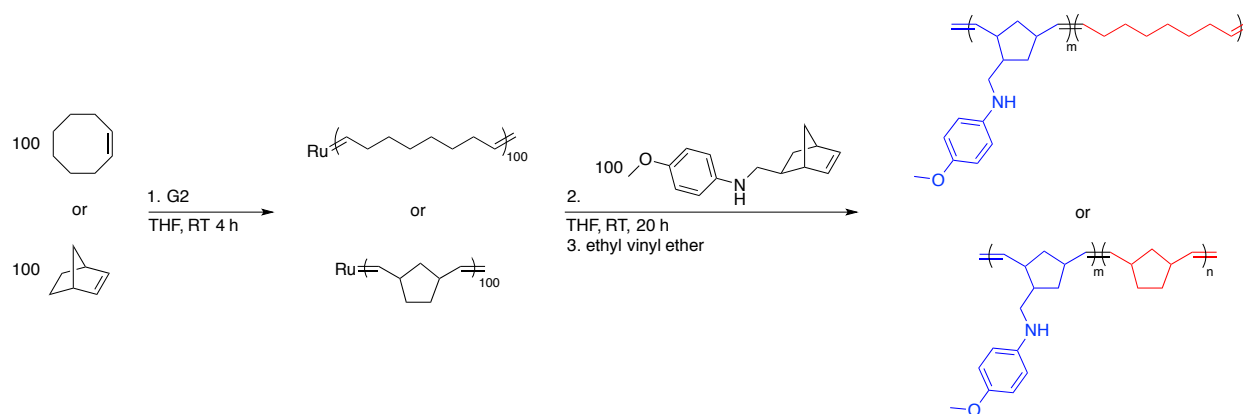


Figure 95 Generation of diblock copolymers from NBE or COE and **6** using a sequential addition protocol

The addition of monomers in a sequential fashion led to polymers that were isolated in good yields, after precipitation, filtration, and drying *in vacuo*, regardless of the hydrocarbon comonomer used (Entries 1 and 2, Table 21). Analysis of the resulting off-white solids by ^1H NMR spectroscopy revealed excellent incorporation values for each monomer. All values were near the expected 50:50 ratio expected from using equimolar amounts of each monomer, indicating near equal incorporation of each monomer in the generated copolymer. A select example of the ^1H NMR spectrum synthesized from NBE and monomer **6** in a sequential addition protocol (Table 21, Entry 1) is displayed below (Figure 96).

Table 21 Copolymers of NBE or COE and **6 synthesized from sequential or single addition protocols**

Entry ^a	Monomers	Addition	Yield (%) ^b	%A : %6 ^c	$M_{n, th}$ ^d	$M_{n, exp}$ ^e	\bar{D} ^f
1	NBE: 6	Sequential	87	47 : 53	32,348	77,420	1.31
2	COE: 6	Sequential	81	45 : 55	33,952	77,620	1.19
3	NBE: 6	Single	70	52 : 48	32,348	76,390	1.37
4	COE: 6	Single	65	11 : 89	-	77,970	1.43

^aAll polymerizations were conducted in THF at RT using monomer-to-monomer ratios of 100:100. All entries represent data obtained from single experiments. ^bCalculated from gravimetric analysis. ^cExperimental monomer incorporation values calculated from ^1H NMR spectroscopy. ^dTheoretical MW, Monomer MW×[M:I]×conversion. ^eDetermined by GPC using dn/dc values calculated by 100% mass recovery methods. ^fDispersity = M_w/M_n .

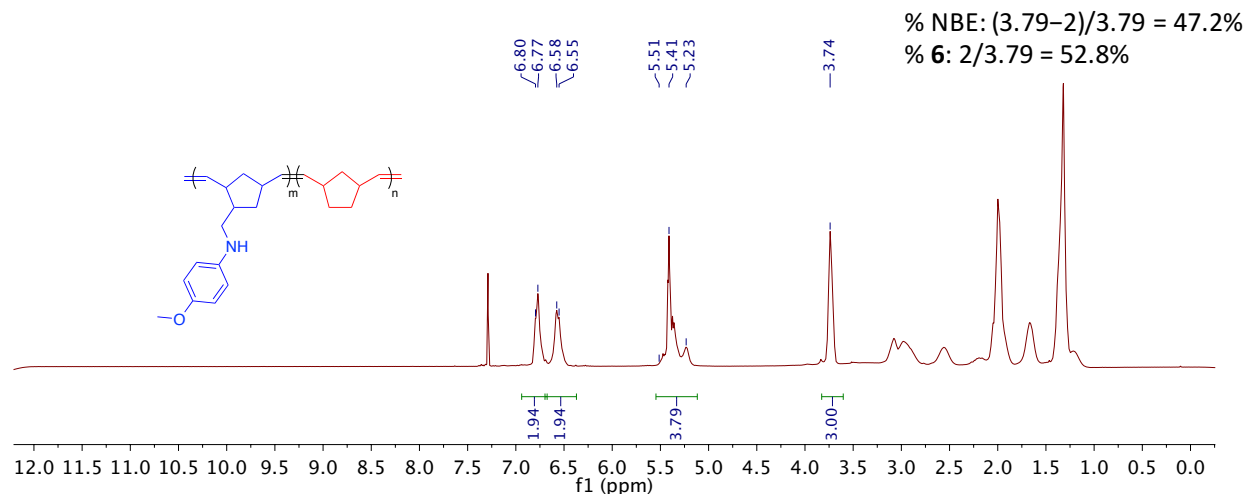


Figure 96 ^1H NMR spectrum (CDCl_3 , 300 MHz, 298 K) of copolymer from 100:100 NBE:6 (Table 19, Entry 1)

Experiments using these monomers were repeated in a single addition procedure. This was done as varying the addition protocol has the potential to generate random or gradient copolymers, however, the significant difference in rates of polymerization between the two monomers make this potential architecture unlikely. Considering this, the single addition protocol is advantageous as it possesses the potential to generate similar materials to the sequential protocol but benefits from an increased ease of synthesis. To conduct single addition polymerizations, G2 was added to a stirring mixture of the two comonomers, negating the need for additional injections of comonomer upon depletion of the first monomer.

Results of this single addition protocol using NBE (Entry 3) and COE (Entry 4) are detailed in Table 21. When using NBE and **6** (Entry 3), initiation and propagation of both monomers proceeded smoothly and gave monomer incorporation values of 52:48 (NBE:**6**) which are in good agreement to the theoretical value of 50:50. The polymer had a $M_{n, \text{exp}}$ value of $76,390 \text{ g mol}^{-1}$ which is higher than the $M_{n, \text{th}}$ of $32,348 \text{ g mol}^{-1}$, but consistent with the other previous AB copolymers discussed in Table 21. Again, this is proposed to be the result of rapid,

less controlled propagation of the hydrocarbon monomer.^{65, 105} The \bar{D} of this sample was measured to be 1.37. Interestingly, when COE was used as the hydrocarbon comonomer, percent incorporation values deviated greatly from the expected 50:50 ratio (Entry 4). In this case, only 11% of COE was incorporated suggesting incomplete conversion of the monomer (although not determined for this reaction). This is potentially due to the decreased propensity of this less strained olefin to ring-open, relative to NBE. The yield of this reaction was decreased as well, although not significantly relative to the other reactions discussed in Table 21, and this is usually attributable to the difficult isolation of these materials on the small scale on which the reactions were performed. The MW of this reaction was measured to be 77,970 g mol⁻¹ and possessed a \bar{D} value of 1.43. Interestingly, this MW value is in line with Entries 1-3, despite lower incorporation of the unfunctionalized block. These polymers were next tested for their thermal properties.

Table 22 Percent composition and thermal properties of copolymers of NBE or COE and 6

Entry ^a	Monomers	Addition	%A : %B ^b	T_g (°C) ^c	$T_{d, 5\%}$ (°C) ^d	$T_{d, 50\%}$ (°C) ^e
1	NBE:6	Sequential	47 : 53	50.9	371.4	427.8
2	COE:6	Sequential	45 : 55	52.6	186.7	426.0
3	NBE:6	Single	52 : 48	54.9	364.2	435.1
4	COE:6	Single	11 : 89	47.5	348.9	421.2

^aAll polymerizations were conducted in THF at RT using monomer-to-monomer ratios of 100:100. All entries represent data obtained from single experiments. ^bExperimental monomer incorporation values calculated from ¹H NMR spectroscopy. ^c T_g as calculated from DSC thermograms. ^d $T_{d, 5\%}$ as calculated by TGA analysis. ^e $T_{d, 50\%}$ as calculated by TGA analysis.

All polymers discussed in Table 21 and Table 22 display similar thermal stabilities, as observed by the $T_{d, 50\%}$ values. These numbers range from 421 °C to 435 °C, with the COE:6 copolymers synthesized through a single addition protocol (Entry 4) having the lowest value,

potentially due to the low values of COE incorporation observed. This polymer possesses the lowest onset decomposition temperature, $T_{d, 5\%} = 349\text{ }^{\circ}\text{C}$, except for the respective polymer synthesized from a sequential addition protocol (Entry 2, $T_{d, 5\%} = 187\text{ }^{\circ}\text{C}$) which displays an unexpected loss of approximately 10% of its mass at these lower temperatures. Barring this unexpected observation, the T_g values displayed in Table 22 and Figure 98 are similar between all copolymers studied. These values range from $48\text{ }^{\circ}\text{C}$ to $55\text{ }^{\circ}\text{C}$ and are displayed in Figure 98.

Despite displaying only small differences in thermal stabilities, the smooth weight loss profiles of these polymers indicate that the synthetic protocol, either sequential or single addition, does not significantly impact the resultant thermal properties.

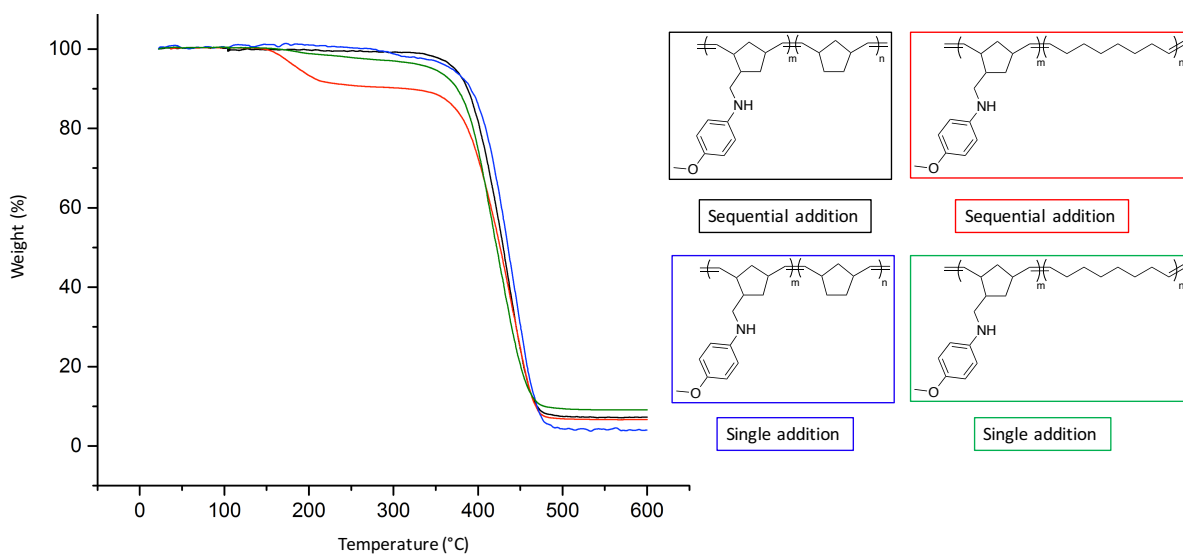


Figure 97 TGA thermograms of copolymers of NBE or COE and 6, described in Table 22

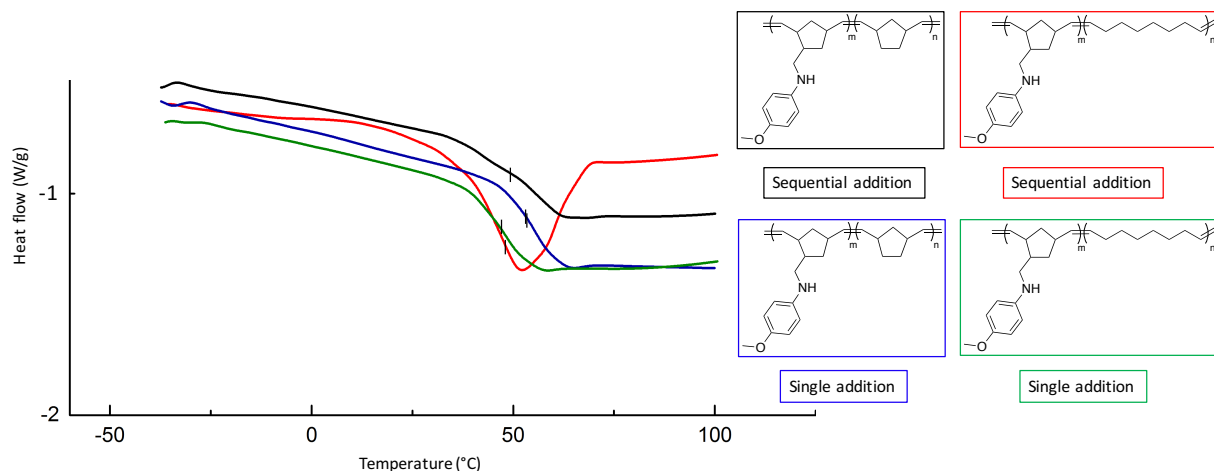


Figure 98 DSC thermograms of copolymers of NBE or COE and **6**, described in Table 22

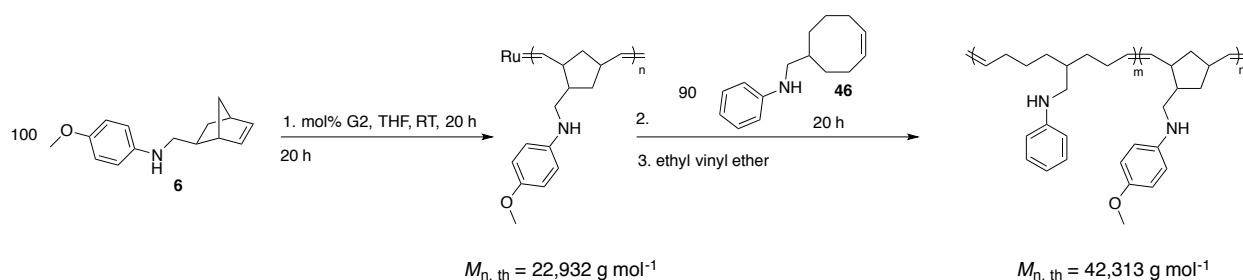
The results presented above indicate that copolymers consisting of amine-containing monomer **6** and either COE and NBE give rise to materials with similar thermal properties. Seemingly, the incorporation of a more flexible, linear hydrocarbon segment (COE) did not drastically influence the thermal behavior of the polymers studied, although problems with equimolar incorporation of this block were encountered. Nevertheless, no significant differences between the sequential and single addition protocols were observed, indicating that the respective reactivity ratios of the two comonomers dictates the molecular architecture, with the more rapidly polymerizing NBE or COE undoubtedly polymerizing first.

4.7.3 Copolymers of Two Amine-Containing Monomers

To compliment the materials discussed in the previous sections, we were curious to synthesize copolymers bearing two amine-containing monomers. Initial investigations began by synthesizing AB-type diblock copolymers in a sequential protocol using two different amine-

containing monomers. Specifically, aminonorbornene **6** and aminocyclooctene **46** were chosen to probe the effect of various backbone structures (Scheme 40).

Monomer **6** (100 eq.) was polymerized using the standard conditions with G2. After 20 h, a sample (100 μ L) was removed from the polymerization mixture, quenched, and precipitated using MeOH to give a flocculent, off-white solid. GPC analysis gave a M_n of 32,310 g mol^{-1} and a D of 1.07, consistent with previous experiments when synthesizing **P6**. Next, an aliquot of aminocyclooctene **46** was added and the reaction left to react for an additional 20 h. Following the termination of this reaction and precipitating into cold MeOH, an off-white polymeric material was isolated in moderate overall yield (*ca.* 60%). This material was observed to be very different to that isolated from the 100 μ L sample (and previous experiments using amine-functionalized norbornenes) and resulted in a less flocculent, more viscous and gum-like polymeric material, attributed to the flexible linear backbone. This physical observation has been observed with homopolymers from aminocyclooctenes, **P46** and **P47**. This copolymer did not require gravity filtration and rather could be isolated simply by decanting off the supernatant.



Scheme 40 Diblock copolymer synthesis using amine-containing monomers

GPC analysis showed an increase in M_n to 45,110 g mol^{-1} and a dispersity of 1.51. This experimental molecular weight is in reasonable agreement with the theoretical value of the

copolymer of 42,313 g mol⁻¹. Interestingly, pairing the aminocyclooctene monomer with an aminonorbornene monomer leads to a more favourable compatibility with THF for analysis by GPC, relative to the homo-aminocyclooctene homopolymers discussed in Chapter 3, which were insoluble once dried *in vacuo*. Also noteworthy is the predictable MW obtained from this copolymer. As discussed previously, copolymers of NBE or COE and aminonorbornenes generate polymers with higher than expected MW values. This result supports that the high values are derived from the difficulties in controlling the polymerization of the unfunctionalized olefin comonomer. However, when the reactivity is reduced (by the incorporation of an amine group) polymeric materials with MW values close to theoretical values are achievable.

An approximate value for percent incorporation of each monomer could be obtained *via* ¹H NMR spectroscopy (Figure 99). Integration of these resonances gave relative incorporation values of NBE monomer **6** of 75% and 25% for the aminocyclooctene monomer **46**, as calculated by the equations in Figure 99. These values deviate from the theoretical ratio of 53:47 (**6:46**). Interestingly, the lower incorporation of unsubstituted COE was observed previously, when synthesizing copolymers of COE and **6** in a single addition protocol (Table 22, Entry 4). This could be caused by problematic initiation and propagation of the sluggish amine-containing cyclooctene, although predictable MW values were obtained. Although it is unclear from where the deviations in the NMR analysis arise, it was pleasing that MW values from GPC are in close agreement to those expected were obtained.

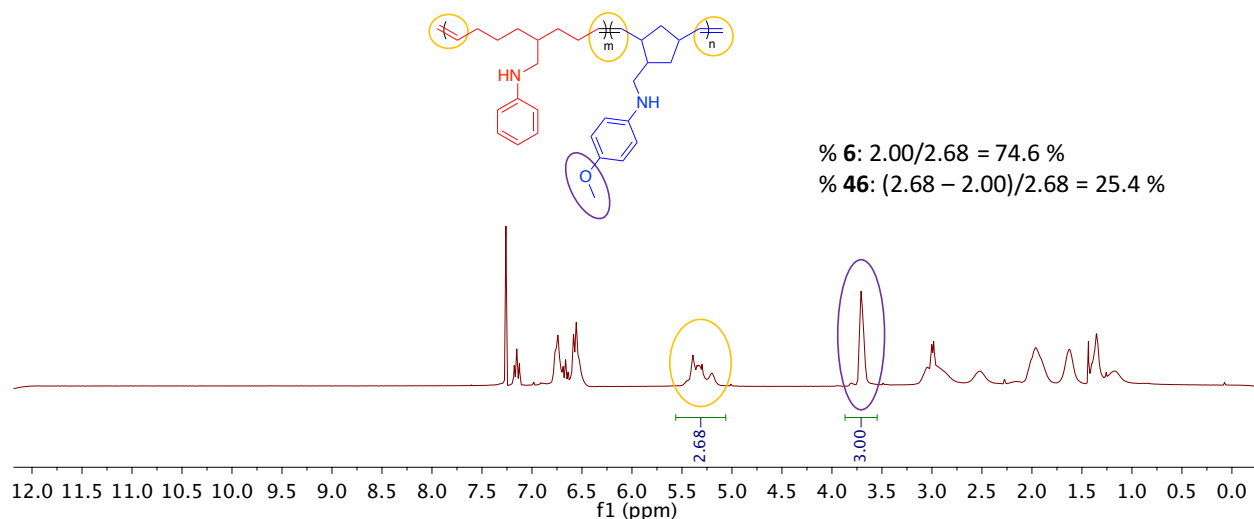


Figure 99 ^1H NMR spectrum (CDCl_3 , 300 MHz, 298 K) of copolymer synthesized from **6** and **46** (100:100)

Elemental analysis was performed on the sample to probe the percentage of nitrogen in the polymer. Experimental values are listed as follows, with theoretical values shown in brackets: 5.69 %N (5.76%); 78.48 %C (81.43%); 8.63% H (9.53%). It should be noted that these theoretical values do not include end groups to maintain consistency with the secondary-amine homopolymers discussed in Chapter 3. Although this analysis technique does not provide direct information regarding monomer incorporation for this particular experiment, as both comonomers contain amine moieties, it can be useful when one comonomer does not contain nitrogen functionality (*vide supra*). Importantly, TGA analysis provides insight into the molecular architecture of the sample. A smooth decomposition trace was observed, indicating that the material is a copolymer, as opposed to a mixture of two homopolymers. The polymer began degradation ($T_{\text{d}, 5\%}$) at 362 °C and reached 50% weight loss ($T_{\text{d}, 50\%}$) at 423 °C. These values are different than those of the homopolymer **P6**, which has a $T_{\text{d}, 5\%}$ and $T_{\text{d}, 50\%}$ of 333 °C and 434 °C, respectively. Interestingly, the thermal properties of this copolymer bearing two

amine-functionalized monomers can be compared to copolymers of COE and **6** discussed in section 4.7.2, where $T_{d\ 5\%}$ and $T_{d\ 50\%}$ were *ca.* 349 °C and 426-441 °C, respectively. The incorporation of an amine-substituted cyclooctene block leads to an increased onset decomposition temperature (362 °C), reflecting the increased initial thermal stability. However, the $T_{d\ 50\%}$ (423 °C) remains relatively comparable to copolymers of unfunctionalized COE and **6**.

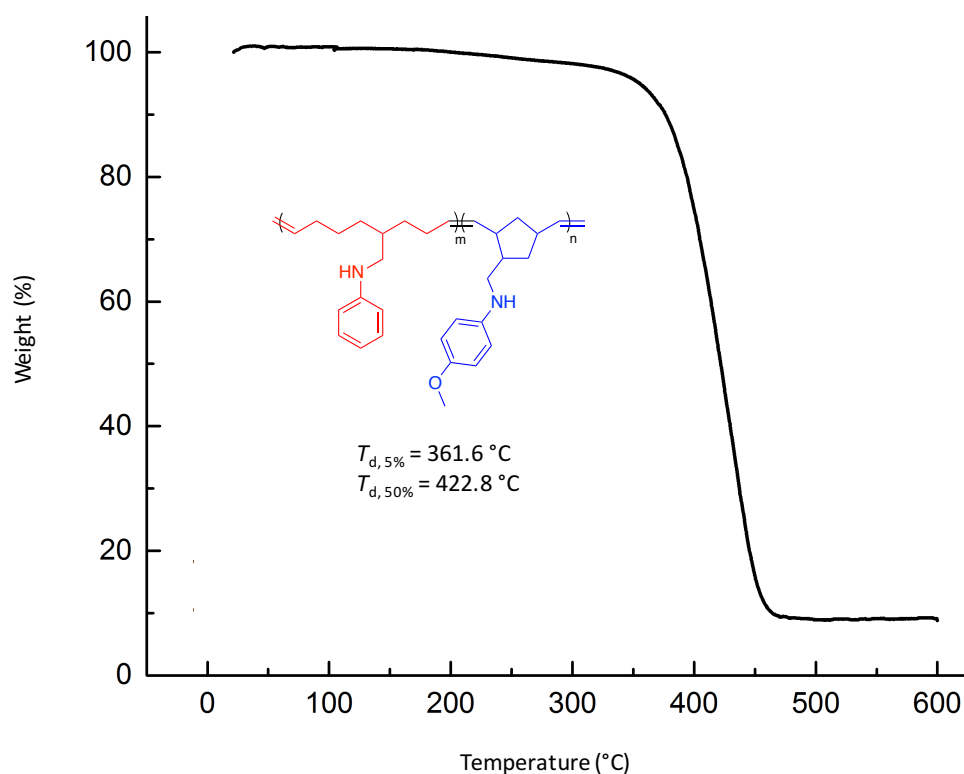


Figure 100 TGA thermogram of amine-containing copolymer comprised of **6** and **46**

Despite deviations from the expected percent incorporation values observed by ^1H NMR spectroscopy, these results indicate that forming copolymeric structures using two monomers containing pendant secondary amines is possible. The development of this synthetic strategy allows for the synthesis of a variety of monomer combinations, with the results of such future

exploits to be assuredly interesting. While the expansion of this protocol to include other monomers is of interest, we were curious to probe the potential uses of some of these amine-containing polymers.

4.8 Potential Applications of Nitrogen-Containing Polymers

Enlightened by the facile monomer synthesis, unexpected compatibility with Grubbs catalysts, and interesting rheological properties of these novel nitrogen-containing polymers discussed in Chapter 3, it was of interest to harness and exploit the power of the amine moiety. Applications targeting the H-bonding and nucleophilic properties of these materials are the focus of the following studies. One intriguing application of nitrogen-containing polymers is their use as anti-microbial materials. Many examples of this application utilize norbornene-based polymers bearing protected or protonated pendant amines, due to the fact that the traditional synthetic protocols do not tolerate unprotected primary or secondary amines.⁸¹⁻⁸² Therefore, we were curious to see if our facile protocol to nitrogen-containing polymers could provide a rapid gateway into potential candidates for these applications.

Selected examples of secondary-amine polymers were analyzed by anti-microbial testing offered by UBC BioServices. Unfortunately, these polymers were not successful candidates for anti-microbial activity towards a variety of microbial strains (MRSA, MSSA, *Enterococcus faecalis*, *Klebsiella pseudomoniae*, *Pseudomonas aeruginosa*, *Candida albicans*) (see Appendix B). This is hypothesized to be due to the inability of the neutral nitrogen moiety to adsorb to the negatively charged cell wall.⁸¹⁻⁸² Regardless, these preliminary studies indicate areas for future investigation. Next, other uses for these novel materials were explored.

One other interesting potential use for polymers bearing pendant amines is metal sequestration, as nitrogen functionalities are often used as ligands and metal-chelators.⁴¹⁵⁻⁴¹⁶ Many examples of amine-containing polymers as effective sequestration materials have been documented in the literature.⁴¹⁶⁻⁴¹⁹ Tertiary amine polymer **P49** was utilized in this study, owing to its greater donor capacity relative to the secondary aryl amine polymers previously discussed. An experiment was designed to test whether **P49** would be suitable to sequester specific metal ions. Specifically, we opted to use Cu(II)SO₄, as it is inexpensive and readily available. Furthermore, Cu(II)SO₄ concentration in solution can easily be determined by UV-Vis spectroscopy ($\lambda_{\text{max}} = 635 \text{ nm}$). A standard curve describing the absorbance values of various concentrations was made through the serial dilution of a 0.40 M Cu(II)SO₄ solution (Table 23, Entry 1-Entry 5).

A filter was prepared using a Pasteur pipette and 50 mg of **P49**. An aliquot of Cu(II)SO₄ (5 mL, 0.40 M) was loaded on the top of this filter and allowed to drip through the plug. This quantity of polymer provided a depth of *ca.* 2 cm inside the pipette, and the 5 mL aliquot required *ca.* 30 min to completely run through the filter. The concentration of the Cu(II)SO₄ filtrate was measured after allowing it to drip through the filter two and three times (Table 23, Entry 7 and Entry 8).

Table 23 Sequestration of Cu(II)SO₄ with tertiary amine polymer P49

Entry ^a	Concentration (M)	Sequestration trial	Absorbance ($\lambda_{\text{max, 635 nm}}$) ^b
1	0.080	-	0.166
2	0.160	-	0.334
3	0.240	-	0.510
4	0.320	-	0.664
5	0.400	-	0.843
6	0.400 ^c	Control	0.843
7	0.400 ^c	Two passes	0.841
8	0.400 ^c	Three passes	0.841
9	0.400 ^c	Stirred overnight	0.839

^aStandard solutions were made by serial dilutions of a 0.40 M solution. ^bAs measured by UV-Vis spectroscopy at $\lambda_{\text{max, 635 nm}}$. ^cCalculated from absorbance values obtained experimentally.

The molar ratios of **P49** to copper sulfate used in this experiment were such that for every nitrogen atom present, there are *ca.* 10 atoms of copper. Therefore, if every molecule of nitrogen were to sequester one atom of copper, the resulting concentration would be reduced to 0.36 M, and a decrease in absorbance value of 0.756 would be observed. Although copper commonly exists with a coordination number of four, we expected this initial experiment to guide our future investigations. Passing the aqueous 0.40 M solution of Cu(II)SO₄ resulted in negligible change to the solutions' concentration after two or three passes (Entry 7 and Entry 8, respectively). Furthermore, a sample of **P49** (*ca.* 50 mg) was stirred overnight in a 0.40 M solution (5 mL) of Cu(II)SO₄. The filtrate was then analyzed by UV-Vis spectroscopy (Table 23, Entry 9). Again, analysis of this filtrate revealed a small change in absorbance, although this change did not result in a significant decrease in copper concentration. Also noteworthy is the fact that the white polymer filter did not display any visible colour change throughout the sequestration experiment, indicating that little or no interaction between the blue copper solution and the white tertiary amine polymer was occurring.

Unfortunately, initial investigations into the potential uses of these amine-containing polymers were met with limited success. No promising anti-microbial activity was observed with polymers such as **P6** and others, and the attempts to sequester copper ions with **P49** were unfruitful. Despite these unproductive efforts, the preliminary synthetic achievements point toward key future developments which will inevitably lead to new and exciting uses for these novel materials.

4.9 Conclusions

This chapter detailed the expansion of monomers and polymers capable of being synthesized by coupling HAA and ROMP. Increasing the size of the functional pendant groups on the nitrogen moiety led to significant changes in the resulting thermal properties of the materials, most clearly observed in DSC and TGA analysis. Larger substituents were appended to the amine moiety and resulted in a decrease in the T_g value relative to the secondary-amine polymers described in Chapter 3. Specifically, the DSC analysis of tertiary-amine polymer **P49**, bearing a benzyl-protecting group led to a decrease in T_g , most likely due to the elimination of the H-bonding ability of the amine group. Conversely, when a TBDMS-protected polymer, **P50**, was studied, a significant increase was observed indicating stronger inter and/or intramolecular interactions occurring through the secondary amine group and the electron-rich TBDMS-protecting group, despite the introduction of larger pendant groups. The investigation into hydroxy-functionalized monomer **51** was hindered by decomposition pathways and led to polymers with unpredictable solubility profiles that prevented adequate characterization and thermal analysis.

Investigations into the synthesis of copolymers began with the generation of oligomers of both hydrocarbon and amine-containing monomers. Initiation from hydrocarbon (NBE) macroinitiators yielded materials with more desirable (lower) dispersity values. These copolymers could be synthesized in a sequential or single addition protocol and the resulting materials show similar thermal properties relative to each other. Elemental analysis and ^1H NMR spectroscopy indicate good levels of monomer incorporation amongst all polymers, except for when poly(COE) was used as a macroinitiator for **6**. This material displayed lower $T_{g, 50\%}$ and T_g values relative to the other copolymers described, potentially due to low levels of COE incorporation.

Diblock copolymers bearing two amine-functionalized monomers were synthesized and showed reasonable experimental molecular weight relative to theoretical values, obtained by GPC analysis. However, levels of aminocyclooctene monomer were decreased from the expected ratio. Thermal analysis indicated that these materials were not mixtures of two homopolymers, and rather a new copolymeric material. The development of a synthetic protocol to generate amine containing monomers and polymers is expected to lead to materials with interesting properties and applications.

4.10 Experimental

4.10.1 Materials and Methods

General Details. All chemistry was performed in a nitrogen-filled glovebox or using standard Schlenk techniques unless otherwise stated. The following chemicals were purchased from Aldrich and used as received: 4-(methylamino)phenol sulfate, imidazole, *tert*-butyldimethylsilyl chloride, 1-bromobutane, methyl iodide, *para*-formaldehyde, propanal, *para*-methyl benzaldehyde, ethyl vinyl ether, copper(II) sulfate, benzyl chloride, and sodium iodide. G1 and G2 were purchased from Aldrich and used as received. G3 was synthesized from G2 per the literature protocol.⁶⁰ Anhydrous solvents were obtained from an activated alumina tower and degassed prior to use. Benzene- d_6 and toluene- d_8 were dried over activated 4 Å molecular sieves and degassed prior to use. IR spectra were obtained on either a Nicolet 4700 FTIR (NaCl) or a Perkin Elmer Frontier (ATR) spectrometer. All absorption data (Uv-vis) was collected using a Varian Cary 5000 UV-vis-near-IR spectrophotometer. All column chromatography was conducted using SiliaFlash F-60, 230-400 mesh and the solvent systems listed below. All polymers were synthesized following the protocol described in Chapter 3, unless otherwise stated.

NMR Spectroscopy

NMR spectroscopy was performed on a Bruker Avance 300 MHz, 400 MHz, or 600 MHz spectrometer at 298 K unless otherwise stated. All coupling values are $^3J_{H-H}$ and reported in Hz. Abbreviations for NMR assignments for peaks are as follows: s = singlet; d = doublet; t = triplet; q = quartet; s = septet, m = multiplet; br = broad. Chemical shift values for polymers are listed as the most abundant peaks in the spectra.

Gel Permeation Chromatography

All GPC analysis was conducted on polymers precipitated 3 times using an appropriate solvent (typically hexanes or methanol) and dried *in vacuo* prior to being dried overnight in a vacuum oven. Analysis was performed using Agilent GPC equipped with a Viscostar-II, opti-lab T-rEX and miniDAWN TREOS detectors. GPC analysis was conducted in THF using a flow rate of 0.5 mL/min at 40 °C. All dn/dc values were calculated from 100% mass recovery methods. All samples were analyzed at a concentration of approximately 2 mg mL⁻¹.

Differential Scanning Calorimetry

Thermal properties of the samples were measured on a TA instruments Q2000 differential scanning calorimeter calibrated using indium. Analyses were performed in an inert atmosphere (nitrogen) with samples of approximately 5-6 mg in an aluminum pan. All analyses were conducted in duplicate to ensure consistency amongst the data. Samples were heated to 200 °C with a heating rate of 10 °C/min. They were held isothermally at 200 °C for 1 min to eliminate any thermal history followed by gradual cooling to -20 °C with a cooling rate of 5 °C/min. The samples were then reheated to 200 °C with a heating rate of 10 °C/min. The glass transition temperatures were determined from the second heating ramp and are reported as the midpoint of the transition.

Thermogravimetric Analysis

Thermal decomposition results were obtained using a thermogravimetric analysis Shimadzu TGA-50 instrument. A heating rate of 20 °C/min was used. Data was typically obtained between 30 to 600 °C. All data was collected for samples under an inert atmosphere of nitrogen. Duplicate runs were performed to ensure consistency amongst the data.

Anti-microbial screening

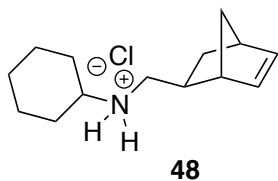
Anti-microbial screening was done in collaboration with UBC BioServices on the following microbial strains: MRSA, MSSA, *Klebsiella pseudomoniae*, Enterococcus, *Pseudomonas aeruginosa*, *Candida albicans*. Images of the anti-microbial screening can be found in Appendix C.3, beginning on page 319.

4.10.2 Synthesis and Characterization

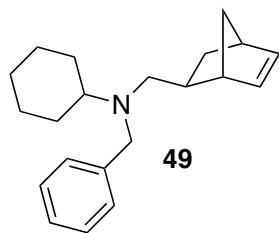
General Procedure for Aminonorbornene Monomer Synthesis

All aminonorbornenes were synthesized using tantalum phosphoramidate precatalysts **2**^{12, 183} described in this chapter and previous chapters and were isolated as colourless or pale yellow oils. HAA produced only one diastereomer of monoalkylated product, as shown by GC-MS analysis of the crude reaction mixture. It was previously confirmed to be the *exo*-diastereomer by X-ray crystallography,¹⁸³ and by comparison to similar compounds in the literature.²⁷¹ All other diastereomers were assigned by analogy to this compound. In some instances, over alkylation of the diene was observed. All monomers were purified by column chromatography (SilicaFlash F-60, 230-400 mesh) using the solvent systems listed below for the individual compounds. All

monomers were dried *in vacuo* before further use. Selected spectra can be found in Supplementary Information for Chapter 4 in Appendix C

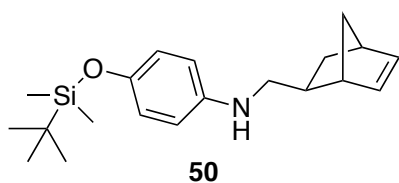


48. Secondary amine **42** (0.10 g 0.49 mmol) was dissolved in ether (50 mL) and stirred vigorously. HCl (6M, ether) was syringed into the mixture in one portion. The mixture was let stir for 1 hour at room temperature before all volatiles were removed *in vacuo*. The crude, off-white solid was washed with cold hexanes until washings became clear and colourless to give white needles (0.10 g, 88%). The white solid could be further purified by recrystallization by slowly evaporating of a saturated solution in DCM. White crystals were collected *via* gravity filtration and washed with cold hexanes. ^1H NMR (300 MHz, C_6D_6): δ 9.35-9.32 (m, 2H, NH_2), 6.07-6.05 (m, 2H, $(\text{CH})_2$), 2.97-2.99 (m, 4H, $2\times\text{CH}_2$), 2.86 (br s, 1H, CH), 2.30-2.36 (m, 2H, CH_2), 1.97-1.93 (m, 1H, CH), 1.86-1.82 (m, 2H, CH_2), 1.73-1.64 (m, 3H, $\text{CH}_2 + \text{CH}$), 1.50-1.23 (m, 7H, $3\times\text{CH}_2 + \text{CH}$). ^{13}C NMR (75 MHz, C_6D_6): δ 137.0 (CH), 136.2 (CH), 57.9 (C), 49.8 (CH), 45.3 ($2\times\text{CH}_2$), 42.0 (CH), 35.8 (CH_2), 32.3 (CH_2), 29.1 (CH_2), 29.0 (CH), 25.0 (CH_2), 24.9 ($2\times\text{CH}_2$). IR (ATR, cm^{-1}): 3400, 3059, 2932, 1581, 1454, 1014. HRMS-EI (m/z): calcd: 205.18305 found; 205.18326.

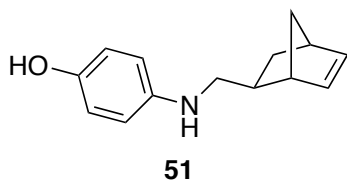


49. Secondary amine **42** (0.82 g, 4.0 mmol) was dissolved in acetone (50 mL) and stirred using a magnetic stir bar. Benzyl chloride (1.5 eq., 0.69 mL, 6.0 mmol) was added *via* syringe in one portion. NaI (1.5 eq., 0.90 g, 6.0 mmol) was added as a solid in one portion. The mixture was refluxed overnight. The mixture was cooled to room temperature and the NaCl was removed *via* gravity filtration. The filtrate was reduced *in vacuo* to reveal an orange liquid which was

subsequently purified by back extraction using HCl (3 M) and NaHCO₃ (aq). The crude product was purified *via* column chromatography (1.04 g, 88%). **¹H NMR** (300 MHz, C₆D₆): δ 7.43-7.41 (m, 2H, 2 \times ArCH), 7.36-7.31 (m, 2H, 2 \times ArCH), 7.27-7.22 (m, 1H, ArCH), 6.07 (s, 2H, CH=CH), 3.69 (s, 2H, CH₂), 2.79-2.76 (m, 2H, 2 \times CH), 2.60-2.44 (m, 3H, CH+CH₂), 1.88-1.80 (m, 4H, 2 \times CH₂), 1.68-1.52 (m, 2H, CH₂), 1.32-1.09 (m, 9H, 4 \times CH₂+CH). **¹³C{¹H} NMR** (75 MHz, CDCl₃): δ 142.2 (C), 137.0 (CH), 136.7 (CH), 128.4 (CH), 128.1 (CH), 126.4 (CH), 59.4 (CH), 55.9 (CH₂), 55.0 (CH₂), 45.2 (CH), 44.6 (CH₂), 41.8 (CH), 38.0 (CH), 31.5 (CH₂), 29.3 (CH₂), 28.4 (CH₂), 26.7 (CH₂), 26.5 (2 \times CH₂), 26.4 (2 \times CH₂). **IR** (ATR, cm⁻¹): 2926, 2852, 1450, 1367. **HRMS-EI** (*m/z*): calcd: 295.23000; found: 295.23016.



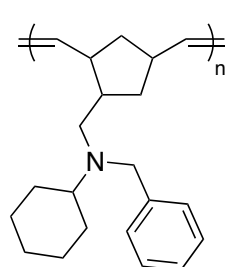
50. Product isolated as a yellow oil after column chromatography (hexanes/ethyl acetate 95:5) 0.69 g, 91%). **¹H NMR** (300 MHz, CDCl₃): δ 6.70 (d, ³*J* = 6.0 Hz, 2H, 2 \times ArH), 6.53 (d, ³*J* = 6 Hz, 2H, 2 \times ArH), 6.10 (m, 2H, (CH)₂), 3.51 (br s, 1H, NH), 3.07 (m, 2H, CH₂), 2.85 (m, 1H, CH), 2.73 (m, 1H, CH), 1.38-1.19 (m, 4H, 2 \times CH₂), 0.98 (s, 9H, 3 \times CH₃), 0.16 (s, 6H, 2 \times CH₃). **¹³C{¹H} NMR** (75 MHz, CDCl₃): δ 147.5 (C), 143.1 (C), 136.9 (CH), 136.6 (CH), 120.8 (2 \times CH), 114.0 (2 \times CH), 50.8 (CH₂), 45.4 (CH₂), 44.7 (CH), 41.8 (CH), 39.2 (CH), 31.5 (CH₂), 25.9 (3 \times CH₃), 18.3 (C), -4.3 (2 \times CH₃). **IR** (ATR, cm⁻¹): 3418, 2957, 2858, 1510, 1472, 1239, 905. **HRMS-ESI** (*m/z*): calcd: 329.21749; found: 329.21706.



51. To a mixture of silyl ether **50** (1.18 g, 3.6 mmol) in THF (10 mL) was added TBAF (1M, 3.6 mL) *via* syringe. The pale yellow mixture turned dark yellow upon addition. TLC analysis showed no

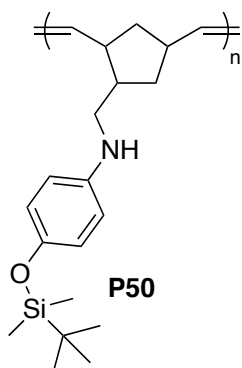
starting material remaining after 10 minutes. Water (10 mL) was added and the mixture was extracted with DCM (3x10 mL), dried over magnesium sulfate, and the solvents were removed *in vacuo* to reveal an off white solid. The mixture was dissolved in DCM and eluted through a plug of silica. Further purification was conducted via sublimation to reveal a pale yellow solid, 0.46 g, 60%. **¹H NMR** (300 MHz, CDCl₃): δ 6.70 (d, ³J = 9.0 Hz, 2H, 2×ArH), 6.53 (d, ³J = 9.0 Hz, 2H, 2×ArH), 6.09 (m, 2H, (CH)₂), 4.32-3.63 (br m, 2H, NH + OH), 3.20-2.96 (m, 2H, CH₂), 2.85 (m, 1H, CH), 2.72 (m, 1H, CH), 1.68-1.65 (m, 1H, CH), 1.37-1.18 (m, 4H, 2×CH₂). **¹³C{¹H} NMR** (75 MHz, CDCl₃): δ 148.1 (C), 142.4 (C), 136.9 (CH), 136.5 (CH), 116.4 (2×CH), 114.8 (2×CH), 51.2 (CH₂), 45.4 (CH₂), 44.6 (CH), 41.8 (CH), 39.0 (CH), 31.4 (CH₂). **IR** (ATR, cm⁻¹): 3304, 3193, 2961, 1505, 1241, 709. **HRMS-EI** (*m/z*): calcd: 215.13101; found: 215.13090. **EA**: calcd: C, 78.10; H, 7.96; N, 6.51; found: C, 78.28; H, 8.07; N, 6.40.

Characterization of Polymeric Materials



P49

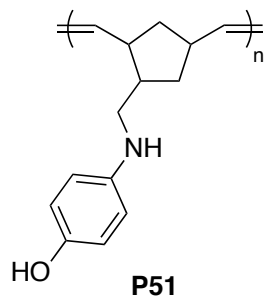
P49. **¹H NMR** (300 MHz, CDCl₃): δ 7.34-7.19 (m, 5H), 5.27-5.15 (m, 2H), 3.73-3.54 (m, 2H), 2.83-2.60 (m, 1H), 2.83-2.60 (m, 1H), 2.41-2.24 (m, 4H), 1.74-1.57 (m, 10H), 1.29-1.11 (m, 5H). **IR** (ATR, cm⁻¹): 2926, 2852, 1449, 733.



P50

P50. **¹H NMR** (300 MHz, CDCl₃): δ 6.68-6.665 (m, 2H), 6.46-6.43 (m, 2H), 5.413-5.41 (m, 2H), 3.45 (br s, 1H), 3.04-2.72 (m, 2H), 2.72-2.41 (m, 1H), 2.03-1.82 (m, 2H), 1.72-1.45 (m, 3H), 1.29-1.05 (m, 1H), 0.95 (s, 9H),

0.13 (s, 6H). **IR** (ATR, cm^{-1}): 3401, 2929, 2856, 1510, 1235.



P51. Characterization of this polymer by ^1H and ^{13}C NMR spectroscopy was complicated by its poor solubility in common NMR solvents. Approximate ^1H NMR data is listed as follows: **^1H NMR** (300 MHz, THF-d_8): δ 7.26 (br s, 1H), 6.53-6.50 (m, 2H), 6.40-6.32 (m, 2H), 5.43-5.17 (m, 2H), 3.98 (br s, 1H), 3.03-2.84 (m, 3 H), 2.67-2.45 (m, 2H), 2.15 (m, 1H), 1.92-1.89 (m, 2H), 1.29-1.03 (m, 4H), 0.91-0.84 (m, 2H). **IR** (ATR, cm^{-1}): 3360, 2930, 2860, 2172, 1513, 1232, 819.

Chapter 5: Conclusions and Future Work

5.1 Summary

The work presented in this thesis focused on the utility of *N,O*-chelated metal complexes in two small-molecule, amine-forming reactions. Hydroaminoalkylation and hydroamination were explored to afford new carbon-carbon and carbon-nitrogen bonds, respectively. Titanium was the focus of much research presented in this thesis, with the aim of developing alternatives to the leading tantalum complexes in the field of hydroaminoalkylation catalysis; namely tantalum precatalyst **2**. The products of HAA were then exploited for their utility in the formation of amine-containing polymers. Homopolymers of various repeat units were studied and a preliminary investigation into the synthesis of copolymeric materials was established.

Chapter 2 focused on expanding the scope of a phosphoramidate tantalum precatalyst, **2**, previously reported by the Schafer Group.¹⁸³ This complex was reported in 2013 and remains the only documented complex that affords HAA at room temperature. The synthetic procedure was expanded and optimized to include a solvent-free protocol. In many cases, **2** was found to generate higher yielding reactions under neat conditions, as compared to its solution-phase reactivity, and retained comparable levels of regioselectivity. An investigation into the synthesis of silylated products was presented with the efficacy of such reactions depending on the aryl-substitution of the starting amine. Most importantly, the HAA of NBD was found to generate monoalkylated products in good yield. Dialkylated products were observed, independently synthesized, and characterized. The desired monoalkylated strained alkene could be isolated and utilized for further chemical transformations, as described in Chapter 3.

Further investigations in Chapter 2 detailed the attempts to generate *N,O*-chelated complexes of titanium. This research was influenced by the relatively low cost, earth abundance,

and low toxicity of this metal, as opposed to tantalum and other metals. Inspired by the mono-ligated titanium complexes developed by Doye^{341, 346} and Chong,²⁴⁶ which show excellent HAA and HA activity, we attempted to synthesize mono-chelated complexes bearing one bulky phosphoramidate ligand. Phosphoramidates are a class of tunable, bulky ligands, where the steric bulk of the *N,O*-chelate lies relatively far from the metal-centre. Whereas the *N,N*-chelating aminopyridonate and formamidinate ligands provide sufficient steric bulk to afford mono-ligated titanium complexes, attempts to generate monophosphoramidate complexes were met with limited success. Ultimately, while substitution about the nitrogen atom can be easily varied, the inherent lack of bulk about the oxygen atom encourages ligand redistribution to form the respective bis-chelated complexes. Fortunately, the solid-state molecular structure of a mono-ligated complex, **18**, was obtained and full characterization could be achieved when bulkier *dipp* ligands were employed, as shown for complex **21**. This change mitigated rapid ligand redistribution and allowed for the collection of all characterization data (although no solid-state molecular structure was obtained), although ligand redistribution was observed in solution over time.

The facile synthesis of bis-ligated phosphoramidate complexes allowed us to prepare a family of new compounds by varying the substitution on the *N*-substituent. Aryl-substituted variants could be analyzed by X-ray crystallography, where a related alkyl-substituted complex was isolated as an oil. The small titanium metal centre could support only three phosphoramidate ligands, with the third chelate adopted a $\kappa^1\text{-O}$ binding geometry to minimize steric repulsion. All attempts to access tetrachelated titanium complexes with phosphoramidate ligands were unsuccessful.

All titanium complexes were screened for HAA and HA activity, with monophosphoramidates outperforming the disubstituted counterparts in all cases. High yielding HAA reactions were observed in some cases, although forcing conditions including 130-165 °C and 96-164 h were required to generate over 90% of the desired product with complex **18** or **34**. Monophosphoramidates were competent HA catalysts, with conversion of primary aminoalkenes **36** to the 6-membered product, **37**, being observed in all cases. Complex **18** gave quantitative conversions in 2 h at 80 °C. The reaction temperature could be lowered to 65 °C, although conversion was reduced to 86% yield after 6 h and quantitative conversion at room temperature required 168 h. Unfortunately, neither monophosphoramidate nor diphosphoramidate complexes were efficient for the mono-alkylation of NBE, with tantalum precatalyst **2** being a far better catalyst for this transformation. These titanium complexes and the catalytic results obtained from their employment represent an interesting proof of concept as few examples of HAA or HA using titanium complexes exist in the literature, and titanium phosphoramidate complexes are newly reported here. Unfortunately, the catalytic activity of these systems is trumped by existing titanium systems where mono-ligated complexes are possible when using *N,N*-chelates capable of possessing large amounts of steric bulk on both chelating atoms. Unfortunately, phosphoramidates, despite being sterically bulky, are not able to mitigate the formation of less active diligated species through ligand redistribution reactions.

Chapter 3 focused on the exploitation of the atom-economic, selective synthesis of monoalkylated products of cyclic dienes, NBD and COD, through HAA. Unfortunately, the titanium species presented in Chapter 2 lacked efficient reactivity to generate these products in sufficient yields. However, tantalum precatalyst **2** was found to be effective at furnishing these valuable products at room temperature and using solvent-free conditions.^{105, 183} The efficient

synthesis of amine-containing monomers for ROMP remains an important area of research, as traditional syntheses are laborious and wasteful. A family of products from NBD and COD was presented and screened for their polymerization behavior with Grubbs metathesis catalysts. Pleasingly, all aryl-substituted aminonorbornene monomers gave amine-containing polymers in good yields with unexpectedly high levels of control, as evidenced by the strong predictability of MW. Furthermore, the \bar{D} remained low. Perhaps unsurprisingly, alkyl-substituted aminonorbornene **42** was not tolerated by catalyst G2 and did not produce any polymeric material. This result is attributed to the stronger nucleophilicity of this alkyl amine, whereas the electron-withdrawing phenyl group renders aryl-substituted aminonorbornenes suitable for this transformation. Monomers derived from COD could be successfully polymerized, however, they resulted in insoluble materials that were unsuitable for traditional characterization techniques such as GPC.

The presence of the coordinating amine group causes sluggish propagation, with monomers requiring *ca.* 20 h to reach full conversion. However, the incorporation of the H-bonding group imparts interesting behavior of these unique materials. Polymers were analyzed by thermal analysis techniques and showed increased T_g values relative to unfunctionalized PNB, indicating the presence of inter- or intramolecular networks. Most convincing was the rheological analysis of these polymers. The viscoelastic properties were found to be dependent on the MW of the polymer. Methoxy-substituted polymer, **P6**, displayed melt-phase behavior indicating the presence of H-bonding. Lower MW samples displayed liquid-like behavior across a range of frequencies. However, higher MW samples behaved as solid-like viscoelastic materials, displaying the effect of increased H-bonding partners and their effect on hindered reptation throughout the polymer network. Furthermore, tunable rheological behavior was

observed when comparing the aryl-substituted polymers. All samples behaved as viscoelastic solids, however, viscosity behavior was found to be dependent upon the substitution and the H-bonding potential of the different amine groups.

Chapter 4 focused on the expansion of amine-containing monomers amenable to ROMP with ruthenium-based catalysts. The inhibition of G2 with alky-substituted monomer was attempted to be overcome by using the more catalytically active G3. No success was achieved and the derivatization of substrate **42** into an appropriate monomer was attempted by a variety of methods. Protonation of the substrate with HCl resulted in a product that yielded no productive polymerization. Alkylation of **42** with benzyl chloride afforded tertiary amine monomer **49**. It is well documented that tertiary amines are compatible with Grubbs catalysts, as the steric hindrance prevents deactivation despite these substrates being more nucleophilic than their secondary analogues.⁶⁴ Thus, **49** could be polymerized rapidly with G2, with full consumption being observed in under 10 minutes. This polymer, **P49**, allowed for direct comparisons of secondary and tertiary amine-containing polymers. **P49** displayed lower T_g and T_d values relative to secondary amine polymers capable of H-bonding. Expansion of this investigation to include the H-bond donating hydroxyl functionality was met with limited success. While polymers could be afforded in good yields with high levels of control, the lack of solubility of **P51** prevented any further investigation to be performed with this polymer. It is hypothesized that the decreased solubility is related to the strong H-bonding interactions present in this polymer. The unfavourable solubility of this polymer was circumvented by the polymerization of the TBDMS-protected variant, **50**, with **P50** being isolated in good yields with high levels of control. Interestingly, the electron-rich silyl protecting group led to increased thermal characteristics consistent with heightened levels of H-bonding throughout the polymer. While it is theoretically

possible to access **P51** by deprotecting **P50**, this was not pursued due to the problems associated with effective characterization of the hydroxyl-substituted **P51**.

Chapter 4 focused on the development of copolymeric materials comprised of these amine-containing monomers. Inexpensive hydrocarbon partners were targeted in hopes that the incorporation of H-bonding amine monomers would offer a way to selectively tailor the properties of the copolymer. Lower levels of D were observed when hydrocarbon monomers were polymerized first, followed by the nitrogen-containing monomer **6**. Therefore, this order of addition was used for the synthesis of block copolymers. The synthesis of copolymers containing varying degrees of amine incorporation were studied. Increasing the level amine was found to have little effect on the T_g values, although two distinct transitions were observed when lower monomer-to-monomer ratios were used. Although accurate MW values were difficult to obtain by end-group (^1H NMR spectroscopy) and GPC analysis, the judicious choice of methoxy-functionalized comonomer **6** provided a convenient handle by which monomer incorporation values could be determined by ^1H NMR spectroscopy. All experimental incorporation values were in good agreement with theoretical values. Furthermore, the levels of amine-incorporation could be measured by elemental analysis. While this technique is not a method for absolute characterization, it was shown to be an excellent supporting technique for the analysis of these materials.

The development of copolymers was expanded to include COE, a flexible, ethylene like alternative to NBE. Monomer-to-monomer ratios of 100:100 were employed and two polymerization protocols were used. Specifically, sequential addition gives rise to block copolymers, where the single addition of monomers theoretically gives rise to potentially random or gradient copolymers. While excellent levels of monomer incorporation were achieved with

NBE using single and sequential protocols, the single addition of COE and **6** led to poor incorporation values of the hydrocarbon comonomer, potentially due to the reduced ring-strain of COE and the sluggish catalytic activity of G2 in the presence of amines. The thermal properties of all copolymers were studied and show comparable T_g values regardless of the synthesis protocol employed. These results indicate that the polymer morphology (either block, random, or gradient) relies on the propensity of each monomer to ring-open, and not the addition protocol employed.

Preliminary synthetic investigations into the generation of copolymers bearing two amine-containing monomers was presented. Specifically, **6** and **46** were used in a sequential protocol to synthesize a block copolymer. Importantly, MW values obtained from GPC were predictable, supporting the hypothesis that deviations from theoretical values observed when NBE and COE were used can be directly attributed to the rapid, less controlled polymerization relative to the amine-containing monomer **6**. Despite the difficulties associated with MW determination, these results show that efficient synthesis of amine-containing copolymers is possible, and provide an interesting avenue for future investigations.

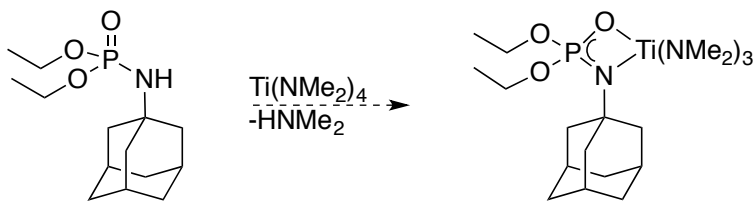
Preliminary studies towards the potential application of these amine-containing polymers were conducted, including the investigations of these unique materials for anti-microbial and metal sequestration activity. Secondary amine-containing homopolymers were not promising candidates for use as anti-microbial materials. This is perhaps unsurprising as many of the leading materials possess protonated amine groups to enhance cell apoptosis.⁸² Attempts to utilize tertiary homopolymer **P49** for metal sequestration were also met with limited success, as insignificant levels of copper ions were removed from solution. Despite the lack of success, this

study points to key amendments to experimental design. Further exploration is warranted to realize the relevant applications of these materials.

5.2 Future Directions

5.2.1 Synthesis of Sterically Bulky Mono-Ligated Titanium Complexes

Chapter 2 detailed the investigation into titanium phosphoramidate complexes. Greater reactivity was observed when mono-ligated titanium precatalysts were employed. However, these complexes were subject to significant ligand redistribution which led to decreased levels of reactivity; the diligated complexes were shown to be much worse catalysts for HAA and HA. This redistribution is caused by an inherent characteristic of the ligand scaffold itself. The O-atom of the phosphoramidate ligand motif does not provide sufficient bulk to prevent this redistribution. The ligand with the highest level of steric bulk investigated in this thesis is that derived from 2,6-diisopropyl aniline. Lower levels of redistribution were observed when this substitution pattern was used. One simple way to potentially mitigate the deleterious reactions observed is the use of ligands possessing higher levels of steric protection about the nitrogen atom. Ligands derived from adamantylamine could potentially offer the necessary steric protection to afford isolable mono-chelated titanium complexes and allow access to reactive precatalysts for these transformations (Scheme 41). Also appealing is the fact that adamantylamine hydrochloride is relatively inexpensive and available from commercial sources.



Scheme 41 Proposed synthesis of an adamantyl-substituted phosphoramidate complex

5.2.2 Further Investigations and Expansion of H-Bonding in Polymers

The investigations presented in this thesis towards homopolymers from amine-containing monomers have generated a foundation of interesting results. This unique family of polymers synthesized from ROMP displayed differing rheological properties depending on the H-bonding potential of the incorporated amine groups. Chapter 4 detailed the synthesis of a tertiary amine monomer, **49**, from alkyl amine **42** and benzyl chloride. Not only did this derivatization result in a marked increase in the polymerization behaviour of this substrate, but it also drastically changed the thermal properties of the resulting polymer, **P49**. Most attractive are the complimentary rheological measurements of viscosity and the viscoelastic moduli of this material. Of course, the rheological results of secondary aryl amine polymers (**P6** and **P43-P45**) cannot be compared directly to tertiary alkyl polymer **P49**, however, the absence of a H-bond donor in **P49** should lead to the absence of H-bonding behaviours present in these secondary amine polymers. Future experiments should probe the deleterious effects of the alkyl amine presence, specifically using monomer **42**, using ^1H and ^{31}P NMR spectroscopy. Furthermore, despite the problems associated with the poor solubility of aminocyclooctene polymers, the rheological analysis of **P46** and **P47** is of interest to probe the relative effect of a flexible ethylene-like backbone.

Related to these suggested future works are the syntheses of other polymers for the comparison of the H-bonding hypotheses put forth in this thesis. Specifically, the derivatization of **42** to form **49** has elucidated the facile methodology required to access these types of tertiary benzyl amine monomers. Of interest is the synthesis of benzyl-derivatives of monomers **6** and **43-45** to form the proposed monomers shown in Figure 101. The formation of the respective macromolecules would not only provide an opportunity to compare the thermal and rheological properties of the derivatized and non-derivatized polymers, but also comparisons between all benzyl-derivatives could be drawn to account for any phenomena arising from potential π -stacking interactions occurring in these polymers.

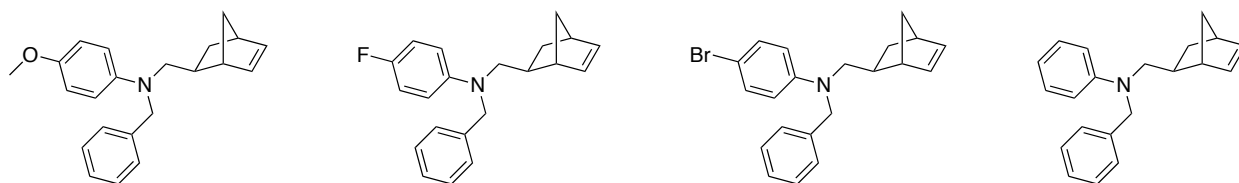
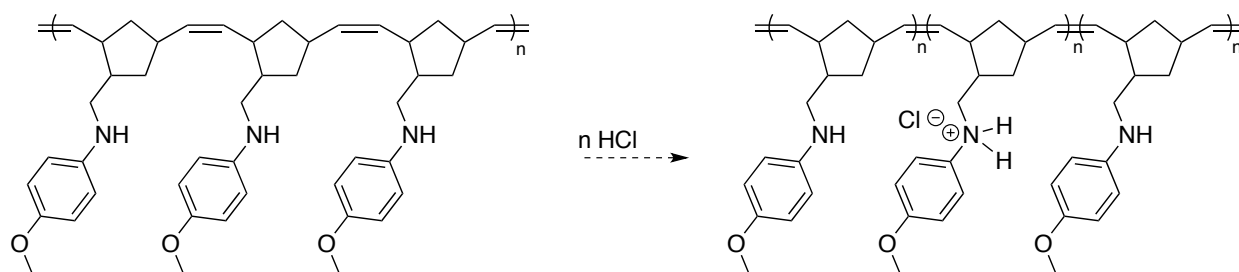


Figure 101 Proposed benzyl-monomers to generate tertiary polymers to probe H-bonding effects

5.2.3 Post-Polymerization Chemistry

One obvious avenue to explore with these novel materials is the post-polymerization derivatization of the amine group. Of immediate interest is the protonation of the secondary amine groups in **P6**, or any other secondary amine polymer discussed in this thesis. Indeed, the protonation of monomer **42** was successful and was the subject of discussion in Section 4.3.4. Hypothetically, a sample of a secondary-amine polymer could be protonated to varying degrees using HCl (Scheme 42). This is appealing as the pronation event would not introduce large amounts of steric bulk, as in the benzyl-derivatives discussed above. The elimination of H-bond

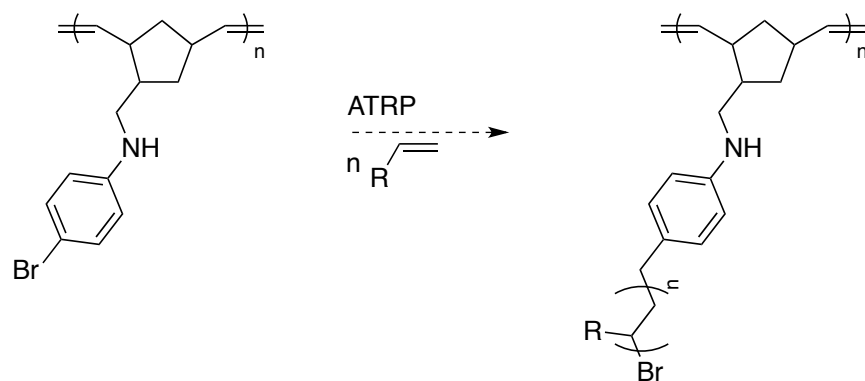
donor from the polymer sample should directly affect the rheological properties of these materials.



Scheme 42 Protonation of P6 to generated quaternary amine moieties

Ideally, trends could be drawn between the level of protonation and the decrease in the materials' storage modulus due to decreased levels of H-bonding. Similar effects have been observed when hydrolyzing poly(*n*-butyl acrylate)s to generate copolymers of the form poly(*n*-butyl acrylate)-*co*-poly(acrylic acid), having various levels of the H-bonding acrylic acid segment.¹⁴⁸

The post-polymerization modification of brominated polymer **P44** is of interest for the synthesis of brush-like copolymers. **P44** possesses the requisite halogen group for use as a macroinitiator in atom transfer radical polymerization (ATRP).¹⁰⁻¹¹ Furthermore, the thermal investigation of **P44** by TGA indicated the loss of the bromine group at *ca.* 230 °C, suggesting it as a potential candidate for radical polymerization protocols. In doing so, advanced molecular architectures, such as polymer brushes, could be achieved in combination with olefin comonomers (Scheme 43).



Scheme 43 Brominated polymer P44 as a macroinitiator for ATRP

The synthetic protocol and development of the novel polymers developed in this thesis has opened the door to several avenues that warrant future exploration. While many of these have been discussed in detail above, there exist a variety of other simple experiments that could be performed. For example, the hydrogenation of homopolymers **P6** and **P43-P45** would be of interest to probe the effect of a more flexible backbone. Furthermore, the thermal characterization of amine-containing copolymers showed no drastic differences in T_g values. It is of interest to test these materials for their viscoelastic properties to gain insight into the H-bonding potential of these novel copolymers. Other direct applications of such materials are discussed below.

5.2.4 Potential Applications for Nitrogen-Containing Polymers

While the investigations towards useful applications in this thesis were met with limited success, the materials and methodologies discussed provide promising avenues for future studies. Importantly, the facile synthesis of amine-containing monomers in a selective, one-step, atom-economic, and waste-limiting transformation was shown to furnish unique molecules for further

transformation. Specifically, HAA provides efficient access to amine-containing monomers which show surprising compatibility with Grubbs catalysts. The unique materials presented in this thesis are believed to possess large amounts of untapped potential. The generation of protonated amine polymers has direct implications towards their use as anti-microbial materials. Efforts to synthesize nitrogen-containing polymers bearing quaternary amine cations using a post-polymerization protocol is a potential avenue for preparing these biocidal materials as many anti-microbial polymers possess positively charged groups to promote this interaction.

Preliminary studies of metal sequestration using **P49** utilized aqueous solutions of Cu(II)SO₄. Insignificant metal binding was observed. Optimization of this experiment should include the use of alcohol-based solutions to promote the interaction between the metal and polymer. Further efforts should focus on the dissolution of the polymer in a solution of metal, and removal of the generated metal-polymer complex by precipitation. Sequestration could also be improved by using hard metal ions, such as chromium, magnesium, or sodium, as these preferentially bind to hard nitrogen ligands.^{417, 420}

Obvious future investigations include the blending of these homo- or copolymeric materials with known, commercially available commodity polymers, such as polyurethanes. Incorporation of these materials could increase the processability and overall thermal properties of these useful polymers. Further applications include their use as compatibilizers between immiscible polymers, such as polyethylene and Nylon, to harness the positive characteristics and improve the processing of these inexpensive commodity plastics.

5.3 Concluding Remarks

The research presented in this thesis highlights the utility of *N,O*-chelated complexes of early transition metals for the synthesis of amines. This begins with catalyst and method development where earth abundant, inexpensive metals of low toxicity are the focus. The judicious pairing of metal and ligand is highlighted to exploit the full potential of these species. The end-products of HA and HAA are of great importance. Furthermore, they lend themselves to further functionalization to generate a wealth of value-added products. ROMP has been shown to be one such avenue, where coupling of efficient, atom economic transformations has been shown to lead to unique polymeric materials with unharnessed potential. The work presented in this thesis serves to guide future experimentalists in their exploration of novel titanium complexes and unique polymeric materials.

References

- [1] R. J. Young, P. A. Lovell, *Introduction to Polymers, Third Edition*, Taylor & Francis, **2011**.
- [2] J. A. Brydson, *Plastics Materials*, Elsevier Science, **2013**.
- [3] M. E. Hermes, *Enough for One Lifetime: Wallace Carothers, Inventor of Nylon*, American Chemical Society and the Chemical Heritage Foundation, **1996**.
- [4] L. Brunsveld, B. J. B. Folmer, E. W. Meijer, R. P. Sijbesma, *Chem. Rev.* **2001**, *101*, 4071-4098.
- [5] Global Plastic Production Rises, Recycling Lags. G. Gourmelon. **2013**. Accessed July 3rd, 2017. <http://www.worldwatch.org/global-plastic-production-rises-recycling-lags-0>
- [6] L. E. N. Allan, M. R. Perry, M. P. Shaver, *Prog. Polym. Sci.* **2012**, *37*, 127-156.
- [7] D. Feldman, A. Barbalata, *Synthetic Polymers: Technology, Properties, Applications*, Springer, **1996**.
- [8] C. S. Brazel, S. L. Rosen, *Fundamental Principles of Polymeric Materials*, Wiley, **2012**.
- [9] K. Matyjaszewski, J. Spanswick, *Mater. Today* **2005**, *8*, 26-33.
- [10] K. Matyjaszewski, *Macromolecules* **2012**, *45*, 4015-4039.
- [11] K. Matyjaszewski, *Isr. J. Chem.* **2012**, *52*, 206-220.
- [12] M. R. Perry, L. E. N. Allan, A. Decken, M. P. Shaver, *Dalton Trans.* **2013**, *42*, 9157-9165.
- [13] G. Moad, E. Rizzardo, in *Nitroxide Mediated Polymerization: From Fundamentals to Applications in Materials Science*, The Royal Society of Chemistry, **2016**, pp. 1-44.
- [14] R. T. A. Mayadunne, E. Rizzardo, J. Chiefari, Y. K. Chong, G. Moad, S. H. Thang, *Macromolecules* **1999**, *32*, 6977-6980.
- [15] R. T. A. Mayadunne, J. Jeffery, G. Moad, E. Rizzardo, *Macromolecules* **2003**, *36*, 1505-1513.
- [16] M. R. Hill, R. N. Carmean, B. S. Sumerlin, *Macromolecules* **2015**, *48*, 5459-5469.
- [17] D. J. Keddie, *Chem. Soc. Rev.* **2014**, *43*, 496-505.
- [18] A. Tardy, J. Nicolas, D. Gigmes, C. Lefay, Y. Guilleaneuf, *Chem. Rev.* **2017**, *117*, 1319-1406.
- [19] O. Dechy-Cabaret, B. Martin-Vaca, D. Bourissou, *Chem. Rev.* **2004**, *104*, 6147-6176.
- [20] C. Samojłowicz, M. Bieniek, K. Grela, *Chem. Rev.* **2009**, *109*, 3708-3742.
- [21] K. A. Ogawa, A. E. Goetz, A. J. Boydston, *J. Am. Chem. Soc.* **2015**, *137*, 1400-1403.
- [22] B. Wei, W. Li, Z. Zhao, A. Qin, R. Hu, B. Z. Tang, *J. Am. Chem. Soc.* **2017**.
- [23] X. Wang, K. Maeda, A. Thomas, K. Takanabe, G. Xin, J. M. Carlsson, K. Domen, M. Antonietti, *Nat Mater* **2009**, *8*, 76-80.
- [24] C. W. Bielawski, R. H. Grubbs, *Prog. Polym. Sci.* **2007**, *32*, 1-29.
- [25] T. M. Trnka, R. H. Grubbs, *Acc. Chem. Res.* **2001**, *34*, 18-29.
- [26] C. Slugovec, *Macromol. Rapid Commun.* **2004**, *25*, 1283-1297.
- [27] K. Nomura, M. M. Abdellatif, *Polymer* **2010**, *51*, 1861-1881.
- [28] S. Sutthasupa, M. Shiotsuki, F. Sanda, *Polym. J.* **2010**, *42*, 905-915.
- [29] M. Szwarc, M. Levy, R. Milkovich, *J. Am. Chem. Soc.* **1956**, *78*, 2656-2657.
- [30] G. Moad, D. H. Solomon, *The Chemistry of Radical Polymerization*, Elsevier, **2006**.
- [31] A. F. Halasa, *Rubber Chem. Technol.* **1981**, *54*, 627-640.

- [32] K. Matyjaszewski, A. H. E. Müller, *Controlled and Living Polymerizations: From Mechanisms to Applications*, Wiley, **2009**.
- [33] D. J. Nelson, S. Manzini, C. A. Urbina-Blanco, S. P. Nolan, *Chem. Commun.* **2014**, 50, 10355-10375.
- [34] E. Kovács, P. Sághy, G. Turczel, I. Tóth, G. Lendvay, A. Domján, P. T. Anastas, R. Tuba, *J. Organomet. Chem.*
- [35] O. Nuyken, S. Pask, *Polymers* **2013**, 5, 361.
- [36] P. v. R. Schleyer, J. E. Williams, K. R. Blanchard, *J. Am. Chem. Soc.* **1970**, 92, 2377-2386.
- [37] B. L. Goodall, L. H. McIntosh, L. F. Rhodes, *Macromol. Symp.* **1995**, 89, 421-432.
- [38] J. C. Mol, *J. Mol. Catal. A: Chem.* **2004**, 213, 39-45.
- [39] C. P. Casey, *J. Chem. Educ.* **2006**, 83, 192.
- [40] S. Hilf, A. F. M. Kilbinger, *Nat Chem* **2009**, 1, 537-546.
- [41] S. Hilf, A. F. Kilbinger, *Nat Chem* **2009**, 1, 537-546.
- [42] J. A. Love, M. S. Sanford, M. W. Day, R. H. Grubbs, *J. Am. Chem. Soc.* **2003**, 125, 10103-10109.
- [43] G. C. Vougioukalakis, R. H. Grubbs, *Chem. Rev.* **2010**, 110, 1746-1787.
- [44] G. Odian, *Principles of Polymerization*, Wiley, **2004**.
- [45] S. K. Armstrong, *J. Chem. Soc., Perkin Trans. 1* **1998**, 371-388.
- [46] J. A. M. Lummiss, F. A. Perras, R. McDonald, D. L. Bryce, D. E. Fogg, *Organometallics* **2016**, 35, 691-698.
- [47] K. Grela, *Olefin Metathesis: Theory and Practice*, Wiley, **2014**.
- [48] C. S. Higman, J. A. M. Lummiss, D. E. Fogg, *Angew. Chem. Int. Ed.* **2016**, 55, 3552-3565.
- [49] P. Schwab, R. H. Grubbs, J. W. Ziller, *J. Am. Chem. Soc.* **1996**, 118, 100-110.
- [50] J. Huang, E. D. Stevens, S. P. Nolan, J. L. Petersen, *J. Am. Chem. Soc.* **1999**, 121, 2674-2678.
- [51] M. Scholl, T. M. Trnka, J. P. Morgan, R. H. Grubbs, *Tetrahedron Lett.* **1999**, 40, 2247-2250.
- [52] L. Ackermann, A. Fürstner, T. Weskamp, F. J. Kohl, W. A. Herrmann, *Tetrahedron Lett.* **1999**, 40, 4787-4790.
- [53] M. S. Sanford, J. A. Love, R. H. Grubbs, *J. Am. Chem. Soc.* **2001**, 123, 6543-6554.
- [54] M. S. Sanford, M. Ulman, R. H. Grubbs, *J. Am. Chem. Soc.* **2001**, 123, 749-750.
- [55] C. Adlhart, P. Chen, *Helv. Chim. Acta* **2003**, 86, 941-949.
- [56] K. Getty, M. U. Delgado-Jaime, P. Kennepohl, *J. Am. Chem. Soc.* **2007**, 129, 15774-15776.
- [57] N. S. Antonova, J. J. Carbó, J. M. Poblet, *Organometallics* **2009**, 28, 4283-4287.
- [58] J. A. M. Lummiss, C. S. Higman, D. L. Fyson, R. McDonald, D. E. Fogg, *Chem. Sci.* **2015**, 6, 6739-6746.
- [59] L. Cavallo, *J. Am. Chem. Soc.* **2002**, 124, 8965-8973.
- [60] J. A. Love, J. P. Morgan, T. M. Trnka, R. H. Grubbs, *Angew. Chem. Int. Ed.* **2002**, 41, 4035-4037.
- [61] R. H. Grubbs, *J. Macromol. Sci., Part A* **1994**, 31, 1829-1933.
- [62] C. F. Hansell, P. Espeel, M. M. Stamenović, I. A. Barker, A. P. Dove, F. E. Du Prez, R. K. O'Reilly, *J. Am. Chem. Soc.* **2011**, 133, 13828-13831.

- [63] A. F. M. Kilbinger, in *Functional Polymers by Post-Polymerization Modification*, Wiley-VCH Verlag GmbH & Co. KGaA, **2012**, pp. 153-171.
- [64] P. Compain, *Adv. Synth. Catal.* **2007**, *349*, 1829-1846.
- [65] A. Leitgeb, J. Wappel, C. Slugovc, *Polymer* **2010**, *51*, 2927-2946.
- [66] F. Sinclair, L. Chen, B. W. Greenland, M. P. Shaver, *Macromolecules* **2016**, *49*, 6826-6834.
- [67] A. E. Madkour, A. H. Koch, K. Lienkamp, G. N. Tew, *Macromolecules* **2010**, *43*, 4557-4561.
- [68] S. Sutthasupa, M. Shiotsuki, H. Matsuoka, T. Masuda, F. Sanda, *Macromolecules* **2010**, *43*, 1815-1822.
- [69] S. Sutthasupa, M. Shiotsuki, T. Masuda, F. Sanda, *J. Am. Chem. Soc.* **2009**, *131*, 10546-10551.
- [70] J. Romulus, J. T. Henssler, M. Weck, *Macromolecules* **2014**, *47*, 5437-5449.
- [71] A.-V. Ruzette, L. Leibler, *Nat Mater* **2005**, *4*, 19-31.
- [72] R. H. Platel, L. M. Hodgson, C. K. Williams, *Polymer Reviews* **2008**, *48*, 11-63.
- [73] M. Labet, W. Thielemans, *Chem. Soc. Rev.* **2009**, *38*, 3484-3504.
- [74] D. Wu, Y. Zhang, M. Zhang, W. Zhou, *Eur. Polym. J.* **2008**, *44*, 2171-2183.
- [75] T. Patrício, P. Bártolo, *Procedia Engineering* **2013**, *59*, 292-297.
- [76] D. J. Gilmour, R. L. Webster, M. R. Perry, L. L. Schafer, *Dalton Trans.* **2015**, *44*, 12411-12419.
- [77] R. L. Webster, N. Noroozi, S. G. Hatzikiriakos, J. A. Thomson, L. L. Schafer, *Chem. Commun.* **2013**, *49*, 57-59.
- [78] S. Tempelaar, L. Mespouille, O. Coulembier, P. Dubois, A. P. Dove, *Chem. Soc. Rev.* **2013**, *42*, 1312-1336.
- [79] C. Bastioli, R. T. Limited, *Handbook of Biodegradable Polymers*, Rapra Technology, **2005**.
- [80] A. E. Madkour, A. H. R. Koch, K. Lienkamp, G. N. Tew, *Macromolecules* **2010**, *43*, 4557-4561.
- [81] K. Lienkamp, A. E. Madkour, K. N. Kumar, K. Nusslein, G. N. Tew, *Chem. Eur. J.* **2009**, *15*, 11715-11722.
- [82] K. Lienkamp, A. E. Madkour, A. Musante, C. F. Nelson, K. Nüsslein, G. N. Tew, *J. Am. Chem. Soc.* **2008**, *130*, 9836-9843.
- [83] B.-S. Kim, S. W. Park, P. T. Hammond, *ACS Nano* **2008**, *2*, 386-392.
- [84] E.-R. Kenawy, S. D. Worley, R. Broughton, *Biomacromolecules* **2007**, *8*, 1359-1384.
- [85] H. Kim, S. Kobayashi, M. A. AbdurRahim, M. J. Zhang, A. Khusainova, M. A. Hillmyer, A. A. Abdala, C. W. Macosko, *Polymer* **2011**, *52*, 1837-1846.
- [86] S. Kobayashi, J. Song, H. C. Silvis, C. W. Macosko, M. A. Hillmyer, *Ind. Eng. Chem. Res.* **2011**, *50*, 3274-3279.
- [87] G. S. Wildes, T. Harada, H. Keskkula, D. R. Paul, V. Janarthanan, A. R. Padwa, *Polymer* **1999**, *40*, 3069-3082.
- [88] Y. Kuwahara, D. Y. Kang, J. R. Copeland, N. A. Brunelli, S. A. Didas, P. Bollini, C. Sievers, T. Kamegawa, H. Yamashita, C. W. Jones, *J. Am. Chem. Soc.* **2012**, *134*, 10757-10760.
- [89] A. Goeppert, M. Czaun, R. B. May, G. K. S. Prakash, G. A. Olah, S. R. Narayanan, *J. Am. Chem. Soc.* **2011**, *133*, 20164-20167.

- [90] H.-B. Wang, P. G. Jessop, G. Liu, *ACS Macro Letters* **2012**, *1*, 944-948.
- [91] B. Smit, J. A. Reimer, C. M. Oldenburg, I. C. Bourg, *Introduction to Carbon Capture and Sequestration*, World Scientific Publishing Company, **2014**.
- [92] S. Colak, G. N. Tew, *Langmuir* **2012**, *28*, 666-675.
- [93] J. Liu, Y. Huang, A. Kumar, A. Tan, S. Jin, A. Mozhi, X.-J. Liang, *Biotechnol. Adv.* **2014**, *32*, 693-710.
- [94] S. Niedermayer, V. Weiss, A. Herrmann, A. Schmidt, S. Datz, K. Muller, E. Wagner, T. Bein, C. Brauchle, *Nanoscale* **2015**, *7*, 7953-7964.
- [95] H. Wu, L. Zhu, V. P. Torchilin, *Biomaterials* **2013**, *34*, 1213-1222.
- [96] S. Binauld, M. H. Stenzel, *Chem. Commun.* **2013**, *49*, 2082-2102.
- [97] Y. Yang, D. Pan, K. Luo, L. Li, Z. Gu, *Biomaterials* **2013**, *34*, 8430-8443.
- [98] S.-H. Park, S. Wei, B. Mizaikoff, A. E. Taylor, C. d. Favero, C.-H. Huang, *Environ. Sci. Technol.* **2009**, *43*, 1360-1366.
- [99] Q. Y. Yue, B. Y. Gao, Y. Wang, H. Zhang, X. Sun, S. G. Wang, R. R. Gu, *J. Hazard. Mater.* **2008**, *152*, 221-227.
- [100] Z.-J. Zheng, L.-X. Liu, G. Gao, H. Dong, J.-X. Jiang, G.-Q. Lai, L.-W. Xu, *RSC Advances* **2012**, *2*, 2895.
- [101] F. Liu, L. Wang, Q. Sun, L. Zhu, X. Meng, F.-S. Xiao, *J. Am. Chem. Soc.* **2012**, *134*, 16948-16950.
- [102] M. R. Buchmeiser, *Macromol. Symp.* **2010**, *298*, 17-24.
- [103] M. Lefèvre, E. Proietti, F. Jaouen, J.-P. Dodelet, *Science* **2009**, *324*, 71-74.
- [104] N. B. McKeown, P. M. Budd, *Chem. Soc. Rev.* **2006**, *35*, 675-683.
- [105] M. R. Perry, T. Ebrahimi, E. Morgan, P. M. Edwards, S. G. Hatzikiriakos, L. L. Schafer, *Macromolecules* **2016**.
- [106] J. K. Kammeyer, A. P. Blum, L. Adamiak, M. E. Hahn, N. C. Gianneschi, *Polym. Chem.* **2013**, *4*, 3929-3933.
- [107] A. Deiters, S. F. Martin, *Chem. Rev.* **2004**, *104*, 2199-2238.
- [108] S. K. Chattopadhyay, S. Karmakar, T. Biswas, K. C. Majumdar, H. Rahaman, B. Roy, *Tetrahedron* **2007**, *63*, 3919-3952.
- [109] F.-X. Felpin, J. Lebreton, *Eur. J. Org. Chem.* **2003**, *2003*, 3693-3712.
- [110] K. A. Günay, P. Theato, H.-A. Klok, in *Functional Polymers by Post-Polymerization Modification*, Wiley-VCH Verlag GmbH & Co. KGaA, **2012**, pp. 1-44.
- [111] C. P. Woodward, N. D. Spiccia, W. R. Jackson, A. J. Robinson, *Chem. Commun.* **2011**, *47*, 779-781.
- [112] F. Sinclair, M. Alkattan, J. Prunet, M. P. Shaver, *Polym. Chem.* **2017**, *8*, 3385-3398.
- [113] G. Godin, P. Compain, O. R. Martin, *Org. Lett.* **2003**, *5*, 3269-3272.
- [114] T. Itoh, N. Yamazaki, C. Kibayashi, *Org. Lett.* **2002**, *4*, 2469-2472.
- [115] G. C. Fu, S. T. Nguyen, R. H. Grubbs, *J. Am. Chem. Soc.* **1993**, *115*, 9856-9857.
- [116] S. H. Hong, R. H. Grubbs, *J. Am. Chem. Soc.* **2006**, *128*, 3508-3509.
- [117] R. Weihofen, O. Tverskoy, G. Helmchen, *Angew. Chem. Int. Ed.* **2006**, *45*, 5546-5549.
- [118] K. Shimizu, M. Takimoto, M. Mori, *Org. Lett.* **2003**, *5*, 2323-2325.
- [119] W. Jaeger, J. Bohrisch, A. Laschewsky, *Prog. Polym. Sci.* **2010**, *35*, 511-577.
- [120] S. Monfette, D. E. Fogg, *Organometallics* **2006**, *25*, 1940-1944.
- [121] S. Monfette, K. D. Camm, S. I. Gorelsky, D. E. Fogg, *Organometallics* **2009**, *28*, 944-946.

- [122] N. J. Beach, J. A. M. Lummiss, J. M. Bates, D. E. Fogg, *Organometallics* **2012**, *31*, 2349-2356.
- [123] B. J. van Lierop, D. E. Fogg, *Organometallics* **2013**, *32*, 7245-7248.
- [124] C. S. Higman, A. E. Lanterna, M. L. Marin, J. C. Scaiano, D. E. Fogg, *ChemCatChem* **2016**, *8*, 2424-2424.
- [125] A. G. Santos, G. A. Bailey, E. N. dos Santos, D. E. Fogg, *ACS Catal.* **2017**, *7*, 3181-3189.
- [126] J. A. M. Lummiss, W. L. McClennan, R. McDonald, D. E. Fogg, *Organometallics* **2014**, *33*, 6738-6741.
- [127] J. A. M. Lummiss, B. J. Ireland, J. M. Sommers, D. E. Fogg, *ChemCatChem* **2014**, *6*, 459-463.
- [128] W. L. McClennan, S. A. Rufh, J. A. M. Lummiss, D. E. Fogg, *J. Am. Chem. Soc.* **2016**, *138*, 14668-14677.
- [129] B. J. Ireland, B. T. Dobigny, D. E. Fogg, *ACS Catal.* **2015**, *5*, 4690-4698.
- [130] G. A. Bailey, D. E. Fogg, *J. Am. Chem. Soc.* **2015**, *137*, 7318-7321.
- [131] S. C. G. Biagini, R. Gareth Davies, V. C. Gibson, M. R. Giles, E. L. Marshall, M. North, *Polymer* **2001**, *42*, 6669-6671.
- [132] S. C. G. Biagini, S. M. Bush, V. C. Gibson, L. Mazzariol, M. North, W. G. Teasdale, C. M. Williams, G. Zagotto, D. Zamuner, *Tetrahedron* **1995**, *51*, 7247-7262.
- [133] S. Sutthasupa, F. Sanda, T. Masuda, *Macromolecules* **2009**, *42*, 1519-1525.
- [134] B. Commarieu, J. P. Claverie, *Chem. Sci.* **2015**, *6*, 2172-2181.
- [135] J. D. Rule, J. S. Moore, *Macromolecules* **2002**, *35*, 7878-7882.
- [136] M. R. Buchmeiser, S. Sen, J. Unold, W. Frey, *Angew. Chem. Int. Ed.* **2014**, *53*, 9384-9388.
- [137] S. H. Lubbad, R. Bandari, M. R. Buchmeiser, *J. Chromatogr. A* **2011**, *1218*, 8897-8902.
- [138] C. D. Han, *Rheology and Processing of Polymeric Materials*, Oxford University Press, **2007**.
- [139] J. M. Dealy, R. G. Larson, in *Molten Polymers*, Hanser, **2006**, pp. I-XIV.
- [140] Basics of Applied Rheology. G. Paroline. **2016**. Accessed July 29th, 2017. http://web.engr.oregonstate.edu/~rochefow/Polymer_Course_Notes_2016/Applied_Rheology_by_Anton_Paar.pdf
- [141] H. A. Barnes, *A Handbook of Elementary Rheology*, University of Wales, Institute of Non-Newtonian Fluid Mechanics, **2000**.
- [142] Graph constructed using fabricated data
- [143] Measuring Polymers using a Rotational Rheometer in Oscillatory Mode. S. Goodyer. **2016**. Accessed July 29th, 2017. http://www.t-p-a.org/archive/papers/15052013/Measuring_Polymers_using_a_Rotational_Rheometer_in_Oscillatory_Mode.pdf
- [144] L. H. Sperling, *Introduction to Physical Polymer Science*, Wiley, **2005**.
- [145] L. L. Blyler, T. W. Haas, *J. Appl. Polym. Sci.* **1969**, *13*, 2721-2733.
- [146] J. M. Dealy, R. G. Larson, in *Molten Polymers*, Hanser, **2006**, pp. 91-130.
- [147] F. Herbst, D. Döhler, P. Michael, W. H. Binder, *Macromol. Rapid Commun.* **2013**, *34*, 203-220.
- [148] A. Shabbir, H. Goldansaz, O. Hassager, E. van Ruymbeke, N. J. Alvarez, *Macromolecules* **2015**, *48*, 5988-5996.

- [149] C.-C. Cheng, J.-H. Wang, W.-T. Chuang, Z.-S. Liao, J.-J. Huang, S.-Y. Huang, W.-L. Fan, D.-J. Lee, *Polym. Chem.* **2017**, *8*, 3294-3299.
- [150] C. L. Lewis, K. Stewart, M. Anthamatten, *Macromolecules* **2014**, *47*, 729-740.
- [151] M. Rubinstein, A. N. Semenov, *Macromolecules* **2001**, *34*, 1058-1068.
- [152] L. Leibler, M. Rubinstein, R. H. Colby, *Macromolecules* **1991**, *24*, 4701-4707.
- [153] P. Cordier, F. Tournilhac, C. Soulie-Ziakovic, L. Leibler, *Nature* **2008**, *451*, 977-980.
- [154] J. Li, C. L. Lewis, D. L. Chen, M. Anthamatten, *Macromolecules* **2011**, *44*, 5336-5343.
- [155] J. Li, J. A. Viveros, M. H. Wrue, M. Anthamatten, *Adv. Mater.* **2007**, *19*, 2851-2855.
- [156] Y. Chen, A. M. Kushner, G. A. Williams, Z. Guan, *Nat Chem* **2012**, *4*, 467-472.
- [157] A. Choperena, P. Painter, *Macromolecules* **2009**, *42*, 6159-6165.
- [158] J. A. Neal, D. Mozhdghi, Z. Guan, *J. Am. Chem. Soc.* **2015**, *137*, 4846-4850.
- [159] M. Garzoni, M. B. Baker, C. M. A. Leenders, I. K. Voets, L. Albertazzi, A. R. A. Palmans, E. W. Meijer, G. M. Pavan, *J. Am. Chem. Soc.* **2016**, *138*, 13985-13995.
- [160] S. Chen, W. H. Binder, *Acc. Chem. Res.* **2016**.
- [161] T. K. Kwei, *Journal of Polymer Science: Polymer Letters Edition* **1984**, *22*, 307-313.
- [162] W. B. Stockton, M. F. Rubner, *Macromolecules* **1997**, *30*, 2717-2725.
- [163] D. J. Skrovanek, S. E. Howe, P. C. Painter, M. M. Coleman, *Macromolecules* **1985**, *18*, 1676-1683.
- [164] D. C. Sherrington, K. A. Taskinen, *Chem. Soc. Rev.* **2001**, *30*, 83-93.
- [165] Y. He, B. Zhu, Y. Inoue, *Prog. Polym. Sci.* **2004**, *29*, 1021-1051.
- [166] J. H. K. K. Hirschberg, L. Brunsveld, A. Ramzi, J. A. J. M. Vekemans, R. P. Sijbesma, E. W. Meijer, *Nature* **2000**, *407*, 167-170.
- [167] T. Kato, H. Kihara, T. Uryu, A. Fujishima, J. M. J. Frechet, *Macromolecules* **1992**, *25*, 6836-6841.
- [168] T. Kondo, C. Sawatari, R. S. J. Manley, D. G. Gray, *Macromolecules* **1994**, *27*, 210-215.
- [169] R. F. M. Lange, M. Van Gurp, E. W. Meijer, *J. Polym. Sci., Part A: Polym. Chem.* **1999**, *37*, 3657-3670.
- [170] M. M. Coleman, P. C. Painter, *Prog. Polym. Sci.* **1995**, *20*, 1-59.
- [171] S. Burattini, B. W. Greenland, D. H. Merino, W. Weng, J. Seppala, H. M. Colquhoun, W. Hayes, M. E. Mackay, I. W. Hamley, S. J. Rowan, *J. Am. Chem. Soc.* **2010**, *132*, 12051-12058.
- [172] O. Ikkala, G. ten Brinke, *Science* **2002**, *295*, 2407-2409.
- [173] X. Liu, M. Jiang, *Angew. Chem.* **2006**, *118*, 3930-3934.
- [174] U. Kumar, T. Kato, J. M. J. Frechet, *J. Am. Chem. Soc.* **1992**, *114*, 6630-6639.
- [175] L. J. Prins, D. N. Reinhoudt, P. Timmerman, *Angew. Chem. Int. Ed.* **2001**, *40*, 2382-2426.
- [176] T. Kato, J. M. J. Frechet, *Macromolecules* **1989**, *22*, 3818-3819.
- [177] J. H. K. K. Hirschberg, F. H. Beijer, H. A. van Aert, P. C. M. M. Magusin, R. P. Sijbesma, E. W. Meijer, *Macromolecules* **1999**, *32*, 2696-2705.
- [178] P. C. Painter, J. F. Graf, M. M. Coleman, *Macromolecules* **1991**, *24*, 5630-5638.
- [179] M. S. Green, A. V. Tobolsky, *J. Chem. Phys.* **1946**, *14*, 80-92.
- [180] S. A. Ryken, P. R. Payne, L. L. Schafer, in *Ligand Design in Metal Chemistry*, John Wiley & Sons, Ltd, **2016**, pp. 364-405.
- [181] S. A. Ryken, L. L. Schafer, *Acc. Chem. Res.* **2015**, *48*, 2576-2586.
- [182] E. Chong, P. Garcia, L. L. Schafer, *Synthesis* **2014**, *46*, 2884-2896.

- [183] P. Garcia, Y. Y. Lau, M. R. Perry, L. L. Schafer, *Angew. Chem. Int. Ed.* **2013**, 52, 9144-9148.
- [184] M. J. Donachie, *Titanium: A Technical Guide, 2nd Edition*, ASM International, **2000**.
- [185] B. Li, J.-B. Sortais, C. Darcel, *RSC Advances* **2016**, 6, 57603-57625.
- [186] Q. A. Acton, *Amines—Advances in Research and Application: 2013 Edition*, ScholarlyEditions, **2013**.
- [187] Amines Market by Amine Type (Ethylene, Alkyl, Fatty, Specialty, & Ethanol), & by Application (Agricultural Chemicals, Personal Care, Cleaning Products, Petroleum, Water Treatment, Pharmaceutical, Textile, & Others) - Global Trends and Forecast to 2020. marketandmarkets.com. **2015**. Accessed June 14th, 2017. <http://www.marketsandmarkets.com/Market-Reports/amines-market-724.html>
- [188] C. A. Olsen, H. Franzyk, J. W. Jaroszewski, *Synthesis* **2005**, 2005, 2631-2653.
- [189] T. Rosenau, *Synth. Commun.* **2002**, 32, 457-466.
- [190] G. Xu, B. Chen, B. Guo, D. He, S. Yao, *Analyst* **2011**, 136, 2385-2390.
- [191] H. Wang, Y. Huang, X. Dai, F. Shi, *Chem. Commun.* **2017**, 53, 5542-5545.
- [192] S. Kobayashi, H. Ishitani, *Chem. Rev.* **1999**, 99, 1069-1094.
- [193] G. W. Gribble, *Chem. Soc. Rev.* **1998**, 27, 395-404.
- [194] S. Gomez, J. A. Peters, T. Maschmeyer, *Adv. Synth. Catal.* **2002**, 344, 1037-1057.
- [195] C. Guyon, E. Da Silva, R. Lafon, E. Metay, M. Lemaire, *RSC Advances* **2015**, 5, 2292-2298.
- [196] U. Ragnarsson, L. Grehn, *Acc. Chem. Res.* **1991**, 24, 285-289.
- [197] S. Gabriel, *Berichte der deutschen chemischen Gesellschaft* **1887**, 20, 2224-2236.
- [198] M. S. Gibson, M. S. Gibson, R. W. Bradshaw, *Angew. Chem. Int. Ed.*, 7, 919-930.
- [199] K. Kunz, U. Scholz, D. Ganzer, *Synlett* **2003**, 2003, 2428-2439.
- [200] F. Monnier, M. Taillefer, *Angew. Chem. Int. Ed.* **2009**, 48, 6954-6971.
- [201] P. T. Anastas, J. C. Warner, *Green Chemistry: Theory and Practice*, Oxford University Press, **2000**.
- [202] C. Valente, S. Çalimsiz, K. H. Hoi, D. Mallik, M. Sayah, M. G. Organ, *Angew. Chem. Int. Ed.* **2012**, 51, 3314-3332.
- [203] B. Schlummer, U. Scholz, *Adv. Synth. Catal.* **2004**, 346, 1599-1626.
- [204] G. Zeni, R. C. Larock, *Chem. Rev.* **2006**, 106, 4644-4680.
- [205] O. Navarro, N. Marion, J. Mei, S. P. Nolan, *Chem. Eur. J.* **2006**, 12, 5142-5148.
- [206] A. Fayol, Y.-Q. Fang, M. Lautens, *Org. Lett.* **2006**, 8, 4203-4206.
- [207] F. Paul, J. Patt, J. F. Hartwig, *J. Am. Chem. Soc.* **1994**, 116, 5969-5970.
- [208] A. S. Guram, S. L. Buchwald, *J. Am. Chem. Soc.* **1994**, 116, 7901-7902.
- [209] O. V. Zatolochnaya, V. Gevorgyan, *Nat Chem* **2014**, 6, 661-663.
- [210] C. G. Espino, P. M. Wehn, J. Chow, J. Du Bois, *J. Am. Chem. Soc.* **2001**, 123, 6935-6936.
- [211] X. Chen, X.-S. Hao, C. E. Goodhue, J.-Q. Yu, *J. Am. Chem. Soc.* **2006**, 128, 6790-6791.
- [212] M. Wasa, J.-Q. Yu, *J. Am. Chem. Soc.* **2008**, 130, 14058-14059.
- [213] J. Yamaguchi, A. D. Yamaguchi, K. Itami, *Angew. Chem. Int. Ed.* **2012**, 51, 8960-9009.
- [214] J. Roane, O. Daugulis, *J. Am. Chem. Soc.* **2016**, 138, 4601-4607.
- [215] J. Jiao, K. Murakami, K. Itami, *ACS Catal.* **2016**, 6, 610-633.
- [216] Y. Park, Y. Kim, S. Chang, *Chem. Rev.* **2017**.
- [217] E. T. Hennessy, T. A. Betley, *Science* **2013**, 340, 591-595.

- [218] K.-H. Ng, Z. Zhou, W.-Y. Yu, *Org. Lett.* **2012**, *14*, 272-275.
- [219] H. Yamamoto, A. Banerjee, *Synfacts* **2017**, *13*, 0519.
- [220] L. Legnani, B. N. Bhawal, B. Morandi, *Synthesis* **2017**, *49*, 776-789.
- [221] B. Zimmermann, J. Herwig, M. Beller, *Angew. Chem. Int. Ed.* **1999**, *38*, 2372-2375.
- [222] M. Ahmed, A. M. Seayad, R. Jackstell, M. Beller, *J. Am. Chem. Soc.* **2003**, *125*, 10311-10318.
- [223] L. Routaboul, C. Buch, H. Klein, R. Jackstell, M. Beller, *Tetrahedron Lett.* **2005**, *46*, 7401-7405.
- [224] M. Ahmed, R. P. J. Bronger, R. Jackstell, P. C. J. Kamer, P. W. N. M. van Leeuwen, M. Beller, *Chem. Eur. J.* **2006**, *12*, 8979-8988.
- [225] D. Crozet, M. Urrutigoity, P. Kalck, *ChemCatChem* **2011**, *3*, 1102-1118.
- [226] J. L. Klinkenberg, J. F. Hartwig, *Angew. Chem. Int. Ed.* **2011**, *50*, 86-95.
- [227] S. Li, K. Huang, J. Zhang, W. Wu, X. Zhang, *Org. Lett.* **2013**, *15*, 1036-1039.
- [228] A. Behr, A. J. Vorholt, K. A. Ostrowski, T. Seidensticker, *Green Chemistry* **2014**, *16*, 982-1006.
- [229] J. Meng, X.-H. Li, Z.-Y. Han, *Org. Lett.* **2017**, *19*, 1076-1079.
- [230] J. P. Wolfe, S. Wagaw, S. L. Buchwald, *J. Am. Chem. Soc.* **1996**, *118*, 7215-7216.
- [231] C. Chen, X.-Q. Dong, X. Zhang, *Org. Chem. Front.* **2016**, *3*, 1359-1370.
- [232] E. Chong, L. L. Schafer, *Org. Lett.* **2013**, *15*, 6002-6005.
- [233] J. A. Bexrud, P. Eisenberger, D. C. Leitch, P. R. Payne, L. L. Schafer, *J. Am. Chem. Soc.* **2009**, *131*, 2116-2118.
- [234] P. Eisenberger, R. O. Ayinla, J. M. P. Lauzon, L. L. Schafer, *Angew. Chem. Int. Ed.* **2009**, *48*, 8361-8365.
- [235] P. R. Payne, P. Garcia, P. Eisenberger, J. C. H. Yim, L. L. Schafer, *Org. Lett.* **2013**, *15*, 2182-2185.
- [236] P. Garcia, P. R. Payne, E. Chong, R. L. Webster, B. J. Barron, A. C. Behrle, J. A. R. Schmidt, L. L. Schafer, *Tetrahedron* **2013**, *69*, 5737-5743.
- [237] Z. Zhang, J.-D. Hamel, L. L. Schafer, *Chem. Eur. J.* **2013**, *19*, 8751-8754.
- [238] E. Chong, J. W. Brandt, L. L. Schafer, *J. Am. Chem. Soc.* **2014**, *136*, 10898-10901.
- [239] L. Schafer, E. Chong, P. Garcia, *Synthesis* **2014**, *46*, 2884-2896.
- [240] J. C. H. Yim, L. L. Schafer, *Eur. J. Org. Chem.* **2014**, *2014*, 6825-6840.
- [241] Z. Zhang, L. L. Schafer, *Org. Lett.* **2003**, *5*, 4733-4736.
- [242] Z. Zhang, D. C. Leitch, M. Lu, B. O. Patrick, L. L. Schafer, *Chem. Eur. J.* **2007**, *13*, 2012-2022.
- [243] D. C. Leitch, P. R. Payne, C. R. Dunbar, L. L. Schafer, *J. Am. Chem. Soc.* **2009**, *131*, 18246-18247.
- [244] D. C. Leitch, R. H. Platel, L. L. Schafer, *J. Am. Chem. Soc.* **2011**, *133*, 15453-15463.
- [245] J. A. Bexrud, L. L. Schafer, *Dalton Trans.* **2010**, *39*, 361-363.
- [246] E. Chong, S. Qayyum, L. L. Schafer, R. Kempe, *Organometallics* **2013**, *32*, 1858-1865.
- [247] J. C. H. Yim, J. A. Bexrud, R. O. Ayinla, D. C. Leitch, L. L. Schafer, *J. Org. Chem.* **2014**, *79*, 2015-2028.
- [248] C. Li, R. K. Thomson, B. Gillon, B. O. Patrick, L. L. Schafer, *Chem. Commun.* **2003**, 2462-2463.
- [249] J. A. Bexrud, J. D. Beard, D. C. Leitch, L. L. Schafer, *Org. Lett.* **2005**, *7*, 1959-1962.
- [250] R. O. Ayinla, L. L. Schafer, *Inorg. Chim. Acta* **2006**, *359*, 3097-3102.

- [251] R. K. Thomson, J. A. Bexrud, L. L. Schafer, *Organometallics* **2006**, *25*, 4069-4071.
- [252] A. V. Lee, L. L. Schafer, *Eur. J. Inorg. Chem.* **2007**, *2007*, 2245-2255.
- [253] M. C. Wood, D. C. Leitch, C. S. Yeung, J. A. Kozak, L. L. Schafer, *Angew. Chem. Int. Ed.* **2007**, *46*, 354-358.
- [254] L. J. E. Stanlake, L. L. Schafer, *Organometallics* **2009**, *28*, 3990-3998.
- [255] D. C. Leitch, C. S. Turner, L. L. Schafer, *Angew. Chem. Int. Ed.* **2010**, *49*, 6382-6386.
- [256] M. A. Antunes, R. F. Munhá, L. G. Alves, L. L. Schafer, A. M. Martins, *J. Organomet. Chem.* **2011**, *696*, 2-6.
- [257] R. O. Ayinla, T. Gibson, L. L. Schafer, *J. Organomet. Chem.* **2011**, *696*, 50-60.
- [258] R. O. Ayinla, L. L. Schafer, *Dalton Trans.* **2011**, *40*, 7769-7776.
- [259] P. R. Payne, J. A. Bexrud, D. C. Leitch, L. L. Schafer, *Can. J. Chem.* **2011**, *89*, 1222-1229.
- [260] C. E. Hayes, R. H. Platel, L. L. Schafer, D. B. Leznoff, *Organometallics* **2012**, *31*, 6732-6740.
- [261] L. L. Schafer, J. C. H. Yim, N. Yonson, in *Metal-Catalyzed Cross-Coupling Reactions and More*, Wiley-VCH Verlag GmbH & Co. KGaA, **2014**, pp. 1135-1258.
- [262] N. Yonson, J. C. H. Yim, L. L. Schafer, *Inorg. Chim. Acta* **2014**, *422*, 14-20.
- [263] J. M. P. Lauzon, L. L. Schafer, *Z. Anorg. Allg. Chem.* **2015**, *641*, 128-135.
- [264] E. K. J. Lui, L. L. Schafer, *Adv. Synth. Catal.* **2016**, *358*, 713-718.
- [265] C. Braun, S. Bräse, L. L. Schafer, *Eur. J. Org. Chem.* **2017**, *2017*, 1760-1764.
- [266] Y. Y. Lau, H. Zhai, L. L. Schafer, *J. Org. Chem.* **2016**, *81*, 8696-8709.
- [267] R. Kubiak, I. Prochnow, S. Doye, *Angew. Chem. Int. Ed.* **2010**, *49*, 2626-2629.
- [268] P. W. Roesky, *Angew. Chem. Int. Ed.* **2009**, *48*, 4892-4894.
- [269] M. G. Clerici, F. Maspero, *Synthesis* **1980**, *1980*, 305-306.
- [270] W. A. Nugent, D. W. Ovenall, S. J. Holmes, *Organometallics* **1983**, *2*, 161-162.
- [271] S. B. Herzon, J. F. Hartwig, *J. Am. Chem. Soc.* **2007**, *129*, 6690-6691.
- [272] N. Chatani, T. Asaumi, S. Yorimitsu, T. Ikeda, F. Kakiuchi, S. Murai, *J. Am. Chem. Soc.* **2001**, *123*, 10935-10941.
- [273] C.-H. Jun, *Chem. Commun.* **1998**, 1405-1406.
- [274] S. B. Herzon, J. F. Hartwig, *J. Am. Chem. Soc.* **2008**, *130*, 14940-14941.
- [275] A. L. Reznichenko, T. J. Emge, S. Audörsch, E. G. Klauber, K. C. Hultsch, B. Schmidt, *Organometallics* **2011**, *30*, 921-924.
- [276] T. E. Müller, M. Beller, *Chem. Rev.* **1998**, *98*, 675-704.
- [277] T. E. Müller, K. C. Hultsch, M. Yus, F. Foubelo, M. Tada, *Chem. Rev.* **2008**, *108*, 3795-3892.
- [278] R. Severin, S. Doye, *Chem. Soc. Rev.* **2007**, *36*, 1407-1420.
- [279] F. Pohlki, S. Doye, *Chem. Soc. Rev.* **2003**, *32*, 104-114.
- [280] L. Huang, M. Arndt, K. Gooßen, H. Heydt, L. J. Gooßen, *Chem. Rev.* **2015**, *115*, 2596-2697.
- [281] A. J. Musacchio, L. Q. Nguyen, G. H. Beard, R. R. Knowles, *J. Am. Chem. Soc.* **2014**, *136*, 12217-12220.
- [282] A. J. Musacchio, B. C. Lainhart, X. Zhang, S. G. Naguib, T. C. Sherwood, R. R. Knowles, *Science* **2017**, *355*, 727-730.
- [283] J.-J. Brunet, D. Neibecker, in *Catalytic Heterofunctionalization*, Wiley-VCH Verlag GmbH, **2001**, pp. 91-141.

- [284] S. Doye, *Synlett* **2004**, 2004, 1653-1672.
- [285] F. Alonso, I. P. Beletskaya, M. Yus, *Chem. Rev.* **2004**, 104, 3079-3160.
- [286] A. L. Odom, *Dalton Trans.* **2005**, 225-233.
- [287] M. Nobis, B. Driëben-Hölscher, *Angew. Chem. Int. Ed.* **2001**, 40, 3983-3985.
- [288] J. Seayad, A. Tillack, C. G. Hartung, M. Beller, *Adv. Synth. Catal.* **2002**, 344, 795-813.
- [289] P. W. Roesky, T. E. Müller, *Angew. Chem. Int. Ed.* **2003**, 42, 2708-2710.
- [290] S. Hong, T. J. Marks, *Acc. Chem. Res.* **2004**, 37, 673-686.
- [291] K. C. Hultsch, *Org. Biomol. Chem.* **2005**, 3, 1819-1824.
- [292] D. V. Gribkov, K. C. Hultsch, *Angew. Chem. Int. Ed.* **2004**, 43, 5542-5546.
- [293] I. Aillaud, J. Collin, J. Hannedouche, E. Schulz, *Dalton Trans.* **2007**, 5105-5118.
- [294] K. C. Hultsch, *Adv. Synth. Catal.* **2005**, 347, 367-391.
- [295] A. G. M. Barrett, M. R. Crimmin, M. S. Hill, P. A. Procopiou, *Proceedings of the Royal Society A: Mathematical, Physical and Engineering Science* **2010**, 466, 927-963.
- [296] J. Hannedouche, J. Collin, A. Trifonov, E. Schulz, *J. Organomet. Chem.* **2011**, 696, 255-262.
- [297] J. Jenter, A. Lühl, P. W. Roesky, S. Blechert, *J. Organomet. Chem.* **2011**, 696, 406-418.
- [298] G. Zi, *J. Organomet. Chem.* **2011**, 696, 68-75.
- [299] J.-J. Brunet, N.-C. Chu, M. Rodriguez-Zubiri, *Eur. J. Inorg. Chem.* **2007**, 2007, 4711-4722.
- [300] K. D. Hesp, M. Stradiotto, *ChemCatChem* **2010**, 2, 1192-1207.
- [301] G. Zi, *Dalton Trans.* **2009**, 9101-9109.
- [302] H. Wang, J. C.-Y. Yang, S. L. Buchwald, *J. Am. Chem. Soc.* **2017**.
- [303] A. L. Reznichenko, K. C. Hultsch, in *Hydrofunctionalization* (Eds.: V. P. Ananikov, M. Tanaka), Springer Berlin Heidelberg, Berlin, Heidelberg, **2013**, pp. 51-114.
- [304] B. Niu, Z. Chen, Z. Xu, *ACS Sustainable Chemistry & Engineering* **2017**, 5, 1376-1381.
- [305] R. G. Eggert, *Nat Chem* **2011**, 3, 688-691.
- [306] R. E. Hester, R. M. Harrison, *Waste as a Resource*, Royal Society of Chemistry, **2013**.
- [307] S. H. Weeden, R. H. Schmidt, *J. Arthroplasty.* **2007**, 22, 151-155.
- [308] Q. V. Le, T. P. Nguyen, K. S. Choi, Y.-H. Cho, Y. J. Hong, S. Y. Kim, *PCCP* **2014**, 16, 25468-25472.
- [309] C. Fitzpatrick, E. Olivetti, T. R. Miller, R. Roth, R. Kirchain, *Environmental Science & Technology* **2015**, 49, 974-981.
- [310] Patrick Flanigan, Varun R. Kshetry, Edward C. Benzel, *Neurosurg. Focus.* **2014**, 36, E22.
- [311] D. I. Bleiwas, J. F. Papp, T. R. Yager Shift in Global Tantalum Mine Production, 2000–2014 2015 Fact Sheet U. S. G. Survey Reston, VA <http://pubs.er.usgs.gov/publication/fs20153079>
- [312] J. F. Caccamo, D. M. McCarthy, *Journal of Moral Theology, Volume 4, Number 1: Technology*, Pickwick Publications, **2015**.
- [313] U.S. Geological Survey. Mineral commodity summaries 2015 2015 Mineral Commodities Summaries U. S. G. Survey Reston, VA Accessed on June 6th, 2017 <http://pubs.er.usgs.gov/publication/70140094>
- [314] SEC Delays Risk Undermining Efforts to Curb Congolese Conflict Minerals. a. A. D. Sophia Pickles. **2015**. Accessed July 16th, 2017. http://www.huffingtonpost.com/sophia-pickles/sec-delays-risk-undermini_b_1438364.html

- [315] X. Feng, K. Shankar, M. Paulose, C. A. Grimes, *Angew. Chem. Int. Ed.* **2009**, *48*, 8095-8098.
- [316] K. G. Budinski, *Wear* **1991**, *151*, 203-217.
- [317] I. Prochnow, P. Zark, T. Müller, S. Doye, *Angew. Chem. Int. Ed.* **2011**, *50*, 6401-6405.
- [318] P. Horrillo-Martinez, D. C. Leitch, S. A. Ryken, R. K. Thomson, J. D. Beard, B. O. Patrick, L. L. Schafer, G. R. Giesbrecht, *Can. J. Chem.* **2015**, *93*, 775-783.
- [319] L. Ackermann, R. G. Bergman, *Org. Lett.* **2002**, *4*, 1475-1478.
- [320] Y. Wang, Y. Qin, X. Wang, F. Wang, *ACS Catal.* **2015**, *5*, 393-396.
- [321] H. Nishikiori, K. Todoroki, R. A. Setiawan, K. Teshima, T. Fujii, H. Satozono, *Langmuir* **2015**, *31*, 964-969.
- [322] D. J. Gilmour, R. L. Webster, M. R. Perry, L. L. Schafer, *Dalton Trans* **2015**, *44*, 12411-12419.
- [323] G. R. Giesbrecht, A. Shafir, J. Arnold, *Inorg. Chem.* **2001**, *40*, 6069-6072.
- [324] P. D. Knight, I. Munslow, P. N. O'Shaughnessy, P. Scott, *Chem. Commun.* **2004**, 894-895.
- [325] D. A. Kissounko, I. A. Guzei, S. H. Gellman, S. S. Stahl, *Organometallics* **2005**, *24*, 5208-5210.
- [326] A. L. Reznichenko, K. C. Hultsch, *Organometallics* **2010**, *29*, 24-27.
- [327] G. Zi, F. Zhang, H. Song, *Chem. Commun.* **2010**, *46*, 6296-6298.
- [328] F. Zhang, J. Zhang, H. Song, G. Zi, *Inorg. Chem. Commun.* **2011**, *14*, 72-74.
- [329] J. A. Thomson, L. L. Schafer, *Dalton Trans.* **2012**, *41*, 7897-7904.
- [330] A. L. Reznichenko, K. C. Hultsch, *J. Am. Chem. Soc.* **2012**, *134*, 3300-3311.
- [331] A. L. Gott, A. J. Clarke, G. J. Clarkson, P. Scott, *Organometallics* **2007**, *26*, 1729-1737.
- [332] M. C. Wood, D. C. Leitch, C. S. Yeung, J. A. Kozak, L. L. Schafer, *Angew. Chem. Int. Ed.* **2009**, *48*, 6937-6937.
- [333] L. J. E. Stanlake, J. D. Beard, L. L. Schafer, *Inorg. Chem.* **2008**, *47*, 8062-8068.
- [334] P. R. Payne, R. K. Thomson, D. M. Medeiros, G. Wan, L. L. Schafer, *Dalton Trans.* **2013**, *42*, 15670-15677.
- [335] J. C. Slater, *J. Chem. Phys.* **1964**, *41*, 3199-3204.
- [336] F. H. Froes, T.-L. Yau, H. G. Weidinger, in *Mater. Sci. Technol.*, Wiley-VCH Verlag GmbH & Co. KGaA, **2006**.
- [337] M. C. Karunaratne, J. W. Baumann, M. J. Heeg, P. D. Martin, C. H. Winter, *J. Organomet. Chem.*
- [338] R. K. Thomson, F. E. Zahariev, Z. Zhang, B. O. Patrick, Y. A. Wang, L. L. Schafer, *Inorg. Chem.* **2005**, *44*, 8680-8689.
- [339] D. C. Leitch, J. D. Beard, R. K. Thomson, V. A. Wright, B. O. Patrick, L. L. Schafer, *Eur. J. Inorg. Chem.* **2009**, *2009*, 2691-2701.
- [340] E. Chong, W. Xue, T. Storr, P. Kennepohl, L. L. Schafer, *Organometallics* **2015**, *34*, 4941-4945.
- [341] J. Dörfler, S. Doye, *Angew. Chem. Int. Ed.* **2013**, *52*, 1806-1809.
- [342] J. Dörfler, T. Preuß, A. Schischko, M. Schmidtman, S. Doye, *Angew. Chem. Int. Ed.* **2014**, *53*, 7918-7922.
- [343] T. Elkin, N. V. Kulkarni, B. Tumanskii, M. Botoshansky, L. J. W. Shimon, M. S. Eisen, *Organometallics* **2013**, *32*, 6337-6352.

- [344] T. Elkin, M. Botoshansky, R. M. Waymouth, M. S. Eisen, *Organometallics* **2014**, *33*, 840-843.
- [345] N. V. Kulkarni, T. Elkin, B. Tumaniskii, M. Botoshansky, L. J. W. Shimon, M. S. Eisen, *Organometallics* **2014**, *33*, 3119-3136.
- [346] J. Dörfler, T. Preuß, C. Brahms, D. Scheuer, S. Doye, *Dalton Trans.* **2015**, *44*, 12149-12168.
- [347] R. Kubiak, I. Prochnow, S. Doye, *Angew. Chem. Int. Ed.* **2009**, *48*, 1153-1156.
- [348] P. Anastas, N. Eghbali, *Chem. Soc. Rev.* **2010**, *39*, 301-312.
- [349] Z. Shi, C. He, *J. Org. Chem.* **2004**, *69*, 3669-3671.
- [350] R. B. Bedford, C. J. Mitchell, R. L. Webster, *Chem. Commun.* **2010**, *46*, 3095-3097.
- [351] S. Bensaid, H. Doucet, *ChemSusChem* **2012**, *5*, 1559-1567.
- [352] A. W. Addison, T. N. Rao, J. Reedijk, J. van Rijn, G. C. Verschoor, *J. Chem. Soc., Dalton Trans.* **1984**, 1349-1356.
- [353] R. Kempe, P. Arndt, *Inorg. Chem.* **1996**, *35*, 2644-2649.
- [354] A. Pöllnitz, S. Irisli, C. Silvestru, A. Silvestru, *Phosphorus, Sulfur Silicon Relat. Elem.* **2010**, *185*, 910-919.
- [355] R. Contreras, J. M. Grevy, Z. García-Hernández, M. Göizado-Rodriguez, B. Wrackmeyer, *Heteroat. Chem* **2001**, *12*, 542-550.
- [356] K. Naktode, R. K. Kottalanka, T. K. Panda, *New J. Chem.* **2012**, *36*, 2280-2285.
- [357] C. Müller, W. Saak, S. Doye, *Eur. J. Org. Chem.* **2008**, *2008*, 2731-2739.
- [358] I. Prochnow, R. Kubiak, O. N. Frey, R. Beckhaus, S. Doye, *ChemCatChem* **2009**, *1*, 162-172.
- [359] P. J. Walsh, A. M. Baranger, R. G. Bergman, *J. Am. Chem. Soc.* **1992**, *114*, 1708-1719.
- [360] J. S. Johnson, R. G. Bergman, *J. Am. Chem. Soc.* **2001**, *123*, 2923-2924.
- [361] B. F. Straub, R. G. Bergman, *Angew. Chem. Int. Ed.* **2001**, *40*, 4632-4635.
- [362] L. K. Lukanov, A. P. Venkov, N. M. Mollov, *Synthesis* **1985**, *1985*, 971-973.
- [363] W. Dabkowski, J. Michalski, C. Radziejewski, Z. Skrzypczyński, *Chem. Ber.* **1982**, *115*, 1636-1643.
- [364] R. Serwa, I. Wilkening, G. Del Signore, M. Mühlberg, I. Claußnitzer, C. Weise, M. Gerrits, C. P. R. Hackenberger, *Angew. Chem. Int. Ed.* **2009**, *48*, 8234-8239.
- [365] B. A. Dar, N. A. Dangroo, A. Gupta, A. Wali, M. A. Khuroo, R. A. Vishwakarma, B. Singh, *Tetrahedron Lett.* **2014**, *55*, 1544-1548.
- [366] M. Meazza, A. Kowalczyk, L. Shirley, J. W. Yang, H. Guo, R. Rios, *Adv. Synth. Catal.* **2016**, *358*, 719-723.
- [367] H. Zhai, A. Borzenko, Y. Y. Lau, S. H. Ahn, L. L. Schafer, *Angew. Chem. Int. Ed.* **2012**, *51*, 12219-12223.
- [368] G. A. Jeffrey, *An Introduction to Hydrogen Bonding*, Oxford University Press, **1997**.
- [369] T. Steiner, *Angew. Chem. Int. Ed.* **2002**, *41*, 48-76.
- [370] B. K. Keitz, A. Fedorov, R. H. Grubbs, *J. Am. Chem. Soc.* **2012**, *134*, 2040-2043.
- [371] A. Lahor, M. Nithitanakul, B. P. Grady, *Eur. Polym. J.* **2004**, *40*, 2409-2420.
- [372] B. A. Miller-Chou, J. L. Koenig, *Prog. Polym. Sci.* **2003**, *28*, 1223-1270.
- [373] G. S. Kirshenbaum, *Polymer Science Study Guide*, Gordon and Breach, **1973**.
- [374] J. Alonso-Villanueva, J. M. Cuevas, J. M. Laza, J. L. Vilas, L. M. León, *J. Appl. Polym. Sci.* **2010**, *115*, 2440-2447.
- [375] R. Walker, R. M. Conrad, R. H. Grubbs, *Macromolecules* **2009**, *42*, 599-605.

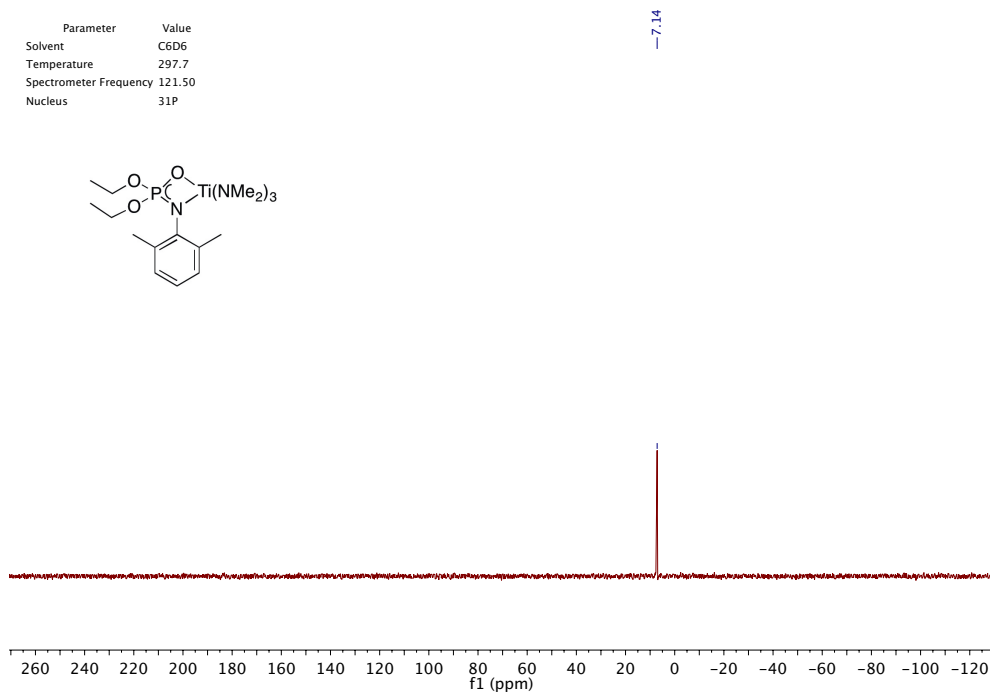
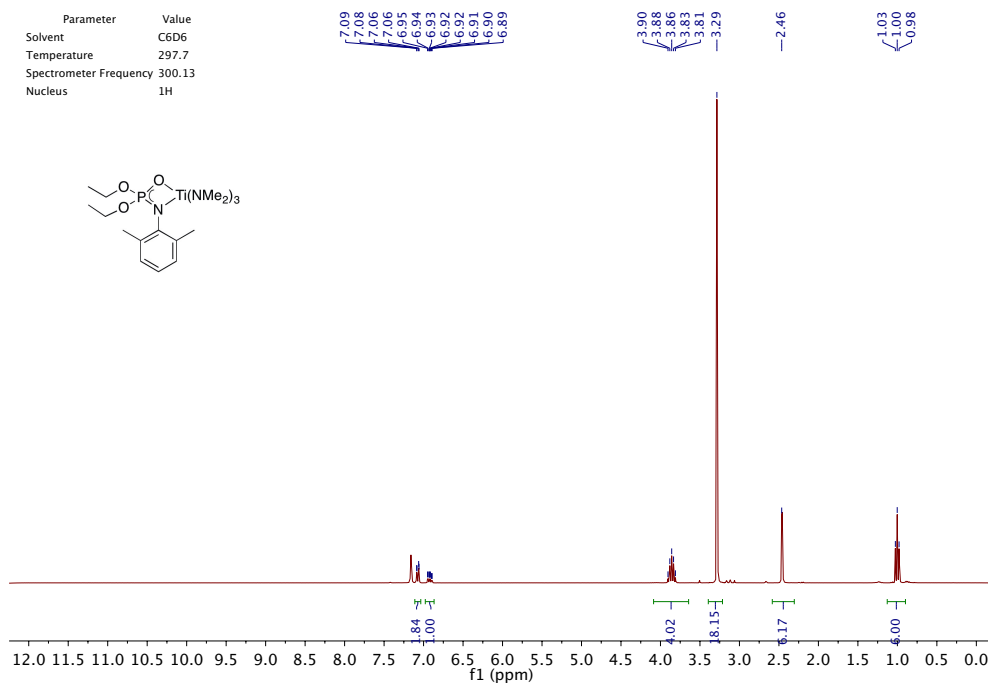
- [376] J. Joseph, E. D. Jemmis, *J. Am. Chem. Soc.* **2007**, *129*, 4620-4632.
- [377] K. Sakurai, T. Takahashi, *J. Appl. Polym. Sci.* **1989**, *38*, 1191-1194.
- [378] T. Ebrahimi, S. G. Hatzikiriakos, P. Mehrkhodavandi, *Macromolecules* **2015**, *48*, 6672-6681.
- [379] K. B. Walters, D. E. Hirt, *Macromolecules* **2007**, *40*, 4829-4838.
- [380] J. Eames, M. Watkinson, *Eur. J. Org. Chem.* **2001**, *2001*, 1213-1224.
- [381] T. J. Clark, N. J. Robertson, H. A. Kostalik Iv, E. B. Lobkovsky, P. F. Mutolo, H. D. Abruña, G. W. Coates, *J. Am. Chem. Soc.* **2009**, *131*, 12888-12889.
- [382] A. F. Abdel-Magid, K. G. Carson, B. D. Harris, C. A. Maryanoff, R. D. Shah, *J. Org. Chem.* **1996**, *61*, 3849-3862.
- [383] G. J. P. Britovsek, M. Bruce, V. C. Gibson, B. S. Kimberley, P. J. Maddox, S. Mastroianni, S. J. McTavish, C. Redshaw, G. A. Solan, S. Strömberg, A. J. P. White, D. J. Williams, *J. Am. Chem. Soc.* **1999**, *121*, 8728-8740.
- [384] W.-J. Yoo, C.-J. Li, *J. Am. Chem. Soc.* **2006**, *128*, 13064-13065.
- [385] S. A. Lawrence, *Amines: Synthesis, Properties and Applications*, Cambridge University Press, **2004**.
- [386] Y. Zhou, C. Yao, R. Ni, G. Yang, *Synth. Commun.* **2010**, *40*, 2624-2632.
- [387] S. D. Bull, S. G. Davies, G. Fenton, A. W. Mulvaney, R. S. Prasad, A. D. Smith, *J. Chem. Soc., Perkin Trans. 1* **2000**, 3765-3774.
- [388] H. Ji, Q. Jing, J. Huang, R. B. Silverman, *Tetrahedron* **2012**, *68*, 1359-1366.
- [389] B. Basu, S. Paul, A. K. Nanda, *Green Chemistry* **2009**, *11*, 1115-1120.
- [390] P. Perlmutter, M. Rose, F. Vounatsos, *Eur. J. Org. Chem.* **2003**, *2003*, 756-760.
- [391] V. Bütün, S. P. Armes, N. C. Billingham, *Macromolecules* **2001**, *34*, 1148-1159.
- [392] K. M. Veccharelli, V. K. Tong, J. L. Young, J. Yang, N. C. Gianneschi, *Chem. Commun.* **2016**, *52*, 567-570.
- [393] K. Mizuta, S. Fukutomi, K. Yamabuki, K. Onimura, T. Oishi, *Polym. J.* **2010**, *42*, 534-539.
- [394] P. Theato, *Multi-Component and Sequential Reactions in Polymer Synthesis*, Springer International Publishing, **2015**.
- [395] P. Espeel, F. E. Du Prez, *Eur. Polym. J.* **2015**, *62*, 247-272.
- [396] P. Chen, *Acc. Chem. Res.* **2016**, *49*, 1052-1060.
- [397] H. Martinez, M. A. Hillmyer, C. J. Cramer, *J. Org. Chem.* **2014**, *79*, 11940-11948.
- [398] J. V. Olsson, D. Hult, S. Garcia-Gallego, M. Malkoch, *Chem. Sci.* **2017**.
- [399] G. Stork, D. Niu, A. Fujimoto, E. R. Koft, J. M. Balkovec, J. R. Tata, G. R. Dake, *J. Am. Chem. Soc.* **2001**, *123*, 3239-3242.
- [400] Y. Hayashi, J. Kanayama, J. Yamaguchi, M. Shoji, *J. Org. Chem.* **2002**, *67*, 9443-9448.
- [401] K. Nakamoto, M. Margoshes, R. E. Rundle, *J. Am. Chem. Soc.* **1955**, *77*, 6480-6486.
- [402] C. Wu, X. Liu, D. Wei, J. Fan, L. Wang, *Water Res.* **2001**, *35*, 3927-3933.
- [403] J. P. Mathias, C. T. Seto, E. E. Simanek, G. M. Whitesides, *J. Am. Chem. Soc.* **1994**, *116*, 1725-1736.
- [404] P. Sun, J. a. Liu, Z. Zhang, K. Zhang, *Polym. Chem.* **2016**, *7*, 2239-2244.
- [405] L. C. Dias, M. A. B. Ferreira, C. F. Tormena, *J. Phys. Chem. A* **2008**, *112*, 232-237.
- [406] M. Schaefer, N. Hanik, A. F. M. Kilbinger, *Macromolecules* **2012**, *45*, 6807-6818.
- [407] Y. C. Simon, E. B. Coughlin, *J. Polym. Sci., Part A: Polym. Chem.* **2010**, *48*, 2557-2563.

- [408] S. T. Nguyen, L. K. Johnson, R. H. Grubbs, J. W. Ziller, *J. Am. Chem. Soc.* **1992**, *114*, 3974-3975.
- [409] F. S. C. Chang, in *Polymer Molecular Weight Methods, Vol. 125*, American Chemistry Society, **1973**, pp. 154-163.
- [410] S. S. Hou, P. L. Kuo, *Polymer* **2001**, *42*, 2387-2394.
- [411] L. H. Tung, *J. Appl. Polym. Sci.* **1979**, *24*, 953-963.
- [412] W. S. Anderson, Google Patents, **1983**.
- [413] K. Komuro, A. Ueda, Google Patents, **1984**.
- [414] H. W. Holland, Google Patents, **1994**.
- [415] D. E. Bergbreiter, P. L. Osburn, J. D. Frels, *J. Am. Chem. Soc.* **2001**, *123*, 11105-11106.
- [416] R. R. Navarro, K. Sumi, M. Matsumura, *Water Sci. Technol.* **1998**, *38*, 195-201.
- [417] E. Fourest, B. Volesky, *Environmental Science & Technology* **1996**, *30*, 277-282.
- [418] C. A. Bell, S. V. Smith, M. R. Whittaker, A. K. Whittaker, L. R. Gahan, M. J. Monteiro, *Adv. Mater.* **2006**, *18*, 582-586.
- [419] M. Kawalec, A. P. Dove, L. Mespouille, P. Dubois, *Polym. Chem.* **2013**, *4*, 1260-1270.
- [420] R. G. Pearson, *J. Am. Chem. Soc.* **1963**, *85*, 3533-3539.

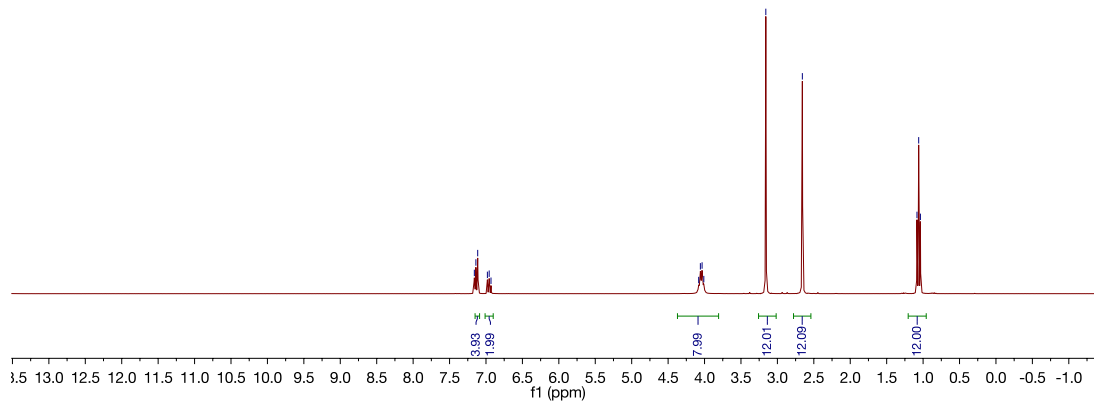
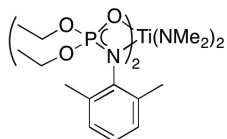
Appendices

Appendix A Supplementary Information for Chapter 2

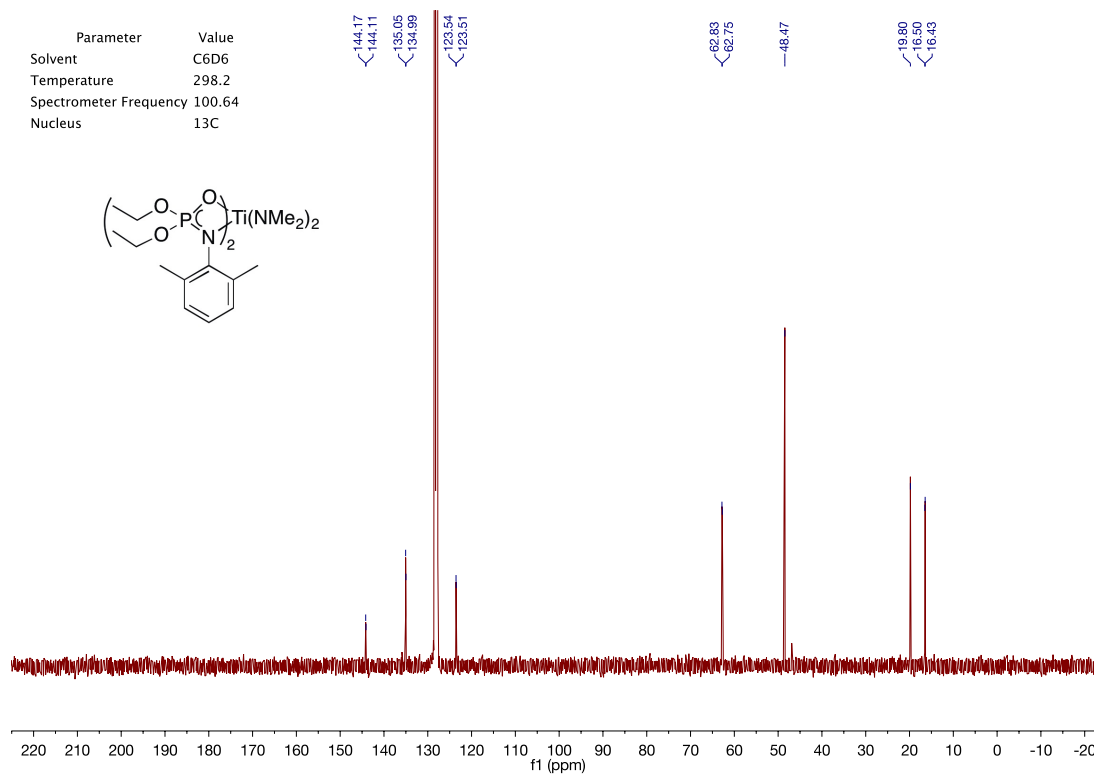
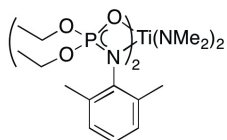
A.1 Selected NMR Spectra



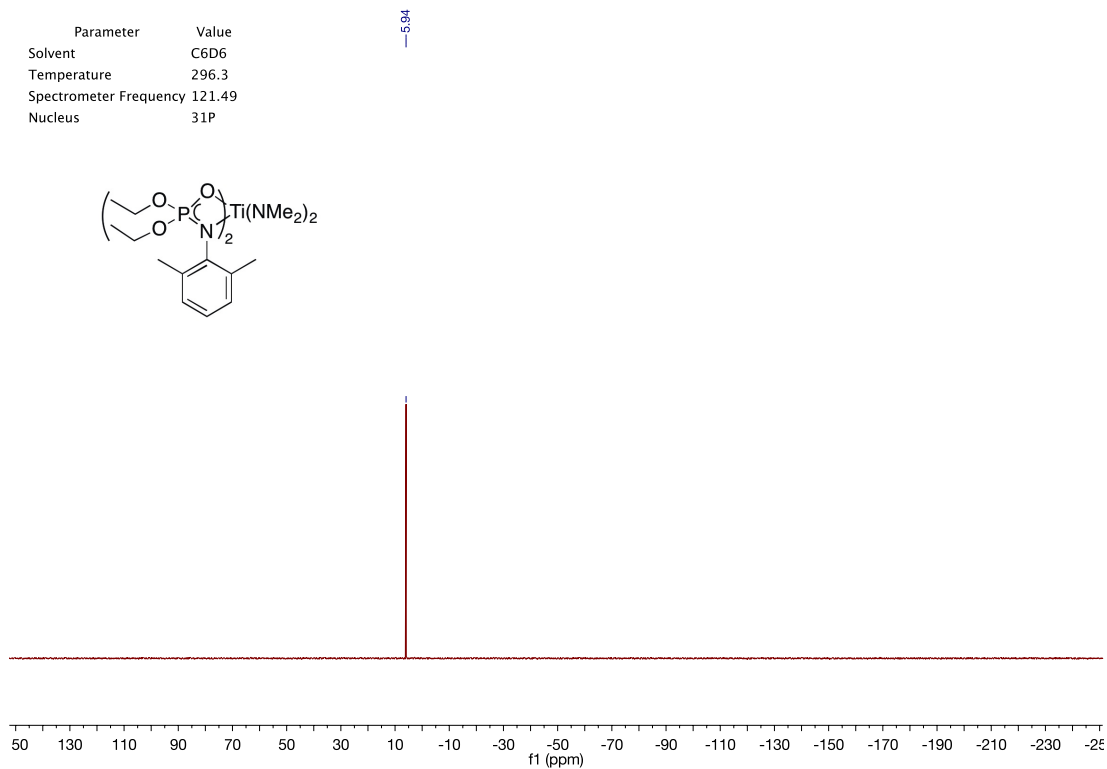
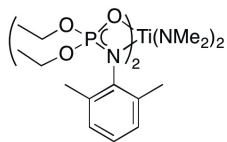
Parameter	Value
Solvent	C6D6
Temperature	298.6
Spectrometer Frequency	300.13
Nucleus	¹ H



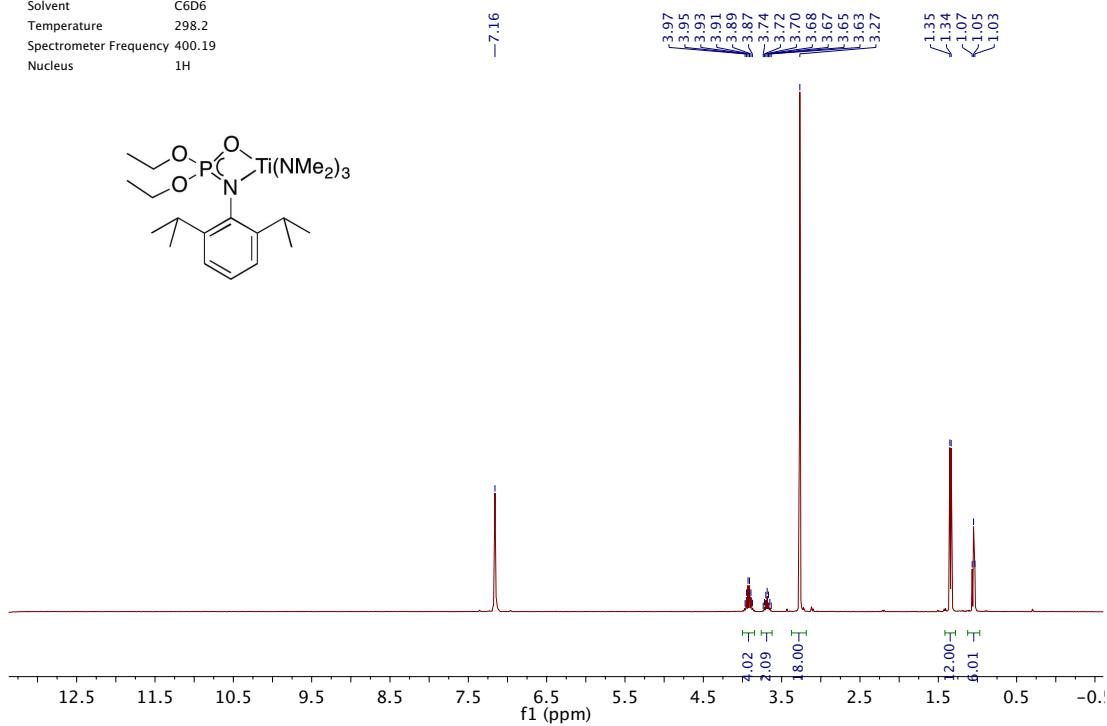
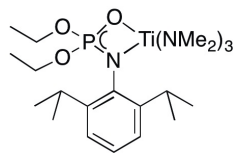
Parameter	Value
Solvent	C6D6
Temperature	298.2
Spectrometer Frequency	100.64
Nucleus	¹³ C



Parameter	Value
Solvent	C6D6
Temperature	296.3
Spectrometer Frequency	121.49
Nucleus	31P



Parameter	Value
Solvent	C6D6
Temperature	298.2
Spectrometer Frequency	400.19
Nucleus	1H



Parameter	Value
Solvent	C6D6
Temperature	297.6
Spectrometer Frequency	100.64
Nucleus	¹³ C

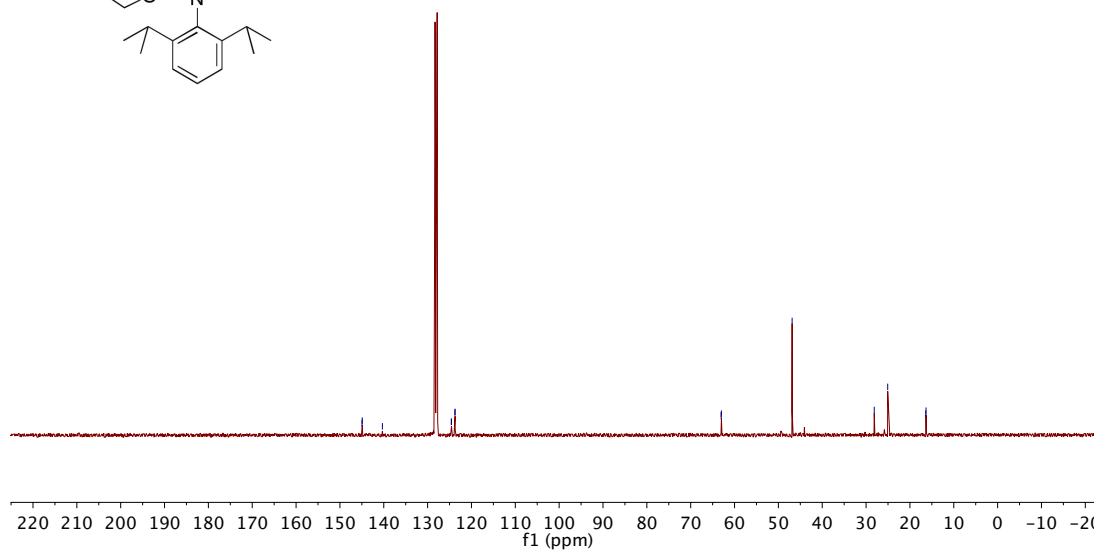
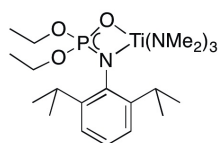
144.96
144.90
140.31
124.60
123.56
123.77
123.73

63.07
62.99

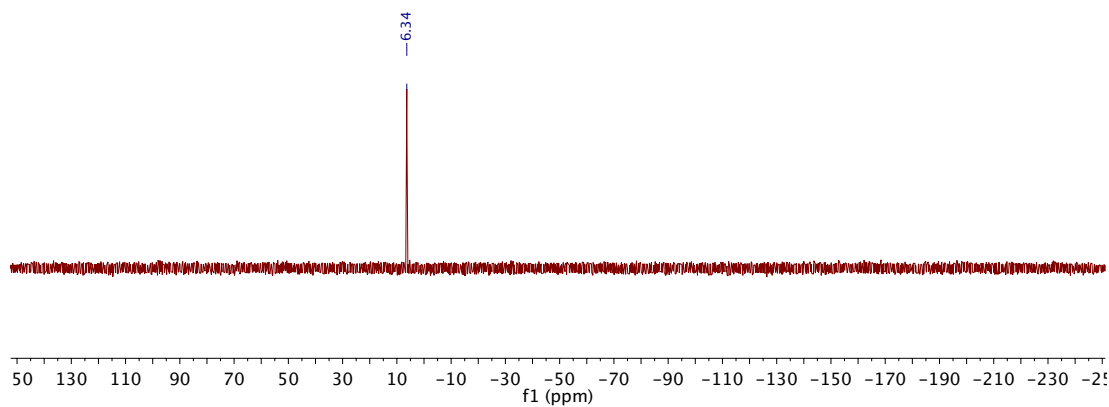
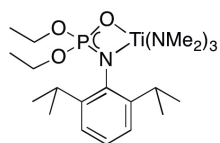
46.87

28.14
25.07

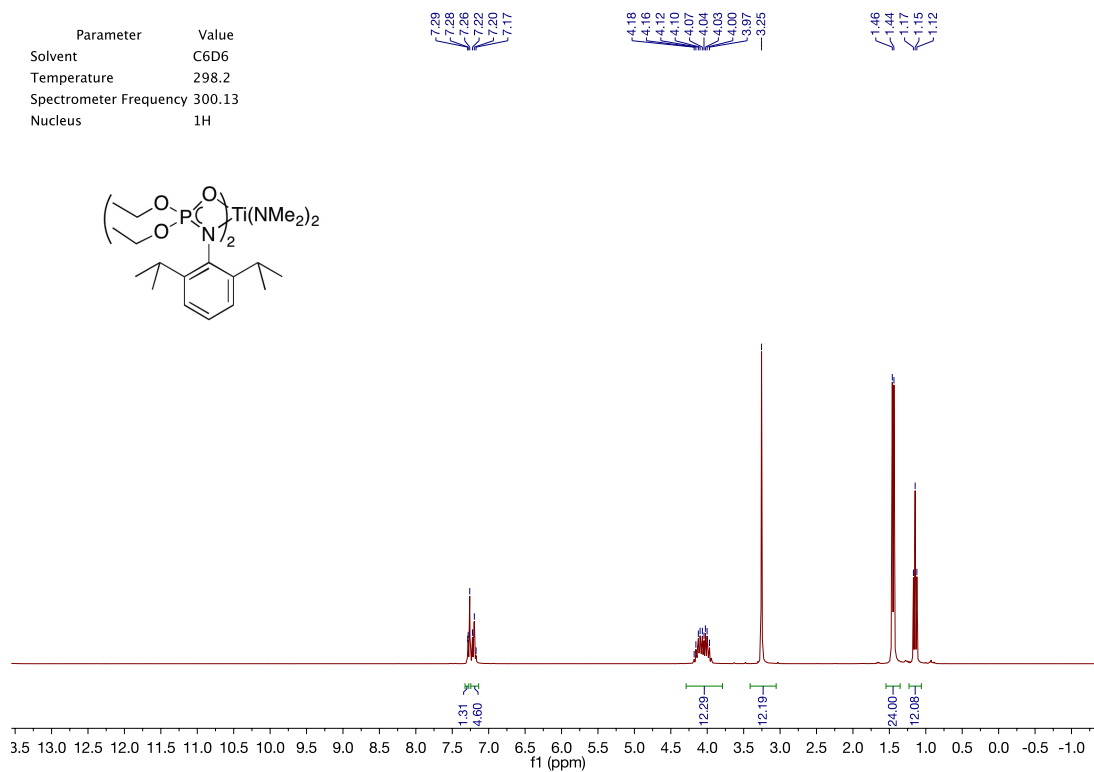
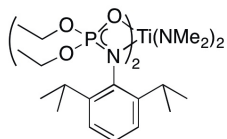
16.39
16.33



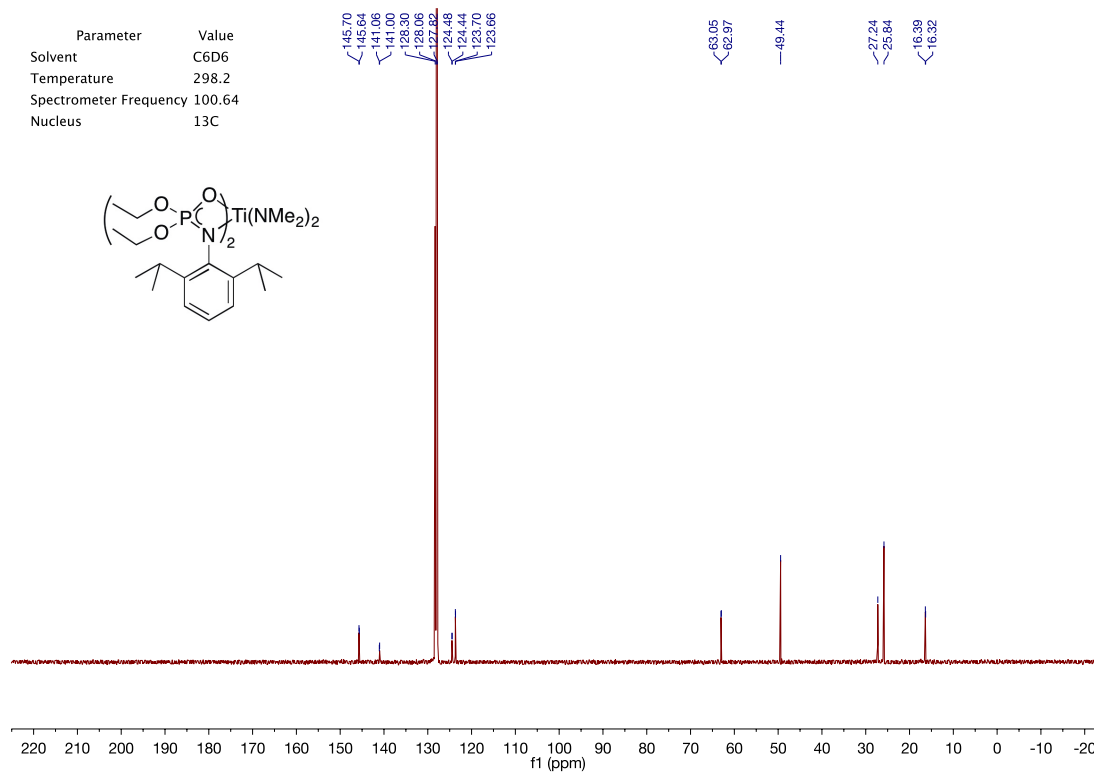
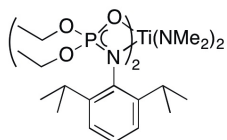
Parameter	Value
Solvent	C6D6
Temperature	297.7
Spectrometer Frequency	121.49
Nucleus	³¹ P



Parameter	Value
Solvent	C6D6
Temperature	298.2
Spectrometer Frequency	300.13
Nucleus	¹ H

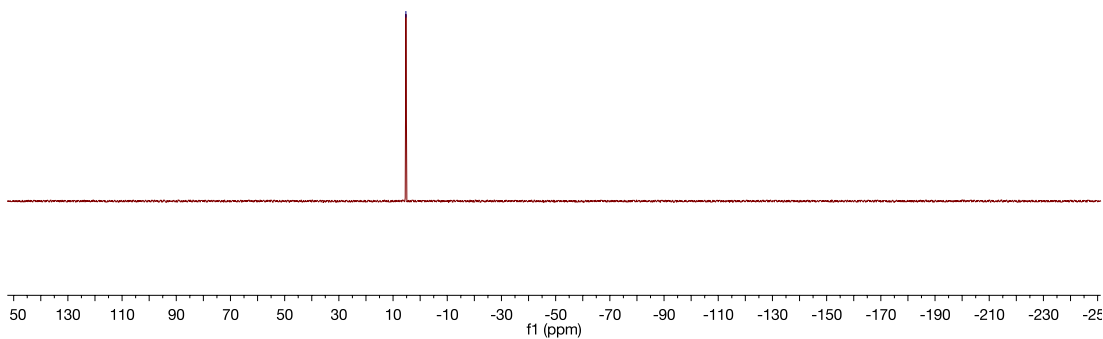
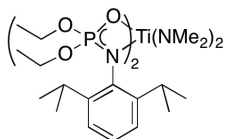


Parameter	Value
Solvent	C6D6
Temperature	298.2
Spectrometer Frequency	100.64
Nucleus	¹³ C

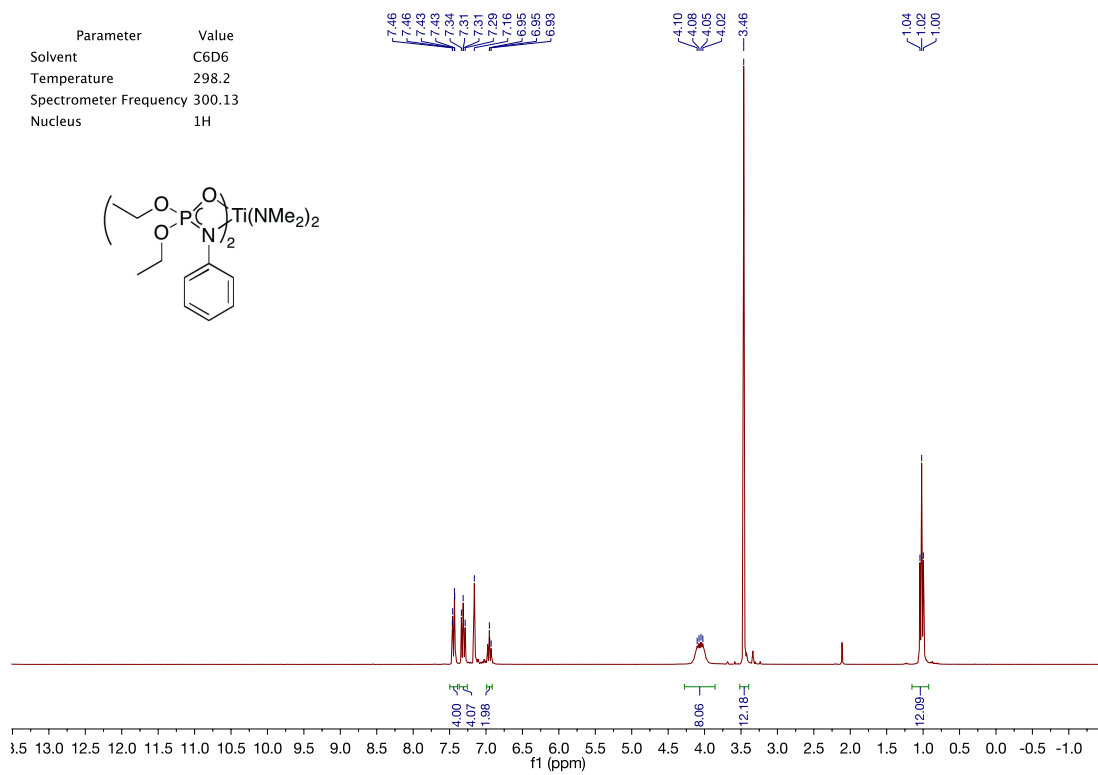
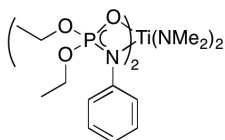


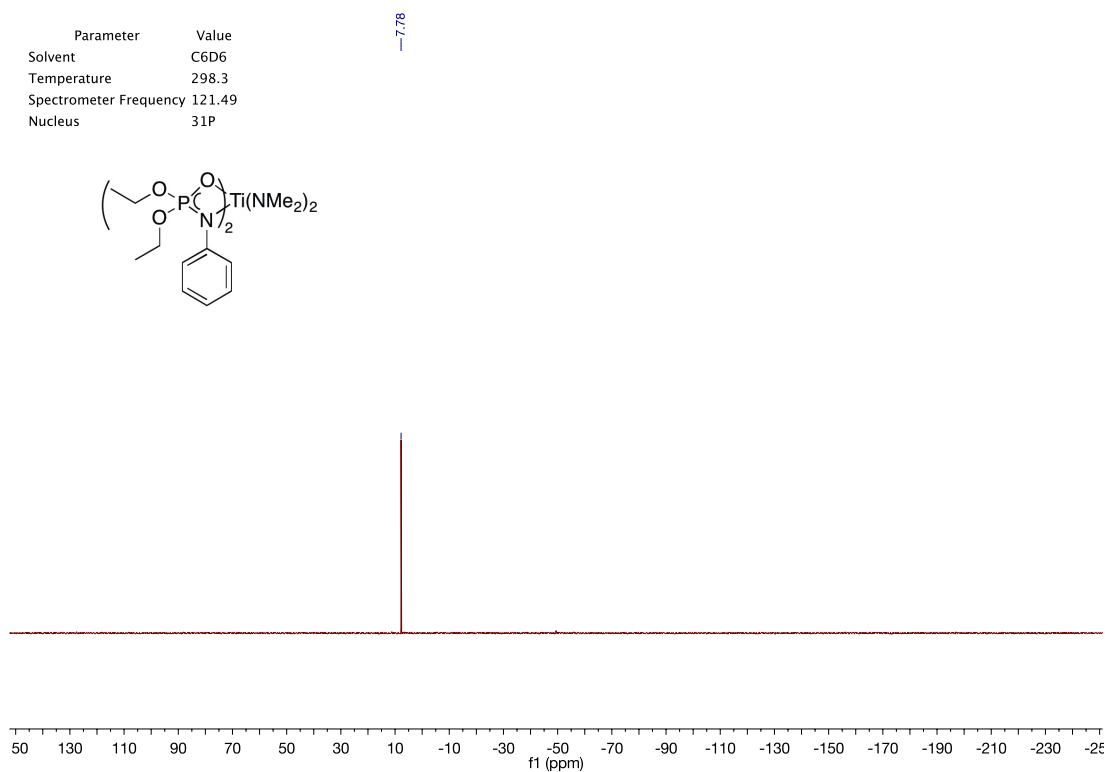
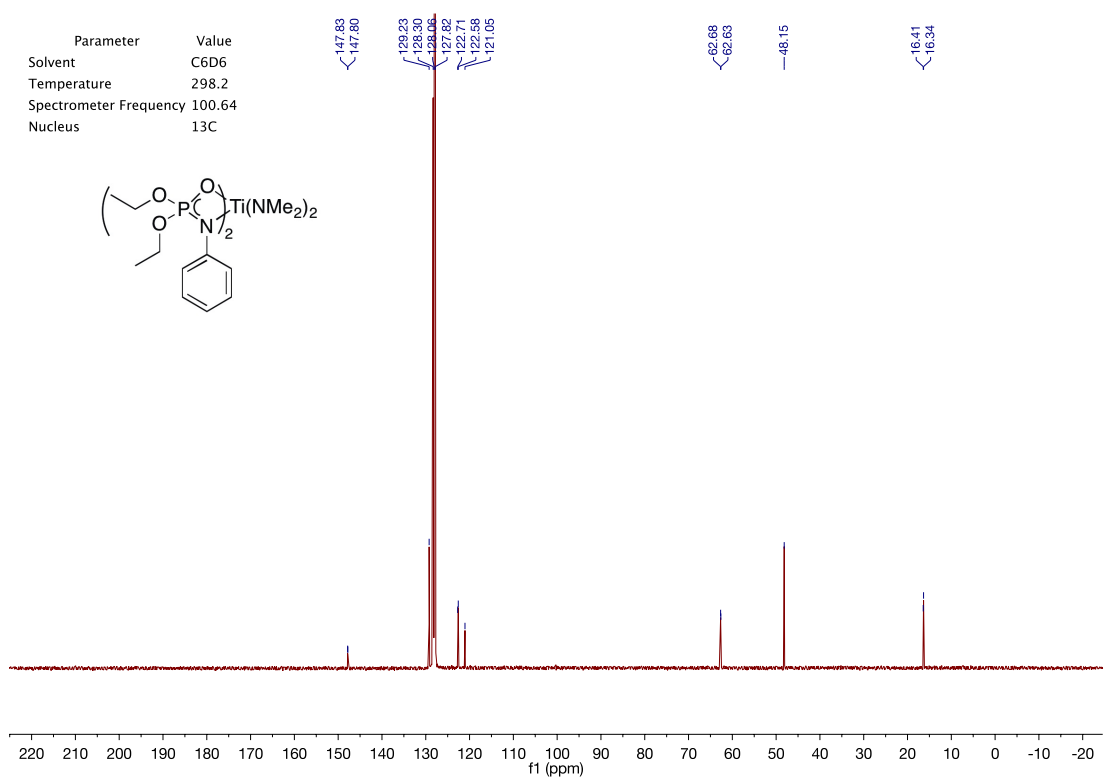
Parameter	Value
Solvent	C6D6
Temperature	298.2
Spectrometer Frequency	121.49
Nucleus	31P

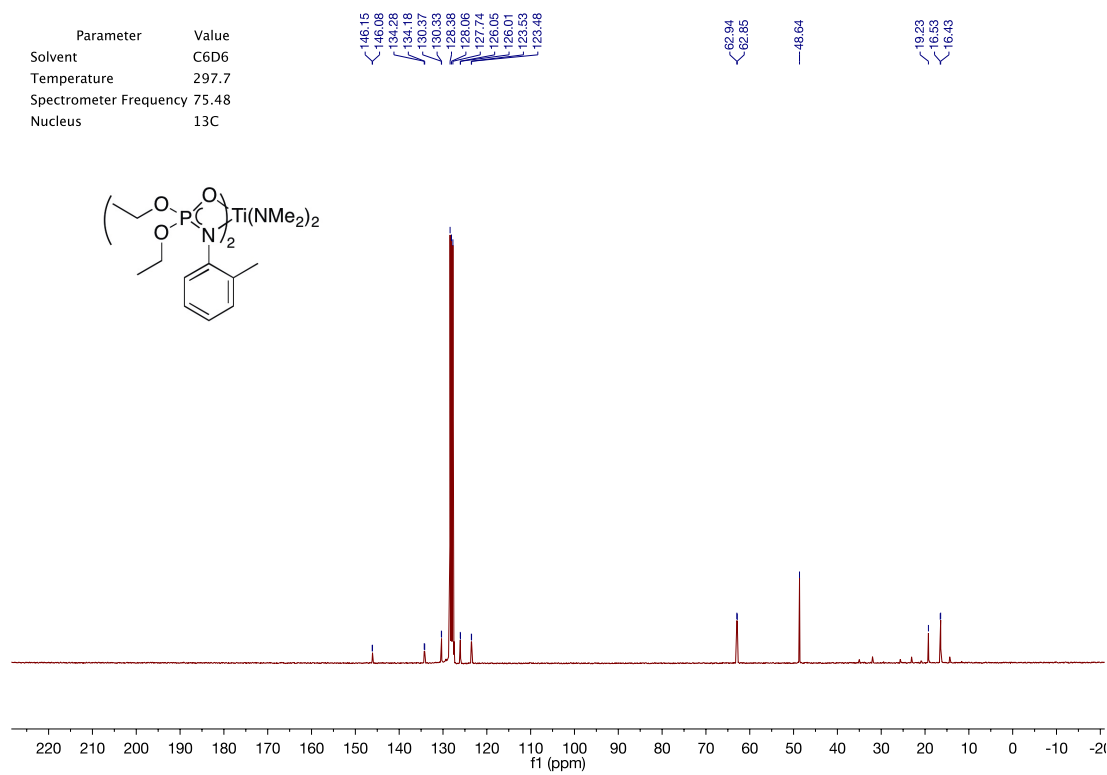
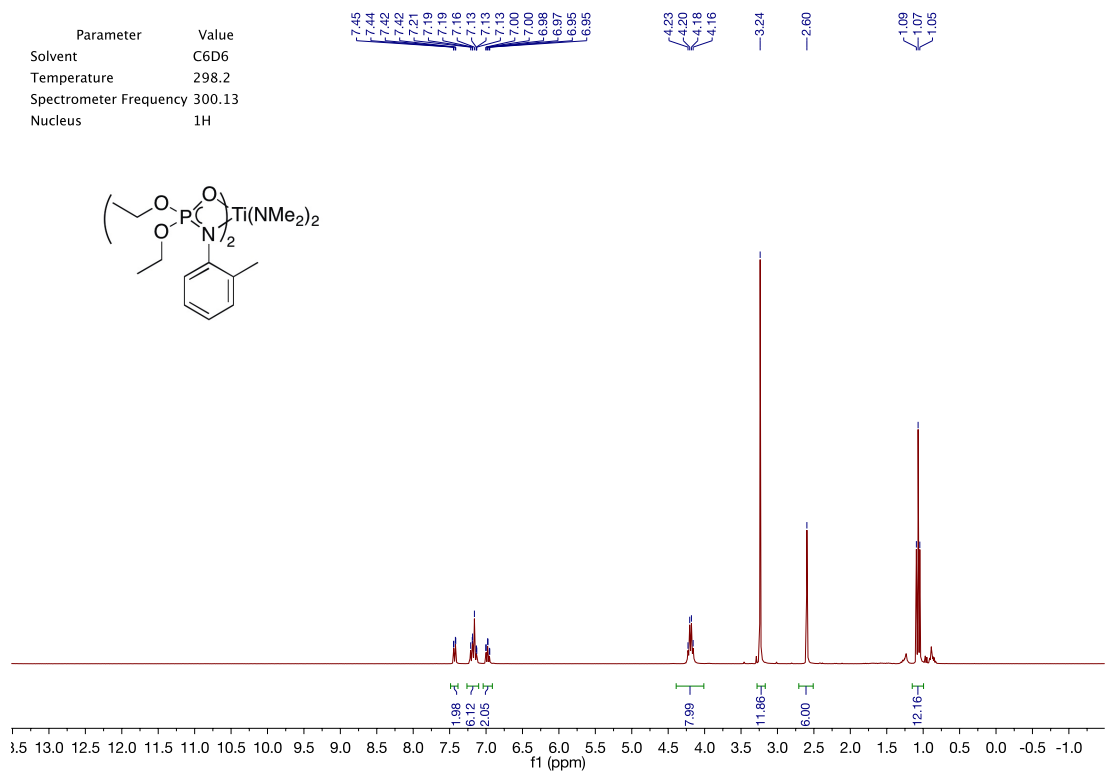
—5.26



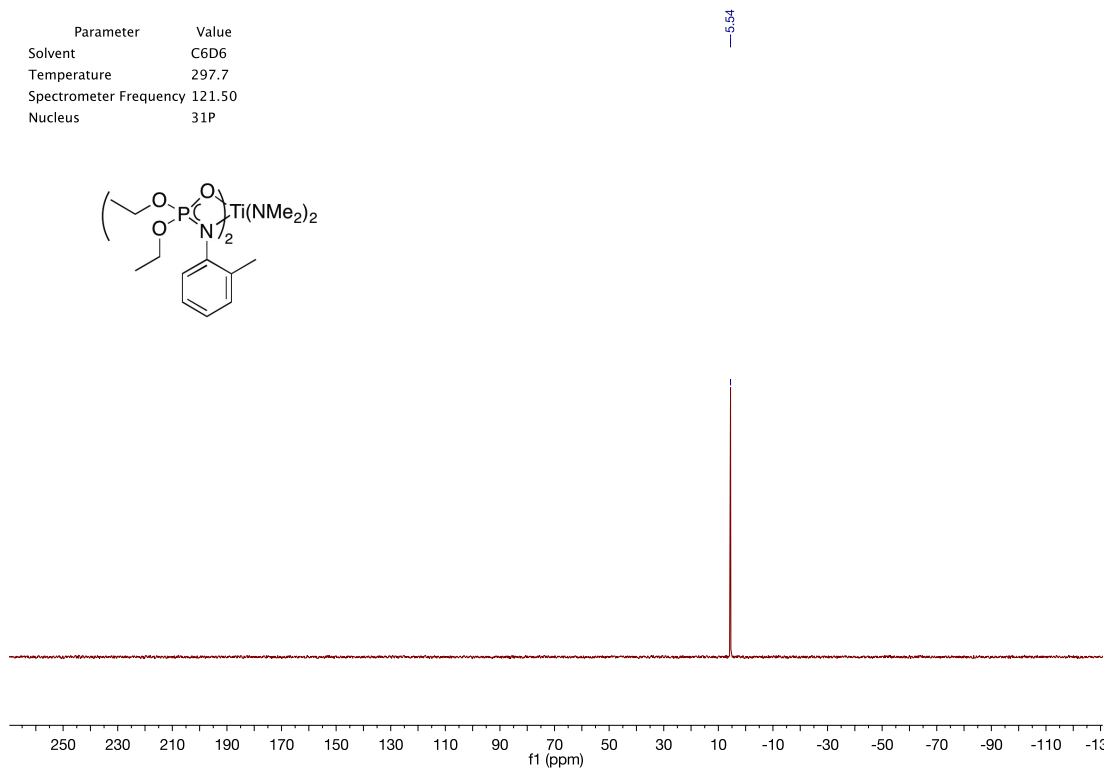
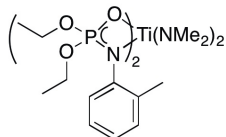
Parameter	Value
Solvent	C6D6
Temperature	298.2
Spectrometer Frequency	300.13
Nucleus	1H



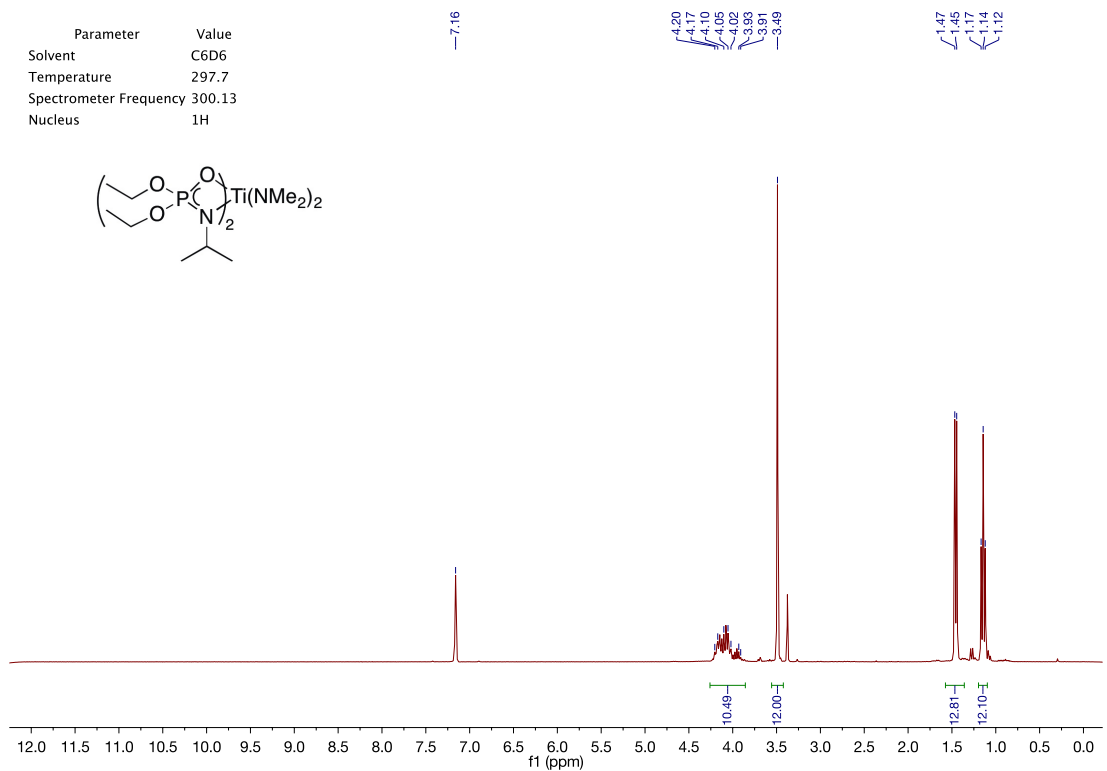
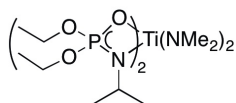


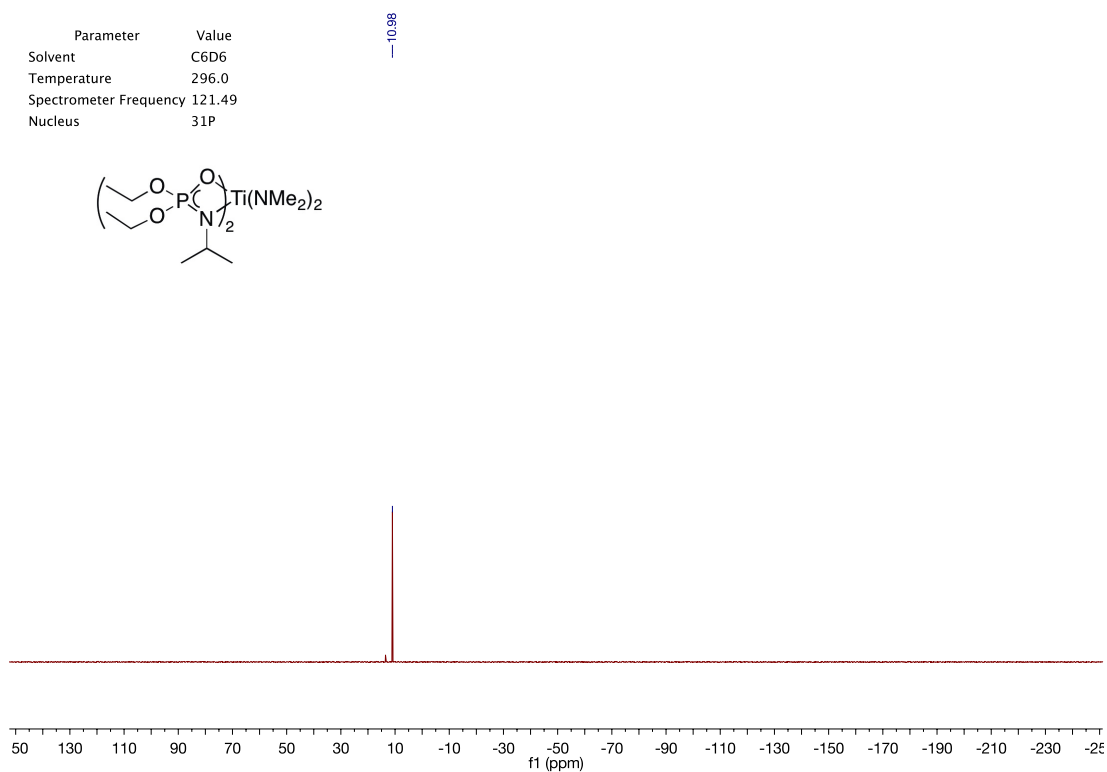
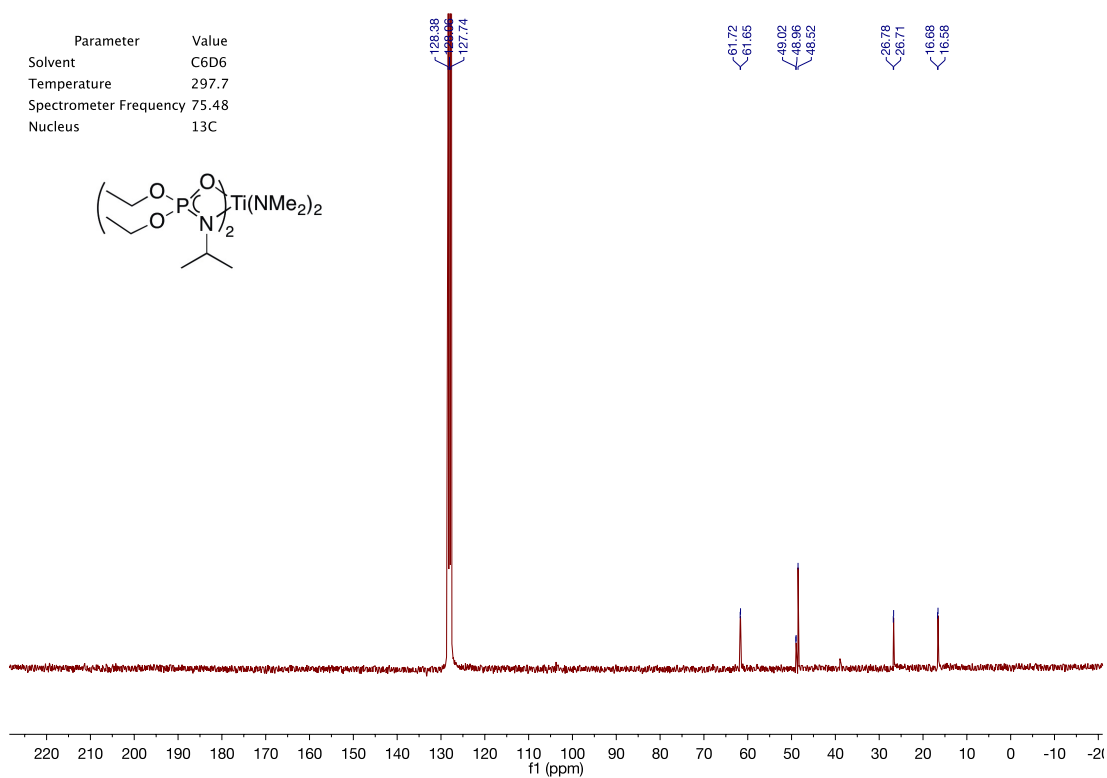


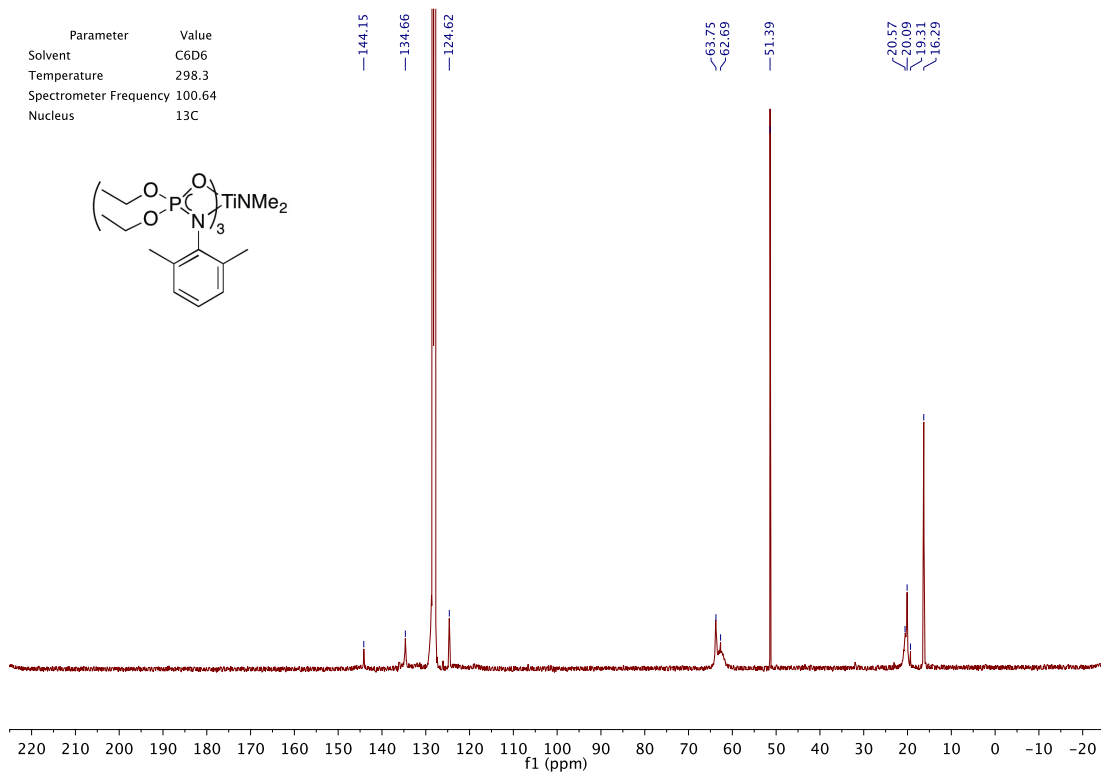
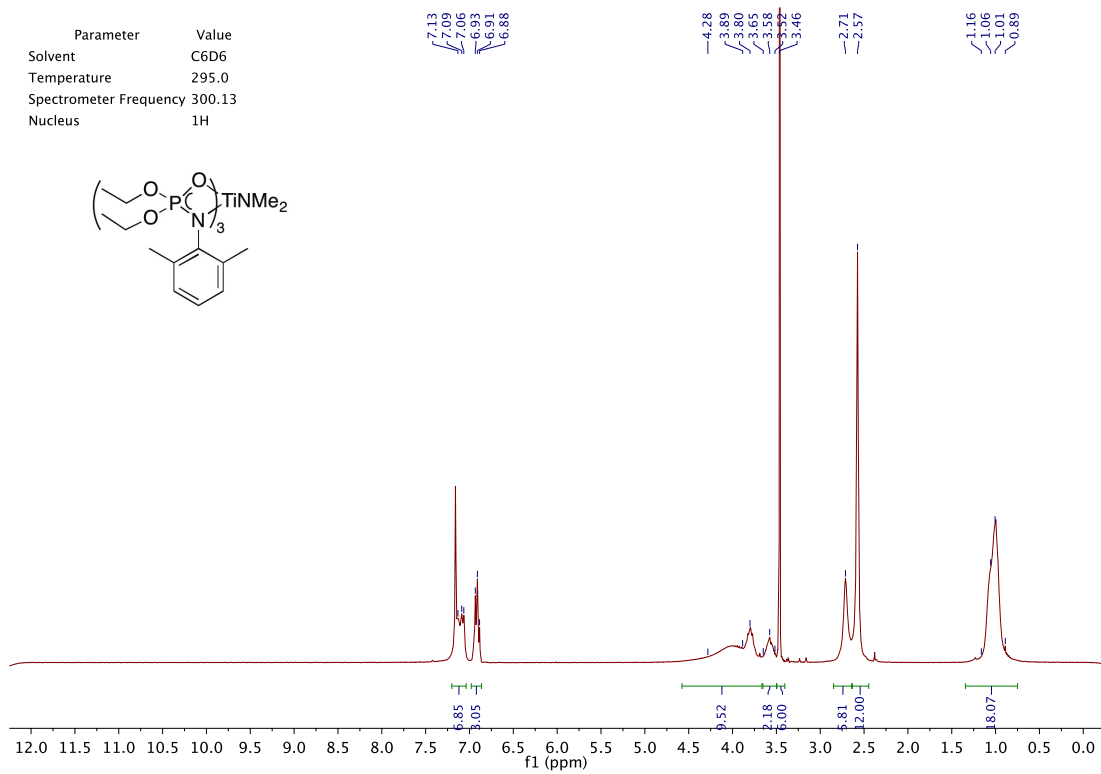
Parameter	Value
Solvent	C6D6
Temperature	297.7
Spectrometer Frequency	121.50
Nucleus	31P



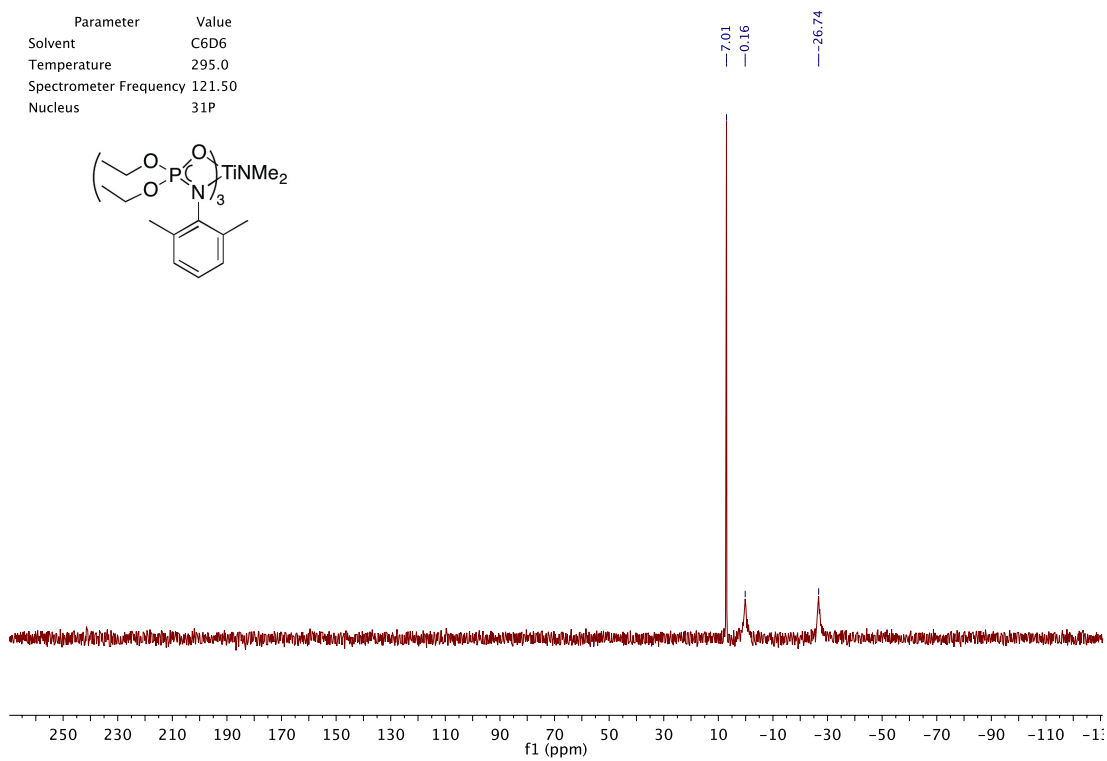
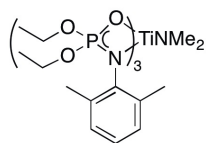
Parameter	Value
Solvent	C6D6
Temperature	297.7
Spectrometer Frequency	300.13
Nucleus	1H



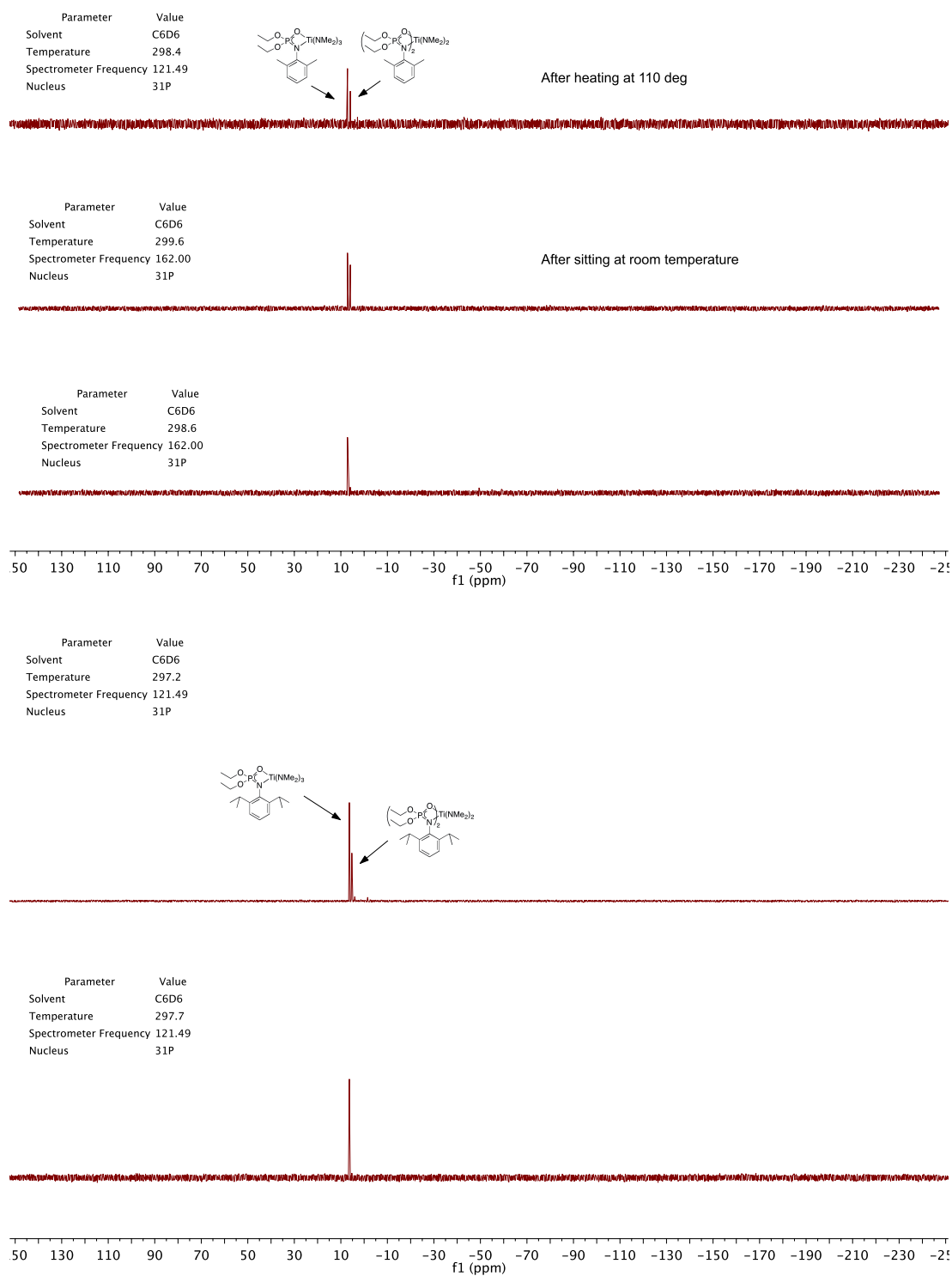




Parameter	Value
Solvent	C6D6
Temperature	295.0
Spectrometer Frequency	121.50
Nucleus	31P



Spectra highlighting ligand redistribution in monophosphoramidate complexes:



A.2 Additional Information Regarding the Geometry Index Parameter

The geometry index or structure parameter classification system was developed by Addison in 1984 and takes into consideration the greatest valence angles about the metal centre.³⁵² The τ_5 is calculated using Equation 1 shown below.

Equation 1 Formula used in the calculation of τ_5 values

$$\tau = \frac{\beta - \alpha}{60^\circ} \approx -0.01667\alpha + 0.01667\beta$$

The variables β and α are the two greatest valence angles as shown below in Figure 26.

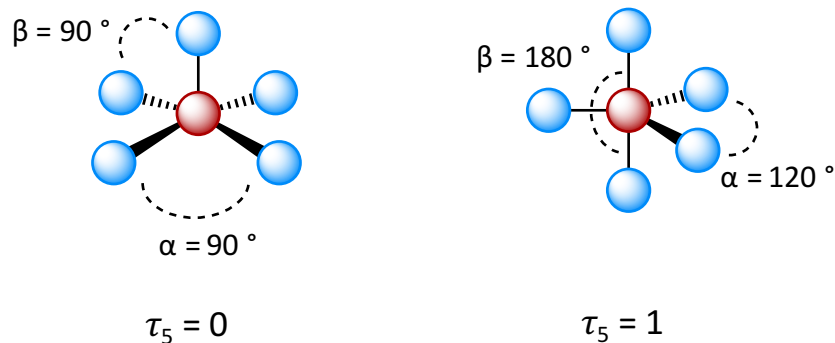


Figure 102 Idealized square pyramidal and trigonal bipyramidal molecular geometries

A.3 Method for Monitoring Hydroaminoalkylation Reactivity

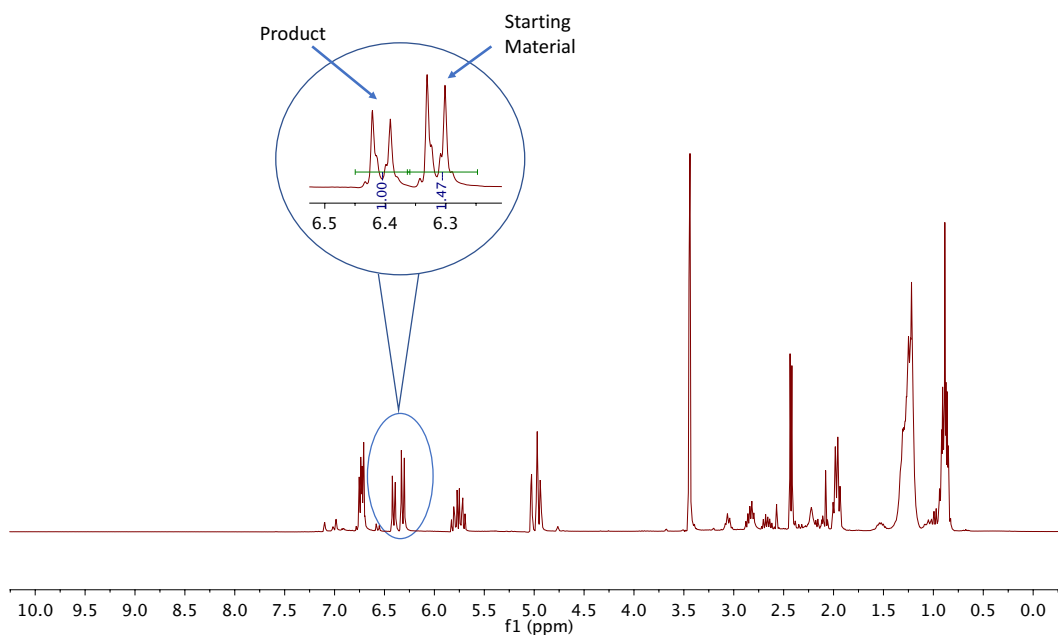


Figure 103 Representative ¹H NMR spectrum (tol-d₈, 300 MHz, 298 K) for monitoring hydroaminoalkylation reactions between 1-octene and 4-methoxy-*N*-methyl aniline, and determining yield by ¹H NMR spectroscopy.

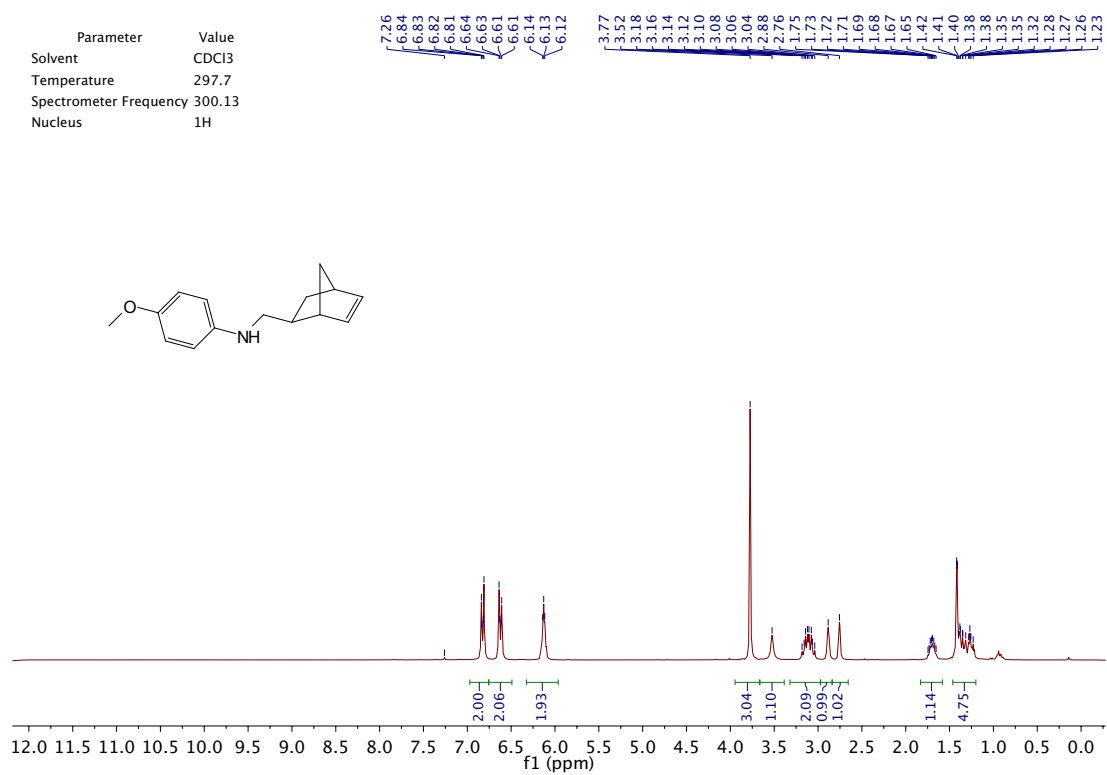
This reaction went to 41% yield using precatalyst 18

$$\text{Yield} = \frac{\text{integration of product signal}}{\text{integration of product} + \text{starting material signal}} \times 100\%$$

Equation 2 Equation for determining percent yield of hydroaminoalkylation reactions

Appendix B Supplementary Information for Chapter 3

B.1 Selected NMR Spectra of Aminonorbornenes and Other Products



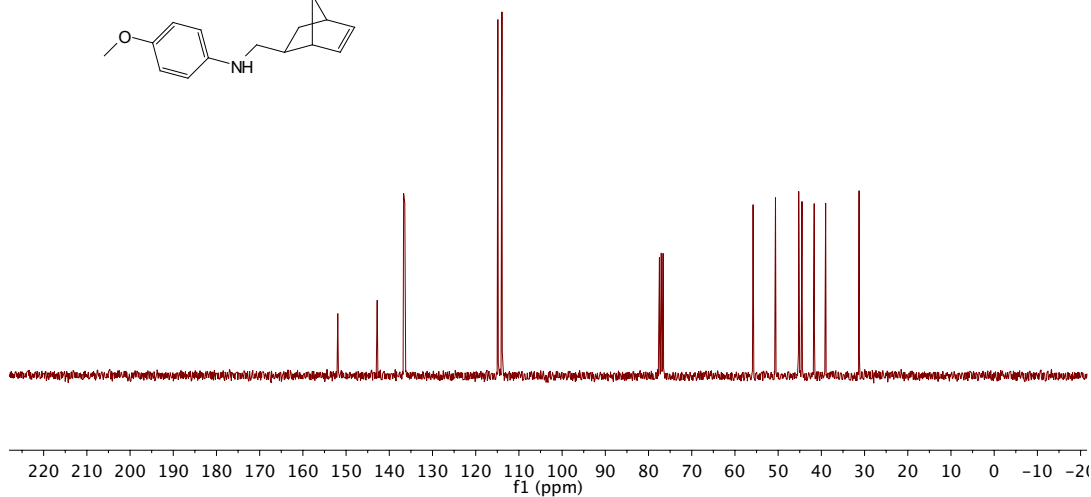
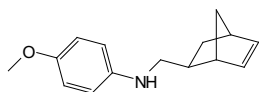
Parameter	Value
Solvent	CDCl ₃
Temperature	297.7
Spectrometer Frequency	75.48
Nucleus	¹³ C

152.03
142.90
136.79
136.52

114.99
114.03

77.58
77.16
76.74

55.91
50.72
45.35
44.59
41.76
39.11
31.38

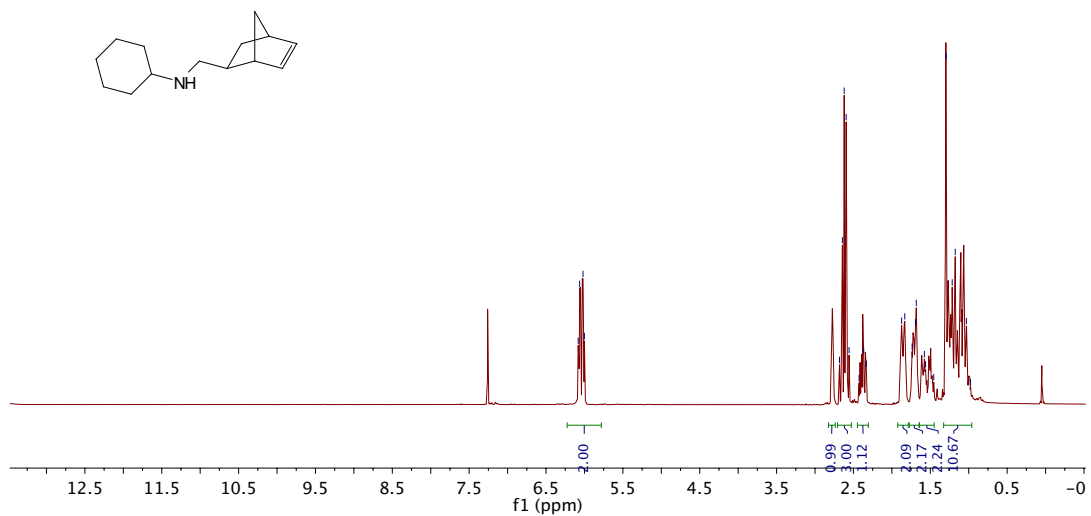
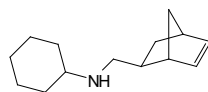


Parameter	Value
Solvent	CDCl ₃
Temperature	298.2
Spectrometer Frequency	300.13
Nucleus	¹ H

6.08
6.06
6.02
6.00

2.68
2.64
2.62
2.59
2.56
2.43
2.37
2.33

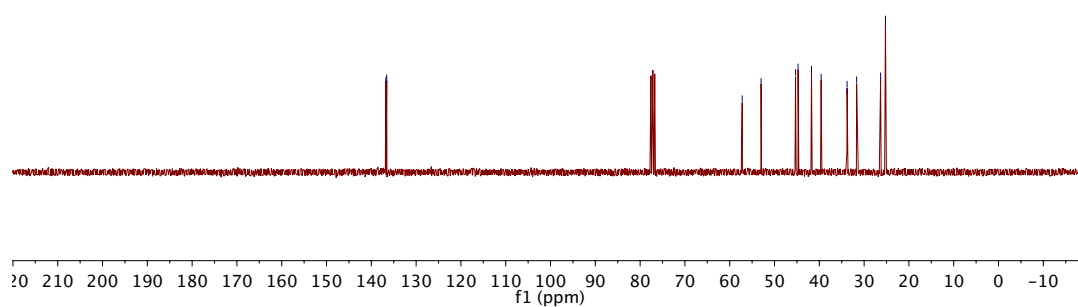
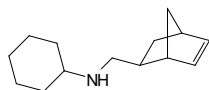
1.87
1.83
1.74
1.69
1.68
1.58
1.56
1.46
1.29
1.21
1.18
1.03



Parameter	Value
Solvent	CDCl ₃
Temperature	298.3
Spectrometer Frequency	75.48
Nucleus	¹³ C

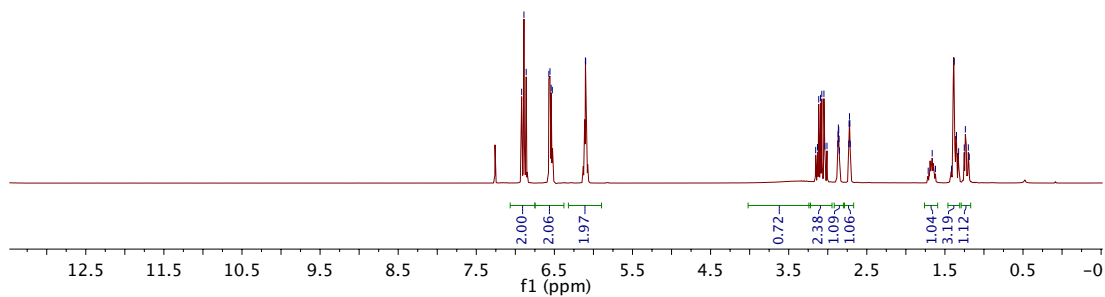
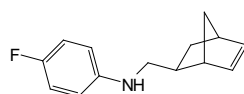
136.74
136.56

57.22
53.00
45.31
44.74
41.75
39.60
33.83
33.80
31.67
26.32
25.24



Parameter	Value
Solvent	CDCl ₃
Temperature	298.3
Spectrometer Frequency	300.13
Nucleus	¹ H

6.92
6.89
6.86
6.57
6.56
6.54
6.53
6.10
6.10
3.15
3.13
3.12
3.09
3.08
3.05
3.04
3.01
2.87
2.86
2.86
2.85
2.85
2.73
2.73
2.72
2.72
2.71
1.71
1.66
1.62
1.41
1.38
1.35
1.32
1.25
1.24
1.20
1.19



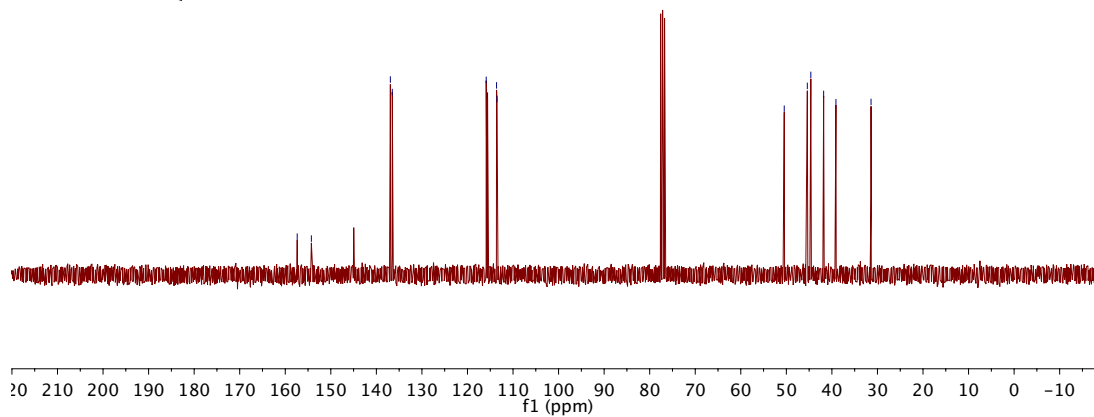
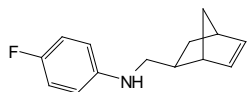
Parameter	Value
Solvent	CDCl ₃
Temperature	298.5
Spectrometer Frequency	75.48
Nucleus	¹³ C

157.38
154.27

136.93
136.51

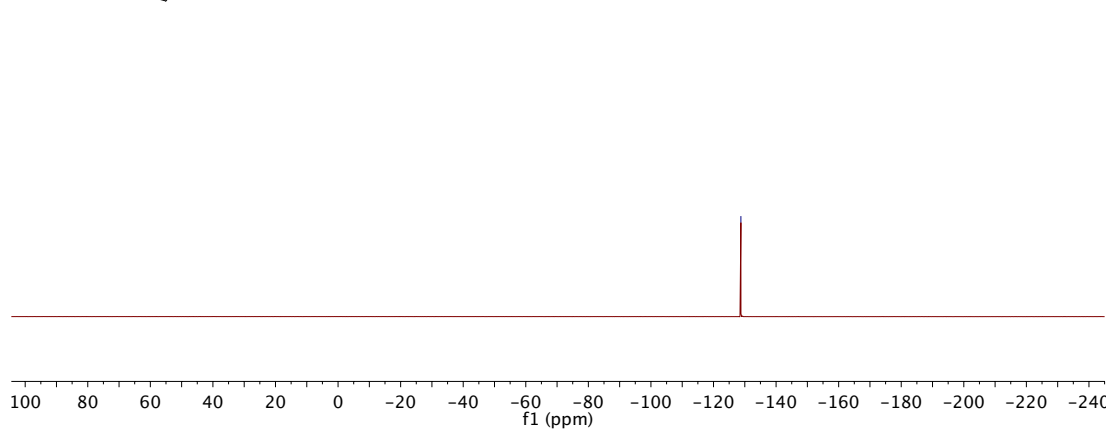
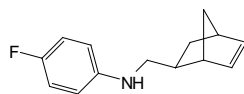
115.89
115.59
113.61
113.51

50.46
45.40
44.63
41.81
39.11
31.41



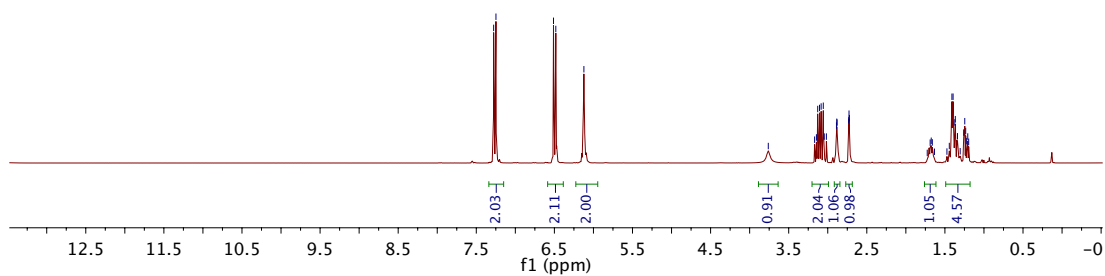
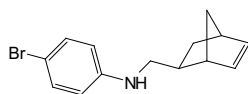
Parameter	Value
Solvent	CDCl ₃
Temperature	298.3
Spectrometer Frequency	282.38
Nucleus	¹⁹ F

-128.75



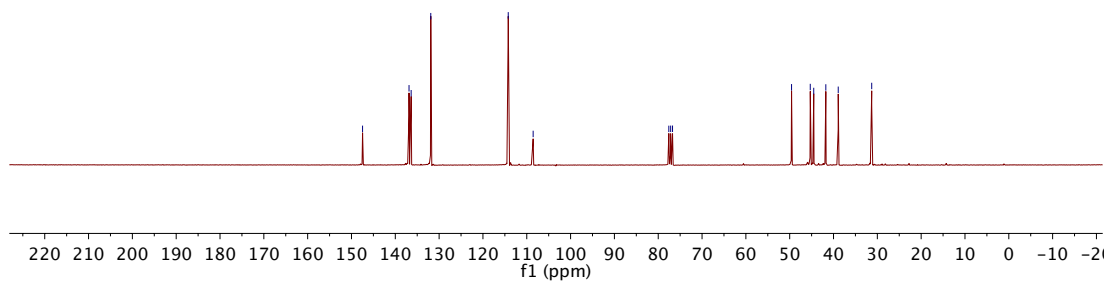
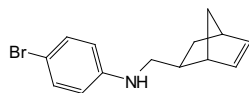
Parameter	Value
Solvent	CDCl ₃
Temperature	298.2
Spectrometer Frequency	300.13
Nucleus	¹ H

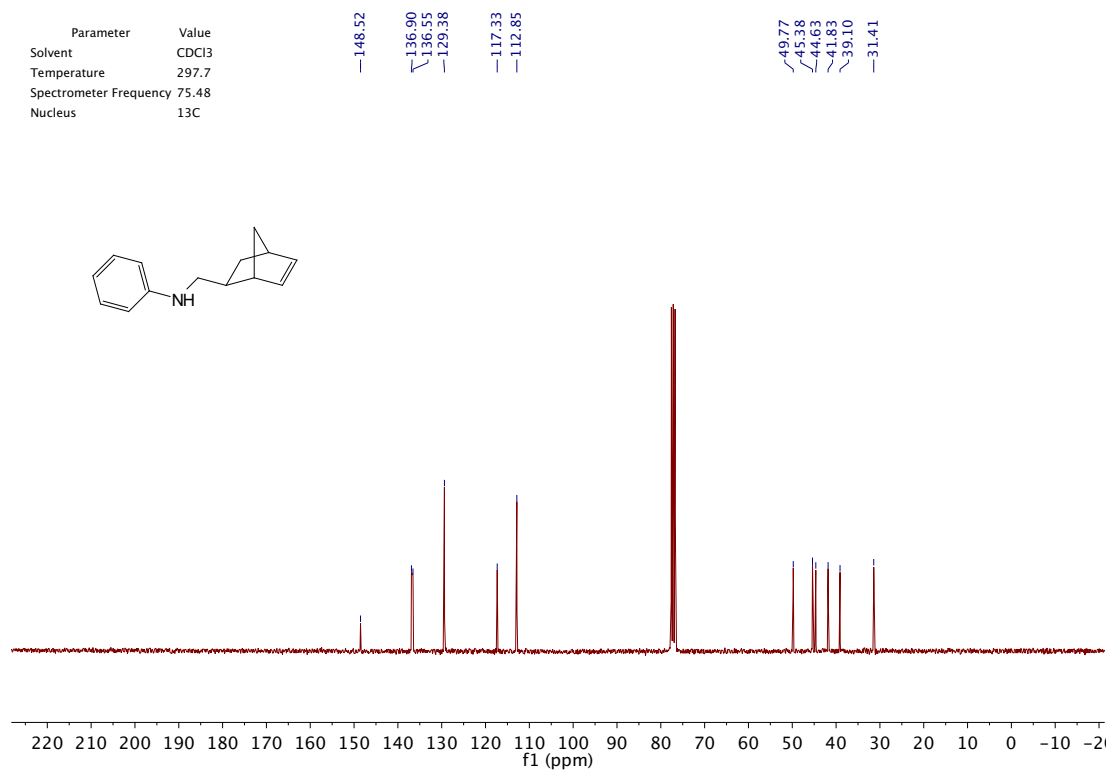
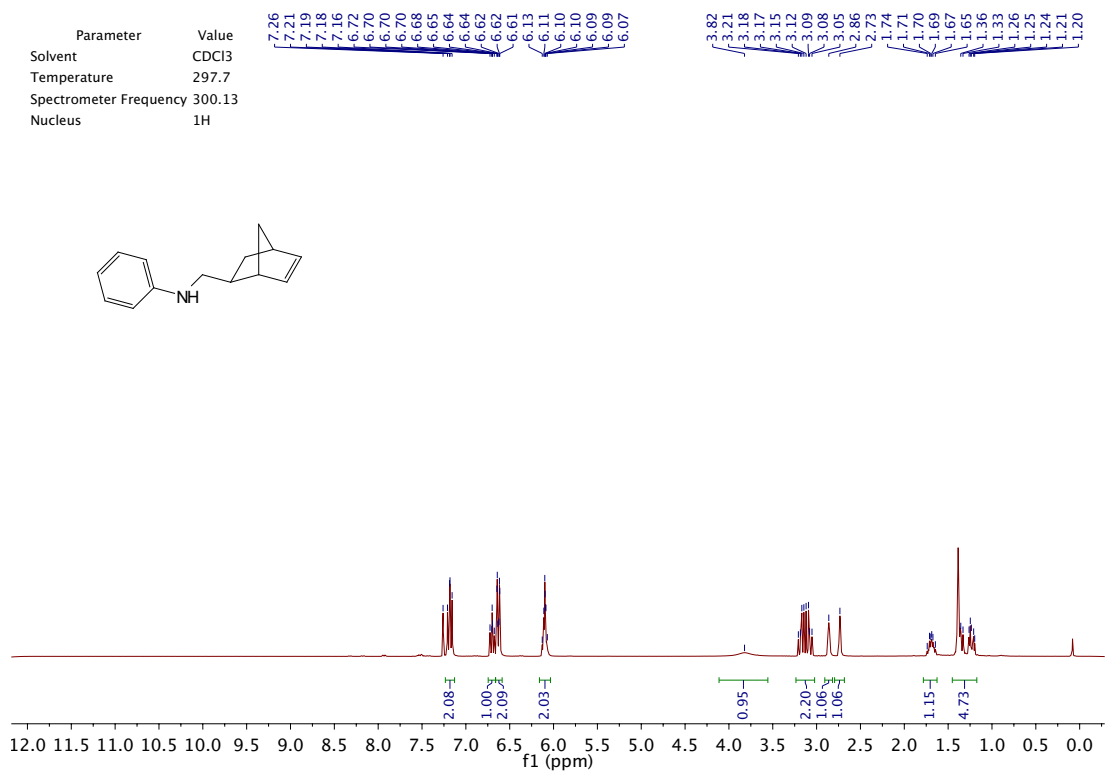
¹H NMR peaks (ppm): 7.28, 7.25, 6.51, 6.48, 6.12, 3.76, 3.17, 3.15, 3.13, 3.11, 3.08, 3.06, 3.04, 3.02, 2.89, 2.88, 2.88, 2.73, 2.72, 1.68, 1.66, 1.41, 1.40, 1.37, 1.34, 1.26, 1.25, 1.23, 1.22, 1.21, 1.20

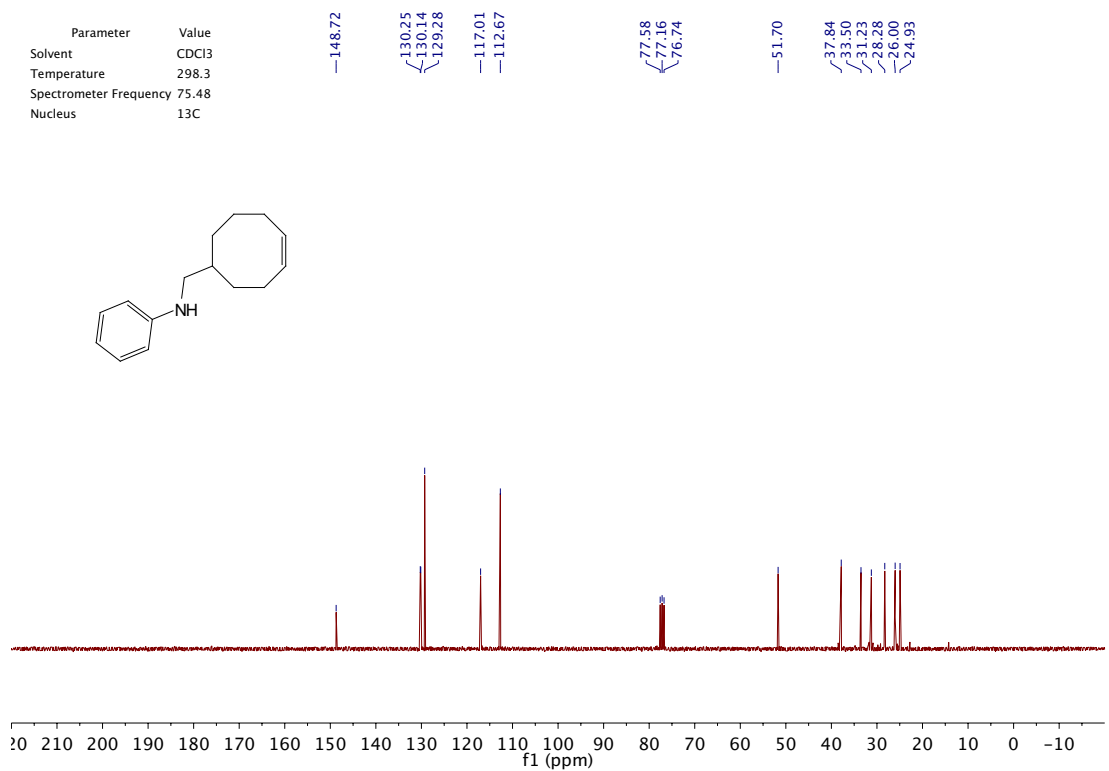
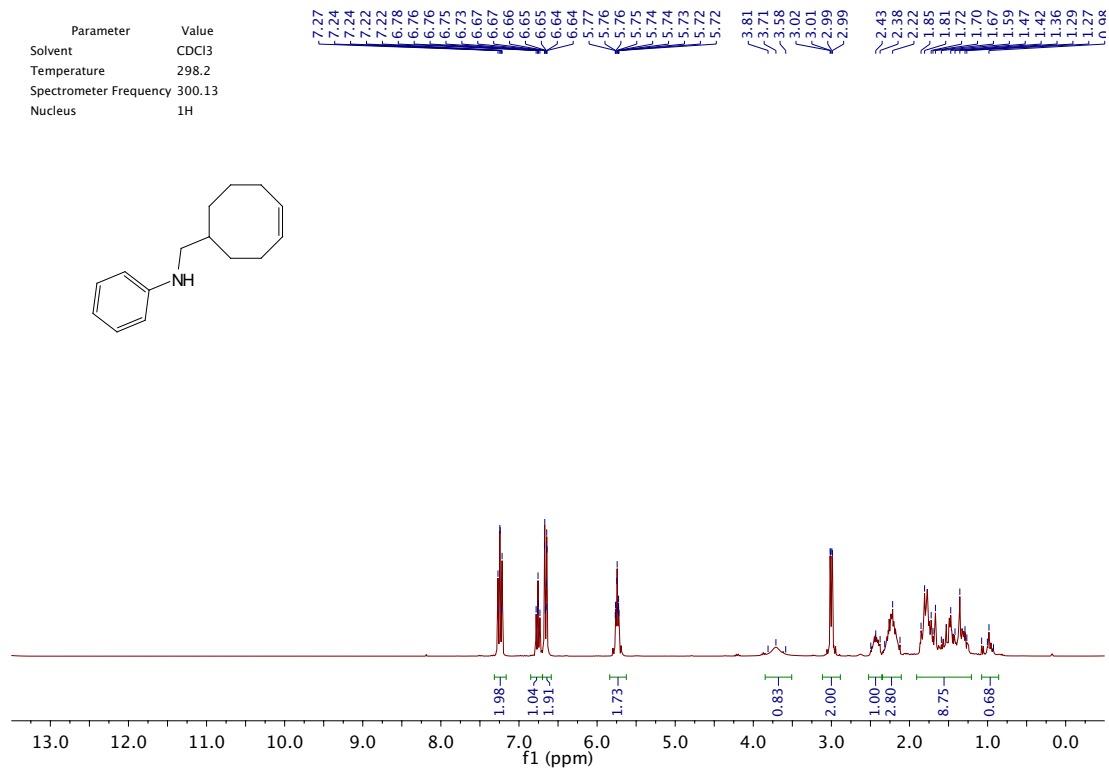


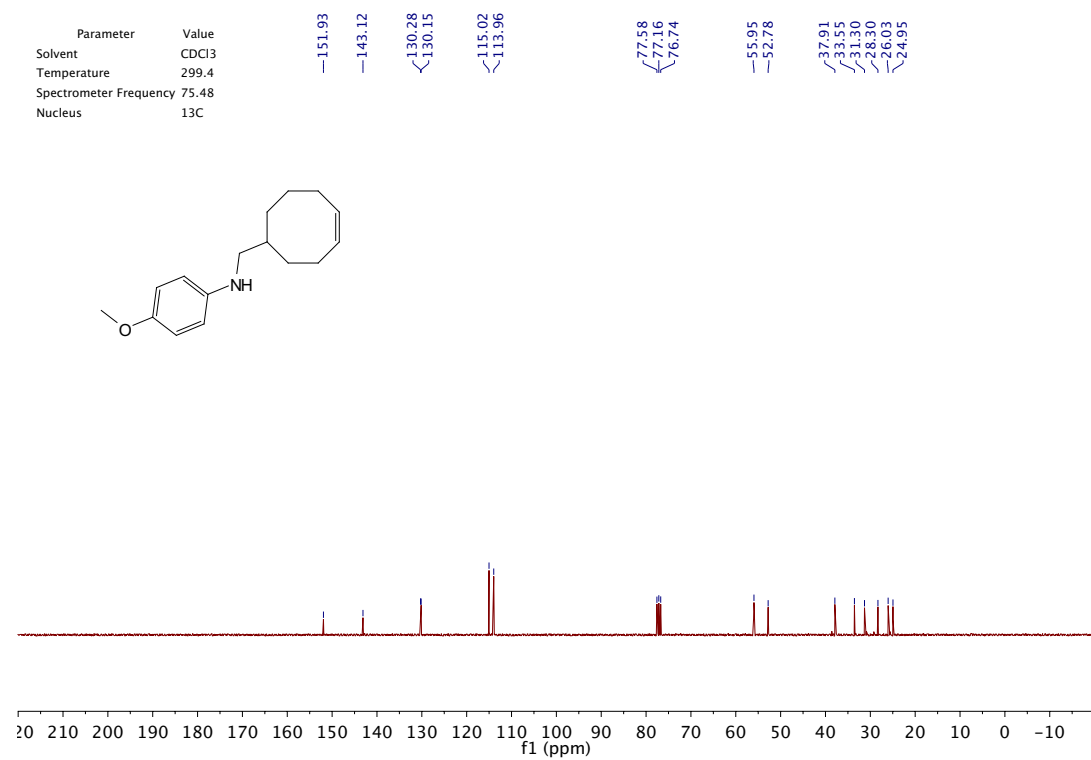
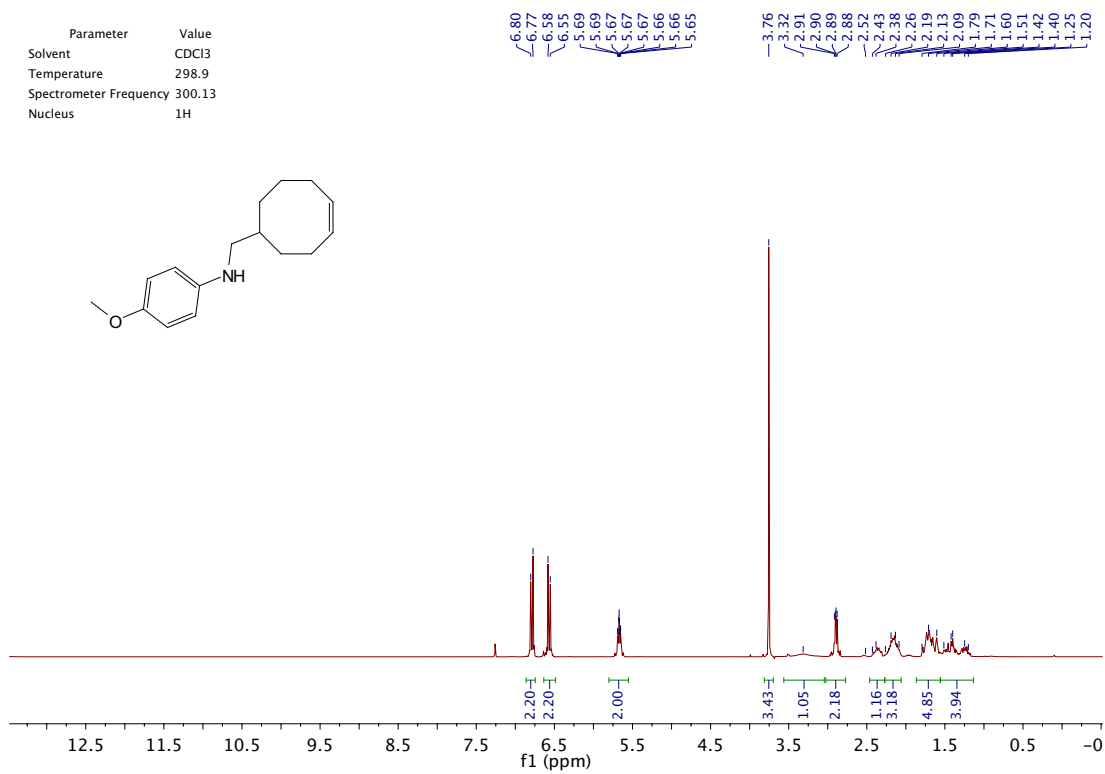
Parameter	Value
Solvent	CDCl ₃
Temperature	297.7
Spectrometer Frequency	75.48
Nucleus	¹³ C

¹³C NMR peaks (ppm): 147.47, 136.87, 136.38, 131.91, 114.23, 108.54, 77.58, 77.16, 76.74, 49.58, 45.31, 44.51, 41.76, 38.92, 31.28

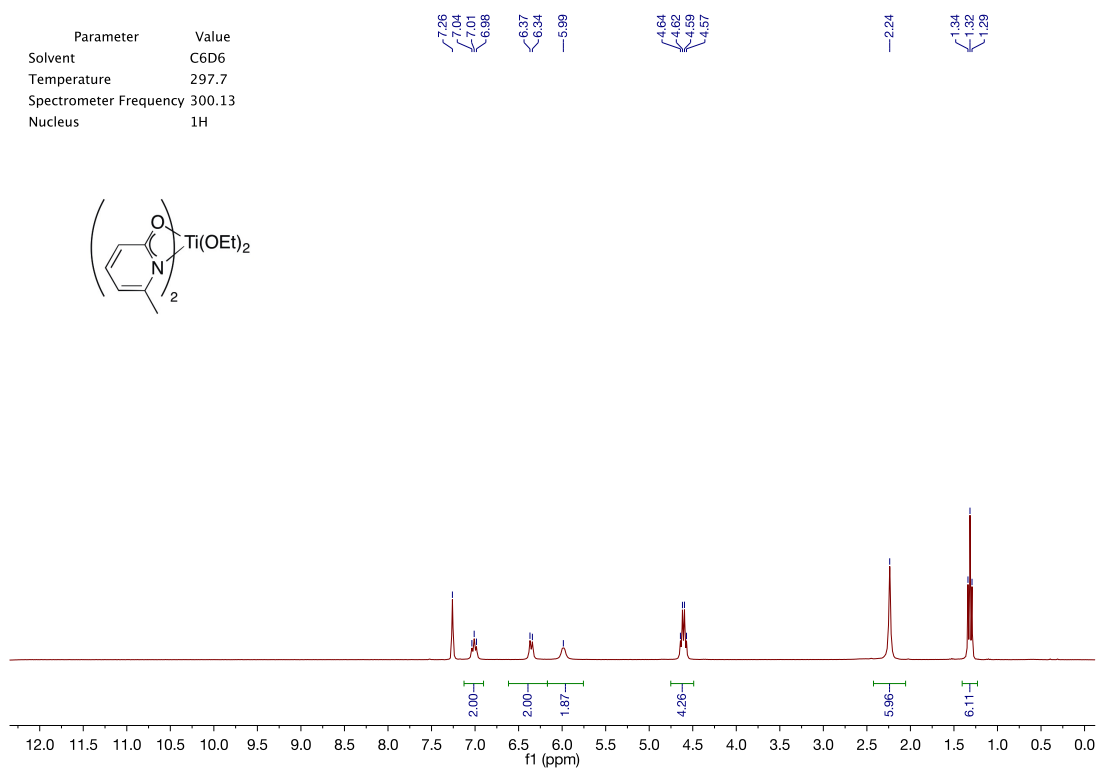
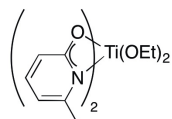




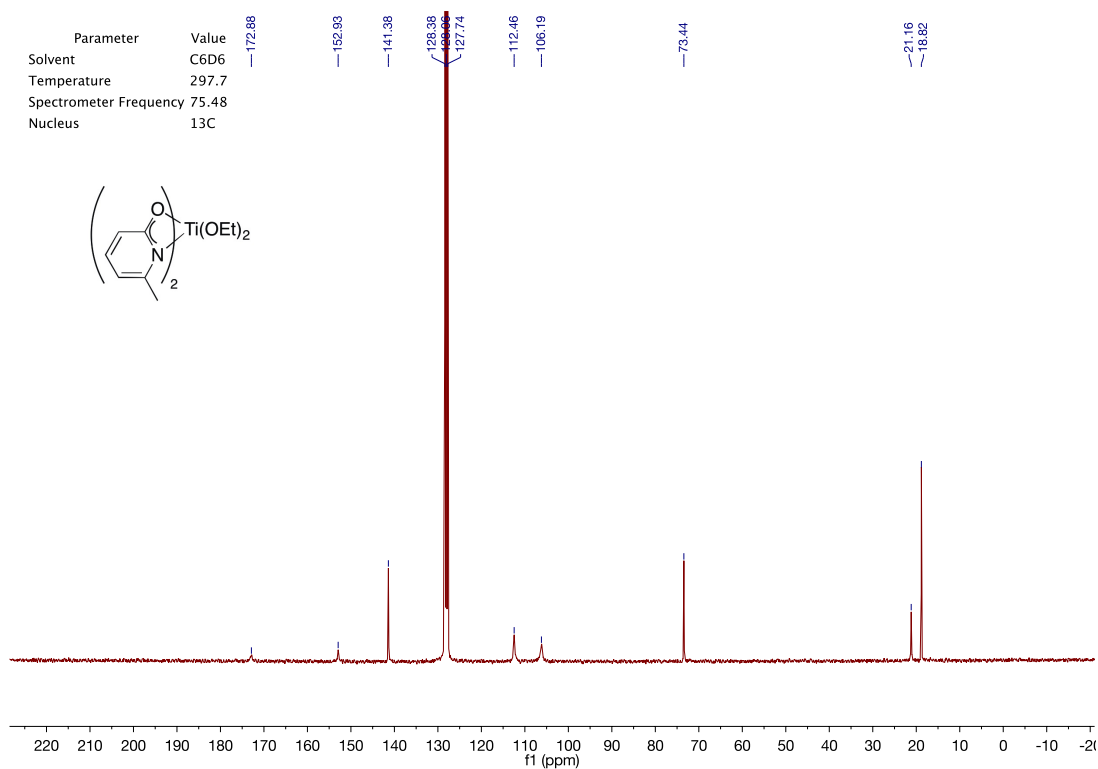
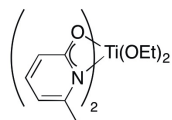




Parameter	Value
Solvent	C6D6
Temperature	297.7
Spectrometer Frequency	300.13
Nucleus	¹ H

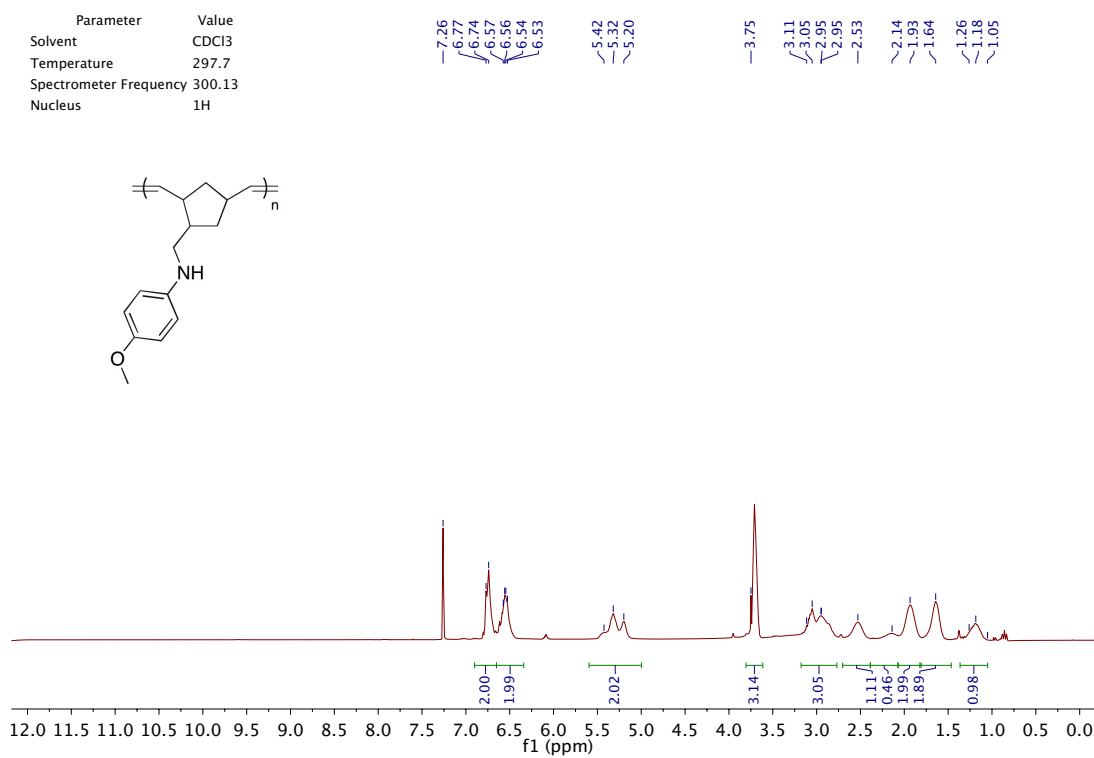


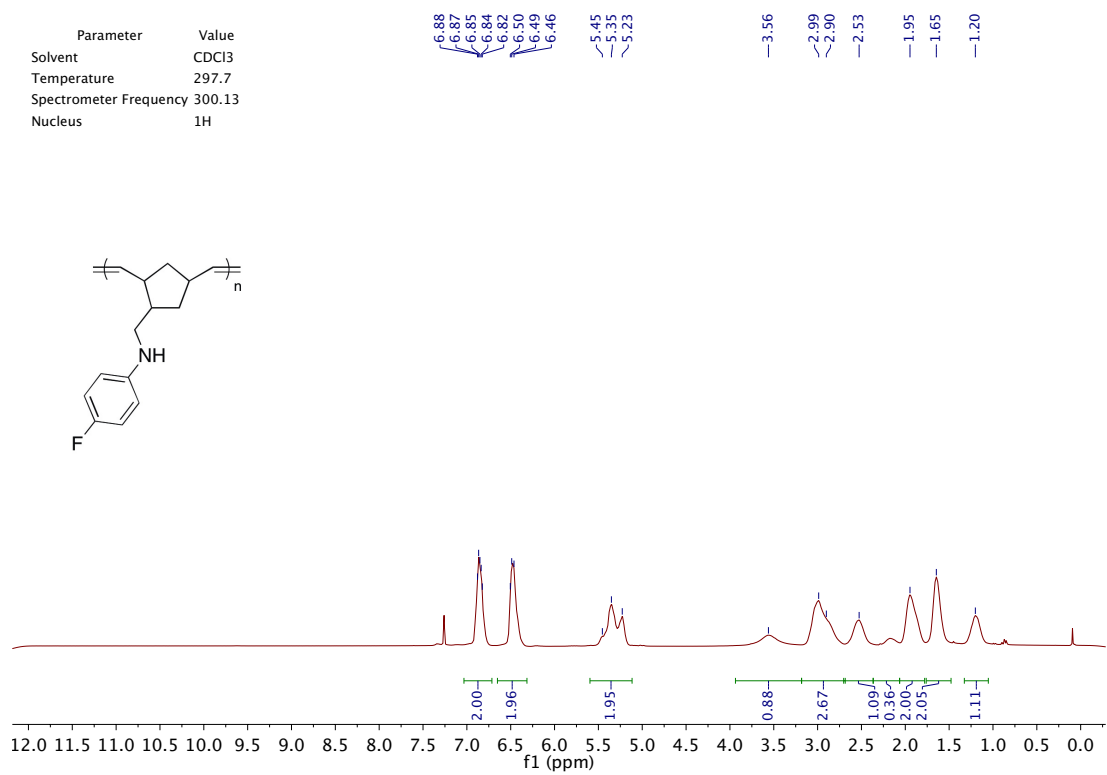
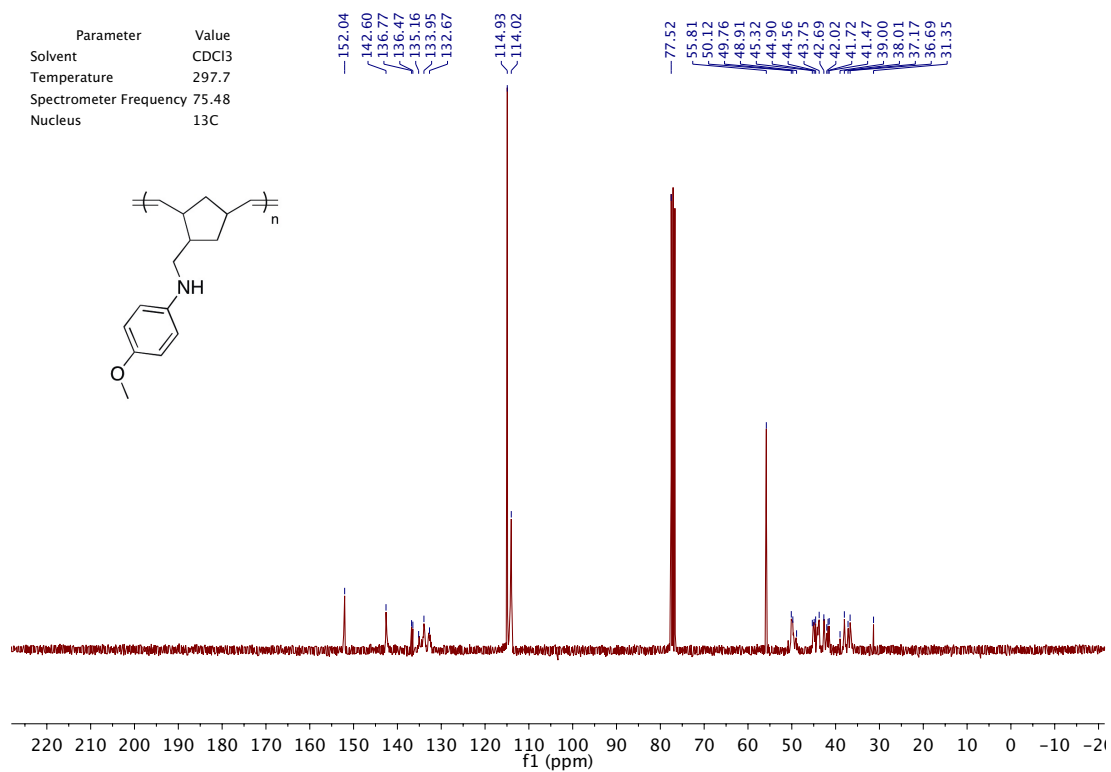
Parameter	Value
Solvent	C6D6
Temperature	297.7
Spectrometer Frequency	75.48
Nucleus	¹³ C

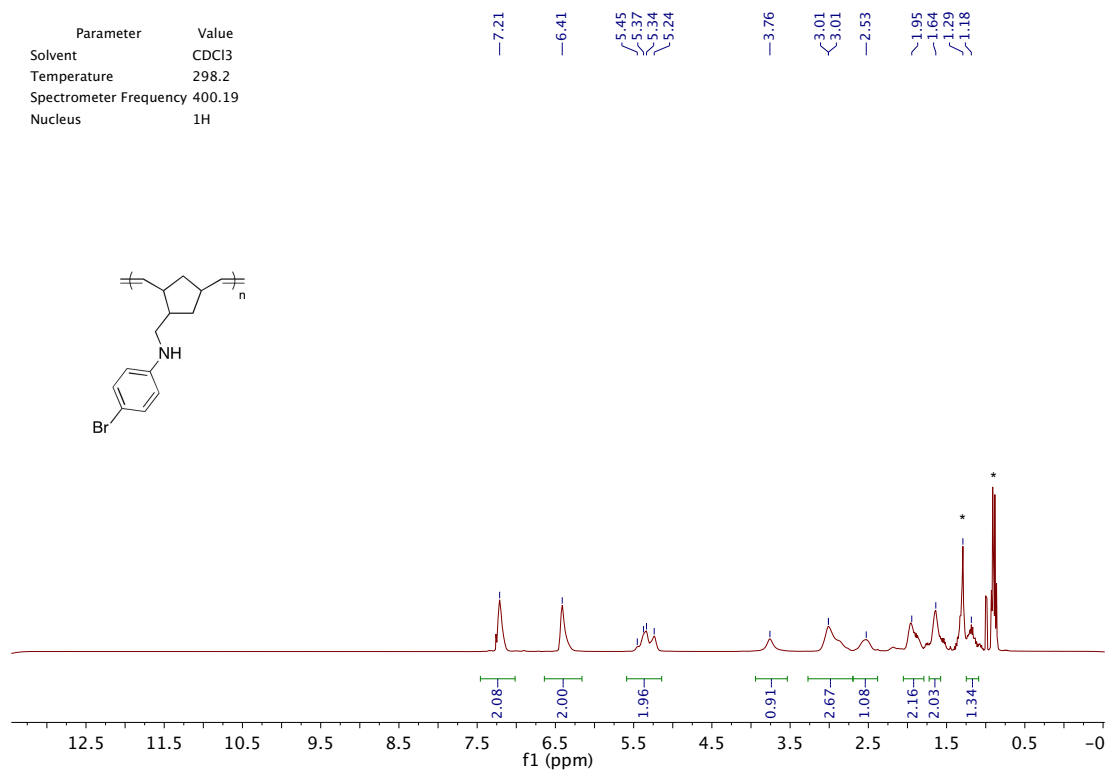
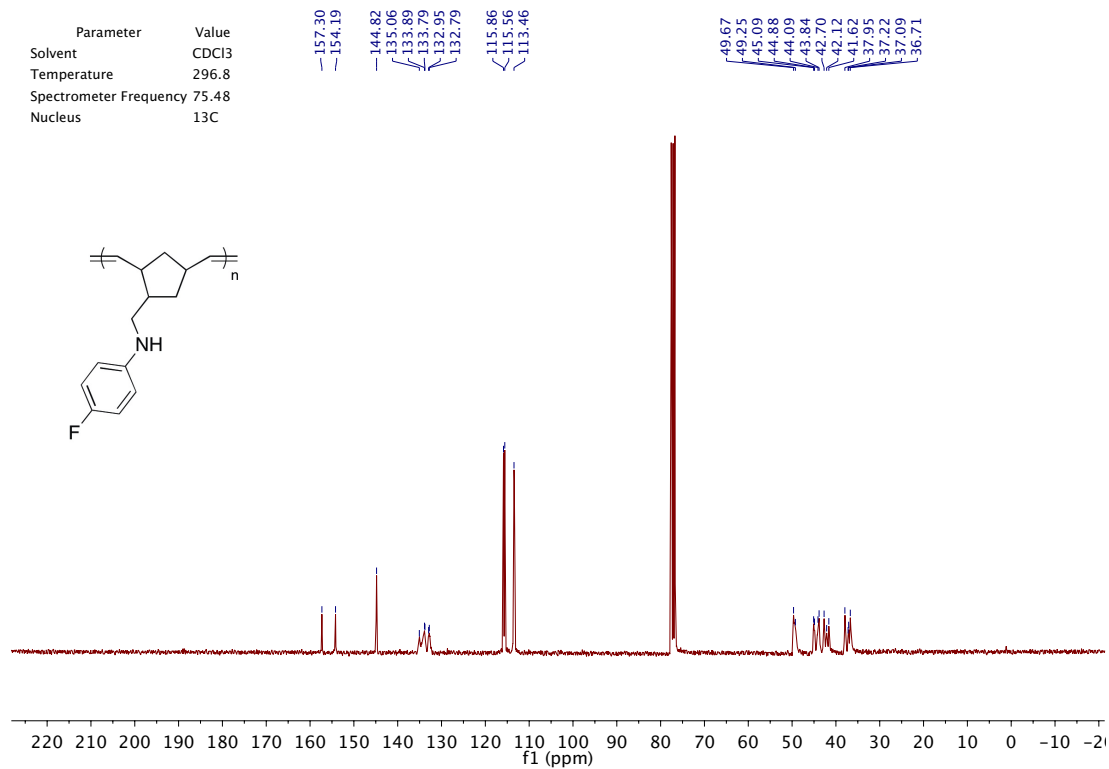


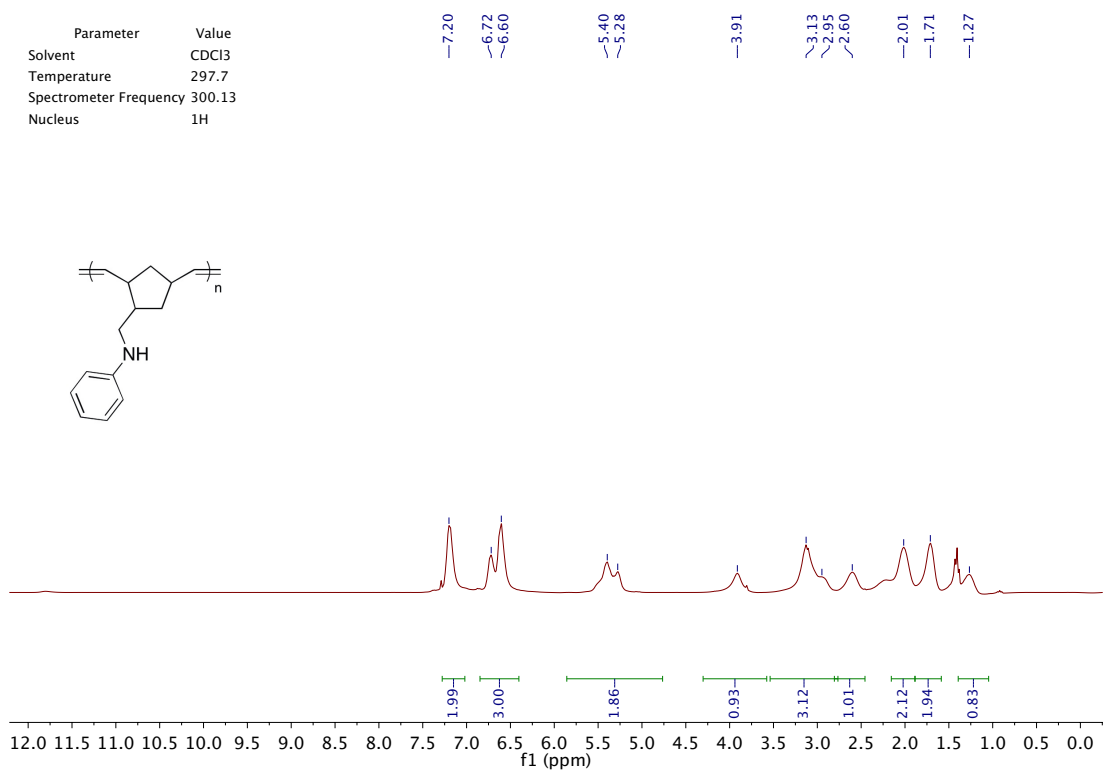
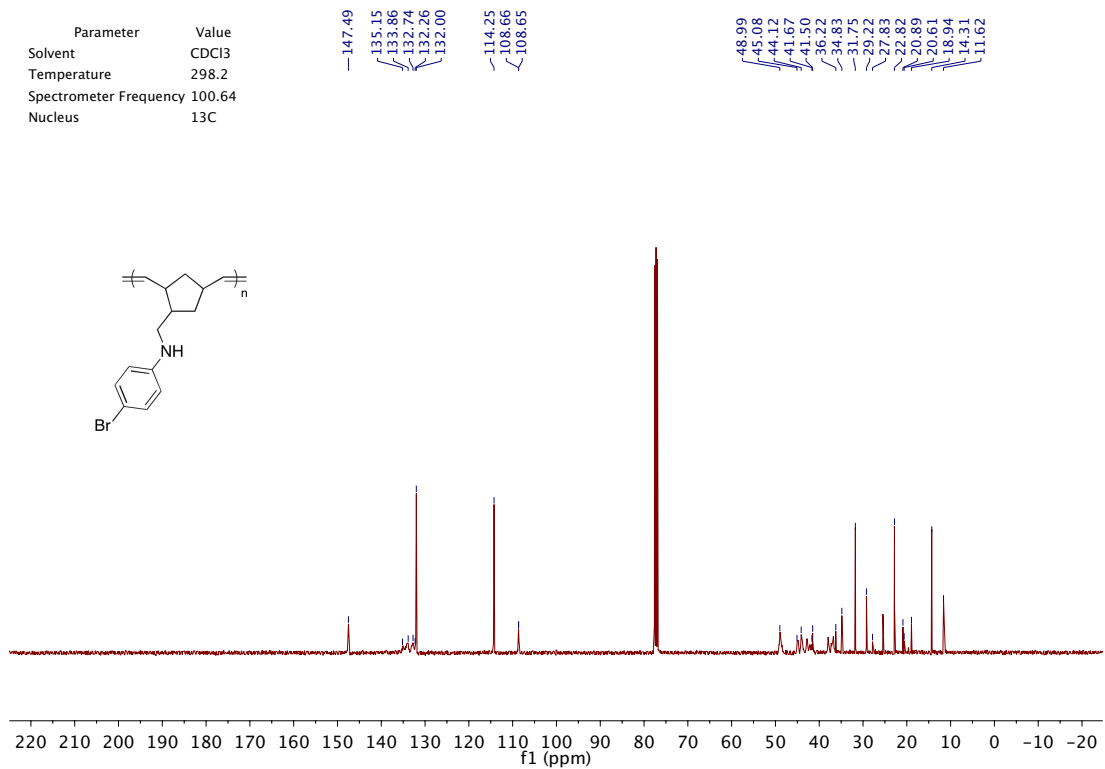
B.2 Selected NMR Spectra of Polymers

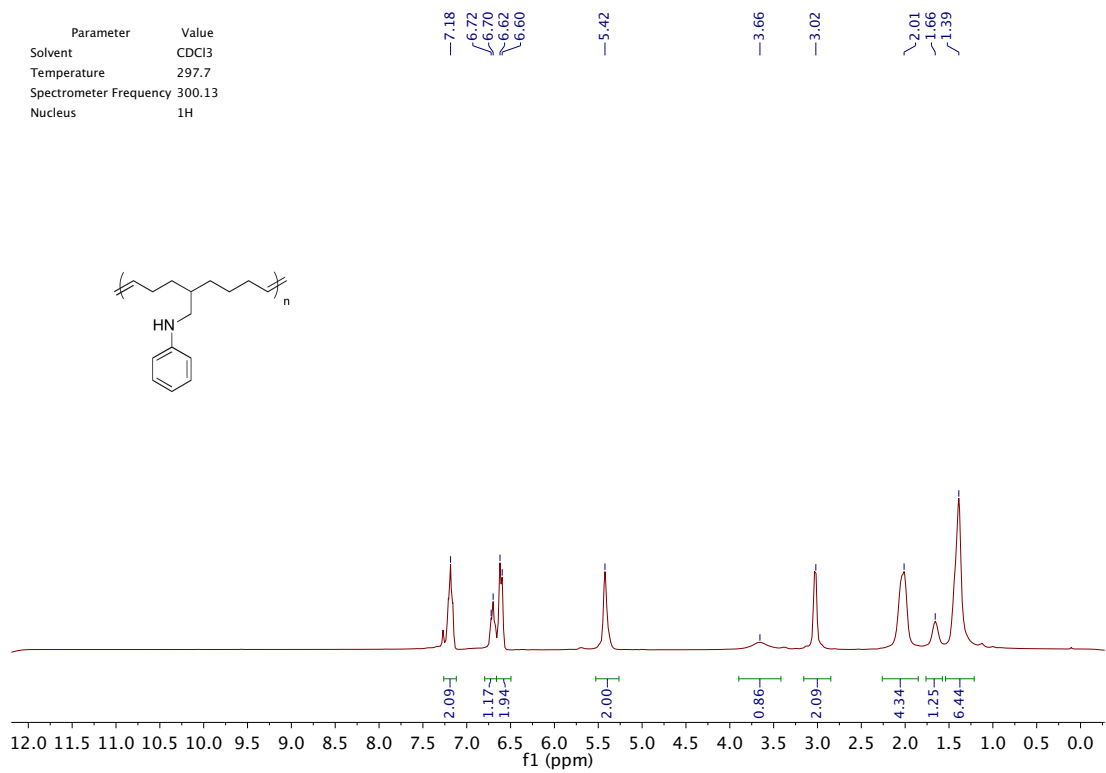
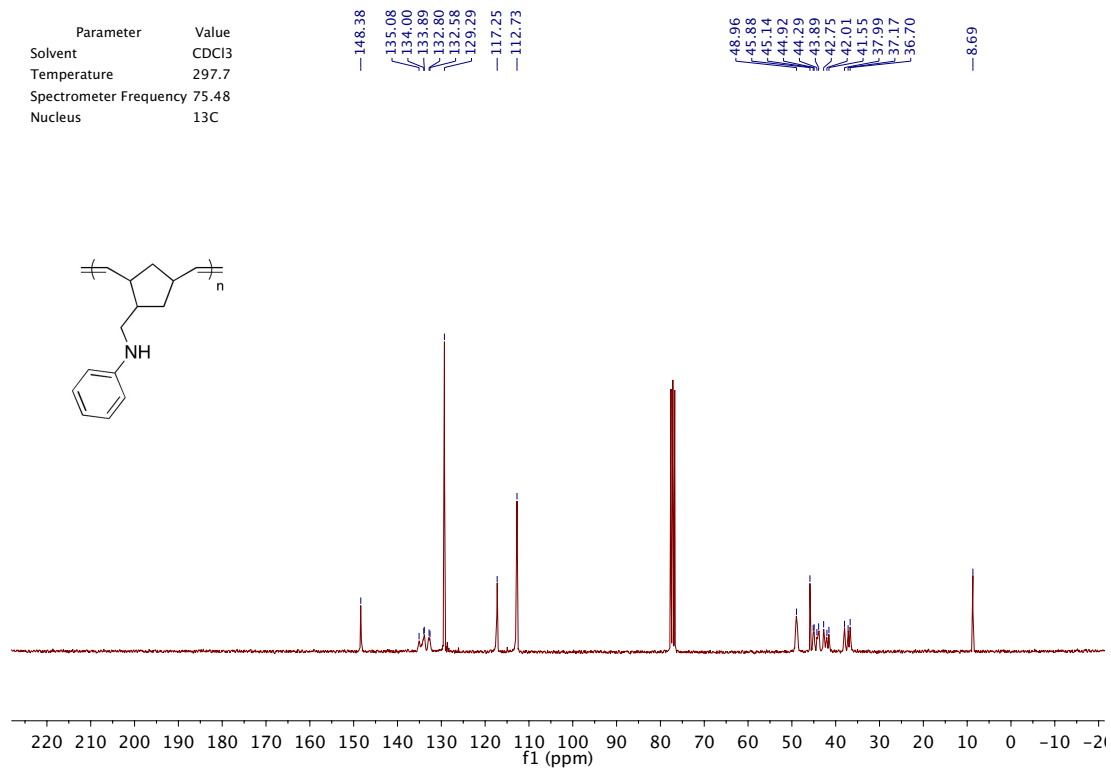
All spectra listed below were synthesized using G2 and M:I = 100.

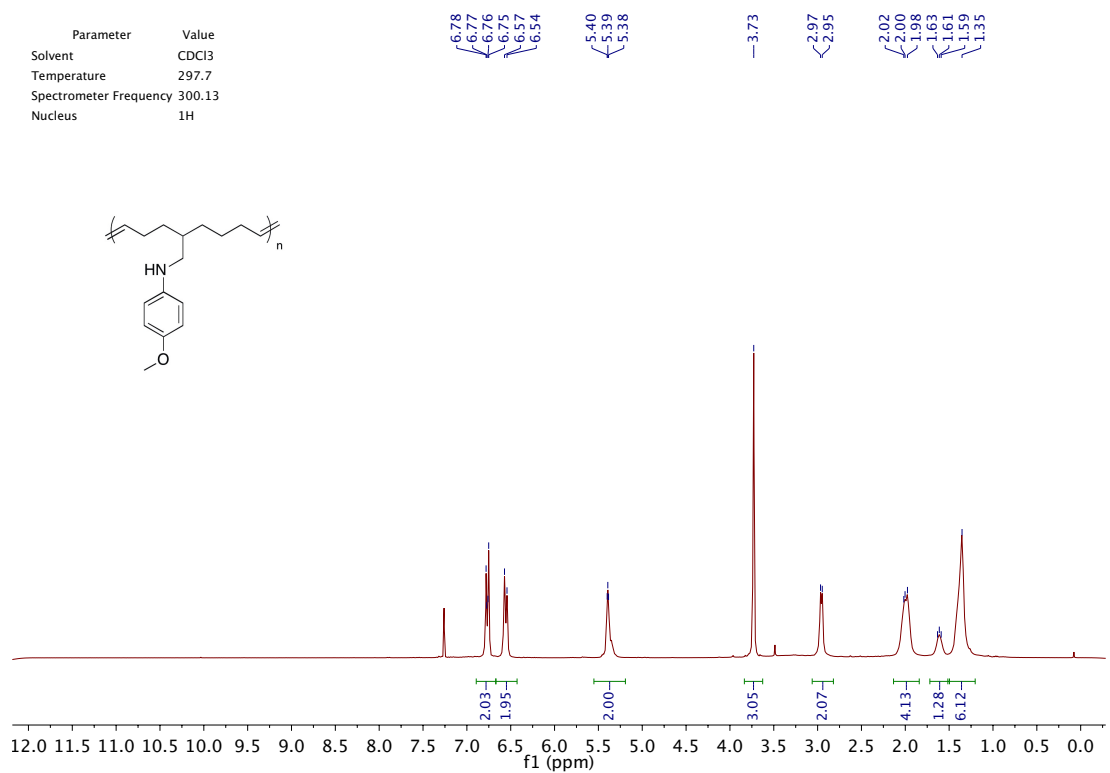
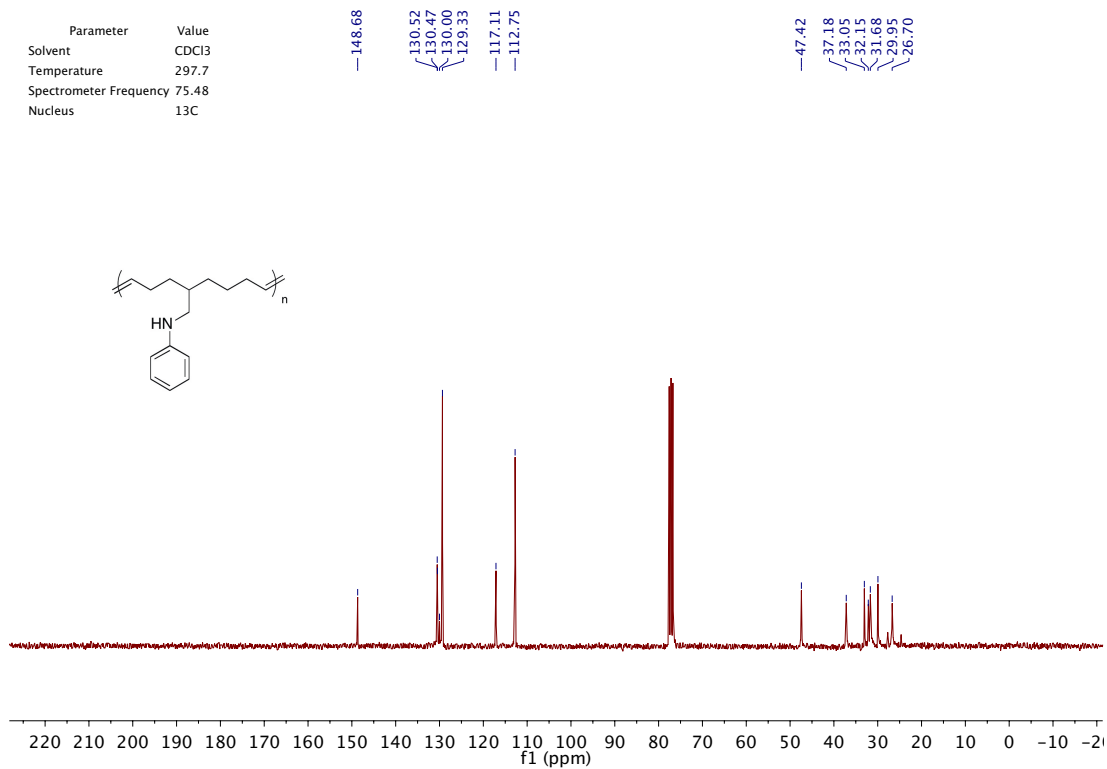


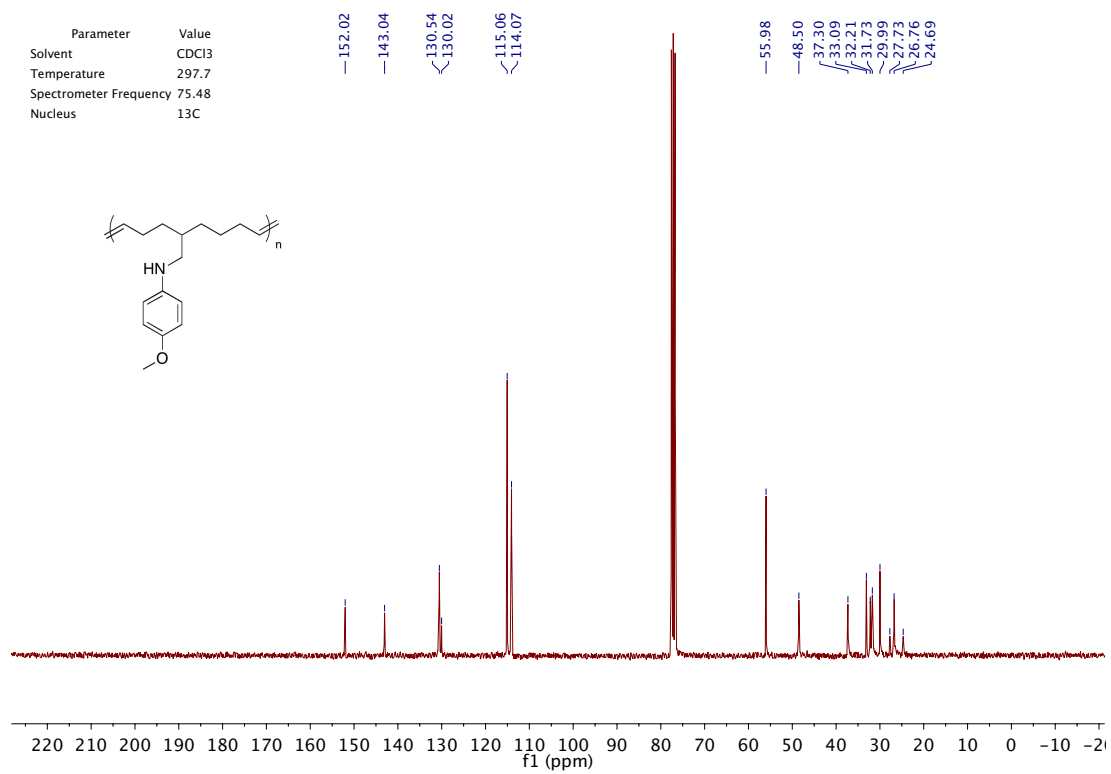




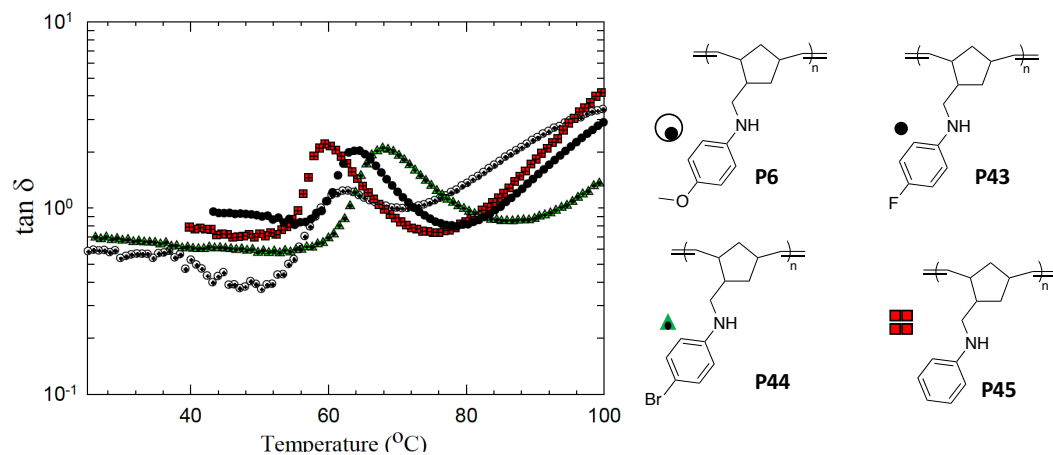






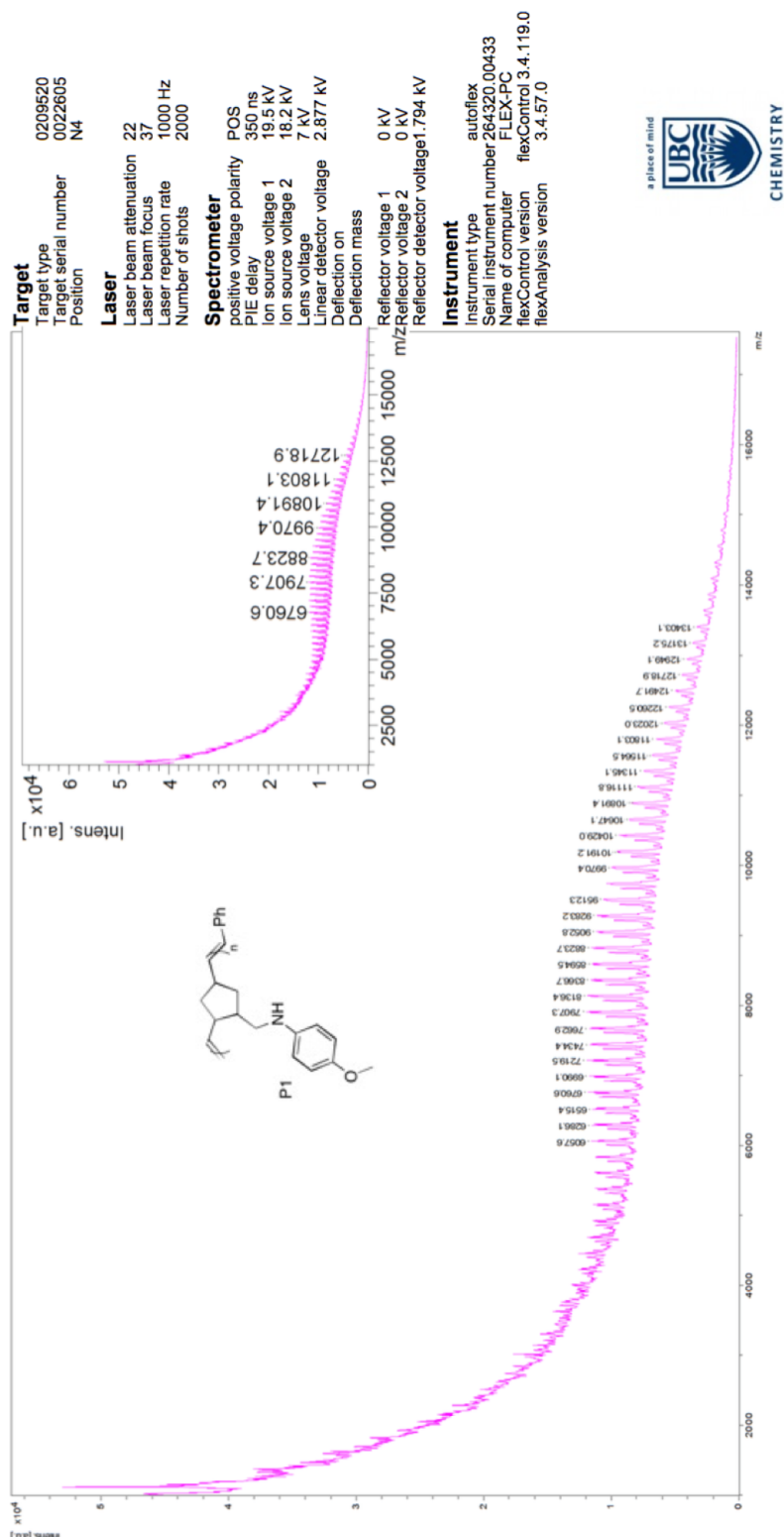


B.3 Additional Information for Chapter 3



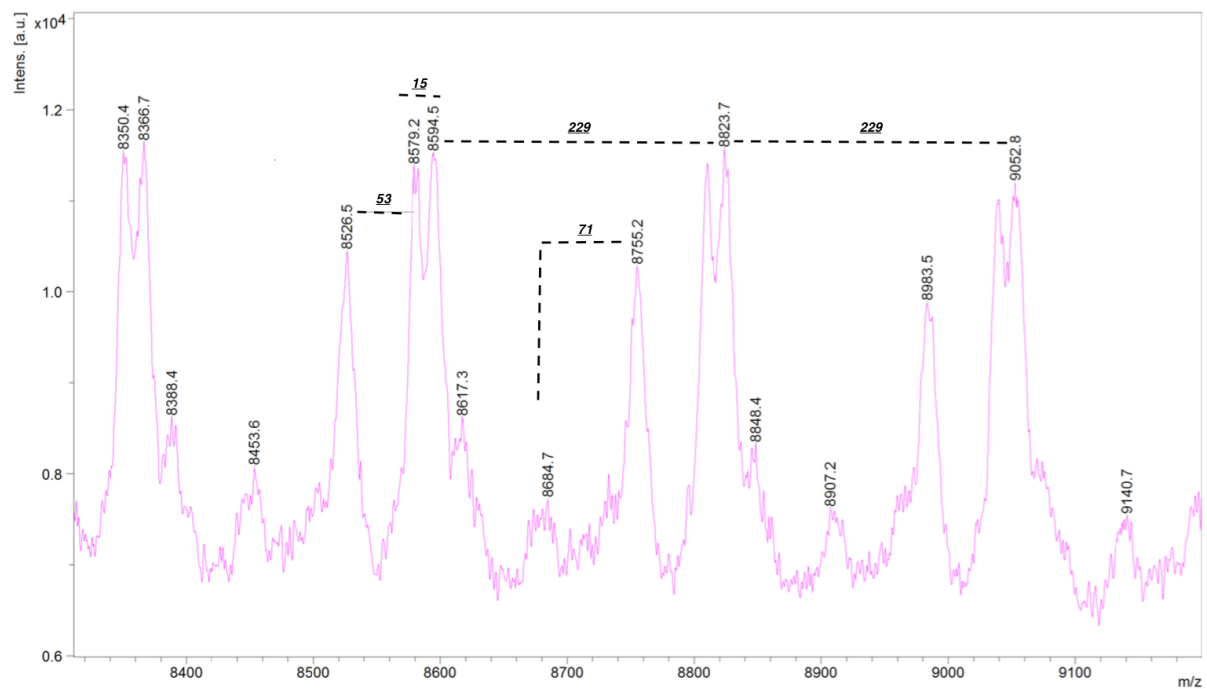
A 1 Tan delta values for T_g calculations by isochronal dynamic temperature sweep tests. Shown by melt rheological loss tangent vs. temperature using 0.1 Hz and heating rate of 1 °C min⁻¹. The maximum temperature indicates the T_g

dhb/TA mix matrix:sample 10:1



A 2 MALDI-TOF mass spectrum of NBD-PMP polymer, P6

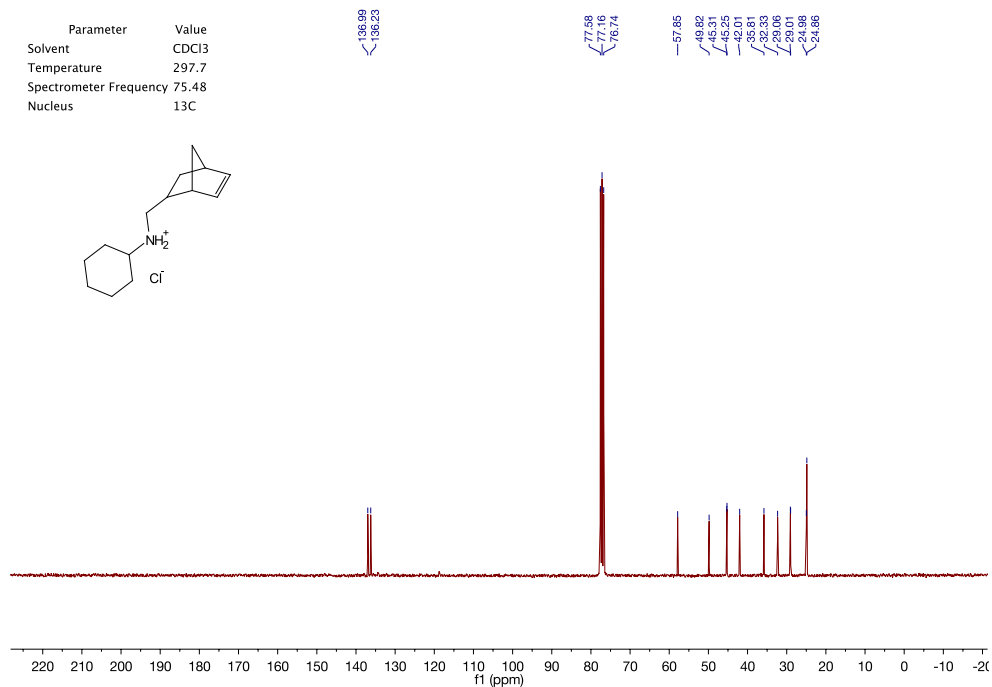
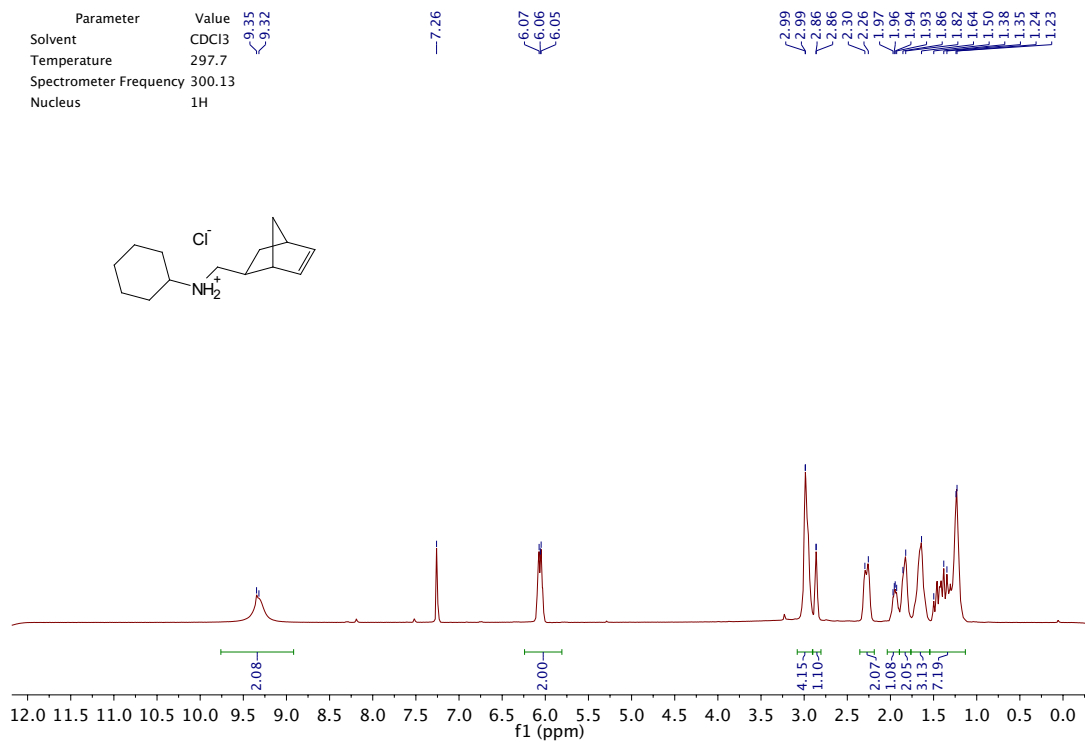
Comment 2 dnb/TA mix matrix:sample 10:1

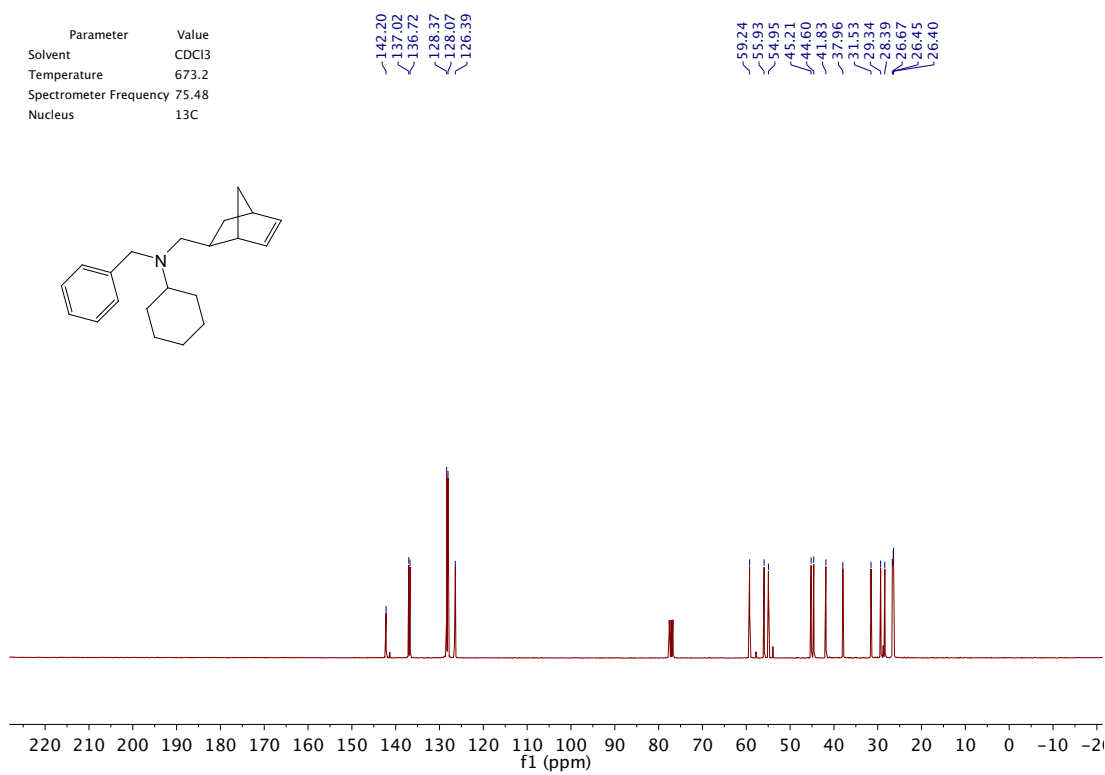
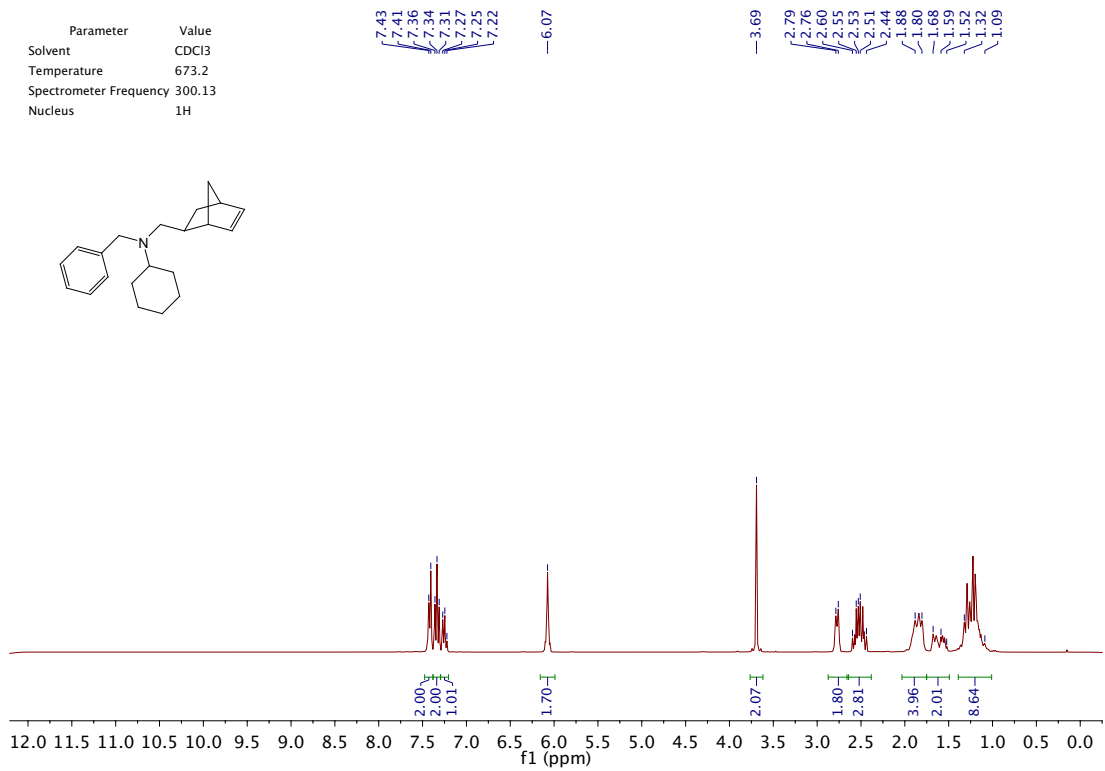


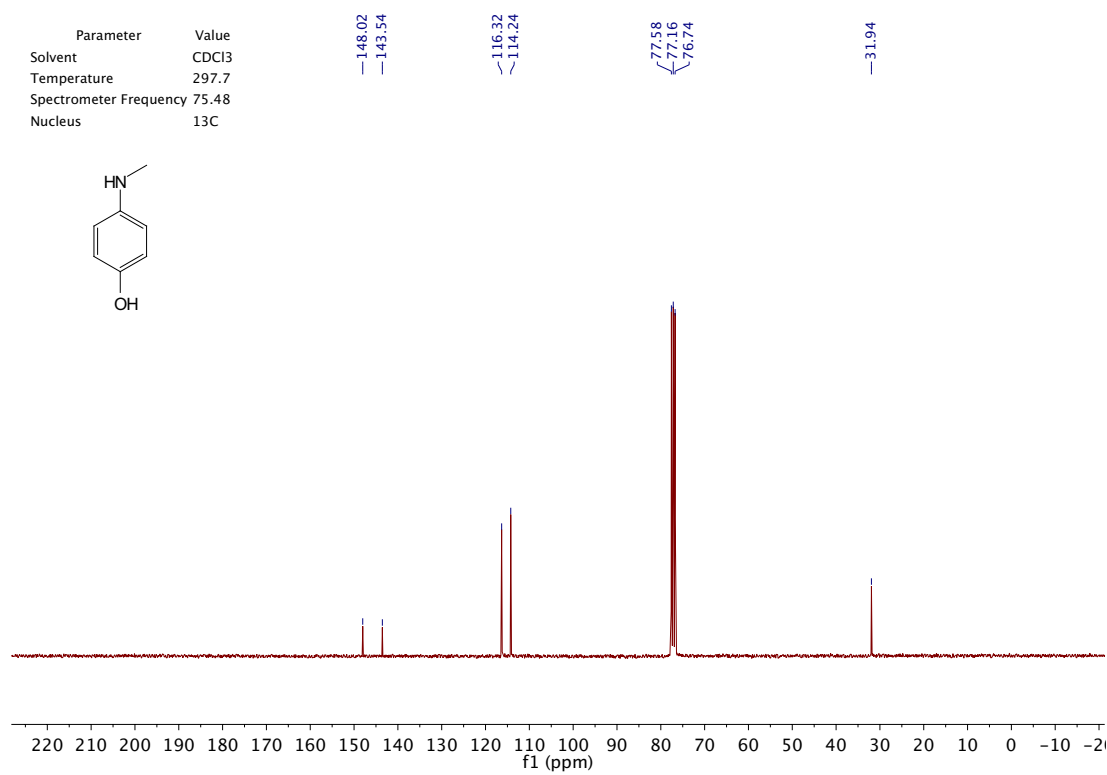
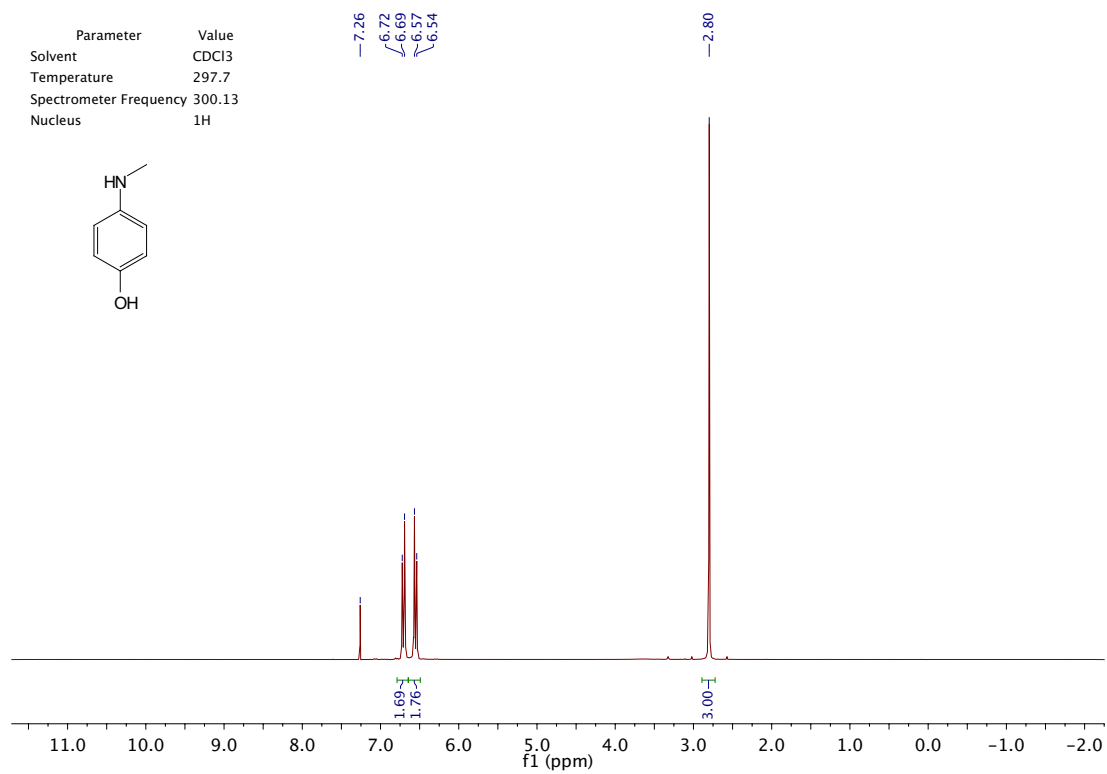
A 3 Expansion of MALDI-TOF mass spectrum of NBD-PMP polymer, P6

Appendix C Supplementary Information for Chapter 4

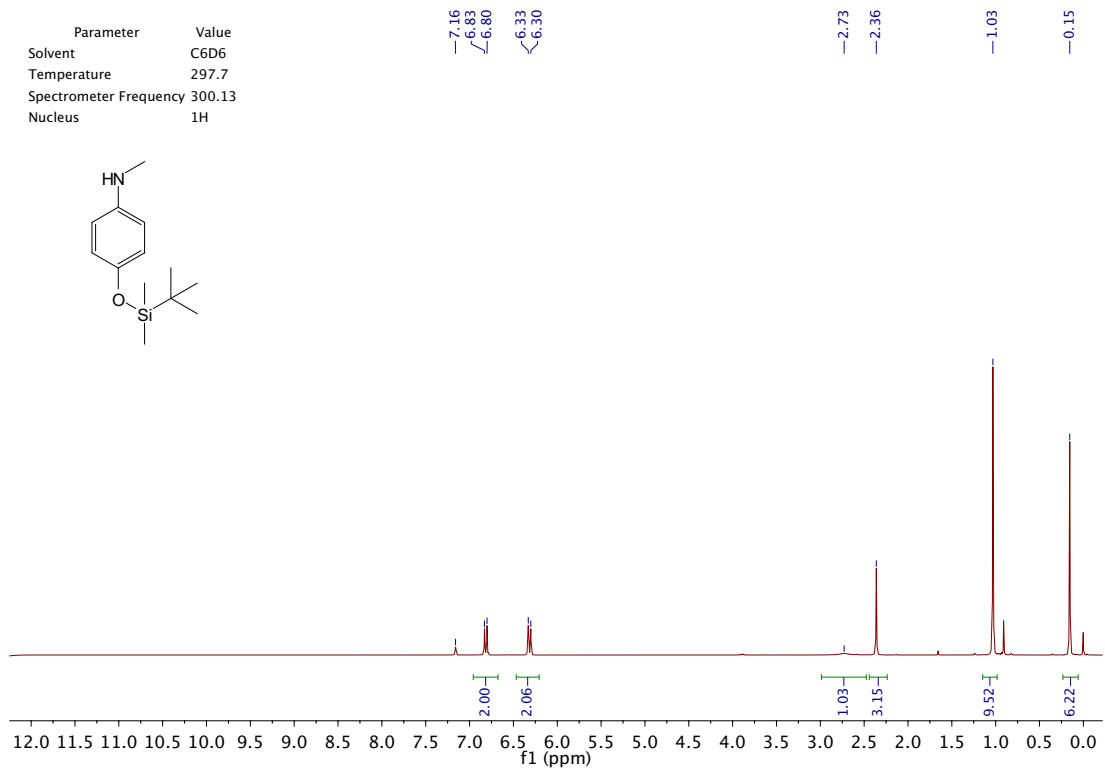
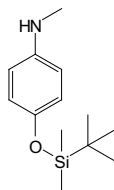
C.1 Selected NMR Spectra of Aminonorbornenes and Other Products



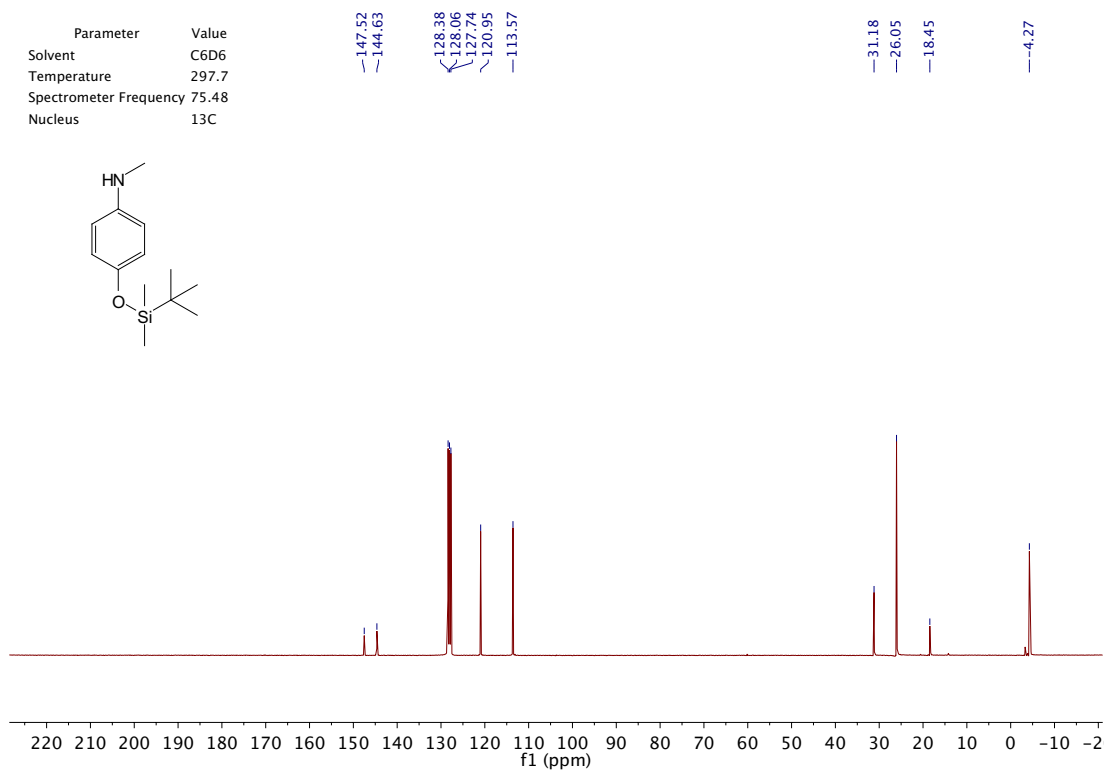
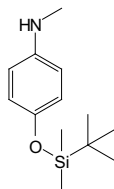


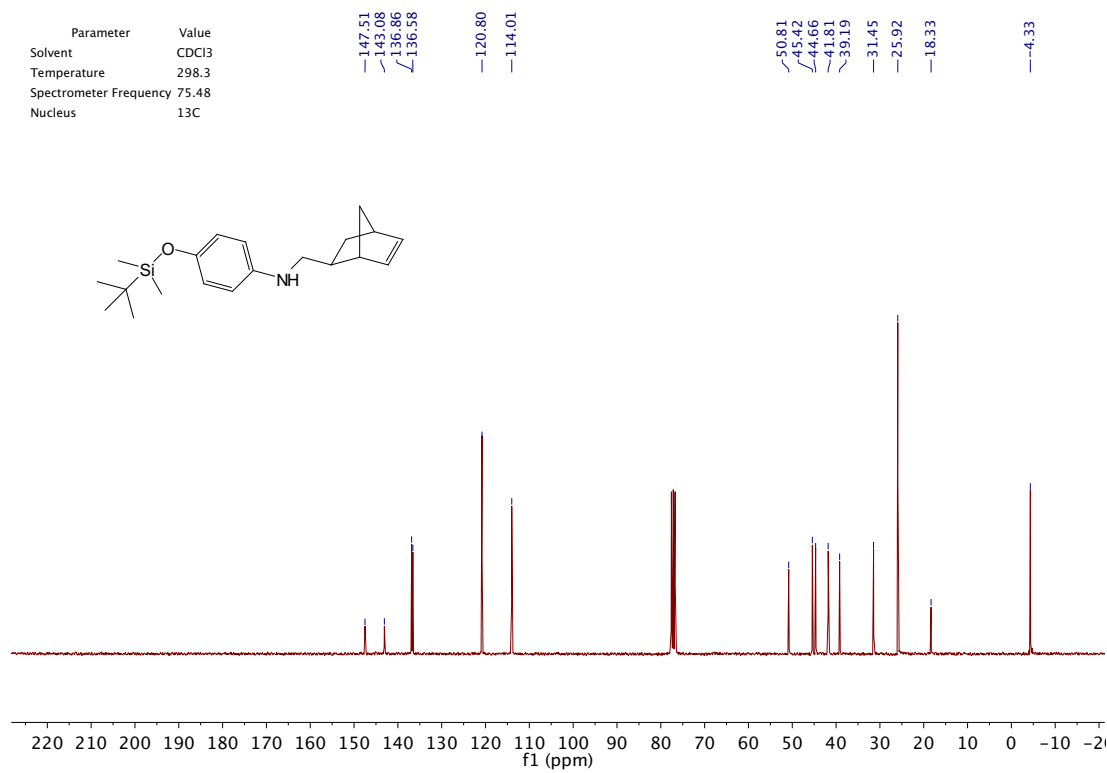
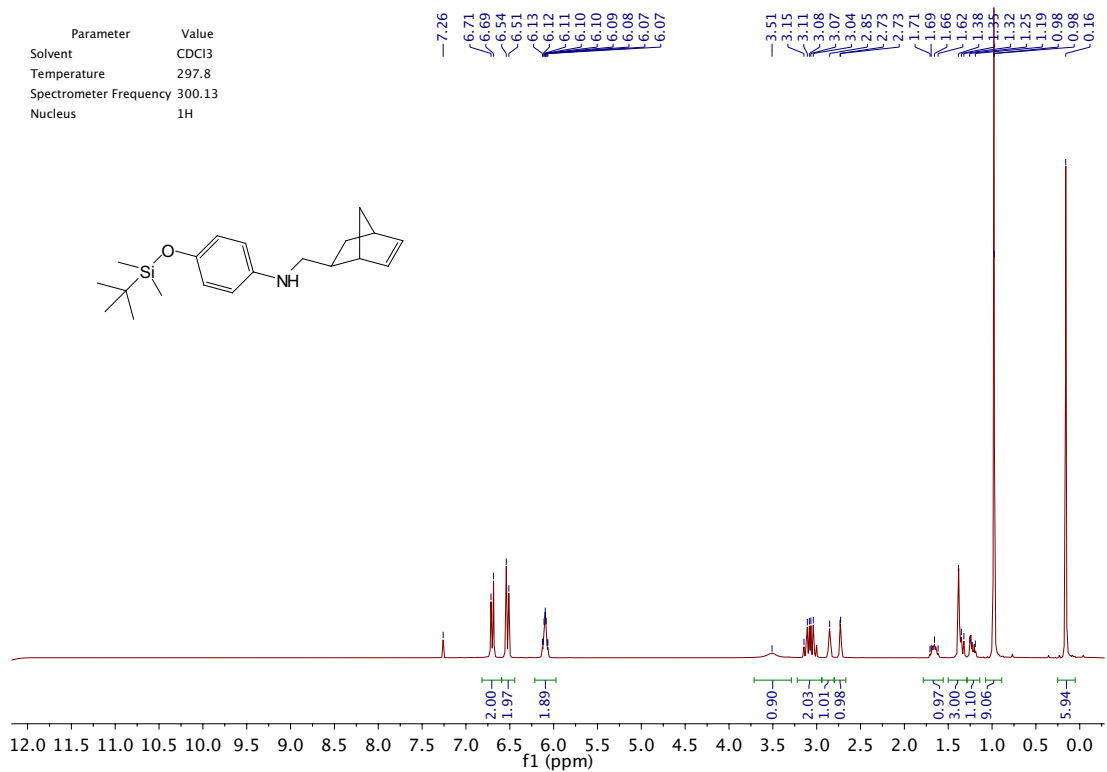


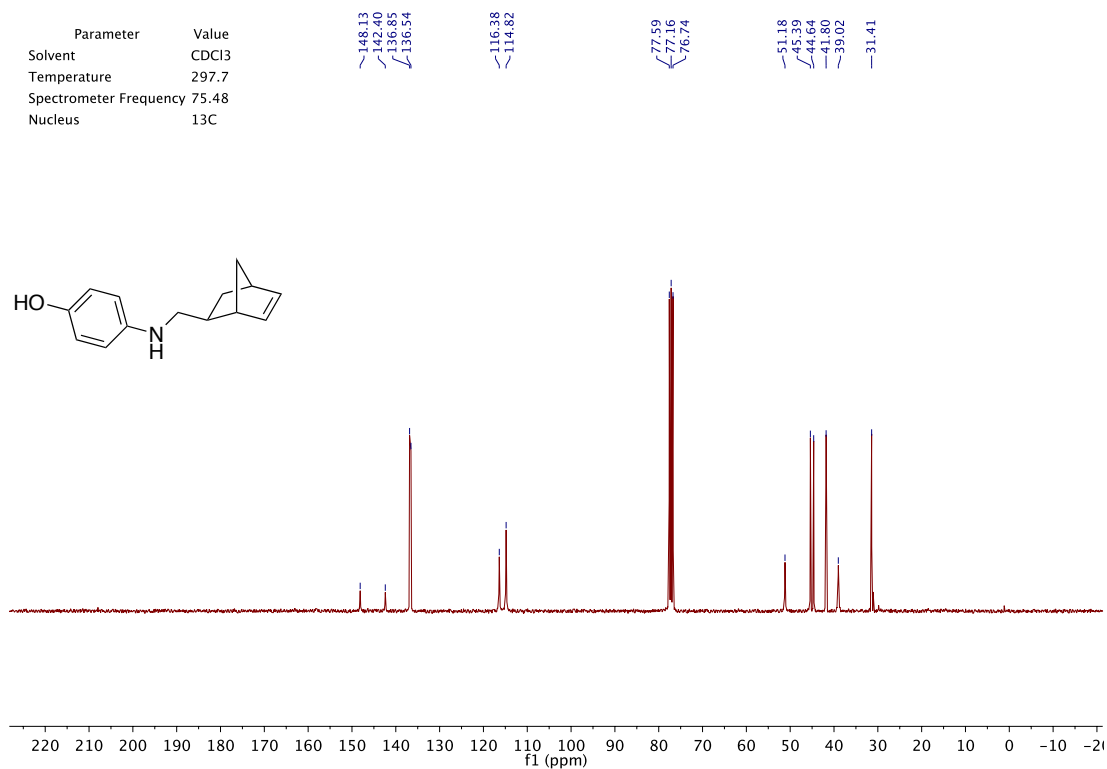
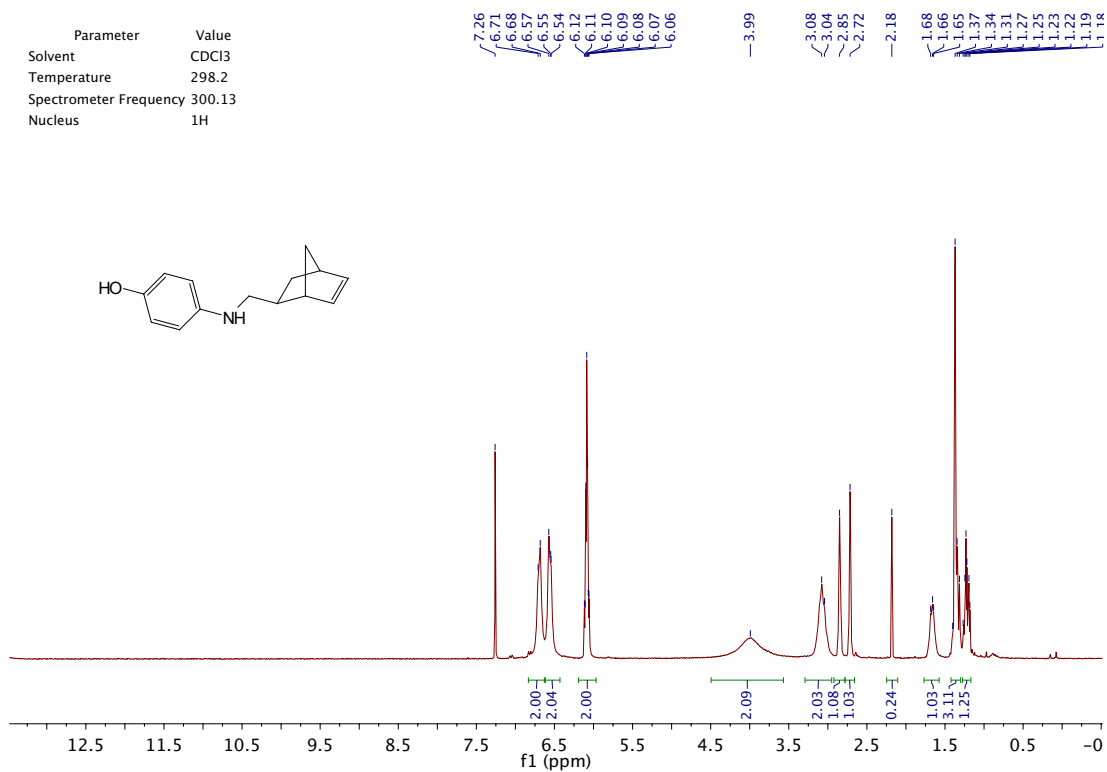
Parameter	Value
Solvent	C6D6
Temperature	297.7
Spectrometer Frequency	300.13
Nucleus	¹ H



Parameter	Value
Solvent	C6D6
Temperature	297.7
Spectrometer Frequency	75.48
Nucleus	¹³ C



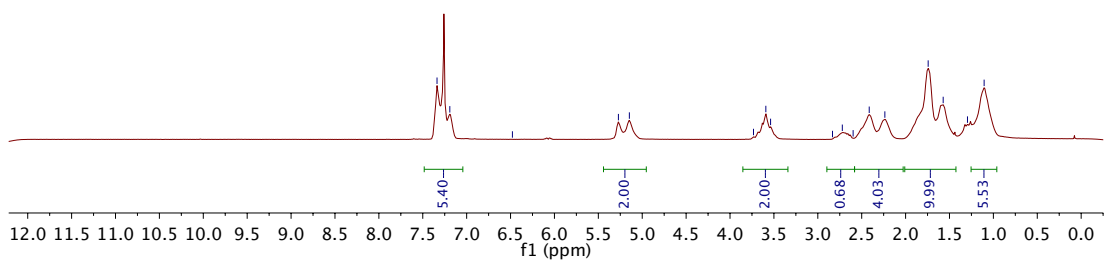
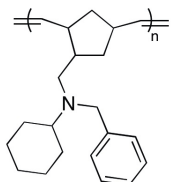




C.2 Selected NMR Spectra of Polymers

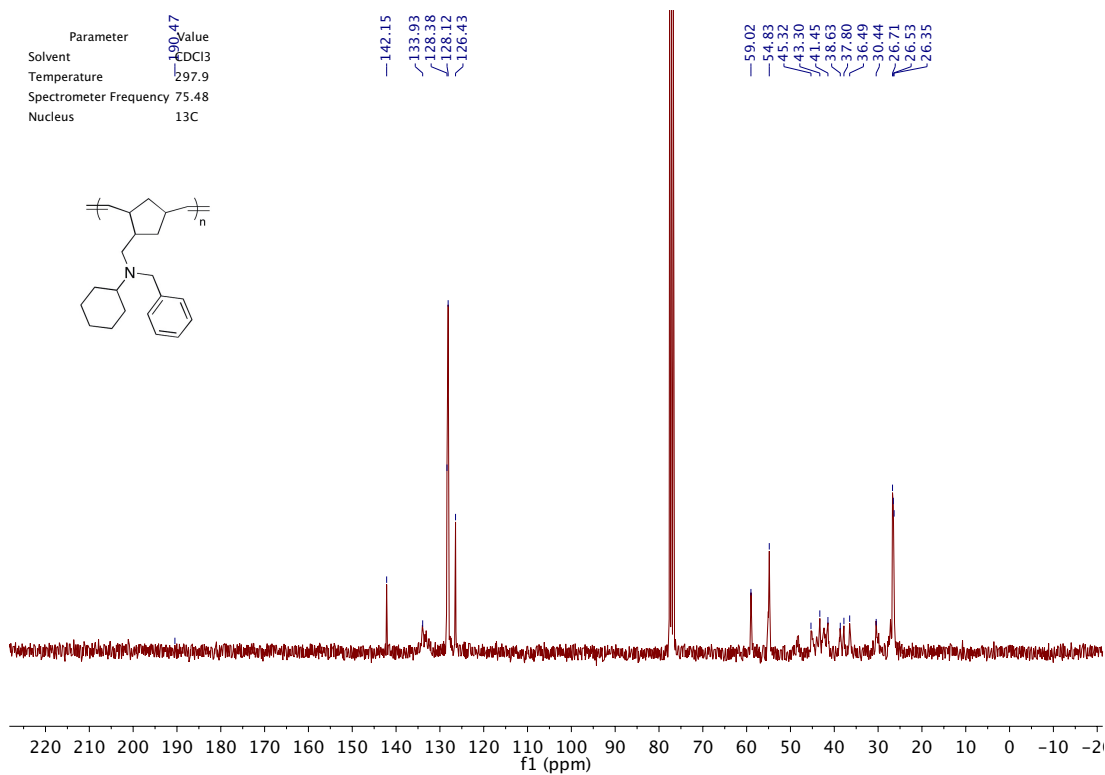
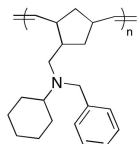
Parameter	Value
Solvent	CDCl ₃
Temperature	297.8
Spectrometer Frequency	300.13
Nucleus	¹ H

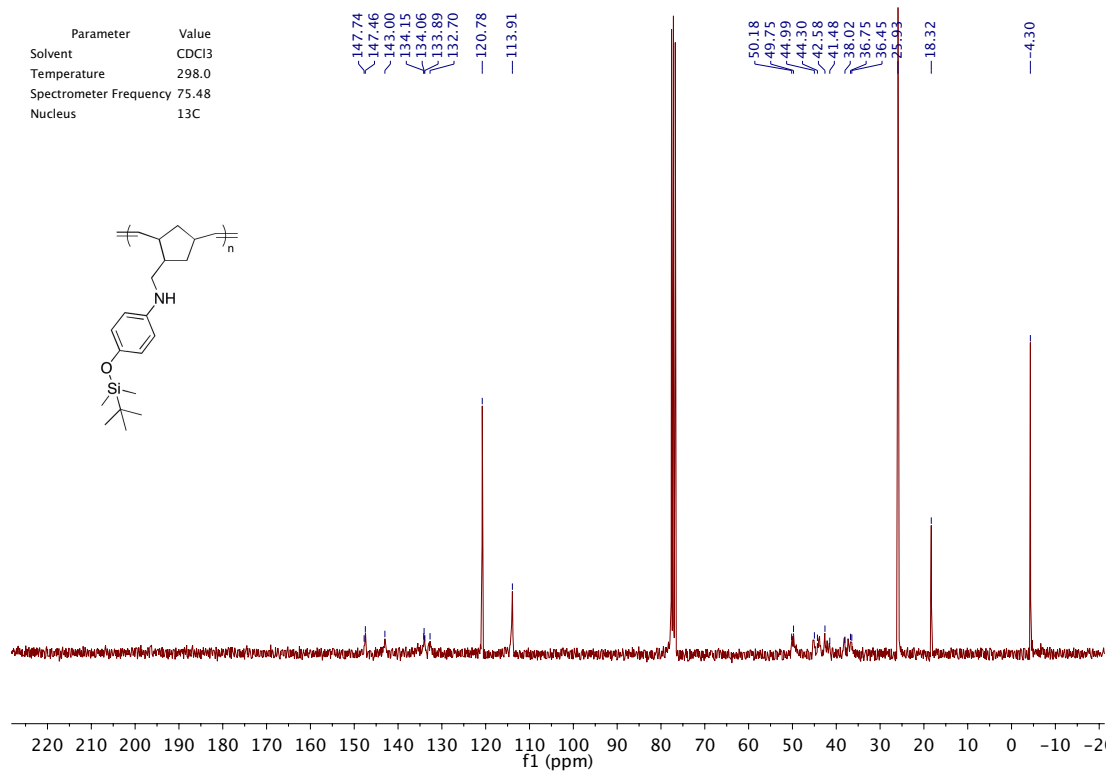
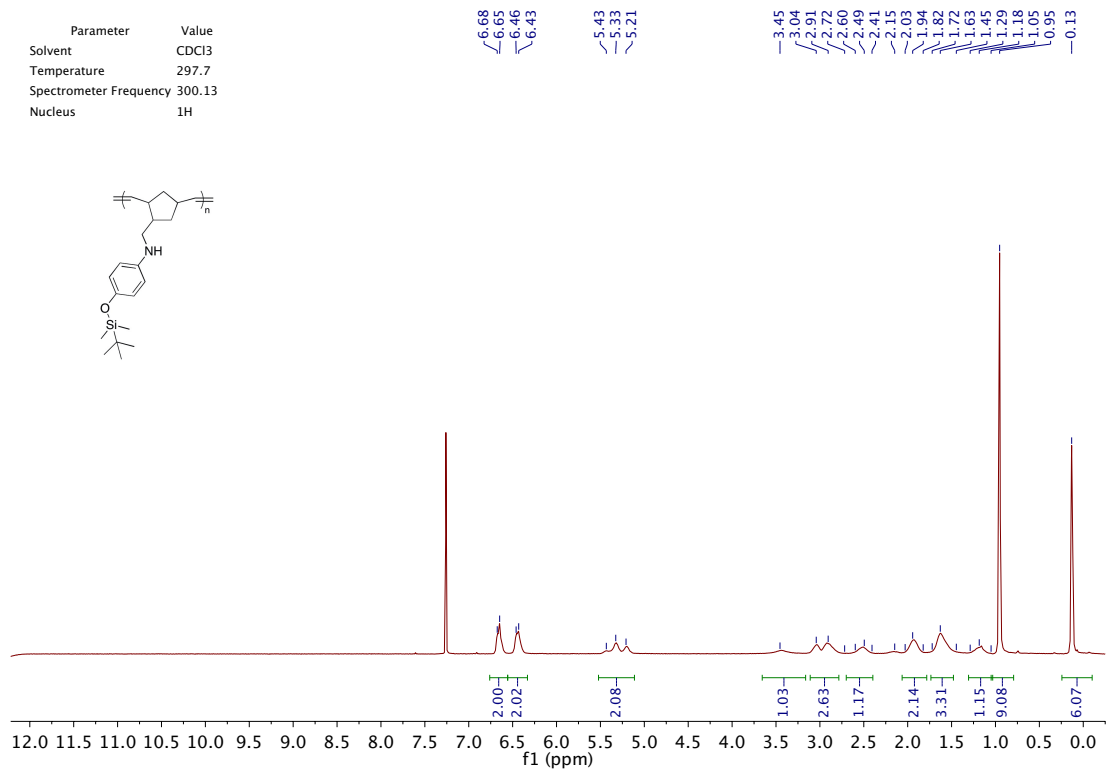
¹H NMR peaks (ppm):
 ~7.34, ~7.19, ~6.48, ~5.27, ~5.15, ~3.73, ~3.59, ~3.54, ~2.83, ~2.72, ~2.60, ~2.41, ~2.24, ~1.74, ~1.57, ~1.29, ~1.11

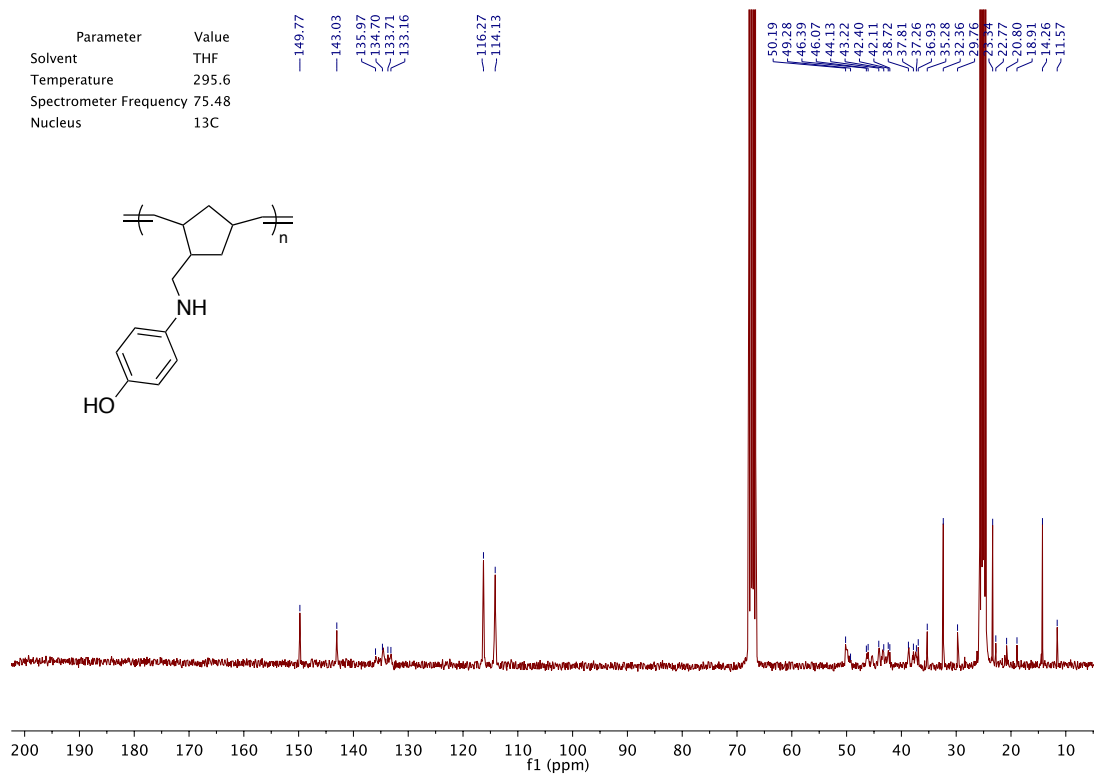
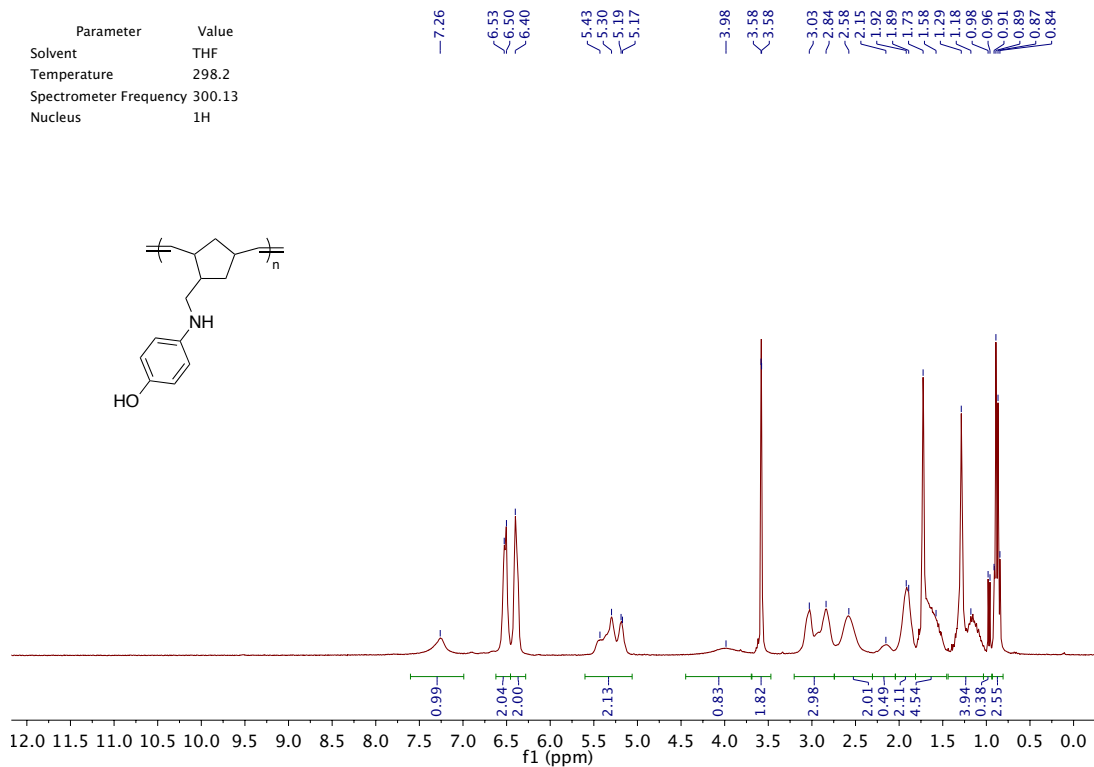


Parameter	Value
Solvent	CDCl ₃
Temperature	297.9
Spectrometer Frequency	75.48
Nucleus	¹³ C

¹³C NMR peaks (ppm):
 ~142.15, ~133.93, ~128.38, ~128.12, ~126.43, ~59.02, ~54.83, ~45.32, ~43.30, ~41.45, ~38.63, ~37.80, ~36.49, ~30.44, ~26.71, ~26.53

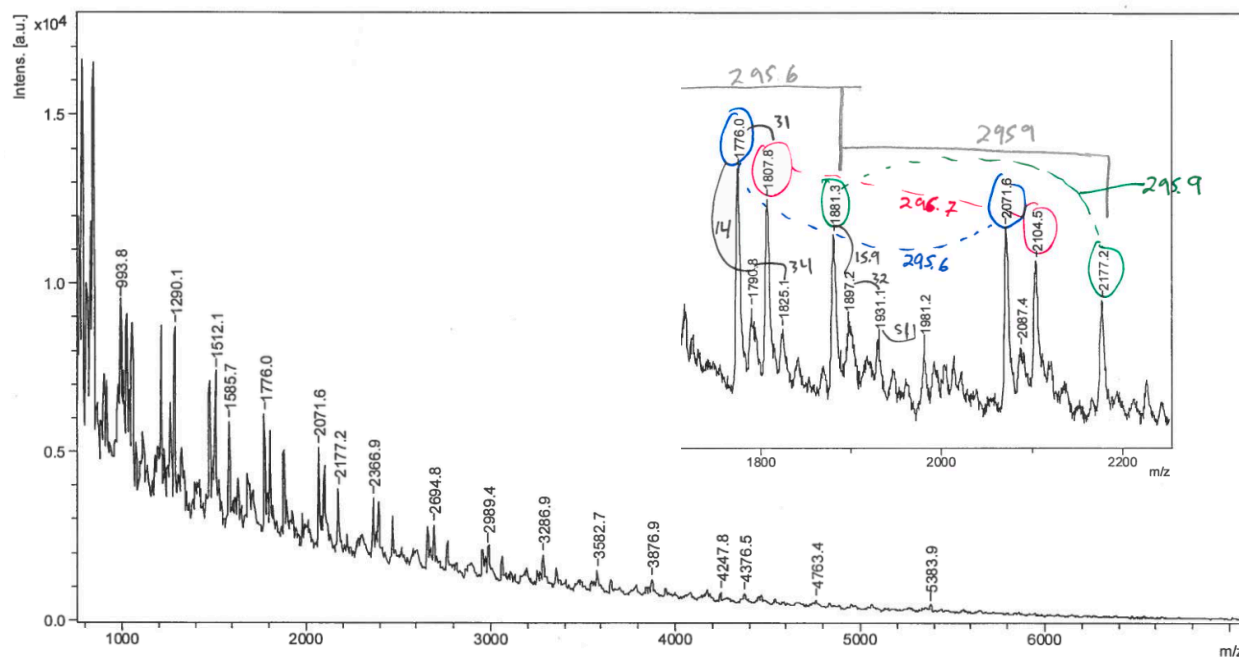




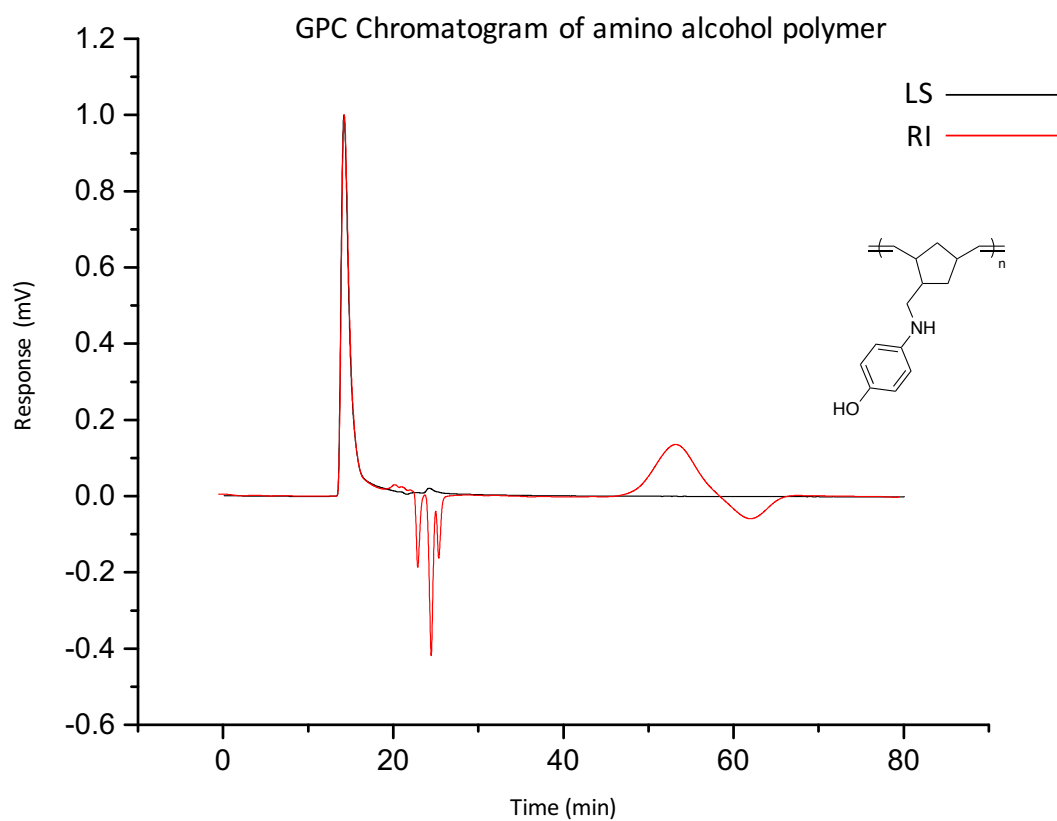


C.3 Additional Information for Chapter 4

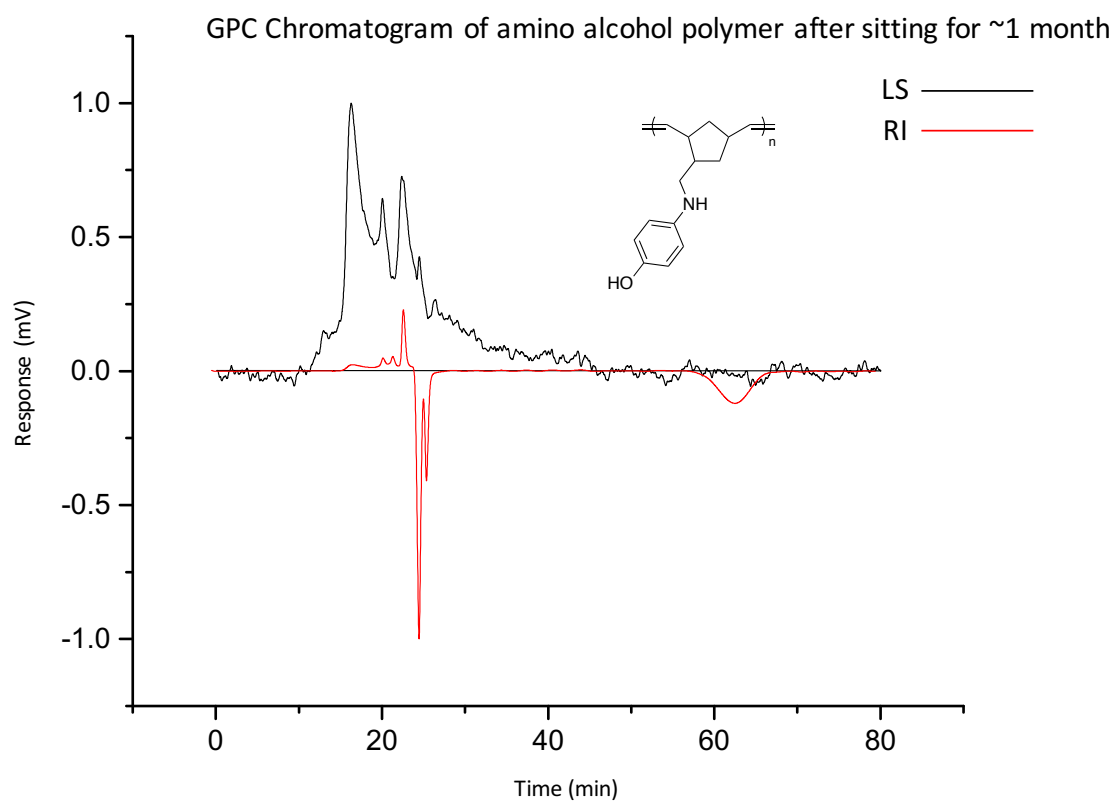
Comment 1 MP-523
 Comment 2 1.9mg/10ul CHCl₃ dil 1:10 1:1:1 dnb



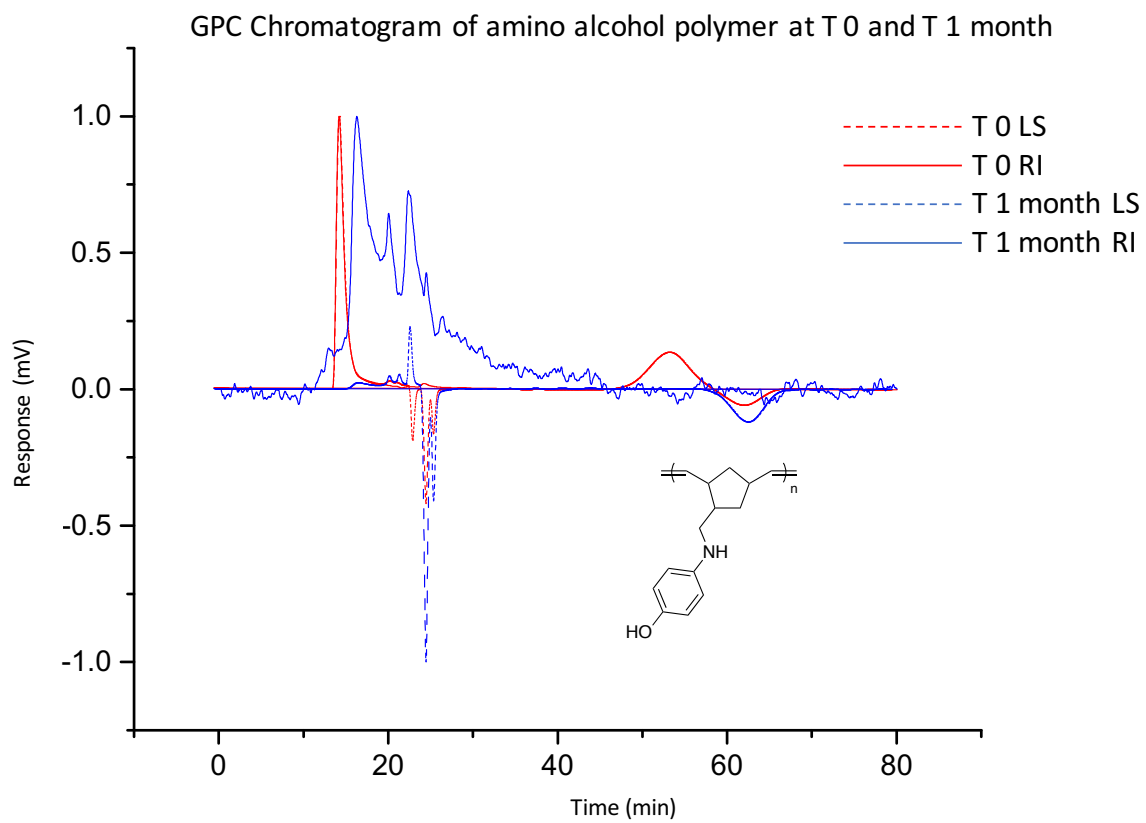
A 4 MALDI-TOF mass spectrum of benzyl-protected polymer P49. Inset shows peak differences corresponding to monomer MW



A 5 GPC Chromatogram of alcohol-substituted polymer, P51. Light-scattering trace is shown in black. Refractive index trace is shown in red

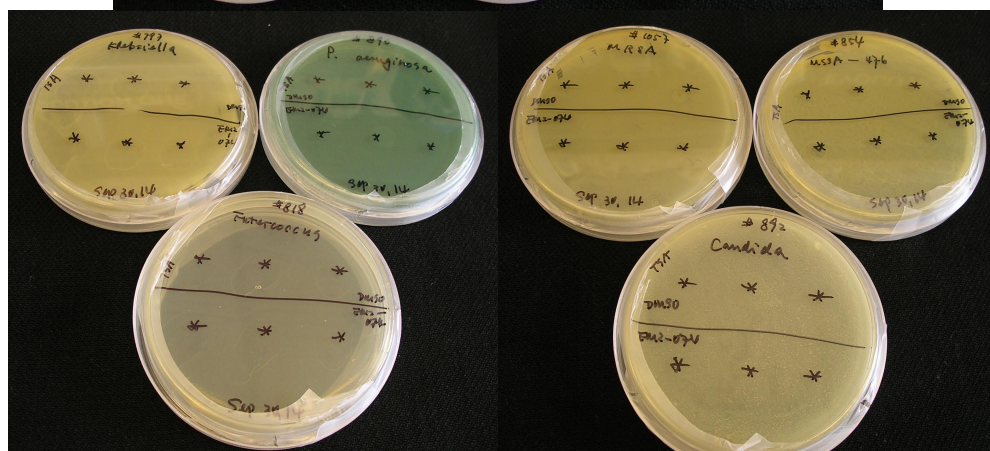
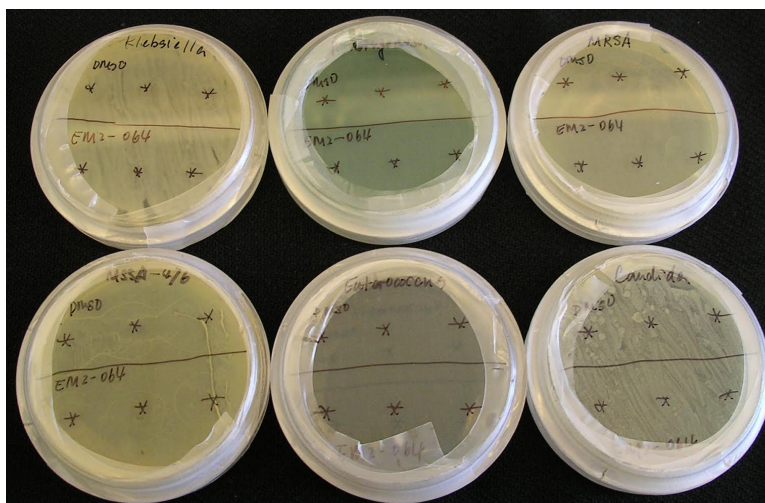
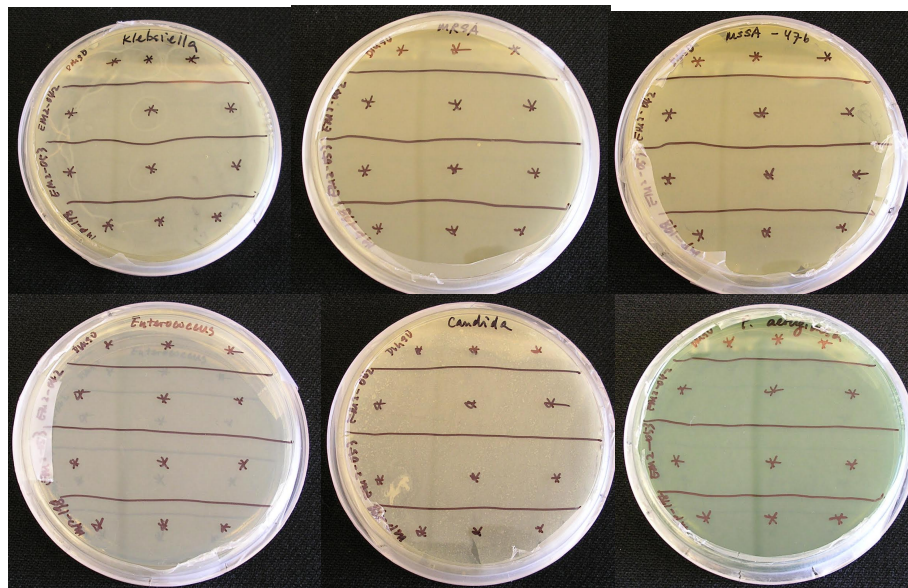


A 6 GPC chromatogram of alcohol-substituted polymer P51 after sitting in solution for 1 month. Light-scattering trace is shown in black. Refractive index trace is shown in red



A 7 GPC chromatogram of amino alcohol polymer at T 0 (red) and 1 month after synthesis (blue)

Anti-Microbial Screening



Appendix D X-Ray Crystallographic Data

D.1 X-Ray Crystallographic Data Presented in Chapter 2

Table A 1 Crystallographic parameters for nosylated aminobornornene 11

	11
Identification code	ls404
formula	C ₂₁ H ₂₂ N ₂ O ₅ S
F_w	414.48
crystal size (mm)	0.20 × 0.05 × 0.04
colour, habit	Colourless, prisms
cell setting	Monoclinic
space group	P2 ₁ /c
a (Å)	6.2153 (11) Å
b (Å)	19.993 (4) Å
c (Å)	15.863 (3) Å
α (°)	90
β (°)	94.665 (4)
γ (°)	90
V (Å ³)	1964.7 (6) Å ³
Z	4
ρ_{calcd}	1.401 g cm ⁻³
$F(000)$	872.0
μ (MoK α) (mm ⁻¹)	0.201
$2\theta_{\text{max}}$ (°)	60.400
total no. of reflns	24989
no. of unique reflns	5757
no. of reflns	4003
with $I > 2\sigma(I)$	
no. of variables	325
R_1 (F^2 , all data)	0.0863
wR_2 (F^2 , all data)	0.1132
R_1 (F , $I > 2\sigma(I)$)	0.0514
wR_2 (F , $I > 2\sigma(I)$)	0.1006
goodness of fit	1.032

Table A 2 Crystallographic parameters for monophosphoramidate complex 18

	18
Identification code	ls466
formula	C ₁₈ H ₃₇ N ₄ O ₃ PTi
F_w	436.36
crystal size (mm)	0.12 × 0.12 × 0.06
colour, habit	Red, prisms
cell setting	Triclinic
space group	P-1
a (Å)	15.486
b (Å)	16.747
c (Å)	17.967
α (°)	91.59
β (°)	91.82
γ (°)	90.66
V (Å ³)	4655.1
Z	2
ρ_{calcd}	1.245
$F(000)$	1872.0
μ (MoK α) (mm ⁻¹)	0.460
$2\theta_{\text{max}}$ (°)	46.276
total no. of reflns	89558
no. of unique reflns	12995
no. of reflns	7390
with $I > 2\sigma(I)$	
no. of variables	1013
R_1 (F^2 , all data)	0.1704
wR_2 (F^2 , all data)	0.2594
R_1 (F , $I > 2\sigma(I)$)	0.0932
wR_2 (F , $I > 2\sigma(I)$)	0.2132
goodness of fit	1.060

Table A 3 Crystallographic parameters for diphosphoramidate complex 19

	19
Identification code	ls627
formula	C ₂₈ H ₅₀ N ₄ O ₆ P ₂ Ti
F_w	648.56
crystal size (mm)	0.252 × 0.133 × 0.103
colour, habit	Red, prisms
cell setting	monoclinic
space group	C ₂
a (Å)	14.113(3)
b (Å)	10.978(2)
c (Å)	11.644(2)
α (°)	90
β (°)	112.550(6)
γ (°)	90
V (Å ³)	1666.2(6)
Z	2
ρ_{calcd}	1.293
$F(000)$	692.0
μ (MoK α) (mm ⁻¹)	0.397
$2\theta_{\text{max}}$ (°)	50.788
total no. of reflns	9380
no. of unique reflns	2916
no. of reflns	2706
with $I > 2\sigma(I)$	
no. of variables	332
R_1 (F^2 , all data)	0.0815
wR_2 (F^2 , all data)	0.1608
R_1 (F , $I > 2\sigma(I)$)	0.0757
wR_2 (F , $I > 2\sigma(I)$)	0.1576
goodness of fit	0.998

Table A 4 Crystallographic parameters for diphosphoramidate complex 22

	22
Identification code	ls558
formula	C ₃₆ H ₅₉ N ₄ O ₆ P ₂ Ti
F_w	753.71
crystal size (mm)	0.357 × 0.257 × 0.207
colour, habit	Red, prisms
cell setting	monoclinic
space group	P2 ₁ /n
a (Å)	11.7429(10)
b (Å)	22.594(2)
c (Å)	16.9276(14)
α (°)	90
β (°)	92.962(5)
γ (°)	90
V (Å ³)	4485.2(7)
Z	4
ρ_{calcd}	1.116
$F(000)$	1612.0
μ (MoK α) (mm ⁻¹)	0.304
$2\theta_{\text{max}}$ (°)	51.194
total no. of reflns	58172
no. of unique reflns	8365
no. of reflns with $I > 2\sigma(I)$	5534
no. of variables	469
R_1 (F^2 , all data)	0.0867
wR_2 (F^2 , all data)	0.1007
R_1 (F , $I > 2\sigma(I)$)	0.0453
wR_2 (F , $I > 2\sigma(I)$)	0.0893
goodness of fit	1.033

Table A 5 Crystallographic parameters for diphosphoramidate complex 23

	23
Identification code	ls592
formula	C ₂₄ H ₄₂ N ₄ O ₆ P ₂ Ti
F_w	592.45
crystal size (mm)	0.3 × 0.21 × 0.17
colour, habit	Orange, prisms
cell setting	Orthorhombic
space group	P 2 ₁ 2 ₁ 2 ₁
a (Å)	9.9388(2)
b (Å)	15.5890(4)
c (Å)	19.0437(5)
α (°)	90
β (°)	90
γ (°)	90
V (Å ³)	2950.55(12)
Z	4
ρ_{calcd}	1.334
$F(000)$	1256.0
μ (MoK α) (mm ⁻¹)	0.441
$2\theta_{\text{max}}$ (°)	60.08
total no. of reflns	20118
no. of unique reflns	8617
no. of reflns	7621
with $I > 2\sigma(I)$	
no. of variables	342
R_1 (F^2 , all data)	0.0435
wR_2 (F^2 , all data)	0.0726
R_1 (F , $I > 2\sigma(I)$)	0.0351
wR_2 (F , $I > 2\sigma(I)$)	0.0757
goodness of fit	1.036

Table A 6 Crystallographic parameters for diphosphoramidate complex 24

	24
Identification code	ls517
formula	C ₂₆ H ₄₄ N ₄ O ₆ P ₂ Ti
F_w	618.49
crystal size (mm)	0.38 × 0.27 × 0.18
colour, habit	Red, prisms
cell setting	tetragonal
space group	I41/a
a (Å)	21.202(5)
b (Å)	21.202(5)
c (Å)	31.436(8)
α (°)	90
β (°)	90
γ (°)	90
V (Å ³)	14131(8)
Z	16
ρ_{calcd}	1.163
$F(000)$	5248.0
μ (MoK α) (mm ⁻¹)	0.371
$2\theta_{\text{max}}$ (°)	60.092
total no. of reflns	156780
no. of unique reflns	156780
no. of reflns	127717
with $I > 2\sigma(I)$	
no. of variables	420
R_1 (F^2 , all data)	0.0708
wR_2 (F^2 , all data)	0.1358
R_1 (F , $I > 2\sigma(I)$)	0.0517
wR_2 (F , $I > 2\sigma(I)$)	0.1227
goodness of fit	1.021

Table A 7 Crystallographic parameters for triphosphoramidate complex 26

	26
Identification code	ls609
formula	C ₃₈ H ₆₃ N ₄ O ₉ P ₃ Ti
F_w	860.73
crystal size (mm)	0.218 × 0.105 × 0.047
colour, habit	Red, prisms
cell setting	monoclinic
space group	P2 ₁ /c
a (Å)	12.2852(7)
b (Å)	17.6497(9)
c (Å)	20.5001(12)
α (°)	90
β (°)	94.609(2)
γ (°)	90
V (Å ³)	4430.7(4)
Z	4
ρ_{calcd}	1.290
$F(000)$	1832.0
μ (MoK α) (mm ⁻¹)	0.355
$2\theta_{\text{max}}$ (°)	50.854
total no. of reflns	45257
no. of unique reflns	8153
no. of reflns	5970
with $I > 2\sigma(I)$	
no. of variables	510
R_1 (F^2 , all data)	0.0745
wR_2 (F^2 , all data)	0.1190
R_1 (F , $I > 2\sigma(I)$)	0.0455
wR_2 (F , $I > 2\sigma(I)$)	0.1035
goodness of fit	1.053

Table A 8 Crystallographic parameters for monophosphoramidate chloro complex 28

28	
Identification code	ls623
formula	C ₂₆ H ₄₄ ClN ₃ O ₆ P ₂ Ti
F_w	639.93
crystal size (mm)	0.31 × 0.213 × 0.18
colour, habit	Red, prisms
cell setting	monoclinic
space group	P2 ₁ /n
a (Å)	9.9879(4)
b (Å)	14.1439(6)
c (Å)	16.0758(7)
α (°)	90
β (°)	107.9120(10)
γ (°)	90
V (Å ³)	2160.92(16)
Z	4
ρ_{calcd} (g cm ⁻³)	1.967
$F(000)$	1352.0
μ (MoK α) (mm ⁻¹)	0.729
$2\theta_{\text{max}}$ (°)	58.272
total no. of reflns	7593
no. of unique reflns	3333
no. of reflns with $I > 2\sigma(I)$	2702
no. of variables	235
R_1 (F^2 , all data)	0.0454
wR_2 (F^2 , all data)	0.0985
R_1 (F , $I > 2\sigma(I)$)	0.0351
wR_2 (F , $I > 2\sigma(I)$)	0.0942
goodness of fit	0.972

D.2 X-Ray Crystallographic Data Presented in Chapter 3

Table A 9 Crystallographic parameters for aminonorbornene monomer 6

	6
Identification code	ls633
formula	C ₁₅ H ₁₉ ON
F_w	229.32
crystal size (mm)	0.150 x 0.210 x 0.420
colour, habit	yellow, prisms
cell setting	monoclinic
space group	P2 ₁ /n
a (Å)	5.4660(11)
b (Å)	18.672(3)
c (Å)	12.310(2)
α (°)	90
β (°)	98.878(5)
γ (°)	90
V (Å ³)	1241.3(4)
Z	4
ρ_{calcd} (g cm ⁻³)	1.090
$F(000)$	439.0
μ (MoK α) (mm ⁻¹)	0.067
$2\theta_{\text{max}}$ (°)	52.096
total no. of reflns	9888
no. of unique reflns	2450
no. of reflns with $I > 2\sigma(I)$	1672
no. of variables	70
R_1 (F^2 , all data)	0.0967
wR_2 (F^2 , all data)	0.1804
R_1 (F , $I > 2\sigma(I)$)	0.0644
wR_2 (F , $I > 2\sigma(I)$)	0.1595
goodness of fit	1.092

Table A 10 Crystallographic parameters for titanium pyridonate complex 41

	41
Identification code	ls371
formula	C ₁₆ H ₂₃ N ₂ O ₄ Ti
F_w	355.26
crystal size (mm)	0.150 x 0.220 x 0.410
colour, habit	yellow, needles
cell setting	orthorhombic
space group	F d d 2
a (Å)	56.949(9)
b (Å)	10.8724(16)
c (Å)	11.2108(17)
α (°)	90
β (°)	90
γ (°)	90
V (Å ³)	6941.4(18)
Z	16
ρ_{calcd} (Mg cm ⁻³)	1.360
$F(000)$	2992
μ (MoK α) (mm ⁻¹)	0.513
$2\theta_{\text{max}}$ (°)	59.60
total no. of reflns	34715
no. of unique reflns	4952
no. of reflns	4596
with $I > 2\sigma(I)$	
no. of variables	212
R_1 (F^2 , all data)	0.0469
wR_2 (F^2 , all data)	0.1233
R_1 (F , $I > 2\sigma(I)$)	0.0422
wR_2 (F , $I > 2\sigma(I)$)	0.1179
goodness of fit	1.005

D.3 X-Ray Crystallographic Data Presented in Chapter 4

Table A 11 Crystallographic parameters for HCl monomer salt 48

	48
Identification code	ls615
formula	C ₁₄ H ₂₁ ClN
F_w	265.78
crystal size (mm)	0.248 × 0.232 × 0.11
colour, habit	Colorless, prism
cell setting	monoclinic
space group	P2 ₁ /c
a (Å)	5.7018(7)
b (Å)	22.876(3)
c (Å)	10.4418(14)
α (°)	90
β (°)	93.642(3)
γ (°)	90
V (Å ³)	1359.2(3)
Z	4
ρ_{calcd}	1.167
$F(000)$	516.0
μ (MoK α) (mm ⁻¹)	0.257
$2\theta_{\text{max}}$ (°)	50.788
total no. of reflns	10453
no. of unique reflns	2497
no. of reflns	2071
with $I > 2\sigma(I)$	
no. of variables	103
R_1 (F^2 , all data)	0.1731
wR_2 (F^2 , all data)	0.5115
R_1 (F , $I > 2\sigma(I)$)	0.1566
wR_2 (F , $I > 2\sigma(I)$)	0.4800
goodness of fit	2.437

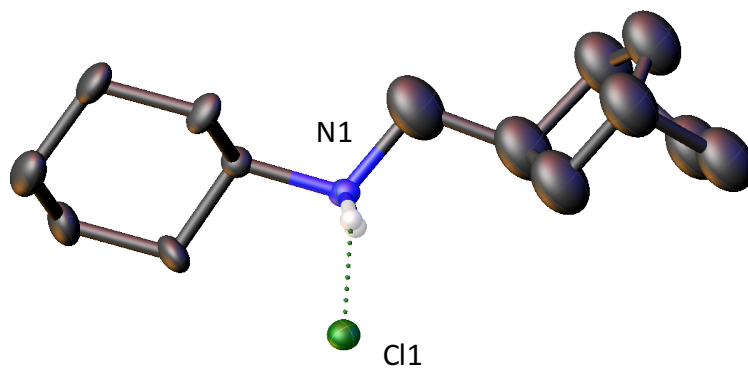


Figure 104 ORTEP of compound 48 synthesized by adding HCl to monomer 42

Appendix E Additional Formulas and Information

The area above the glass transition temperature (T_g) and below the melt is known as the rubbery plateau. The rubbery plateau modulus, G_p , is inversely proportional to the molecular weight between the entanglements, M_e . The value of the plateau modulus, G_n^o , can be estimated from several sets of experimental data for PNB samples of various molecular weights.

$$M_e \cong \frac{\rho_o R T}{G_n^o}$$

M_e = entanglement molecular weight

ρ = polymer density

R = gas constant

T = glass transition temperature